Oil and Natural Gas Technology

Cooperative Research Agreement Award Number DE-FC26-01NT41332

Final Technical Report

September 30, 2001 – March 31, 2014

Resource Characterization and Quantification of Natural Gas Hydrate and Associated Free-Gas Accumulations in the Prudhoe Bay – Kuparuk River Area on the North Slope of Alaska

Submitted by:
BP Exploration (Alaska), Inc. (BPXA)
P.O. Box 196612
Anchorage, Alaska 99519-6612

Robert Hunter (Principal Investigator, 2001-2009)
(Petrotechnical Resources of Alaska)

with Scott Digert (BPXA Principal Investigator)

Prepared for:
United States Department of Energy
National Energy Technology Laboratory

December 3, 2014

Office of Fossil Energy

DISCLAIMER

ABSTRACT

Industry and government have noted and studied natural gas hydrate accumulations on the Alaska North Slope since the 1960's. ARCO and Exxon drilled, logged, cored, and tested a dedicated gas hydrate exploration well (Northwest Eileen State-02) in 1974, after which gas hydrate became better known as a shallow gas hazard necessary to avoid by using conventional well casing and cementing operations to properly isolate these shallow intervals during oil field development. In the 1980's, industry and government renewed desire to better understand the potential productivity of these large natural gas hydrate accumulations within and near North Slope oil field infrastructure areas and whether or not they might contribute to commerciality of stranded gas resources. On April 23, 2001, application for this award resulted in Cooperative Research Agreement DE-FC26-01NT41332 on October 21, 2002 (retroactively effective to September 30, 2001). The project was structured with progression decision gates between 3 phases and significant achieved milestones. A project team assembled in 2001-2002 consisted of a consultant program manager with supporting staff from contractors, universities, and government; this team helped ensure continued industry support by minimizing industry staff distraction from their primary oil field operations responsibilities and by maintaining alignment of stakeholders while accomplishing project objectives. From 2003-2004, Phase 1 reservoir characterization studies confirmed a large in-place potential gas hydrate resource and acquired additional shallow log data in wells-of-opportunity during oil field development operations. Phase 1 reservoir modeling scoping studies indicated the potential for conventional subsurface production using depressurization to dissociate gas hydrate into producible gas and water. In 2005, Phase 2 studies developed more detailed reservoir models, which confirmed this potential production capability and encouraged project progression into 2006 planning of Phase 3 field operations. These 2007 Phase 3a field operations occurred at one of fourteen identified gas hydrate-bearing prospects within the 100% BPXA owned and operated Milne Point Unit. The 2007 Mount Elbert #1 gas hydrate stratigraphic test well confirmed validity of geophysical prospecting techniques and achieved several first Alaska North Slope gas hydrate milestones including acquisition of multi-day open-hole data, 100-feet gas hydrate-bearing core, and dual-packer open-hole Modular Dynamics Testing, sampling, and temperature monitoring. Operations were considered for extension into a Phase 3b long-term production test at the Prudhoe Bay Unit L-pad site in 2008. However, BPXA was debarred from receiving Federal funding in this area due to a March 2006 pipeline oil spill. Continued project no-cost extensions and significantly reduced scope project activities transpired during stakeholder deliberations from 2009-2014.

ACKNOWLEDGEMENTS

This DOE-BPXA Cooperative Research Agreement (CRA) facilitated significant industry interest in the resource potential of ANS natural gas hydrate accumulations. We gratefully acknowledge DOE, USGS, BPXA, industry, government, and academic support of these studies. DOE NETL through the efforts of Brad Tomer, Ray Boswell, Richard Baker, Edith Allison, Tom Mroz, Kelly Rose, Eilis Rosenbaum, and others enabled success of this and associated research projects. Scott Digert and others at BPXA have promoted the importance of this cooperative research within industry. BPXA staff Micaela Weeks, Larry Vendl, Dennis Urban, Dan Kara, Paul Hanson, and others supported stratigraphic test well plans and successfully implemented these Phase 3 well operations and data acquisition. The State of Alaska Department of Natural Resources through the efforts and leadership of Dr. Mark Myers, Bob Swenson, Paul Decker, Diane Shellenbaum, and others has consistently recognized the contribution of this research toward identifying a possible additional unconventional gas resource and has actively supported the Methane Hydrate Act to support continued funding of these studies.

The USGS has led ANS gas hydrate research, especially through the efforts of Dr. Timothy Collett, whom coordinated USGS partnership in the BPXA-DOE CRA. Seismic prospecting and associated reservoir characterization studies accomplished by Tanya Inks (Interpretation Services) and by USGS scientists Tim Collett, Myung Lee, Warren Agena, and David Taylor identified multiple MPU gas hydrate prospects. Support by USGS staff Bill Winters, Bill Waite, and Tom Lorenson and Oregon State University staff Marta Torres and Rick Colwell are gratefully acknowledged. Steve Hancock (RPS Energy) and Peter Weinheber (Schlumberger) helped design and implement Modular Dynamics Test (MDT) field operations. Scott Wilson (Ryder Scott Co.) enhanced reservoir models from studies by the University of Calgary and Fekete Associates (Dr. Mehran Pooladi-Darvish and Huifang Hong) and by the University of Alaska Fairbanks (UAF). Dr. Shirish Patil and Dr. Abhijit Dandekar have maintained UAF School of Mining and Engineering as an arctic region gas hydrate research center. University of Arizona reservoir characterization studies led by Dr. Bob Casavant with Dr. Karl Glass, Ken Mallon, Dr. Roy Johnson, and Dr. Mary Poulton described the structure and stratigraphy of ANS Eileen accumulation Sagavanirktok formation gas hydrate-bearing reservoirs.

Studies of gas hydrate resource potential are numerous, but we are particularly grateful to the following organizations. National Labs studies include those of Dr. Pete McGrail, CO_2 injection experiments, and Dr. Mark White, reservoir modeling, at Pacific Northwest National Lab (PNNL) and Dr. George Moridis, reservoir modeling, and Dr. Jonny Rutqvist, geomechanics, at Lawrence Berkeley National Lab (LBNL). Dr. Joe Wilder and Dr. Brian Anderson (West Virginia University) led significant efforts of an International Reservoir Modeling Code Comparison team. The Colorado School of Mines (CSM) under the leadership of Dr. Dendy Sloan and Dr. Carolyn Koh continue to progress laboratory and associated studies of gas hydrate. The significant efforts of international gas hydrate research projects such as those supported by the Directorate General of Hydrocarbons by the government of India and by the Japan Oil, Gas, and Metals National Corporation (JOGMEC; formerly JNOC) with the government of Japan and by others are significantly contributing to a better understanding of worldwide major resource potential of natural methane hydrate. JOGMEC and the government of Canada support of the 2002 and 2007-2008 Mallik project gas hydrate studies in Northwest Territories, Canada are gratefully acknowledged. This DOE-BPXA cooperative research project builds upon the accomplishments of many prior government, academic, and industry studies.

TABLE OF CONTENTS

1.0 EXECUTIVE SUMMARY

Significant methane hydrate deposits have formed within and below the permafrost in the uppermost reservoirs of the Alaska North Slope (ANS) petroleum system. A desire to better understand the potential productivity of these large natural gas hydrate accumulations and whether or not they could become a commercially viable part of stranded ANS gas resources inspired this multi-year Cooperative Research Agreement (CRA) between BP Exploration (Alaska), Inc. (BPXA) and the U.S. Department of Energy (DOE) National Energy Technology Laboratory (NETL) in close collaboration with the United States Geological Survey (USGS).

Lowered geothermal gradients associated with permafrost growth to depths approaching 2,000 feet (610 meters) over the past 1.2 Million years before present (MMybp) converted ANS shallow free gas-bearing reservoirs within conventional structural and stratigraphic traps into gas hydrate accumulations. Reservoir characterization, reservoir modeling, and associated studies indicate that 0 to 12 Trillion Cubic Feet (TCF) gas may be technically recoverable from 33-44 TCF gas-in-place (GIP) within the ANS Eileen gas hydrate accumulation encompassing portions of the Milne Point Unit (MPU), Prudhoe Bay Unit (PBU), and Kuparuk River Unit (KRU) oil fields and production infrastructure areas.

To better constrain these resource estimates, the USGS reprocessed and interpreted MPU 3D seismic data provided by BPXA and delineated 14 MPU prospects interpreted to contain significant highly saturated gas hydrate-bearing sand reservoirs. The “Mount Elbert” prospect was selected to drill a gas hydrate stratigraphic test well to acquire wireline log, core, and formation pressure test data. Drilling results and data interpretation confirmed pre-drill predictions and thus increased confidence in both the prospect interpretation methods and in the wider ANS gas hydrate resource estimates. The interpreted data from the Mount Elbert #1 well provided insight into and reduced uncertainty of key gas hydrate-bearing reservoir properties, enabled further refinement and validation of the numerical simulation of production potential of both MPU and broader ANS gas hydrate resources, and helped determine viability of field sites for potential future long-term production testing. Successful operations demonstrated that gas hydrate scientific research, drilling, data acquisition, and testing programs can be safely, effectively, and efficiently conducted within ANS infrastructure.

The stratigraphic test program success may help future stakeholders design, drill, and complete a long-term production test within ANS infrastructure to better constrain the potential gas rates and volumes that could be produced from gas hydrate-bearing sand reservoirs and to provide a unique, valuable dataset that cannot be obtained from existing or planned desktop research or laboratory studies. Proximity to resource, industry technology, and infrastructure combine to make the ANS an ideal site to evaluate gas hydrate resource potential through long-term production testing. Such a future test may occur to determine whether or not gas hydrate could help supplement fuel gas requirements for local (MPU or KRU) field development. Test designs could initially evaluate depressurization technologies and if necessary, extend into a sequence of increasingly complex stimulation procedures, possibly including thermal, chemical, and/or mechanical.

2.0 LIST OF TABLES AND FIGURES

2.1 Tables

2.1.1 Appendix A Tables

2.2 Figures

2.2.1 Appendix A Figures

2.2.2 Appendix B Figures

3.0 INTRODUCTION

This Cooperative Research Agreement (CRA) between BP Exploration (Alaska), Inc. (BPXA) and the U.S. Department of Energy (DOE) in collaboration with the U.S. Geological Survey (USGS) stands on the shoulders of many prior efforts (Table 1). Studies within this CRA helped to characterize and assess Alaska North Slope (ANS) methane hydrate resources and to identify technical and commercial factors, which enabled a better understanding of the future development potential of this unconventional energy resource. Results of reservoir characterization, reservoir modeling, regional schematic modeling, and associated studies culminated in the 2007 Mount Elbert-01 Stratigraphic Test, which acquired extensive core, wireline log, and formation pressure data to help mitigate uncertainty of potential recoverable gas hydrate resource and risk of operations within these gas hydrate-bearing shallow reservoirs. Future long-term production testing remains a key goal of worldwide gas hydrate research and development (R&D), but that objective was unable to proceed under this project.

3.1 Project Structure

The project was structured in 3 phases with 7 major elements: (1) Award, contracts, and project management, (2) Geologic framework for reservoir and fluid characterization, (3) Engineering including reservoir modeling, experiments, and operations standards, (4) Regional resource assessment of Eileen gas hydrate accumulation and future production potential, (5) Gas hydrate prospects assessment, test site identification, and resource characterization, (6) Mount Elbert #1 stratigraphic test well planning, operations, and results, and (7) Gas hydrate long-term production test planning and implementation (did not proceed).

Phase 1 desktop studies established project award, contracts, and management; developed project phases, gates, and milestones; setup relevant supporting experimental and reservoir modeling studies; developed field engineering operations standards; and initiated reservoir and fluid characterization studies that led to additional shallow data acquisition within development wells targeting deeper oil-bearing horizons and that also identified viable candidate sites for a dedicated gas hydrate stratigraphic test well.

Phase 2 desktop studies continued the reservoir and fluid characterization, reservoir modeling, and experimental studies and demonstrated the possibility of future regional Alaska North Slope gas hydrate resource commercial development scenarios within the Eileen gas hydrate accumulation. In recognition of the significant regional resource potential, project stakeholders selected a viable site, Mount Elbert #1, for additional data acquisition in a dedicated gas hydrate stratigraphic test well within the Milne Point Unit (MPU).

Phase 3 field operations studies were planned as 2 sub-phases, 3a and 3b. Phase 3a planned and implemented operations that acquired the core, log, and experimental data within Mt Elbert #1. Importantly, this gas hydrate stratigraphic test validated the seismic interpretation methodology and confirmed the gas hydrate petroleum system. Project stakeholders then recommended a site within the Prudhoe Bay Unit (PBU) L-pad area for additional Phase 3b gas hydrate data acquisition and long-term production testing. Phase 3b was planned to extend field operations into long-term gas hydrate production testing, but Phase 3b did not proceed. A future long-term production test could help address remaining technical uncertainties including reservoir continuity, reservoir productivity under various production methods, ability to propagate and maintain a gas hydrate dissociation pressure front under depressurization, ability to sustain near-wellbore and reservoir thermodynamics of gas hydrate dissociation, and determination of gas hydrate dissociation effects on sand and water production within unconsolidated shallow sediments.

3.2 Project Accomplishments Summary

Section 5 of this report fully documents all major and detailed project accomplishments and is structured by project phase and task. Section 5.1 documents detailed Phase 1 accomplishments, tasks 1-13, in Sections 5.1.1 through 5.1.13. Section 5.2 documents detailed Phase 2 accomplishments, tasks 1-10 in Sections 5.2.1 through 5.2.10. Section 5.3 documents detailed Phase 3 accomplishments, tasks 1-9 in Sections 5.3.1 through 5.3.9.

Significant Phase 1 project accomplishments (2001-2004) compiled from Section 5.1 included:

- Defined overall project objectives and summarized technical objectives and approach
- Created, monitored, and maintained task schedules, milestones, and budget estimates
- Released Limited Rights NWEileen and Milne survey 3D seismic data within MPU
- Acquired shallow log data in MPU and PBU wells drilling to deeper oil-bearing targets, including MPE-26, MPS-15i, PBL-106, PBV-107, and MPI-16
- Presented project briefings to DOE, AAPG sectional and national meetings
- Investigated seismic attribute analyses for direct free gas and gas hydrate indicators
- Interpreted multiple potential MPU area gas hydrate play fairways and prospects
- Developed gas hydrate volumetrics, uncertainty analyses, and comparative ranking of 14 MPU prospects with 668 BCF GIP for Phase 2 progression recommendation
- Determined a relation between seismic amplitude attribute and gas hydrate-bearing zone thickness and saturation
- Calculated GIP range from distribution of gas hydrate saturation (40%-90%), net-to-gross (70%-90%), porosity (34%-40%), and BRV
- Developed industry-standard reservoir models to help determine potential gas hydrate-bearing reservoir producibility and assist in phase progression decisions

- Evaluated, ranked, and selected viable candidate areas for gas hydrate and associated free gas drilling, data acquisition, and potential production testing operations
- Considered future gas hydrate regional development potential and calculated project appraisal economics and risk for input into project phase progression decisions

University of Arizona studies (also see Appendix A) included:

- Demonstrated significant role of faults in migration and trapping of gas within gas hydrate-bearing reservoirs, including ESP (coherency) volumes interpretation
- Calculated base of the gas hydrate stability zone using log-interpreted base of ice-bearing permafrost (BIBPF) depths and high resolution borehole temperature surveys
- Correlated gas hydrate-bearing reservoir stratigraphy using both seismic and log data
- Analyzed log data and developed methods for Rw, Sw, resistivity, porosity, Vp/Vs
- Distinguished faulting versus velocity pull-ups associated with gas hydrate prospects
- Distinguished coal-prone sequences versus interpreted prospective gas anomalies
- Validated and reviewed published stratigraphic correlations and compared well log correlations to USGS, and other work, and resolved discrepancies between models
- Compiled representative sample or cuttings data, drilling data, wireline data and petroleum engineering data (casing, perforations, logs, tracer data, temperature data)
- Established and optimized graphic output for well and cross-section displays
- Normalized lithologic responses in multiple generations of wireline log data
- Correlated detailed stratigraphic sequences and parasequences (non-lithostratigraphic)
- Integrated regional structural characterization studies to stratigraphic interpretation
- Included structural analysis mapping fault throws and growth using Milne 3D data
- Calculated fault-seal based on modified shale gouge ratio (SGR) and clay smear potential (CSP) algorithms to show lateral variability in fault seal and trap potential
- Interpreted gas hydrate-bearing reservoirs strongly controlled by N-NE-trending faults
- Developed unique Sagavanirktok stratigraphic column integrating USGS framework
- Correlated 20 Sagavanirktok parasequence units and related bed successions and created correlative sequence stratigraphic framework to guide maps and volumetrics
- Calculated fault heaves from seismic data interpretation and combined with shale thickness data to predict fault-seal, sand body continuity, and reservoir connectivity
- Calculated MPU gas hydrate and free gas volumes to support Phase 2 progression using lithostratigraphic, sequence stratigraphic, and seismic methods
- Confirmed spatial correlation between current shoreline and river trends with certain fault zones and structural trends
- Identified effects of syndepositional faults, permafrost thickness, net-gross sand ratios and locations of "gas chimneys"
- Compared gas hydrate zone thickness to fault proximity and determined possible relation to show sealing syndepositional faults can influence gas hydrate distribution
- Studied timing and influence of fault reactivation on deposition of reservoir sand
- Developed theory for transtensional basin architecture within MPU structural setting
- Created shallow fault map from upper 950 ms seismic data in Milne Point 3D survey and overlapping area of Northwest Eileen 3D survey
- Extracted Amplitude along prominent reflections for possible correlation with gas hydrate and free gas occurrences and performed AVO analyses

- Created grid-illumination-horizon structure maps to interpret subtle structural features and faults and confirmed strong N-NE and more subtle NW structural trends become apparent as termini of N-NE-trending faults, fault zones, and fault seal
- Investigated petrophysical and artificial neural network modeling techniques for log and seismic data analyses
- Performed unsupervised classification using 3D seismic attributes instantaneous frequency, amplitude acceleration, and dominant frequency
- Developed expert system to interpret reservoir fluid types, including gas hydrate, free gas, water, and ice based on resistivity, sonic, porosity, and other logs
- Applied artificial neural network analysis to help characterize and predict lithologies (sand, coal, shale) and fluids (gas hydrate, gas, water) in normalized log data

University of Alaska Fairbanks (UAF) studies included:

- Ran Pressure-Temperature phase behavior experiments; developed thermodynamic models to cover the range of gas hydrate compositions and temperatures
- Conducted 2-phase relative permeability experiments to quantify multiphase flow and assess possible gas productivity from gas hydrate-bearing porous media
- Evaluated drilling mud system chiller options to reduce formation damage and enhance well operations and data acquisition within gas hydrate-bearing sediments
- Evaluated cementing techniques to minimize formation damage and cement volumes and to maximize flow potential and cement bond within gas hydrate-bearing intervals
- Assessed ANS coring technologies and applicability to gas hydrate-bearing reservoirs
- Assessed and comprehensively reviewed commercially available coring systems

Significant Phase 2 project accomplishments (2005-2006) compiled from Section 5.2 included:

- Prepared detailed characterization summaries for 14 MPU gas hydrate prospects
- Compared and ranked 14 prospects and selected Mt Elbert as most highly ranked
- Planned Mt Elbert-01 stratigraphic test well operations and data acquisition program
    - Identified critical tasks and path for well permits, materials, contracts, and rig
    - Documented risks, addressed concerns, and developed plans to mitigate risks
    - Developed contacts and contracts with appropriate operations subcontractors
    - Developed LWD, wireline, core, and MDT evaluation programs
    - Evaluated cement program and initiated discussions with Schlumberger
    - Evaluated drilling mud program and DrillCool, Inc. mudchilling system
    - Planned wireline retrievable core program with Corion (ReedHycalog)
    - Planned core handling and processing program with OMNI Lab and others
    - Prepared procedures, plans, and cost estimates for well operations
- Confirmed Mt Elbert-01 prospect viability from Sagavanirktok formation sequence stratigraphic and structural interpretations in MPU and in PBU L- and V-pad areas
- Completed drilling mud system and formation damage experimental studies
- Completed reservoir modeling and characterization studies to support stakeholder decision to proceed into Phase 3a gas hydrate well stratigraphic test operations
- Used single well, pattern and sectional models to help determine viable candidate sites, design well operations, and predict potential productivity characteristics

Significant Phase 3 project accomplishments (2006-2014) compiled from Section 5.3 included:

- Designed and implemented dedicated gas hydrate stratigraphic test well plans
  - Developed critical tasks, schedules, and path for well permits, materials, contracts, rig, and ice pad/road; modified task schedules as needed
  - Evaluated drilling and data acquisition risks and developed risk mitigations
  - Developed contacts and contracts for well permitting, operations, wireline coring, core processing, wireline and MDT evaluation program, and other
  - Obtained permit to drill from Alaska Oil and Gas Conservation Commission
- Safely implemented Stratigraphic Test Well operations and data acquisition plans
- Successfully demonstrated ability to safely and effectively acquire data within shallow gas hydrate-bearing reservoirs over 7-10 day operations period
- Validated seismic interpretation of gas hydrate-bearing MPU area Mt Elbert prospect
- Acquired 430 feet of 3-inch diameter core (100 feet gas hydrate-bearing) and collected 261 onsite subsamples for preservation and laboratory analyses (also see Appendix B)
- Acquired extensive open-hole wireline logs and 4 long shut-in period MDTs within 2 gas hydrate-bearing reservoirs
- Accomplished several “firsts” in well operations and data acquisition program
  - First significant ANS gas hydrate-bearing core (100 feet of 430 feet acquired)
  - First wireline retrievable coring system application using ANS drilling rig
  - First extensive ANS gas hydrate open hole multi-day data acquisition program
  - First in world gas hydrate-bearing reservoir open-hole dual packer MDT
  - First ANS gas hydrate-bearing reservoir MDT sampling of both gas and water
  - First in world sand face temperature data in both MDT flow and shut-in period
- Acquired data to determine long-term gas hydrate production test program feasibility
- Collaborated with international reservoir model code comparison group and applied gas hydrate numerical simulators to idealized problems of increasing complexity
- Documented reservoir simulator agreement for gas production rates, character, and times and modeled warmer and deeper gas hydrate as more productive with higher initial and sustained rates as well as less time required to initiate gas dissociation from gas hydrate
- Simulated field-scale gas hydrate-bearing reservoirs, history matched the Mt Elbert-01 stratigraphic test MDT data, and evaluated ANS potential production test options
- Completed from 2002 through 2009, project related studies and final report with University of Arizona, supporting a total of 13 students, including 5 Masters theses
- Completed from 2002 through 2009, project related studies with University of Alaska Fairbanks, supporting a total of 8 students, including 5 Masters theses
- Established preliminary designs for a potential future ANS long-term production test
- Completed additional resource characterization and reservoir modeling studies to evaluate potential production test sites within the Eileen gas hydrate accumulation
- Evaluated 4 Eileen accumulation areas for gas hydrate-bearing reservoir properties
- Selected 3 of these 4 areas for input to 3 primary reservoir model simulation studies
- Selected PBU L-106 area as high-potential area for recommended test operations
- Collaborated with gas hydrate research programs, including support to DOE-ConocoPhillips’ Ignik Sikumi (CRA DE-NT0006553) PBU L-106 area test program

3.3 Journal of Marine and Petroleum Geology Special Publication

The Phase 3a field operations program at the MPU Mount Elbert site provided a unique opportunity to acquire and integrate numerous datasets related to the prediction and description of naturally-occurring gas hydrate-bearing reservoirs. The field program included a science team drawn primarily from the USGS, BPXA, DOE-NETL, and Oregon State University (OSU), augmented in collaboration with leading groups worldwide in the post-field program analyses of acquired data and samples. Comprehensive test results and data analyses were published in the Journal of Marine and Petroleum Geology (JMPG; Table 2; Boswell, Collett, Anderson, and Hunter, 2011). Section 7.2 provides links to abstracts for the 24 JMPG Volume papers published.

The *Journal of Marine and Petroleum Geology* (JMPG) thematic volume is entitled "Scientific Results of the Mount Elbert Gas Hydrate Stratigraphic Test Well, Alaska North Slope". This special publication serves as a Scientific Results documentation of the February 2007 Mount Elbert-01 gas hydrate stratigraphic test well data acquisition and interpretation conducted by the DOE, BPXA, USGS, and affiliated scientists. Four guest editors of the JMPG volume helped ensure peer review by project-external subject matter experts to meet JMPG standards: Dr. Ray Boswell, DOE NETL; Dr. Timothy Collett, USGS; Dr. Brian Anderson, West Virginia University/NETL; and Robert Hunter, consultant to BPXA.

The JMPG Volume presented critical data acquired and analyses conducted within the project and integrated findings across multiple disciplines. The 328 page volume (Volume 28, Issue 2, Feb. 2011, ISSN 0264-8172, pp. 279-607) included 24 original scientific research papers within primary topic areas of introductory project review and data synthesis; validation of the seismic data analysis used to site the well; interpretation of advanced well logs; geological, geochemical and petrophysical analyses of sediment core samples; results of pressure testing of reservoir response; and numerical simulations of potential reservoir productivity (Table 2).

This final report of CRA DE-FC26-01NT41332 describes detailed project achievements, milestones, products, and references for all tasks throughout phases 1-3. However, the 24 papers published in the JMPG volume (Table 2 and Section 7.2) represent the most comprehensive review of Phase 3a stratigraphic test studies and readers of this report are encouraged to also fully review this JMPG Volume (Boswell, Collett, Anderson, and Hunter, 2011).

3.4 Alaska North Slope Gas Hydrate Accumulations and Resource Potential

Gas and water combine under appropriate pressure-temperature conditions within both subsea and onshore arctic region sediments to form gas hydrate, a solid that may contain a significant portion of worldwide natural gas resources (Collett, 2002). Natural gas hydrate accumulations require presence of all petroleum system components (source, migration, trap, seal, charge, and reservoir) within the gas hydrate stability conditions depicted in Figure 1. For example, in the right hand portion of Figure 1, the temperature profile projected to an assumed permafrost base of 610m intersects the 100% methane-hydrate stability curve at about 200m, thus marking the methane-hydrate stability zone upper boundary. A geothermal gradient of 4.0°C/100m projected from base of permafrost at 610m intersects the 100% methane-hydrate stability curve at about 1,100m; thus, the methane hydrate stability zone in this example is approximately 900m thick.

The USGS systematically assessed the in-place natural gas hydrate resources of the United States (Collett, 1995) and estimated that ANS gas hydrates within and beneath permafrost contain a mean 590 trillion cubic feet (TCF) gas-in-place (GIP) (Figures 2 and 3). Of this total, 100 TCF estimated GIP may be trapped within the gas hydrate - bearing formations of the "Eileen" and

Timeframe	**Significant ANS Gas Hydrate R&D Historical Events and Milestones**
1960's – 1970's	Early industry and government memorandums and studies of ANS gas hydrate-bearing reservoirs, reservoir characterization, and resource potential
1974	ARCO-Exxon drilling, data acquisition, and testing of Northwest Eileen #2, first ANS dedicated gas hydrate exploration well with logs, core, and Drill Stem Tests (DST)
1984-present	Industry supports and discusses ANS gas hydrate R&D with DOE and USGS
1992	Cirque-02 well control issue related to shallow gas hydrate-bearing reservoir
1996	University of Alaska Fairbanks and Japan R&D on possible ANS gas hydrate test well
1996 – 1999	Industry discusses possible joint DOE-USGS-Industry gas hydrate R&D
January 2001	DOE-USGS-BPXA-Industry resume discussions of gas hydrate R&D project
April 2001	BPXA submits proposal response to DOE, aligned with Alaska gas strategy
October 2002	BPXA initiates desktop studies, reservoir characterization and modeling
February 2007	BPXA/DOE complete Mt Elbert-01 gas hydrate stratigraphic test well in MPU
2008 – 2013	EPA debarment limits BPXA-DOE R&D due to ineligibility to receive Federal funds within PBU
2008 – 2013	ConocoPhillips completes Ignik-Sikumi gas hydrate test well and R&D within PBU
2013 – current	Alaska DNR sets aside 11 ANS leases specifically for gas hydrate research
March 31, 2014	BPXA-DOE CRA project contract termination
2014 – future	DOE continues gas hydrate program with ANS long-term production test a key goal

Table 1: Partial listing of ANS Gas Hydrate R&D Studies, Events, and Milestones

"Tarn" gas hydrate accumulations (Collett, 1993) in close proximity to established ANS oil and gas production infrastructure within the Prudhoe Bay Unit (PBU), Kuparuk River Unit (KRU), and Milne Point Unit (MPU) field areas (Figures 3, 4, and 5). Over 33 TCF GIP hydrate resources are interpreted within gas hydrate-bearing Sagavanirktok reservoir units E, D, C, B, and A within the Eileen accumulation in this area (Figures 4, 5, and 6). The probabilistic volumetric assessment (Collett, 1995) did not identify or characterize the nature of individual gas hydrate accumulations nor assess estimated ultimate recovery (EUR). A future long-term production test could resolve significant remaining challenges of quantifying the fraction of these in-place resources that might become a technically-feasible or possibly a commercial natural gas reserve. USGS studies estimated a mean 85.4 TCF undiscovered, technically recoverable gas hydrate resources beneath the North Slope of Alaska (Table 3) (Collett et al., 2008).

Section / Page	Primary Topic	Primary Author	Author Affiliation
Introduction			
279	ANS Regional Geology	T. Collett	USGS[1]
295	Program Overview	R. Hunter	Consultant/BPXA
Core Program			
311	Coring and Sedimentology	K. Rose	DOE NETL[1]
332	Pore Fluid Geochemistry	M. Torres	OSU
343	Gas Geochemistry	T. Lorenson	USGS[1]
361	Physical Properties	W. Winters	USGS[1]
381	Core Examination / Effects	T. Kneafsey	LBNL[1]
394	SEM Grain Scale Imaging	L. Stern	USGS[1]
404	Microbiology	F. Colwell	OSU[2]
411	Hydrate Characteristics	H. Lu	NRC, Canada[1]
419	Relative Permeability	A. Dandekar	UAF
427	Sediment Properties	S. Dai/C. Lee	Georgia Institute Tech.[1]
Log Program			
439	Gas Hydrate Saturation	T. Collett/M. Lee	USGS[1]
450	Dielectric Properties	Y. Sun	Texas A&M[2]
Simulation			
460	ANS Regional Modeling	S. Wilson	Ryder Scott, Inc.
478	MDT Program & Results	B. Anderson	West Virginia Univ.[1]
493	Long-term Modeling	B. Anderson	West Virginia Univ.[1]
502	MDT Analyses & Modeling	M. Kurihara	Japan Oil Engineering[1]
517	Mt Elbert Site Modeling	G. Moridis	LBNL[1]
535	MDT / Long-term Modeling	M. Pooladi-Darvish	Univ. Calgary/Fekete[2]
546	Modeling & CO_2 Injection	M. White	PNNL[1]
Summary			
561	Log/Core Montages	T. Collett	USGS[1]
578	Pre- Post-drill Comparison	M. Lee/T. Inks	USGS/ Interp. Services[1]
589	Hydrate Geologic Controls	R. Boswell	DOE NETL[1]

Table 2: JMPG Volume Special Publication of Mt Elbert-01 Well Results. Abstracts and papers available at: http://www.sciencedirect.com/science/journal/02648172/28/2

[1] Support for this publication was provided separately from funding for this project
[2] Support for this publication was partially provided separately from funding for this project

In association with this DOE-BPXA CRA project, the USGS interpreted a MPU 3D seismic volume provided by BPXA to characterize gas hydrate resource potential. The study identified 14 sub-permafrost gas hydrate prospects containing an estimated mean 668 BCF GIP within the MPU portion of the Eileen accumulation (Figures 4, 5, 6, and 7; Table 4) (Lee et al., 2009; Lee et al., 2010; Inks et al., 2009). The Mount Elbert prospect was selected after comparative review of these 14 prospects indicated a greater probability of achieving stratigraphic test program data acquisition objectives at this site.

Historically, ANS gas hydrates were considered a shallow drilling hazard to the hundreds of well penetrations targeting deeper oil-bearing formations rather than a potential gas resource. Interpreted occurrence of gas hydrate within Eocene Sagavanirktok Formation shallow sand reservoirs was originally confirmed by log, core, and Drillstem Test (DST) data acquired in the first ANS dedicated gas hydrate test within the Northwest Eileen State-02 (NWEIL-02) well, drilled in 1972 (Table 1, Figures 4 and 5; Collett, 1993). NWEIL-02 DST data indicate limited gas production at a calculated maximum rate of only 3,960 cubic feet/day (CF/d). Since that time, active investigation of gas hydrate recoverable resource potential has been limited due to no ANS gas export infrastructure, assumed low-rate production potential, unknown production methods, and lack of real-world, field-scale data to validate laboratory experiments and reservoir models. However, studies within and supported by this CRA and other studies have improved characterization of ANS gas hydrate-bearing reservoirs, provided reservoir simulations to help better understand gas hydrate dissociation processes, and recognized significant natural gas hydrate energy resource potential.

Research and development of unproven unconventional resources are typically hindered by a lack of proven positive examples necessary before generating stand-alone interest from industry. This pre-development condition held true for tight gas resources in the 1950's-1960's, coalbed methane plays in the 1970's-1980's and shale gas/oil resources in the 1990's-2000's. In each case, the resource was considered technically infeasible and uneconomic until the unique combination of market, technology (new or newly applied), and positive field experience helped motivate industry to implement unconventional recovery techniques in an effort to prove whether or not the resource could be technically and commercially produced.

In an attempt to bridge this gap, gas hydrate reservoir modeling efforts were coupled with an initial regional schematic model to quantify potential recoverable resource within the Eileen accumulation (Figure 6; Wilson, et al., 2011). Production forecast and regional schematic modeling studies included downside, reference, and upside cases. Reference case forecasts with type-well depressurization-induced production rates of 0.4-2.0 MMSCF/D predicted that 2.5 TCF of gas might be produced within 20 years, with up to 10 TCF ultimate recovery after 100 years from the Eileen accumulation 33 TCF GIP. The downside case envisioned research pilot failure and economic or technical infeasibility. Upside cases identified additional potential recoverable resource. These studies included rate forecasts and hypothetical well scheduling, methods typically employed to evaluate potential large conventional gas development projects (additional detail available from June 2006 Quarterly Technical Report Fifteenth Technical Quarterly Report, July 31, 2006 and also from Wilson, et al., 2011).

These reservoir simulation and regional schematic studies culminated in recommendations to drill the Mount Elbert Stratigraphic Test (Figure 7, Tables 4 and 5), which acquired reservoir data including extensive core, wireline log, and formation pressure data between February 3-19, 2007. Significantly, this well effectively proved the ability to safely conduct drilling and extended data acquisition and pressure testing operations within the hydrate-bearing formations. Stratigraphic Test technical success and data interpretation improved understanding of uncertainties, validated reservoir production simulations, and led to an evaluation of potential long-term production test sites in one of four general areas within ANS infrastructure (Figure 8). A future long-term ANS test would build on successful short-term production tests at the Mallik site in March 2008 and at the ANS Ignik Sikumi site in 2012, both of which indicated the technical feasibility of gas production from gas hydrate by conventional depressurization and by CO_2-replacement technology, respectively.

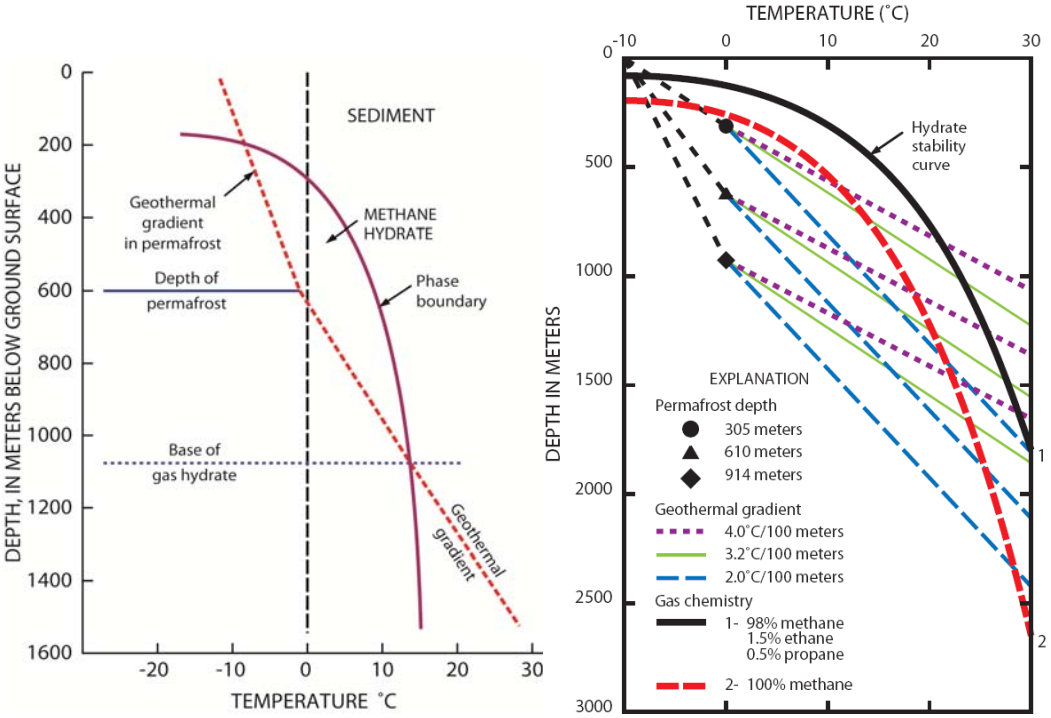

Figure 1: Gas Hydrate Stability Phase Diagrams (after Collett et al., 2010); right-hand figure shows effects of formation temperature, pore pressure, and gas composition on gas hydrate stability with depths between intersections of geothermal gradient and gas hydrate stability curve

Although the technical recovery has been modeled for the ANS and proven possible in these short-term production tests, the economic viability of gas hydrate production remains uncertain until sufficient field testing constrains long-term production rates, predicts EUR volume, and defines and implements applicable production technologies. Additional data acquisition and future production testing would help determine the technical feasibility of depressurization-induced or stimulated dissociation of gas hydrate into producible gas. Long-term production testing was not approved for this CRA, although implementation of the designs at one of the sites (Figure 8) would provide a unique, valuable dataset that cannot be obtained from existing or future desktop research or laboratory studies. Proximity to resource, industry technology, and infrastructure combine to make the ANS an ideal site to evaluate gas hydrate resource potential.

In recognition of this principle, in August of 2013, the State of Alaska DNR set aside 11 leases from the ANS and Beaufort sale areas for purposes of gas hydrate resource research (Figure 9).

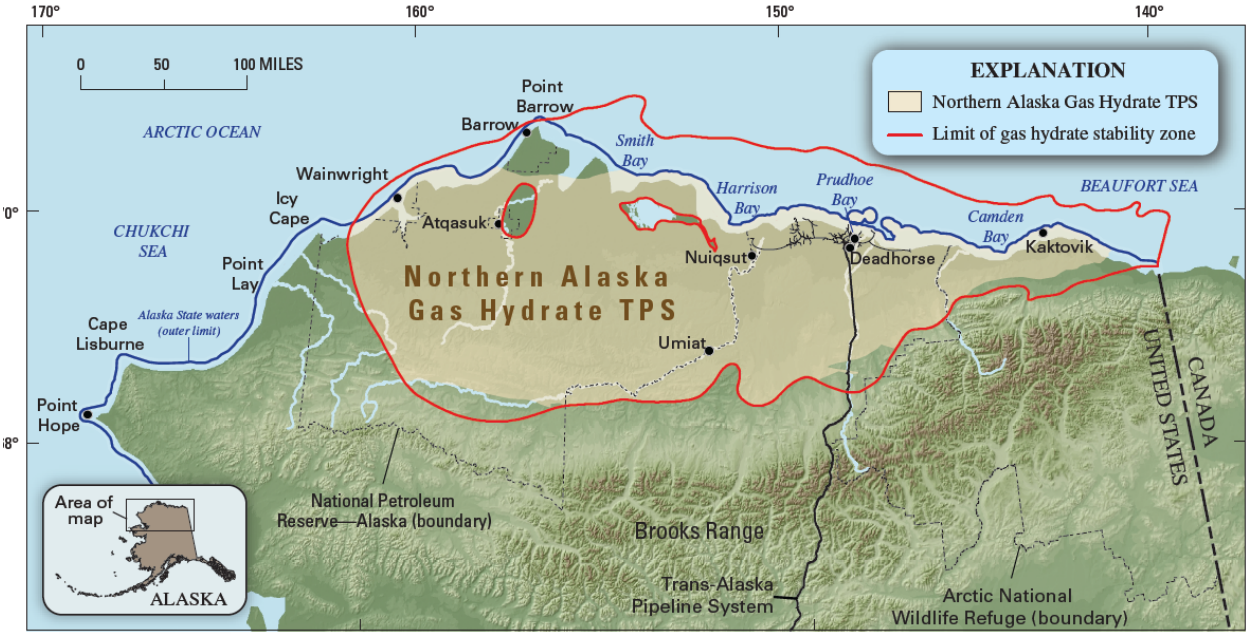

Figure 2: Northern Alaska Gas Hydrate Total Petroleum System (TPS) (shaded in tan), and the limit of gas hydrate stability zone in northern Alaska (red outline); USGS Fact Sheet 2008-3073.

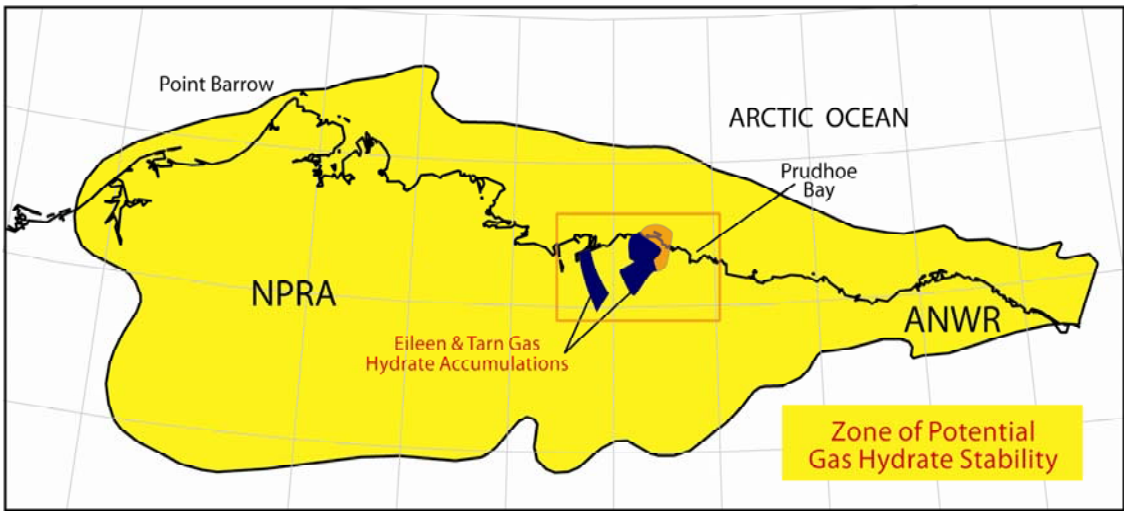

Figure 3: ANS gas hydrate stability zone (red outline of Figure 2) containing an estimated mean 590 TCF GIP showing Eileen and Tarn gas hydrate accumulations after Collett (1993 and 1995).

Future exploitation of gas hydrate would require developing feasible, safe, and environmentally-benign production technology, initially within areas of industry infrastructure. The ANS onshore area within the Eileen accumulation area favorably combines a well-characterized gas hydrate petroleum system with accessible infrastructure and technology. Future long-term production testing might initially evaluate depressurization technologies and if necessary, extend into a sequence of increasingly complex thermal, chemical, and/or mechanical stimulation procedures. The information and technology developed in an onshore ANS program might also help determine the resource potential of the potentially much larger marine gas hydrate resources in

the GOM and in other offshore continental shelf areas. If gas can be technically produced from gas hydrate and if future studies help prove production capability at economically viable rates, then methane dissociated from ANS gas hydrate could possibly help supplement future field operations fuel-gas, provide additional lean-gas for reservoir energy pressure support, sustain long-term production of portions of the geographically-coincident 20-25 billion barrels viscous oil resource, and/or supplement conventional export-gas in the longer term.

Total Petroleum System and Assessment Unit	Field Type	*Total Undiscovered Resources*							
		Gas (BCFG)				*NGL (MMBNGL)*			
		F95	F50	F5	Mean	F95	F50	F5	Mean
Northern Alaska Gas Hydrate TPS									
Sagavanirktok Formation Gas Hydrate AU	*Gas*	6,285	19,490	37,791	20,567	0	0	0	0
Tuluvak-Schrader Bluff-Prince Creek Formations Gas Hydrate AU	*Gas*	8,173	26,532	51,814	28,003	0	0	0	0
Nanushuk Formation Gas Hydrate AU	*Gas*	10,775	35,008	68,226	36,857	0	0	0	0
Total Undiscovered Resources		**25,233**	**81,030**	**157,831**	**85,427**	**0**	**0**	**0**	**0**

Table 3: ANS EUR gas hydrate resource (USGS Fact Sheet 2008-3073). Sagavanirktok Assessment Unit (AU) includes Eileen accumulation infrastructure area (Figure 4).

3.5 Future Recommendations

This DOE-BPXA CRA built upon the accomplishments of many prior studies and the research accomplishments of this project may be applied to a future ANS long-term gas hydrate production test pilot project. A location for this pilot test was identified in 2008 at the PBU L-pad site (Figure 8). This site or alternate sites may offer the unique combination of low geologic risk, maximum operational flexibility (multiple zones), low operational risk (near-vertical wells adjacent to infrastructure) and near-term meaningful reservoir response (Figure 8 and Table 5; Collett and Boswell, 2009). The ConocoPhillips-DOE Ignik-Sikumi well successfully tested this PBU L-pad site in a short-term CO_2/CH_4 exchange and depressurization gas hydrate test in 2012 (DE-NT0006553). The final report for that project documented a successful wellbore and completion design (Schoderbek, et al, 2013, pp.34-40). Successful future long-term gas hydrate production testing would help motivate industry to implement unconventional recovery techniques on either local fuel-gas or regional gas development scales.

Large scale potential future development of gas hydrate resources might occur if initial local test results promisingly indicate commercial viability. Regional development of ANS gas hydrate resources may occur in the future, but only if commercially viable and synergistic with conventional gas resource development. Certain ANS field areas such as MPU and KRU may become short of fuel gas for local facility power generation. One option to supplement these fuel gas needs may be the locally abundant gas hydrate accumulations. Rather than transport PBU gas via pipeline, a local shallow gas hydrate pilot test production well might help meet this local fuel gas demand. If proven capable of commercial gas production for local use, gas hydrate may eventually be used to supplement a long-term regional conventional gas supply.

Prospect	Bulk Rock Volume (m^3)	Acres	Porosity	Net to Gross	Gas Hydrate Saturation	Gas-in-Place (BCF)	Gas-in-Place (Billion M^3)
Mt Antero "C"	66,545,880	955	38%	80%	66.1%	75.2	2.13
Mt Bierstadt "D"	31,704,181	268	37%	80%	49.8%	32.3	0.91
Mt Bierstadt "E"	34,891,823	332	39%	80%	66.9%	41.8	1.18
Blanca Peak "C"	20,977,026	328	38%	80%	55.1%	22.4	0.63
Crestone Peak "C"	179,796,792	1728	38%	80%	49.8%	185.8	5.26
Mt Elbert "C"	84,961,956	1106	38%	80%	59.7%	93.3	2.64
Mt Elbert "D"	49,876,375	267	37%	80%	52.6%	52	1.47
Grays Peak "B"	5,771,419	85	38%	80%	47.2%	5.8	0.16
Maroon Peak "A"	26,261,864	375	38%	80%	81.2%	32.8	0.93
Mt Princeton "D"	36,580,949	449	37%	80%	53.2%	38.2	1.08
Pikes Peak "B"	11,261,848	298	38%	80%	68.8%	13.2	0.37
Redcloud Peak "B"	16,580,030	194	38%	80%	58.1%	18	0.51
Mt Sneffels "D"	42,949,487	516	37%	80%	57.6%	46.2	1.31
Uncompahgre Pk "D"	11,056,564	167	37%	80%	49.3%	11.2	0.32
E Combined	**34,891,823**	**332**	**39%**	**80%**	**66.9%**	**41.8**	**1.18**
D Combined	**172,167,556**	**1667**	**37%**	**80%**	**52.5%**	**179.9**	**5.09**
C Combined	**352,281,654**	**4117**	**38%**	**80%**	**57.7%**	**376.7**	**10.7**
B Combined	**33,613,297**	**577**	**38%**	**80%**	**58.03%**	**37**	**1.04**
A Combined	**26,261,864**	**375**	**38%**	**80%**	**81.2%**	**32.8**	**0.93**
TOTAL	**619,216,195**	**7068**	**38%**	**80%**	**63.3%**	**668.2**	**18.9**

Table 4: MPU gas hydrate prospect reservoir properties (Hunter et al, 2011; Inks et al, 2009).

Studies for commercialization of conventional ANS gas have been underway since discovery and development of the PBU field. While these large gas reserves currently remain stranded, a future development may be associated with the recently approved Pt Thomson gas condensate field. PBU conventional ANS gas development would require separation and sequestration of 10-12% CO_2 prior to pipeline shipment. Since ANS gas hydrate reservoirs are likely not filled to spill-point due to their significant volume reduction with conversion from originally-migrated free gas, these gas hydrate-bearing reservoirs are likely not filled to spill point. The transformation of the trapped free gas into gas hydrate when combined with available pore waters would commonly lead to what was a free gas at spill point being converted to a gas hydrate accumulation with a hydrate-water contact well above the former spill-point free-gas to water contact. Thus, abundant natural gas traps could be available for injection of CO_2 into the now water-bearing lower portions of these accumulations and may become a significant available proven sink for future CO_2 sequestration that could occur, perhaps in combination with CO_2/CH_4 exchange method production. Some evidence for this was interpreted with perched water within the MPU Mount Elbert prospect area (this report; Hunter, et al, 2011; and Boswell, et al, 2011).

Field Area / Risk Parameter	MPU E-pad (area 1)	MPU B-Pad (area 1)	PBU L-pad (area 2)	PBU Kup St. 3-11-11 (area 2)	PBU Downdip L-pad (area 3)	KRU WSak-24 (area 4)	KRU 1H-Pad (area 4)
Temperature	H	H	M	M	L	H	H
Ownership	L	L	H	H	H	M-L	M-L
Gravel Access	M	M	L	L	H	L	L
Geologic	L	L	L	L	H	M	M
Data Constraints	L	L	L	M	H	M	M
Well / Drilling	L-M	L-M	M	M	H	M	M
Facilities	L	L	L	M	H	M	L
Gas Handling	H	H	H	H	H	H	H
Water Handling	L	L	L	M	H	M	L
Simultaneous Operations	L	M	H?	L	L	L	H?
Operations Link	L?	L?	M	M	M	L	L?
Multi-zone	M-H	M-H	L	L	M-H	H	H
AVERAGE	**L-M**	**L-M**	**L-M**	**M**	**M-H**	**M**	**M**

Unit	Depth meters (feet)	Lower Contact	Thickness meters (feet)	Gas Hydrate Saturation (%)	Porosity (%)	Intrinsic Permeability (mD)	Temperature (^{o}C)	Pressure Gradient	Salinity (ppt)
Milne Point Unit – Mount Elbert Prospect (area 1 of Figure 8)									
C	650 (2132)	Water	16 (52)	65	35	1000	3.3 - 3.9	Hydrostatic	5
D	614 (2014)	Shale?	14 (47)	65	40	1000	2.3 - 2.6	Hydrostatic	5
Prudhoe Bay Unit – L-V-Z pad vicinity (area 2 of Figure 8)									
C2	707 (2318)	Shale	19 (62)	75	40	1000	5.0 – 6.5	Hydrostatic	5
C1	679 (2226)	Shale	17 (56)	75	40	1000	5.0 – 6.5	Hydrostatic	5
D	628 (2060)	Shale	15 (50)	70	40	1000	3.0 – 4.0	Hydrostatic	5
E	584 (1915)	Shale	15 (50)	60	40	1000	2.0 – 3.0	Hydrostatic	5
Prudhoe Bay Unit Down-Dip (area 3 of Figure 8)									
C	762 (2500)	Shale	18 (60)	75	40	1000	~12	Hydrostatic	5
Kuparuk River Unit – West Sak 24 vicinity (area 4 of Figure 8)									
B	689 (2260)	Shale?	12 (40)	65	40	1000	2.0 – 3.0	Hydrostatic	5

Table 5: Review of risk factors and reservoir properties for long-term production test sites. H=high risk parameter (unfavorable); M=medium risk; L=low risk (Collett and Boswell, 2009).

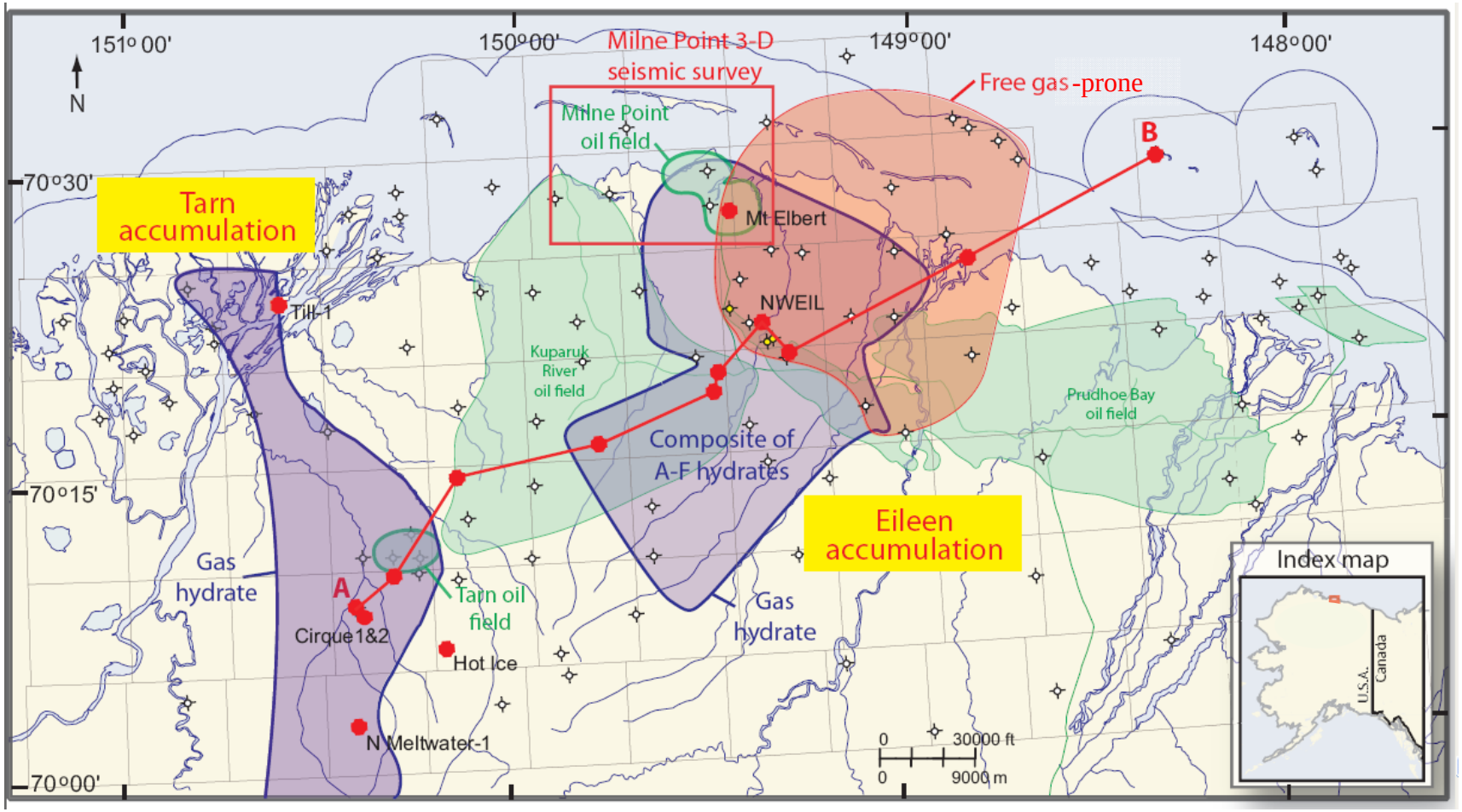

Figure 4: Eileen and Tarn Gas Hydrate Accumulations and ANS Field Infrastructure (modified after Collett et al, 2010). Estimated Eileen accumulation GIP = 33 TCF with EUR = 2 - 12 TCF (Wilson et al., 2011).

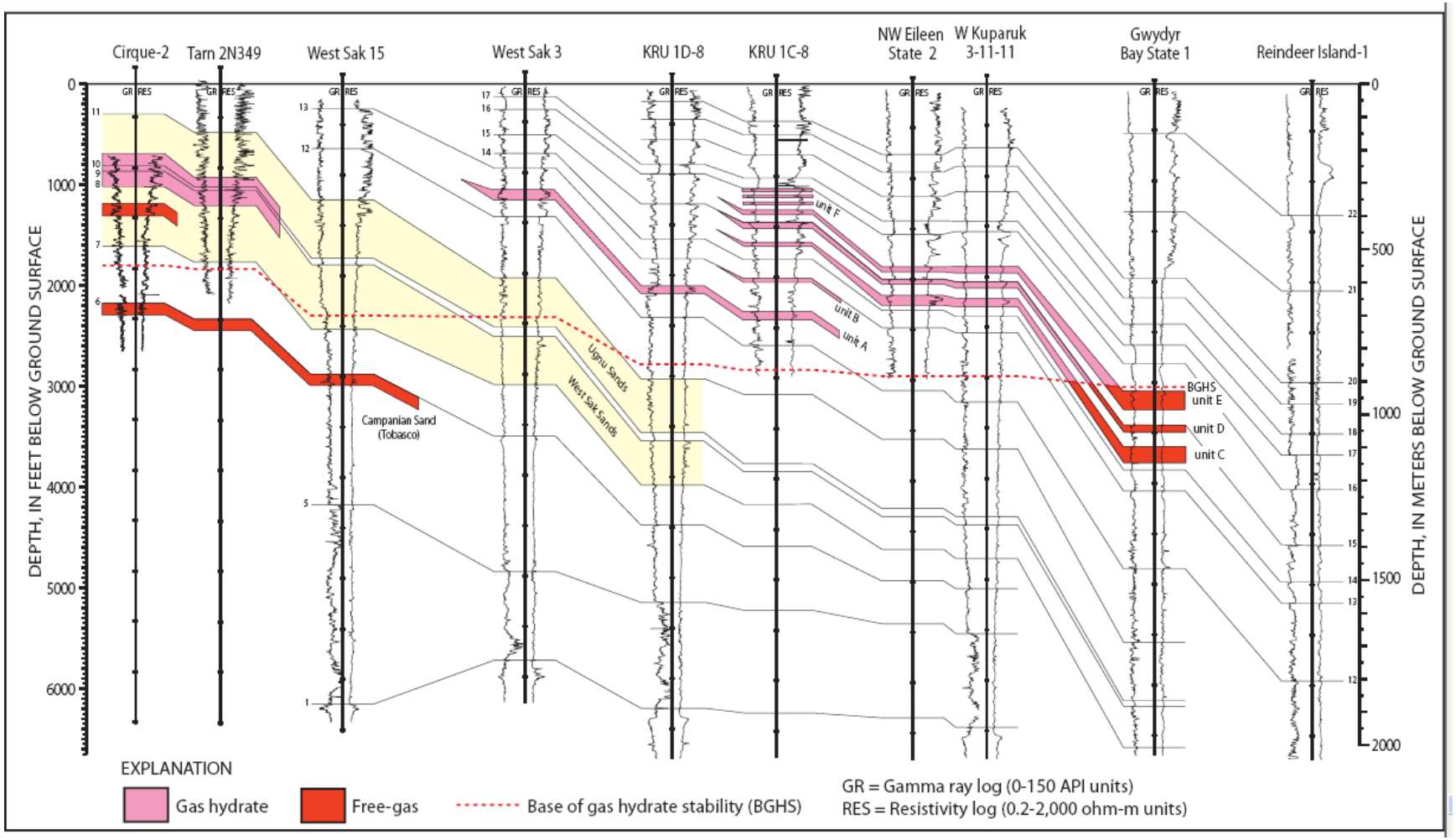

Figure 5: Well log cross-section (Red line of section A-B shown in Figure 4) illustrating gas hydrate-bearing formations within the Eileen and Tarn accumulations (Collett, et al, 2011). Informal Sagavanirktok formation units A through F are shown within the Eileen accumulation. Gas hydrate (pink) and free gas (red) schematic to respectively indicate sediments within and below gas hydrate stability field. Log correlation markers, shown by numbered solid lines, are used to construct a regional stratigraphic framework (modified from Collett, 1993, Collett, et al, 2011).

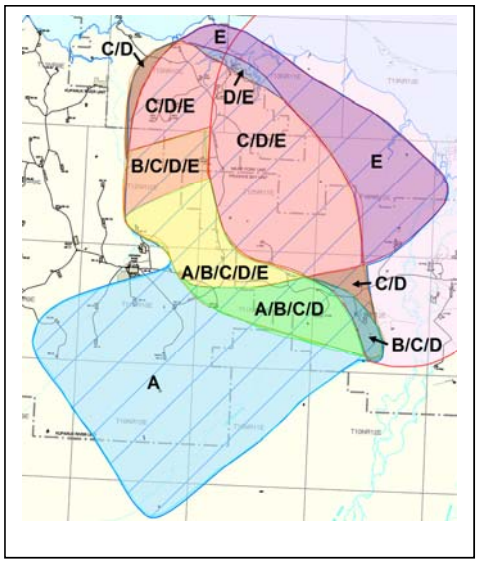

Figure 6: Interpreted gas hydrate-bearing Sagavanirktok units A through E in map of Eileen accumulation (modified from Collett, 1993); used to construct regional schematic model (Wilson, et al., 2011).

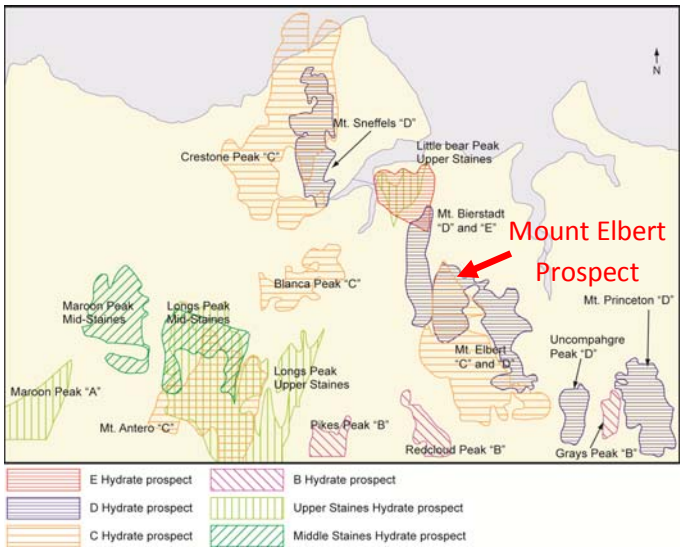

Figure 7: MPU gas hydrate prospects interpreted from 3D seismic, including Mount Elbert (Inks, T., Lee, M., Taylor, D., Agena, W., Collett, T. and Hunter, R., 2009), also Figure 35.

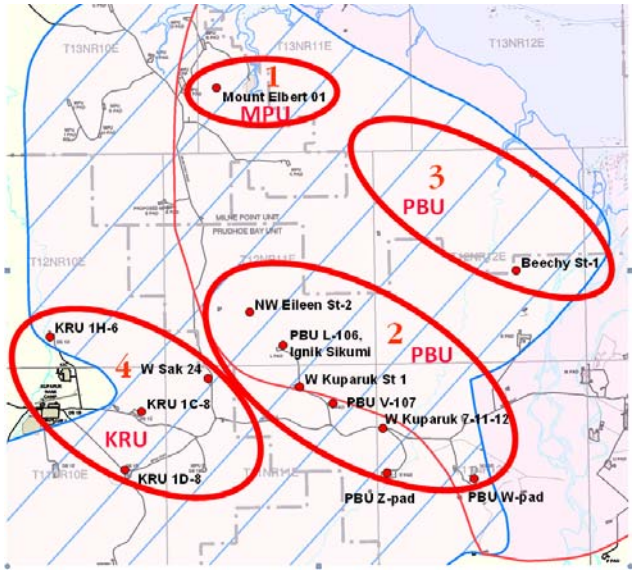

Figure 8: Eileen gas hydrate accumulation composite Sagavanirktok zones A, B, C, D, E (blue striped area; also Figure 6) with 4 areas-of-interest for a potential future long-term production test site.

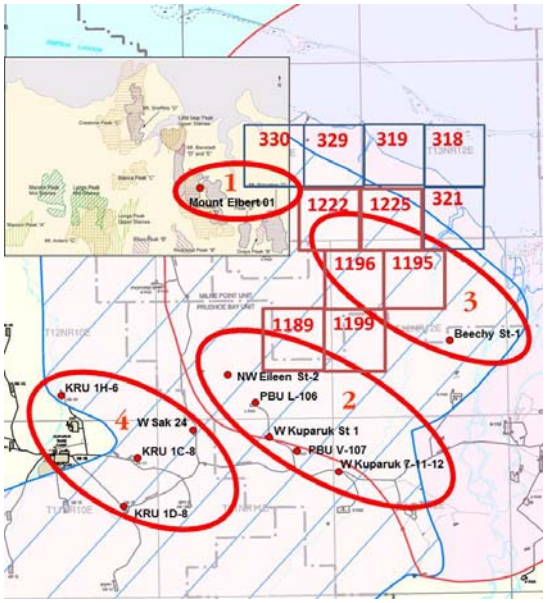

Figure 9: Eileen gas hydrate accumulation with non-georeferenced overlays of MPU gas hydrate prospects (Figure 7) and of August, 2013 DNR 11 Beaufort and North Slope State leases set aside for future gas hydrate research.

4.0 CONTRACT AND COST SUMMARY

4.1 Contract Amendments

Table 6 summarizes CRA project contracts and amendments. Following a 2008 recommendation to consider a long-term gas hydrate production test within PBU, it was determined that BPXA was ineligible to receive Federal funds for operations within PBU due to EPA debarment associated with the March 2006 pipeline spill. Project activities remained at a reduced scope from 2008 through 2014. From 2008 through 2013, under separate agreement DE-NT0006553 with DOE, ConocoPhillips (CoP) successfully accomplished a short-term gas hydrate production test at Ignik-Sikumi near PBU L-pad. In 2014, CRA project stakeholders elected to not submit a Continuation Application request for Phase 3 long-term gas hydrate production test operations.

Amendment	Date	DOE Funding	Total Federal	Primary Purpose
0 – Contract	10/1/2001	$1,300,000	$1,300,000	Contract 10/23/02 retroactive to 9/30/01
1 – Phase 1	10/1/2001	$573,546	$1,873,546	Added Phase 1 funds
2	9/30/2002	$400,000	$2,273,546	Included $195,718 funds for Phase 2*
3	12/22/2003	$0	$2,273,546	Time Extension only
4	1/26/2004	$0	$2,273,546	Patent Waiver
5	8/9/2004	$500,000	$2,773,546	Additional funds & Cost share update
6	11/2/2004	$0	$2,773,546	Budget Period extension
7	11/16/2004	$34,000	$2,807,546	Reservoir characterization funds added
8	1/5/2005	$0	$2,807,546	*Obligated $195,718 for formal Phase 2
9 – Phase 2	3/3/2005	$674,767	$3,482,313	Obligated full Phase 2 funds
10	7/6/2005	$0	$3,482,313	3-month Phase 2 time extension
11 – Phase 3	9/3/2005	$2,257,000	$5,739,313	Phase 3a SOW & initial funds obligation
12	4/21/2006	$1,853,584	$7,592,897	Additional Phase 3a operations funds
13	7/21/2006	$734,809	$8,327,706	Additional Phase 3a operations funds
14	9/28/2006	$10,000	$8,337,706	Additional Phase 3a operations funds
15	12/6/2006	$0	$8,337,706	"Definitized" Phase 3a budget
16	12/18/2006	$0	$8,337,706	Cost overrun approval contingencies
17	1/24/2007	$0	$8,337,706	DOE COR to Richard Baker
18	9/13/2007	$1,083,982	$9,421,688	Phase 3a documented cost-overrun
19	12/3/2007	$0	$9,421,688	9-month extension; new BPXA officer
20	3/7/2008	$397,728	$9,819,416	Additional planning & analyses costs
Extensions				
21	8/25/2008	$0	$9,819,416	No-cost extension
22	9/4/2008	$0	$9,819,416	$230,000 change DOE to Arctic Energy
23	9/17/2008	$0	$9,819,416	$167,728 change DOE to Arctic Energy
24	12/19/2008	$0	$9,819,416	No-cost extension
25	4/2/2009	$0	$9,819,416	No-cost extension; PI Gordon Pospisil
26	7/7/2009	$0	$9,819,416	No-cost extension
27	9/16/2009	$0	$9,819,416	No-cost extension
28	3/24/2010	$0	$9,819,416	No-cost extension
29	6/30/2010	$0	$9,819,416	No-cost extension
30	9/30/2010	$0	$9,819,416	No-cost extension
31	3/31/2011	$0	$9,819,416	No-cost extension; Alter BPTA to BPXA
32	9/20/2011	$0	$9,819,416	No-cost extension
33	9/21/2012	$0	$9,819,416	No-cost extension; PI Scott Digert
34	9/20/2013	$0	$9,819,416	No-cost/Project extension to 3/31/14

Table 6: CRA project contract amendments and primary purpose

4.2 Cost Summary

Table 7 estimates project cost status through end-2Q14. Project cost-share remained above the contractually required 20% through contributions of in-kind data utilized by the project and by paying 100% contributing BP staff and 25% lead consulting staff.

US Treasury Account Total Federal Share Funds (Phases 1-3)	$9,819,416.00
Total Federal-share invoices (end-2Q14)	$9,629,796.30
Estimated Project Reimbursement (6/23/2014)	$122,046.57
Estimated pre-closeout costs final invoices	$12,819.75
Pre-project closeout final costs	$134,866.32
Estimated US Treasury Account Balance as of 6/17/2014	$189,619.70
Estimated DOE Funds after pre-closeout cost reimbursement	$54,753.38
Estimated DOE cost April-July, 2014 Project Closure Activity	$48,600.00
Calculated BPXA Cost-Share (March, 2014)	20.66%
Estimated DOE funds remaining at close-out (August, 2014)	**$6,153.38**

Table 7: Estimated project cost status from Phase 1 through Phase 3 and project closeout

5.0 PROJECT PHASES, TASK DESCRIPTIONS, AND ACCOMPLISHMENTS

This section summarizes detailed project accomplishments by project phase and task, but does not comprehensively review all previously reported project work. Additional detailed project technical reports and associated information covering specific timeframes are available from DOE website link at:
http://www.netl.doe.gov/research/oil-and-gas/project-summaries/methane-hydrate.

Table 8 provides a comprehensive listing of all project technical reports. For certain project accomplishments, this section references prior reports containing additional detailed information by their indicated number in the left-most column in Table 8 (e.g. R01 for first quarterly report for time period ending December, 2002). Where significant supplemental information is available, such reference includes specific page number(s) from that prior report. Table 9 lists additional project documents currently available on the DOE website link.

One of the most significant project accomplishments established this Cooperative Research Agreement to enable, align, and formalize industry and government cooperation to help determine the resource potential of ANS natural gas hydrate-bearing reservoirs. Prior studies establish that the majority of worldwide carbon and gas resources are contained in gas hydrate accumulations (Figure 10) and that the easiest place to determine technical feasibility of production would be within ANS industry infrastructure (Figure 11).

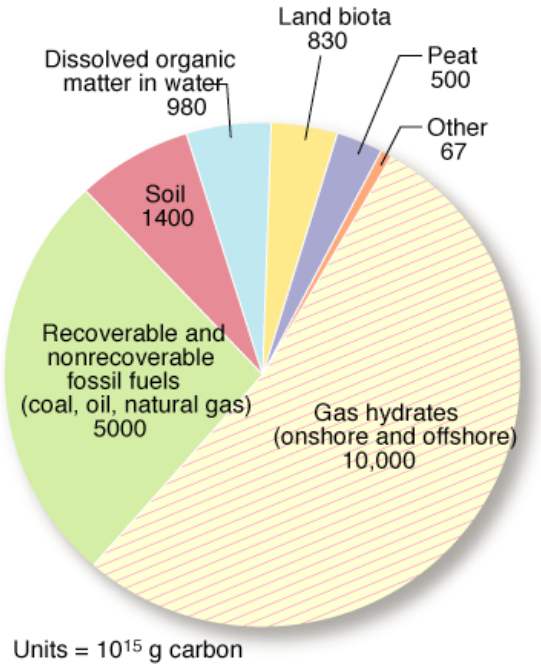

Figure 10: Distribution of Organic Carbon Worldwide (after Kvenvolden, 1988)

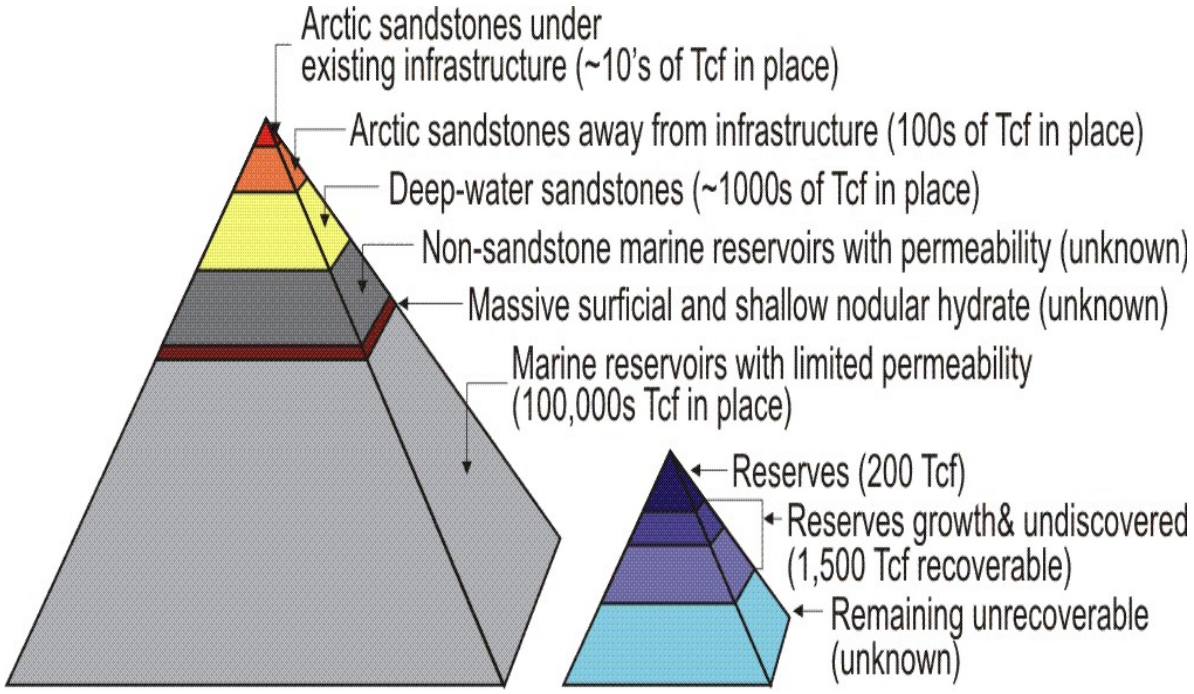

Figure 11: Gas hydrate worldwide resources pyramid (after Boswell, et al, 2007)

#	Timeframe	Report Description	Length, Size (pdf)
	PHASE 1		
R01	Sept 2001-Dec 2002	1st Quarterly	62pp, 0.6MB
R02	Jan-Mar 2003	2nd Quarterly	54pp, 0.5MB
R03	Apr-June 2003	3rd Quarterly	51pp, 2.5MB
R04	July-Sept 2003	4th Quarterly	29pp, 1.9MB
R05	Oct-Dec 2003	5th Quarterly	53pp, 1.9MB
R06	Jan-Mar 2004	6th Quarterly	53pp, 0.9MB
R07	Apr-June 2004	7th Quarterly	72pp, 3.1MB
R09	July-Dec 2004	8th-9th Quarterly	83pp, 7.5MB
	PHASE 2	*10th-14th Quarterly waived*	
T01	June 2005	Topical: Drilling / Planning	36pp, 8MB
	PHASE 2-3		
R15	Jan 2005-June 2006	15th Quarterly	212pp, 7.4MB
	PHASE 3		
R16	July-Sept 2006	16th Quarterly	51pp, 1MB
R17	Oct-Dec 2006	17th Quarterly	108pp, 10.5MB
R18	Jan-Mar 2007	18th Quarterly	117pp, 34MB
R19	Apr-June 2007	19th Quarterly	37pp, 2.3MB
R20	July-Sept 2007	20th Quarterly	100pp, 16MB
R22	Oct 2007-Mar 2008	4Q07 – 1Q08 Semi-Annual Q21-22	66pp, 11.9MB
R24	Apr 2008-Sept 2008	2Q08 – 3Q08 Semi-Annual Q23-24	62pp, 1.2MB
R26	Oct 2008-Mar 2009	4Q08 – 1Q09 Semi-Annual Q25-26	133pp, 14.6MB
	PHASE 3 Extensions		
R28	Apr 2009-Sept 2009	2Q09 – 3Q09 Semi-Annual Q27-28	65pp, 3.5MB
R30	Oct 2009-Mar 2010	4Q09 – 1Q10 Semi-Annual Q29-30	63pp, 3.8MB
R32	Apr 2010-Sept 2010	2Q10 – 3Q10 Semi-Annual Q31-32	59pp, 3.4MB
R34	Oct 2010-Mar 2011	4Q10 – 1Q11 Semi-Annual Q33-34	60pp, 3.4MB
R36	Apr 2011-Sept 2011	2Q11 – 3Q11 Semi-Annual Q35-36	60pp, 3.4MB
R38	Oct 2011-Mar 2012	4Q11 – 1Q12 Semi-Annual Q37-38	59pp, 3.4MB
R40	Apr 2012-Sept 2012	2Q12 – 3Q12 Semi-Annual Q39-40	59pp, 2.2MB
R42	Oct 2012-Mar 2013	4Q12 – 1Q13 Semi-Annual Q41-42	59pp, 1.7MB
R44	Apr 2013-Sept 2013	2Q13 – 3Q13 Semi-Annual Q43-44	59pp, 1.6MB
		4Q13 – 1Q14 Semi-Annual waived	
F01	Sept 2001-June 2014	Final Report, December 2014	360pp, 30.8MB (pdf), 120MB (WORD)

Table 8: Listing of Submitted Project Technical Reports

Document	Year	Description
JIP_Hunter_PrudhoeBay.pdf	2003	30 Slide DOE Conference Presentation
char-41332-hydrate-poster.pdf	2004	Seismic Modeling Poster
ArcticEnergySummitPaper-2008.pdf	2008	Preliminary Results of 2007 Stratigraphic Test (Hunter, et al, 2008)
ICGH_5730_1_41332.pdf	2008	Analysis of MDT Results, Mount Elbert-01 Stratigraphic Test (Anderson, et al, 2008)
ICGH_5727_2_CodeComp.pdf	2008	International Effort to Compare Gas Hydrate Reservoir Simulators (Wilder, et al, 2008)
ICGH_5498_1_41332.pdf	2008	Preliminary Assessment of Hydrocarbon Gas Sources from Mt Elbert-01 (Lorenson, et al, 2008)
ICGH_5794_41332.pdf	2008	Analyses of Production and MDT Tests at Mallik and Alaska (Kurihara, et al, 2008)
ICGH_5755_41332.pdf	2008	Investigation of Gas Hydrate-Bearing Sandstone Reservoirs at Mount Elbert (Boswell, et al, 2008)
NT41332_BPXA-Wilson.pdf	2009	49-Slide Reservoir Modeling Summary (Wilson, 2009)
NT41332_BPXA-Hancock.pdf	2009	13-Slide ANS Production Test Well Considerations (Hancock, 2009)
NT41332_BPXA-Hunter.pdf	2009	60-Slide Project Summary (Hunter, 2009)

Table 9: Listing of Additional Project Documents Currently Available on DOE website: http://www.netl.doe.gov/research/oil-and-gas/project-summaries/methane-hydrate

5.1 Phase 1 Tasks, Milestones, and Accomplishments, 2002-2004

U.S. Department of Energy Milestone Log, Phase 1, 2002-2004

Program/Project Title: DE-FC26-01NT41332: Resource Characterization and Quantification of Natural Gas Hydrate and Associated Free-Gas Accumulations in the Prudhoe Bay - Kuparuk River Area on the North Slope of Alaska.

Phase 1 desktop and laboratory studies in tasks 1-13 are summarized in Tables 10 and 11. These studies facilitated gas hydrate-bearing reservoir characterization, laboratory studies, reservoir modeling, data acquisition, and planning of production test technologies used to select viable drilling location candidates and to help determine whether or not to proceed into additional Phase 2 studies. Phase 1 scope-of-work was outlined in contract amendments 1-8 (Table 6). Phase 1 accomplishments are summarized for each task in this section. Significant accomplishments also reference prior reports containing additional detailed information by their indicated number in the left-most column in Table 8.

Identification Number	Description	Planned Completion Date	Actual Completion Date	Comments
Task 1.0	Research Management Plan	12/02 – 12/04	12/02 – 12/04	Subcontracts Completed, Section 5.1.1
Task 2.0	Provide Technical Data and Expertise	MPU: 12/02 PBU: * KRU: *	MPU: 12/02 PBU: * KRU: *	See Technical Progress Reports, Section 5.1.2
Task 3.0	Wells of Opportunity Data Acquisition	Ongoing	Ongoing	See Technical Progress Reports, Section 5.1.3
Task 4.0	Research Collaboration Link	Ongoing	Ongoing	See Technical Progress Reports, Section 5.1.4
Subtask 4.1	Research Continuity	As-Needed	As-Needed	
Task 5.0 (USGS)	Logging and Seismic Technology Advances	12/04	12/04	See Technical Progress Reports, Section 5.1.5
Task 6.0 (UA)	Reservoir and Fluids Characterization Study	12/04	final report received 9/09	2004 Hedberg Conference, See Section 5.1.6
Subtask 6.1	Characterization and Visualization	12/04	final report received 9/09	2004 Hedberg Conference, See Section 5.1.6
Subtask 6.2	Seismic Attributes and Calibration	12/04	final report received 9/09	2004 Hedberg Conference, See Section 5.1.6
Subtask 6.3	Petrophysics and Artificial Neural Net	12/04	final report received 9/09	2004 Hedberg Conference, See Section 5.1.6
Task 7.0 (UAF)	Laboratory Studies for Drilling, Completion, Production Support	6/04	6/04	See Technical Progress Reports, Section 5.1.7
Subtask 7.1	Characterize Gas Hydrate Equilibrium	6/04	6/04	2004 Hedberg Conference, See Section 5.1.7
Subtask 7.2	Measure Gas-Water Relative Permeabilities	6/04	6/04	2004 Hedberg Conference, See Section 5.1.7
Task 8.0 (UAF)	Evaluate Drilling Fluids	12/04	12/04	See Section 5.1.8
Subtask 8.1	Design Mud System	11/03	12/03	See Section 5.1.8
Subtask 8.2	Assess Formation Damage	9/05	Into Phase 2	See Section 5.1.8
Task 9.0 (UAF)	Design Cement Program	12/04	Into Phase 2	See Section 5.1.9
Task 10.0 (UAF)	Study Coring Technology	2/04	2/04	See Section 5.1.10
Task 11.0	Reservoir Modeling	12/04	12/04 & into Phase 2-3	2004 Hedberg Conference, See Section 5.1.11
Task 12.0	Select Drilling Location and Candidate	9/05	Ongoing into Phase 2-3	Topical Report, June 2005, See Section 5.1.12
Task 13.0	Project Commerciality & Phase 2 Progression Assessment	9/05	Redesigned 2005 Phase 2	BPXA and DOE decision, See Section 5.1.13

* Not released to CRA as limited-rights data due to dependent on industry partner agreement

Table 10: Phase 1 Task Descriptions and Milestones

DOE F 4600.3# TABLE 11: U.S. DEPARTMENT OF ENERGY FEDERAL ASSISTANCE MILESTONE PLAN: PHASE 1 (2002-2004)

1. Program/Project Identification No. DE-FC26-01NT41332

2. Program/Project Title Resource Characterization and Quantification of Natural Gas Hydrate and Associated Free-Gas Accumulations in the Prudhoe Bay - Kuparuk River Area on the North Slope of Alaska

3. Performer (Name, Address)
BP Exploration (Alaska), Inc., 900 East Benson Blvd, P.O. Box 196612, Anchorage, Alaska 99519-6612

4. Program/Project Start Date 10/22/02*

5. Program/Project Completion Date 3/31/11 (through Phase 3a)

6. Identification Number	7. Planning Category (Work Breakdown Structure Tasks)	8. Program/Project Duration (Phase 1, 2002-2004) O N D J F M A M J J A S O N D J F M A M J J A S-D	9. Comments (Primary work Performer)
Task 1.0	Research Management Plan	>>>!>	BPXA
Task 2.0	Technical Data and Expertise	>>>>>>----->>>>------>>>>>>>>------------->>>>>>>>-------->>>>>>>>-->>>>>>>>--!-	BPXA
Task 3.0	Wells of Opportunity - Data	------>>>>>------------------->>>>>---------->>>>>>>>>>>>>>>----------->>>>>>>>>>>>>>>>!-	BPXA
Task 4.0	Research Collaboration Link	>>!>	BPXA, USGS, UAF, UA
Task 5.0	Logging/Seismic Technology	>>!	USGS, BPXA
Task 6.0	Characterize Reservoir/Fluid	------->>!>>	UA
Task 7.0	Lab Studies: Ph Behav, Rel k	-- ----->>!----------	UAF
Task 8.0	Evaluate Drilling Fluids	------->>>>>>>>>>>>>>>>>>>>>>>>>>>>>>>>>>>>--->>>>>>>>>>>>>>>>>>>>>>>>>>>>>>>>>>>>>	UAF
Task 9.0	Design Cementing Program	------->>>>>>>>>>>>>>>>>>>>>>>>>>>>>>>>>>>	UAF
Task 10.0	Study Coring Techniques	-------->>>>>>>>>>>>>>>>>>>>>>>>>>>>>>>>>>>>>- --	UAF
Task 11.0	Reservoir Modeling	>>>>----------------------------->>>>>>>>>------------------>>>>>>>>>>>>>>>>>>>>>>>>!>>>	UAF, RyderScott
Task 12.0	Drilling Candidate Selection	>>>------ ----->>>>>------->>>>>>>>>>>>---->>>>>>>>>>>>>!	BPXA, UA, USGS, RyderScott
Task 13.0	Commerciality Assessment	>>>>>>---------------------------------->>>>>>>>-------------->>>>>>>----->>>>>>>>>>	BPXA, UAF, Ryder Scott

10. Remarks * Official Contract Date 10/22/02; Funded reduced-cost pre-Phase 1 from 10/01-10/02. Phase 1 project from 10/02 through 12/04.
Explanation of Symbols: (> = Major Task Work); (- = Minor Task Work); (! = Milestones).
Additional significant milestones presented in Quarterly Technical Progress Reports.

Table 11: Phase 1 (2002-2004) USDOE Milestone Plan and Task Descriptions

5.1.1 Phase 1, Task 1 – Research Management

The research management task established project plans, tracked progress against project milestones (Tables 10 and 11), monitored project costs, and helped determine progression through the gates between project phases. Significant Phase 1, Task 1 accomplishments included:

- Maintained BPXA management support for Cooperative Research Agreement
- Held February, 2002 kick-off meeting at UA with BPXA, UA, UAF, and DOE
- Coordinated project work and planning meetings with USGS, UA, and UAF
- Finalized and executed project contract (BPXA-DOE) and subcontracts (UA and UAF)
- Submitted application documents and finalized patent waiver (no CRA patents recorded)
- Defined overall project objectives and summarized technical objectives and approach
- Created, monitored, and maintained task schedules, milestones, and budget estimates
- Maintained accounting procedures linked to project tasks, subcontracts, and reports
- Maintained project financial and technical progress reports

5.1.2 Phase 1, Task 2 – Technical Data and Expertise

BPXA provided technical data and industry perspective to help maintain overall project objectives and synergy with other projects and research. Accomplishments included coordinating release of shallow seismic, well log, and other data to project partners, universities, and others and maintaining industry-standard scope of work. Significant accomplishments included:

- Released Limited Rights NWEileen and Milne survey 3D seismic data within MPU
- Drafted data confidentiality agreements for MPU, PBU, KRU for WIO review/input
- Reviewed shallow seismic data quality and finalized 3D seismic survey selection
- Provided Limited Rights MPU VSP, seismic velocity, and check-shot data to UA, USGS
- Compiled Eileen accumulation shallow well log data within gas hydrate intervals
- Unsuccessfully attempted WIO approval to release shallow portion PBU 3D seismic data
- Helped plan agenda and presentations for 2004 AAPG Hedberg Gas Hydrate Conference
- Reviewed and provided technical input to UA and UAF MS theses and associated studies

5.1.3 Phase 1, Task 3 – Wells of Opportunity (WOO) Data Acquisition

Adequate data quality and quantity within the shallow gas hydrate-bearing intervals was an ongoing challenge throughout the project. Industry infrastructure and data acquisition focused on development of the deeper oil-bearing formations in the MPU, KRU, and PBU areas. Therefore, acquisition of shallow data was commonly limited to relatively sparse and inconsistent data from older exploration wells and minimal data from development wells. An initial priority project objective involved reviewing and enhancing data gathering opportunities within these shallower gas hydrate and associated free gas horizons near ongoing development drilling operations. Significant accomplishments included:

- Monitored drilling schedule for potential log data acquisition in wells-of-opportunity
- Acquired shallow log data in MPU and PBU wells drilling to deeper oil-bearing targets
    - MPE-26, April, 2001
    - MPS-15i, January, 2002, including gas compositional analyses
    - PBL-106, January, 2002, including dipole sonic, thickest (200-feet) ANS hydrate
        - (type-log for 2011-12 CoP Ignik Sikumi DOE-CoP project NT0006553)
    - PBV-107, October, 2002, including dipole sonic, complex fluids and geology

- MPI-16, late 2004, which delineated only low gas hydrate saturation within Staines Tongue reservoir sands versus Task 5 (Section 5.1.5) seismic interpretation that indicated possibility for gas hydrate accumulation

5.1.4 Phase 1, Task 4 – Research Collaboration Link

Coordinating project activities and establishing clear point-of-contact research links with other gas hydrate research programs helped maximize synergies with industry, academic, government, and other projects both domestically and internationally. Project objectives and accomplishments were presented to industry partners to help facilitate cooperation. Project presentations were provided on a minimum annual basis to DOE and to public and industry forums such as American Association of Petroleum Geologists (AAPG) meetings. The presentations were well attended and the project received awards from the AAPG Mineral and Energy Division (EMD) for best poster (Hunter, et al, 2003) and for best presentation (Hunter, et al, 2007). Significant project results were extensively published (See References Section 7). Phase 3 accomplishments were published in a special issue of the Journal of Marine and Petroleum Geology (Volume 28, Issue 2, February 2011). Phase 1 Task 4 accomplishments included:

- Coordinated project research, including with other methane hydrate research programs
- Presented project to industry partners, Exxon-Mobil and Conoco-Phillips
- Presented project to 2002 AAPG-SPE Western Region Meeting in Anchorage
- Drafted BPXA-Japan National Oil Company (JNOC) Collaborative Research Agreement
  - Provided JNOC gas hydrate program review and well cost estimates
  - Met with JNOC to discuss potential cooperative research programs and studies
  - Led ANS MPU and PBU field and facilities tour to four JNOC representatives
- Worked with AETDL and DOE to sponsor separate UAF/PNNL research proposal to study the potential for CO_2 as a possible methane hydrate enhanced recovery mechanism
- Held BP-internal project briefings: MPU, PBU, KRU, and BP Canada
- Provide project briefings to Congressional and other inquiries
- Exchanged ideas and information with Chevron GOM JIP DOE CRA program
- Participated in technical briefings with Anadarko during preparations for Hot Ice #1
- Presented project to State of Alaska (DNR, AOGCC) and Federal (MMS) agencies
- Presented project to DOE Interagency Coordination and other Washington, D.C. events
- Presented project to and participated in planning meetings with CSM industry consortium
- Presented project poster to May, 2003 AAPG; awarded best-EMD poster
- Presented project progress summary to AAPG sectional and national meetings (2003-05)
- Provided briefings to DOE Methane Hydrate Advisory Committee and DOE conferences
- Drafted agreement for Mallik data sharing and attended Mallik project review meetings
- Considered electromagnetic thermal heating technology application to gas hydrate testing
  - Met with Dr. Bruce McGee and with Dr. Pooladi-Darvish (Calgary)
- Provided project summary briefings and held discussions with various stakeholders, including BPXA, XOM, CoP, BP GOM, DOI, BLM, DOE, NETL, LBNL, PNNL, JNOC

5.1.5 Phase 1, Task 5 – USGS Data, Logging, and Seismic Technology

The USGS, under the leadership of Dr. Tim Collett provided project team members with a technical resource link to valuable past and current research associated with downhole logging and shallow seismic evaluation of gas hydrate-bearing reservoirs. Significant technology developed over the course of the project to advance downhole logging (wireline and

MWD/LWD) and shallow seismic evaluation of gas hydrate reservoirs. Maintaining and helping to advance knowledge of gas hydrate related petrophysical/geophysical technology and transferring this information to the project team ensured adequate, timely and efficient gathering of shallow seismic and log data. The USGS provided interpretive reports and data from the analyses of shallow seismic and downhole logs from well(s) to be used in reservoir characterization (Task 6.0) and reservoir modeling (Task 11.0). Significantly, in 2004, this task progressed into studies of the full-depth Milne 3D seismic volume which delineated the MPU gas hydrate prospects introduced in Table 4 and Figure 7 and which culminated in the Phase 3 Mt Elbert-01 drilling and data acquisition program. Task 5 accomplishments included:

- Compiled gas hydrate distribution maps and supporting data developed in USGS/USDOE Alaska gas hydrate research during the 1980's
    - Provided nine well log correlation sections (120 wells) through PBU-KRU area
- Updated Eileen-accumulation gas hydrate reservoir model and provided to LBNL and BPXA
- Prepared report and mapped KRU gas hydrate accumulations from 16 well log analyses
- Prepared nine-section report containing all USGS-internal gas hydrate assessment notes and a comprehensive listing of all ANS wells known to contain gas hydrate
    - Annotated each well with indication and depth of gas hydrate and free-gas
    - Listed recently drilled wells requiring assessment for gas hydrate
- Prepared preliminary report for Tarn gas hydrate accumulation open-hole log data
- Maintained linkages to Schlumberger and logging technology advances
- Evaluated Baker-Hughes INTEQ's 6 3/4" APX LWD tool for gas hydrate data acquisition
- Provided input to future wireline and LWD logging data acquisition WOO plans
- Investigated seismic attribute analyses for direct free gas and gas hydrate indicators (R06, R09 pp. 9-19 and summarized below)
    - Applied developed synthetic models illustrating seismic attribute response to fluid (gas hydrate – free gas – water) and reservoir changes to MPU interpretation
    - Interpreted multiple potential MPU area gas hydrate play fairways and prospects (Figures 7, 12, 13; Tables 4, 5, 12) in parallel to UA characterization Task 6
    - Developed volumetrics and uncertainty analysis methods for 14 specific MPU gas hydrate prospects for input into Phase 2 progression decision

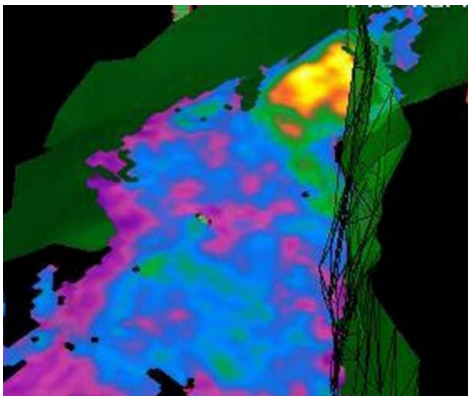

Figure 12: Gas hydrate fault-bounded trap of MPU Mt Elbert prospect

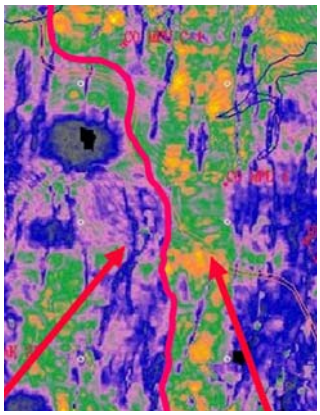

Figure 13: Gas hydrate (left) – free gas (right) prospect fairway in seismic amplitude time slice

- Determined a relation between seismic amplitude attribute and gas hydrate-bearing zone thickness and saturation
- Confirmed with modeling and interpretation that seismic velocity, amplitudes, and wavelet character may respond to gas hydrate-bearing reservoir and fluid changes
- Finalized, ranked, and compared MPU gas hydrate-bearing prospects (Figure 7, Table 4; R09); Table 12 illustrates the prospect ranking methodology (Mt Elbert highest rank)
- Recommended log and core data acquisition to help prove feasibility of direct seismic detection of gas hydrate-bearing reservoirs of Mt Elbert prospect (Figure 12)

Mt Elbert Zones C and D: E-Pad, B-Pad

Estimated Rank - #1	
POSITIVE QUALITY (PQ)	**NEGATIVE QUALITY (NQ)**
135 BCF Gas Hydrate In-Place	Requires Delineation
Stacked Prospects (C and D horizons)	No Staines Tongue gas hydrate or free gas
Conventional, Fault-bounded structural trap	
	No well penetration, fault-separated from correlative wells
Well organized and consistent amplitude anomaly	
MPB-02 and MPE-26 confirm gas hydrate in C and D	
Both MPB-02 and MPE-26 have excellent synthetic ties	
Gas hydrate in C/D causes velocity pull-up in Staines T.	
Interpreted 45 feet C-hydrate thickness	Requires Delineation
Interpreted 45 feet D-hydrate thickness	Requires Delineation
Interpreted high-saturation gas hydrate at structure crest	Requires Delineation
Potential movable connate waters in downdip position	Requires Delineation
Facilities	
E-pad gas compression and injection available	
Good distance from E-pad for horizontal well	Need delineation well and data before production testing
3000 feet from E-pad, 3500 feet from B-pad	Possible limitations for wireline & core acquisition?
Reservoir Model	
Import Structure, thickness, saturation grids	
Test water saturation and connate water mobility	
Horizontal well test	
Depressurization test (connate water mobility)	
Test hot gas injection/circulation	
Test hot water injection/circulation	

Blanca Zones C and D: A-Pad

Estimated Rank - #2	
PQ	**NQ**
23 BCF Gas Hydrate In-Place (C-horizon only)	
Stacked Prospects (C and D horizons)	
Penetrated/delineated by MPA-01	
35+ feet D; 30+ feet C	
Thicknesses nearer seismic resolution limits	Less well-organized amplitudes
Possible destructive interference affecting amplitudes	Less well-organized amplitudes
Possibly more stratigraphically controlled	Flat structure, less 4-way-type closure
Possibly more lateral extent and thickness upside	
Possibly more thickness upside	
Facilities	
On A-pad; readily accessible from A-pad	No facility infrastructure other than gravel

Table 12: Continued – MPU Gas Hydrate Prospect Ranking and Criteria

Crestone Zones C and D: C-Pad

Estimated Rank - #3

PQ	NQ
186 BCF Gas Hydrate In-Place (Crestone C-horizon)	Gas Chimney in updip position to SW may be leaky seal
46 BCF Gas Hydrate In-Place (Sneffels D-horizon to SE)	
4.8+ BCF upside free gas in Shavano Mid-Staines with Crestone	
MPC-01 has good gas shows in Mid-Staines	
Fault-bounded and 4-way closure traps	Structurally compartmentalized into 6 fault blocks
MP18-01 delineated good C and D gas shows in NE	
Best amplitudes in North and Northeast Crestone	Not as well-organized amplitudes in South and SW
Interpret ~40 feet Crestone C hydrate reservoir thickness	
Interpret ~45 feet Sneffels D hydrate reservoir thickness	
Interpret 60-70% Saturation gas hydrate in C and D	

Facilities

SW corner directly beneath C-pad (Crestone C)

Actions

Potential for C-pad WOO - Review drilling schedule

Princeton Zone D: K-Pad

Estimated Rank - #4

PQ	NQ
38 BCF Gas Hydrate In-Place in D-horizon	Very structurally complex and likely compartmentalized
Good K-pad delineation in MPK-38 and MPK-25	
K-pad area very active gas-prone area	Very structurally complex and likely compartmentalized
200 feet free gas in C and D zones delineated in wells	
Stacked prospect potential in Staines Tongue	
Staines Tongue Yale prospect with 3.6-10 BCF	Probable low-saturation Staines tongue

Facilities

K-pad area not very active; Minimal disruption/distraction

Antero Zone C: H-Pad

Estimated Rank - #5

PQ	NQ
68 BCF Gas Hydrate In-Place in C-horizon	No confirmation wells; seismic-only anomaly
Interpreted 45 feet C-horizon reservoir thickness	Structurally compartmentalized, may require delineation
	Patchy gas hydrate saturation interpretation
Stacked with Staines Tongue Prospect	Staines Tongue likely low-saturation: logged at MPI-16
Fresh water likely	Possible coal-associated gas versus free gas?
Gas Hydrate in upper Staines	Closely associated with updip-edge gas chimney
Free gas potential in middle Staines	Gas Chimney may indicate leaky seal
	Free gas requires delineation

Facilities

Prospect very near road access - 100 feet from road	
Prospect near H-pad - 1,600 feet from pad	
Possible option inject produced gas into Staines Tongue	Question if hi-pressure gas injection option available

Actions

Check for new well data over shallow intervals

Table 12: Continued – MPU Gas Hydrate Prospect Ranking and Criteria

Pikes Peak Zone B: S-Pad

Estimated Rank - #6

PQ	NQ
13-26 BCF Gas Hydrate In-Place in B-horizon	Low-Saturation B-horizon directly below S-pad
Upside as off 3D survey edge on NW Eileen Structure	
B-zone is clean marine sandstone	
Additional upsides in C, D, E, F horizons	
Stacked with Mt Holy Cross Staines Tongue Prospect	
Upper Staines Tongue Free Gas - 3.5 BCF w/ upside	Low Saturations calculated in Staines Tongue (25%)
Downdip Staines Longs Peak gas hydrate prospect (23 BCF w/ upside potential if > saturations)	MPI-16 was low-saturation in Staines Tongue
Mid-Staines Tongue free gas potential 9+ BCF	Likely low saturation in Staines Tongue
Facilities	Long Stepout, 6,840 feet from S-pad may be prohibitive

Bierstadt Zone E: B and D-Pads

Estimated Rank - #7

PQ	NQ
42 BCF Gas Hydrate In-Place in E-horizon	Very cold & near Permafrost
Opportunity for E-horizon evaluation	Possible Ice formation on production testing
Interpreted to 50 feet E-horizon reservoir thickness	Possible Paleosol alternative interpretation
Excellent geophysically-constrained prospect	
Very organized amplitude anomaly	Not an obvious velocity pull-up in Staines Tongue below
Fault closure with downdip amplitude dimming	
Saturation may have significant upside	Surface statics (inlet) may decrease amplitude anomaly
Stacked with Little Bear Staines Tongue Prospect	Amplitude anomaly is limited in Staines Tongue
Well-constrained prospect	Low Saturations are likely (10-40%)
Gas hydrate/free gas/water contacts follow contours	MPD-01 well is only 20 ohm*m resistivity
	Small volumes in Staines Tongue
Facilities	
B-pad on location	Horizontal well option may be limited from B-pad
Consider horizontal well design turn up into gas hydrate	E-horizon penetration may not allow Staines penetration
This design could help mitigate water production	(may be possible to mitigate with well design)
D-pad near location & may provide better horizontal well	

Table 12: MPU Gas Hydrate Prospect Ranking and Criteria

Beginning in September 2003 through December 2004 and extending into Phase 2, Task 5 collaborative studies were expanded in scope in parallel to similar UA Task 6 activities. 3D seismic in the Milne Point area of northern Alaska was interpreted in detail to help answer questions about gas hydrate reservoir characteristics and properties as input to possible production methods, commercial viability, and Task 12 candidate drilling site selection. Historical log correlation work and analysis of gas hydrates in the Milne Point area (Collett, et al., 1993, 2001) was used as a starting point for a seismic driven analysis of the Milne Point 3D survey area. Interpretation of modern seismic data helped to gain a better understanding of geologic controls related to gas hydrate petroleum systems in the MPU area. The Landmark software suite was used to integrate and analyze detailed log correlations, specially processed log data, gas hydrate composition information and specialized 3D seismic volumes. Structural and stratigraphic interpretations encompassed the interval from the Base of Ice-Bearing Permafrost

(BIBPF), into the Gas Hydrate Stability Zone (GHSZ), and into potential gas-bearing reservoirs immediately below the Base of the Gas Hydrate Stability Zone (BGHSZ).

The seismic data was also used to analyze reservoir fluid properties in comparison to theoretical modeling results by Lee (2005). The modeling showed that a relatively strong impedance contrast will occur when moderate to highly saturated gas hydrate-bearing reservoirs exist within the GHSZ. Modeling showed that shallow gas hydrate and associated trapped sub-hydrate free gas may cause velocity anomalies that would affect the depth conversion of deeper, conventional ANS hydrocarbon targets. Primary study results delineated interpretation of "intra-hydrate" stability zone prospects and "sub-hydrate" free gas prospects. These prospects have been analyzed relative to the petrophysical parameters in analog wells, for comparable reservoir intervals. Monte Carlo style volumetrics were performed using Crystal Ball™ software to calculate the potential range of in-place resources from the interpreted range (in triangular distribution) of potential reservoir properties, including gas hydrate saturation (40%-90%), reservoir net-to-gross (70%-90%), and reservoir porosity (34%-40%). In addition, the Bulk Rock Volume (BRV) was calculated in Zmap by integrating reservoir thickness over each prospect area and applying a normal distribution using a 10% standard deviation from the calculated BRV values. The gas expansion (or formation volume) factor (1/Bg) was defined as 164. Fourteen gas hydrate-bearing prospects were identified and calculated to contain a total of 668 BCF gas in hydrate in-place (Figure 7, Table 4).

Task 5 studies focused on the Milne Point 3D seismic survey within the MPU (Figure 7), provided to the USGS by BPXA as co-sponsor of this research. A small portion of the NW Eileen 3D survey just to the south of the Milne Point survey within the MPU was also provided. However, poor shallow (<950 ms) data resolution within the NW Eileen 3D survey prevented extension of the full interpretation methods into this area. Regional 2D seismic data, licensed by the USGS, supplemented the 3D seismic data and was used along with well data to constrain and improve the quality of critical maps, such as time structure maps, fault maps and base hydrate stability zone maps within the MPU.

The initial interpretation of the structural framework in the Milne Point 3D seismic survey within the MPU shows that faulting plays a significant role in the migration and trapping of gas associated with gas hydrate-bearing reservoirs. North Slope gas hydrate-bearing reservoirs contain mostly methane gas sourced from more deeply buried hydrocarbon-bearing formations, which likely accumulated as free gas in conventional traps prior to formation of the gas hydrate stability zone within and beneath permafrost with onset of arctic conditions. Therefore, a detailed fault interpretation is critical to understanding the relationship between faults, as the gas conduits, and shallow gas hydrate accumulations. The age relationship between various fault sets may play a significant role in determining migration pathways and the compartmentalization of these gas hydrate-bearing reservoirs. Fault analyses on a 3D seismic volume enhanced by ESP (coherency) processing showed that the fault orientation, above and below the Canning Formation, is distinctly different, and as such, the secondary and tertiary migration from deeper hydrocarbon reservoirs may be complex. Some faults may not be connected through the Canning Formation to deeper hydrocarbon-bearing reservoirs.

The interpretation of faulting on the ESP (coherency) volume greatly improved the overall understanding of fault compartmentalization at each mapped horizon. An example time structure map for the Top of the Staines Tongue horizon is shown in Figure 14. Figure 15 shows the same map in North-perspective view. Notice that some faults trend more North-South, similar to the predominant younger fault trend. Some of the larger-offset faults within the Staines Tongue interval trend more NNE to SSW, similar to the older sub-Canning fault trend. These faults may be better connected to deeper hydrocarbon systems and may serve as gas migration conduits.

Theoretical seismic modeling of boundaries between ice-bearing permafrost to gas hydrate-bearing reservoirs, shale to gas hydrate-bearing reservoirs, and shale to free gas-bearing reservoirs as well as transitional gas hydrate to free gas reservoirs at the base of the gas hydrate stability zone was used to understand the acoustic properties of these complex systems in the pre and post stack domain. The similarity in acoustic properties between ice and gas-hydrate makes it difficult to differentiate between ice- and gas hydrate-bearing sediments. Therefore, gas hydrate within to permafrost, while prospective, is both more difficult to quantify and to produce. In the Milne Point 3D area, some assumptions can be made to constrain modeled results describing the relationship of these boundaries in the stack and offset domains. First, if thermogenically-derived gas originally migrated into what are now fully saturated gas hydrate-bearing reservoirs, then a gas hydrate concentration within the pore system of a sandstone reservoir might also range between 80 - 85%, similar to saturations within conventional gas

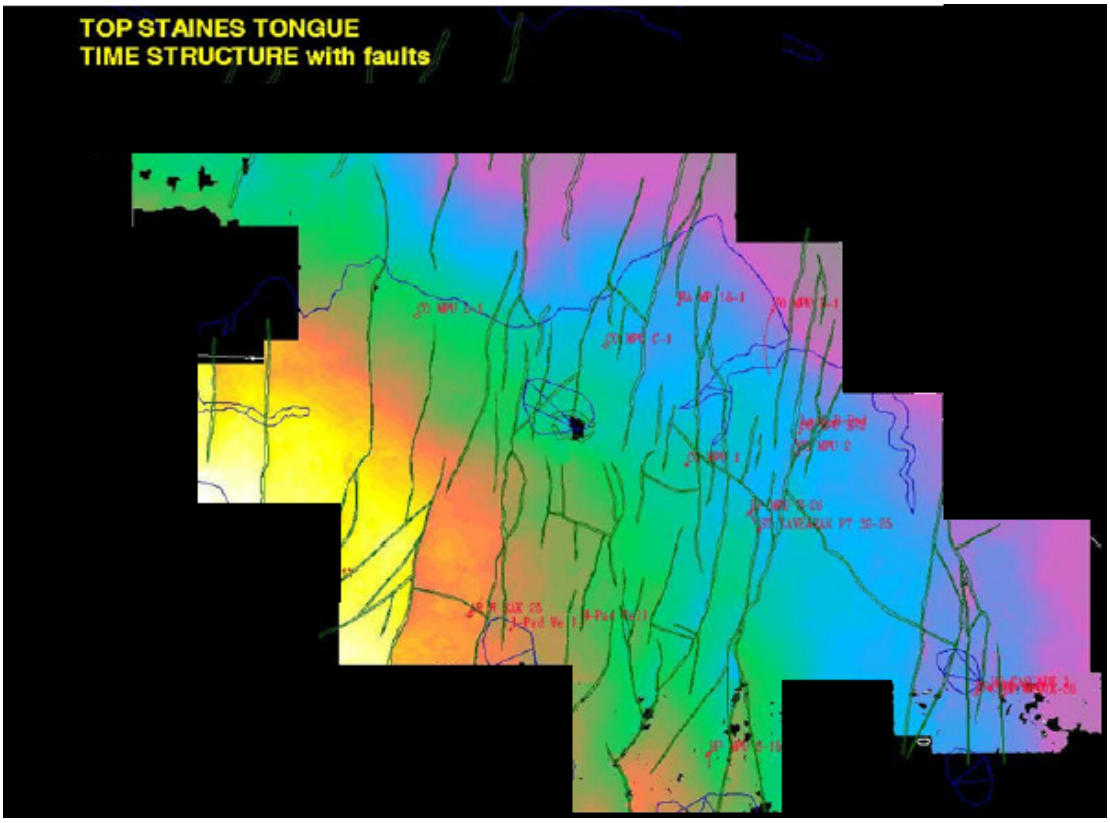

Figure 14: Top Staines Tongue time structure map with interpreted shallow faults

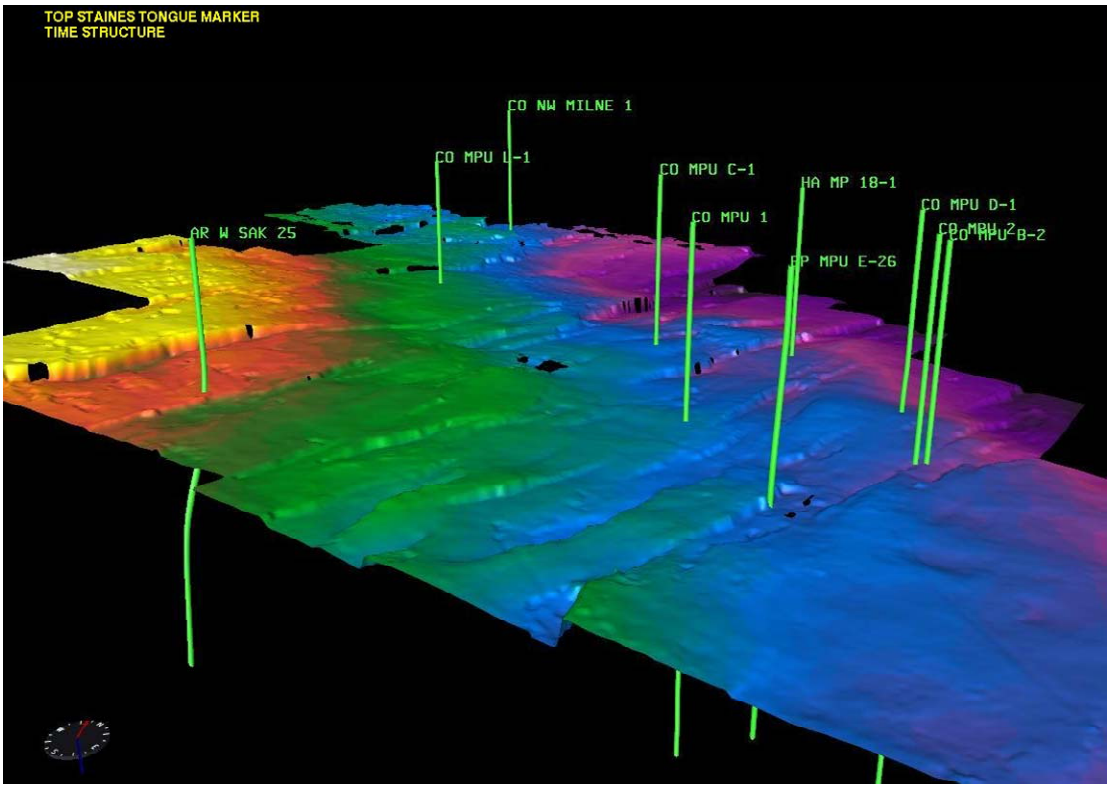

Figure 15: Top Staines Tongue time horizon in North-perspective view

reservoirs. Thin bed seismic modeling shows that hydrate saturation is variable and that these gas hydrate-bearing reservoirs may be under-saturated with respect to gas hydrate, and may, therefore, possibly contain movable connate waters in some areas. Undersaturation could occur possibly due to the gas volume reduction occurring when a free gas-bearing reservoir is transformed into gas hydrate in the presence of water within the GHSZ. Unconsolidated sandstone reservoirs within the Sagavanirktok formation that contain the majority of gas hydrates within the MPU area typically have 30-40% porosity. Reservoir thickness is the main variable used in modeling acoustic attributes and in calculating volumetrics. However, thickness can be calculated using "thin-bed" modeling where these reservoirs are isolated and in a single pore-filling phase.

The base of the gas hydrate stability zone was computed using well log-interpreted base of ice-bearing permafrost (BIBPF) depths and high resolution borehole temperature surveys. Figure 16 shows an Eileen accumulation gas hydrate log correlation for interpreted KRU-MPU gas hydrate-bearing reservoirs. This study confirms the stratigraphic consistencies of this correlation within the MPU. Gas hydrate-bearing reservoir stratigraphy interpreted within MPU area wells were correlated using both seismic and well log data. A pair of horizons representing the upper and lower limits of the base gas hydrate stability zone were mapped and displayed on the seismic data. The error range of the base gas hydrate stability zone was considered to be plus or minus 75 feet, or plus or minus 15 milliseconds. Gas hydrate reservoirs below the BIBPF and within the hydrate stability zone ("intra"-gas hydrate prospects) have acoustic properties allowing them to be interpreted by several simple seismic attributes. Several candidates for intra-hydrate prospects were found during reconnaissance mapping of this interval as shown in Figure 17.

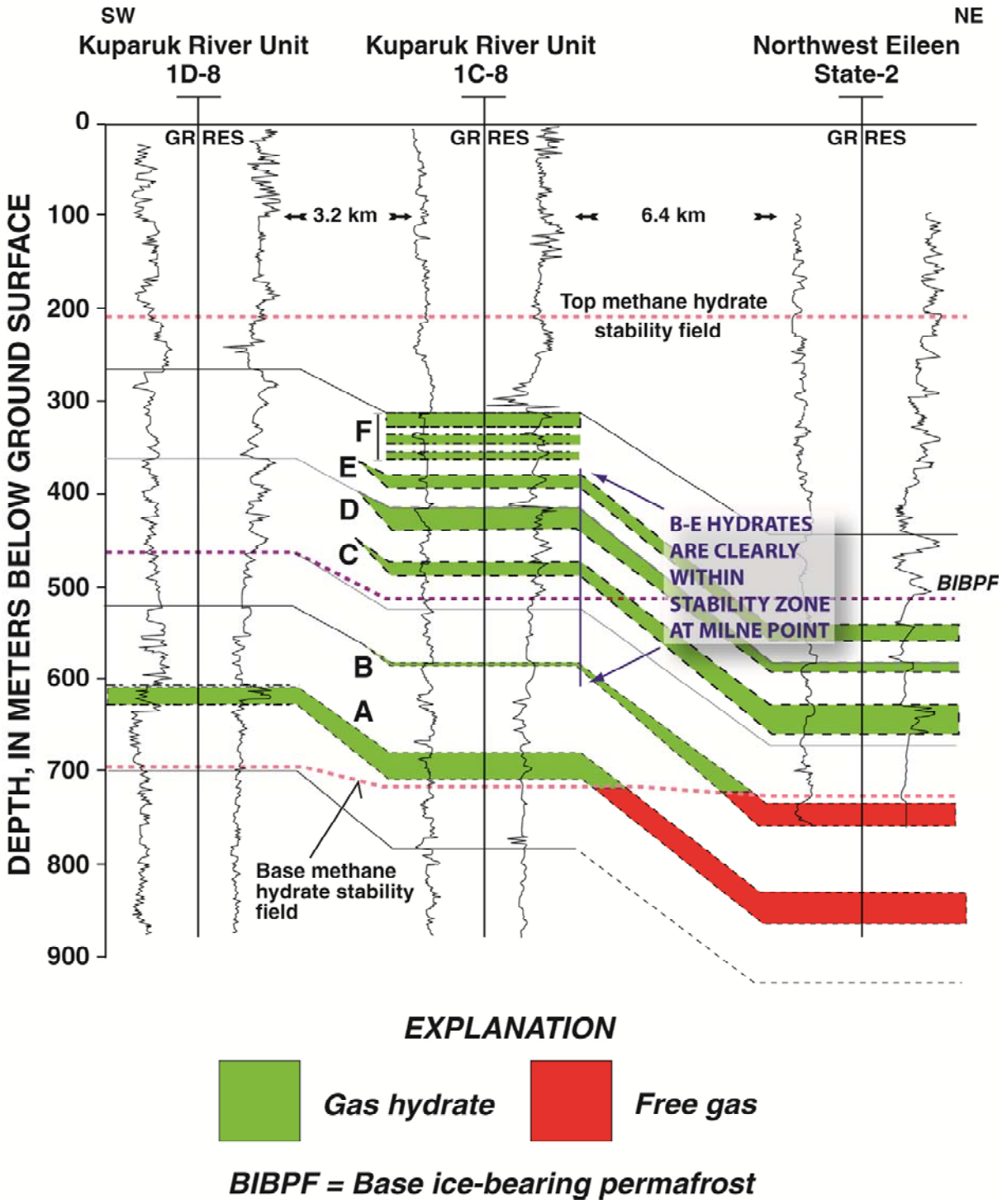

Figure 16: Eileen gas hydrate accumulation log correlations (Collett, USGS). In the Milne Point area, the base of the hydrate stability field is generally near the Top of the Staines Tongue, or approximately the A to B unit hydrates of Collett, 1993 (Lee, et al, 2011, modified from Collett, 1993, 2002).

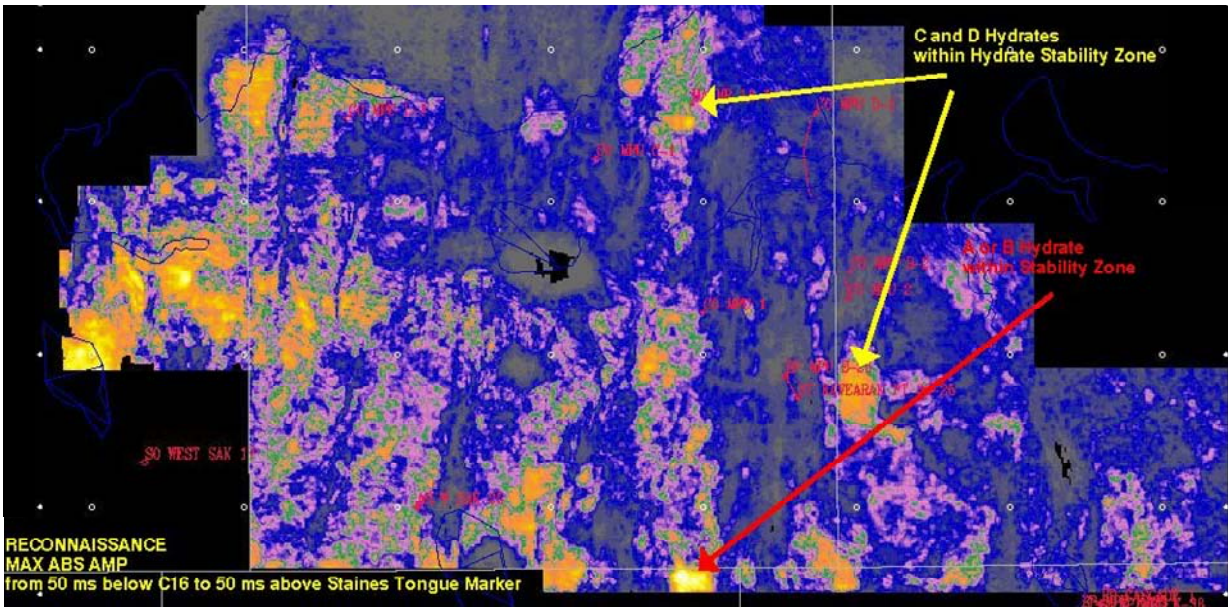

Figure 17: Reconnaissance mapping of 100 millisecond interval around Staines Tongue marker

Free gas trapped below gas hydrate and/or below the gas hydrate stability zone can be identified by seismic attributes in this geologic setting. However, relatively low saturation free gas can give nearly the same acoustic signature as higher saturation free gas reservoirs. The seismic amplitude anomalies are commonly associated with free gas near the base of the interpreted gas hydrate stability field and may be connected to up-dip gas hydrate-bearing reservoirs in some cases (Figure 18). In other cases, no distinct amplitude anomalies attributed to gas hydrates above the free gas to gas hydrate boundary were identified, even though convention would indicate that gas hydrates must be present to form a hydrate-seal trap. One hypothesis would be that there were changes in migration pathways and the rate of migration during the formation of the gas hydrate stability zone, or that the hydrates never reach the minimum values for thickness and/or saturation that would allow them to be imaged by the seismic data. The recent movement along younger faults in the post-Canning interval likely influenced migration pathways and may affect the location of sub-hydrate free gas accumulations. Another hypothesis would be that the charge is limited and/or the seal leaky for some of these systems.

From seismic data analyses, 14 intra-gas-hydrate stability zone prospects were identified in the Milne Point 3D survey area (Table 4). Interpreted intra-gas-hydrate prospects are typically conventional fault bounded traps and are identified primarily by their acoustic properties. As a rule, areas that are currently structurally high within prospective fault blocks can be shown to have acoustic properties that are interpreted to correspond to higher concentrations of gas hydrate. This structural relationship is similar to conventional gas prospects, pointing back to the likely free gas origin of these gas hydrates during migration and trapping before permafrost conditions prevailed. Some of these fault blocks are interpreted as not “fully charged”, as there are down-dip limits to the mapped acoustic anomalies, again pointing back to the likely originally trapped free gas prior to onset of permafrost and hydrate stability conditions. Several of these intra-hydrate prospects might be candidates for gas hydrate data acquisition and/or production testing, due to their proximity to existing roads and infrastructure (Table 12).

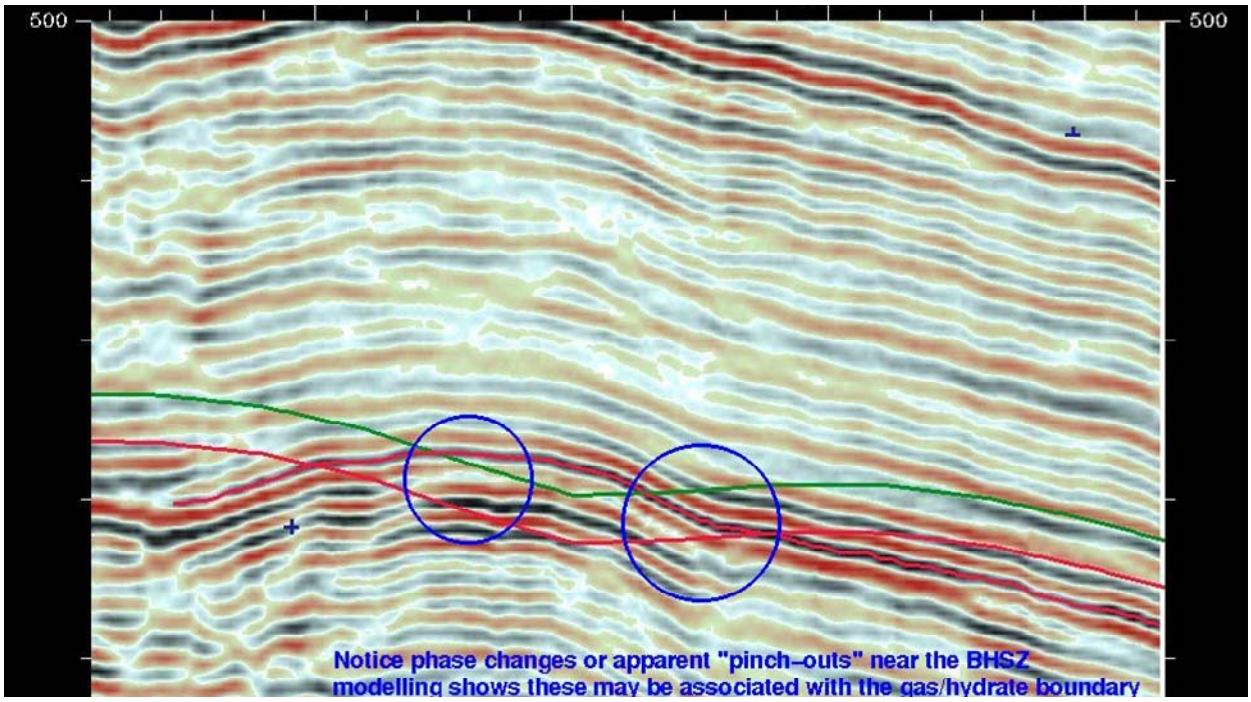

Figure 18: The minimum (green line) and maximum (red line) BHSZ relative to truncated high amplitude seismic reflections that are interpreted to be sub-gas hydrate accumulations of free gas. However, as shown in well-of-opportunity log data collected in this study from MPS-15i and MPI-16, saturations in the interpreted free gas may be lower than 10% in some cases.

The MPU area study identified both intra-gas hydrate and possible sub-gas hydrate free gas prospects that may become candidate areas for future data acquisition and may also be local fuel gas targets. In the MPU area, seismic amplitudes lessen dramatically above the base of the gas-hydrate stability zone. This sedimentary section could contain numerous prospects comprised of thick reservoirs that potentially host both gas hydrate and conventional free gas accumulations.

The historical log analysis work conducted by the USGS in this area combined with interpretation of 3D seismic attributes has promoted a better understanding of the geologic setting for gas hydrate-bearing reservoirs. Delineation of prospects through additional well-log data acquisition would help verify assumptions used to evaluate the candidate prospects.

Additional USGS-supporting studies contributed to the success of this work:

- Enhancement of data with post-stack seismic processing
- Definition of geometrical configuration of data traces using ProMAX
- Analyses of velocity for developing poststack and prestack migration velocity model
- Correlation of seismic reflections to well data, synthetic ties, and time/depth conversion
- Documentation of sources for seismic and well data
- Procedures for loading of data into Landmark software systems
- Incorporation of historical work and formation nomenclature (see Section 7.3)
- Petrophysical analyses of digital log data, including methodologies for Rw, Sw, and cutoffs for resistivity, porosity, Vp/Vs, etc.

- Determination of seismic reflection coefficient versus angle-of-incidence and relation to interpreted gas hydrate and free gas saturations
- Modeling of intra-hydrate prospect saturation and thickness using "thin-bed" approach
- Calculations of reservoir thickness for both intra-hydrate and free gas prospects
- Estimations of saturations for both intra-hydrate and free gas prospects
- Generation of trace models for both varied hydrate thickness and section across BHSZ
- Interpretation of structure including fault methodology, ESP coherency volume, and ties to deep-seated fault systems and transfer zones
- Distinguished faulting versus velocity pull-ups associated with gas hydrate prospects
- Interpretation of regional stratigraphy with excellent synthetic ties for correlation
- Distinguished coal-prone sequences versus interpreted prospect-associated gas anomalies
- Calculation and mapping of base permafrost and hydrate stability zone (Table 13)
- Methodology for intra-hydrate and free gas prospecting and volumetrics calculations

Well	IBPF depth (MD, ft)	Temperature at base of IBPF (deg F)	Depth to BHSZ (MD, ft)	Pressure at BHSZ (psi) (from CSM)	Temp. at BHSZ (deg F) (from CSM)	Sub-IBPF geothermal gradient (deg F/100 ft)
MPU E-26	1760	30.2	2820	1221.1	53	2.15
Kavearak Pt 32-25	1796	30.2	2856	1236.6	54	2.25
MPU A-01	1708	30.2	2741	1186.9	53	2.21
MPU D-01	1783	30.2	2836	1228.0	53	2.17
WSak 25*	1821	30.2	2899	1255.3	54	2.21
MPU C-01	1678	30.2	2688	1163.9	53	2.26
MPU B-01	1808	30.2	2853	1235.3	54	2.28
MPU B-02	1806	30.2	2852	1234.9	54	2.28
MPU S-15i*	1910	30.2	3051	1321.1	55	2.17
MPU L-01	1858	30.2	2918	1263.5	54	2.25
West Sak 17	1738	30.2	2788	1207.2	53	2.17
					Average	2.22
Cascade-01	1674	30.2	2711	1173.9	53	2.2

* West Sak 25 and MPS-15 difficult to interpret BIBPF due to hydrate-permafrost commingling

Table 13: Well-log based Depth to base IBPF and BHSZ within and near MPU study area

5.1.6 Phase 1, Task 6 – UA Reservoir and Fluids Characterization, Seismic Studies

Reservoir and fluid characterization studies of the Sagavanirktok formation across the MPU, KRU, and PBU areas were accomplished in subtask 6.1 by the University of Arizona (UA) department of Mining and Geological Engineering (MGE) under the leadership of Dr. Bob Casavant. The initial data gathering portion of these studies confirmed that industry had acquired only relatively sparse and inconsistent shallow log data within the Sagavanirktok formation gas hydrate-bearing sands since the primary industry targets were deeper, oil-bearing horizons. MGE setup a secure lab area with industry-standard computing capabilities for these studies. In concert with MGE, UA's department of Geology and Geophysics (GEOS) under the leadership of Dr. Roy Johnson accomplished subtask 6.2 studies of shallow 3D seismic data released by BPXA within the MPU area. This Limited Rights seismic data was vertically truncated to 950ms

(to help maintain confidentiality of the deeper oil-bearing horizons) and horizontally truncated to the MPU boundaries (the development infrastructure study area-of-interest) and consisted of the majority of the Milne Point 3D seismic survey acquired in 1991 and of a small portion of the NW Eileen 3D seismic survey acquired in 1994. The project was unable to gain data co-owner approval for release of additional confidential 3D seismic data within either the PBU or KRU areas (Table 10). Subtask 6.3 studies included investigation of petrophysical and artificial neural network modeling to determine capabilities to improve log and seismic data analyses. Phase 1 accomplishments for these 3 subtasks are summarized below in chronological order. However, full integration of well and seismic data interpretations remained incomplete due to various issues, including limited available data, contract discontinuities, UA IT computing funding cuts, and 950ms truncation of seismic data causing difficulties in ties to well log data. In addition, certain out-of-scope accomplishments helped meet project demands, including stratigraphic interpretation in MPU Mt Elbert prospect area, PBU L-pad area, and PBU Z-pad area in support of Task 12 drilling candidate selection and also including MPU S-pad area volumetrics calculations. Phase 1 Task 6 results, recommendations, and supporting documentation were presented at the 2004 AAPG Hedberg Conference in Vancouver, B.C. and summarized in detail in R09, Section 5.6, pp. 20-53.

5.1.6.1 Subtask 6.1, UA Reservoir and Fluids Characterization Studies

This section documents Phase 1 accomplishments from subtask 6.1 studies, which included:

- Validate and review published stratigraphic correlations and compare well log correlations to USGS, and other work, and resolve discrepancies between models
- Compile representative sample or cuttings data, drilling data, wireline data and petroleum engineering information (casing, perforations, spinner logs, tracer data, temperature logs)
- Establish and optimize graphic output for well and cross-section displays
- Normalize lithologic responses in multiple generations of wireline log data
- Correlate detailed stratigraphic sequences and parasequences (versus lithostratigraphy)
- Integrate regional structural characterization studies to stratigraphic interpretation
- Build geologic reservoir and visualization model within local area of interest for input into Task 11.0 (Reservoir Modeling).

Naturally occurring gas hydrates on the North Slope of Alaska represent a potentially large resource of methane gas. Within the MPU, gas hydrates occupy thin, highly faulted, syndepositional sand intervals in the Tertiary Sagavanirktok formation within and below ice-bearing permafrost within the gas hydrate stability zone. Detailed structural analysis, including mapping of fault throw and growth using the Milne Point 3D seismic volume constrain the recent faulting history. Time- and space-variant fault activity during gas migration through and into shallow reservoir sands imply models for 1) initial migration of deeper thermogenic gas into the current gas hydrate stability zone (GHSZ) and 2) deposition of reservoir and gas hydrate-prone facies. Field-wide fault-seal calculations, based on modified shale gouge ratio (SGR) and clay smear potential (CSP) algorithms show lateral variability in fault seal potential along gas hydrate-bearing horizons and suggest a mechanism for trapping initial free gas which later combined with water to form gas hydrate. Seismic waveform classification along with well-log-interpreted gas hydrate-bearing horizons helps define distributions of gas hydrate-similar waveforms, representing potential gas hydrate, whose lateral variations are consistent with fault

location, fault activity and fault-seal calculations. Potential gas hydrate distributions bounded by faults with greater sealing potential yield potential future production targets.

Detailed analyses of fault trends, throw, growth, and seal with respect to interpreted gas hydrate accumulations within 3 major stratigraphic intervals were presented in R07 (pp. 15-28, figures 1-12, and table 2) and at the AAPG Hedberg Research Conference in September 2004, summarized in R09 (pp. 20-53). Interpreted gas hydrate distributions strongly controlled by N-NE-trending faults, especially in the eastern MPU, which is consistent with trends observed in fault activity and fault-seal potential. These results support a model in which thermogenic free gas migrated up active faults into permeable sand reservoir intervals and was subsequently trapped by sealing faults (Figure 19). This trapped free gas later formed gas hydrate by combining with connate waters under conditions of regional geothermal gradient depression (Collett, 1993). Distribution of gas hydrate within the MPU is likely controlled by sealing/barrier/baffle-faults, original gas conduit/migration faults, and depositional and structural geometry of gas hydrate-bearing sands.

Phase 1, subtask 6.1 accomplishments included:

- Obtained $750,000 software for UA through BPXA/Landmark University Grant Program
- Planned and designed secure labs for UA hardware, software, and network system
- Installed six BPXA-donated SGI Octane and two Sun Ultra 30 workstations
- Reviewed ANS and world gas hydrate literature and references
- Loaded ANS well data to geological Petra software and initiated reservoir/fluid studies
- Reviewed and compiled literature regarding Sagavanirktok stratigraphy and structure
- Produced a working base map of Sagavanirktok formation available log data
    - Determined 67 out of 90 wells provided contain suitable logs for both GR correlation and comprehensive petrophysical interpretation
- Developed unique Sagavanirktok stratigraphic column and integrated USGS framework
- Correlated 20 Sagavanirktok parasequence units and genetically related bed successions and identified correlative marine flooding surfaces (R03, R04, Appendix A)
    - Established chronostratigraphic versus lithostratigraphic correlation framework (R04, Appendix A)
    - Created gross interval horizon isopachs (30-29, 33-31, 34-33, 35a-35, 36-35a)
- Identified significant lateral and vertical heterogeneity in Sagavanirktok reservoir quality
- Generated net/gross and net sand isopachs based on well log data
    - Compared well log-based gross isopachs maps with seismic-based isopachs
    - Revealed significant variation between the two grids for respective intervals
    - Advised caution in using seismic gross isopachs to guide net sand mapping
    - Used well log-based bulk volumetric analysis for volumetric calculations
- Compared USGS gas hydrate zones with UA lithostratigraphic framework
    - Noted some USGS zones cross some UA lithostratigraphic unit correlations
- Developed new sequence stratigraphic framework within MPU Sagavanirktok formation
- Determined that this framework will guide final volumetric and mapping exercises
- Revealed more complex stratigraphic relationships in the Sagavanirktok, which will affect lateral continuity and connectivity of gas hydrate and associated free gas resources
    - Calculated fault heaves from seismic data interpretation and combined this interpretation with shale thickness data to predict sealing/non-sealing nature of faults, sand body continuity, and connectivity of reservoir pore-fluids

- Completed preliminary analysis of MPU seismic traverse from Simp32-14 to MPD-01
    - Identified major intraformational unconformities and their relationship to UA log-based sequence stratigraphic framework
    - Located reflector terminations at areas of potential downlap, onlap and erosion
- Calculated MPU gas hydrate and free gas volumetrics in support of Phase 2 progression decision (Tables 14 and 15; R07, pp. 12-13; R09, table 2, pp. 38)
    - Incorporated new gas hydrate probability predictor (expert system)
    - Created PETRA data set distinguishing gas hydrate, free gas, ice, oil and coal
    - Finalized MPU S-pad preliminary comparative volumetric study/chart (Table 15)
    - Adjusted net pay calculations related to base of ice and gas hydrate stability fields
    - Determined gas expansion factor and unit porosity on each of 12 mapped sequences and completed MPU gas and gas hydrate volumetric calculations
- Confirmed spatial correlation between current shoreline and river trends with certain fault zones and structural trends
- Identified and characterized a northeast-trending pull apart basin in the central MPU
    - Identified effects of syndepositional faults, permafrost thickness, net-gross sand ratios and locations of "gas chimneys"
- Identified another possible transtensional basin, the western margin of which is located in the vicinity of the MPK-38 and Cascade-01 wells
    - Basin margins appear to be characterized by discontinuous narrow grabens
- Reviewed GR log normalization in regionally extensive marine shale interval, marker 36-36a and net sand cutoff to incorporate cased-hole GR data
    - Validated 55 API GR cutoff for net sand (Geauner and Manual, et al, 2004)
- Compared gross interval and net sand isopach maps using lithostratigraphic and sequence stratigraphic frameworks
    - Show both normal and abrupt (between some zones) strike/dip interval changes
- Attempted to reconcile seismic gross interval thickness and well log interval thickness for several wells located near fault zones
- Compared gas hydrate zone thickness to fault proximity and determined possible relation suggesting syndepositional faults, if sealing, influence gas hydrate distribution
- Studied shallow fault throw variation in and fault seal potential across the MPU area
- Studied timing and influence of fault reactivation on deposition of shallow reservoir sands
- Studied sedimentary facies-related gas emplacement in gas hydrate-bearing reservoirs

Assessment Method	**Gas Hydrate In-Place**	**Free Gas In-Place**	**Total Gas In-Place**
USGS Lithostrat	1.46 – 2.73 TCF	Not Determined	1.46 – 2.73 TCF
UA Waveform Class.	0.77 – 1.31 TCF	Not Determined	0.77 – 1.31 TCF
UA Lithostrat.	Not Determined	Not Determined	Not Determined
UA Sequence Strat. 1	1.03 – 1.22 TCF	0.77 – 1.31 TCF	1.8 – 2.53 TCF
UA Sequence Strat. 2	1.28 – 1.51 TCF	1.6 TCF	2.88 – 3.11 TCF
UA Seq. Strat. MPS-pad, 2-mile radius	0.64 TCF (Table 15 shows detailed inputs)	Not Determined	Not Determined
Contrast USGS Task 5	*0.67 TCF (Table 4 MPU)*		

Table 14: Summary of UA well log-based volumetric calculations and methodologies (R07 pp.12-13)

Sequence	Area (ft^2)	Thickness (ft)	Porosity	Saturation	1/Bg	Pore-filling Fluid Type	Volume (BCF)
35-34	188958626	19	43%	80%	164	Gas Hydrate	199
34-33	188958626	36	40%	80%	164	Gas Hydrate	355
33-31	58222494	19	37%	80%	164	Gas Hydrate	55
30-29	123231091	2	40%	80%	83	Gas	6
29-28	58222494	13	38%	80%	87	Gas	20
Total	**617593333**	**88**					**635**
Average			**40%**	**80%**			

Table 15: MPU S-pad area preliminary, UA sequence stratigraphic correlation-based volumetrics calculations for gas hydrate and associated free gas

- Interpreted a diffuse and segmented northwest-trending structural hingeline controlled deformation of shallow sequence of gas hydrate-bearing rocks by north-northeast trending syn- and post-depositional faults
- Linked northwest-trending hingeline to deeper fault zones within oil-bearing reservoirs
- Interpreted fault complexity including differential offset near fault terminus, en echelon faults, relay zones, and possible rotation
- Developed theory for transtensional basin architecture within MPU structural setting
    - Interpreted small, northeast-trending pull-apart basin that may have influenced sediment deposition and the later accumulation of gas hydrate
    - Interpreted local structural controls on sediment deposition and gas migration
    - Observed higher net/gross sand ratio within basin, suggesting syndepositional faults may have influenced facies distributions and depositional environments
    - Observed anomalous stratigraphic thickening and thinning correlative to graben distribution within Marker 34 (USGS Zone C equivalent)
    - Interpreted probable gas hydrate-bearing reservoirs to be nearer faults within basin
- Interpreted sigmoidal fault geometries and related to transtensional deformation in weak sedimentary cover above a deeper left-stepping sinistral strike-slip fault system
    - Considered linkage of sinistral shear zone to gas migration conduits or barriers
- Confirmed six distinct, laterally continuous gas hydrate-bearing reservoir units with lithostratigraphic correlations
    - Applied sequence stratigraphic framework to show more reservoir heterogeneity
    - Identified numerous intraformational unconformities defining many sequences
- Studied possible gas hydrate occurrence connections including active deeper-seated fault-related migration conduits and possible gas source from coalbed methane
- Considered sealing faults, gas-conduit/migration faults, reservoir depositional geometry, and structural framework as controlling factors of gas hydrate-bearing sands

5.1.6.2 Subtask 6.2, UA Seismic Studies

Subtask 6.2 studies helped delineate the extent of in-situ gas hydrate and free gas zones based on seismic character and seismic attributes from shallow seismic reflection data. These studies also helped determine the relationship between occurrences of gas hydrate and free gas based on seismic character, seismic attributes, model waveform character, and seismic attributes.

Phase 1, subtask 6.2 accomplishments included:

- Created synthetic seismograms for tying well logs (such as MP18-01, WSAK-25, MPS-15, MPA-01, MPB-01, MPC-01, and MPD-01) to seismic data
- Calculated initial attribute cubes on original stacked data, and modeled acoustic properties of gas/water and hydrate/gas contacts to confirm seismic response
- Successfully loaded NWEileen and Milne survey 3D seismic data to computing system
    - Tested and calibrated UA seismic finite-difference modeling algorithms
- Created shallow fault map from upper 950 ms seismic data in Milne Point 3D survey and overlapping area of Northwest Eileen 3D survey (R03, figure 5)
- Extracted Amplitude along prominent reflections for possible correlation with gas hydrate and free gas occurrences (R03, figure 6) and performed AVO analyses
- Analyzed seismic wavelet/waveform classification to determine potential relationship to gas hydrate occurrence in seismic-equivalent horizons 30, 26, 33, 36, and 39 (R04)
- Developed waveform classification along known gas hydrate horizons on trace-equalized predictive deconvolution data (R05, figures 1-4; USGS Units E, D, and C)
- Concluded that waveform classification anomalies are primarily fault-controlled, particularly near faults with higher sealing potential
- Completed time-depth conversion of Milne Point 3D survey using improved synthetics and checkshots (R05, figure 5)
- Completed post-stack wavelet processing (25-50 foot tuning thickness) and discovered significant enhancement of signal within gas hydrate stability field
- Calculated fault heaves across all interpreted faults for 14 UA stratigraphic horizons
- Calculated fault frequency for four intervals and revealed a distinctly lower frequency over NW trend in cube, indicating a deep structure accommodating offset at depth, or many smaller faults below seismic resolution that accommodate offset
- Calculated fault seal CSP (Clay Smear Potential) and SGR (Shale Gouge Ratio) across gas hydrate Unit C, using fault throws from seismic and shale thickness from well logs to predict sealing/non-sealing nature of faults (Figure 19)
- Correlated fault heave magnitude, sealing nature, and relative time of faulting to known/interpreted gas hydrate occurrences as interpreted from waveform classification
    - Concluded that waveform-classification anomalies are fault controlled, specifically around faults with high sealing potential (R07, pp. 17-28)
- Created grid-illumination-horizon structure maps to interpret subtle structural features and faults and confirmed strong N-NE and more subtle NW structural trends become apparent as termini of N-NE-trending faults, fault zones, and fault seal (Figures 20-21)
    - Northwest trending zone indicated by Figure 20 box
    - Arrows show major “basin-bounding” faults that may cut deeper reservoir levels
    - Location of seismic cross-section (Figure 21) shown by dashed line
- Performed unsupervised (untrained) classification using three seismic attributes
    - Extracted instantaneous frequency, amplitude acceleration, and dominant frequency from 3D seismic data
    - Matched classification of interpreted gas hydrate-bearing zones in several areas with gas hydrate-bearing zones identified in well logs
    - Determined zones identified as possible gas hydrate-bearing layers predominantly characterized by relatively high dominant frequency

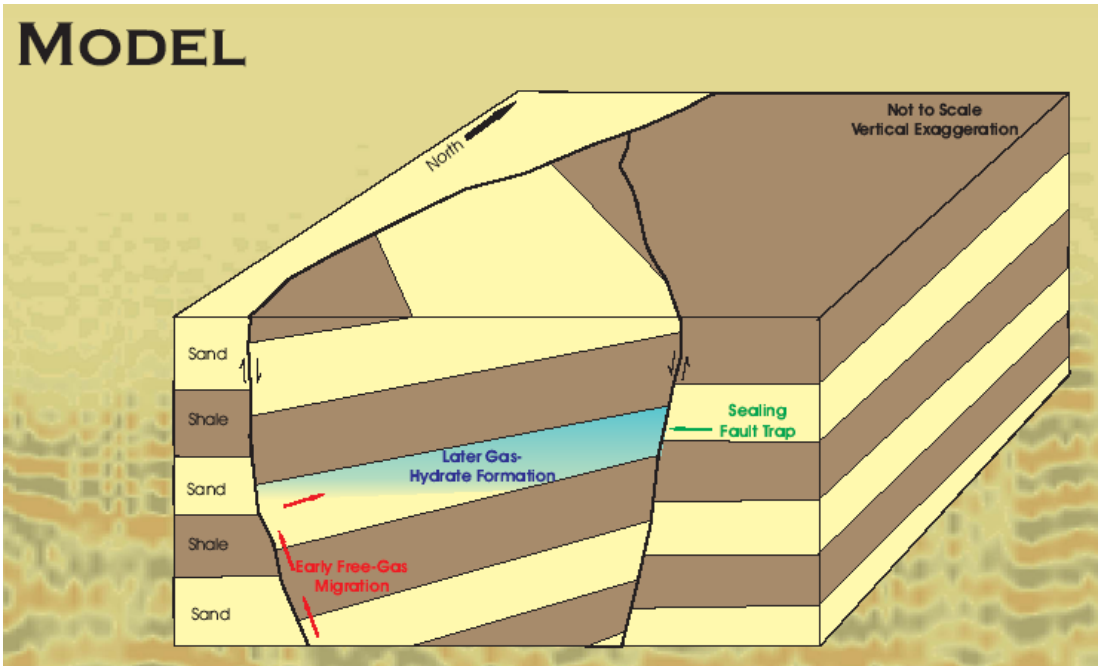

Figure 19: Diagrammatic gas migration model showing migration of thermogenic free gas up faults into reservoir sands with trap by sealing faults due to CSP and SGR.

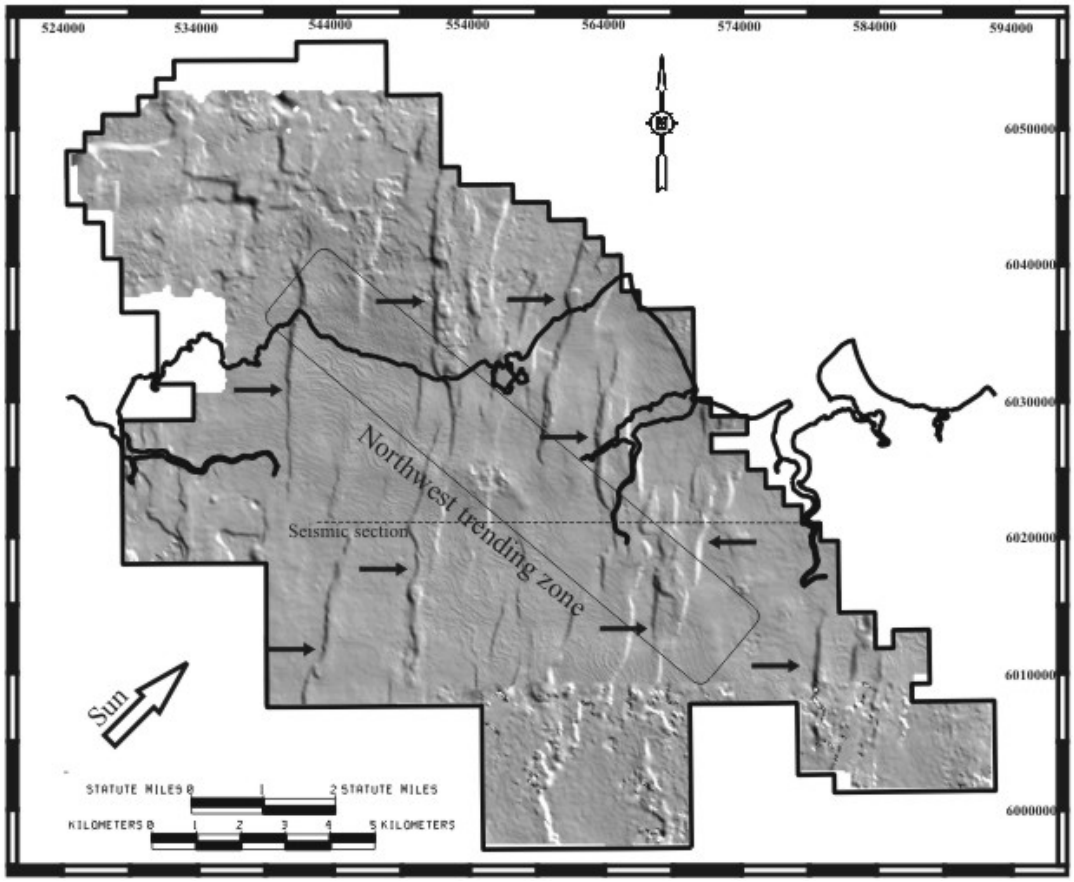

Figure 20: Shaded illumination map for the seismic horizon 34 surface. "Sun" direction is S45W with an altitude of 25 degrees.

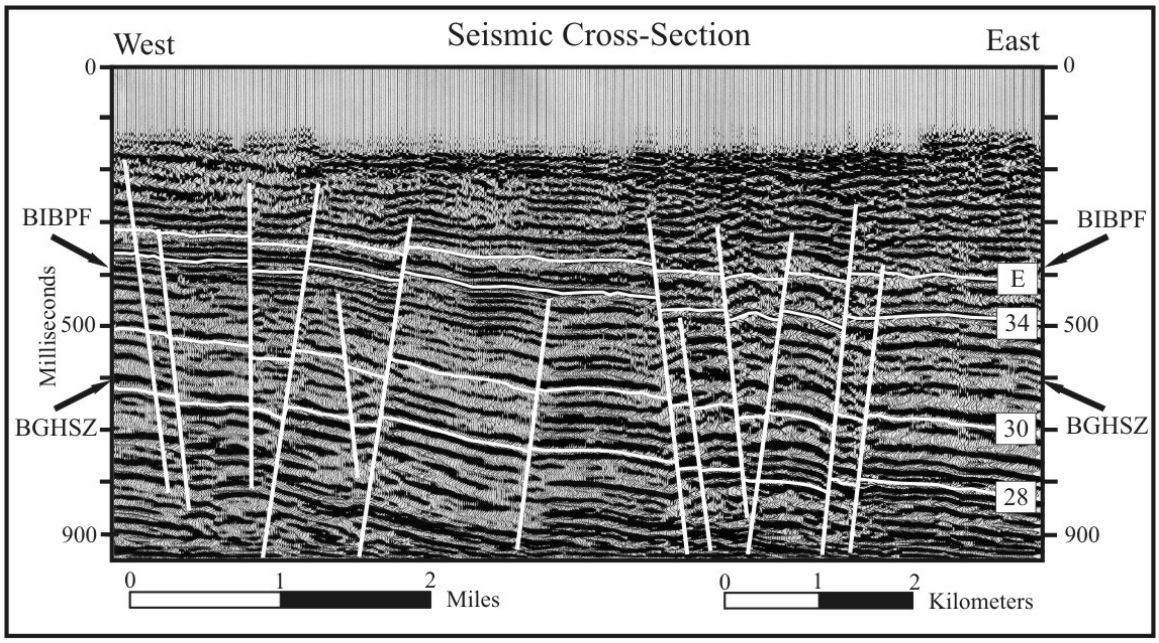

Figure 21: West to East seismic cross section (in milliseconds) of the wavelet processed Milne Point Survey; location is shown in Figure 20. Near vertical lines indicate seismically interpreted faults and near horizontal lines show four seismic horizons considered in this study: 28, 30, 34, and Unit E. Arrows show approximate location of base ice-bearing permafrost (BIBPF) and base gas hydrate stability field (BGHSZ).

5.1.6.3 Subtask 6.3, Petrophysical and Artificial Neural Network Modeling

Subtask 6.3 studies investigated petrophysical and artificial neural network modeling techniques for log and seismic data analyses. Studies included analyses of seismic waveform characteristics to identify and map hydrate facies through the shallow seismic volume. Studies also included using neural networks to help normalize and correlate well log signatures to seismic data.

One study component applied artificial neural network analysis (ANN) to help characterize and predict gas hydrate and free-gas resources. In this subtask, trained neural networks classified lithologies (sand, coal, shale) and fluids (gas hydrate, gas, water) in 0.5 foot increments from normalized gamma ray, resistivity, sonic, density, and neutron porosity well log curves.

A neural network is also able to analyze seismic waveform characteristics that represent a horizon and form robust templates that can be used to match waveforms through a seismic volume (Poulton, 2001, 2002). Phase 1 studies used neural networks to identify and map interpreted gas hydrate-bearing facies within the MPU seismic volume by analyzing the morphology of wavelets within a specified horizon. An initial ANN model for methane hydrate formation in the MPU used a self-organizing map (SOM) (Zhao, 2003). An unsupervised (untrained) classification was performed using three seismic attributes: instantaneous frequency, amplitude acceleration, and dominant frequency extracted from 3D seismic data. The classification results of the seismic attributes showed that the SOM classification of interpreted gas hydrate-bearing zones correlated in several areas with gas hydrate-bearing zones identified in well logs. The dominant frequency attribute produced the most consistent results for tracking layers of suspected methane hydrate. In general, zones identified as possible gas hydrate-bearing

layers were characterized by relatively high dominant frequency. Early SOM classifications were completed before completing satisfactory time-depth corrections for the seismic data, full stratigraphic analyses, chronostratigraphic sequencing, and fault pattern analyses. Subsequent studies included tying lithology and fluid classifications for each well to seismic data and conducting a detailed investigation of the wavelet morphology for each class. Refined volumetric estimates of gas hydrate and gas within the MPU were also planned based on the identification of waveform signatures for gas hydrate- and associated gas-bearing reservoirs. An expert system was developed to interpret the type of fluids present within reservoir intervals from the well logs (Glass, 2003) and results compare well to the ANN results for NWEileen-02.

Phase 1 subtask 6.3 results are summarized in R09 (pp. 41-53) and accomplishments included:

- Began research on neural network mapping and analyses
- Investigated petrophysical model to predict gas hydrate concentrations using sonic and bulk density logs in conjunction with seismic attributes such as compressional velocity
- Completed gas hydrate and free gas log-based fluid predictor
    - Adapted predictor to generated a pseudo log of missing curve for intervals where sonic, density and resistivity log were absent
- Completed log-based fluid prediction algorithm: "Estimating Pore Fluid Concentrations Using Seismic and Electrical Attributes"
- Estimated pore fluid concentrations of ice, free gas, water, and gas hydrate using down-hole measurements of electrical resistivity, bulk density and compressional wave velocities using the following eight techniques, which produced similar patterns
    - Lee equation for seismic compressional wave velocity
    - Archie equation for electrical resistivity
    - Fuzzy membership functions using seismic compressional wave velocity
    - Maximum likelihood probability using seismic compressional wave velocity
    - Modeling using seismic compressional wave velocity and electrical resistivity
    - Bulk elastic moduli (BEM) estimation
    - Reister Model using seismic compressional and shear wave velocity and porosity
    - Pore fluid density estimation as predicted from resistivity logs (dependent upon porosity and saturations)
- Determined free gas concentration dominated by compressional wave velocities and tend to be high even where electrical resistivity values do not support the existence of free gas
- Corrected free gas concentrations by computing second probability to ensure estimates of free gas concentrations occur only where electrical resistivity values are suitably high
- Determined gas hydrate concentration also affected by compressional wave velocity bias, especially near the base of gas hydrate stability
- Noted ice and gas hydrate cannot be distinguished using available well log data
    - Distinguished by estimating gas hydrate below base ice-bearing permafrost
    - Where gas hydrate may occur above base permafrost, no distinction is possible
- Completed expert system algorithms to classify fluid saturation, estimate confidence, and detect coal occurrence
    - Evaluated and compared results to manual interpretations
    - Determined velocity and resistivity response for water saturated zones
    - Trained neural network to predict gas hydrate, free gas, coal, clean sand, and water saturation components within reservoir sands from well log signatures

- Applied artificial neural network analysis (ANN) to help characterize and predict lithologies (sand, coal, shale) and fluids (gas hydrate, gas, water) in normalized log data
    - Created two basic types of training sets using various combinations of log data
    - Determined good match of ANN to well log expert system of Glass (2003)
    - Determined good correlation of ANN classification and expert system results to cored hydrate interval of the 1972 NWEileen-02 well

5.1.7 Phase 1, Task 7 – UAF Drilling, Completion, and Production Studies

Laboratory studies included designing experiments to characterize the formation and dissociation of gas hydrate in porous media at or near reservoir conditions. Two primary subtasks included characterizing gas hydrate phase behavior (7.1) and measuring gas-water relative permeabilities in gas hydrate-bearing sediment (7.2).

5.1.7.1 Subtask 7.1, Characterize Gas Hydrate Equilibrium

These studies designed phase behavior experiments and generated hydrate curves (Pressure-Temperature diagrams) for methane, ethane and standard natural gas mixtures, determined the reliability of experimental techniques, and developed thermodynamic models to cover the range of gas hydrate compositions and temperatures. Results of non-porous media and Anadarko Hot Ice porous media are presented in R05, pp. 22-26.

Phase 1 subtask 7.1 accomplishments included:

- Planned, designed, and setup UAF Phase Behavior experimental apparatus (Figure 22)
- Acquired DBR Phase Behavior apparatus and "HYDRATE 5.1" software
- Calibrated Phase Behavior apparatus and conducted experiments (R02, R03)
    - Conducted experiments using varied brine concentrations and using CO_2

5.1.7.2 Subtask 7.2, Measure Gas-Water Relative Permeabilities in Gas Hydrate

Subtask 7.2 studies designed original experimental apparatus to help determine relative permeability function relationships by conducting two-phase relative permeability experiments, quantifying multiphase flow, and assessing gas productivity from hydrate-bearing porous media. Relative permeability measurements on gas hydrate-bearing sediments used the unsteady-state technique with formation water-saturated core plugs, absolute permeability base, two-phase production data, pressure drop on core plug dimensions using the Johnson-Bossler-Naumann (JBN) method. Interim results of these experiments are presented in R05, pp. 26-30.

Phase 1 subtask 7.2 accomplishments included:

- Designed apparatus, theory, and procedures for two-phase (gas, hydrate-water) relative permeability experiments (R02; R03 pp.23-27; R04 pp.25-31) (Figure 23)
- Redesigned experimental apparatus to form synthetic gas hydrate and measure relative permeability across cores by the unsteady state method (R06, pp. 16-20; R07, pp. 29-40)
    - Used coarse sand particles to create synthetic gas hydrate in the lab (Figure 24)
    - Calculated relative permeability at gas hydrate saturations of 10%, 17%, and 29%
    - Relative permeability considerably changed at higher gas hydrate saturations

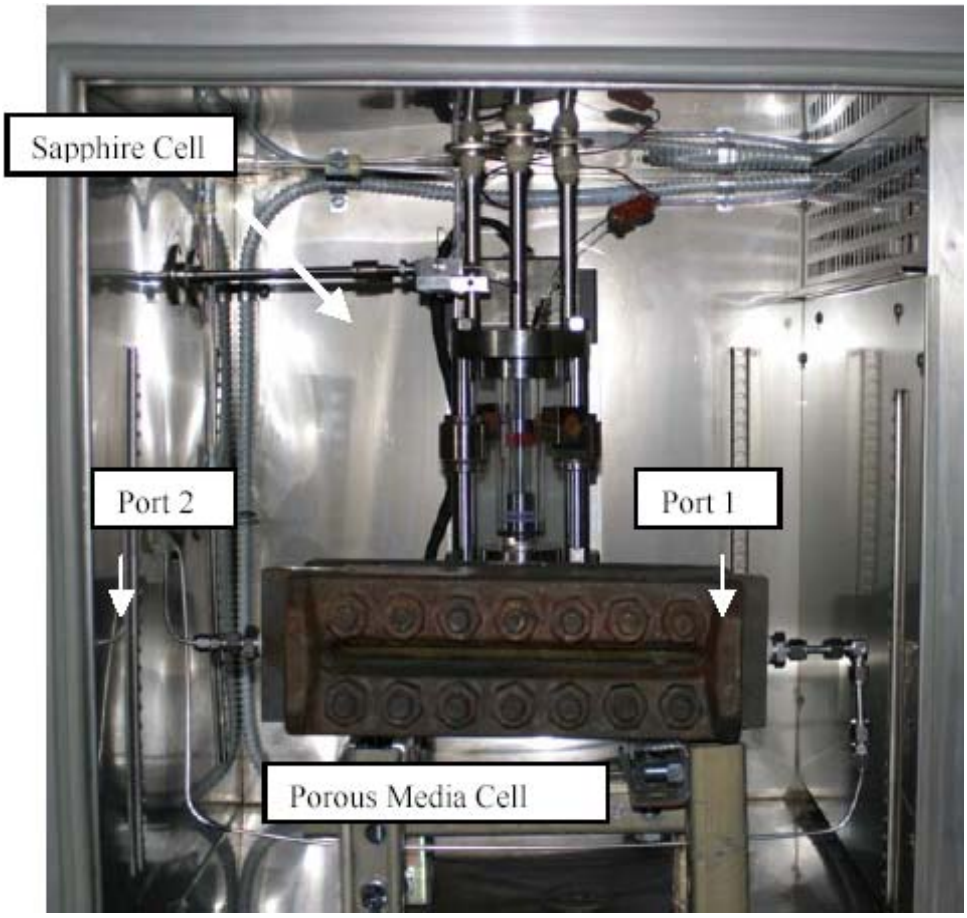

Figure 22: UAF Phase Behavior apparatus, temperature controlled air bath with sapphire cell and porous media cell

These experimental studies supported the following main conclusions:

- Gas hydrate was successfully formed by this new method within the core holder
- Relative permeability measurements were achieved on both the Oklahoma 100 mesh sand sample and shallow field samples obtained from the Anadarko Hot Ice # 1
- The type of gas hydrate growth influences the mechanism of formation and the gross morphology of gas hydrate occurrence; this not only depends on a number of sediment parameters, including grain size, porosity, and pore structure, but also parameters such as non-uniform dissociation, fluid parameters such as viscosity, and also the method of forming hydrates
- The relative permeability inferred from unsteady-state core floods conducted in this study is a lumped parameter; this not only includes hydrate saturation, but also the effects of dissociation instabilities caused by fluid flow, fines migration due to gas production, and local compaction in porous media at low temperatures
- These relative permeability curves generated in the laboratory for sand samples and field samples could, to some extent, describe the field behavior of two phase flow in the presence of gas hydrates and could improve reservoir modeling of the dynamic flow behavior expected during gas production from gas hydrate-bearing reservoirs

The gas-water relative permeability data for gas hydrate systems is essential when either considering the depressurization methods or inhibitor injection methods for dissociation and recovery of gas from gas hydrate-bearing formations. Such types of data are virtually non-existent in the literature. UAF indigenously designed and developed a displacement apparatus capable of forming gas hydrate and conducting relative permeability experiments. UAF successfully measured the gas-water relative permeability functions, in the presence of gas hydrate saturations ranging from 5-36%, for unconsolidated Oklahoma sand and for Anadarko Hot Ice #1 core samples. The key gas-water relative permeability results are shown in Figure 25 (also R07, pp. 29-40 and R06, pp. 16-20). Results indicate a reduction in relative permeabilities as gas hydrate saturation increases.

Recommended additional relative permeability experimental studies could include:

1. These gas-water relative permeability data experiments for gas hydrate systems used reconstituted sediment samples. Actual field samples from the Sagavanirktok reservoir interval within MPU were unavailable during these Phase 1 studies. Sediment samples from field areas would help refine results of procedures pioneered in these experiments. Input from potential future experiments run with field samples could help refine reservoir simulation work with important gas-water relative permeability measurements (Mt Elbert-01 core samples provided following Phase 3a operations – Section 5.3.8.8.6).
2. Dynamics of growth and dissociation of gas hydrate in presence of fluid flow are not yet fully known. Thus, additional experimental measurements are recommended to help predict relative permeability curves for formation, distribution, and dissociation of gas hydrate within the pore structure of porous media. Conducting laboratory displacements in a fully scaled model of field-scale displacement may help enable prediction of a functional relationship between permeability, porosity, pore structure discontinuities, tortuosity, and fluid parameters such as viscosity and dissociation instability.
3. Additional relative permeability tests should be performed at different temperature conditions, which could significantly improve understanding of the relative permeability characteristics of gas hydrate-bearing petroleum systems.

Figure 23: Relative permeability experimental apparatus at UAF laboratory (9/22/2003)

Figure 24: The experimental set-up constructed for forming gas hydrate and measuring relative permeability (April 2004)

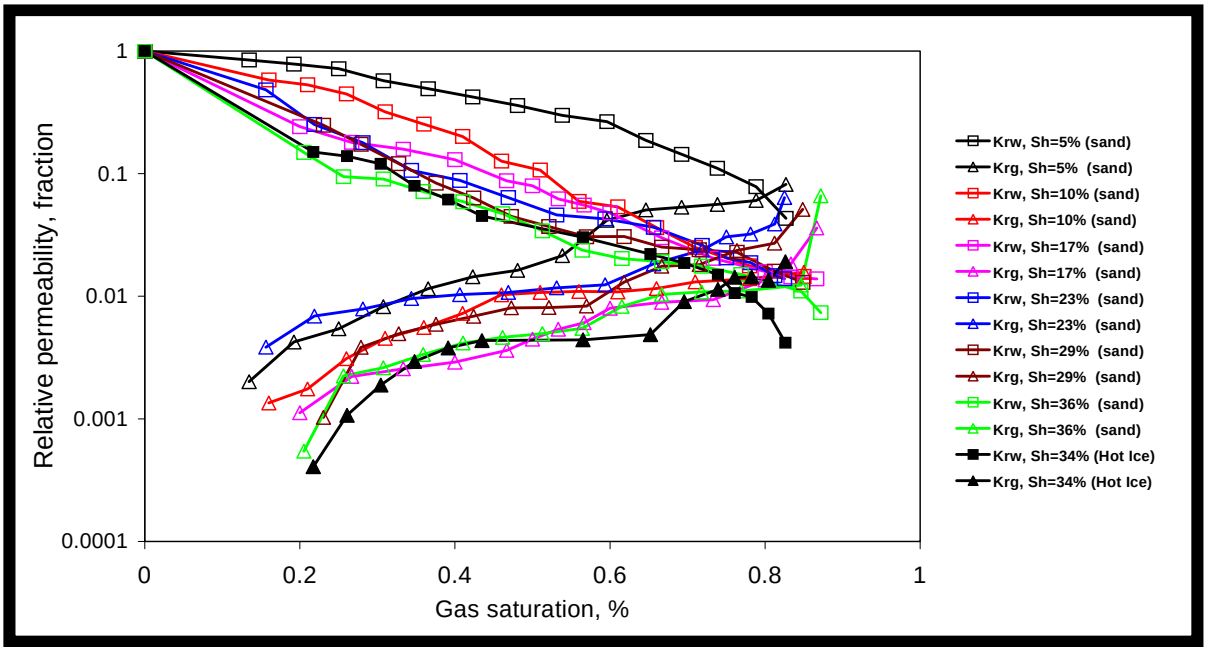

Figure 25: Relative Permeability Plots

5.1.8 Phase 1, Task 8 – UAF Drilling Fluids and Formation Damage Evaluation

Task 8 studies evaluated available options and design for a temperature-controlled drilling mud system to help ensure effective well operations and data acquisition programs within gas hydrate-bearing sediments. Studies included assessment of formation damage prevention and included evaluation of mud chilling systems to enhance borehole stability, maintain borehole gauge, and maximize flow potential of gas hydrate and associated free gas during test operations. Detailed plans for these experiments are presented in R05, pp. 31-33.

Phase 1 Task 8 accomplishments included:

- Reviewed drilling fluids literature pertaining to gas hydrate-bearing reservoir intervals
- Evaluated rheological properties of Mackenzie Delta and Japan Offshore drilling fluids
- Evaluated mud chiller systems to determine applicability to ANS operations (R02, R03)
    - Design to prevent gas hydrate and/or permafrost thawing during operations
    - Enable multi-day data acquisition programs within gas hydrate-bearing reservoirs
    - Evaluated mud additives, hydrate stabilization, and hydrate inhibitors
        - Compared Anti-agglomerates to Kinetic inhibitors
    - Determined systems significantly contributed to success of Canada programs
    - Included recommendation of Drill Cool Systems (Figure 26) for operations
- Sized and defined specifications of some components in the experimental apparatus setup, including methane gas and drilling fluid separator, floating piston accumulator, gas mass flow meter, pressure gauges etc.
- Positioned items including back pressure regulators and gas-liquid separators in the experimental apparatus to allow for consideration of the possibility of compression of gas and the requirement to analyze and measure the gas flow with time
- Procured critical parts of the testing apparatus, including Dynamic filtration core holder, dual action recirculation pump, floating piston accumulator, gas drilling fluid and other gas and liquid measurement devices
- Developed an understanding of standardized testing procedure for formation damage assessment and defined experiment parameters with methane gas and shallow sand cores
- Developed key testing procedures and addressed experiment challenges (R06, pp. 21-23)
- Erected experimental apparatus and refined standard testing procedures (R07, pp. 40-44)

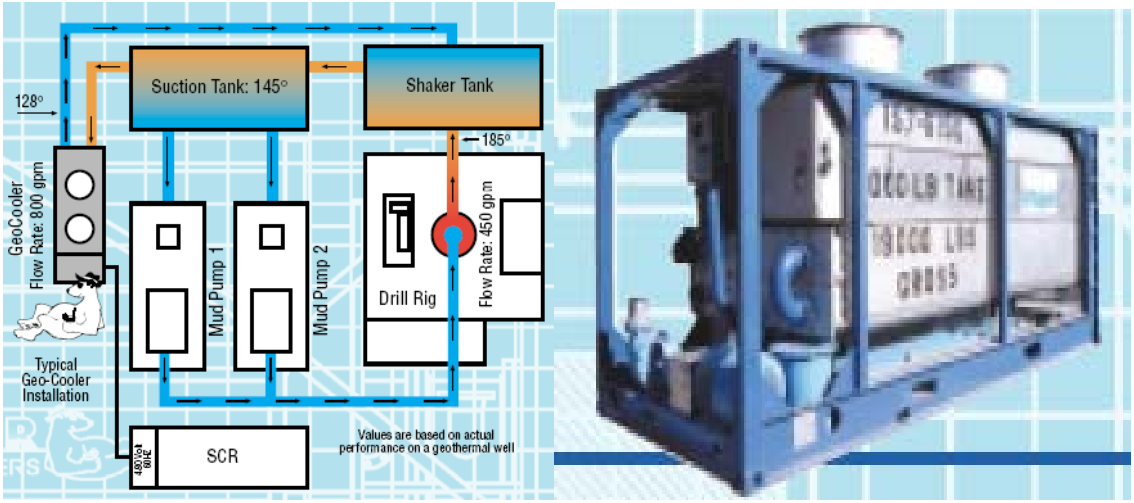

Figure 26: Mud Cooling System configuration (After, Drill Cool Systems, Inc.)

5.1.9 Phase 1, Task 9 – UAF Cementing Program Design

Task 9 studies evaluated cementing techniques to help minimize formation damage, minimize required cement volumes, maximize flow potential, and maximize cement strength and bond within gas hydrate-bearing intervals. Accomplishments included:

- Reviewed drilling cement literature pertaining to gas hydrate-bearing reservoir intervals
- Considered Ceramicrete (Bindan Corporation product) for downhole application

5.1.10 Phase 1, Task 10 – UAF Coring Technology Studies

Task 10 studies investigated core tools, recovery techniques, preservation means and transportation methods. Standard industry methods were compared to existing and new techniques within gas hydrate-bearing reservoirs to help determine the ability to recover an undisturbed pressurized core of gas hydrate-bearing reservoir. The results were applied to Phase 3 core program operations and enhanced core recovery, preservation, transportation, and analyses. Accomplishments included:

- Reviewed core technology literature pertaining to gas hydrate-bearing reservoir intervals
- Assessed ANS coring technologies and applicability to gas hydrate-bearing reservoirs
- Assessed and comprehensively reviewed available core systems including Pressure Core Sampler (PCS), Hydrate Autoclave Coring Equipment (HYACE), HYACE tools In New Tests on Hydrates (HYACINTH), OMEGA Multiple Autoclave Corer (OMEGA MAC), Pressure-Temperature Core Sampler (PTCS), and core storage/transport (R03 pp. 32-37)

5.1.11 Phase 1, Task 11 – Reservoir Modeling

The reservoir modeling Task 11 studies helped determine whether or not the gas hydrate-bearing reservoirs were theoretically capable of production and thus figured prominently in phase progression decisions. Data from gas hydrate reservoir and fluids characterization studies were used to build new and/or optimize existing reservoir models. The reservoir models incorporated available gas hydrate production test data and were used to help calculate potential reserves, productivity and development costs, which helped determine possible future development economics and project progression from desktop studies into field operations. Industry perspective was applied and linked to various gas hydrate reservoir models such as the TOUGH2 gas hydrate module developed by Lawrence Berkeley National Laboratory (LBNL). Accomplishments included:

- Modeled a 1-mile by 4-mile fault block within CMG STARS (Figure 27, R06, pp.28-33)
- Completed BPXA-LBNL pre-Phase 1 scoping reservoir model (Figures 28, 29)
- Incorporated Mallik data to help calibrate reservoir model code
- Collaborated with LBNL on TOUGH2 and EOSHYDR2 simulation module
- Evaluated STARS multi-component, multi-phase, thermal simulator developed by the Computer Modeling Group (CMG) and adapted to use in gas hydrate-bearing reservoirs
- Evaluated ProCast simulator with RyderScott Co.
- Documented gas hydrate decomposition kinetics (R06, pp. 23-28)
- Simulated reservoir cooling during endothermic gas hydrate dissociation (R06, pp. 34-35)
- Noted CMG Model limitations at temperatures below 0^{o} C prevented thorough analyses
- Initiated ProCast beta modeling to more quickly forecast possible development scenarios
- Continued to adapt CMG STARS to gas hydrate reservoir characteristics (R07, pp.44-58)
    - Built on foundational work of Hong and Darvish (2003) and by Howe (2004)

- Developed theory (Hunter, 2004 personal communication) to depressurize available mobile connate water to initiate gas production from gas hydrate-bearing reservoirs
  - Evaluated partial hydrate saturation and potential for mobile connate waters
  - Determined potential for relative permeability in pore-filling gas hydrate reservoir
  - Mobile Connate waters could enable in-situ depressurization drive (CBM analog)

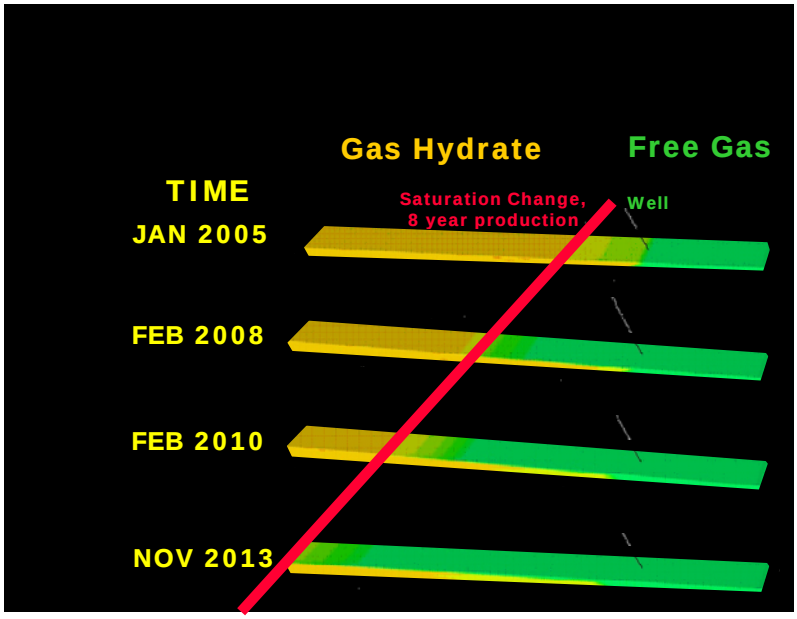

Figure 27: Gas hydrate saturation profiles, initial CMG STARS model over 8 years

5.1.12 Phase 1, Task 12 – Drilling Location and Candidates

Task 12 required input from all tasks to help evaluate viable candidate areas for gas hydrate and associated free gas drilling, data acquisition and production testing operations. Once a site was selected, project Phase 3 operations maximized synergies with field development activities, ensuring safe facility access and drilling rig availability (compiled in Report T01, June, 2005).

5.1.13 Phase 1, Task 13 – Commerciality and Phase 2 Progression Assessment

To help determine project progression, Task 13 considered future potential regional gas hydrate development and included calculating project appraisal economics and risk. Accomplishments included:

- Demonstrated potential gas production commerciality from scoping study of gas hydrate across broad regional contact with adjacent free gas depressurization (Figure 28, R01)
- Collected public domain input data (gas price, transportation tariff, capital expense estimates) for economic model of potential gas hydrate reservoir regional development
- Completed economic model template and ran 2 test simulations with positive results (R03 pp. 37-40)

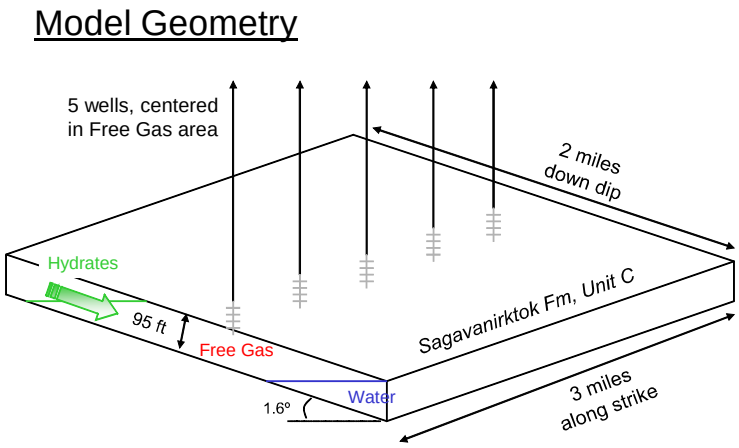

Figure 28: ANS scoping study reservoir model showing free gas depressurization leading to gas hydrate dissociation across a broad regional contact (R01)

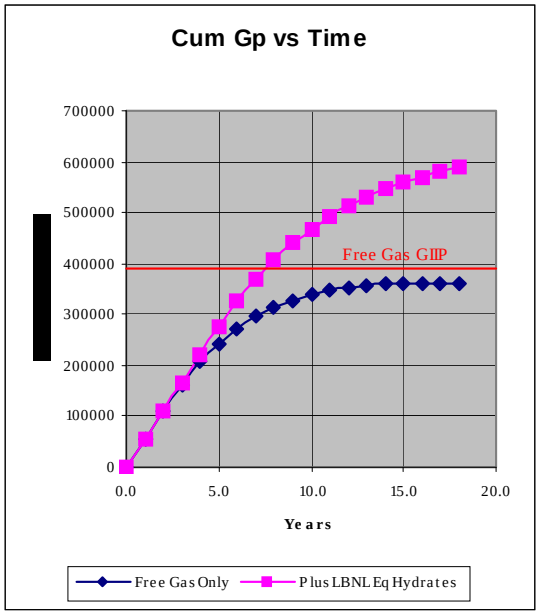

Figure 29: Cumulative production plot showing significant increase with hydrate dissociation from model in Figure 28 (R01).

5.2 Phase 2 Task Schedules, Milestones, and Accomplishments

U.S. Department of Energy Milestone Log, Phase 2, 2005-2006
Program/Project Title: DE-FC26-01NT41332: Resource Characterization and Quantification of Natural Gas Hydrate and Associated Free-Gas Accumulations in the Prudhoe Bay - Kuparuk River Area on the North Slope of Alaska.

Phase 2 continued the desktop studies initiated in Phase 1 and added additional focused reservoir characterization and modeling activities that culminated in a decision to proceed into Phase 3 drilling and data acquisition operations (Tables 16 and 17). Phase 2 scope-of-work was outlined in contract Amendment 9 (Table 6). Reporting was limited during Phase 2 as project work focused on recommending progressing desktop studies into field operations and data acquisition. Topical report T01 summarized these drilling operations plans (T01, 36pp.).

Identification Number	Description	Planned Completion Date	Actual Completion Date	Comments
Task 1.0	Research Management Plan	1/05 – 1/06	1/06	Subcontracts Completed; Also see Section 5.2.1
Task 2.0	Provide Technical Data and Expertise	MPU: 12/02 PBU: * KRU: *	MPU: 12/02 PBU: * KRU: *	See Technical Progress Reports and Section 5.2.2
Task 3.0	Wells of Opportunity Data Acquisition	Ongoing	Ongoing	See Technical Progress Reports and Section 5.2.3
Task 4.0	Research Collaboration Link	Ongoing in Phase 2-3	Ongoing in Phase 2-3	See Technical Progress Reports and Section 5.2.4
Subtask 4.1	Research Continuity	Ongoing in Phase 2-3	Ongoing in Phase 2-3	
Task 5.0	Logging and Seismic Technology Development and Advances	Ongoing in Phase 2-3	Ongoing in Phase 2-3	See Topical Report T01 and Section 5.2.5
Task 6.0	Reservoir and Fluids Characterization Study	12/06	final report received 9/09	See Technical Progress Reports and Section 5.2.6
Subtask 6.1	Structural Characterization	12/06	final report received 9/09	
Subtask 6.2	Resource Visualization	12/06	final report received 9/09	
Subtask 6.3	Stratigraphic Reservoir Model	12/06	final report received 9/09	
Task 7.0	Laboratory Studies for Drilling, Completion, Production Support	12/06		Some Hiatus; also see Section 5.2.7
Subtask 7.1	Design Mud System	12/05	Completed	
Subtask 7.2	Assess Formation Damage	1/06	Completed	
Subtask 7.3	Measure Petrophysical and Other Physical Properties	9/06	Into Phase 3a	No Samples Acquired; await Phase 3a acquisition
Task 8.0	Design Completion / Production Test for Gas Hydrate Well	4/06	Mt Elbert-01 stratigraphic test 2/07	Design of Phase 3a Strat Test operation Complete; See Section 5.2.8
Task 9.0	Field Operations and Data Acquisition Program Planning	4/06	Mt Elbert-01 stratigraphic test 2/07	Planning for Potential operations: Section 5.2.9
Task 10.0	Reservoir Modeling and Project Commercial Evaluation	1/06	Ongoing in Phase 2-3	Regional Resource Review & Development Planning: Section 5.2.10
Subtask 10.1	Task 5-6 Reservoir models	Ongoing in Phase 2-3	Ongoing in Phase 2-3	
Subtask 10.2	Hydrate Production Feasibility	1/06	Phase 2-3	
Subtask 10.3	Project Commerciality & Phase 3a Progression Assessment	1/06	Phase 2-3	January 2006 approval for Phase 3a Stratigraphic Test

* Not released to CRA as limited-rights data due to dependent on industry partner agreement

Table 16: Phase 2 Task Descriptions and Milestones

DOE F 4600.3# TABLE 17: U.S. DEPARTMENT OF ENERGY FEDERAL ASSISTANCE MILESTONE PLAN: PHASE 2-3a (2005-2006)

1. Program/Project Identification No. DE-FC26-01NT41332	2. Program/Project Title Resource Characterization and Quantification of Natural Gas Hydrate and Associated Free-Gas Accumulations in the Prudhoe Bay - Kuparuk River Area on the North Slope of Alaska
3. Performer (Name, Address) BP Exploration (Alaska), Inc., 900 East Benson Blvd, P.O. Box 196612, Anchorage, Alaska 99519-6612	4. Program/Project Start Date 10/22/02* 5. Program/Project Completion Date 3/31/11 (through Phase 3a)

6. Identification Task Number	7. Planning Category (Work Breakdown Structure Tasks)	8. Program/Project Duration (Phases 2-3, 2005 - 2006) ← Planning/Analysis → ← DECISION---→ ←Planning--------→← IMPLEMENTATION deferred to 2007→ J F M A M J J A S O N D J F M A M J J A S O N D	9. Comments (Primary work Performer)
Task 1.0	Contracts and Research Management Planning	>>>>>>>!>>>---->>>>>!--->>>>>>>>>>>>>>>>>>!----------------------->>----->>-->>>>>>>	BPXA, AES
Task 2.0	Technical Data and Expertise	-->>>>>>----->>>>--!---->>>>>>>>>-------!---->>>>>>>>--------->>>>>>>>-->>>>>>>>--	BPXA, AES
Task 3.0	Wells of Opportunity - Data	------------->>>>>-!------------>>>>>---!----->>>>>>>>>>>>>>>----------->>>>>>>>	BPXA, AES
Task 4.0	Research Collaboration Link	---------->>>>>>>>>!---------->>>>>>>>>>!>>	BPXA, USGS, AES, UAF,UA
Task 5.0	Logging/Seismic Technology	>>>>>>>>>>>>>>>>>>!>>>>>>>>>>>>>>>>>>>!>>>>>>>>>--------------------------->>	USGS, BPXA
Task 6.0	Characterize Reservoir/Fluid	------->>>>>>>>>>>>>!---------->>>>>>>>>>!>>>>>>>>>>>>>>>>>---------->>>>>>>>>>>>>	UA, USGS
Task 7.0**	Lab Studies: Drilling, Completion, Production	------------>>>>>>>!---------->>>>>>>>>>!>>>>>>>----------------->----->>>>>>>>>	UAF
Task 8.0**	Stratigraphic Test Decision, Design, and Implementation	-->>>>>>>>>>>>!>>>----->>>>>>>>>>>>!>>>>>>>--------------------->>>>>>>>>>>	APA, BPXA, AES, UAF
Task 9.0**	Field Operations Planning and Implementation	---->>>>>>>>>>!>>>------->>>>>>>>>>!>>>>>>>--------------------->>>>>>>>>>>	APA, BPXA, AES, UAF
Task 10.0**	Reservoir Modeling and Commercial Evaluation	----->>>>>>>>>>>>>>>!>>>>>>>>>>>>>>>>>>---!------------------------------------	RS, AES, BPXA, UAF

10. Remarks * Schedule shows Phases 2-3a from 2005 through end-2006. Phase 2 project from 1/05 through 12/05. Phase 3a stratigraphic test initiated 6/05 and included 9/05 Continuation Application culminating in 1/06 decision to Drill. Explanation of Symbols: >> Major Task Work; -- Minor Task Work; ! Milestone. Significant technical work and milestones presented in Technical Progress and Topical Reports. **Note new (Phase 2-3a) Task numbers.

Table 17: Phase 2-3a (2005-2006) USDOE Milestone Plan and Task Descriptions

5.2.1 Phase 2, Task 1 – Research Management

The research management Task 1 studies continued to establish project plans, track progress against project milestones (Tables 16 and 17), monitor project costs, and help determine progression through the gates between project phases. Significant efforts were added to contract for services associated with the planned Mt Elbert-01 well.

5.2.2 Phase 2, Task 2 – Technical Data and Expertise

Task 2 desktop studies progressed into Mt Elbert-01 well operations and data acquisition planning, which utilized significantly more BPXA staff time contributed as cost-share. Regular weekly meetings were held with the BPXA MPU and drilling teams. Accomplishments included:

- Developed and implemented task schedules for well permits, materials, and plans
- Identified critical tasks and path for well permits, materials, contracts, and rig
- Documented risks, addressed concerns, and developed plans to mitigate risks
- Developed contacts and contracts with appropriate operations subcontractors
- Prepared and checked surface ice pad/road and well bottom hole location (BHL)
- Developed agenda, convened, and moderated weekly well planning meetings
    - Provided task status updates and coordinated well operations plans
- Evaluated and selected ice road route to ensure safe access within existing infrastructure
- Developed logging-during-drilling, wireline, core, and MDT evaluation program
- Evaluated cement program options and initiated discussions with Schlumberger
- Evaluated drilling mud program and incorporated DrillCool, Inc. mudchilling system
- Planned wireline retrievable core program and procedures with Corion (ReedHycalog)
- Planned core handling and processing program with OMNI Lab and others
- Completed detailed plan of operations and supporting documentation for well permits
- Initiated and reviewed drilling and data acquisition time and cost plans
    - Determined inability to drill well in 2006 due to third party rig delays and approaching end-of-tundra travel and ice season drilling (March 14, 2006)
    - Notified DOE and subcontractors of drilling delay and test deferral to early 2007
- Developed, reviewed, and submitted detailed Phase 3a program drilling, data acquisition, and data evaluation budget
- Initiated review of possible alternative gravel pad options for future production test site(s)

5.2.3 Phase 2, Task 3 – Wells of Opportunity Data Acquisition

Task 3 studies continued to monitor drilling schedules for additional data acquisition opportunities, but focused efforts on MPU Mt Elbert-01 well and data acquisition planning.

5.2.4 Phase 2, Task 4 – Research Collaboration Link

Task 4 studies continued to coordinate project activities and maintain clear point-of-contact research links with other gas hydrate research programs to maximize synergies with industry, university, government, and other projects both domestically and internationally. Project objectives and accomplishments were presented to industry partners to help facilitate cooperation. Project presentations were provided on a minimum annual basis to DOE and to public and industry forums such as American Association of Petroleum Geologists (AAPG) meetings. Accomplishments included:

- Prepared agendas, briefed management, and held meetings with DOE, industry, Alaska State, and Federal government in Houston and Anchorage (June 2005)

- Contributed to April 2006 meetings on Barrow, Alaska gas hydrate research proposal
- Prepared agendas, briefed management, and held meetings with DOE, industry, Alaska State, and Federal government in Houston and Anchorage (June 2005)
- Participated in invited technical conferences, including:
  - Provided project input to State Department gas hydrate conference (April 2005)
  - Presented project summary for DOE Advisory Committee meeting (June 2005)
  - Prepared and presented 3-panel project poster, AAPG Calgary (June 2005)
  - Helped plan, presented project summary, and contributed to gas hydrate workshop, co-sponsored by State of Alaska and USGS (August 2005)
  - Presented project summary for DOE Advisory Committee meeting (April 2006)
  - Presented project summary to AAPG/SPE Pacific Section Conference (May 2006)
- Presented project results and plans to BP Technical Advisory Committee (August 2005)

5.2.5 Phase 2, Task 5 – USGS Data, Logging, and Seismic Technology

To help ensure timely selection of a viable site for Phase 3 drilling and data acquisition operations, in parallel to the UA Task 6 activities, Task 5 studies were expanded in late Phase 1 through Phase 2 and augmented by supporting industry consultants. These expanded reservoir characterization activities identified multiple gas hydrate prospects within the MPU (Tables 4, 5, 12; Figure 7) through detailed investigation of the full volume MPU 3D seismic data (see also Section 5.1.5 above and Section 5.2.9 below).

Studies included detailed calculation of well log-based reservoir quality (sand quality, thickness, areal extent, porosity, net/gross, and saturation) as input to volumetric calculations for each of the 14 identified prospective areas within MPU (Tables 4 and 12). Uncertainty calculations using Monte Carlo principles were used to calculate the potential resource in-place distribution.

5.2.6 Phase 2, Task 6 – UA Reservoir and Fluids Characterization, Seismic Studies

Reservoir and fluid characterization studies continued into Phase 2 at the University of Arizona. Full documentation of accomplishments during this time period is available in prior reports (R15, pp. 17-76) and in Appendix A. Certain relevant accomplishments and activities are also summarized in this section. In particular, the studies relating to confirming the Mt Elbert-01 site gas hydrate prospectivity from Task 5 studies as well as studies relating to UA's Sagavanirktok formation sequence stratigraphic interpretations in MPU and in the PBU L- and V-pad areas. Note that mapping pertaining to these studies is available in supporting documentation from the University of Arizona final report and from excerpts of that report published in prior project report R26 (pp. 36-89) and in Appendix A.

The University of Arizona continued studies on faulting and clay smear. These assessments showed promise in helping to delineate prospective areas for trapping of gas hydrate-bearing sediments (Figures 30-31). Isopach mapping such as illustrated in Figure 32 also continued in support of UA gas hydrate prospect interpretations.

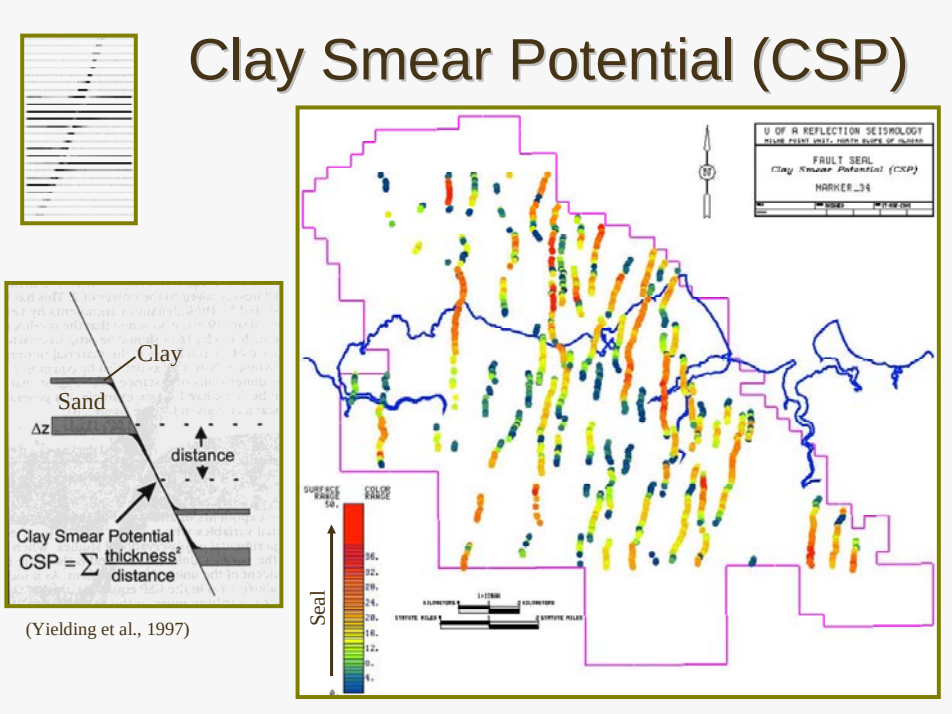

Figure 30: UA Fault interpretation of the MPU 3D seismic dataset enabled interpretation of "clay-smear potential", which may correlate to gas hydrate traps within the area-of-interest

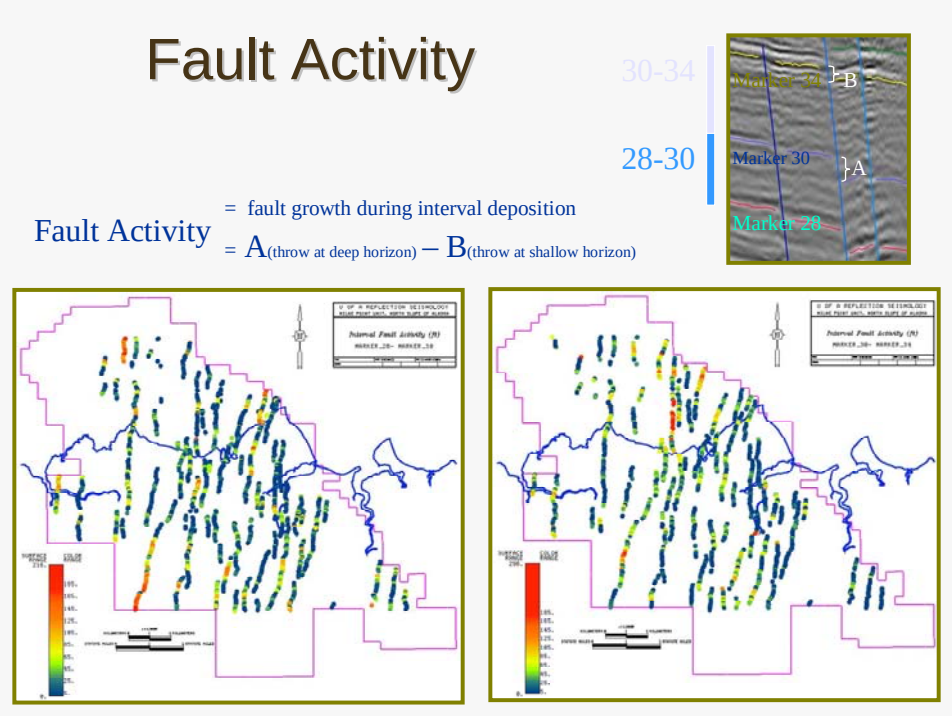

Figure 31: Pre- and syn-depositional faulting as interpreted by UA from the MPU 3D seismic dataset which may influence gas hydrate trapping and thickness of gas hydrate-bearing sediments

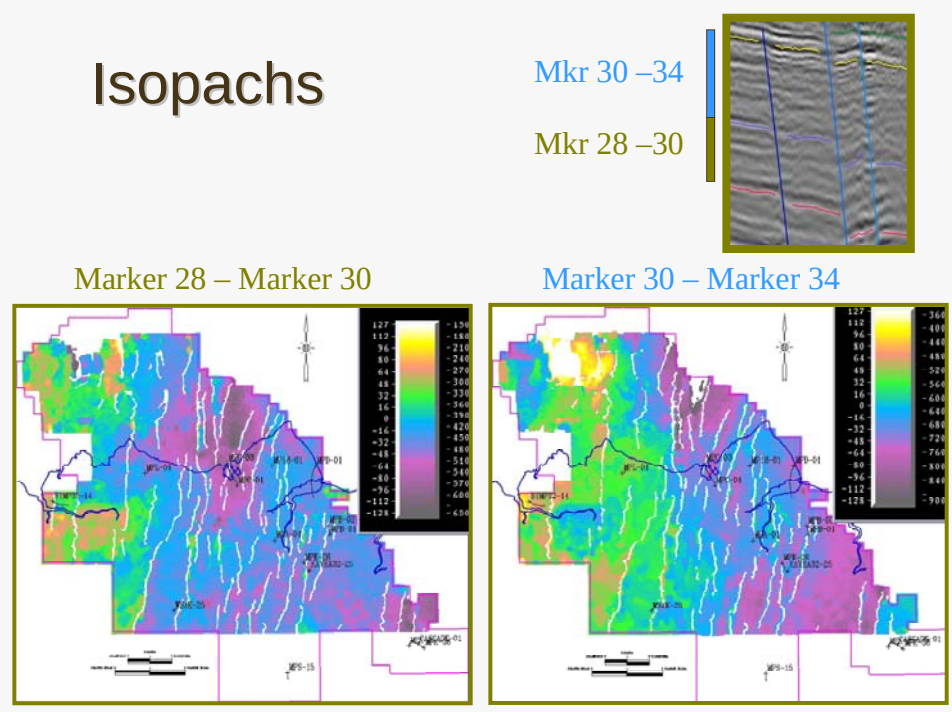

Figure 32: Example of isopach mapping between chronostratigraphic markers that may reveal a linkage between faulting, sediment deposition, and gas hydrate occurrence.

5.2.6.1 Comparison of Phase 2, Task 6.0 Studies to Phase 1, Task 5.0 MPU Prospects

As of March 2005, the UA fluid prediction studies, stratigraphic-structural analyses, and seismic attribute studies all suggested that the models presented at the September 2004 Hedberg conference remained viable for interpretation of gas hydrate-bearing reservoirs within the MPU. Post-conference analyses across the KRU and PBU illustrated a structural-stratigraphic linkage between fluvial source regions, confirming the role of channel pathways and depocenters that were interpreted to have accumulated reservoir-quality gas hydrate-bearing sands within structural traps. This was first interpreted with Phase 1 isopach and structural mapping at several levels within and below the gas hydrate-bearing Sagavanirktok formation. A review of the 2004 Hedberg presentations (also documented in R09) revealed the limits of a deeper inverted basin and resulting change in depositional dip that was interpreted as associated with prospective gas hydrate resources in the region. This section provides a qualitative ranking based on UA studies within the MPU of several potential gas hydrate-bearing prospect areas recommended for future data collection and resource testing.

The UA studies concluded that most gas hydrate-bearing reservoirs within the MPU occur within a general area in the eastern MPU where thick and coarser marine and non-marine sands were deposited downdip of the eastern flank of the Colville high and along strike where inflections and a lessening of dip are interpreted. One such site was reported at the 2004 Hedberg conference and related to structural-stratigraphic elements associated with transtensional deformation that resulted in the formation of a small pull-apart basin within the eastern portion of the MPU (Casavant et al., 2004). This area is characterized by a persistent increase in sand deposition and gross unit thickness of stacked sequences as noted in isopach maps and cross-sections and by the presence of minor structural inversion and the downdip flattening of horizons

along the eastern flank of the Colville high. Within this general structural-stratigraphic framework, gas hydrate resources in the MPU appear be localized within updip traps, defined in part by variations in sealing capacity along north-northeast-trending faults (Hennes, et al., 2004), as well as by the location of older, deeper transtensional fault systems that are well expressed immediately below the Sagavanirktok formation.

The deeper Northwest-trending fault fabric, which is manifested as a monoclinal or hingeline in the shallower Sagavanirktok sediments, is a subset of a larger and wider Northwest Eileen fault complex that is interpreted to relate to the Late Jurassic to Early Cretaceous rifting of the Alaska Arctic terrane. Interpretations reveal that the nature of this fault system at depths below 4,000-feet BMSL is partly transtensional in character. The latter may provide key linkages for sourcing and updip leakage of gas resources from the underlying Early Tertiary to Cretaceous Ugnu, West Sak and Kuparuk sandstone reservoirs as suggested by previous studies.

Table 18 summarizes zone fluid and depositional environment interpretations for several wells within and near the MPU. The general interpreted western limit of gas hydrate prospectivity may impact the Mt Elbert gas hydrate prospect interpretation (Phase 1-2 Task 5.0) within the MPU and is best shown by net sand maps. That limit is represented by a line roughly connecting the MPU C-pad to the WestSak-25 well area. At this point the margin of the prospective area is interpreted to bend to the southeast approximately 1 mile south of the MPS-15 well. The interpreted easternmost margin of gas hydrate prospectivity is less well defined, but could be crudely described by a line drawn roughly from the MPU D-01 well south into the MPU E-26 well area. The approximate limits of the most prospective area for gas hydrate occurrence within the MPU appears to be related to a depositional basin or structural flat within the MPU that includes an area that extends south and southwest of the MPU B-pad and includes the MPU A-pad area. Interpretation of seismic and stratigraphic data indicates that the structurally flat character of this depositionally low area may be due also in part to the partial structural inversion of a former basin with the greatest amount of inversion occurring along the former basin axis.

The westward limits of the prospective area have yet to be well defined and include potential gas hydrate accumulations localized by both structural and stratigraphic trapping in the vicinity of the MPU J-, G-, I- and H-pad areas. Shallow WOO data acquisition within MPU I-16 (Phase 1, late-2004, Task 3), confirmed earlier models for the potential updip stratigraphic as well as structural trapping of gas hydrate resource to the west and northwest of the NWE2-01, MPU A-01, MPU S-15, and MPU E- 26 well areas. The UA lithostratigraphic zones involved include L_31, 33, 34a, and 35a. The upper sands of zones 34a and 35a include the USGS C and D gas hydrate-bearing intervals, respectively. The structural and stratigraphic location of the MPU S-15 well places it in an approximate axial position within this structural-stratigraphic basin mentioned above. The western margin of the basin is defined by an increase in dip along the eastern flank of the Colville high and is characterized by one or two North-Northeast-trending upthrown fault blocks bordered by en echelon faulting. The easternmost block contains the West Sak-25 well (herein referred to as WS25 block), while the westernmost block is bordered by a fault west of WS25 and another east of the West Sak-17 well. The WS25 block and the complex fault zone that marks its eastern flanks just east of West Sak-25 is interpreted to be of high risk, and as such, it marks the westernmost limit of the prospect area. Although previous Task 5.0 analysis does extend correlative gas hydrate-prone units into the updip WS25 fault block, any

prospective gas hydrate-bearing zones would likely lie within or near the lower portion of the ice-bearing permafrost (IBPF). Consequently this makes it difficult from a geophysical standpoint to distinguish gas hydrate-bearing zones from ice-bearing intra-permafrost sands.

Although the lithostratigraphic and sequence stratigraphic correlations show that the gas hydrate-prone units are common to MPU wells S-15, I-16 and A-01, independent log-based fluid-prediction analysis, extrapolation of the base IBPF from the NW Eileen wells, and current structural characterization do not provide definitive support for the WS25 interpretation. The footwall position and close proximity of the West Sak-25 well to a major north-northeast-trending fault that has undergone repeated reactivation suggests that the fault zone has a high potential for being a sealing fault near West Sak-25. There is the potential that gas may not have migrated beyond this fault zone near West Sak-25, but could have migrated up dip to the north before resuming migration to the west. Waveform classifications indicated gas hydrate-like classification interpreted in the vicinity of West Sak-25 also exists north within the block; however, this interpretation might be invalid considering that early UA seismic attribute analysis and waveform classification had designated West Sak-25 as a training well for gas hydrate-bearing reservoirs per early USGS published interpretation of gas hydrate within that well. The recent analysis based on structural and stratigraphic mapping suggests caution in extrapolating gas hydrate-bearing sediments from MPU A-pad southwest to West Sak-25. This area should be considered higher risk; however, confirmation of gas hydrate existence in WS25 by additional drilling and shallow data acquisition is recommended. Data to evaluate would include drilling and fluid shows as well as, resistivity and density/neutron/sonic porosity logs.

The northwest hingeline or monocline apex of Hennes et al. (2004) is interpreted to be the shallow expression of a Northwest-trending wrench fault at depth. The hingeline continues just north of the MPU A-01 well area and defines what is interpreted to be the northern limit of the gas hydrate-prospective area. Analyses of potential gas hydrate-bearing reservoirs within the MPU B-, C-, and D-pad areas differs from Task 5.0 Phase 1 studies in that much of the gas hydrate-bearing log signatures interpreted in these areas are interpreted to be better attributed to the presence of low-permeability fluvial units associated with the development of intraformational unconformities and associated interpreted paleosols (See Appendix A, Section 9.5.6). The 2005 studies were planned to distinguish from seismic response whether or not these dense zones serve to trap and seal gas hydrate-bearing reservoirs just northeast and downdip of these pad areas (and associated with the north-dipping flank of a northwest-trending monocline). In that sense, a cluster of northwest-trending prospect polygons located north of these pads as interpreted in Task 5.0 seismic-based studies may be either (1) interpreting actual potential gas hydrate accumulations or (2) misidentifying the high-velocity responses of these cement-prone units as gas hydrate-bearing reservoir sands.

Net sand and Net-Gross ratio maps show a depositional or erosional southern limit of the prospective area interpreted to extend to the south from MPU. The E-26 and S-15 wells occur along the eastern margins of this prospective polygon area. Log and seismic-based gas hydrate-bearing prospect leads within the MPU A-pad area are located within the northeast quadrant of what is interpreted as a north-northeast trending elliptical polygon that is structurally controlled by north-northeast-trending faults on its eastern and western flanks and by underlying northwest-trending fault zones on its northern and southern flanks. The UA structural-stratigraphic model,

artificial neural net (ANN), and expert system (ES) fluid analyses, coupled with the supervised seismic waveform classification scheme independently converge on the gas hydrate prospectivity presented for this region.

5.2.6.2 Phase 2 (2005) Geologic Setting Studies

MPU Cross sections and geologic mapping show gas hydrate (GH) and free gas (FG) resources are typically contained within distal deltaic and nearshore marine sand units. Gamma-Ray (GR) and Resistivity deep (Rd) log pattern interpretations indicate that higher quality MPU gas hydrate-bearing reservoirs are contained mostly within thin sand-rich distributary channel and in some cases the upper portions of relatively thicker distributary mouth bar parasequences (Table 18). Some resistive "hydrocarbon" zones thought to be prospective may instead be related to thin point bar units that log responses suggest could be paleosol horizons (see Appendix A).

Stratigraphic analysis of interpreted gas hydrate-bearing reservoirs to the south within the KRU and NW Eileen area of western PBU indicates that the majority of GH and FG zones are stratigraphically lower than those within the MPU and are constrained to mostly stacked fluvial and delta plain deposits related to incised valley deposits that have cut into distributary mouth bar units during low-stand deposition. Distributary mouth bar units are the subsidiary reservoir facies as indicated in Table 18.

Shallow seismic mapping within most of the MPU reveals that numerous north-northeast-trending, mostly down-to-the-east normal faults compartmentalize interpreted nearshore marine and fluvio-deltaic reservoir sands within the shallow Sagavanirktok formation. In some locales, these faults appear to extend to surface, offsetting the coarser, gravel-rich units of the upper Sagavanirktok and overlying Gubik formations.

Seismic interpretation within the MPU reveals the presence and influence of at least two northwest-southeast-trending basement fault zones that underlie the shallow strata of the Sagavanirktok and Gubik formations and that have slightly deformed (minor lateral translation, little or no dip slip) and influenced deposition of these formations. Although these fault zones are not directly imaged because they exist just below the extent of the shallow seismic data truncated at 950ms, their presence is expressed by an inflection in the regional dip of the shallow strata. Detailed 3D analyses of this seismic data shows that where north-northeast-trending normal faults intersect the underlying northwest-trending faults, the amount of dip slip on the north-northeast faults either decreases or terminates; there is commonly an associated inflection and/or termination in fault trend in map view and in some locations, fault polarity switches. These faults define major structural blocks and are interpreted to represent the northern continuation of a northwest-trending basement trend commonly referred to as the Northwest Eileen (NWE) trend. Related fault-bounded highs are interpreted to continue to the southeast and may control deeper hydrocarbon production within the western third of the Prudhoe Bay field.

The basement faults that core these structures represent only a subset of the complexly faulted north-dipping eastern flank of the Colville High. Consisting of a mostly down-to-the-northeast horst-graben architecture, variable displacement along these faults may be linked to a late Jurassic to early Cretaceous-age rifting of the Alaska Arctic Terrane (AAT) and subsequent Cenozoic reactivation associated with shortening of the Brooks Range and consolidation, differential uplift and minor translation of basement blocks that characterize the northern margin

(Barrow Arch) of the rifted terrane (Casavant, 2001). The apex of east-west Barrow Arch can be tracked within the adjacent KRU to the west and again is picked up within the PBU area to the east and northeast. A left-stepping offset or northeast bend in the axis of this regional basement uplift occurs along an approximate line that may equate to the eastern margins of the MPU and KRU field areas.

Within the MPU, stratigraphic pinchouts occur at subtle structural inflections that overly the margins of Northwest Eileen fault blocks. Where shallower north-northeast-trending faults with greater displacement intersect underlying northwest-trending fault zones, structural trap doors may exist. In these 3-way closures, hanging wall traps of GH and associated FG are interpreted in updip positions. These gas- and gas hydrate-bearing reservoir sands within these hanging wall traps are thicker as a result of syndeposition or fault-related sand preservation (isolated from erosional scouring and truncation associated with the formation of numerous intraformational unconformities that defined sequences within the Sagavanirktok formation). However, their role in updip trapping of GH remains inferred. Net sand and net-gross maps indicate potential areas exist such as the area around and/or east of the MPU E-pad and also east of the MPU S-15 well. This interpretation may corroborate the Phase 1, Task 5.0 studies of the Mt Elbert prospect area.

Based on wireline data, stratigraphic maps, and fault architectures, many of the UA-defined prospective GH sites within the MPU seem to be located above or just downdip of hingeline(s) where dips have lessened. At the shallow levels in which GH occurrence is inferred, these underlying fault zones are expressed only as hingelines. Both the MPU A-01 and MPU S-15 well areas, which both contain relatively thick sand reservoirs, lie above or near two different Northwest-trending hingelines.

Linkages between gross isopachs and net/gross sand maps and distribution of GH as defined by well log analysis and fluid prediction algorithms (e.g. UA expert system and artificial neural network) reinforce the premise that GH-bearing reservoirs will most likely be limited to intervals of adequate reservoir sand quality and thickness in updip structural-stratigraphic traps such as those interpreted by Phase 1 Task 5.0 and Task 6.0 studies. Phase 1 Task 6.0 studies show that increases in the accumulated thicknesses of stacked nearshore and fluvio-deltaic sands are noted where decreases in structural dip occur down the flank (half-graben settings). Isopach maps and structural analyses within the MPU reveal influence of two underlying northwest-trending normal fault zones characterized by down-to-north displacement (Werner, 1987; Hennes et al., 2004; Casavant et al., 2004). Fault morphologies suggest a complex fault zone marked by transtensional or oblique-normal displacement (Casavant, 2001; Casavant et al., 2004).

Wells associated with candidate areas for GH occurrence and associated wireline and seismic leads are summarized in Table 18. Based on UA time-depth relationships, fluid predictors, and structural and stratigraphic mapping, a reasonable potential for GH exists within the “C-Unit” interval (L_35-34) in an area south and southwest of a line connecting the MPU D-01 and West Sak-25 wells. Net/Gross sand ratio maps indicate a structurally-controlled fairway (paleo-shoreline or trend of sand preservation) that likely reflects influence of the Northwest-trending and North-Northeast-trending fault sets. The most prospective gas hydrate-bearing reservoir site includes an area due south of the MPU B-pad, which coincides with the planned Mt Elbert-01 well site area selected from Task 5 studies.

Well	USGS Zone E USGS Marker 15a UA Zone L_35a-35	USGS Zone D USGS Marker 15 UA Zone L_35-34	USGS Zone C USGS Marker ~14 UA Zone L_34-33	USGS Zone B USGS Marker 13 UA Zone L_33-31	USGS Zone A or Staines Tongue USGS Marker 12-13 UA Zone L_31-29	FREE GAS Undifferentiated Zone Intervals
3K-06	PF, MB	PF, MB	PF, MB	PF, MB	NLS, L_31-30 Rd inc, but not Vel, N-D near cross-over in channel sands	
BEECHYPT-01	NLS	NLS (wet)	NLS	NLS	NLS	
CASCADE-01	NA, no MG	Fair LS, MG, SW of Mt Princeton prospect, SA,WF, DMB	LS, fair MG, good ES/ANN for FG, CH	LS, good MG, no logs through upper 1/3 interval, zone faulted?, CH, PB	Similar to MPK-38	
EUGNU-01	PF, neg. ES/ANN	PF, V poor, neg. ES, ANN coals	Faulted out, neg. ANN	NLS, Rd inc, Vel poor, faulted section	NLS, 1/2 of L_30 to L_31 appears faulted out	
KAVEARAK-32	PF?, no Rhob/Vel logs, NLS, small Rd inc. and correl to MPE-26, PAL? PB, no logs for ES/ANN	NLS, DMB, v poor Rd inc., no Rhob/Vel logs, no ES/ANN, SA,WF	Good 10'+ Rd inc, DMB, no Rhob/Vel logs, no logs for ES or ANN, SA,WF, far W of Mt Elbert	NA, log gap, thin Rd zones correl to MPE-26	NLS, small Rd w/coals	
KRUGNU	PF	PF	PF, neg. ES except 2 thin sands ~1940, 1960	NLS, ES saw water zone, but Rd is too high	NLS, some thick coals	N FG on ANN
MP18-01	NA, SA,WF	NA, MG, SA does not appear unique to horizon or prospect location,	NA, within Crestone prospect, SA does not appear unique to horizon	NA	NA	Y within Mt Shavano prospect
MPA-01	PF?, PB, NLS, v poor Rd, Vel, inc., no MG, potential PAL that is correlative thru B, E & K-pads, etc., CH/PB, SA,WF	Mod-good LS, DMB, good ANN, ES, good MG starts, increase in N/G; "East basin" model, increase in net sands on east flank of Kuparuk structure; updip of gas charged sands to SE, SA,WF	LS, MG, ES, ANN (1-5' coals), CH, PB within prospect, SA appears more robust relative to locations outside prospect, N-G mapping and "East basin" model predict mod-good GH to the SW & S SA,WF	NLS, no Rd/Vel inc, FG indicated on USGS x-sect?	NLS, oil?, low Rd & Vel., poor-fair MG, neg. ES, neg, ANN, correlates to section showing oil and low Vp indicate on USGS x-sect for WSAK25	
PB-01	LS, PB, mod Rd, V, no RHOB log, correl well w/MPB-02, PAL, SA,WF	poor LS, DMB, thin Rd/Vel inc, no Neut & Rhob logs, potential	NLS, CH/PB, thin Rd & Vel, assoc w/ shale, SA,WF	NLS, up half faulted out, looks wet	NLS	

Table 18: Continued – UA Sagavanirktok facies interpretations

		PAL, SA,WF				
Well	**USGS Zone E**	**USGS Zone D**	**USGS Zone C**	**USGS Zone B**	**USGS Zone A**	**Free Gas**
MPB-02	NLS? mod Rd & Vel increase, however, RHOB also inc.= potential PAL?, PB, SA,WF	LS? DMB, thin zone of Rd inc, ES show w/coals, neg. ANN, SA,WF	NLS, CH/PB, SA,WF	NLS	NLS	
MPC-01	PF, NLS, SA,WF	Good MG, DMB, far west of Snuffles prospect, SA does not appear unique to horizon or prospect location, SA,WF	NLS, DCH, within Crestone prospect, well located W of SA anomaly, SA appear unique to horizon and prospect location	NLS	NLS	Y within polygon W of Mt Shavano prospect
MPC-03	NA, SA,WF	NA,	NA, within Crestone prospect, SA does not appear unique to horizon or prospect location	NLS	NLS	Y within prospect W of Mt Shavano prospect
MPD-01	LS, PB, poor Rd, Vel. inc, close to BIBPF), neg. ES or ANN; potential PAL, SA,WF	Thin LS, DCH, signif, Vel, inc. Rhob NA, PAL?, SA,WF	NLS	NLS	NLS	Y within Little Bear prospect (Staines)
MPE-26	NLS, poor ANN, neg. ES, mod Rd & Vel inc. and RHOB inc.= PAL?, noted same zone in NorthWest Eileen State-02, but Rhob decreasing in NEW, SA,WF	NLS, DCH/DMB, W of Mt Bierstadt & Mt Elbert prospects, SA,WF	v poor LS, DCH/DMB, v thin Rd inc., neg ES/ANN, far W of Mt Elbert prospect, SA,WF	NLS, v poor Rd, thin zones of Rhob/neu cross-over, good ES, neg. ANN, minor FG reported on USGS x-sect	NLS, neg. ES/ANN	
MPI-16	NA, GR only	NA, GR only	NA, GR only, possible updip play to NWE2-01 and MPS-15,depends on BIBPF, maybe better than Rd inc in NWE2-01, south & updip to MPS-15	NA, GR only, possible updip play to MPS-15 & NWE2-01, maybe better Rd inc than in NWE2-01 which is south and updip to MPS-15	Inc. in Rd observed in several thin zones, look like crevasse splays sands	

Table 18: Continued – UA Sagavanirktok facies interpretations

MPK-25	NA	NA	NA	LS, GF, ~80' gross, 50' net	LS, FG, better than K-38	SA
Well	**USGS Zone E**	**USGS Zone D**	**USGS Zone C**	**USGS Zone B**	**USGS Zone A**	**Free Gas**
MPK-38	NLS, PB, v. poor Rd inc., but w/ RHOB inc.= PAL stack?	Good LS, DCH, GH?, only Rd, thin zone of Rhob/Neut x-over below GH, but neg. Rd inc (FG), correl to Cascade MG show, neg. Vel, good ES GH, good ANN (GH & FG, SW of Princeton	LS, DCH, fair MG correl to Cascade, SA,WF	LS, DCH, FG, >40-50 ohm, 55' gross, 35' net, good ES/ANN FG	LS, CH/CV/PB, FG, neg. ES/ANN despite Rd inc, thin ANN coals	SA
MPL-01	PF, NA	PF	PF or near BIBPF	NA	NLS	
MPS-15	PF or interval pinched out, large washout	good LS, good ES/ANN, SA,WF NA	v thin LS, good ANN FG, neg. ES, coal? SA,,WF NA	NLS, no Rhob , neg. ES, ANN	NLS, coals, thick sds, neg. ES/ANN,	Prospective play updip to the west of this well
PRUDHOE-01	NA, no MG, ES/ANN unknown	NA, probable LS, good MG, unknown ES/ANN equiv shows in NWE2-01, NEW-2, BeechSt-01 FG, K071112 MG, poss. Chev. 18111	NA, thus no ES/ANN, excellent MG, probable GH	MG, no logs over upper 2/3 of interval	thin prominent MG zones, 3 v thin sds w/ Rhob/Neut x-over, thin ES/ANN zones	
SIMPSON-01	PF, NA	PF, NA	PF, NA	NA	NA L_33-30, NLS L_30-29	
WS-17	PF	PF	PF	PF	NLS, Rd inc w/coals	
WS-25	PF, NLS, DCH/DMB, MG w/coals @2400', SA,WF	PF, DCH/DMB, slight MG, neg. ES/ANN, SA,WF	LS f(BIBPF), correl. to NWE-2 well suggests zone just within PF, CH, well located W of prospect, SA of polygon does not appear unique within sequence given UA T-D conv., SA,WF	NLS, CH/DMB, poor Rd, MG, neg. ES/ANN	NLS, CH/PB, CV, DCH, DMB, thin Rd inc w/coals, MG inc. only w/ coals, oil & low Vp noted on USGS x-sect, neg. ES/ANN	

Table 18: UA Sagavanirktok sequences facies interpretations from well data and seismic attribute analysis; blue text color indicates well within/adjacent to UA prospect site; relation to Phase 1, Task 5.0 prospects (see Tables 4, 5, and 12) are noted where applicable)

Table 18: Continued – UA Sagavanirktok facies interpretations

Table 18 Legend:

ANN = GH inferred by artificial neural network
BIBPF = base of ice-bearing permafrost
ES = GH show inferred by expert system predictor
FG = associated free gas (interpreted)
GH = gas hydrate (interpreted)
LS = GH show inferred by wireline log responses (e.g. favorable Rd, sonic, Rhob, & GR responses)
MG = mud gas present (total background gas)
NA = no logs available through interval
Neut = neutron log response
NLS = no GH/FG show based on log curve responses (e.g. insufficient Rd, sonic, & porosity log responses)
PF = interval lies within permafrost, making log interpretation ambiguous with IBPF log response
Rd = resistivity log responses
Rhob = bulk density log response
SA = total amplitude response observed on UA seismic line(s) in/adjacent to USGS polygon (UA Time-Depth conversion)
Vel = sonic, delta time log
WF = in/near area identified in UA waveform classification as "gas hydrate consistent anomaly" (scheme derived from Phase 1, Task 5.0 gas hydrate picks of variable quality, analysis done only for gas hydrate zones E, D, & C within MPU)
Y = well lies within or near Phase 1, Task 5.0 free gas prospect polygon

FACIES of reservoir unit containing resource (log pattern-based)

Fluvio-deltaic Facies
CH = channel
PB = point bar sand
L = channel levee
CV = crevasse sand
PAL = paleosol, cemented zone

Deltaic-Marine Facies
DMB = distributary mouth bar
DCH = distributary channel
RW = reworked marine sand

Table 18: Continued – UA Sagavanirktok facies interpretations

5.2.6.3 Phase 2 Interpretation of PBU L-pad and V-pad Area

In March 2005, a request was made for UA input into the regional development scenario modeling studies conducted under Task 10 and documented in R15. The response was preliminary and compiled over a 2-day period, but is included here to document the interpretation status and discussion. Benefits of this exercise were anticipated to assist the development scenario modeling by adding some stratigraphic trend lines to help determine where to start "development" in certain potential sweet spots. This was a high-level exercise, so detailed interpretation was not incorporated at this stage of studies.

The interpretation indicated that the PBU L-pad area is more prospective than the V-pad area. Interpretation of Sagavanirktok channel complex trends are not currently well understood, but in general may trend from west-southwest to northeast. Future mapping should better constrain this interpretation. Wells that are currently interpreted to represent depositional axes of eight individual channel complexes include: 1. West Sak-25 to MPU E-26, 2. KRU 1H-06 to MPU S-15, 3. KRU 1D-05 to West Sak-24, 4. NWE1-01, 5. WT-01, 6. West Sak-06, 7. WETW, and 8. KUPST-01.

Good channel development and associated potential gas hydrate-bearing reservoir sands should be expected in and around both PBU L- and V-pads at various stratigraphic levels. The recommendation is to place a west-southwest-northeast trend in modeling of gas hydrate resource in the area of both pads. This trend of gas hydrate and free gas resource is a function of not only the general trend of reservoir facies (primarily channel deposits incising high-stand distributary channel-mouth bar units), but also the trend and limits of the Base of Ice-bearing Permafrost (BIBPF) located just to the northwest, which trend varies with depth (and structure) and ranges from north-south to southwest-northeast depending on stratigraphic horizon. The role of fault containment can only be inferred given the data restriction to shallow intervals.

The characterized "sweet spot" stratigraphic units are both updip and downdip of the PBU L-pad and V-pad areas. Sweet spot is actually a misnomer for there can be several within a single sequence as well as being vertically stacked. Their position varies slightly from layer to layer and appears to be a function of channel position/dimension (width/thickness) and the structural position (updip trapping related to either an inferred fault or stratigraphic pinchout).

At this time, individual channels or channel meander belts were not yet mapped at the various levels, although this was planned. They have been noted and generally discussed within a detailed correlation exercise across the KRU-PBU areas. This updated stratigraphic framework was used to guide detailed stratigraphic and facies studies. A new set of fieldwide picks for all the wells is anticipated to be completed during Phase 2 studies to capture the detailed log-based characterization across the AOI scheduled for summer and fall 2005. Completion of the tighter vertical stratigraphic framework would allow more precise mapping of variations in individual parasequences and parasequence sets and would be an improvement over the earlier gross correlations completed in the preliminary regional correlation and mapping studies within the MPU that were provided to guide Phase 1 seismic attribute analysis and time-depth conversion studies. This more detailed framework would be used to re-evaluate the MPU seismic cube as it relates to finalizing Time-Depth discrepancy between the Task 5 and Task 6 studies and to assisting with Phase 2 attribute mapping and associated neural network studies.

5.2.6.3.1 Upper Sagavanirktok Stratigraphy, PBU L-pad and V-pad Area

The upper prospective intervals in the L-pad area include the UA litho- and sequence-stratigraphic units 35a-35, 35-34a, and 34a-34. These resource prone units are best shown in the nearby NW Eileen State 2 well. The 35a-35 unit includes the poorly developed USGS Zone E gas hydrate-bearing unit, which is commonly interpreted as a relatively thin point bar sequence (pb) above an unconformity that cuts into both distributary mouth bar (dmb) units as well as laterally equivalent fluvial channel (fch) and composite point bar (cpb). In areas such as the MPU B- and D-pad areas, the resistive character of the unit appears to be in some locales associated with a cemented and less permeable strata (possible paleosol?) that can be tracked for some distance (e.g. BeechyPt, etc.) rather than a gas hydrate-bearing unit. In some locales, the earlier USGS correlations have the zone E hydrate pick crossing UA-defined stratigraphic intervals (e.g. zone E crosses down to the 35-34a zone in the nearby 33-29E well and unit 35-34a elsewhere is typically equivalent to the USGS Zone D gas hydrate-bearing unit.

In the L-pad area, however, the zone E gas hydrate-bearing unit is reasonably consistent with UA sequences and can be expected to pinchout updip to the northwest between well 33-29E and NWEileen St 2 and downdip some unknown distance to the northeast. To the southeast, the unit structurally rises again and is present in the KUPST-01 according to the Expert System/Artificial Neural Network (ES/ANN) fluid predictors and log analysis. This agrees well with the net sand map trends and the slight increase in total background gas seen on mud logs for this zone.

The Zone D gas hydrate-bearing unit lies within the upper sand units of the UA litho unit 35-34a and anticipated gas hydrate resource in this zone may extend northwest updip to a location beyond 33-29E to as far as NWE2-01. This conclusion depends on interpretation of the BIBPF. If the BIBPF pick is placed below the upper sand as interpreted by UA ES fluid/facies model (C. Glass), then the gas hydrate resource limit would extend to just beyond the 33-29a well. If the BIBPF is interpreted to be shallower (as direct correlation from the NW Eileen St 2 well over to West Sak-25 might indicate), and therefore, above Zone D, then gas hydrate resource potential in this interval could possibly extend to the NWE2-01 well and beyond into the next depositional trough to the northwest ("East basin"), which contains the sand-rich zones penetrated by the MPU S-15 well (2004 Hedberg Casavant et al. and Poulton papers). To the northwest and updip is MPU I-16 in which recently acquired (late-2004) GammaRay (GR) logs indicate that Zone D sands are still well-developed in this area. This zone is prospective if a shallower BIBPF is picked in the MPU S-15 well. To the southeast, the Zone D gas hydrate-bearing unit is interpreted to extend to the CHEV181112 well, but terminates before the WETW well, which exhibits no increase in resistivity response over background. Prospectivity of Zone D in the WETW, if any, is attributed to only several thin zones of moderate gas increase in the mud logs. To the west, the limits of gas hydrate-bearing Zone D are interpreted to extend nearly to or just beyond the West Sak-24 well, again depending on the depth of the BIBPF.

Most promising for gas hydrate-bearing reservoirs in the PBU L-pad is unit 34a-34 (upper well-developed sand(s) containing the USGS Zone C-hydrate). This unit is characterized by well-developed channel units (fch) that like the other zones incise to various degrees mixed dmb and fluvial units in the upper part of the underlying 34-33a unit. Palinspastic reconstructions in some locales indicate that some of the better developed dmb, dch, and fch occur together in the same area because of the persistence of paleo-depositional lows that apparently created significant

accommodation space for depocenters. Whether these depocenters are derived from structure or incision, is not always easily to interpret. The northwestern limits of the 34a-34 hydrate-bearing sands are interpreted to be just north-northwest of NWE2-01 well.

The upper sands of unit 33-34 in NWE2-01, which is updip of well 33-29E, contain several stacked cpb sequences below the Zone C-hydrate that appear to contain prospective gas hydrate-bearing sands (no sonic, porosity logs). These reservoir sands exhibit a similar response, gain, and separation of deep to shallow resistivity logs as seen in the NW Eileen St 2 well area. These same units appear wet in MPU S-15 which is to the northwest and downdip and many of these units shale out farther north in the updip MPI-16 well. However, the uppermost sand in this unit remains well-developed and could contain gas hydrate, depending on where the BIBPF is interpreted. Except for GR, there are no logs available over this interval. Reservoir sands in MPU S-15 and MPU I-16 appear to be in a separate southwest-northeast channel complex whose trend is not well constrained, but approximates the Eileen accumulation interpretation to the south.

5.2.6.3.2 Lower Sagavanirktok Stratigraphy, PBU L-pad and V-pad Area

Lithostratigraphic unit L_33-31 may contain some gas hydrate-bearing reservoir sands based on UA analysis and fluid predictors. This unit is just above the upper Staines(?) and includes USGS Zone B gas hydrate-bearing unit (where picked). Unit L_33-31 may represent a west-southwest-trending channel complex, informally referred herein as the "Eileen complex". In the NWE2-01 well, a gas prospect may be present updip as interpreted from the mudlog gas show in the nearby 33-29E well to the south. The deep resistivity reading is beginning to increase in the NWE2-01 well in this interval. The 33-29E well shows mudlog gas increases within the L_33-31 interval, but the deep resistivity appears to indicate primarily water-saturated sands. The WS-24 well log interpretation reveals thinner stacked cpb sands, a good response for gas hydrate-bearing sands incised into shales, not dmb as in the downdip NWE1-01 well.

South of the "Eileen complex", another west-southwest trending channel complex is interpreted, informally referred to herein as the “WETW complex” and present within the CHEV181112 well. This well and the area just updip exhibit excellent free gas response in a regionally persistent and well-developed uppermost sand of unit L_33-31. The interpretation indicates that a northwest-trending fluvial channel (fch) incises into a well-developed and thick dch/dmb parasequence unit bordered by marine shales. This zone is correlative to gas-bearing sands in the MPU K-Pad-Cascade-01 well area. The WETW well is downdip of CHEV181112, but still exhibits the same free gas response in channel sand. The WKUPSt-01 and NWE1-01 wells also show channel sand developed in this interval and within lithostratigraphic unit L_30-29 (USGS Zone A).

Lithostratigraphic unit L_30-29 sands are well developed in the NW Eileen St #2 well area. Updip of the NWE1-01 well, the L_30-29 sands are also well developed with a significant deep resistivity response to interpreted gas within several stacked fch-coal-crevasse splay(cv) facies. This response may increase updip in the NW Eileen St 2 well area in a potential fault trap. The L_30-29 sands are also present in the WETW and CHEV181112 wells and still exhibit some interpreted free gas responses within this channel sand.

5.2.7 Phase 2, Task 7 – UAF Drilling, Completion, and Production Studies

Task 7 laboratory studies and experiments continued into Phase 2 to characterize the formation and dissociation of gas hydrate in porous media at or near reservoir conditions. Two Phase 1 subtasks were essentially completed in Phase 1, including characterizing gas hydrate phase behavior (Section 5.1.7.1) and measuring gas-water relative permeabilities in gas hydrate-bearing sediment (Section 5.1.7.2). Primary Phase 2 experimental procedures included drilling mud and formation damage studies (Figure 33), the results of which are available in prior reports (R15, pp. 79-97).

Figure 33: UAF drilling fluid and formation damage analyses laboratory setup, 2006

5.2.8 Phase 2, Task 8 – Gas Hydrate Well Design

Project studies and stakeholder consensus concluded that field operations should be split into 2 distinct phase 3 activities. Phase 3a would design and implement a dedicated gas hydrate stratigraphic test well and data acquisition program to determine the feasibility of a possible future Phase 3b long-term gas hydrate production test program.

Task 8 accomplishments culminated with the January 11, 2006 approval for drilling the Phase 3a stratigraphic test well:

- Initiated long-lead well permit discussions to allow potential future well operations
- Developed long-lead materials and rig plans to allow possible future well operations
    - Data acquisition to include wireline core, full open-hole logging, and MDT
    - Met with Corion for wireline core technical discussion and applicability
    - Met with OMNI Lab for core processing and analyses
    - Evaluated core storage options with ASRC Energy Services (AES) and others
    - Evaluated mud-chilling options and providers and selected DrillCool, Inc.
    - Evaluated and planned open-hole logging program and met with Schlumberger
- Prepared Continuation Application, Budget, Decision Support Package, and “Authority to Negotiate” documents to support Phase 3a stratigraphic test approval (January 11, 2006)

  - Met with BPXA Gas and MPU management for discussions and decisions
  - Developed stratigraphic test plans with BPXA MPU technical and drilling staff
  - Completed "Authority to Negotiate" document and worked through approvals
  - Obtained Stratigraphic Test well operations approval January 11, 2006
- Provided operational integrity and HSE requirements for stratigraphic test operations
  - Provided justification for rig operations and safety requirements
  - Assured clarified processes and procedures conformed to BPXA standards
  - Proposed turnkey operation with newly consigned rig, Doyon Arctic Fox
  - Selected BPXA-led operation with Doyon Arctic Fox and AES
- Prepared initial procedures, plans, and cost estimates for stratigraphic test well operations

5.2.9 Phase 2, Task 9 – Site Selection and Data Acquisition Program

Reservoir characterization (tasks 5-6) and well design (Task 8) studies were used to determine viable sites for Phase 3a dedicated gas hydrate stratigraphic test well operations. Viable sites were characterized and ranked (Tables 4 and 12) and the Mt Elbert prospect was the highest ranked site, although it was also classified as a higher risk site due to it not being penetrated by existing wellbores. Detailed prospect characterization summaries such as that presented below for the Mt Elbert C and D prospects were evaluated for each of the 14 prospects (Tables 4, 5, and 12) identified during Phase 1, Task 5 studies.

Phase 2, Task 9 was modified by mutual agreement between BP and DOE to split Phase 3 well operations into a Phase 3a stratigraphic test and a potential future Phase 3b long-term production test. The modified task was carried forward into Phase 3a well operations as documented in contract Amendment 11 and reported in Section 5.3.8 in Phase 3, Task 8.

5.2.9.1 Mt Elbert Prospect Characterization Summary

Task 5 studies revealed that the gas hydrate-bearing zones of the Mt Elbert prospect are fault separated from the MPU E-pad and the B-pad well penetrations that contain only thin gas hydrate-bearing zones C and D. The highest amplitude and interpreted highest saturation are in the most up-dip portion of the prospect. Both the Zone C and D hydrate anomalies may be directionally drilled from the same surface location from either MPU B or E pad or vertically drilled from an ice pad (Figure 34). This prospect was ranked as one of the most promising "intra-hydrate" prospects (Tables 4 and 12). The proximity to the existing infrastructure and processing facilities near E-pad make it one of the most convenient opportunities in the Milne Point field area (Figures 34 and 35). From the proposed Mt Elbert prospect location, which is optimized for both C and D hydrate targets, the road is 2,370 feet, the Kavearak pad is 2,740 feet, and the E-pad area Central Production Facility and Drillsite is 3,020 feet away. The C and D hydrates are found in wells adjacent to the prospect in the MPU B-02 and MPU E-26 wells, although these hydrates are thought to be thinner and of lower saturation than that expected in the up-dip portion of the Mt Elbert prospect. Good synthetic seismic ties to both of these wells give a high confidence level in the interpretation of the C and D zone gas hydrate-bearing reservoirs in the prospect. The prospect is fault separated from the E-pad, on the west side, by a large regional normal fault. Sequence stratigraphic correlation and fault studies by UA (Task 6, Section 5.2.6.2) corroborated the significant potential of the Mt Elbert prospect area.

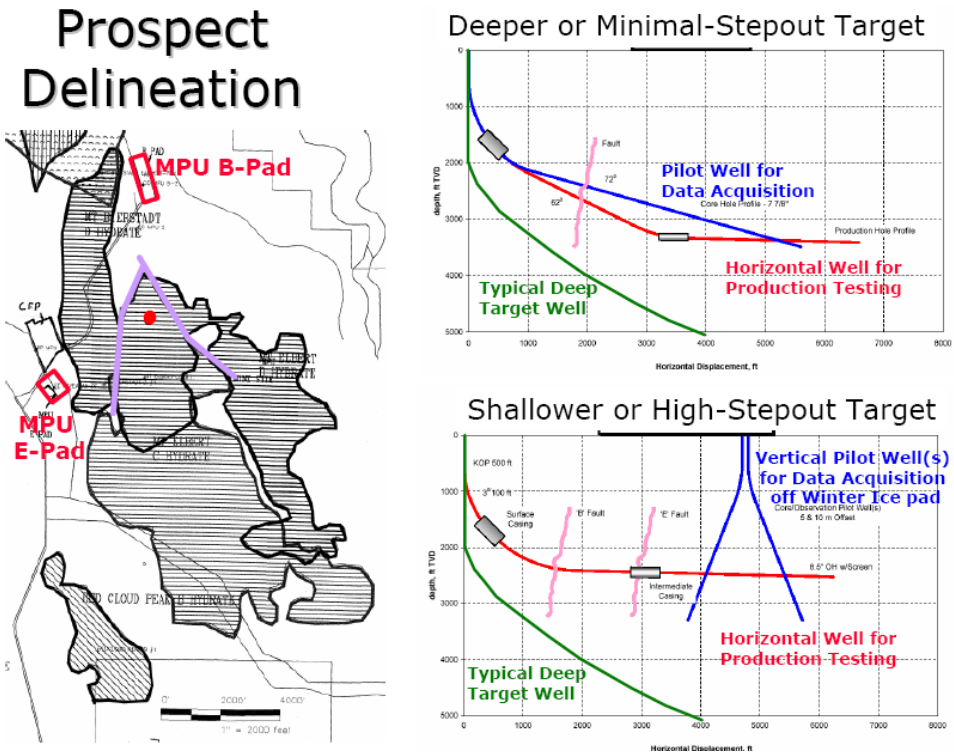

Figure 34: 2005 Mt Elbert prospect map with potential delineation (vertical) and production testing (horizontal) well plan schematics

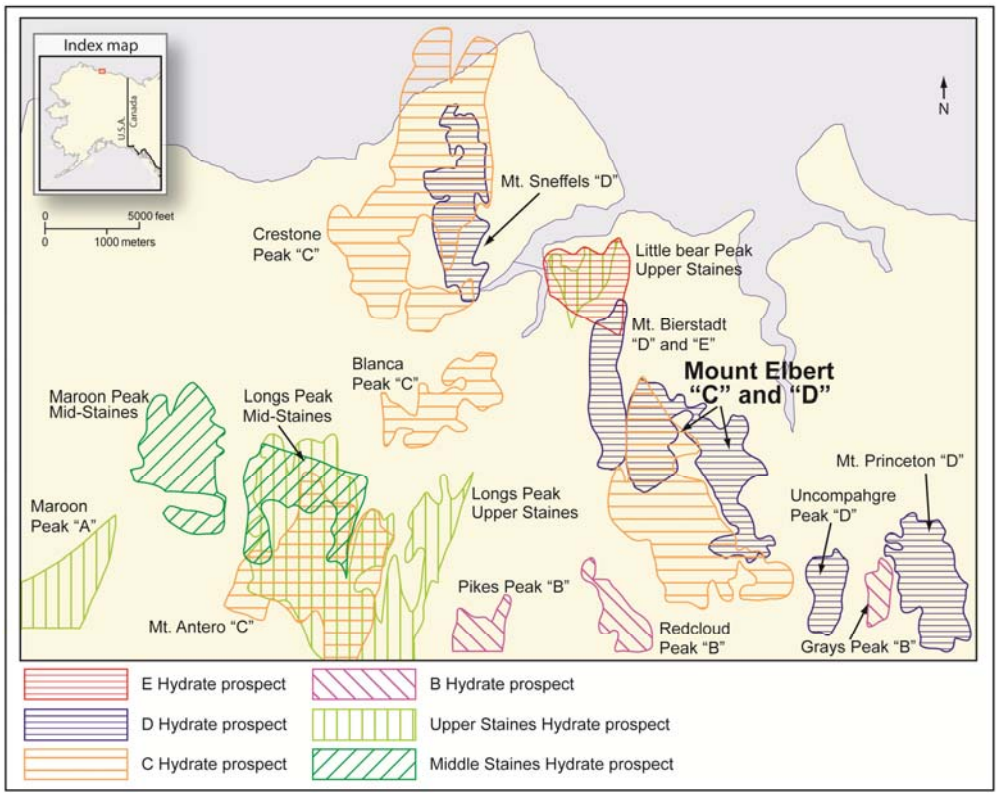

Figure 35: Location of Mt Elbert Zone C and D prospects as well as other gas hydrate prospects of Tables 4 and 12, MPU area (also Figure 7)

5.2.9.2 Mt Elbert Zone D Prospect Characterization

The Zone D hydrate horizon correlates to the D hydrate found in the MPU B-02 well, on the down-dip side of a large regional fault. A single well or 2 wells (updip and downdip) could delineate both the D and C hydrates at the Mt Elbert Prospect. Figure 36 illustrates the seismic amplitude attribute defining this Zone D hydrate accumulation. Figure 37 shows the west to east seismic cross-section E-A to E-A' of Figure 36. Figure 38 shows the south to north seismic cross-section E-B to E-B' of Figure 36. Figure 39 shows the Zone D reservoir thickness in the Mt Elbert prospect as interpreted from seismic attribute analyses. Figure 40 shows the Zone D reservoir gas hydrate saturation in the Mt Elbert prospect as interpreted from seismic attribute analyses.

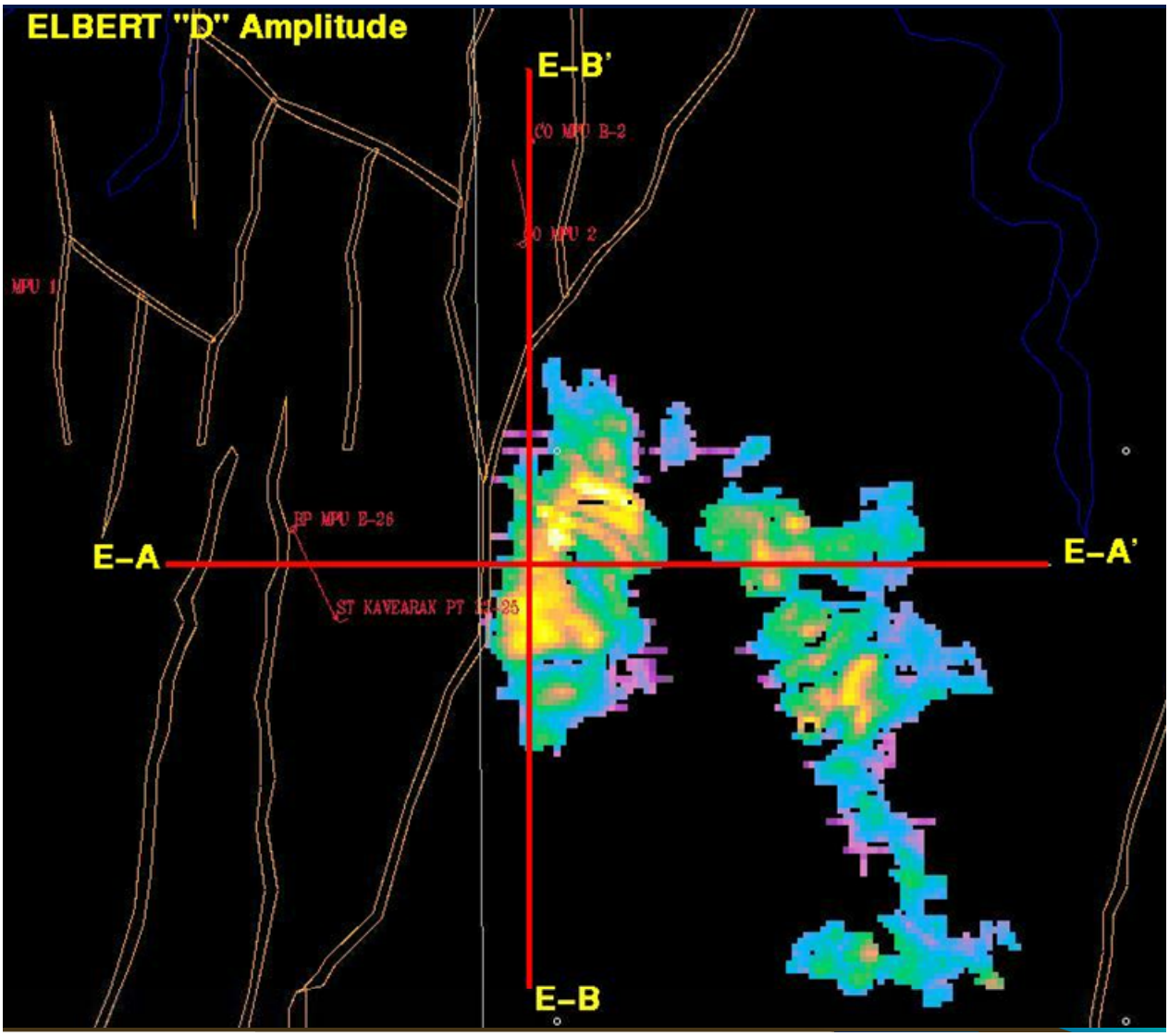

Figure 36: Seismic Amplitude of Zone D horizon with lines of seismic cross-sections displayed in Figure 37 (E-A to E-A') and Figure 38 (E-B to E-B'), Mt Elbert Prospect

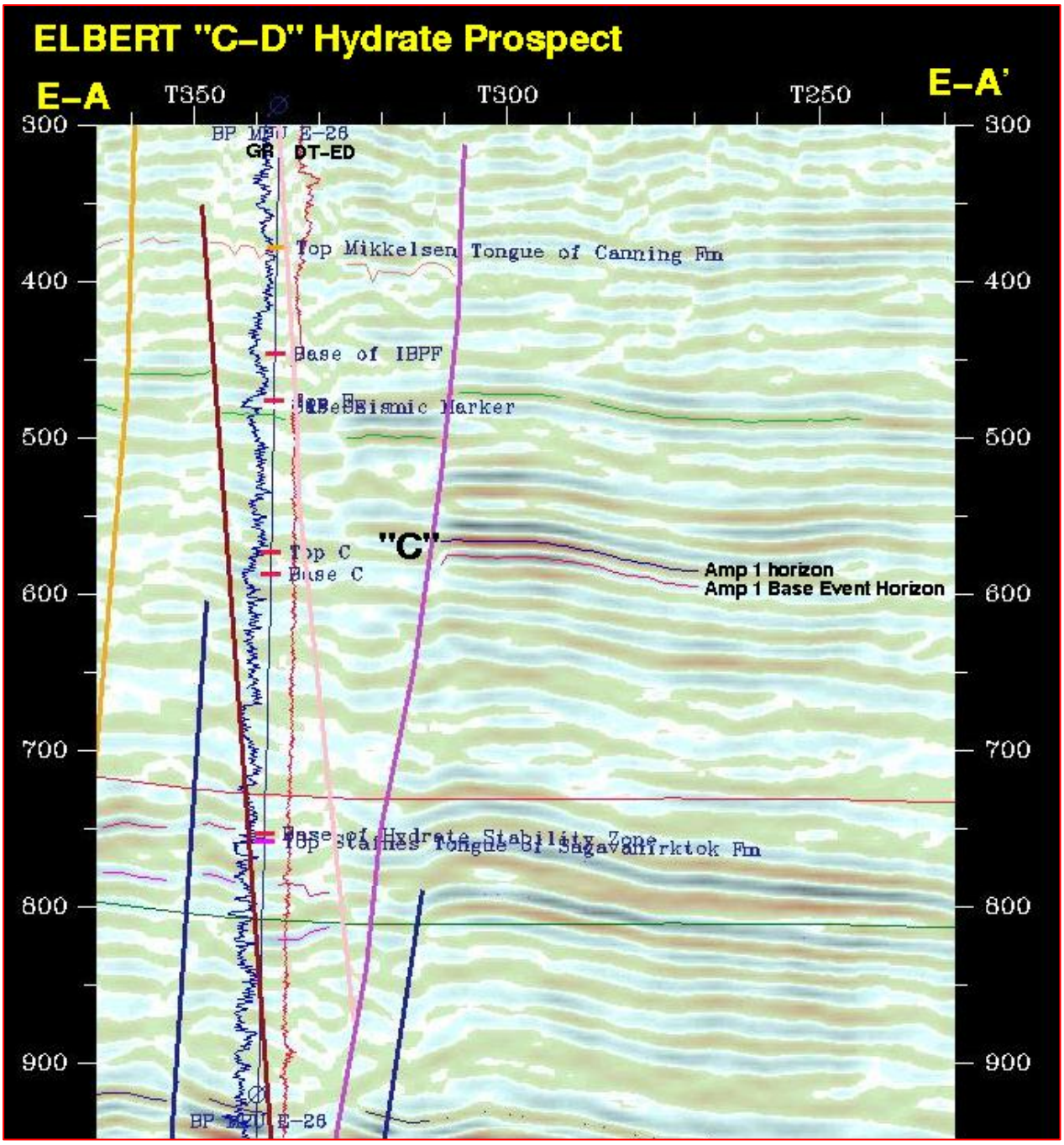

Figure 37: West-East Seismic cross-section E-A to E-A' (location shown in Figure 36), showing Zone C, Mt Elbert Prospect (Time in ms); also Figure 45

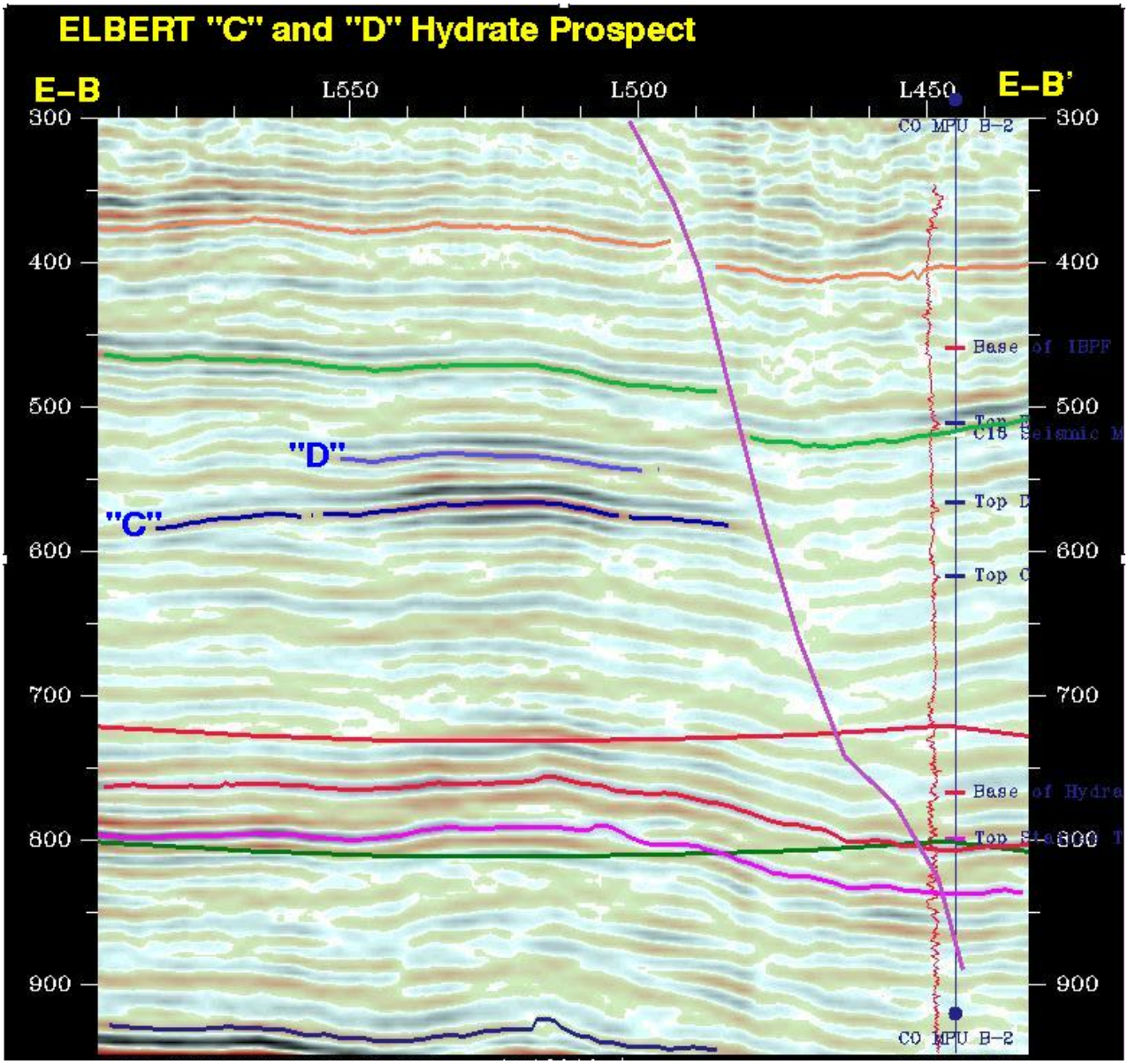

Figure 38: South-North Seismic cross-section E-B to E-B' (location shown in Figure 36), showing Zones C and D, Mt Elbert Prospect (Time in ms); also Figure 46

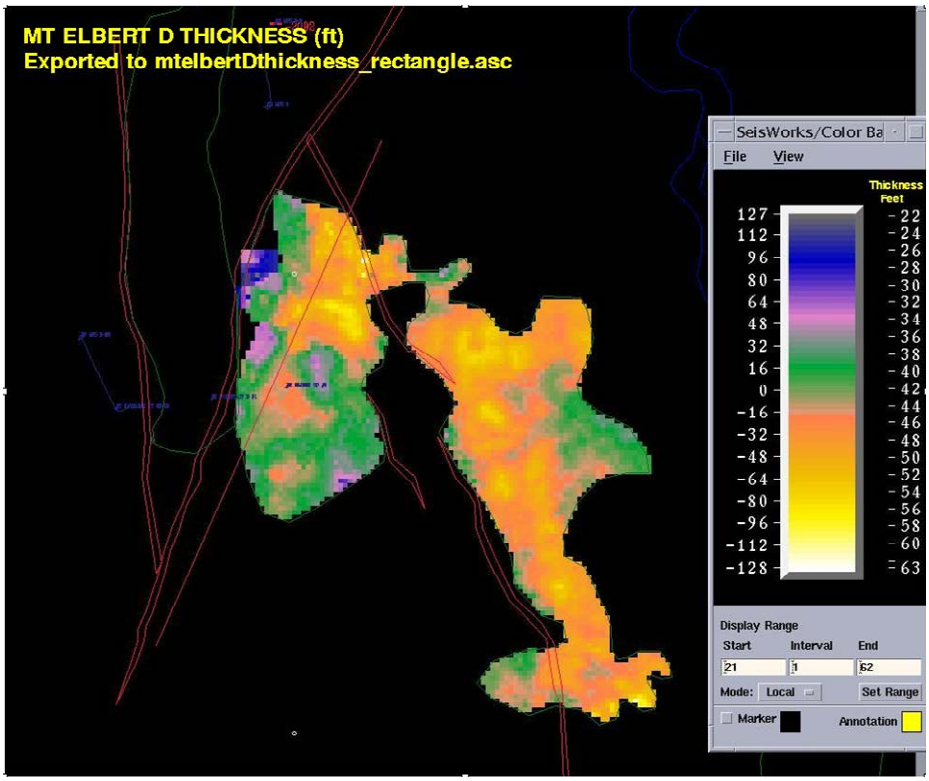

Figure 39: Zone D reservoir thickness (feet) as interpreted from seismic attribute analyses, Mt Elbert prospect

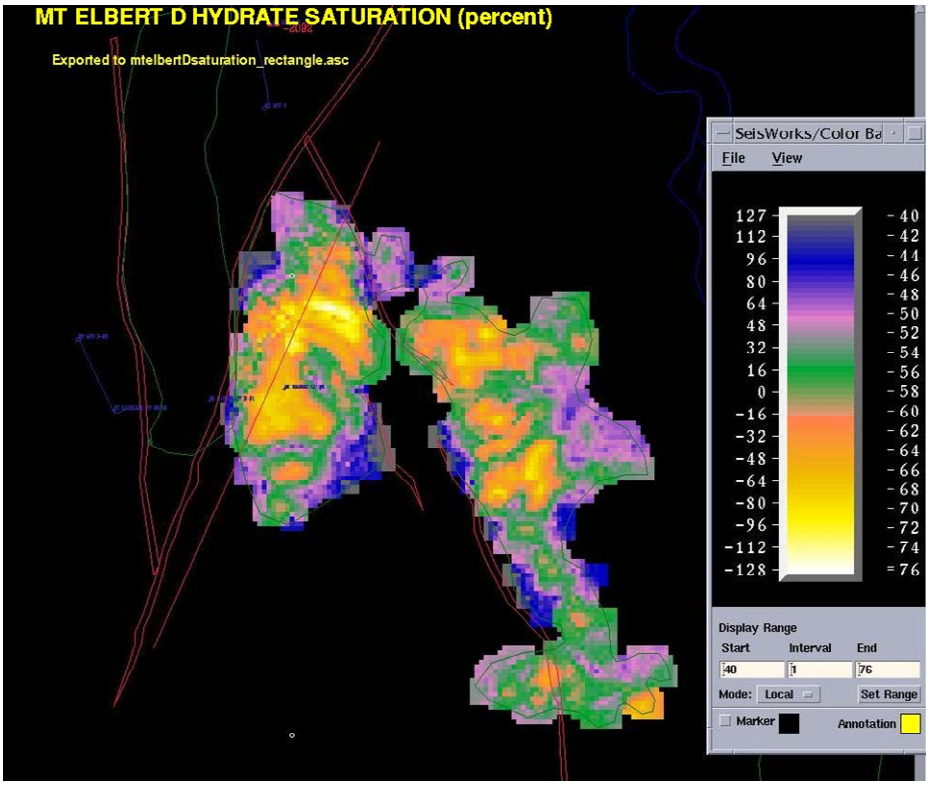

Figure 40: Zone D reservoir gas hydrate saturation as interpreted from seismic attribute analyses, Mt Elbert prospect

5.2.9.3 Mt Elbert Zone C Prospect Characterization

The Mt Elbert C Hydrate prospect is, in part, coincident with the Mt Elbert D Hydrate prospect, but is interpreted to be more laterally extensive, thicker, and of higher saturation than the D Hydrate prospect at this location. Figures 41-42 illustrate the seismic amplitude attribute defining this Zone C hydrate accumulation. Figure 43 shows the Zone C reservoir thickness in the Mt Elbert prospect as interpreted from seismic attribute analyses. Figure 44 shows the Zone C reservoir gas hydrate saturation in the Mt Elbert prospect as interpreted from seismic attribute analyses. Figure 45 (also Figure 37) shows the west to east seismic cross-section E-A to E-A' from Figure 42 with stratigraphy. Figure 46 (also Figure 38) shows the south to north seismic cross-section E-B to E-B' from Figure 42 with stratigraphy.

The "C" hydrate amplitude (Figures 41 and 42) shows that the highest amplitude portion of the Mt Elbert Prospect anomaly is on the highest up-dip portion of the prospect to the Northwest. The same is true for the less dramatic "D" hydrate mapped amplitude shown in Figure 36. These higher amplitudes are interpreted to correspond to the highest saturation portions of the prospect based on the thin bed analysis technique. The location of these higher amplitudes, in the most up-dip portion of the prospect, also point to the likelihood that these hydrate accumulations were originally emplaced as gas and later converted with available connate water into gas hydrate within the hydrate stability zone.

Figure 45 shows West-East seismic cross section E-A to E-A' through the MPU E-26 well and across the Mt Elbert Prospect anomaly. The prospect is separated from E-26 by the large down-to-the-west normal fault shown in black. Notice that the higher amplitude "C" hydrate zone in the prospect correlates to the thin "C" hydrate in the E-26 well. Figure 46 shows South-North seismic cross section E-B to E-B' through the Mt Elbert Prospect. The "C" and "D" hydrates which appear in the prospect, on the left of the black fault, can be correlated to thin "C" and "D" hydrate intervals in the MPU B-02 well. The reduction in amplitude to the south and east shown in Figures 41-42 is probably largely due to a decrease in hydrate saturation (Figure 44). Figure 47 shows a three dimensional display of the prospect with the bounding faults and adjacent key wells.

5.2.9.4 Mt Elbert Prospect Data Acquisition Planning

Phase 3 operations delineated the seismically-defined Mt Elbert prospect and implemented these 2005-2006 plans for additional static data acquisition. Since the prospect lies 3,000 to 4,000 feet from MPU E and B pads, data was better acquired from a vertical well drilled from an ice pad directly over the prospect during the winter drilling season (Figures 34 and 48). If acquired data confirmed the geophysical interpretation, then a horizontal production test well drilled from MPU E or B pads was considered at that time to potentially follow the delineation well. The B-pad location would have offered the best orientation with respect to the interpreted faults which define the western and eastern boundaries of the prospect. Table 19 illustrates the type of data acquisition that was considered, both from the vertical delineation well and from the potential future production test.

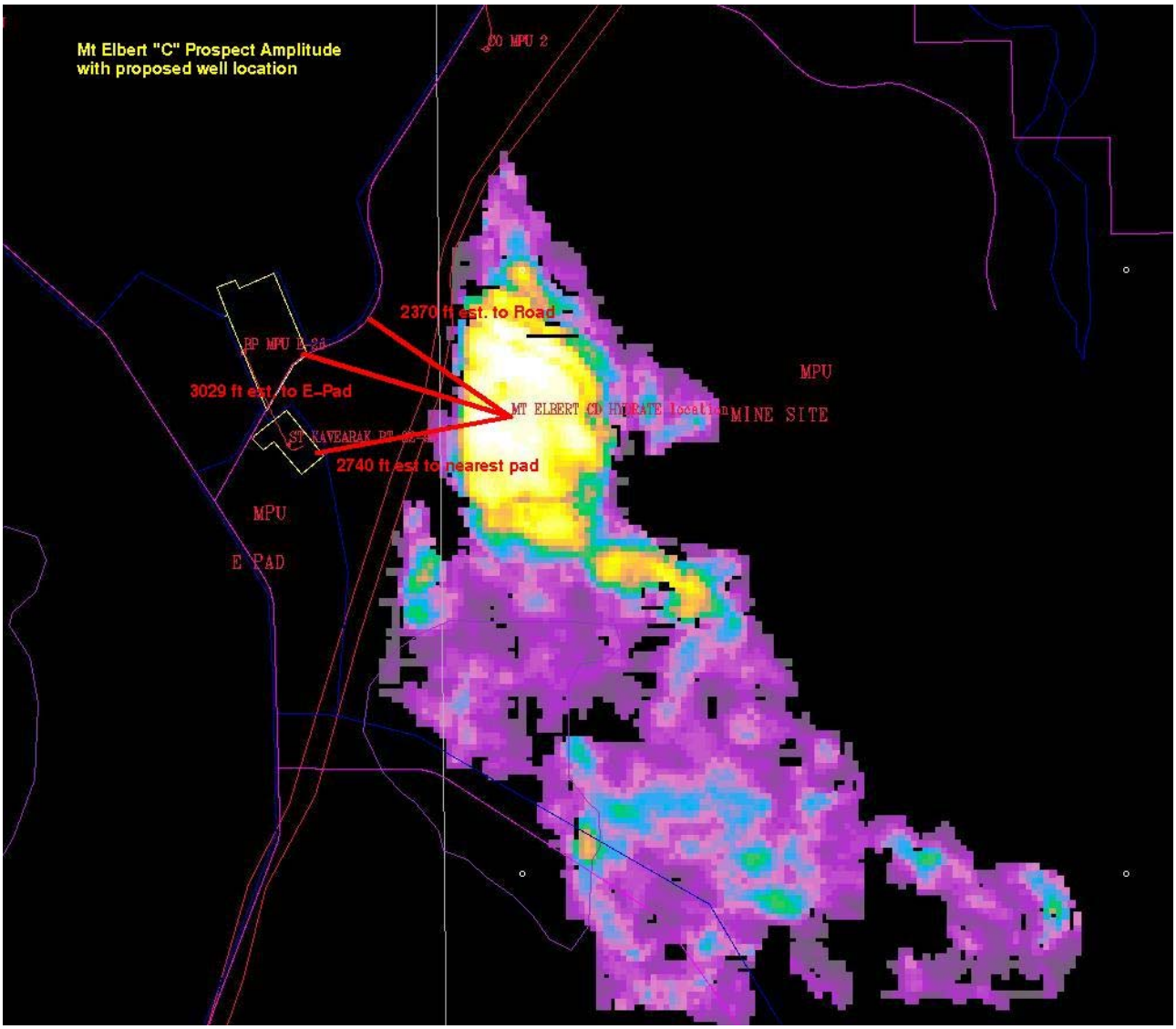

Figure 41: Seismic amplitude of Zone C horizon, Mt Elbert Prospect, showing proposed well location and distance to infrastructure at MPU E-pad and Central Facilities pad

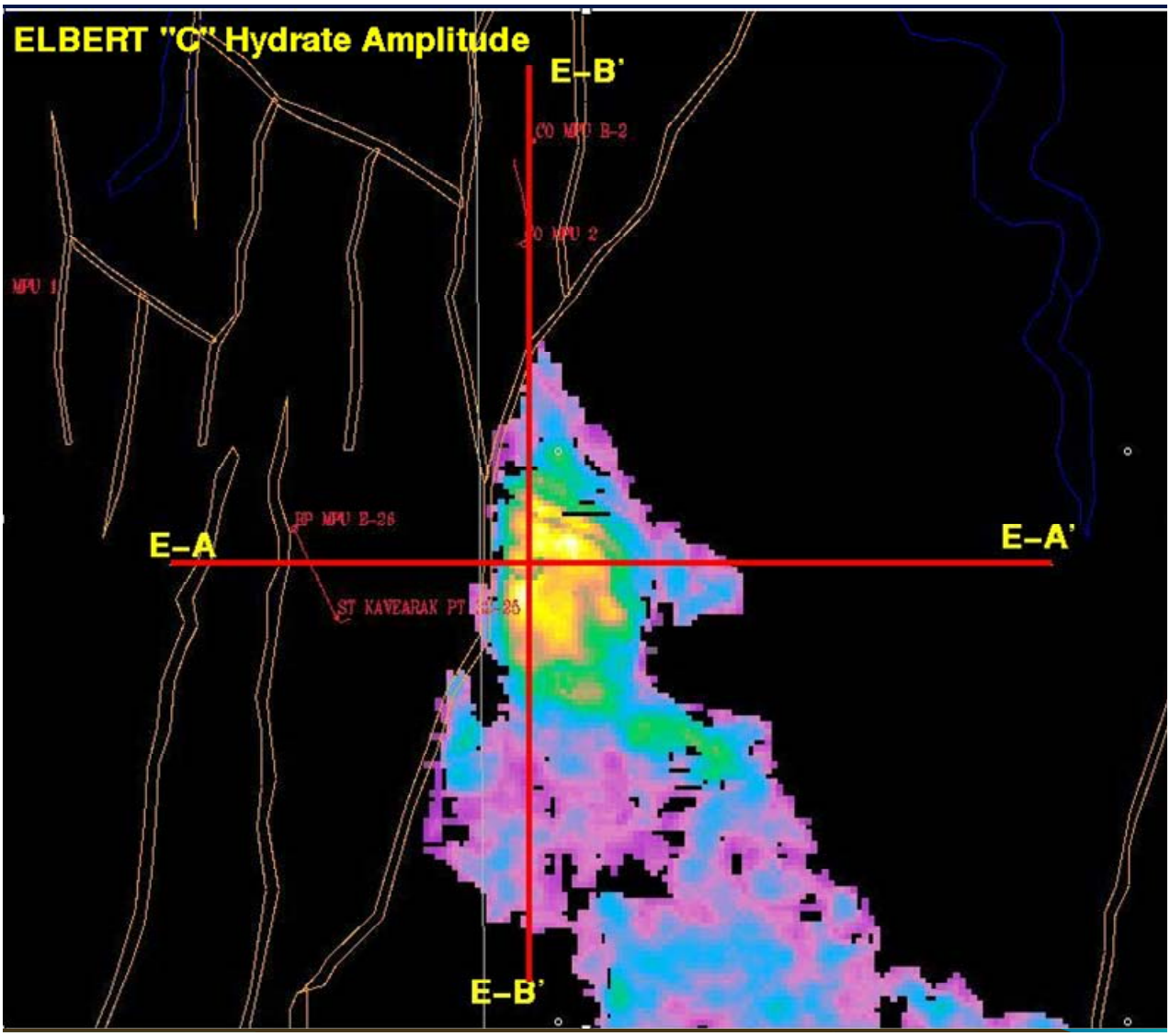

Figure 42: Zone C seismic amplitude, Mt Elbert prospect, showing location of seismic cross-sections in Figures 37-38 and with stratigraphy in Figures 45 and 46

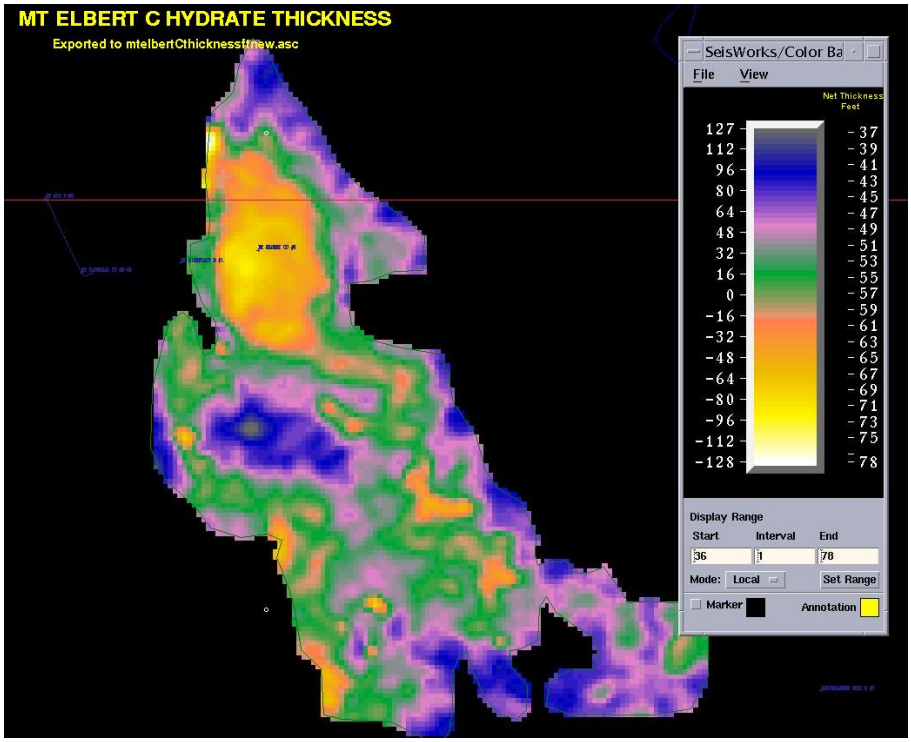

Figure 43: Zone C reservoir thickness (feet) as interpreted from seismic attribute analyses, Mt Elbert prospect

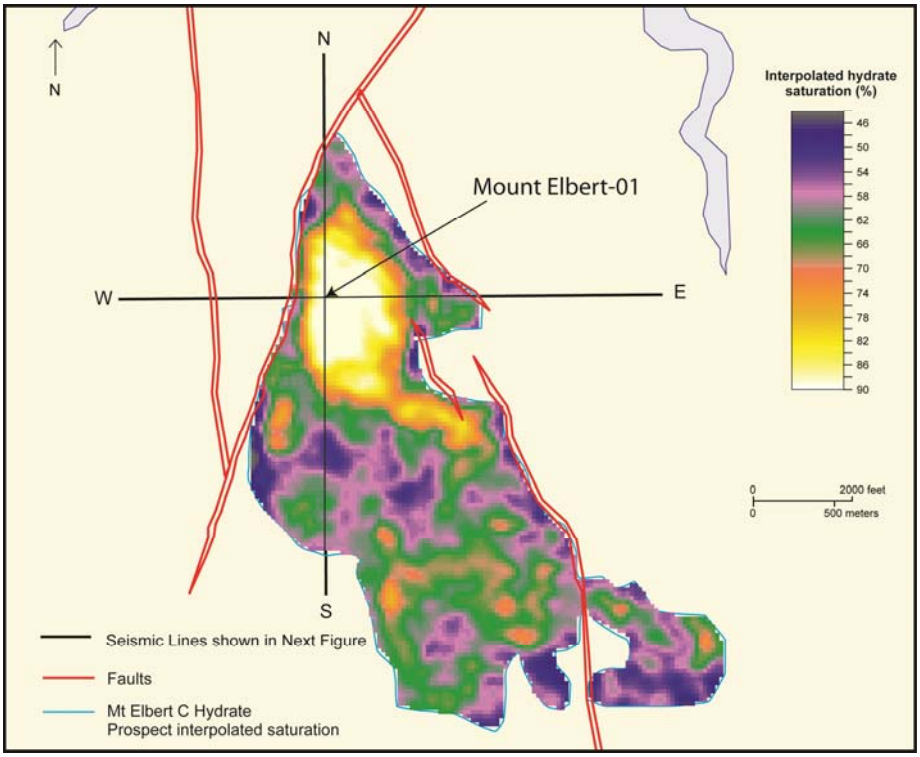

Figure 44: Zone C reservoir gas hydrate saturation as interpreted from seismic attribute analyses, Mt Elbert prospect (Hunter, et al, 2011)

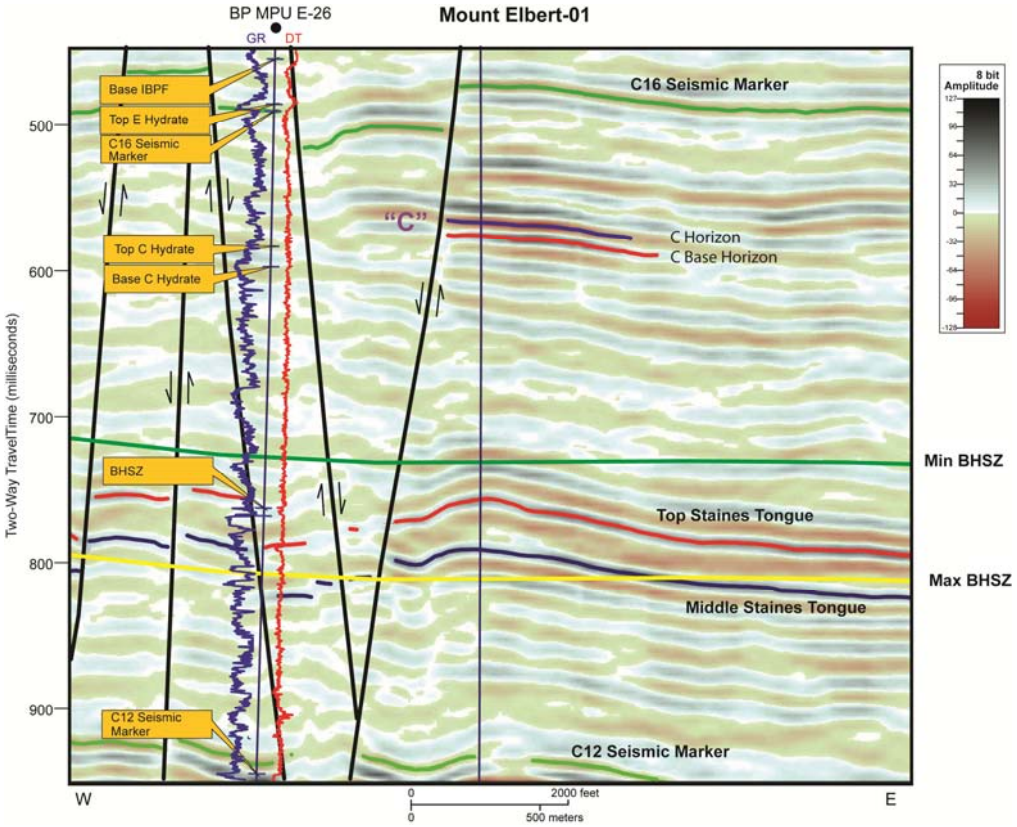

Figure 45: West-East Seismic cross-section E-A to E-A' with stratigraphy (also Figure 37) (Hunter, et al, 2011)

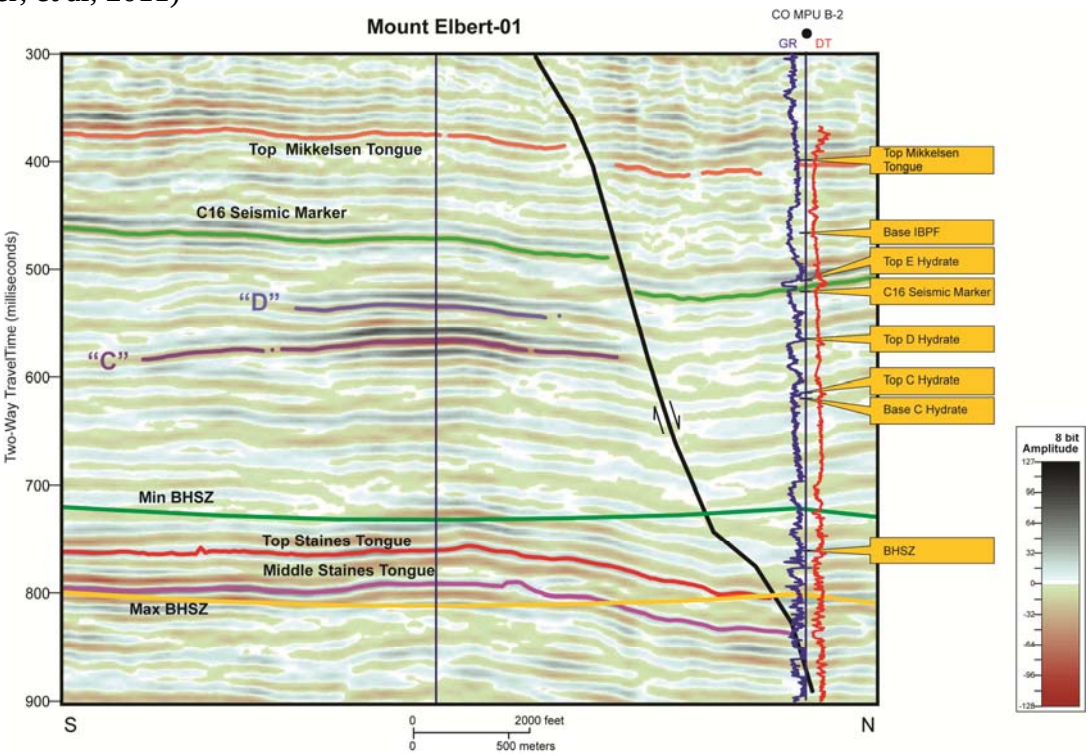

Figure 46: South-North Seismic cross-section E-B to E-B' with stratigraphy (also Figure 38) (Hunter, et al, 2011)

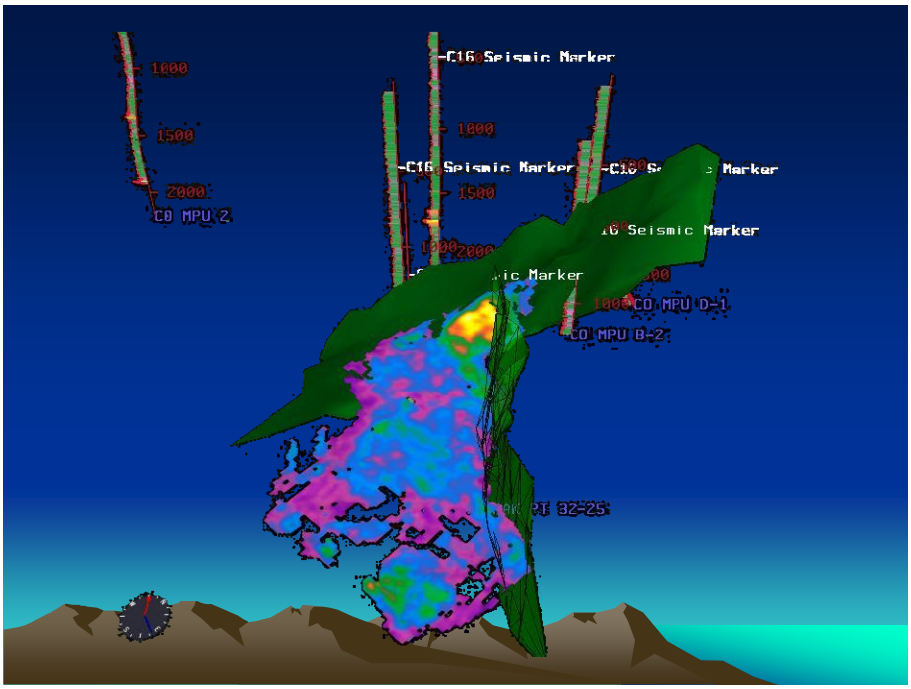

Figure 47: Three dimensional display of the Mt Elbert Prospect with bounding faults and adjacent key wells

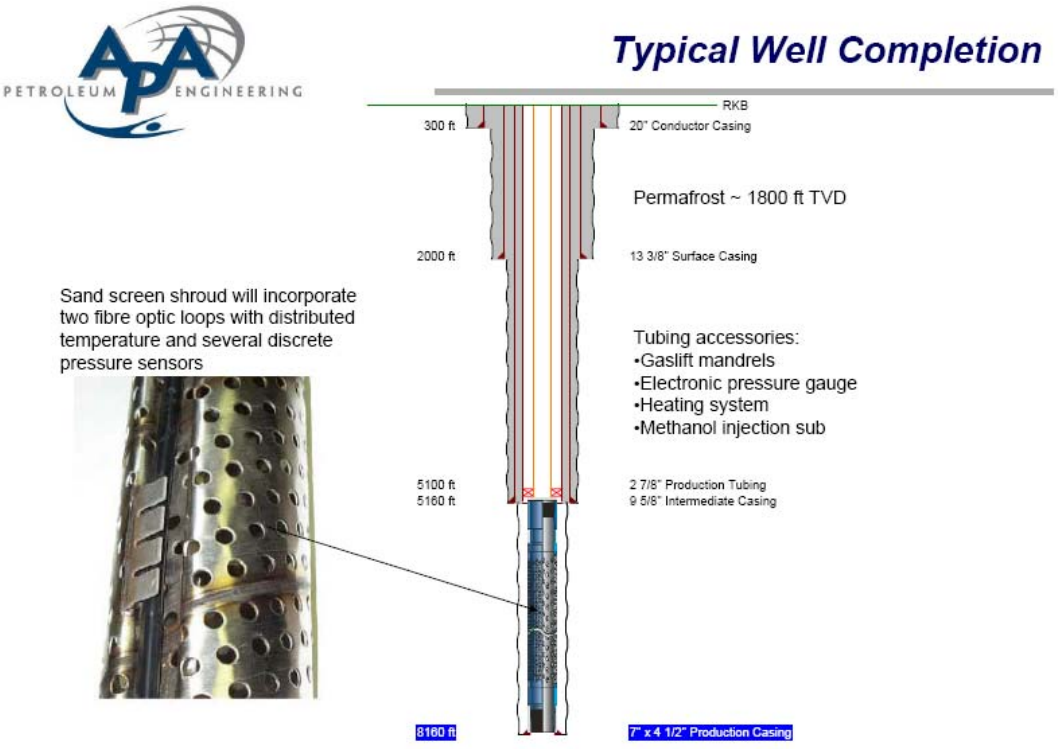

Figure 48: Example Well Design, 2005 Mt Elbert Prospect

Gas Hydrate-only prospect	**Recommended Data Acquisition**	**Data Issues**
	Core	Requires nearly vertical well
	Wireline &/or MWD/LWD logs	Requires nearly vertical well
	MDT testing and samples	Requires nearly vertical well
		Dedicated sidetrack an option
Possible Testing Sequence:	1. Vertical Well for data and observations	
	2. Horizontal sidetrack for testing	
	3. Fracturing and Huff-Puff testing	
	4. Chemical treatment testing?	
	Method of Production Test	**Production Testing Issues**
	Temperature	Hot Water Injection
		Hot Gas Injection
		Chemical Injection
		In-situ Combustion?
		Near-wellbore electro-magnetics
	Pressure	In-situ water production (?Sw?)
		Horizontal well setup options
		circulation with gas lift mandrel
		fracture with Huff/Puff
	Chemical	CO2 injection?
		Salt additives
		Methanol
	Other	Possible motor at/near surface
		Rod in-hole to 45 degrees
		Water & Sand Production Handling
		SSRDPCP
		(surface sucker-rod driven
		progressive cavity pump)
Gas Hydrate/Free Gas prospect	**Recommended Data Acquisition**	**Data Issues**
	Core	Requires nearly vertical well
	Wireline &/or MWD/LWD logs	Requires nearly vertical well
	MDT testing and samples	Requires nearly vertical well
		Dedicated sidetrack an option
		Depressurization Case Test
	Method of Production Test	**Production Testing Issues**
	Pressure	Produce well-constrained Free Gas
		Gas disposal/facilities issue
	Temperature	Combat near-wellbore drawdown
		Could reform hydrate &/or ice
		gas/water cycling/hot gas/water
	Chemical	CO2 injection?
		Salt additives
		Methanol
	Other	Possible motor at/near surface
		Rod in-hole to 45 degrees
		Water & Sand Production Handling
		(possible surface sucker-rod driven
		progressive cavity pump)

Table 19: Example Data Acquisition Program Considerations, 2005, Mt Elbert Prospect

5.2.9.5 Mt Elbert Prospect Area 2005 Facility Infrastructure Considerations

Several options could help facilitate potential production testing operations from MPU B-pad. During 2005 considerations of these operations, only one production line was not in use to B-pad (an 8" water line, ANSI 600) that at one time was used to bring source water from B-pad to the Central Production Facility (CFP). However, the 14" 3-phase pipeline could have been used as it was bringing produced fluids from B-pad to the CFP at E-pad, but was nowhere near its hydraulic limit with 2006 B-pad production rates. Also, there was active gas-lift at B-pad with room to add additional wells. 2006 gas-lift supply pressure at B-pad was about 1325 psi, while the E-pad 3-phase header pressure was about 205 psi and the header pressure at B-pad was about 160 psi.

5.2.9.6 Mt Elbert Prospect Phase 2 Recommendation for Phase 3 Operations

Reservoir characterization, reservoir modeling, prospect ranking, and facilities infrastructure indicated that the MPU Mt Elbert prospect was a good candidate for additional data acquisition. If data acquired during prospect delineation confirms the seismic interpretation and reservoir modeling, then the site was also a good candidate for production testing operations conducted from the nearby MPU B-pad facilities. Mt Elbert site field operations were determined to provide a suitable candidate for data acquisition and also potential future production testing operations to help narrow the uncertainties regarding gas hydrate-bearing reservoir productivity, saturations, and absolute and relative permeabilities.

5.2.10 Phase 2, Task 10 – Reservoir Modeling and Commercial Evaluation

Input from reservoir modeling and characterization studies supported the stakeholder decision to proceed into dedicated gas hydrate well stratigraphic test operations in Phase 3a. These studies used the reservoir characterization (Phase 1, tasks 5-6 and Phase 2, tasks 5-6) to build and/or update reservoir models and to help design a dedicated gas hydrate well for Phase 3a operations. Collaborations continued with LBNL and other active hydrate modeling research and code development efforts. Single well, pattern and sectional models were used to help determine viable candidate sites, design well operations, and predict productivity characteristics. Phase 2 Task 10 accomplishments included:

- Planned and coordinated Phase 2 reservoir modeling and regional resource assessments
    - Provided input to DOE NETL-coordinated reservoir model comparison studies
    - Coordinated and implemented regional Eileen accumulation fieldwide potential development scenario studies
        - Input Sagavanirktok zone A, B, C, D, and E polygons from USGS studies
        - Developed statistical approach and sequential development scenario
        - Reviewed preliminary study results and implemented improvements
        - Ranked potential future regional development areas
        - Documented study results as discussed below
- Completed reservoir simulation studies using CGM STARS and coupled these studies with regional Eileen accumulation (50 TCF GIP) potential field development scenario
    - Supported decision to proceed into Phase 3a stratigraphic test well operations
    - Regional modeling documented in R15, pp. 99-131 (also see Wilson, et al, 2011)
    - Additional reservoir modeling studies by UAF documented in R15, pp. 131-141

5.3 Phase 3 Task Schedules, Milestones, and Accomplishments

U.S. Department of Energy Milestone Log, Phase 3a, 2006-2014
Program/Project Title: DE-FC26-01NT41332: Resource Characterization and Quantification of Natural Gas Hydrate and Associated Free-Gas Accumulations in the Prudhoe Bay - Kuparuk River Area on the North Slope of Alaska.

Phase 3 continued some desktop studies initiated in Phase 1 tasks 1-6, but primarily focused on Task 8, planning and implementing gas hydrate well (Tables 20, 21, and 22). Phase 3a scope-of-work was defined in contract Amendment 11 with additional detail provided in contract amendments 18 and 20 (Table 6).

Identification Number	Description	Planned Completion Date	Actual Completion Date	Comments
Task 1.0	Research Management Plan	1/06 – 10/08	12/08	Section 5.3.1
Task 2.0	Provide Technical Data and Expertise	MPU: 12/02 PBU: * KRU: *	MPU: 12/02 PBU: * KRU: *	See Technical Progress Reports and Section 5.3.2
Task 3.0	Wells of Opportunity Data Acquisition	Ongoing	Completed	See Technical Progress Reports Section 5.3.3
Task 4.0	Research Collaboration Link	Ongoing	Completed	See Technical Progress Reports and Section 5.3.4
Subtask 4.1	Research Continuity			
Task 5.0	Logging and Seismic Technology Development and Advances	Ongoing	Completed	See T01 Report and Sections 5.1.5, 5.2.5, 5.3.5
Task 6.0	Reservoir and Fluids Characterization Study	12/07	9/09	UA contract completed; See Section 5.3.6 and see Appendix A
Task 7.0	Laboratory Studies for Drilling, Completion, Production Support	9/08	Completed	See Technical Progress Reports and Section 5.3.7
Subtask 7.1	Design Mud System	9/07	Completed	
Subtask 7.2	Assess Formation Damage	9/07	Completed	
Subtask 7.3	Measure Petrophysical and Other Physical Properties	9/07	Completed	
AEO Task 1	Relative Permeability Studies	9/08	Completed	
AEO Task 2	Minipermeameter Studies	6/08	Completed	
Task 8.0	Plan and Implement gas hydrate well completion & production test	3/07	3/07	Mt Elbert-01 2/3-19, 2007 See Section 5.3.8
Task 9.0	Reservoir Modeling and Project Commercial Evaluation	9/08	Completed	Regional Resource Review and Section 5.3.9
Subtask 9.1	Task 5-6 Reservoir models	9/08	As-needed	
Subtask 9.2	Project Commerciality and Phase 3b Production Test Decision	9/08	Did not proceed to test	Phase 3b planning/design, but not implemented

* Not released to CRA as limited-rights data due to dependent on industry partner agreement

Table 20: Phase 3a Task Descriptions and Milestones. Note this table is consistent with Tables 21-22, Phase 3a Milestone Plans. Section 5.3 is organized by the 9 tasks listed in Tables 20-22.

DOE F 4600.3# Table 21: U.S. DEPARTMENT OF ENERGY FEDERAL ASSISTANCE MILESTONE PLAN: PHASE 3a (2007-2008)

1. Program/Project Identification No. DE-FC26-01NT41332	2. Program/Project Title Resource Characterization and Quantification of Natural Gas Hydrate and Associated Free-Gas Accumulations in the Prudhoe Bay - Kuparuk River Area on the North Slope of Alaska
3. Performer (Name, Address) BP Exploration (Alaska), Inc., 900 East Benson Blvd, P.O. Box 196612, Anchorage, Alaska 99519-6612	4. Program/Project Start Date 10/22/02* 5. Program/Project Completion Date 3/31/14(through Phase 3a)

6. Identification Task Number	7. Planning Category (Work Breakdown Structure Tasks)	8. Program/Project Duration (Phase 3a, 2007-2008) ←Phase 3a Strat Test→←3a Analyses/Audit → 3bPlanning→←3a Analyses, 3b Decisioning & 3b Planning→ J F M A M J J A S O N D J F M A M J J A S O N D	9. Comments (Primary work Performer)
Task 1.0	Contracts and Research Management Planning	!>>>>>>!>>>--->>>>>--->>>>>>>>>>>>>>>>>>!----------!---------->>!>>>>>>>>	BPXA, AES
Task 2.0	Technical Data and Expertise	!->>>>>>----->>>>------->>>>>>>>>-------!--->>>>>>>>-------!>>>>>>>>-->!>>>>>>--	BPXA, AES
Task 3.0	Wells of Opportunity - Data	!------------>>>>>--------------->>>>---!----->>>>>>>>>>>>!>----------!>>>>>>>>	BPXA, AES
Task 4.0	Research Collaboration Link	!>>>>>>>>>>>>>>>>>>>>----------->>>>>>>>>>!>>>>>>>>>>>>>>>>>!>>>>>>>>>>!>>>>>>>>	BPXA, USGS, AES, UAF
Task 5.0	Logging/Seismic Technology	!>>>>>>>>>>>>>>>>>>>->>>>>>>>>>>>>>>>>>!>>>>>>>>>>>>>>>>>!>>>>>>>>>>!>>>>>>>>	USGS, BPXA
Task 6.0	Characterize Reservoir/Fluid	!------>>>>>>>>>>>>>----------->>>>>>>>>>!>>>>>>>>>>>>>>>---!------>>>>>!>>>>>>>>	UA, USGS
Task 7.0	Lab Studies: Drilling, Completion, Production	!----------->>>>>>>----------->>>>>>>>>>!>>>>>>>>>>>>>>>>>!>>>>>>>>>>!>>>>>>>>	UAF
Task 8.0	Drill/Analyze Strat Test Evaluate/Design Production Test & Phase 3b progression	! -->>>>>>>>>>>->>>----->>>>>>>>>>>>!>>>>>>>>>>>>>>>>>!>>>>>>>>>>!>>>>>>>>	APA, BPXA, AES, UAF
Task 9.0	Reservoir Modeling and Commercial Evaluation	!---->>>>>>>>>>>>>>->>>>>>>>>>>>>>>>>>!>>>>>>>>>>>>>>>>>!>>>>>>>>>>!>>>>>>>>	RS, AES, BPXA, UAF

10. Remarks * Schedule shows Phases 3a from 2007 through end-2008. Phase 3a stratigraphic test deferred until early 2007 by 3rd party rig delay. Explanation of Symbols: >> Major Task Work; -- Minor Task Work; ! Milestone. Significant technical work and milestones presented in Technical Progress and Topical Reports.

Table 21: Phase 3a (2007-2008) USDOE Milestone Plan and Task Descriptions

DOE F 4600.3# Table 22: U.S. DEPARTMENT OF ENERGY FEDERAL ASSISTANCE MILESTONE PLAN: Phase 3a (2009-2013)

1. Program/Project Identification No. DE-FC26-01NT41332	2. Program/Project Title Resource Characterization and Quantification of Natural Gas Hydrate and Associated Free-Gas Accumulations in the Prudhoe Bay - Kuparuk River Area on the North Slope of Alaska
3. Performer (Name, Address) BP Exploration (Alaska), Inc., 900 East Benson Blvd, P.O. Box 196612, Anchorage, Alaska 99519-6612	4. Program/Project Start Date 10/22/02* 5. Current Program/Project Completion Date 3/31/14

6. Identification Task Number	7. Planning Category (Work Breakdown Structure Tasks)	8. Program/Project Duration (continuing Phase 3a, 2009-2013) ← Phase 3a and Phase 3b Stakeholder alignment →+ J F M A M J J A S O N D J F M A M J J A S O N 2013	9. Comments (Primary work Performer)
Task 1.0	Contracts and Research Management Planning	!>>>>>>>>!>--->>>>>!-->>>>>>>>>>>>>>>>>>---------------------------------------	BP
Task 2.0	Technical Data and Expertise	!->>>>>>>!--->>>>--!---->>>>>>>>>----------->>>>>>>>--------------------------	BP
Task 3.0	WOO Data Acquisition	!---	BP
Task 4.0	Stakeholder Communications	!>>>>>>>>!>>>>>>>>>!---------->>>>>>>>>>>>>>>>>>>>>>>>>>>>>--------------------	BP
Task 5.0	Logging/Seismic Technology	!>>>>>>>>!>>-------!--	USGS, BP
Task 6.0	Characterize Reservoir/Fluid	--------------->>>>>>>>>>>>!	UA, USGS
Task 7.0	Lab Studies: Drilling, Completion, Production	!--------------------------	UAF
Task 8.0	Long-term Production Test Drill, Complete, Test Plan	!------->!>>>>>>>>>!>>>>>>>>>>>>>>>>>>>>>>>>>>>>>>>>>>>>>----------------------	BP
Subtask 8.1	Finalize Test Site Location	!>>>>>>>>!>>>>>>>>>!-------->>>>>>>>>>>>>>>>>>>>>>>>>>>>>>>--------------------	BP, USGS, DOE
Subtask 8.2	Production Test Plan	!--------!---------!-------------->>>>>>>>>>>>>>>>>>>>>>>>--------------------	RPS, RS, BP
Subtask 8.3	Implement Production Test	!------------------!--	RS, RPS, BP
Task 9.0	Reservoir Modeling	!------------------!--	RS

10. Remarks * Schedule does not show Phase 3b (not currently approved) with primary objective to complete a detailed design and implement a long-term gas hydrate production test.
Explanation of Symbols: >> Major Task Work; -- Minor Task Work; ! Milestone.

Table 22: Phase 3a (2009-2013) USDOE Milestone Plan and Task Descriptions

5.3.1 Phase 3, Task 1 – Research Management

The research management task continued to establish project plans, track progress against project milestones (Tables 20, 21 and 22), manage project subcontracts, monitor project costs, submit project technical and cost reports, and help determine progression through the gates between project phases.

5.3.2 Phase 3, Task 2 – Technical Data and Expertise

Phase 3 Task 2 project activities consisted primarily of recognizing and recommending synergies with exploration season ice-pad operations in conjunction with planning and implementing the Mt Elbert-01 Stratigraphic Test well. Synergies were recognized and input provided into the 2007 MPU 2-well Ugnu and Schrader Bluff formations appraisal program.

5.3.3 Phase 3, Task 3 – Wells of Opportunity Data Acquisition

During Phase 1-2, wireline log data was acquired within shallow gas hydrate-bearing intervals in 5 primary wells (MPU E-26, MPU S-15i, MPU I-16, PBU L-106, and PBU L-107) targeting deeper oil-bearing horizons and thus termed "wells-of-opportunity" (WOO). While drilling schedules continued to be monitored during Phase 3 for additional WOO, project activities focused primarily on the Mt Elbert-01 Stratigraphic Test well. This well would acquire the first (since the 1972 NWEileenState-02) dedicated wireline log and core data over an interpreted gas hydrate-bearing prospect (Mt Elbert, Figures 7 and 35, Table 4) from a vertical penetration beneath an exploration ice pad (Figures 49-50) within an area of the MPU not penetrated by another well.

5.3.4 Phase 3, Task 4 – Research Collaboration Link

With research progression into Phase 3 operations, evaluated technologies included gas hydrate production techniques such as thermal, chemical, and mechanical stimulation to enhance gas dissociation if the project had proceeded into Phase 3b production testing. Advances in electromagnetic thermal stimulation techniques may benefit potential future production test operations. Coiled-tubing unit-supported completions may offer sufficient flexibility to support various completion options during potential future production test operations. DOE granted an advance patent waiver to the project in 2003, but no project-related patents are currently recorded. The project received awards from the AAPG Mineral and Energy Division (EMD) for best poster (Hunter, et al, 2003) and for best presentation (Hunter, et al, 2007). Phase 3 accomplishments were extensively published in the JMPG Volume. Collaborations with other gas hydrate research programs continued throughout Phase 3. Project objectives also benefited from support and recognition of the following studies.

5.3.4.1 ConocoPhillips-DOE CRA DE-NT0006553

Support was provided to DOE-ConocoPhillips' Ignik Sikumi (CRA DE-NT0006553) project based on lessons learned in the Mt Elbert-01 drilling and data acquisition operations. ConocoPhillips and DOE conducted this cooperative research agreement from 2008-2013 to design and field test CO_2 as a potential enhancement to recover gas from CH_4 hydrate-bearing reservoirs beneath ANS industry infrastructure. The goal of this project was to define, plan and conduct a field trial of a methane hydrate production methodology whereby carbon dioxide molecules are exchanged in-situ for the methane molecules within a methane hydrate structure, releasing the methane for production. The project evaluated the viability of this hydrate production technique and promoted understanding of implications of the process at a field scale.

The success of this field trial can help advance larger-scale, longer-term tests needed to test viability of production technologies for methane hydrates. The exchange technology could prove to be a critical tool for unlocking the methane hydrate resource potential in a manner that minimizes potential adverse environmental impacts such as water production and/or subsidence while simultaneously providing a synergistic opportunity to sequester carbon dioxide. Project results are available at:

http://www.netl.doe.gov/technologies/oil-gas/FutureSupply/MethaneHydrates/rd-program/ANSWell/co2_ch4exchange.html

and final project report (August 2013) at: http://www.netl.doe.gov/technologies/oil-gas/publications/Hydrates/2013reports/nt0006553-final-report.pdf.

5.3.4.2 Reservoir Model Comparison studies

DOE NETL and West Virginia University (Dr. Brian Anderson) reservoir modeling coordination significantly contributed to collaborative reservoir modeling efforts with Japan, Lawrence Berkeley National Lab (LBNL), Pacific Northwest National Lab (PNNL), UAF, and University of Calgary and Fekete. This important work has simulated field-scale gas hydrate-bearing reservoirs, history matched the Mt Elbert-01 stratigraphic test MDT data, and evaluated ANS potential production test options (Figure 8, Table 5). These studies improved understanding of how these different gas hydrate reservoir models handle the basic physics of gas hydrate dissociation processes within gas hydrate-bearing formations. Significant contributors to this effort included: Masanori Kurihara (Japan Oil Engineering Co., Ltd.), Yoshihiro Masuda (University of Tokyo), George Moridis (Lawrence Berkeley National Laboratory, University of California), Hideo Narita (National Institute of Advanced Industrial Science and Technology), Mark White (Pacific Northwest National Laboratory), Joseph W. Wilder (University of Akron), Brian Anderson (West Virginia University), Scott Wilson (Ryder Scott Company), Mehran Pooladi-Darvish and Huifang Hong (University of Calgary and Fekete), Shirish Patil and Abhijit Dandekar (UAF), Timothy Collett (USGS), and Robert Hunter (BPXA contractor).

5.3.4.3 CO_2 Enhanced Recovery Mechanism (DE-FC26-01NT41248)

This UAF/PNNL/BPXA study investigated the potential effectiveness of CO_2 as a possible enhanced recovery mechanism for gas dissociation from methane hydrate. DOE supported this associated project research.

5.3.4.4 Efficacy of Ceramicrete Cold Temperature Cement

This project was funded by the Arctic Energy and Technology Development Lab (AETDL) / Arctic Energy Office (AEO) in mid-2004. The project was designed to determine the efficacy of Ceramicrete cold temperature cement for possible application to future gas hydrate drilling and completion operations. Evaluating the stability and use of an alternative cold temperature cement may enhance ability to maintain lower temperatures within the gas hydrate stability field during drilling and completion operations and also may help ensure safer and more cost-effective operations. In early 2006, the Ceramicrete material was approved for field testing at the BJ Services yard in Texas. Although Ceramicrete was not field tested in time to be evaluated for use in 2007 Alaska operations, successful future yard testing of the material may enable future testing in Alaska project operations as discussed in Section 5.3.8.2.3.8.

5.3.4.5 Thermal Tool Prototype (Precision Combustion, Inc. (PCI) – DOE)

Potential synergies from this DOE-supported research project with the BPXA – DOE gas hydrate research program were recognized in December 2003 by Edie Allison (DOE). Communications

with Precision Combustion researchers indicated possible synergies, particularly regarding potential in-situ reservoir heating. Successful modeling and lab work could potentially lead to application in future gas hydrate field operations. In April 2004, BPXA provided a letter in support of progression of PCI's project into their phase 2: prototype tool design and possible surface testing. A thermal component of Phase 3b production testing was considered and a viable future delivery mechanism could potentially incorporate this technology.

5.3.4.6 Thermal Electromagnetic Tool (McGee-McMillan, Inc.)

Dr. Bruce McGee led application of downhole thermal electromagnetic production stimulation for a pilot viscous oil project at Fort McMurray, Canada. Discussions with Dr. McGee continued from 2004 through 2009; potential adaptation of downhole thermal technology is recommended for a potential future ANS long-term production test.

5.3.4.7 Japan Gas Hydrate Research

Progress toward completing the objectives of this project and the DOE gas hydrate R&D program remain aligned with gas hydrate research by Japan Oil, Gas, and Metals National Corporation (JOGMEC), formerly Japan National Oil Corporation (JNOC). JOGMEC remains interested in research collaboration, particularly if the BPXA-DOE CRA would have proceeded into long-term production testing operations. JOGMEC successfully accomplished short-term gas hydrate production test operations in 2007-2008 at the Mallik field site in Canada's MacKenzie Delta and continues activities in the Nankai Trough offshore Japan.

5.3.4.8 India Gas Hydrate Research

India's Institute of Oil and Gas Production Technology (IOGPT) also maintained interest in the BPXA – DOE CRA. BPXA sponsored a technical observer from IOGPT during Phase 3a Mount Elbert Stratigraphic Test operations and data acquisition. Results of the 2007 India offshore program are available at: http://energy.usgs.gov/other/gashydrates/india.html.

5.3.4.9 China Gas Hydrate Research

China has developed a gas hydrate R&D program. BPXA presented project accomplishments in August 2013 to a delegation from the China National Offshore Oil Corporation (CNOOC).

5.3.4.10 U.S. Department of Interior, USGS, BLM, State of Alaska DGGS

A gas hydrate resource assessment research project sponsored by the Department of Interior (DOI) provided significant benefits to this project. To help develop a more complete regional understanding of this potential energy resource, the BLM, USGS and State of Alaska Division of Geological and Geophysical Surveys (DGGS) entered into an Assistance Agreement in 2002 to assess regional gas hydrate energy resource potential in northern Alaska. This agreement combined the resource assessment responsibilities of the USGS and the DGGS with the surface management and permitting responsibilities of the BLM. Information generated from this agreement helped guide these agencies to promote responsible resource development if research proves technical and/or commercial feasibility of this potential arctic energy resource. The DOI project has worked with the BPXA – DOE CRA project to assess the regional recoverable resource potential of onshore natural gas hydrate and associated free-gas accumulations in northern Alaska, initially within current industry infrastructure. A report, Assessment of Gas Hydrate Resources on the North Slope, Alaska, 2008, was issued in October 2008 estimating 85.4 TCF mean technically recoverable undiscovered resources (Figure 2, Table 3).

5.3.5 Phase 3, Task 5 – USGS Data, Logging, and Seismic Technology

To help ensure timely selection of a viable site for Phase 3 drilling and data acquisition operations, in parallel to the UA Task 6 activities, these Task 5 studies were expanded in late Phase 1 through Phase 2 and augmented by supporting industry consultants. These expanded reservoir characterization activities identified multiple gas hydrate prospects within the MPU (Tables 4 and 12, Figure 7) through detailed investigation of the full volume MPU 3D seismic data previously released to the USGS as documented above in Sections 5.1.5, 5.2.5, and 5.2.9. These studies significantly contributed to the selection of the Mt Elbert prospect for the Phase 3a stratigraphic test. The majority of the research and contributions of USGS staff were funded internally by the U.S. Department of Interior and funded incrementally by this project. Major results of this study were also reported in Report T01 and the technical progress report R09.

5.3.6 Phase 3, Task 6 – UA Reservoir and Fluids Characterization, Seismic Studies

Reservoir and fluid characterization studies continued into Phase 3 at the University of Arizona. Significant project final accomplishments are documented above in Sections 5.1.6 and 5.2.6 as well as R26 (pp. 36-89) and Appendix A. From 2002 through 2009, a total of 13 students completed project related studies under this UA program, including 5 Masters theses (Table 23).

5.3.6.1 Phase 3, Task 6 – UA Reservoir Characterization and Supporting Studies

UA studies also supported selection of the Mt Elbert prospect for a gas hydrate stratigraphic test and data acquisition. UA studies also indicated that this MPU prospect is interpreted to contain gas hydrate-bearing reservoir sands. This prospect was interpreted on a structurally-high horst block near the eastern edge of the UA-interpreted “East basin”, but within what may be the western portion of another Sagavanirktok depocenter basin. The frequency of current well control used in the East basin interpretation (since most well penetrations of the shallow Sagavanirktok interval occur within a few hundred feet of existing gravel production pads) may be less than the interpreted frequency of the fluvio-deltaic Sagavanirktok stratigraphic reservoir variation. Thus, a delineation well in the Mt Elbert prospect location would help assess both the structural and stratigraphic controls of gas hydrate accumulation within the shallow Sagavanirktok reservoir.

The Mt Elbert prospect location occurs above what are interpreted to be regionally wet Ugnu sands (below the regional Ugnu reservoir viscous oil to water contact). A petroleum system linkage between viscous oil biodegradation in the Ugnu to gas migration through the Ugnu top seal and into the shallower Sagavanirktok sands remains unproven, but is theorized by some researchers. The seismic interpretation clearly indicates gas hydrate-bearing sands in the Sagavanirktok interval as documented in prior reports. The Mt Elbert-01 stratigraphic test well was initially planned to penetrate the upper Ugnu above 4,000 feet TVDss to investigate this potential petroleum system linkage, but cost-cuts implemented to offset increased costs of oil-based mud and wireline logging necessitated limiting the well total depth to 3,000 feet TVDss.

During Phase 3, UA continued to document the Phase 1-2 regional MPU, KRU, and PBU reservoir characterization Task 6 studies of gas hydrate and associated free gas resources. This regional reservoir characterization is based primarily on well-log-based sequence stratigraphic correlation interpretations within the area-of-interest. A suite of maps is provided in Appendix A.

In December 2007, the University of Arizona was notified of plans to terminate the reservoir characterization studies following the successful Mt Elbert-01 stratigraphic test. A formal letter was issued in early January 2008 to terminate this contract. UA initiated this work under contract in 2002 and had operated under a no-cost extension for some continuing work since 2005. Remaining obligated funds were used in final report preparation.

Student	Dept/Degree/Yr	Topic
Casey Hagbo*	GEOS/MS/ 2003	Characterization of gas-hydrate occurrences using 3D seismic data and seismic attributes, Milne Point, North Slope, Alaska
Bo Zhao*	MGE/MS/2003	Classifying Seismic Attributes in the Milne Point Unit, North Slope of Alaska
Andy Hennes*	GEOS/MS/2004	Structural constraints on gas hydrate formation and distribution in the Milne Point Unit, North Slope of Alaska
Scott Geauner*	MGE/MS/2006	Fault analysis, seismic facies modeling and volumetric reassessment of gas hydrates in the Milne Point Unit, North Slope, Alaska
Lynn Peyton	GEOS/PhD/2007	Research Associate work on seismic and synthetic seismogram analysis, well log to seismic correlation, Milne Point Unit
Justin Manuel*	MGE/MS/2008	A chronostratigraphic framework of the Sagavanirktok Formation, North Slope Alaska: Incorporating facies characterization, reservoir continuity and dimensions in relation to gas-hydrate and associated free-gas resources
M. Serkan Arca	GEOS/PhD/2008	Research Associate work on seismic data analysis, Milne Point Unit
Margaret Barker	GEOS/BS/~2009	Work on interpretation and spectral analysis of seismic data, Milne Point Unit
Shanda Wagner	MGE/BS/2004	Various project support (Also, Preliminary kinematic study of the "Kartchner Block", Southeastern Arizona)
Gwyn Smith	MGE/BS/~2006	Digitize, georegister and synthesize a regional fault map and produced graphics for the 2004 AAPG Hedberg conference presentations and posters
Greg Gandler	MGE/BS/2004	Preliminary spatial analysis of hydrate occurrence with respect to faulting Milne Point Unit, Northern Alaska
Keith Mitchell	MGE/BS/2005	Preliminary Investigation of Structural Control on Deposition of the Nanushuk Formation; Implications to CBM Exploration in the NPRA
Dustin Meisburger	MGE/BS	Various project support

Table 23: University of Arizona student thesis and other work associated with this project
* Project-sponsored MS Thesis

5.3.6.2 Phase 3, Task 6 – UA Final Report Summary

The full UA final report (Table 24, September, 2009 revision, 279pp. with 4 appendices) and associated draft hardcopy files are preserved within project files in BPXA offsite storage in Anchorage and at DOE NETL. Appendix A provides significant excerpts from the University of Arizona final report. Relevant additional work is also described above in Section 5.1.6 and Section 5.2.6.

UA Final Report	#	Pages	Section Accomplishments Summary
Executive Summary	1	12	Summary of 20 key accomplishments (see below) and shallow MPU and KRU stratigraphy, structure, and hydrate distribution
Regional Geologic Framework	2	8	Documentation of robust petroleum system for generation and emplacement of shallow gas hydrate- and associated free gas-bearing fluvio-deltaic and near-shore Sagavanirktok reservoirs
Description of Available Data	3	3	Complete description of available seismic and well data utilized
Processing	4	3	Documentation of GR normalization and seismic processing
Modeling and Synthesis	5	98	Intrapermafrost, base hydrate stability zone, seismic attribute, petrophysical, and neural network modeling and results
Mapping and Analysis	6	106	Characterization of structural, sequence stratigraphic, reservoir, time-slice, faults, seal, and seismic waveform classification
Reservoir Characterization	7	30	Detailed reservoir characterization studies including time-slice net pay maps and gas hydrate/gas AOI volumetrics calculations
Workforce	8	5	Summary of UA staff and studies (also Table 23)
Bibliography	9	4	Summary of publications resulting from these project studies
References	10	10	References cited in these studies
Appendix A	11	7	List of wells used in UA studies and wells used for Net Sand
Appendix B	12	13	Identification of hydrate by expert system and Neural Network
Appendix C	13	5	Sequence stratigraphic framework and 2005 Interpretation
Appendix D	14	9	Coal and paleosol studies

Table 24: UA Final Report Sections and Accomplishments Summary

Significant findings from Phase 1-3 University of Arizona studies (finalized in 2009) included:

1. The structure in the area-of-interest MPU, KRU, and PBU is highly complex with leaky seals
2. Faults extend to surface, which poses risk for both reservoir continuity and seal
3. Seismic analysis reveals that both NS-trending faults NW trending faults extend to surface
4. Both NE-SW and EW trending faults break strata within the gas hydrate-bearing intervals
5. Large faults are imaged in seismic data whereas small faults (less than 45 feet displacement) may significantly segment the reservoir (no modeling has been done on small faults)
6. Stratigraphic horizons are highly compartmentalized and segmented by faults
7. A clay smear factor was assigned to determine fault seal potential in thick reservoir sands
8. Stratigraphic heterogeneity is high, leading to limited dimension of individual reservoir units
9. Gas hydrate-bearing units are thin bedded, laterally discontinuous, and regionally truncated
10. Study area is actively deforming, likely causing gas leakage from hydrate-bearing reservoirs
11. Pull apart basins based on fault morphologies may guide areas of thicker sand deposition and favorable locations for leakage from deeper gas reservoirs into the gas hydrate stability zone
12. Coal horizons and methane hydrate occurrence qualitatively correlate (UA report appendix D)
13. Noticed no irrefutable evidence for discerning difference between seismic imaging of gas hydrate zones versus imaging other lithologic features, given their thin bedded nature

14. Well log distribution was not dense enough with complete sets of logs in the shallow depths (above base of gas hydrate stability zone) to validate response in areas of gas hydrate occurrence and the available 3D seismic data set was limited to within the Milne Point Unit
15. Well log studies and calculations successfully modeled the presence or absence of gas hydrate with an expert system and neural network for interpretation
16. This expert system discerned 316 hydrate layers in 28 wells with 9 feet average thickness and 4 feet median thickness. Neural network identified 65 layers in 15 wells (remaining wells not analyzed) with 10 feet average thickness and 4 feet median thickness. 75% of gas hydrate layers identified within wells were less than 10 feet. B-pad area interpreted as paleosols versus the Task 5 interpreted gas hydrate-bearing zones (UA report appendix D).
17. Interpretations provide detailed Lower Sagavanirktok formation stratigraphic architecture
18. Calculated volumetric estimates of 6.131 trillion cubic feet (TCF) of gas in place in area of interest employed several methods which all revealed lower (approximately half) versus prior USGS gas hydrate and free gas estimates
19. Identified prospective areas within permafrost on western side of Milne Point field based on reservoir sand mapping and recommended future drilling acquire well logs within permafrost
20. Sand and shale are important in picking the base of the ice-bearing permafrost (BIBPF) as the BIBPF and gas hydrate stability zone undulate based on sand and shale content

5.3.7 Phase 3, Task 7 – UAF Drilling, Completion, and Production Studies

Laboratory studies and experiments continued into Phase 3 to characterize gas hydrate in porous media at or near reservoir conditions. From 2002 through 2009, a total of 8 students completed project related studies under this program, including 5 Masters theses (Table 25) supporting Phase 1 tasks 7, 8, 9, 10, and 11; Phase 2 tasks 7 and 10; and Phase 3 tasks 7, 8, and 9.

Name	Dept./Degree/Year	Topic
Namit Jaiswal*	PETE/MS/2004	Measurement of Gas-Water Relative Permeabilities in Hydrate Systems
Stephen Howe*	PETE/MS/2004	Production Modeling and Economic Evaluation of a Potential Gas Hydrate Pilot Production Program on the ANS
Jason Westervelt*	PETE/MS/2004	Determination of Methane Hydrate Stability Zones in the Prudhoe Bay, Kuparuk River, and Milne Point Units, ANS
Prasad Kerkar*	PETE/MS/2005	Assessment of Formation Damage From Drilling Fluids Dynamic Filtration in Gas Hydrate Reservoirs of ANS
Andrew Johnson*	PETE/MS/2009	Experimental and Simulation Studies in Support of the Mt Elbert Gas Hydrate Prospect on the Alaska North Slope
Phillip Tsunemori	PETE/BS/2005	Phase Behavior of Natural Gas Hydrates With and Without the Presence of Porous Media (SPE student paper presented)
Aaron White	PETE/MS	CO2 Injection Grant and 1 semester supporting Gas Hydrate Project
Narender Nanchary	PETE	Research Associate for Gas Hydrate Project

Table 25: UAF student thesis and other work associated with this project
* Project-sponsored MS Thesis

5.3.8 Phase 3, Task 8 – Dedicated Gas Hydrate Well Drilling Program

Well plans were designed and implemented to drill a dedicated gas hydrate stratigraphic test well and acquire data to help determine the feasibility of a possible future Phase 3b long-term gas hydrate production test program. Task 8 work scope included:

- Implement appropriate data acquisition consisting of a drilling and evaluation program based on a single vertical stratigraphic test well with appropriate logging, coring and MDT testing of the previously documented "Mt Elbert" or comparable prospect (Table 4 and figures 7 and 35) within the Milne Point Unit
- Design the field activity to determine the validity of pre-drill seismically-based predictions (Task 5) of gas hydrate occurrence and reservoir quality and to collect other data as necessary to enable a decision whether or not to conduct future dedicated gas hydrate reservoir long-term production testing on the Alaska North Slope
- Maximize synergies with existing and planned ANS developments and either plug and abandon the well before moving off or suspend the well with or without instrumentation for future use as an observation well

5.3.8.1 2005 through 2006 Well Planning Summary

- Completed NEPA Environmental Questionnaire with inputs from BP HSE and Drilling
    - Prepared list of questions and requirements and compiled BP HSE/Drilling input
    - Compiled inputs from newly consigned/constructed Doyon Arctic Fox rig
    - Defined stratigraphic test operation plans as Categorical Exclusion within MPU
- Planned Stratigraphic Test Well and held regular weekly BPXA/DOE/team meetings
    - Developed and implemented task schedules for well permits, materials, plans
    - Identified critical tasks, schedules, and path for well permits, materials, contracts, rig, and ice pad/road; modified task schedules as needed
    - Evaluated drilling and data acquisition risks and developed risk mitigations
    - Developed contacts and contracts with appropriate subcontractors for well permitting, operations, wireline coring, core processing, wireline and MDT evaluation program, and other
    - Prepared and checked surface ice pad/road and bottom hole location (BHL)
        - Discovered and corrected BHL discrepancy
    - Developed agenda, convened, and moderated weekly well planning meetings for Mt Elbert prospect location beginning mid-January 2006
        - Setup planning meetings, agendas, and timelines to accomplish 2006 well
        - Provided task status updates and coordinated well operations and data acquisition plans
        - Developed “statement of risks” document, addressed concerns, and developed plans to mitigate risks
    - Selected ice road route to ensure safe access within existing infrastructure, roads, pads, pipelines, and power lines
        - Evaluated ice pad access from MPU E- and B-pads
        - Selected B-pad route to minimize traffic and infrastructure disturbance
    - Developed detailed wireline and MDT evaluation program with team
    - Determined well casing cementing program with Schlumberger, MPU provider
        - Evaluated alternate Ceramicrete technology, and selected conventional cementing program due to no viable Ceramicrete field tests

        - Met with ASRC Energy Services, Argonne National Lab, BJ Services, and UAF to discuss status of Ceramicrete cement testing (2/1/06)
    - Evaluated drilling mud technology: incorporated DrillCool, Inc. mudchill system
    - Planned core program and wireline retrievable procedures with Corion
        - Planned compatibility of Corion and Doyon Arctic Fox rig equipment
            - Helped ensure 5" RAMS available for hookup to Corion tubulars
    - Initiated planning of core handling and processing program with OMNI Lab
    - Initiated and reviewed detailed plan of operations for well permitting
        - Discussed and reviewed well plans and permits with appropriate industry and State of Alaska representatives
        - Developed and reviewed figures for drilling permit
    - Initiated and reviewed drilling and data acquisition time and cost plans
        - Determined inability to drill well in 2006 due to third party rig delays and approaching end-of-tundra travel and ice seasonal drilling (3/14/06)
        - Notified DOE and subcontractors of decision to defer drilling to 2007
    - Developed, reviewed, and submitted program drilling, data acquisition, and data evaluation budget
        - Identified areas for potential cost savings for desktop and field operations
        - Calculated potential cost savings and evaluated budget options
        - Provided backup documentation for materials, contractors, and budget
- Initiated review of potential alternative, gravel pad options for future stratigraphic and/or potential future Phase 3b production test
    - Prepared and reviewed draft proposal for evaluation
    - Evaluated potential gas handling options for possible future production test well
        - Evaluated potential synergy with Alchem Field Services, Inc – DOE project which developed skid-mounted gas-to-liquid facility
            - Multiple units may be constructed in commercial venture with Waste Management, Inc. and be available for lease by early 2007
            - Units apparently have capability to convert 0.5-2.0 MMCF/d methane into approximately 25-100 BPD #1 low-sulfur diesel fuel
            - Unit construction/operating costs may be up to $3MM; however, leased unit may alternatively be available as demonstration plant

5.3.8.2 Phase 3, Task 8, Initial Mt Elbert Well Planning

In 1Q06, BP Exploration (Alaska) Inc. (BPXA) prepared a Plan of Operations (R15, Appendix B1) to support permit applications to drill the Mt Elbert-01 stratigraphic test well in the northern portion of the Eileen gas hydrate accumulation within the MPU (Figure 35). The surface owner at this location is the State of Alaska and BPXA had valid rights to drill and operate at this site on lease number ADL 255231 within the MPU. BPXA would retain a working interest in the prospect after the well is drilled. Synergies with existing and planned ANS developments were maximized by the utilization of existing BPXA drilling engineering and operations staff to plan and manage the drilling concurrent with ongoing drilling operations within the MPU and adjacent fields. Operations support infrastructure includes the MPU production complex and existing drilling rig service and support contracts. All required environmental permits were obtained under both existing and operation specific permitting criteria and the final permit to drill was obtained from the Alaska Oil and Gas Conservation Commission.

5.3.8.2.1 Drilling Operation Schedule

The initial Plan of Operation called for the Mt Elbert #1 well to have been drilled in March and April of 2006 from an ice pad with ice road access. Regulatory and operational criteria dictated that drilling and plugging be completed by April 30 and site clearance operations be completed by May 15, the end of the seasonal cross tundra travel period. By the end of February 2006, all well design, permit applications, equipment specification and location surveying had been accomplished. Contracts for services were in place and mobilization plans were complete. The drilling rig selected for the project was the Doyon Drilling Arctic Fox rig, which was at the time under contract to another operator, but scheduled to transfer to BPXA for these operations. A BPXA rig contract was prepared contingent upon timely completion of prior wells. In the final week of February and the first week of March 2006, it became increasingly obvious that there were significant delays in rig availability due to drilling operations difficulties for the contracted third-party wells. Support equipment mobilization and ice construction were suspended. By mid-March, it was confirmed that the rig would not be released to BPXA in time to meet the planned operational schedule. On March 16, 2006 the BPXA / DOE project management team reached the decision to defer the program until the 2007 winter drilling season. In early 2006, BPXA re-evaluated the rig selection for this project and chose to utilize Doyon Drilling Rig #14, which was under contract to BPXA. It was anticipated that this rig would be available to begin drilling the Mt Elbert #1 well by early 2007.

5.3.8.2.2 Drilling and Evaluation Program Design

As operator of the Milne Point Unit, BPXA has collected considerable area-specific engineering and operational data relating to drilling mechanics, formation characteristics and reservoir fluids. This data was evaluated and utilized in the engineering design of the Mt Elbert #1 well. It was determined that the well objectives could be met by an up to 4,000 foot vertical hole design using standard MPU drilling engineering criteria. The well design was collated into a Drilling Plan Summary. This summary contained information on all technical aspects of the drilling plan and was the data packet submitted to the Alaska Oil and Gas Conservation Commission (AOGCC) in support of an application for Permit to Drill (AOGCC Form 10-401). On March 6, 2006 the AOGCC issued Permit No: 206-033 (R15, Appendix B2) granting approval of and stipulations to the Drilling Plan Summary.

The drilling procedure sequence did not vary significantly from standard MPU practice. Minor variations for utilizing a Kelly rig and incorporating the mud cooler and wireline retrievable coring equipment were adopted. The general procedure consisted of constructing the location and mobilizing the rig. Surface hole of 12 ¼ inches would be drilled to 1,950 feet and 9 5/8 inch casing would be set and cemented. Next the interpreted gas hydrate-bearing interval from 1,950 feet to up to 2,600 feet would be cored with a 7 7/8 x 3 inch core bit. The hole would then be opened to 8 1/2 inches and drilled out to up to 4,000 feet total depth. Well evaluation logging with electric line tools would be conducted in the open hole and multiple wireline formation tests would be run using the Modular Formation Dynamics Tester (MDT) tool conveyed on drill pipe. The well abandonment would be conducted in conformance with AOGCC requirements and BPXA MPU standard practice. Sections of the open hole would be plugged with balanced cement plugs and cement would be lapped into the casing shoe. The casing would be plugged near the surface and the casing and wellhead would be cut off below tundra level. The location

would be cleared and cleaned to ADEC specification and inspected after the ice pad melts. A Time versus Depth plot for this early well plan is available (R15, appendix B3).

5.3.8.2.3 Well Plan Engineering Detail

Discussion of engineering and operational details of the well plan is presented. Specific design data can be found in the Drilling Plan Summary (R15, appendix B2) and referenced attachments.

5.3.8.2.3.1 Drill Site Location

The Mt Elbert-01 location is 1,242 feet from-north-line (FNL) and 4,183 feet from-east-line (FEL) of Section 30, T13N, R11E UM onshore on State of Alaska lands approximately one half mile east of MPU E-Pad, North Slope Borough (NSB) Resource Development District in the Prudhoe Bay area of Alaska (Figures 49 and 50). The ice road and pad would be constructed on frozen tundra to mitigate potential impacts to wetlands. Water and ice aggregate for ice road and pad construction and maintenance, rig operations, camp and maintenance use would be obtained from permitted sources within the area. Ice construction methods of spraying and flooding would be employed. The ice road to the ice pad would be a spur from MPU B-Pad to the drill site location (Figures 49 and 50). Ice road sections would be of sufficient thickness (6 to 12 inches) and width (50 feet) to provide adequate surface protection and allow safe transport of personnel, equipment, and supplies to the drill site. Ice pad dimensions would be 400 feet by 400 feet and occupy an area of approximately 3.7 acres. Pad thickness would be a minimum of 6 inches or as required for pad leveling and bearing capacity. A working surface of timbers and matting boards would be placed on the ice pad to support the rig structure, and an impermeable plastic membrane would be placed in the well cellar area. Maintenance activities for the ice pad and water source ice roads include plowing, and resurfacing and re-grading with water as needed. The ice structures would thaw during breakup. Security markers and remnant debris would be collected for disposal prior to summer compliance inspection.

5.3.8.2.3.2 Rig Selection

Rig mobilization to the Alaska North Slope is expensive and time consuming. Rig selection was consequently limited to rigs already present in the area. The selection criteria were further narrowed to specify rigs not obligated under existing contracts or involved in pre-established drilling schedules. As the well design is simple and shallow by local standards, rig capabilities were not a significant criterion. It was found that the Doyon Drilling rig Arctic Fox was the only unit that appeared to be available for the project in early 2006, but this was later revised to use the Doyon #14 drilling rig for early 2007 operations (Section 5.3.8.3).

5.3.8.2.3.3 Thermal Modeling and Mud Chiller

The most atypical design criterion for this well is the requirement to minimize the disruption of the thermal regime through the gas hydrate stability zone. This element was critical to the entire evaluation program and especially to the recovery of relatively undisturbed cores from the interpreted gas hydrate-bearing interval. Previous drilling results utilizing chilled mud were reviewed and thermal flux computer models were run. It was concluded that the target temperature for mud going down hole was 2º C. An analysis of the market and availability of qualified rental mud chillers resulted in the selection of Drill Cool Systems Inc. to install and supply a modular mud cooling system like the one used during operations of the 2002 Mallik gas hydrate program.

5.3.8.2.3.4 Coring Technology

The well evaluation program called for continuous coring through the primary zones of interest within the gas hydrate-bearing intervals and quick recovery of the cores in a relatively undisturbed state. Wireline retrievable coring technology including the ability to run drilling bit inserts was required. REED Hycalog Coring Services (Corion) was selected as the vendor for this service. Corion expertise and equipment contributed to the approximately 95-100% gas hydrate-bearing core recovery during the 2002 Mallik gas hydrate program. Detailed equipment specifications and operational procedures were developed for inclusion in the well plan.

5.3.8.2.3.5 Pore Pressure and Fracture Gradient

Pore pressure and fracture gradient were evaluated through analysis of offset well data. Prospect-specific seismic data was reviewed for any indications of pressure anomalies. No unusual indications were noted other than those associated with the interpreted presence of gas hydrate-bearing intervals. The pressure gradient appeared typical for the area at 0.433 psi per foot and the fracture gradient was expected to equal 1.0 psi per foot.

5.3.8.2.3.6 Mud Program

The well would be drilled in two sections. The surface hole to 1,950 feet would be drilled with a fresh water gel mud system. To meet temperature requirements, the final hole section to up to 4,000 feet would be drilled with a potassium chloride-polymer Low-Solids Non-Dispersed (LSND) system with 8% KCl. This concentration would allow mud temperature depression to -3.87 º C. For 2007 operations, the mud for the final hole was revised to a mineral oil-based system to minimize erosivity, enhance borehole stability, and maximize log and core data acquisition (Section 5.3.8.3).

5.3.8.2.3.7 Casing Program

In order to utilize existing casing inventory and to accommodate the coring and MDT logging tool assemblies required for the evaluation program, a standard MPU casing design was selected (Figure 48). Twenty inch conductor would be set at 80 feet subsurface. A 9 5/8-inch casing would be set at 1,950 feet, just above the interpreted gas hydrate-bearing coring interval. A 7 inch contingency liner would be available if hole conditions required isolating the permafrost section and/or the gas hydrate-bearing section prior to MDT logging operations.

5.3.8.2.3.8 Cement Program

The standard surface casing cement utilized in the MPU is formulated to be mixed with 70 º F water. This would enable the slurry to set at the sub-freezing temperatures in the permafrost region. The setting process is an exothermic reaction and a significant amount of heat is released. Laboratory tests to determine the effects of lowering the mix temperature were conducted. It was noted that no significant reduction could be made without adversely affecting the setting time and compressive strength build rate of the slurry. It was decided that the ArcticSet cement, which was available from the contracted service company, should be used in its normal fashion. If unacceptably high temperatures were to occur in the well after cementing, chilled mud would be circulated prior to further drilling into the interpreted gas hydrate-bearing interval. An alternative cementing program was considered using the experimental “Ceramicrete” cement under development as discussed above. However, this cement had not yet completed yard testing, a necessary precursor to field testing. If future field testing of this cement were to occur,

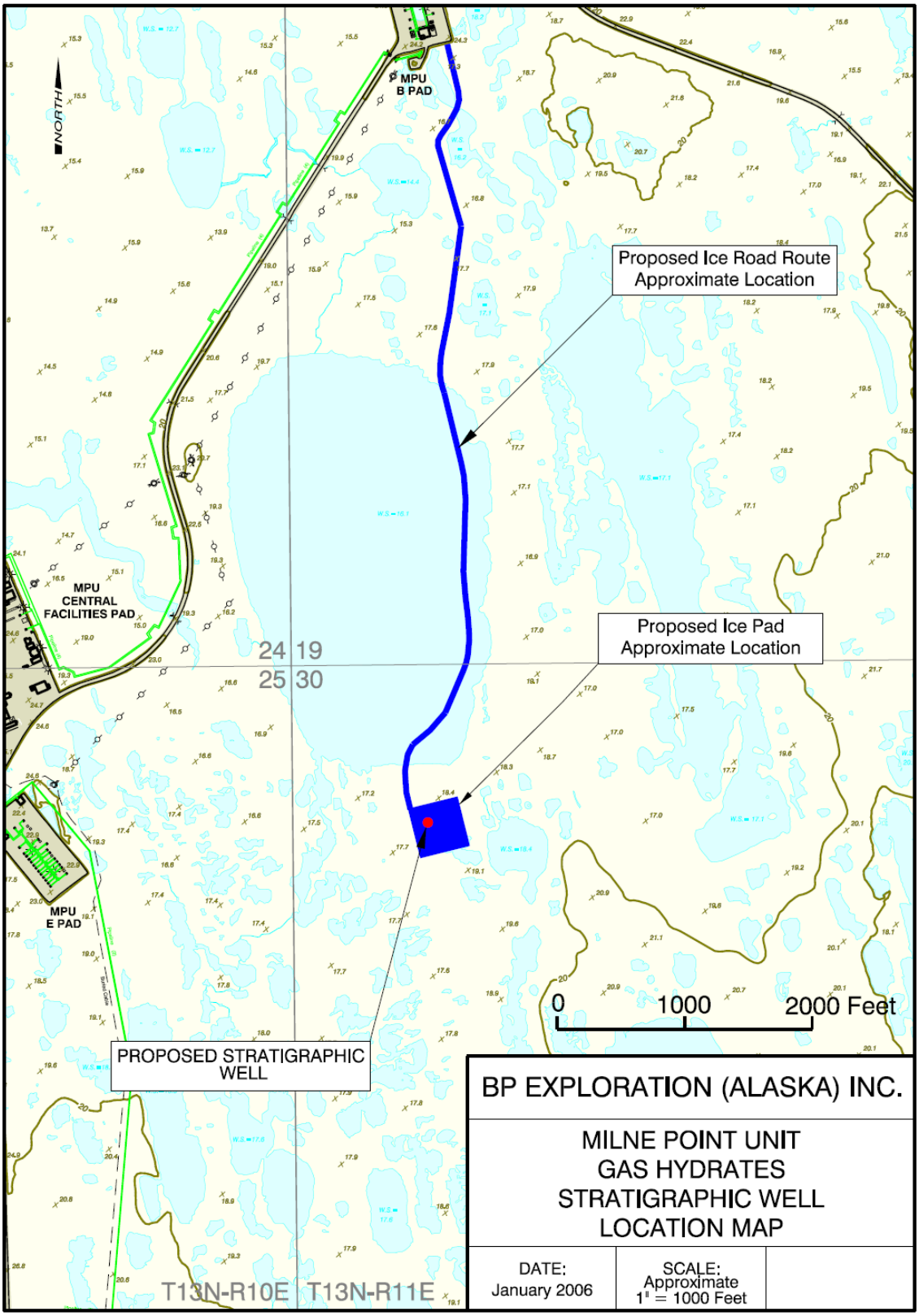

Figure 49: Mt Elbert-01 Stratigraphic Test Well Location Map Showing Ice Road and Pad

Figure 50: Aerial view of Mt Elbert Ice Pad and Road Location

then it is recommended the cement is first attempted on a well conductor, second (if conductor successful) on a well surface casing, and third (if surface casing successful), on a later well production casing. Advantages of this experimental cement may include minimizing formation and/or annular space damage while maintaining gas hydrate temperature stability during completion operations.

5.3.8.2.3.9 Drilling Mechanics and Bit Program

The Doyon Arctic Fox rig was a mechanical drive unit with a kelly rotary rather than a top drive. It was planned to utilize standard rotary bottom hole assembly design and a 12 ¼ inch milled-tooth tricone bit in the surface hole to 1,950 feet. The intermediate interval would be rotary-cored with a 7 7/8 inch core bit to 2,600 feet and then opened to 8 1/2 inches and drilled to total depth of up to 4,000 feet with rotary equipment and a milled-tooth roller bit. Drilling mechanics and mud hydraulics were based on standard practice.

5.3.8.2.3.10 Well Control

The maximum anticipated bottom hole pressure and maximum surface pressure were calculated to be 1,740 psi and 1,340 psi, respectively. A standard 3,000 psi Blow-out Preventer (BOP) stack would be utilized and all well control procedures consistent with AOGCC regulations and BPXA standard practice would be utilized. A formation integrity test would be performed after drilling out the surface casing shoe. Chilled mud, proper hole cleaning and controlled drilling rates would be used to control gas breakout from drilled gas hydrate-bearing reservoirs. A wireline BOP, circulating sub and packoff would be utilized when retrieving cores.

5.3.8.2.3.11 Drilling Hazards and Contingencies

The drilling and coring of highly-saturated gas hydrate-bearing intervals presented a potential severe hazard in this well. Gas hydrate was interpreted to be present from the base of the permafrost to approximately 2,850 feet Measured Depth (MD) at this location. Early mud system design specified a 8% KCl LSND system which would have had a thermal crystallization temperature of -3.78ºC. Operating temperature of mud being pumped down hole would have been maintained at 2.0ºC. Circulating temperature, mud chemistry and drilling mechanics would have been optimized to minimize gas hydrate dissociation while maintaining primary well control. All circulating system components would have been monitored and actively protected from freeze up, both while circulating and during static periods. Cores would be allowed to pressure stabilize below the wellhead and flow checks would be conducted prior to continuing the retrieval and opening the wireline riser to lay down cores. The core would be laid down, removed from the floor, sectioned, and containerized at sub-freezing temperatures. All core storage and any onsite geoscience or analytical studies would be conducted in a refrigerated, containerized unit remote from the wellbore.

The risk of stuck pipe, pack off or lost circulation was mitigated through BPXA and industry standard drilling practices. Proper drilling mechanics and operational techniques, mud chemistry and adequate hole cleaning would be exercised to minimize these risks. Hydrocarbons in the form of methane hydrate were expected from the base of the permafrost through the base of the gas hydrate stability zone at ± 2,850 feet. Neither liquid hydrocarbons nor free gas hydrocarbons were anticipated in any drilled section. No faults or hydrogen-sulfide-bearing intervals were interpreted for the well location and there were no anti-collision issues with existing wellbores.

5.3.8.2.3.12Evaluation Program and Data Acquisition

Much remains unknown regarding gas hydrate-bearing reservoir sand petrophysical properties and lateral continuity based on sedimentary characteristics and depositional environment. Although the gas hydrate stability zone has been safely and successfully penetrated by hundreds of wells within the AOI, the primary targets of these wells are deeper, oil-bearing reservoirs and very few of these wells have specifically acquired complete data sets within the gas hydrate-bearing intervals of interest to this study. Furthermore, since ANS oil reservoir development occurs from centralized gravel pads which access these deeper reservoirs through directional drilling, the data collected within shallow sands (500-2,500 feet below surface) is typically only within a few hundred feet of the gravel pads since most wells do not begin to build angle until near or below the base of ice-bearing permafrost (approximately 1,800 feet below surface). Prior to this effort, the last dedicated well to acquire data within gas hydrate-bearing reservoir sands was the Northwest Eileen-02, drilled in 1972. That well acquired a few feet of conventional core data and tested several zones using Drill Stem Testing (DST) techniques (Figure 51).

The possibility to induce in-situ gas hydrate dissociation through producing connate waters from within an under-saturated gas hydrate-bearing reservoir establishes saturation and permeability as key variables which, when better understood, could help mitigate productivity uncertainty. Approved field operations were designed to enable acquisition of gas hydrate-bearing reservoir data within Phase 3a studies (2006-2007). A key part of this analysis was targeted acquisition of cores and wireline logs within gas hydrate-bearing reservoir sands and associated sediments. The wireline logging was planned to include Modular Dynamic Testing (MDT). Analyses of these core, log, and MDT data were designed to help reduce the uncertainty regarding gas hydrate-bearing reservoir productivity. The Mt Elbert-01 well was planned to be a vertical penetration from an ice pad located directly above the Mt Elbert gas hydrate prospect within the MPU. The vertical well design facilitated safer and more successful acquisition of core, log, and MDT data as illustrated in the type log from MPE-26 (Figure 52).

One of the most diagnostic tools indicative of shallow gas hydrate-bearing sands is the mud log with gas detection. Mud logs were planned to be acquired in the surface and production holes to help identify gas hydrate-bearing sands within the gas hydrate stability zone. The base plan for log data acquisition during drilling operations (LDD) was planned to be limited to gamma-ray, resistivity, and directional at the bit to facilitate correlating stratigraphy, picking surface casing point near base permafrost, and selecting core intervals. The chilled drilling fluids were designed to maintain the stability of the gas hydrate-bearing zones and preserve the integrity of the wellbore, allowing high-quality wireline log and MDT in-situ data acquisition. However, MPU field well operations experience in wells drilled without chilled fluids suggested adding a full suite of logging-during drilling (LDD) tools, including NMR, dipole sonic, and acoustic caliper through the production hole, as a contingency in case hole stability problems occur and since acquisition of log data remains a high-priority objective for this project. The base plan was to acquire only limited LDD data with full-suite open-hole wireline data acquired after the core is cut and the well drilled to total depth (TD). An alternate contingency LDD program could be implemented in recognition and risk-mitigation for the potential for hole stability problems to develop during the several days required for coring and drilling to TD. As of 2006, field experience indicated that attempts to acquire data with the Schlumberger LDD CMR+ tool do not yield the data quality of that acquired with the Halliburton LDD NMR tool; Schlumberger’s

wireline dipole sonic was considered to be better than the Sperry-Sun LDD BAT sonic for low velocity shear wave data acquisition; and Baker Hughes INTEQ has a full waveform LDD sonic (the older APX model did not deliver as high a data quality as was expected in early trials, but the redesigned tool was supposed to work better in this environment). There were also alternative ways to design this program to eliminate all wireline except the MDT, but this was not the primary plan.

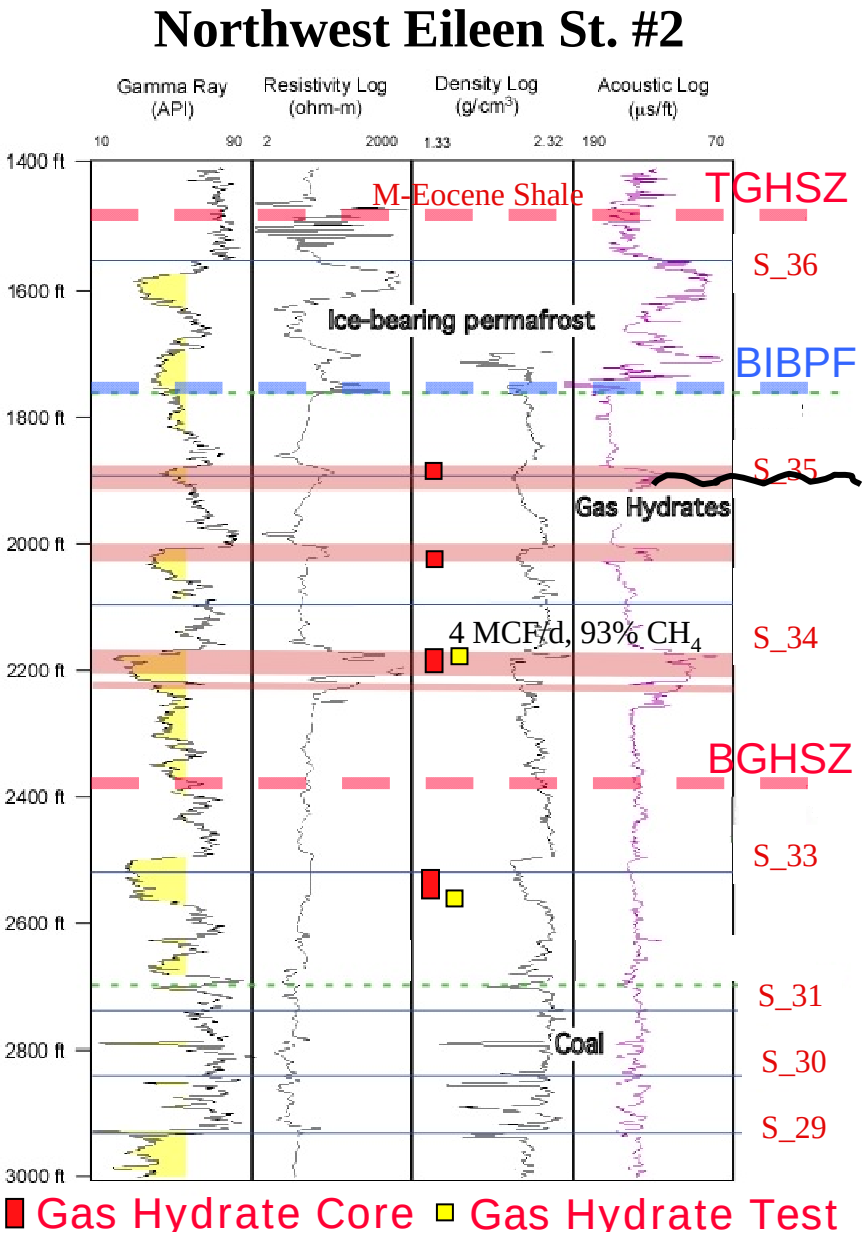

Figure 51: Northwest Eileen State-02 Type Well and data acquired within gas hydrate-bearing zones of interest.

Drilling a near-vertical well and maintaining borehole stability with chilled drilling fluids was planned to help enable acquisition of quality log and core data within the interpreted gas hydrate-bearing intervals and associated sediments. No studies of significant ANS gas hydrate-bearing

porous media had been made in the past. From 400-600 feet of continuous core was planned within the interpreted reservoir sands and associated sediments within the gas hydrate stability zone (Figure 52). Wireline coring was planned to facilitate quick core acquisition and tripping to help preserve gas hydrate-bearing core once overburden pressures are removed during core recovery to surface. Analyses of core was planned to include petrophysical, mineralogical, depositional environment, and select sampling for experimental studies, including phase behavior, relative permeability, formation damage, geomechanical, and other assessments.

An optional drill stem testing program was considered, but rejected due to abandonment and cost concerns regarding downhole electrical submersible pump (ESP) cables and equipment on an exploration ice pad.

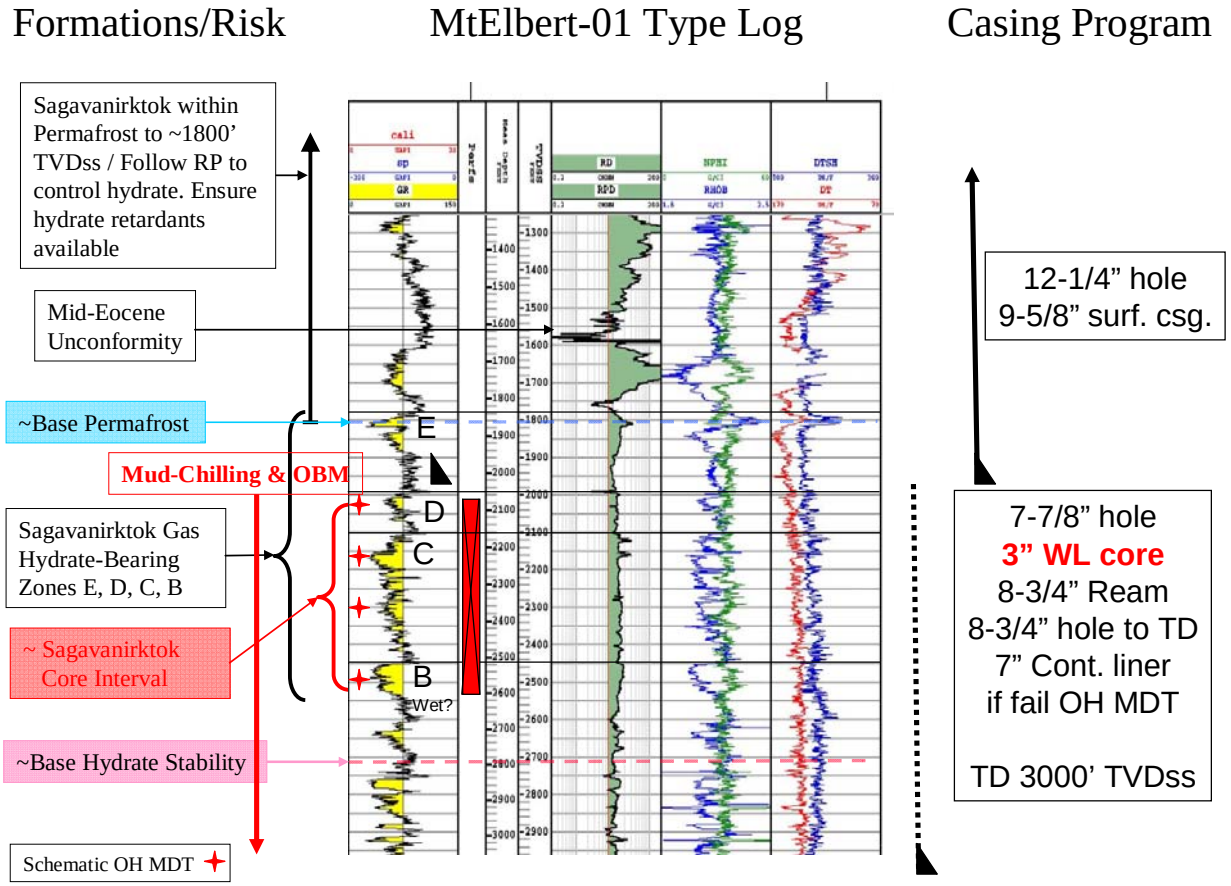

Figure 52: MPE-26 Type Log showing planned intervals of wireline log and core data acquisition between Base of Ice-Bearing Permafrost (BIBPF) and Base Gas Hydrate Stability Zone (BGHSZ) and showing planned drilling/casing program

5.3.8.3 Phase 3, Task 8, Final Mt Elbert Well Planning

Pre-operational drilling engineering, permitting and equipment selection for the Mt Elbert #1 stratigraphic test well was complete at the time of project deferral in March 2006. The deferral, combined with the change in drilling rig selection, resulted in several issues which were addressed before 2007 operations could commence. These considerations and required actions are summarized in this section.

5.3.8.3.1 Final Mt Elbert Well Plan Summary

Following project deferral, the well was listed on the BPXA drilling schedule for drilling by Doyon Drilling Rig #14 beginning in early 2007. Before resuming activity, permits were reviewed and updated and the application for Permit to Drill was modified to reflect a change in drilling rig assignment. The well plan engineering and operations procedures were reviewed with the rig assignment to Doyon 14. The priority of objectives were: 1. Wireline Logging, 2. MDT Pressure Testing, and 3. Core Acquisition. Core acquisition, processing, and transportation plans were prepared as additional documents in support of the well planning documentation for this well. Lessons learned from previous gas hydrate-bearing cored wells, such as the Mallik 1998 and Mallik 2002 onshore and certain offshore research programs were incorporated into the well plan. In September, 2006, 27 project and supporting staff attended a core program workshop held to address core operations plans, concerns, and risk mitigation contingencies. Detailed notes from this workshop were reported in R16, pp. 20-26.

The program was designed to deliver the primary objectives identified by the Gas Hydrate project research team and by the MPU development team; it was reviewed and refined through a number of meetings leading up to well spud in early February 2007. In addition, Job Risk Assessments (JRA) and dry-run pre-operations onsite training were conducted prior to and during the wireline coring, logging, and MDT operations on the Doyon-14 rig.

Mt Elbert-01 was the first of three (2 were non-hydrate) planned appraisal wells to be drilled in MPU during the 2007 ice-pad exploration season. The objectives of the well included acquisition of approximately 400 to 600 feet of low invasion 3-inch whole wireline-retrievable core, wireline logging, and MDT testing within 2-3 interpreted gas hydrate-bearing Sagavanirktok reservoirs beneath the permafrost within the Eileen gas hydrate accumulation to improve reservoir characterization and resource determination. This program was planned to acquire the first conventional rig wireline core on the Alaska North Slope using an improved version of the ReedHycalog (Corion) Wireline Express tool that successfully retrieved, via wireline, the inner core barrel through the drill string in the Mallik 2002 gas hydrate project. A separate coring protocol document (R17, appendix B) gives technical justifications and methods for acquiring, subsampling, transporting, and storing core to meet the project objectives.

In addition, the layout of the mud cooling and coring equipment was integrated with the newly selected rig. This work was accomplished and equipment lists finalized significantly in advance of equipment being mobilized from California and Canada, respectively. All service companies were contacted to ensure current contract status and availability of required equipment and personnel. The well plan engineering and operations procedure were reviewed in light of the change in rig assignment. In particular, the change from a kelly rotary to top drive system affected both specification of down hole drilling assemblies and specific operational sequences.

The final Operational Well Plan incorporated all equipment specifications, operational sequences and specialized service procedures, and was completed well in advance of rig mobilization to the location in February, 2007. The well planning team included experts on gas hydrate, well operations, and data acquisition from BPXA, USGS, and DOE NETL working with staff from the drilling rig contractor (Doyon), core acquisition company (National Oilwell Varco, formerly ReedHycalog), core handling and analyses company (Weatherford, formerly OMNI), water

chemistry and microbiology research group (Oregon State University), wireline log and pressure testing experts (Schlumberger and RPS Energy), and gas geochemistry and physical properties experts (USGS). Together, this team safely accomplished project data acquisition objectives through extensive planning, risk assessments, and risk mitigations.

5.3.8.3.2 Mt Elbert-01 Core Program Objectives

Core acquisition was planned to provide critical information on reservoir quality, interpreted reservoir lateral continuity, reservoir fluids, hydrocarbon in-place, resources, potential deliverability, well placement and drillability:

- Confirm gas hydrate and reservoir characterization interpretation
- Obtain whole-round cores for porosity, permeability, and fluid saturations determination for log calibration, and potential resource assessments
- Sample mineralogy and lithology for log calibration, and understanding formation physical and mechanical properties
- Sample gas hydrate and pore water geochemical and microbiological properties to understand the origin of gas hydrate and implications for vertical and lateral compartmentalization within variable lithologies
- Sample biostratigraphic markers to aid in constraining and/or defining regional stratigraphic correlation horizons

Specific post-well core studies were designed to include the following:

- Core-derived Rw/Sw (gas hydrate-in-place)
- Sedimentology (well placement, reserves)
- Poroperm (reserves, well productivity)
- Reservoir quality (well placement)
- High resolution biostratigraphy (well placement)
- Vertical and horizontal heterogeneity description (compartmentalization, depletion plan)
- Coreflood tests (relative permeability, well productivity)
- Petrophysical tests (gas hydrate-in-place, well productivity)

Primary risks, impacts, and mitigations to good coring performance and the overall well objectives on Mt Elbert-01 were detailed in a Core Risk Register. The top 6 risks included:

1. **Stage:** Planning and preparation / **Risk**: Coring equipment and personnel not available when needed (Corion's wireline system, Drill Cool mud chilling system, USGS/DOE equipment and supplies, Core trailers) / **Impact**: Unable to core well, possible rig standby waiting on equipment / **Mitigation**: Prepare detailed coring plan. Work with vendors to confirm equipment and personnel are available (and properly certified and trained for ANS methods and operations). Prepare checklist and distribute. Prepare checklist for training and ANS clearance.
2. **Stage:** Planning and preparation / **Risk**: Coring procedure and processes and core handling procedure poorly understood leading to HSE incident / **Impact**: Cannot proceed with work or HSE impact / **Mitigation**: Proper Front-End-Loading (FEL) planning and documentation, proper Authority-to-Proceed (ATP). Proper JSA/JRA at rigsite pre-core with dress rehearsal. Detailed coring pre-spud on rig with rig and coring crews.

3. **Stage:** Operations **/ Risk:** Mud chiller fails / **Impact:** Cannot proceed with drilling/coring well, poor data acquisition, poor borehole conditions, loss of borehole, potential well control issue / **Mitigation**: DrillCool equipment must be checked out and working ahead of time, and working at Doyon 14 location on ice pad prior to well spud in early February, 2007.
4. **Stage:** Operations **/ Risk:** Core point picked too shallow or too deep (core point based on isopach ahead from casing shoe) / **Impact:** Core the wrong interval. Pick too shallow and not enough time to obtain up to 600-feet of cored interval. Pick too deep and drill up desired cored interval. Not enough contingency time to have mis-picked core point / **Mitigation**: Have rig geologists and USGS/DOE in agreement for core point.
5. **Stage**: Operations / **Risk**: Swabbing during POOH / **Impact**: Well control incident / **Mitigation**: Prepare tripping guidelines to include maximum speed per wireline run, pump out of open hole. Model swab prior to coring and develop tripping schedule. There is a great deal of flexibility here. If the top valve on the diverter sub is closed, wireline can be pulled at up to 200 feet per minute and likely will not swab the well. If the valve is left open, then approximately 10 gallons may be swabbed. There is no perceived downside to leaving the valve closed and pulling at the above rate. The rates are dealing with gas expansion in the core, if no free gas is expected, then pulling at 200 feet per minute could occur with minimal to no swabbing.
6. **Stage**: Operations / **Risk**: Gas liberation at rig floor / **Impact**: HSE incident, poor core quality / **Mitigation**: Prepare tripping guidelines to include maximum speed per stand and per #5 Corion input. Use chilled MOBM to maximize borehole stability and to enhance data acquisition.

Additional concerns included, but were not limited to:

- Core jam within semi-consolidated water-bearing Sagavanirktok reservoir sands
- Poor recovery of the gas hydrate-bearing reservoir intervals
- Poor displacement of water based drilling mud with oil-based coring fluid or excess water in MOBM system
- Borehole problems due to mud-chilling difficulties or gas dissolution from gas hydrate or associated free gas-bearing formations
- Core face obscured by opaque oil-based mud with black Gilsenite additive causing difficulty in subsampling

All Risks to coring performance were examined in detail and prevention/mitigation agreed with the operations team during the pre-coring risk register assessment. Above all, Mt Elbert-01 coring operations must be done without hurting people or damaging the environment in any way. BPXA HSE practices will be rigorously followed at all times.

5.3.8.3.3 Mt Elbert-01 Logging Requirements

A primary objective of the stratigraphic test was to acquire high-quality wireline logs across the interpreted gas hydrate-bearing intervals of the shallow Sagavanirktok reservoir sands and shales. Since the well was planned to be near-vertical, wireline logs were planned to acquire high-quality gas hydrate-bearing reservoir petrophysical data, provided that the mud-chilling operations maintained adequate borehole stability and in-situ conditions (preventing borehole washouts and gas hydrate dissociation during drilling, coring, and data acquisition operations).

Wireline logs would be run from approximately 1,950 to 3,000 feet (or TD) in the "production" hole below surface casing below BIBPF as shown in Figures 51-52.

The MPU E-26 type log (Figure 52) is directly beneath MPU E-pad within the shallow zones of interest, approximately 1,500 feet west of the proposed Mt Elbert-01 well location (Figures 49-50). Wireline logs planned would include gamma-ray, resistivity, neutron-density in the "platform-express" along with dipole sonic (with shear wave data), nuclear magnetic resonance (NMR), RtScanner, and oil-based formation micro-imager (OBMI) to help determine gas hydrate-bearing reservoir properties. Planned data acquisition is summarized in Table 26.

Wireline Logging Runs from Surface Casing to TD
Run-1
PEX - Platform Express
AIT - Array Induction-SP Log
RtScanner (AIT or RtScanner)
Electromagnetic Propagation Tool (EPT) Log
Run-2
DSI - Dipole Shear Imager Log - expert mode; stonely
GR - Gamma Ray Log
OBMI - Formation MicroImager for oil-based mud
Run-3
CMR - Combinable Magnetic Resonance Tool
NGT - Spectral Gamma Ray Log
ECS - Elemental Capture Sonde
Run-4
MDT Open Hole – 2 test points per sand (2 sands expected) – up 10 hrs/each; 7-inch cased hole MDT contingency

Table 26: Planned Wireline Logging Runs

5.3.8.3.4 Mt Elbert-01 MDT Pressure Testing Requirements and Procedure

During the 2002 Mallik gas hydrate program, Modular Dynamic Test (MDT) data provided valuable insight into the potential productivity of gas hydrate-bearing reservoir sands. These tests revealed for the first time that movable connate waters could be produced through the MDT tool within gas hydrate-saturated reservoir sand intervals. This revelation may importantly indicate an ability of the gas hydrate-saturated reservoir to transmit a pressure pulse with offtake of mobile connate waters. The Mt Elbert-01 open hole, dual packer MDT tests were expected to yield important data regarding gas hydrate-bearing reservoir connate water mobility, permeability, relative permeability, dynamic permeability (changing during dissociation of gas hydrate), and other data in combination with core and wireline logs. Analysis of this data was anticipated to help promote a better understanding of the potential productivity and potential production methods of these gas hydrate-bearing reservoirs. Three to four separate MDT sites within 2-3 interpreted gas hydrate-bearing reservoir sands were anticipated to be tested for up to 10.5 hours per test (Figure 52).

The MDT plan was flexible to account for onsite interpretations and an ability to conduct pressure tests both within and outside gas hydrate equilibrium conditions. The MDT tool basically allows a limited down-hole production test, which can yield this very important data.

MDT testing was planned for a dual-packer, open-hole approach. This approach is commonly run on the North Slope, but had never before been attempted anywhere within a gas hydrate-bearing interval in an open hole. A contingency 7-inch liner was planned to allow running MDT in cased hole should the preferred open hole method have unacceptable operational difficulties. Planning meetings held with Schlumberger MDT experts in Houston included the team that designed and implemented the Mallik 2002 MDT program. The head of the Mallik 2002 MDT testing program, Steve Hancock, APA Engineering, was onsite to help maximize data acquisition and flexibility. MDT results were planned to be applied to reservoir model calibration to help understand the importance of gas hydrate-bearing reservoir relative and dynamic dissociating permeabilities, all very important parameters to modeling of production potential.

The onsite criteria evaluated for selection of MDT test intervals included:

- MDT tool packer section 9 feet overall length (2 x 3-feet packer elements with 3 feet spacing in between packers)
- Do not set packer in previous disturbed area
- Uniform sand quality and reservoir saturation preferable
- Sufficient separation of test intervals so all tests conducted in undisturbed gas hydrate
- Packer set 3 feet minimum away from water zone (tool inlet 6 feet from water)

The sequence of MDT test procedure included:

1) Safety Meeting: Review wireline log operations, job responsibilities, and job hazards
2) Setup MDT logging tool, stub lubricator, and wireline BOP's; Pressure test to 2,000 psi with 40/60% water/Methyl Ethyl Glycol (MEG); Run-In-Hole on Drillpipe and log on depth using GR at first MDT test interval
3) Monitor MDT tool temperature read-out until rate of tool temperature change <1 ^{o}F/hour Expected duration: 1-2 hrs
4) First MDT Packer test Procedure: Move MDT tool to the first straddle packer gas hydrate test interval. Set packers and test seal. Initiate flow using Pump-out sub (POS) to remove mud, filtrate (if any) and reservoir fluids.
    - First flow period planned for 10 minutes or until gas and/or formation water has been detected. Maintain pressure at or below stability pressure while pumping. Shut in if pressure drops below 300 psi while pumping. The first build-up period will be 3-times the flow period duration.
    - Second flow period planned for 50 minutes. Maintain pressure at or below gas hydrate stability pressure while pumping, and at a lower pressure than during flow period 1 if pump control allows. Shut in if pressure drops below 300 psi while pumping. The second build-up period is planned for 100 minutes.
    - Gas and/or water samples will be taken early in the second flow period when near steady state flow conditions have been obtained, or as directed.
5) Subsequent MDT Packer test Procedure: Move MDT tool to the next straddle packer gas hydrate test interval. Set packers and test seal. Initiate flow using POS to remove mud, filtrate (if any) and reservoir fluids. Note that the second and subsequent MDT straddle tests may include optional fluid mobility and fracture (pump-in/break-down) testing
    - Optional: Conduct a mobile fluids test by pumping slowly (or on-off operation) keeping the sandface pressure above gas hydrate stability point. Continue pumping

well until reservoir fluids are identified. Mobile formation water sample(s) may be taken and followed by a build-up period depending upon reservoir response.

- First flow period planned for 10-15 minutes or until gas and/or formation water has been detected. Maintain pressure at or below gas hydrate stability pressure while pumping. Shut in if pressure drops below 300 psi while pumping. The first build-up period planned for 6-times the flow period duration.
- Second flow period planned for 60-120 minutes. Maintain pressure at or below hydrate stability pressure while pumping, and at a lower pressure than during flow period 1 if pump control allows. Shut in if pressure drops below 300 psi while pumping. The second build-up period will be 2-times the flow period or as directed.
- Gas and/or water samples will be taken early in the second flow period when near steady state flow conditions have been obtained, or as directed.
- Optional: Conduct fracture stimulation test. Release and re-set packer elements (to release free gas in the near wellbore area). Reverse POS and pump into the hydrate interval to initiate a fracture. Step up pressure slowly in 250 psi increments. Shut-in and monitor fluid loss for approximately 10 minutes at each step. Continue until fracture initiation is observed. After the fracture is initiated, pump approximately 0.5 gallons at maximum rate to extend the fracture and Shut-in. Monitor pressure fall-off for approximately 15 minutes or until fracture closure is not observed (or as directed).

6) MDT Probe test Procedure (Optional): Move MDT tool to the first probe hydrate test interval. Set probe and test seal. Initiate flow using POS to remove filtrate (if any) and reservoir fluids. Flow until gas and/or water is detected and temperature trend has been established (or as directed depending upon formation response). No samples will be taken during probe tests. Shut-in will be for approximately 30 minutes or as directed. Release probe and move tool down to next interval and repeat as directed if time permits.

5.3.8.3.5 Mt Elbert-01 Operations Safety, Selected Notes

Chilled (0 to 4 degrees Centigrade) mineral oil-based mud drilling fluid is critical to maintaining borehole stability, safe operations, and high-quality data acquisition. Coring is a non-routine activity; most of the below safety considerations, therefore, apply primarily to the coring operations and associated activities.

- Pick core point within interpreted gas hydrate-bearing reservoir section
- Geologists, mudloggers, and driller work closely together to ensure effective well control
- During wireline retrieval of core, care must be taken to not “swab” excessive pore fluids up the drill-string as this interval has not been penetrated at this location and the exact nature of the pore fluids, while interpreted to contain gas hydrate, is not known; pore fluids may include water, gas hydrate, and/or free gas
- Well control and assurance of delivery of the total objectives of the well will take precedence over geological core acquisition and termination criteria
- Coring will commence in open reservoir and well control requirements take precedent over technical recommendations made for improved coring practice
- Coring is not a routine activity, the coring engineer, core specialist, core shift team leads, and BP Operations Geologist will lead Job Risk Assessments (JRA’s) and discussions with

the rig crew involved to ensure that safe and effective procedures are used before picking up the core barrel and beginning coring

- JRAs will be reviewed with each crew as program and shift changes occur
- The core barrel will be large diameter within drillpipe; therefore, calculate the wireline-retrievable tripping rates to prevent swabbing
- Normal drillfloor procedure for safe tripping and wire-lining is required
- The reservoir sections may be cored with moderate overbalance so the adoption of procedures to avoid differential sticking of the coring assembly is essential until BHA is safely tripped into the surface casing
- All core handling presents a manual handling risk and requires careful review with the team to eliminate or minimize risks; a manual handling refresher training will be held with the team before the first core is handled and will be refreshed as required
- Any misalignment of the inner tube during the cutting and the application of the shear boot may result in dropping the core onto the drill floor; therefore, this activity must be conducted with great care
- Stringent precautions for heavy lifting must be followed with care; this is one of the most potentially dangerous parts of the whole coring operation
- Gas monitoring (sniffers) will be provided by BP HSE in the core processing trailer(s) to provide assurance for electrical or non-intrinsically safe equipment operations during hot-work permitted operations; detailed protocols will be developed onsite during JRA's
- Core handling will involve cleaning oil-based mud from the outside core surface; use proper PPE, wiping rags, and rag disposal to eliminate environmental impacts
- The core will be cut with chisel and hammer; proper PPE and precaution must be used to avoid rock chipping hazard and potential eye damage
- Certain subsamples will be removed from the Corion processing trailer, marked with Styrofoam insert, and destroyed in the Core Press to obtain pore water samples; drill press operation, while simple, must employ proper use and adequate cleaning between samples
- Apply appropriate caution to required compressed air line for the presses in the geo trailer; note that if air line is needed to the cold trailer that it will not last very long in cold environment (i.e. pneumatic saw to cut inner barrel tabs)
- Apply appropriate caution to required outdoor methane and nitrogen stations near the core trailer; stabilize methane and nitrogen bottles using a standard bottle rack assembly which is protected from the elements by placing them on the leeward side of the trailer and possibly constructing a temporary shelter, if needed
- Core barrels have tabs which require cutting using a small abrasion air saw which must only be used by qualified operators (suppliers) with appropriate personal protective equipment including gloves, goggles, dust mask and earplugs; all non-essential staff should stand clear; a hot-work permit must be maintained for electrical equipment in the presence of potential out-gassing from gas hydrate dissociation of the core
- Core processing is a non-routine activity; pre-job briefings and training will also be provided to any staff who temporarily assist (e.g. rig crew, mudloggers)

- Team work hours will be monitored and a 12-hour shift system implemented with a maximum of 16 hours worked for each of 2 12-hour 6-man shifts; the team of 12 is needed to maintain safe work hours for 2-3 days of successive 24 foot core acquisition, with approximately 90 minutes between cores and with a 30-90 minute shift change-over time required, depending on operations and difficulties
- Core acquisition turn-around is expected to take 75 to 90 minutes per 24 foot core with the Corion system at optimum usage; core processing and subsampling is estimated to require 60 minutes per 24 foot core
- The planned Mt Elbert-01 core operation will be the longest yet in MPU experience with up to 600 feet of core (25 24-foot cores); change out of team members over the anticipated 2-3 day coring time will be managed to minimize loss of learning and impact of handover
- A number of air-lines and power cables will be routed to the core processing area and these must be properly located and connected; they must not constitute a trip hazard
- All core processing activities must be discussed with and approved by the BPXA Drilling Supervisor before work begins; proper permits must be obtained for any specialized procedures and equipment and proper BPXA authorization is required for special required equipment such as power saws, centrifuge, rock press, etc.

5.3.8.3.6 Mt Elbert-01 Mudlogging Requirements

Mudlogging requirements for the planned operations include:

- Mudlogging interval is from surface to TD (~3,000’ TVDss)
- Gas detection and Gas chromatograph is required from surface to TD
- Catch and describe samples at: 60 foot spacing from 0-1,900’ TVDss (Surface Casing Point) and at 30 foot spacing from 1,900’ TVDss to TD
- Head space gas samples
- Reporting requirements (regular morning report and lithology/gas logging)
- Washed cuttings for the State per State AOGCC requirements for exploration ice pad
- Aerosol cans and isotubes in production hole only where gas shows 5 times over background and additional samples every 10 feet in the anomaly
- Recommend paired samples (i.e., one aerosol can and one isotube together) on every gas anomaly about 5 times over background
- Obtain drill cutting samples for geochemical analysis and preserve the samples in pint or quart size paint cans; collect cuttings directly from the shaker table with a trowel as a single "grab" sample not a composite of the entire interval
- Gas sampling summary:
    - Collect cuttings directly from the shaker table using trowel
    - Place cuttings in pint size can and fill can to half full (do not add water)
    - Add a teaspoon of table salt, which is acts as a bactericide (provided), to cuttings
    - Wipe can rim clean and seal can with lid
    - Label can (depth and well name), both on the side and the bottom of the can
    - Turn the cans upside down and freeze
    - Ship samples in provided coolers and maintain samples as frozen, if possible

5.3.8.4 Mt Elbert-01 Operations, Data Acquisition, and Results Summary

Mt Elbert-01 operations accomplished all major research objectives outlined above and included safely drilling and acquiring all recommended Phase 3a stratigraphic test well data. Acquired data included 430 feet core (100 feet gas hydrate-bearing), extensive wireline logging, and wireline pressure testing operations using the Modular Dynamic Testing (MDT) downhole tool. Significant pre-well planning, inclusion of world hydrate experts, and onsite vigilance were key elements to safely drilling and acquiring this data in February 2007 at Mt Elbert-01 within the Milne Point Unit using the Doyon 14 rig on an exploration ice pad (Figures 49, 50, and 53). Chilled oil-based drilling fluid mitigated operational safety concerns by maintaining gas hydrate and borehole stability during openhole drilling and data acquisition operations. The use of this mud chiller, operated by DrillCool, Inc. (Figure 54), was a key element to the successful acquisition of both core and log data. The chilled mineral oil-based drilling fluid was cooled to approximately -1^{o}C (30^{o}F) and when coupled with borehole conditioning and good drilling practices provided an in-gauge, stable borehole which enhanced stability of both gas hydrate and water-bearing sediments during drilling and extensive data acquisition operations. After setting surface conductor pipe, the surface hole was drilled to 1,952 feet measured depth (MD) where the 9-5/8-inch surface casing and core points were picked from LWD correlation to shallow sections in nearby wells. Table 27 summarizes LWD logs and Bottom Hole Assembly (BHA) configurations. Following installation of surface casing, the formation was cored for 500 feet and drilled to total depth (TD) of 3,000 feet, after which wireline logs were acquired from TD to surface casing (Table 28).

BHA or LWD Component	Component Length (ft / m)	Cumulative Distance from Bottom Hole (ft / m)
BHA Hughes MXL-1 Bit	1.15 / 0.35	1.15 / 0.35
BHA Bit Sub	3.00 / 0.91	4.15 / 1.26
LWD Resistivity/Gamma-ray	23.53 / 7.17	27.68 / 8.44
LWD Directional	9.08 / 2.77	36.76 / 11.20
LWD Neutron/Density Porosity with Caliper	37.66 / 11.48	74.42 / 22.68
LWD Telemetry Module	9.63 / 2.94	84.05 / 25.62

Table 27: Bottom hole drilling assembly (BHA) and Logging While Drilling (LWD) tools

The stratigraphic test validated the 3D seismic interpretation of the MPU gas hydrate-bearing Mount Elbert prospect (Figures 55-56). Importantly, these operations demonstrated the ability to safely and effectively acquire core, log, and wireline pressure test data within shallow gas hydrate-bearing reservoirs over seven to ten days (versus the standard approach to drill and case this interval within two to four days), helping to set the stage for future operations such as the 2012 CoP Ignik Sikumi well testing. Following successful Stratigraphic Test operations and data acquisition, interpretation results were extensively published and presented. In April 2007, these results were shared in “Gas Hydrate Resource Potential” (Hunter, et al, 2007), which won the Frank Kottlowski Memorial Presentation Award for best oral presentation, Energy and Minerals Division, at the 2007 AAPG annual meeting.

Preliminary interpretation results were reported in R18, pp. 20-38. Expanded results were published and presented at the Arctic Energy Summit conference in Anchorage, Alaska in October, 2007 (Hunter, Digert, Boswell, and Collett, 2007). The resulting paper from this conference was also published in-full as appendix A of R20, pp. 88-100. Many other papers (see References Section 7.2) provide additional detail on data interpretation. Finalized results were extensively published in the Journal of Marine and Petroleum Geology Vol. 28, Issue 2, Feb. 2011, edited by Boswell, Collett, Anderson, and Hunter (2011).

Figure 53: Doyon 14 rig and pipeshed during Mt Elbert-01operations, Milne Point Unit, Alaska North Slope, February 2007

In summary, significant Stratigraphic Test Well results included:

- Safely implemented well operations and data acquisition plans
- Successfully demonstrated ability to safely and effectively acquire data within shallow gas hydrate-bearing reservoirs over 7-10 days (versus the normal approach to drill and case within a maximum 2-4 days)
- Validated seismic interpretation of gas hydrate-bearing MPU Mt Elbert prospect
- Acquired 430 feet total and 100 feet gas hydrate-bearing 3-inch diameter core
- Collected 261 onsite subsamples for preservation and laboratory analyses
  - 4 samples preserved in methane-charged pressure vessels (later converted to LN)
  - 7 samples preserved in LN

  - 52 samples for physical property analyses
  - 46 samples for interstitial water geochemistry
  - 5 samples for thermal property study
  - 86 samples for microbiological study
  - 46 samples for organic geochemistry study
  - 15 samples for detailed petrophysical analyses
- Acquired extensive open-hole wireline logs including gamma-ray, caliper, resistivity, neutron-density porosity, Dipole Sonic Acoustic porosity, Nuclear Magnetic Resonance, Formation Imaging, Electromagnetic Propagation, and Modular Dynamics Testing
- Acquired 4 extensive, long shut-in period MDT within 2 gas hydrate-bearing reservoirs
  - MDT analyses improved understanding of gas hydrate dissociation, gas production, formation cooling, and long-term production potential
  - MDT analyses provided calibration of reservoir simulation models
  - Obtained 4 gas samples from each test interval
  - Obtained 1 pre-dissociation formation water sample and demonstrated ability to flow mobile connate formation water from hydrate-saturated interval
  - Observed rapid formation cooling during gas hydrate dissociation and gas flow and demonstrated gas dissociation from gas hydrate with pressure drawdown

The 2007 Gas Hydrate Stratigraphic Test accomplished several ”firsts”, including:

- First significant ANS gas hydrate-bearing core (100 feet of 430 feet acquired)
- First wireline retrievable coring system application using conventional ANS drill rig
- First ANS open hole multi-day data acquisition program in gas hydrate-bearing reservoir zones
- First in world open-hole dual packer MDT program in gas hydrate-bearing sections
- First ANS MDT sampling of both gas and water in gas hydrate-bearing reservoirs
- First in world sand face temperature data during MDT flow and shut-in periods

The acquired data helped calibrate reservoir simulation models and greatly improved understanding of gas hydrate dissociation, gas production, formation cooling, and future long-term production test design. Importantly, analyses of the stratigraphic test core, log, and MDT data has significantly enhanced understanding of gas hydrate-bearing reservoir properties, permeabilities and saturations. These variables are very leveraging to understanding potential gas producibility from gas hydrate-bearing reservoirs and to design, assess, and plan potential future production test operations.

5.3.8.5 Mt Elbert-01 Wireline Log Data Analyses and Interpretation Summary

Obtaining high-quality open hole logs was a primary data acquisition priority (Figure 57). High-quality open hole logs were obtained, due in large part to the chilled, oil-based drilling fluids maintaining gas hydrate and borehole stability (Figure 54). A full suite of wireline logs was obtained, some with initial difficulties due to the cold (-1 degree C; 30 degree F) wellbore temperatures (Figures 58 and 59). Open-hole logs acquired included gamma-ray, caliper, resistivity, neutron-density porosity, Dipole Sonic Acoustic porosity, Nuclear Magnetic Resonance, Formation Imaging, Electromagnetic Propagation, geochemical neutron activation

logging, and Modular Dynamics Testing (MDT). CMR logs (Figure 60) were a direct indicator of gas hydrate saturation and formation permeability, and helped finalize MDT wireline data acquisition. Table 28 summarizes open hole wireline and also LWD logging runs.

Figure 54: DrillCool, Inc. Heat Exchange Mud Chilling Unit at Mt Elbert-01

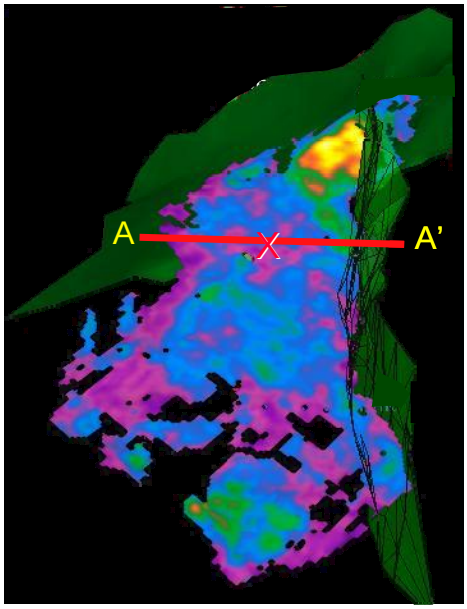

Figure 55: Seismic Amplitude map of Mt Elbert Prospect within 3-way fault-bounded closure. The X marks the Mt Elbert-01 location.

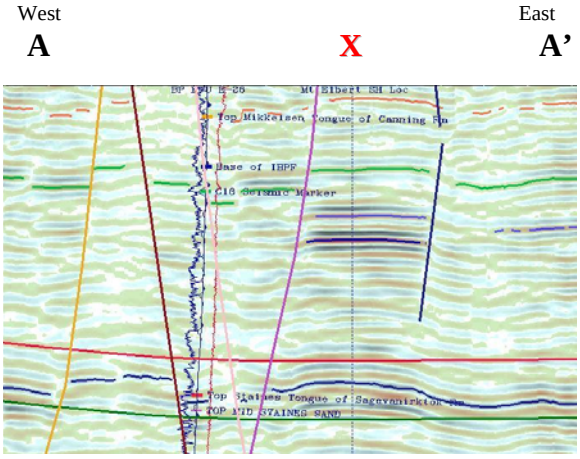

Figure 56: Seismic traverse A-A' (Figure 55) from West to East illustrates interpreted zone C and D gas hydrate-bearing intervals used for thickness and saturation calculations. The X marks the approximate location of the Mt Elbert-01 well. Note corroborating evidence of gas hydrate within zones C and D seen at the Staines Tongue horizon level in the prominent velocity pull-up directly beneath the zone C and D horizons.

Type	Run	Depth (feet)	Depth (m)	Log Combination and Comments
LWD	1-2	275-1,960	84-597	Drilling Performance; Gamma-Ray (GR); EWR-resistivity; neutron-density porosity
LWD	3	1,960-3,000	597-914	LWD GR only
Mud				Mud Temperature and Gas Log (Figure 58)
OH	1	1,952-2,994	595-913	Platform Express (PEX); Resistivity with Array Induction (AIT), RtScanner, and ZAIT; Spontaneous Potential (SP); Compensated Neutron-LithoDensity; Electromagnetic Propagation Tool (EPT)
OH Fail	2	none	none	MSIP/OBMI: MSIP failed no log data collected
OH fail	3	none	none	DSI/OBMI: DSI failed no log data collected (MSIP replaced with DSI)
OH	4	1,952-2,944	595-897	Dipole Shear Imager (DSI) in expert mode, DSST-P, GPIT, EDCT for GR; Formation MicroImager for oil-based mud (OBMIR); Environmental Measurement Sonde (EMS: PPC1-P)
OH	5	1,952-2,996	595-913	Combinable (or Nuclear) Magnetic Resonance Tool (CMRT-B or NMR) – CMR failed, logged with ECS/HNGC); Natural Spectral Gamma Ray as Hostile Environmental Natural Gamma Ray Spectrometry Cartridge (HNGC); Elemental Capture Sonde (ECS: ECC-A, ECS-A)
OH	6	2,000-2,648	610-807	Combinable Magnetic Resonance Tool (CMR); CMR worked after multiple attempts; Hostile Environmental Natural Gamma Ray Spectrometry Cartridge (HNGC)
OH	7	various	various	Modular Dynamics Pressure and Formation Testing (MDT), various depth and time intervals as indicated on Figure 60

Table 28: Mount Elbert-01 Logging-While-Drilling (LWD) and Open-Hole (OH) Wireline Programs

Figure 59 summarizes the Mount Elbert-01 wireline log data between the base permafrost and the base gas hydrate stability zone. Sagavanirktok zones D and C are gas hydrate-bearing. Notably, the reservoir-quality sands of Zone C are not fully charged (to spill point), possibly due to a reservoir charge or seal limit, but likely due to transformation and associated volumetric reduction when originally trapped free gas was converted to gas hydrate with onset of permafrost conditions. Zones A and B are water-bearing and contain no gas hydrate at this location.

Figure 60 illustrates a gas hydrate saturation and permeability log based on the Combinable Magnetic Resonance (CMR) log acquired in the Mount Elbert-01 stratigraphic test well. Based on geophysical interpretations, the well was predicted to encounter two gas hydrate-bearing sands from 7.6 to 22.9 meters (25-75 feet) thick within an upper zone (D) and a lower zone (C).

Well logging and core results show these two sands contain a combined 30.5 meters (100 feet) of gas-hydrate-bearing section (Figures 59 and 60). Within these sections, gas hydrate saturation varies primarily as a function of sand content and silt/clay interbeds. In the cleanest sand zones, saturation reaches a maximum of 75% within the pore volume. The remaining 25% saturation is interpreted as split between a mobile water phase and an irreducible water phase (bound to sand grains and clays) within the tight, hydrate-cemented sands.

Figure 57: Wireline logging operations at Mt Elbert-01 Gas Hydrate Well

Analysis of the Electromagnetic Propagation Tool (EPT) log data used methods developed from the Mallik research. Details of the research plan are presented in R22 (pp. 27-30) and final results were published in the JMPG volume (Sun, et al, 2011).

5.3.8.6 Mt Elbert-01 MDT Data Analyses and Interpretation Summary

Following the major logging runs, the second major data priority was to perform extensive wireline pressure testing using the Modular Dynamics Testing (MDT) tool. MDT wireline pressure testing was accomplished within two gas hydrate-bearing reservoir intervals and acquired four extensive, long shut-in period tests (Table 29) using the drillpipe-conveyed configuration to mitigate risk of tool sticking. Even though the MDT wireline production tests are small-scale, MDT analyses helped improve understanding of gas hydrate dissociation, gas production, formation cooling, and long-term production potential as well as helped calibrate

reservoir simulation models. Four gas samples and one pre-gas hydrate dissociation formation water sample were also obtained. Comprehensive results were published in the JMPG Volume (Anderson, et al, 2011), and much of the below discussion refers to that paper.

The Mt Elbert MDT tests were the first in the world open-hole, dual packer tests within gas hydrate-bearing sediments. The Mallik 2002 MDT tests were similar in design, but within perforated cased-hole. The Mt Elbert MDT data acquired also included the first reservoir temperature measurements at the tool inlet using a small programmable capsule to measure time, temperature, and pressure (Figure 61) mounted to the tool within a screen welded to the tool (Figure 62). One of several emplaced devices survived the test and provided temperature data with time that was interpreted and matched to the various stages of the test. However, this capsule did not have surface read-out as part of the MDT tool string. Therefore, recorded temperatures during testing were not observed until after the MDT was recovered to surface.

Recorded observations indicated major formation cooling during gas hydrate dissociation and gas production during pressure draw-down. The response of the formation during shut-in and pressure build-up following production indicated that gas production during gas hydrate dissociation may have reduced formation permeability to flow, possibly due to the reformation of gas hydrate or formation of ice during the testing. An alternative interpretation involves potential gas storage effects within the tool or borehole due to minimal produced gas.

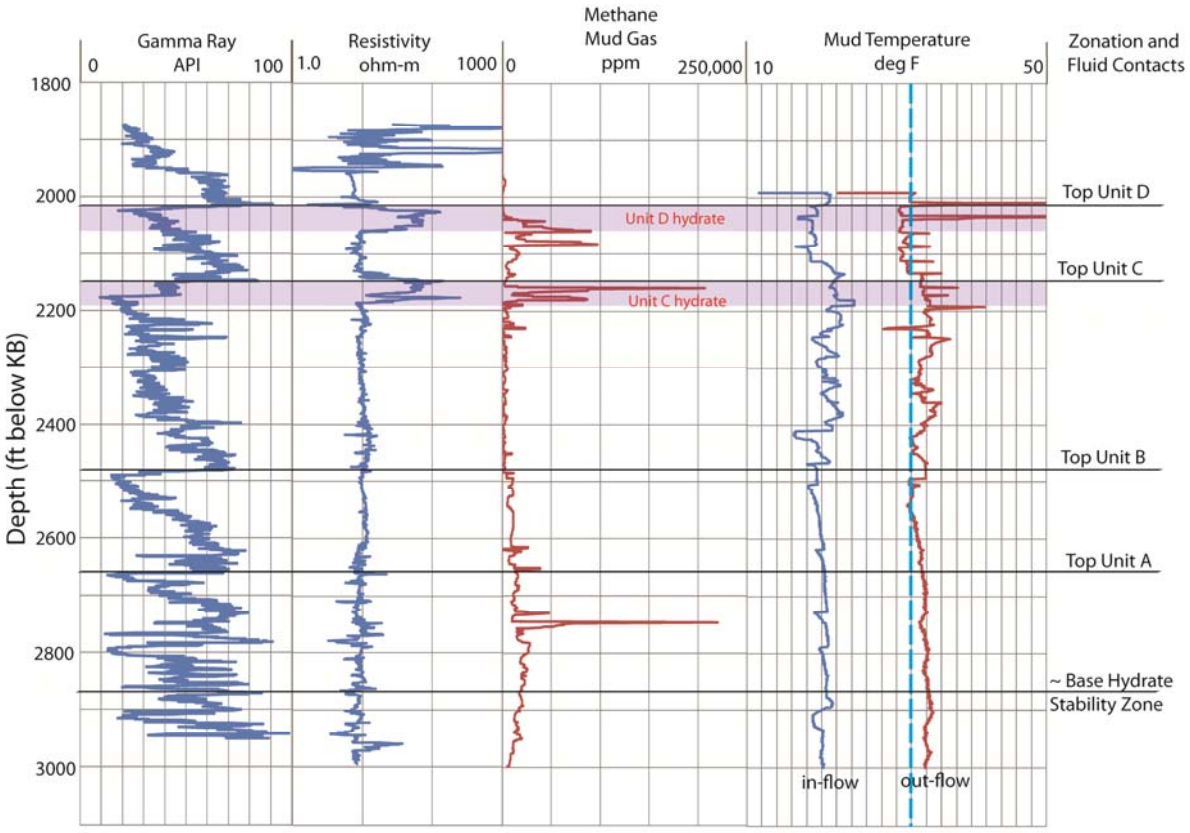

Figure 58: Wireline log data with mudlog gas and temperature with zonation (Hunter, et al, 2011)

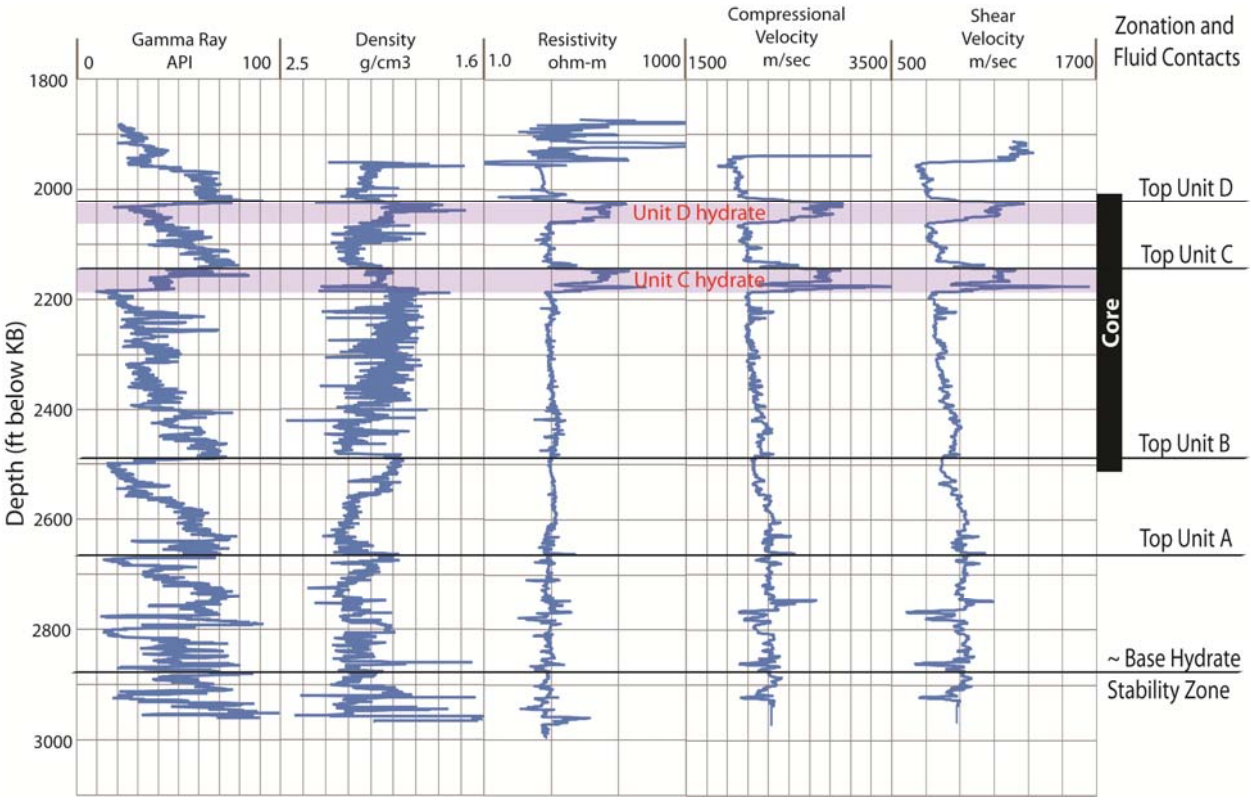

Figure 59: Mount Elbert-01 wireline log data and zonation summary (Hunter, et al, 2011)

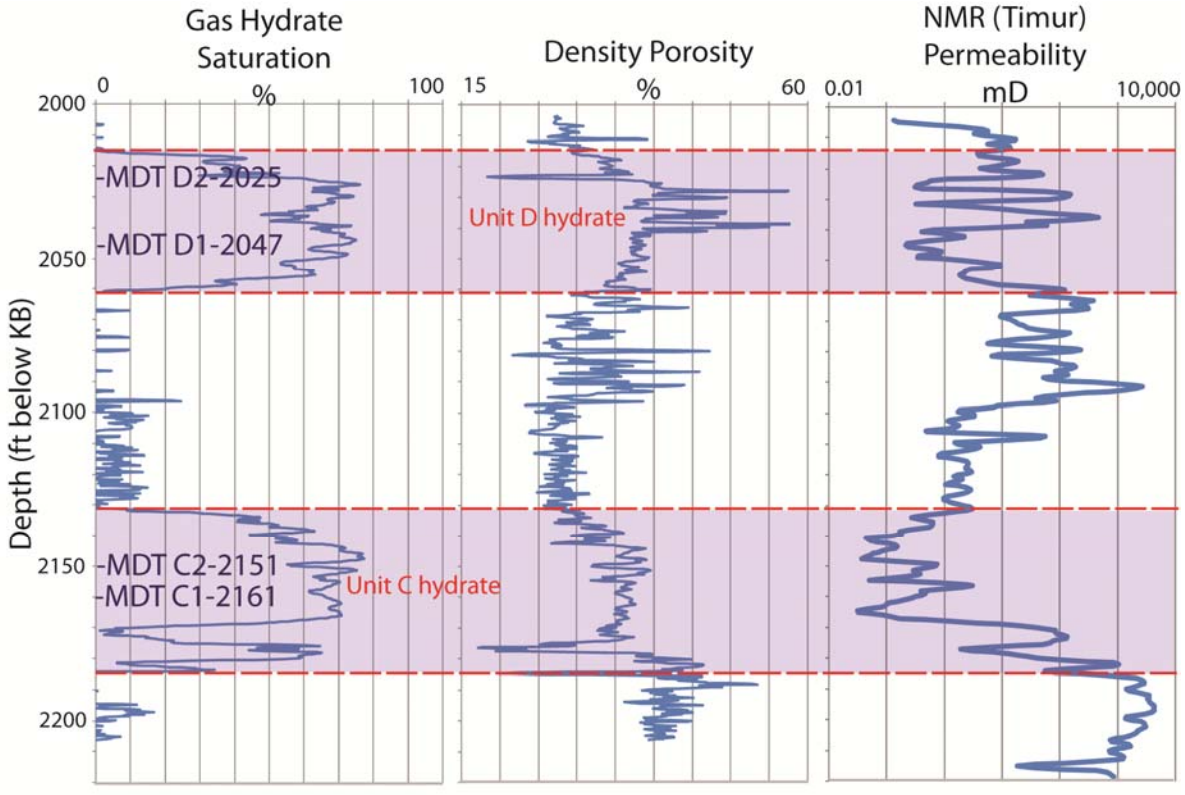

Figure 60: Gas Hydrate saturation and permeability based on Combinable Magnetic Resonance Log for Mt Elbert-01 with density porosity, zonation and MDT points (Hunter, et al, 2011)

Primary MDT test intervals were selected after evaluation of the CMR log (Figure 60) and were based on reservoir quality and fluid saturation criteria, resulting in the four test zones-of-interest, C1, C2, D1, and D2. Each of the four tests included a series of stages that included continuous pressure and temperature monitoring during alternating periods of flow (pressure drawdown) and shut-in (pressure build-up). Samples of produced fluids were also taken and the nature of produced fluids was continuously monitored using the tool optical fluid analyzer, which approximately measured fluid volume ratios for each component (formation water, gas, and OBM).

During the flow (pumping) periods, fluids (typically containing a mixture of formation water, free methane gas, and OBM) were extracted by the tool, thereby reducing the formation pressure in the near-wellbore area. While short-term MDT testing does not typically provide reliable information on reservoir deliverability or potential production rate, especially in tight formations, examination of formation pressure recovery following fluid withdrawal during each flow period allowed interpretation of key reservoir parameters (Anderson, et al, 2011).

MDT analyses and reservoir modeling history match studies were extensively published in the JMPG Volume (Anderson, et al, 2011). History matches of one multi-stage, 12-hour test (Zone C2 test) were accomplished using 5 different reservoir simulators, including CMG STARS, HydrateResSim, MH-21 HYDRES, STOMP-HYD, and TOUGH+HYDRATE (Anderson, et al, 2011). Simulations utilized detailed information collected across the reservoir determined from well logs, including thickness (11.3 m, 37 feet), porosity (35%), hydrate saturation (65%), both mobile and immobile water saturations, intrinsic permeability (1000 mD), pore water salinity (5 ppt), and formation temperature (3.3 - 3.9°C).

The maximum gas hydrate saturation as calculated by the CMR and associated logs is approximately 75% (Figure 60). Data analyses indicated that although there is some mobile water in the hydrate-bearing formation, it might not be enough to maintain dissociation of gas hydrate through depressurization alone by producing the mobile water component. The pressure build-up periods during MDT testing were extensive (up to 12 hours) and the abnormal build-ups after drawdown below gas hydrate stability pressure suggest either a tool configuration effect or that gas production from gas hydrate at these temperatures closer to the base permafrost may not be sustainable over a potential future long-term production test without thermal and/or chemical stimulation. However, it needs to be emphasized that this is only a single well location, and that alternate cases could be considered at higher temperatures and/or where conditions could better allow unstimulated production.

The 4 MDT test intervals are described below in order of operations. MDT results included:

- Star-Oddi pressure and temperature data at MDT inlet
- MDT probe tests of gas hydrate zones 621.5 Meters (2,039 feet) and 619.4 Meters (2,032 feet) failed due to lack of seal (soft water-bearing sediments)
- MDT packer test of water zone at 620.6 Meters (2,036 feet) failed due to inlet plugging (fines migration); noted declining pump performance
- MDT packer test of water zone 613.3 Meters (2,012 feet) failed: pump failed, sediment wear and plugging

- MDT testing terminated (extended initial testing in gas hydrate-bearing zones enabled MDT tool to remain in-hole until testing terminated by probe and pump failures due primarily to anticipated fines migration)

Figure 61: DSTmicro capsule data logger used to record time, temperature, and pressure during coring and during MDT logging operations (data logger on right was destroyed during operations outside the pressure rating of logger)

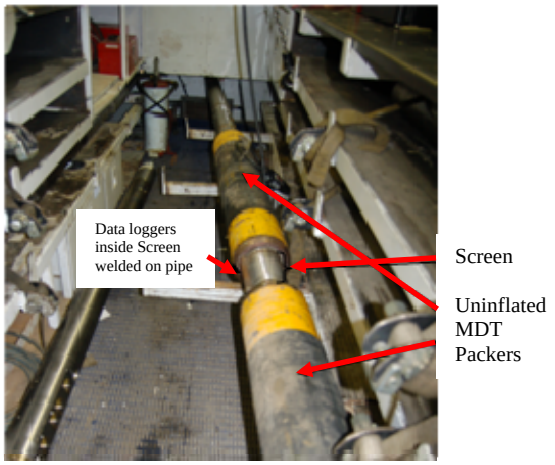

Figure 62: Photo of MDT tool with screen-mounted DSTmicro capsules welded to tool (Photo courtesy Ray Boswell)

Test Zone	Test Type	MDT Intake Depth (Ft)	Pressure Mud Column	Pore Pressure	Hydrate Stability Pressure	Temperature (Degrees F)
C1	Packer	2161	1045	938	547	38.8
C2	Packer	2151	1040	934	535	38.4
D1	Packer	2047	990	889	484	36.5
D2	Packer	2025	979	879	474	36.1

Table 29: MDT test summary in gas hydrate-bearing reservoir zones C and D, Mt Elbert-01

5.3.8.6.1 Zone C1 MDT Flow Test

Figures 63-64 illustrate Zone C1 MDT results. The Zone C1 MDT test was purposely of short-duration. At the MDT intake depth of 2,161 feet (658.7 m), the initial hydrostatic pressure of the formation is 7.66 MPa, indicated on the graph in psi (Figure 63). The first flow period occurred over 16.6 minutes with a flowing bottom-hole pressure (FBHP) less than estimated hydrate stability pressure (Figure 64) at the flowing bottom-hole temperature (FBHT). The subsequent build-up appeared to include non-porous media effects such as a slow pressure increase and an inflection in the pressure curve near 1.4-hours (Figure 63). The first build-up period totaled 52.9 minutes and reached only 6.1 MPa prior to beginning the second flow period (Figure 63). This dampened pressure build-up was characteristic of both C-unit MDT tests and further examined in the history-matching modeling of the Zone C2 test. The second flow period of the C1 test was again conducted with a FBHP less than hydrate stability pressure. During this longer, 58.9 minute flow period, a gas sample was taken at 2.67 hours (Figure 63). The pressure build-up following the second flow period was severely dampened and ended after 104.9 minutes.

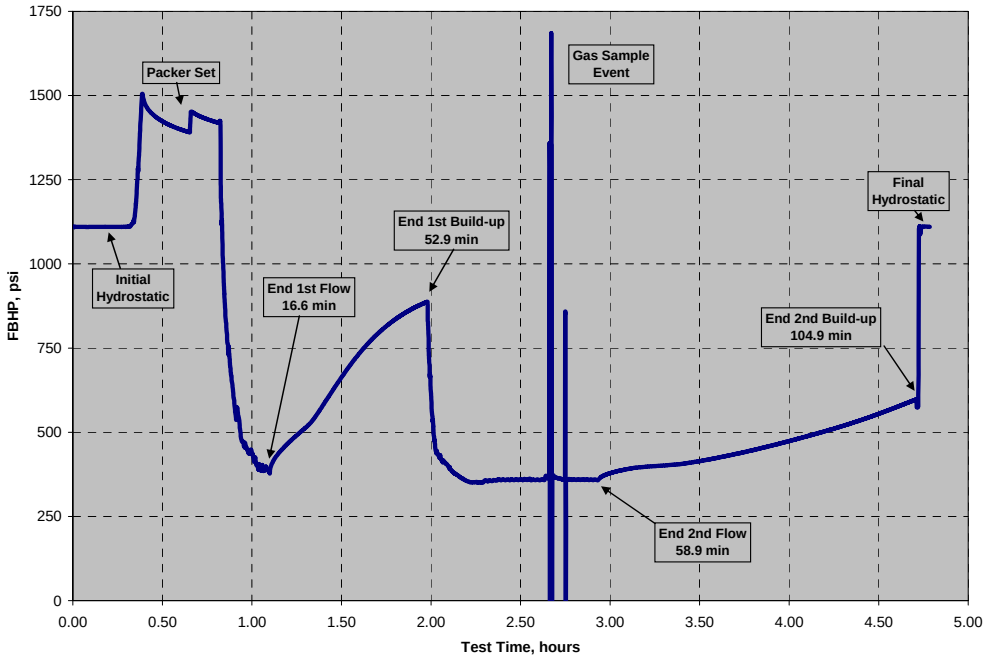

Figure 63: Gas hydrate Zone C1 MDT test pressures, flow, and build-up periods

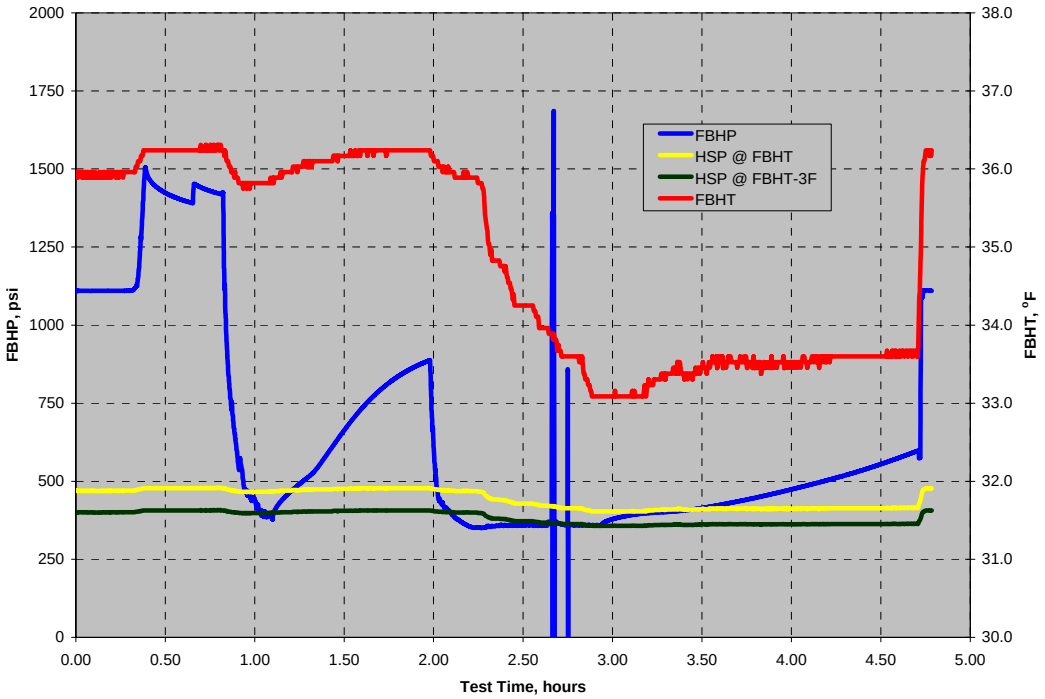

Figure 64: Gas hydrate Zone C1 MDT test pressures and temperatures. The blue line shows FBHP; the yellow line indicates predicted gas hydrate stability at hydrostatic pressure at measured temperature (Moridis, 2003); the dark green line shows gas hydrate stability at hydrostatic pressure with temperature 3^{o} below measured temperature to illustrate range of possible near-wellbore temperature effects; and the red line shows FBHT at MDT inlet port.

5.3.8.6.2 Zone C2 MDT Flow Test

Figures 65-69 illustrate the 11-hour Zone C2 MDT test profiles with flow and build-up periods. The Zone C2 MDT test differed from the Zone C1 test by maintaining pressure above the gas hydrate dissociation pressure during the initial flow period (Figure 65). This experiment design ensured that formation pressure remained above the gas hydrate equilibrium pressure estimate based on in-situ temperature and FBHT (Figure 66). Therefore, methane produced from Zone C2 during this period included only a very small amount dissolved from extracted formation water. Verifying this condition, no free gas was detected at the MDT intake port during this first drawdown period.

Analyses of reservoir pressure response after the first flow period allowed estimating the hydrate-bearing formation effective permeability of 0.12 to 0.17md. The effective permeability is an important key parameter controlling reservoir productivity. Determination of effective permeability is a significant result and indicates the potential for flow of mobile connate water during depressurization of a gas hydrate-bearing reservoir. Formation pressure was reduced below expected gas hydrate equilibrium pressure during the second and third flow periods, dissociating gas hydrate and releasing free gas into the formation (Figure 66). The optical analyzer indicated no to very little methane pumped through the MDT tool during the second pressure drawdown period. This contrasted the expectation of gas production with gas hydrate dissociation at pressures below gas hydrate stability. Evidence of produced gas, however, was indicated during the pressure buildup response to the second pressure drawdown. The pressure buildup response following the first pressure drawdown was characteristic of the recovery in a confined aquifer. The prolonged pressure recovery after the second pressure drawdown indicated compressible gas in the annular space of the MDT above the screened inlet port.

During the third flow period, formation pressure was again reduced below gas hydrate equilibrium pressure. This significantly longer period resulted in measurable production of both formation water and methane gas. The pressure recovery after this flow period was even more prolonged than that after the second flow period. Both the second and third pressure recovery curves display inflection points in the experimentally observed pressure (Figures 65 and 66), potentially indicating a flow regime transition or other significant change in the physical processes influencing pressure buildups.

In summary, the Zone C2 MDT included:

- Planned longer duration test
- First flow with FBHP above gas hydrate stability pressure
- Classic porous media response on first build-up
- Second flow with FBHP below hydrate stability pressure
- Second build-up distinctly different from first build-up
- Extended third flow with FBHP below hydrate stability pressure; subdued third build-up
- 400 psi purposefully maintained in third flow period
- Acquired gas sample
- Fourth flow ended with no inflow

The C2 MDT test shown in the annotated graph preliminary interpretation (Figure 67) indicated that the formation response to initial drawdown is typical of porous media (albeit tight

formation) response when pressures were maintained above the gas hydrate stability zone; this initial drawdown indicates only free connate water was flowing during the initial portion of the test. However, once pressures were allowed to draw-down below the gas hydrate stability pressure to induce gas (and water) dissociation, the following two shut-in periods show an abnormal pressure rebound. This abnormality may be caused by reformation of gas hydrate or possibly by formation of ice within the porous media or alternatively may be a tool configuration artifact (see below discussion and Figures 68-69).

Modeling of MDT Zone C2 test revealed that wellbore (or tool) storage alone can also history-match the pressure curves. Fluid segregation in this annular space plays a key role in the general shape of the recovery curves. No models explicitly represent open space and the overall history-match parameters may reflect this error. It is also possible that formation kinetics may also affect the shape of the pressure recovery curve.

Experimental studies accomplished by M. Batzle at the Colorado School of Mines (CSM) in association with this project modeled the predicted response encountered during MDT wireline production testing of the gas hydrate-bearing reservoir intervals (figure 19 of Anderson, et al, 2011) and as shown in Figures 69-70. Results confirm that the configuration of the MDT coupled with the low-flow rates led to the abnormal pressure recovery profiles (Figure 68) and demonstrated that it was possible to replicate the acquired pressure data in an experimental setup configuration of a simulated MDT tool independent of gas hydrate dissociation or formation. During the entire experiment, the gas and water valve settings remained the same, effectively ensuring the flow rate of gas and liquid into the system would model Darcy flow into the void space around the simulated MDT tool. The flow and build-up period lengths were proportional to the times used in the reservoir tests and resulted in an excellent proportional pressure response (Figures 69-70). Applying Occam's razor ("the simplest explanation is usually correct"), the anomalous pressure build-up response in the C2 MDT (and others) flow test was probably caused by changing wellbore storage effects.

5.3.8.6.3 Zone D1 MDT Flow Test

Figures 71-72 illustrate the 11-hour Zone D1 MDT test profiles with flow and build-up periods. The 3 flow periods of Zone D1 MDT flow test were similar to the Zone C1 and C2 tests. The initial 11.1 minute flow period and the extended second flow period of 229.4 minutes were both conducted with a FBHP higher than gas hydrate stability pressure. Therefore, the gas hydrate remained undissociated during these 2 flow periods as evidenced by the characteristic tight porous media response of the pressure build-up curves in Figure 71. The third flow period of Zone D1 MDT test drew down FBHP below gas hydrate stability pressure and resulted in gas hydrate dissociation and gas production (Figure 72). A gas sample was obtained during this third flow period. Throughout the Zone D1 test, a decreasing pump performance was detected, likely due to extended pumping times and wear due to fine-grained sediments released into the flow stream during gas hydrate dissociation within these unconsolidated sediments. The third buildup period ended prematurely due to a packer seal failure and the system abruptly returned to in situ hydrostatic conditions (Figure 71).

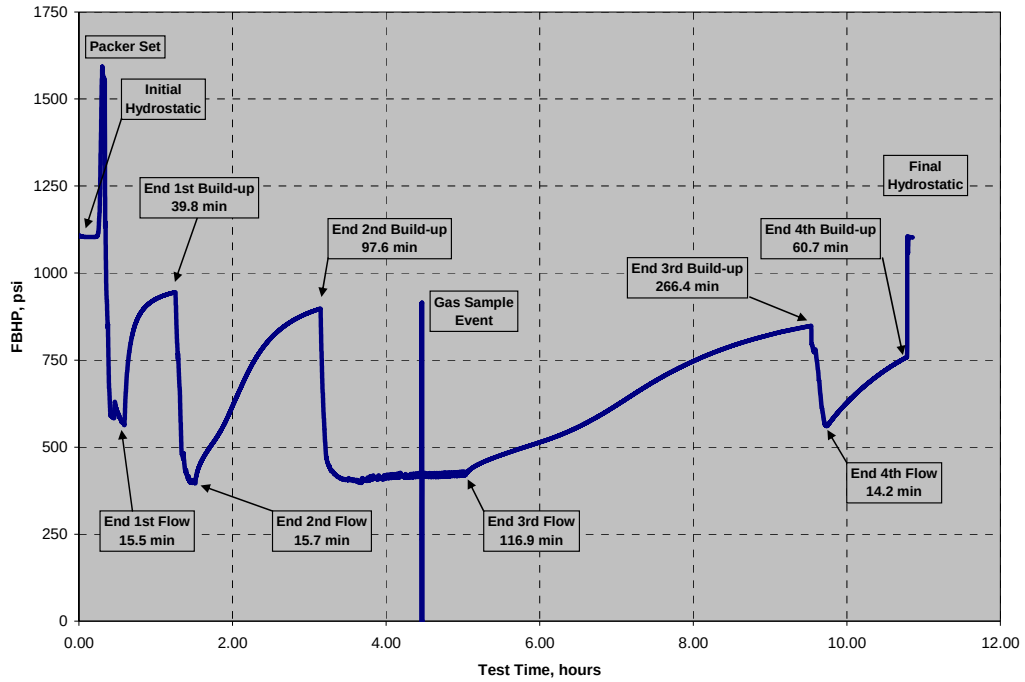

Figure 65: Gas hydrate Zone C2 MDT test pressures, flow, and build-up periods

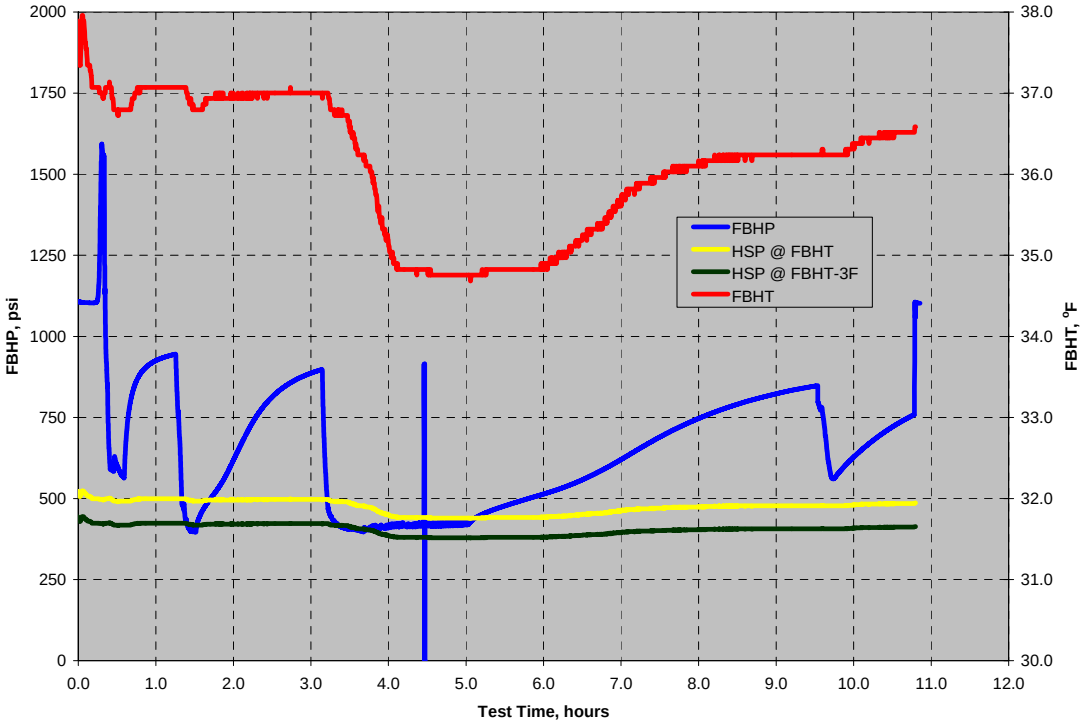

Figure 66: Gas hydrate Zone C2 MDT test pressures and temperatures. The blue line shows FBHP; the yellow line indicates predicted gas hydrate stability at hydrostatic pressure at measured temperature (Moridis, 2003); the dark green line shows gas hydrate stability at hydrostatic pressure with temperature 3^{o} below measured temperature to illustrate range of possible near-wellbore temperature effects; and the red line shows FBHT at MDT inlet port.

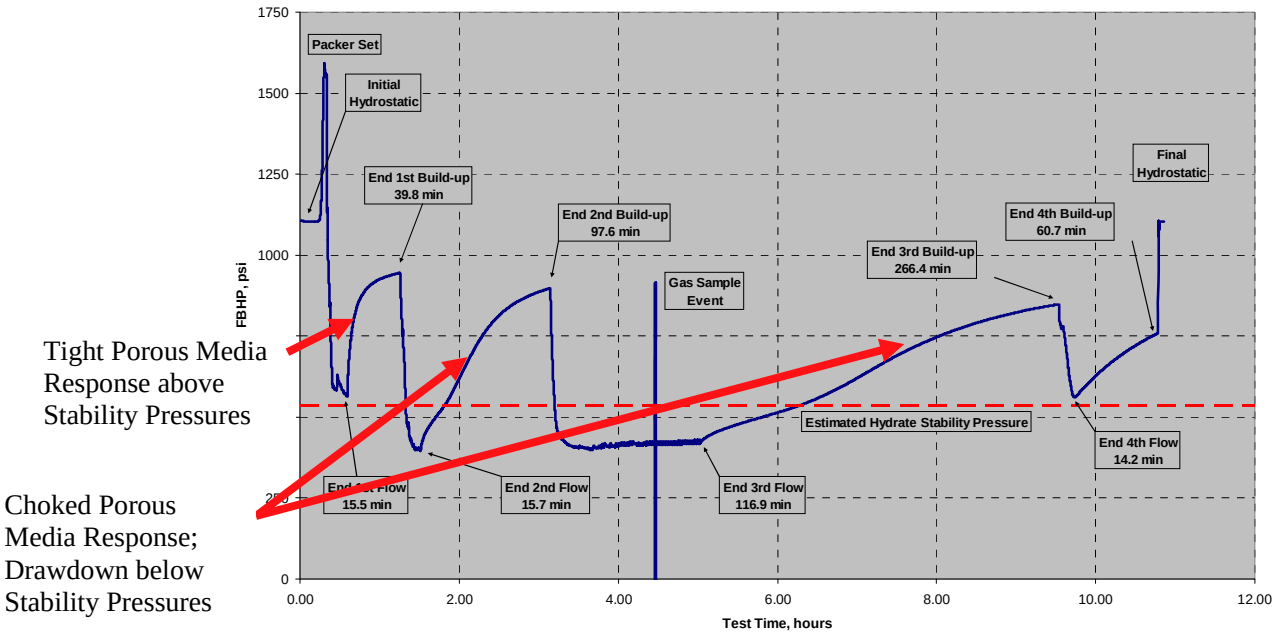

Figure 67: Zone C2 MDT test preliminary interpretations prior to CSM wellbore/tool storage experiment

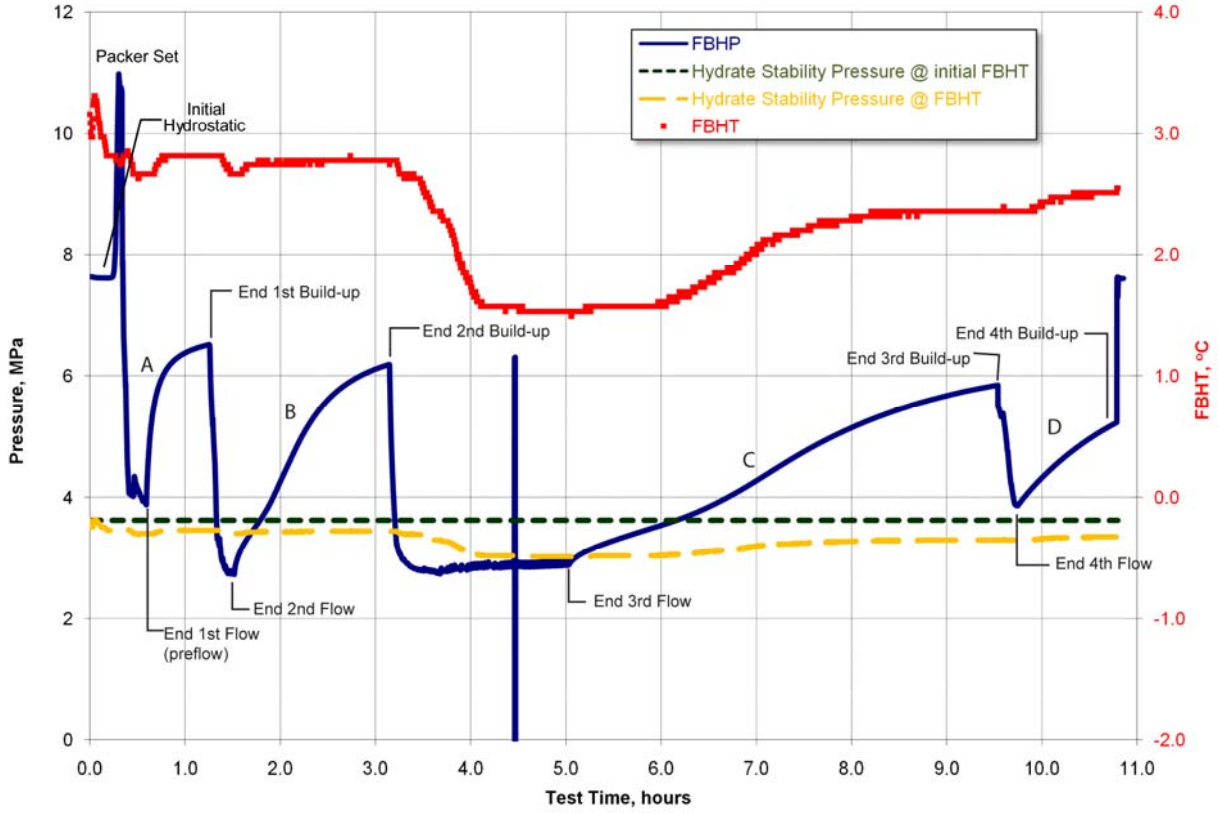

Figure 68: Zone C2 MDT test interpretation summary

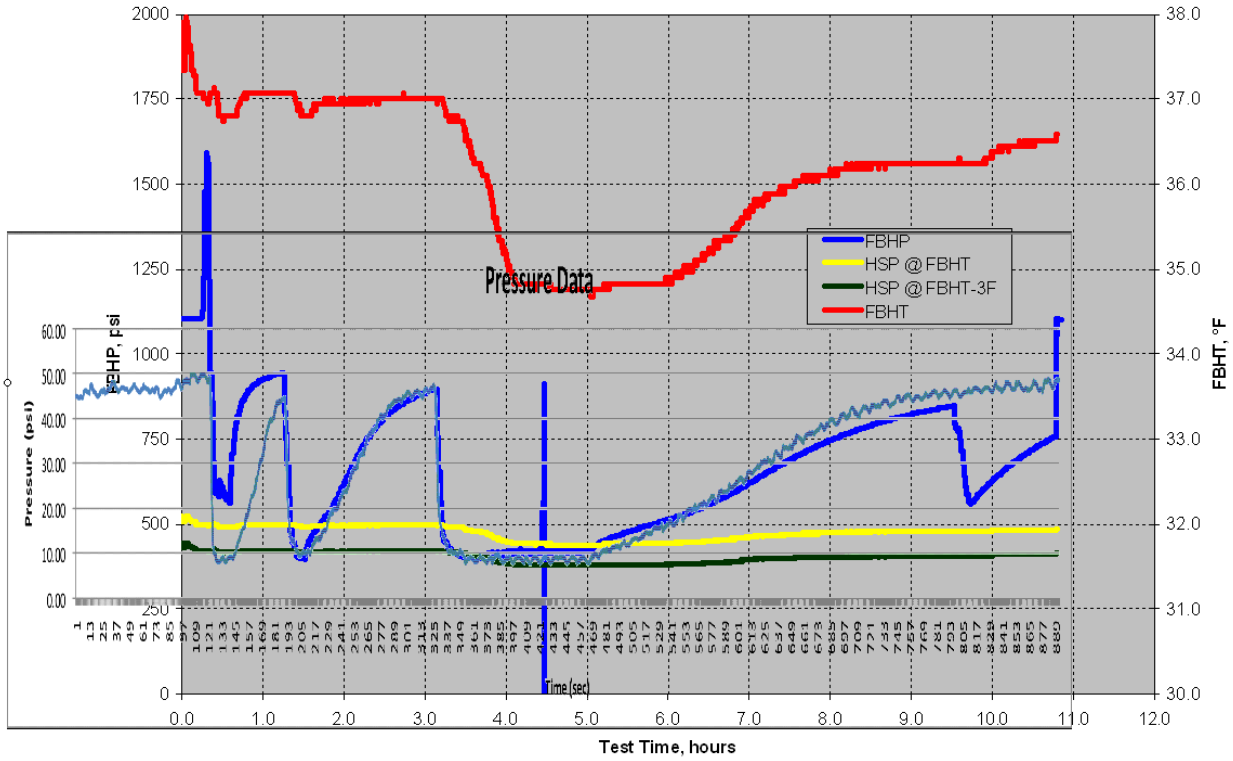

Figure 69: Preliminary pressure history match of CSM MDT tool experiment (jagged lighter blue line) to Mount Elbert-01 C2 MDT (blue line)

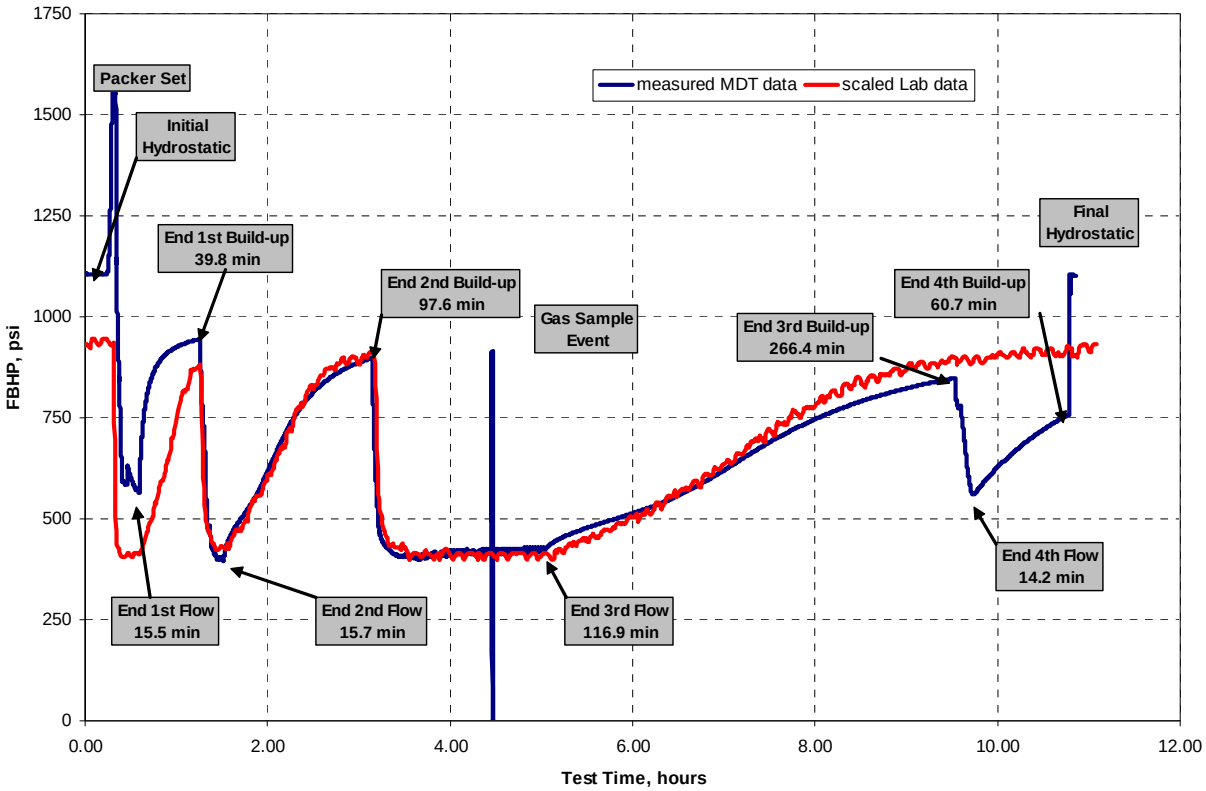

Figure 70: Final CSM scaled laboratory data pressures (jagged red line) versus observed Zone C2 MDT pressures (blue line); (figure 20 of Anderson, et al, 2011)

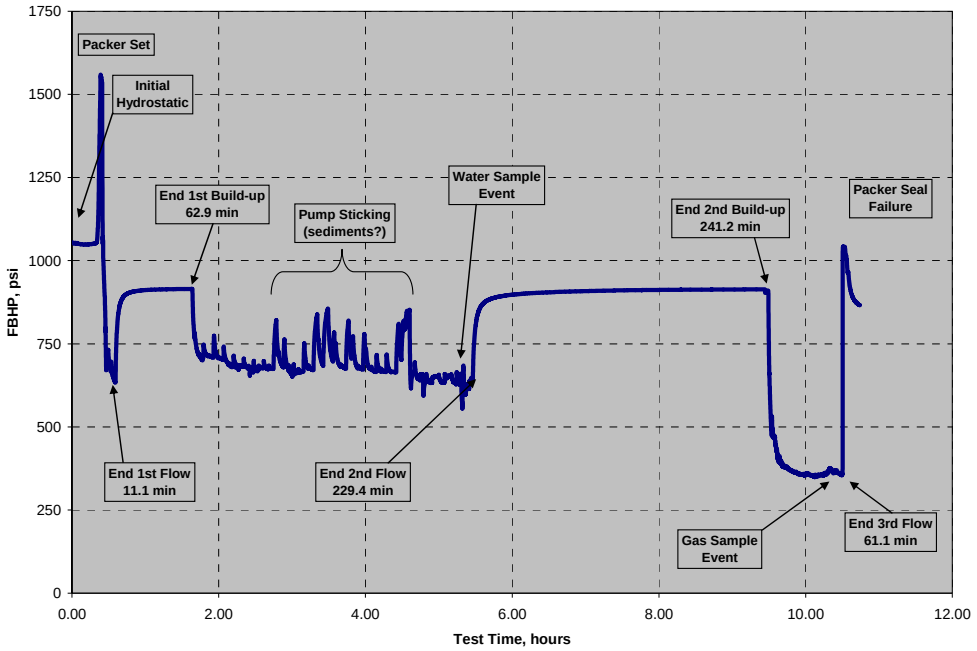

Figure 71: Gas hydrate Zone D1 MDT test pressures, flow, and build-up periods

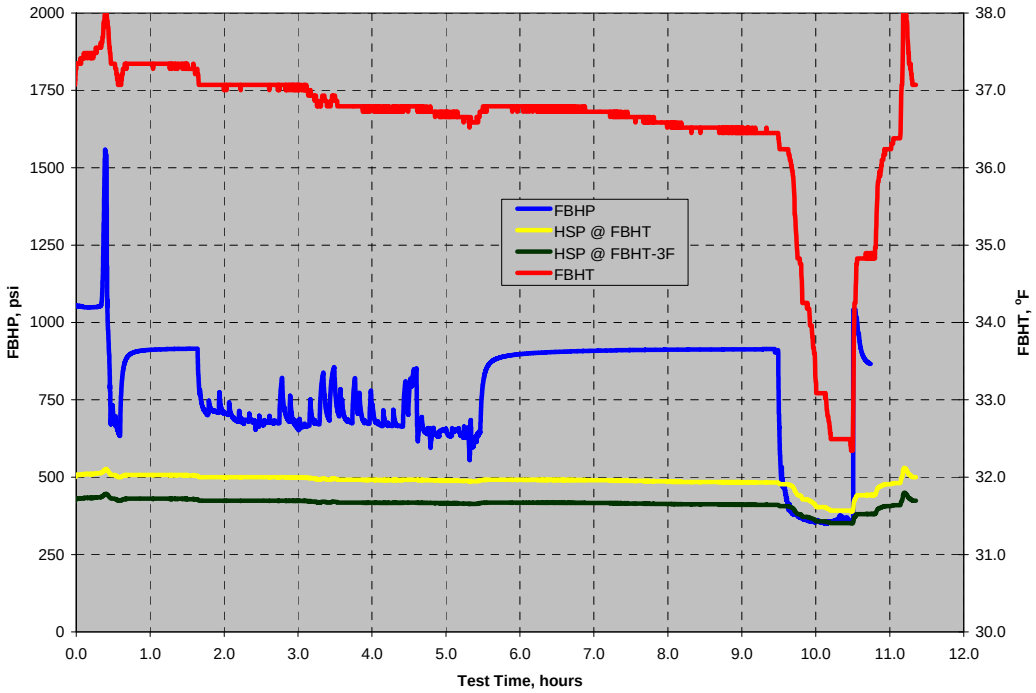

Figure 72: Gas hydrate Zone D1 MDT test pressures and temperatures. The blue line shows FBHP; the yellow line indicates predicted gas hydrate stability at hydrostatic pressure at measured temperature (Moridis, 2003); the dark green line shows gas hydrate stability at hydrostatic pressure with temperature 3^{o} below measured temperature to illustrate range of possible near-wellbore temperature effects; and the red line shows FBHT at MDT inlet port.

5.3.8.6.4 Zone D2 MDT Flow Test

Figures 73-74 illustrate the 2.7-hour Zone D2 MDT test profiles with flow and build-up periods. The Zone D2 flow test consisted of 2 different flow periods (Figure 73). The initial 12.4 minute flow maintained a pressure greater than gas hydrate stability pressure (Figure 74) and again displayed a classic porous media response during the initial buildup period. The ability to repeatedly maintain a FBHP above gas hydrate stability pressure and to observe a response characteristic of classic porous media allowed estimating effective initial permeability of the gas hydrate-bearing reservoir as discussed above in the Zone C2 test section. The second flow period of the Zone D2 flow test was conducted at a pressure below gas hydrate stability pressure; however, pump wear impeding the ability to compress gas shortened this flow test period. Nevertheless, a gas sample was obtained from the gas hydrate dissociation during the second Zone D2 flow period and the similar dampened pressure buildup was again observed (Figure 74).

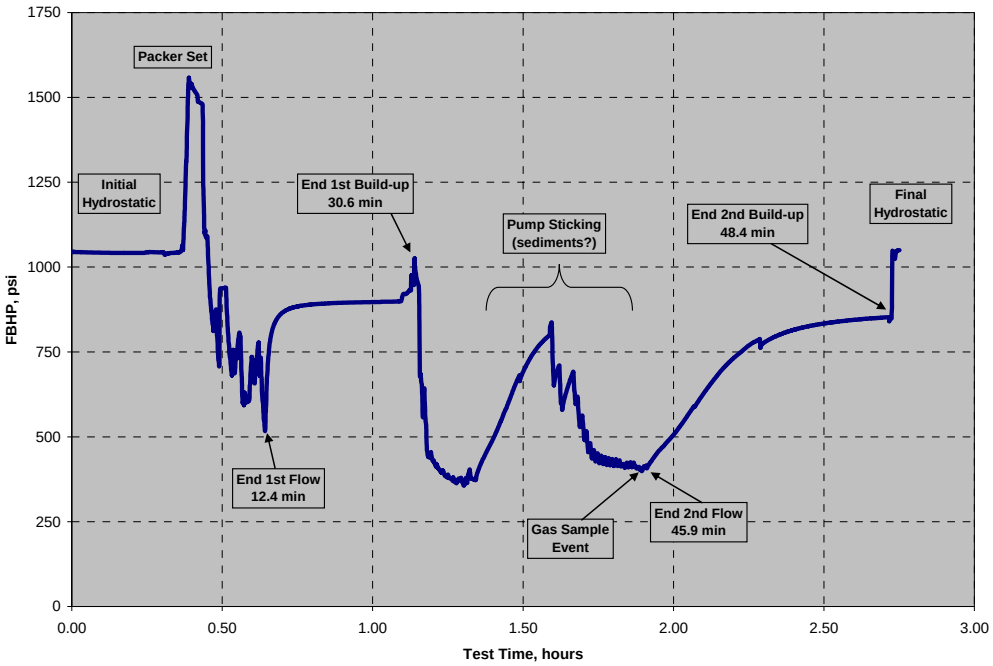

Figure 73: Gas hydrate Zone D2 MDT test pressures, flow, and build-up periods

5.3.8.7 Mt Elbert-01 Gas Data Analyses and Interpretation Summary

The gas sampling program for the Mount Elbert #1 well was conducted to primarily study the geologic controls on the formation and presence of gas hydrate from a depth of about 2,000 feet to the bottom of coring at 2,500 feet. More specific goals of the program included determining: (a) the concentration of hydrocarbon gases (b) the source of hydrocarbon gases; and (c) the relationship of the gas hydrate gas composition to surrounding non-gas hydrate-bearing strata. Five types of samples were collected by the organic geochemistry sampling team from the 23 recovered cores, from the drill cuttings, and from the MDT depressurization tests. Tables 30-34 summarize gas compositional analyses published in the JMPG Volume by Lorenson, et al (2011).

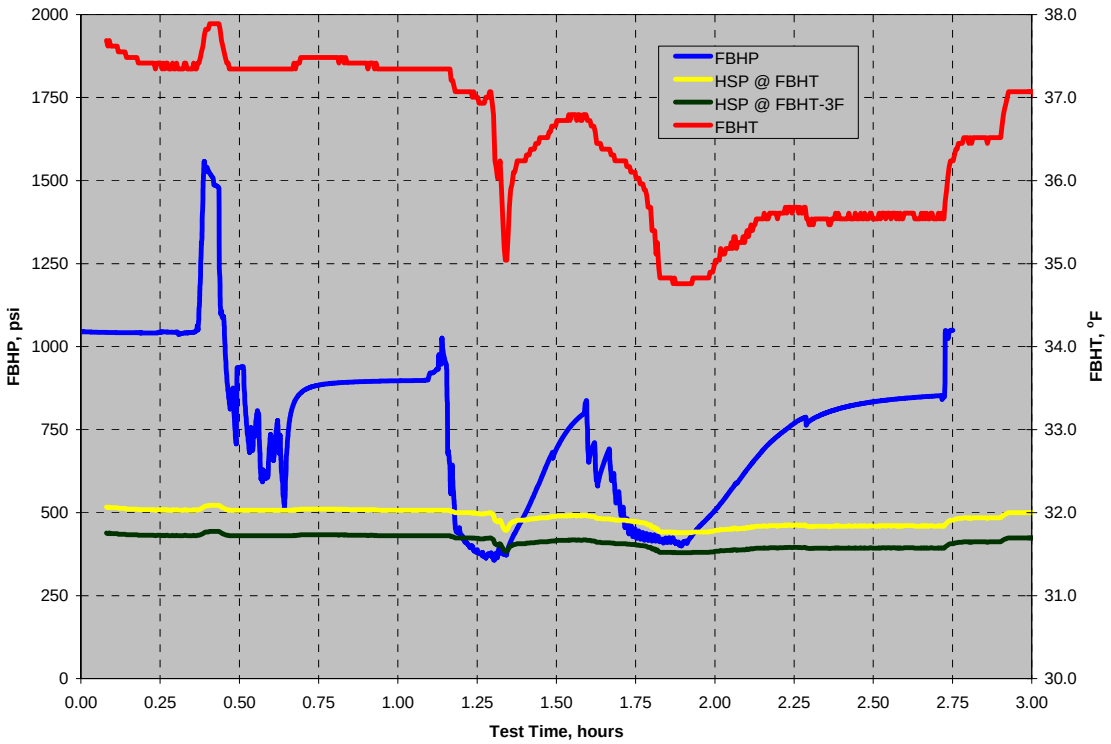

Figure 74: Gas hydrate Zone D2 MDT test pressures and temperatures. The blue line shows FBHP; the yellow line indicates predicted gas hydrate stability at hydrostatic pressure at measured temperature (Moridis, 2003); the dark green line shows gas hydrate stability at hydrostatic pressure with temperature 3^{o} below measured temperature to illustrate range of possible near-wellbore temperature effects; and the red line shows FBHT at MDT inlet port.

Lorenson, et al (2011) gas compositional analyses conclusions from the JMPG Volume indicate:

- The Eileen accumulation is part of the Alaska North Slope gas hydrate petroleum system
- C_1 and C_2 show evidence of oil migration and generation from biodegraded oil or gas
- Gas likely migrated up from the West Sak Oil field (Schrader Bluff sand in MPU area)
- Gas has also microbially biodegraded resulting in removing higher molecular weights
- Based on hydrocarbon gas and C_1 and C_2 carbon isotopic compositions, gases are derived from two main sources and are grouped into three zones with increasing depth
- Within the upper 200 m, the gas is mainly C_1 at low concentration, with very little to no thermogenic hydrocarbon gases
- Dissolved microbial methane is revealed by very light methane isotopic composition
- A transition zone between 200 to 600 m contains sparse thermogenic hydrocarbon gases, very small concentrations of ethane and propane, and 71 to 4500 range $C_1/(C_2+C_3)$ ratios
- Carbon isotopic composition of methane becomes heavier with depth suggesting a thermogenic source augmented by biodegraded oil-sourced methane

- Coal beds underlying the gas hydrate sands may also contribute gases especially rich in methane, nitrogen, and carbon monoxide
- Gas hydrate accumulations between 614 to 665m are entirely thermogenically sourced
- Ethane and propane concentrations remain low and $C_1/(C_2+C_3)$ ratios increase modestly within gas hydrate units, confirming the methane hydrate is primarily Structure I hydrate
- The hydrate gas composition resembles the thermogenic gas in surrounding sediments
- Gas concentrations and isotopic compositions suggest that the gas hydrate zone may act as a partial barrier to gas migration or may scavenge these gases into the hydrate structure
- Methane isotopic composition of 4 Unit D hydrate samples indicated a thermogenic source for methane and carbon dioxide: average -49.4‰, δD -240‰, and $\delta^{13}C$ CO_2 -6.9‰
- Methane isotopic composition of 8 Unit C hydrate samples indicated a thermogenic source for methane and carbon dioxide: average -48.8‰, δD -247‰, and $\delta^{13}C$ CO_2 -14.0‰
- Slight differences in methane and carbon dioxide isotopic composition show that Unit C may be more influenced by a coal gas source than Unit D
- The hydrocarbon gas composition of gas hydrate in both D and C units is nearly 100% C_1
- Minor components include up to 1.46% CO_2 and 61 ppm C_2, consistent with a composition expected of a Structure I gas hydrate; the deeper Unit C gas hydrate has more abundant CO_2 and C_2
- The presence, stratigraphic location, and gas composition suggests that coal seams contributed gas to hydrate, and mainly to hydrate in the deeper Unit C
- Gas concentrations from samples collected during the MDT production test were composed mainly of methane (96.9 to 99.4%) with up to 3.1% N_2 and 284 ppm C_2
- Methane isotopic compositions were very similar to core and gas hydrate samples (Unit D: –47.7‰, δD -236‰ and Unit C: –48.1‰, δD -230‰)
- The gas wetness ratio $C_1/(C_2+C_3)$ was in a similar range as the gas hydrate samples
- The MDT test yielded the highest concentration of C_2, which is anomalous when compared to core and hydrate samples

5.3.8.7.1 Cuttings Samples for Headspace Analyses

A total of 67 cuttings samples in both coarse- and fine-grained sediment were collected for gas and methane carbon isotopic composition analyses. These samples were collected by the mud loggers at 60 foot spacings from 60 to 1,980 feet and then at 30 foot spacings from surface casing to TD at 3,000 feet (Tables 30 and 31). Each sample was scooped into a septa-equipped metal 500 ml can, a teaspoon of salt was added as a preservative, and the can was sealed. The samples were stored outside (frozen) and shipped to Menlo Park, California for analyses. Samples were maintained in a frozen state until thawed for analyses. Analyses targeted the hydrocarbons gases (methane through hexane), carbon dioxide, nitrogen, and oxygen. Subsamples were taken for methane isotopic compositional analyses (Table 30).

5.3.8.7.2 Core Gas, Gas Hydrate Dissociation Gas, and MDT Gas

A total of 46 core samples (HS) in both coarse- and fine-grained sediment were collected for gas and methane carbon isotopic composition analyses. Each sample was scraped to remove excess drilling fluid and placed into a septa-equipped metal 1 liter can. The samples were weighted and sealed inside the core receiving lab. The samples were stored outside (frozen at ambient temperatures) and shipped to Menlo Park, California for analyses (Table 32, Lorenson, 2011). Samples were maintained in a frozen state until thawed for analyses. Analyses targeted the hydrocarbon gases (methane through hexane), carbon dioxide, nitrogen, and oxygen. Subsamples were taken for methane isotopic composition.

Thirteen (13) gas hydrate-bearing core samples (QD) of about 10cc volume were placed into 140 ml plastic syringes equipped with 3-way luer-lock valves and allowed to dissociate at 20° F in the cold laboratory core processing unit. The evolved gas was transferred to evacuated 30 ml serum vials for transport and analyses. Table 33 summarizes gas hydrate compositional analyses results (Lorenson, et al, 2011).

Five (5) samples of formation gas were collected during the MDT test and stored in metal cylinders under pressure. The gas was transferred and sent to both the USGS gas laboratory in Menlo Park and to Isotech laboratories for gas analyses similar to that described in the cuttings section. Table 34 summarizes MDT gas compositional analyses (Lorenson, et al, 2011).

5.3.8.7.3 Isotube Flowed Gas Samples for Headspace Analyses

A total of 35 flowed-gas samples collected in "isotubes" were collected by the mud loggers during drilling operations. These samples were collected at 30 foot spacings from 1,980 feet to TD at 3,000 feet (Table 35). The samples were sent directly to Isotech Laboratories for analyses and results are similar to those described in the cuttings sample scheme. Table 35 illustrates these gas analyses and confirms that the predominantly methane composition and carbon isotope data are consistent with gas hydrate-derived gases.

5.3.8.8 Mt Elbert-01 Core Data Analyses and Interpretation Summary

This section describes the Mt Elbert-01 core data analyses and interpretation from onsite activities through later project studies. Final results from these studies were published in the JMPG Volume (Boswell, et al, 2011).

Over the 2.5 day coring program, 153 meters (504 feet) of mixed gas hydrate and water-bearing sediments were cored in 23 core runs. A total of 131 meters (430 feet) core was recovered, yielding an approximately 85% core recovery efficiency, comparable to that recovered by similar methods in the 2002 Mallik gas hydrate core as reported in GSC Bulletin 585. The wireline core recovery enabled quick drilling and recovery of each core. Maximum core recovery possible per core run was up to 7.3 meters (24 feet) plus a few centimeters in core-catcher.

Approximately 30.5 meters (100 feet) of 153.5 meters (503 feet) cored was gas hydrate-bearing as shown in Figure 59. These results validated the 3D seismic interpretation of the Mount Elbert prospect (Figures 55-56). During core retrieval to the surface, the core passes through the upper limit of the gas hydrate stability zone (Figure 1) and any gas hydrate-bearing sediment begins to dissociate into gas and water. Therefore, the core is kept as cold as possible, and rapid core processing facilitated wireline retrieval from reservoir to surface at the rig floor, to the pipe shed,

Depth	Depth	Gas	O2 + Ar	CO2	N2	N2	CO	C1	C2	C2H4	C3	C3H6	iC4	nC4	iC5	nC5	C6+	d13C1
Feet	m	Units	ppm	ppm	ppm	calc. ppm	ppm	ppm	ppm	ppm	ppm	ppm	ppm	ppm	ppm	ppm	ppm	‰
1980	603.504	144	219200	130	780400	-1800	0	241	0	0	0	0	0	1	1	1	5	
2010	612.648	0	217700	420	781900	5000	0	6	0	0	0	0	0	0	0	0	0	
2040	621.792	364	207400	180	739800	-300	0	52600	0	0	0	0	0	0	0	0	2	-49.5
2070	630.936	125	210900	180	749600	-3000	0	39300	0	0	0	0	0	0	0	0	2	-48.9
2100	640.08	114	215900	150	768000	-2400	0	15900	0	0	0	0	0	0	0	0	2	-47.5
2130	649.224	54	218300	170	775000	-4000	0	6520	0	0	0	0	0	0	0	0	2	-47.5
2160	658.368	646	200400	140	708300	-6800	0	91200	0	0	0	0	0	0	0	0	2	-49
2190	667.512	91	218400	200	776000	-3400	0	5430	1	0	0	0	0	0	0	0	2	-49.4
2220	676.656	93	217100	180	770700	-4000	0	12000	0	0	0	0	0	0	0	0	2	-49
2250	685.8	17	219100	180	778300	-3600	0	2430	0	0	0	0	0	0	0	0	1	-48.4
2280	694.944	22	218500	130	776900	-2800	0	4510	0	0	0	0	0	0	0	0	1	-48.4
2310	704.088	22	219100	180	777800	-4100	0	2870	0	0	0	0	0	0	0	0	2	-48.9
2340	713.232	45	218100	140	775900	-2400	0	5890	0	0	0	0	0	0	0	0	2	-50.1
2370	722.376	11	219300	150	779200	-3400	0	1350	0	0	0	0	0	0	0	0	2	-49.2
2400	731.52	4	219800	330	779800	-4600	0	52	0	0	0	0	0	0	0	0	2	
2430	740.664	20	218100	140	779500	1200	0	2260	0	0	0	0	0	0	0	0	2	-48.9
2460	749.808	21	218700	130	778600	-1800	0	2570	0	0	0	0	0	0	0	0	2	-48.5
2490	758.952	39	218400	180	777000	-2400	0	4420	0	0	0	0	0	0	0	0	2	-49.4
2520	768.096	45	217300	130	774600	-800	0	7950	0	0	0	0	0	0	0	0	2	-48.3
2550	777.24	81	215600	130	772300	2900	0	12000	0	0	0	0	0	0	0	0	2	-48.1
2580	786.384	73	215600	130	773600	4200	0	10700	0	0	0	0	0	0	0	0	2	-48.3
2610	795.528	70	215900	130	774400	4000	0	9570	0	0	0	0	0	0	0	0	2	-48.1
2640	804.672	56	217200	130	774800	-300	0	7840	0	0	0	0	0	0	0	0	2	-48
2670	813.816	124	214000	140	770000	6300	0	15900	0	0	0	0	0	0	0	0	2	-48.2
2700	822.96	95	215600	220	771400	2000	0	12800	0	0	0	0	0	0	0	0	2	-47.8
2730	832.104	389	208000	140	743100	800	0	48800	0	0	0	0	0	0	0	0	2	-48.9
2760	841.248	152	213400	140	766600	5100	0	19900	0	0	0	0	0	0	0	0	2	-47.5
2790	850.392	208	216700	230	772800	-500	0	10300	0	0	0	0	0	0	0	0	2	-47.4
2820	859.536	152	214200	150	765500	1100	0	20100	0	0	0	0	0	0	0	0	2	-47.9
2850	868.68	212	211100	130	761500	8200	0	27300	0	0	0	0	0	0	0	0	2	-47.8
2880	877.824	133	213300	130	768800	7600	0	17800	0	0	0	0	0	0	0	0	2	-47.2
2910	886.968	147	211900	140	768500	12300	0	19500	0	0	0	0	0	0	0	0	1	-47.9
2940	896.112	105	213800	140	772400	9400	0	13700	0	0	0	0	0	0	0	0	2	-47.6
2970	905.256	55	214300	130	773500	8800	0	12100	0	0	0	0	0	0	0	0	2	-48.4
3000	914.4	61	216500	130	775700	3100	0	7690	0	0	0	0	0	0	0	0	2	-47.8

Table 30: Flowed gas composition from cuttings shaker table, surface casing to TD (chemical analyses based on standards accurate to within 2%) (Lorenson, et al, 2011)

Depth (ft)	Depth (m)	O2+Ar µL/L	N2 µL/L	N2 Calc. µL/L	CO µL/L	H2 µL/L	CO2 µL/L	C1 µL/L	C2 µL/L	C2H4 µL/L	C3 µL/L	C3H6 µL/L	iC4 µL/L	nC4 µL/L	iC5 µL/L	nC5 µL/L	C6+ µL/L	C1/C2+C3	C1/CO2	$\delta^{13}C\ CO_2$ ‰	$\delta^{13}C1$ ‰	$\delta^{13}C1$-CO2
150	45.72	199000	822000	112000	0	1040	9330	6390	0	0	0.21	0	0	0	0	0	13.48	30800	0.7	-11.8	-83.4	1.078
210	64.01	202000	879000	159000	0	380	9870	5950	1.43	0	0.55	0	0	0.22	0	0	9.65	3020	0.6			
270	82.3	209000	847000	102000	0	1160	4140	1760	0.74	0	0.32	0	0	0	0	0	10.51	1660	0.4			
330	100.58	306000	1259000	166000	0	1160	18500	660	0.79	0	0	0	0	0	0	0	17.9	830	0	-18.3	-86.4	1.075
390	118.87	280000	1199000	201000	0	1150	14300	580	0.6	0	0	0	0	0	0	0	17.18	970	0			
450	137.16	232000	952000	125000	0	1080	13100	450	1.08	0	0	0	0	0	0	0	12.34	410	0			
510	155.45	202000	843000	123000	0	1130	8010	240	2.53	0	0.84	0	0	0	0	0	9.38	70	0			
570	173.74	223000	934000	138000	0	1010	6870	250	0.7	0	0	0	0	0	0	0	17.47	360	0			
630	192.02	222000	967000	176000	0	860	8500	580	2.04	0	0	0	0	0	0	0	13.77	290	0.1			
690	210.31	406000	2093000	643000	430	2320	19200	2550	10.84	0	0.76	0	0	0	0	0	23.45	220	0.1	-18.3	-80.6	1.068
750	228.6	216000	1219000	450000	250	1100	7510	2210	11.13	1.44	0.58	0	0	0	0	0	13.58	190	0.3			
810	246.89	384000	1625000	255000	0	1730	10700	1060	5.25	0	0	0	0	0	0	0	17.79	200	0.1			
870	265.18	260000	1170000	240000	70	1130	8060	490	3.6	0	0.29	0	0	0	0	0	16.4	130	0.1	-16.5	-79.5	1.068
930	283.46	231000	1067000	244000	0	1000	5090	910	4.17	0	0.26	0	0.26	0	0	0	14.61	210	0.2			
990	301.75	226000	1053000	248000	100	1080	13100	1010	3.62	0	0.39	0	0	0	0	0	13.71	250	0.1			
1050	320.04	287000	1324000	299000	110	1680	15500	4780	3.59	0	0.33	0	0	0	0	0	12.56	1220	0.3		-74.2	
1110	338.33	291000	1288000	248000	50	1480	11300	460	2.86	0	0	0	0	0	0	0	10.98	160	0			
1170	356.62	283000	1184000	175000	60	1160	11100	3480	2.52	0	0.3	0	0	0	0	0	25.48	1240	0.3			
1230	374.9	246000	1303000	426000	90	1420	10500	10800	6.75	0	0.47	0	0	0	0	0	47.12	1490	1	-10.3	-65.9	1.06
1290	393.19	272000	1158000	187000	0	1430	11500	8850	4.06	0	0	0	0	0	0	0	17.7	2180	0.8			
1350	411.48	91000	1406000	1083000	310	1240	9150	18600	13.42	0.92	0.76	0.46	0	0	0	0	14.18	1310	2			
1410	429.77	200000	941000	228000	30	1020	2980	2290	7.68	1.15	0.34	0	0	0	0	0	11.34	290	0.8	-12	-54	1.044
1470	448.06	211000	1314000	560000	80	1010	3120	29300	15.73	0	1.09	0	0	0	0	0	19.47	1740	9.4			
1530	466.34	190000	1378000	701000	90	1460	1880	1240	6.75	0.94	0.63	0.47	0	0	0	0	13.19	170	0.7			
1590	484.63	291000	1775000	736000	0	1560	2700	8040	7.27	0	0.42	0	0	0	0	0	19.94	1050	3		-28.3	
1650	502.92	180000	807000	164000	0	770	6600	5990	4.5	0	0.4	0	0	0	0	0	10.6	1220	0.9			
1710	521.21	372000	1541000	213000	0	1460	16300	11500	6.02	0	0	0	0	0	0	0	18.83	1920	0.7			
1770	539.5	192000	995000	311000	0	810	6790	18500	6.55	0	0.36	0	0	0	0	0	10.31	2680	2.7	-14.8	-53.6	1.041
1830	557.78	302000	1326000	250000	0	1560	8590	16300	4.79	0	0.33	0	0	0	0	0	26.44	3190	1.9			
1890	576.07	221000	1015000	226000	0	1200	10600	20700	4.56	0	0	0	0	0	0	0	22.69	4530	1.9			
1980	603.5	179000	2908000	2269000	0	2740	1150	27100	5.3	2.8	14.64	1.56	0.62	0.62	0	0	45.17	1360	23.5	-15.7	-47.9	1.034
2010	612.65	94000	2260000	1927000	0	980	470	1290	2.59	2.36	8.24	1.18	0	0	0	0	22.61	120	2.7			
2040	621.79	75000	1560000	1293000	0	810	360	2670	1.31	1.15	3.77	0.49	0.49	0	0	0	21.46	530	7.4			
2070	630.94	77000	1541000	1266000	0	1190	520	5380	1.3	0.97	2.27	0.49	0.32	0	0	0	21.93	1500	10.3		-45.5	
2100	640.08	99000	2402000	2048000	350	1740	680	7000	2.51	1.76	12.04	1	0	0	0	0	21.32	480	10.3			
2130	649.22	119000	2428000	2005000	330	2000	770	22900	3.6	1.29	14.4	1.54	0.77	0	0	0	34.46	1270	29.7			
2160	658.37	94000	2124000	1789000	220	1430	360	17700	2.01	0.89	6.71	0.89	0.45	0	0	0	25.27	2030	49.5		-45.5	
2190	667.51	258000	1816000	894000	290	1700	350	1380	1.66	0.83	1.87	0.42	0	0	0	0	38.22	390	3.9			
2220	676.66	166000	3118000	2527000	920	2490	690	6160	2.3	2.3	9.55	1.65	0	0	0	0	37.86	520	8.9			
2250	685.8	255000	3226000	2317000	910	2610	770	1820	2.09	2.09	6.62	1.39	0	0	0	0	39.72	210	2.4		-42.9	

Depth (ft)	Depth (m)	O2+Ar µL/L	N2 µL/L	N2 Calc. µL/L	CO µL/L	H2 µL/L	CO2 µL/L	C1 µL/L	C2 µL/L	C2H4 µL/L	C3 µL/L	C3H6 µL/L	iC4 µL/L	nC4 µL/L	iC5 µL/L	nC5 µL/L	C6+ µL/L	C1/C2+C3	C1/CO2	$\delta^{13}C\ CO_2$ ‰	$\delta^{13}C1$ ‰	$\delta^{13}C1$-CO2
2280	694.94	159000	2146000	1578000	690	2010	440	4300	6.47	1.16	3.47	0.69	0	0	0	0	30.28	430	9.8			
2310	704.09	313000	2903000	1785000	770	2180	580	2070	1.61	1.29	2.58	0.97	0	0	0	0	37.67	490	3.6			
2340	713.23	318000	2127000	993000	270	1610	640	2620	1.47	0	1.47	0	0	0	0	0	30.11	890	4.1		-43.7	
2370	722.38	348000	2601000	1358000	440	1980	740	1740	2.36	0	2.66	0	0	0	0	0	38.38	350	2.4			
2400	731.52	80000	1804000	1520000	130	1330	420	14600	4.75	1.14	5.7	0.76	0	0	0	0	17.28	1400	35			
2430	740.66	112000	2332000	1933000	1180	2010	730	1930	4.16	1.96	7.59	1.22	0	0	0	0	21.79	160	2.6		-41.9	
2460	749.81	234000	2042000	1208000	300	1580	550	2270	1.82	0	1.82	0	0	0	0	0	22.33	620	4.1			
2490	758.95	87000	1931000	1620000	490	1370	750	1920	4.24	1.41	5.86	0.81	0	0	0	0	10.11	190	2.6			
2520	768.1	95000	1050000	712000	180	1030	290	4760	0.92	0.46	0.69	0.35	0	0	0	0	7.36	2960	16.6		-45.2	
2550	777.24	244000	1874000	1002000	280	1620	1060	5400	1.28	0	1.28	0	0	0	0	0	13.39	2120	5.1			
2580	786.38	165000	1358000	770000	180	1020	520	8470	1.53	0	1.07	0	0	0	0	0	9.65	3250	16.3			
2610	795.53	194000	1664000	972000	210	1300	390	6850	1.68	0	1.31	0	0	0	0	0	10.26	2290	17.5		-44.1	
2640	804.67	100000	1684000	1326000	270	1230	140	8460	1.97	0.9	2.15	0.54	0	0	0	0	13.27	2050	59			
2670	813.82	100000	1031000	672000	180	920	310	14400	1.26	0	0.8	0.23	0	0	0	0	6.3	7000	46.7			
2700	822.96	136000	1271000	784000	150	990	330	43200	0	0	1.74	0.29	0	0	0	0	7.98	24800	129.6		-45.5	
2730	832.1	85000	1752000	1447000	340	1610	420	51600	0	0	3.59	0.57	0	0	0	0	11.15	14400	124.1			
2760	841.25	233000	1651000	819000	330	1270	480	30800	1.53	0	1.92	0.38	0	0	0	0	12.45	8940	64.4			
2790	850.39	79000	1662000	1380000	520	1510	570	35400	0	0	3.73	0.71	0	0	0	0	11.2	9480	62.2		-45.5	
2850*	868.68*	77000	1748000	1475000	130	1310	680	56100	2.26	0	5.27	0.56	0	0	0	0	12.23	7450	82.8			
2880*	877.82*	75000	1565000	1297000	310	1170	290	62100	2.72	0	4.09	0.51	0	0	0	0	9.36	9130	214.7		-47	
2890*	880.87*	49000	1181000	1008000	250	1060	160	32200	1.14	0	3.03	0.5	0	0	0	0	6.44	7730	196.2			
2910	886.97	79000	1839000	1557000	160	1640	400	66500	6.55	0	5.36	0.79	0	0	0	0	11.51	5580	167.5			
2940	896.11	104000	2371000	2001000	0	1910	590	70800	9.42	1.27	8.15	1.27	0	0	0	0	16.04	4030	120.9			
2970	905.26	73000	1752000	1492000	300	1640	410	39400	0	0	3.73	0.56	0	0	0	0	12.31	10600	95.9		-46.8	
3000	914.4	50000	1092000	914000	380	1040	240	17400	0	0	1.62	0.23	0	0	0	0	7.07	10700	71.4			

Table 31: Cuttings gas compositional analyses (chemical analyses based on standards accurate to within 2%) (Lorenson, et al, 2011)
* Anomalous depths in this sequence (2850, 2880, and 2890) may be erroneous in Lorenson (2011) where depths listed above could be: 2850 = 2820; 2880 = 2850; and 2890 = 2880

Depth (ft)	Depth (m)	O2+Ar µL/L	N2 µL/L	N2 Calc. µL/L	CO µL/L	H2 µL/L	CO2 µL/L	C1 µL/L	C2 µL/L	C2H4 µL/L	C3 µL/L	C3H6 µL/L	iC4 µL/L	nC4 µL/L	iC5 µL/L	nC5 µL/L	C6+ µL/L	C1/C2+C3	C1/CO2	iC4/nC4 ‰	$\delta^{13}C\ CO_2$ ‰	$\delta^{13}C1$ ‰	δC1 ‰	$\delta^{13}C1$-CO2
1993.04	606.57	120000	640000	210000	0	540	520	16600	2.5	0	2.1	0	1.3	0	0	0	7.7	3640	32		-4	-43.9		1.042
1999.21	608.45	80000	490000	200000	0	480	490	35800	2.6	0	2	0	1.5	0	0	0	7.1	7920	72					
2027.58	617.1	150000	680000	150000	0	420	160	138800	0	0	0.6	0	0.4	0	0	0	7	238000	893			-48.9	-257	
2029.5	617.68	90000	370000	70000	0	360	110	329200	0	0	0.2	0	0.2	0	0	0	6.5	2090000	2982					
2041.42	621.31	200000	1860000	1160000	0	1640	9200	127700	4.6	0	1.1	0	0.7	0	0.7	0	14.5	22400	14			-38.6		
2053.21	624.91	460000	2650000	1020000	0	2840	10100	19200	11	0	1.6	0	0.9	0	0	0	22.9	1530	2					
2066.5	628.96	290000	1830000	810000	110	1500	1780	7320	0	0	2.3	0	0	0	0	0	15.5	3140	4		8.8	-30		1.040
2081.42	633.5	440000	1930000	370000	0	2050	8310	240	0	0.9	1.7	0	0	0	0	0	38.2	140						
2084.17	634.34	120000	2720000	2290000	0	1920	14800	47100	0	0	5.2	0.6	0.6	0	0	0	46.5	9000	3		8.5	-45.4		1.056
2101.92	639.75	540000	1930000	20000	0	2070	3470	150	0	0	0	0	0	0	0	0	16.8							

Depth (ft)	Depth (m)	O2+Ar µL/L	N2 µL/L	N2 Calc. µL/L	CO µL/L	H2 µL/L	CO2 µL/L	C1 µL/L	C2 µL/L	C2H4 µL/L	C3 µL/L	C3H6 µL/L	iC4 µL/L	nC4 µL/L	iC5 µL/L	nC5 µL/L	C6+ µL/L	C1/C2+C3	C1/CO2	iC4/nC4 ‰	$\delta^{13}C\ CO_2$ ‰	$\delta^{13}C1$ ‰	δC1 ‰	$\delta^{13}C1$-CO2
2111.71	642.74	300000	1740000	670000	230	1990	10100	420	2.5	1	2.5	0.6	0.8	0	0	0	13.1	90						
2123.75	646.41	170000	1610000	1010000	0	1280	25500	310	2.2	1.6	3.1	0.9	1.1	0.4	0	0	12.5	60		3				
2147.08	653.52	290000	1560000	530000	0	2090	7070	1869800	0	0	2.2	0	1.1	0	0	0	26	838000	264		-4.6	-43.6	-229	1.041
2154.04	655.64	700000	2760000	260000	0	2260	17400	16190	5.6	0	2.4	0	1.4	0	0	0	27.9	2020	1					
2158.38	656.96	480000	2810000	1090000	0	3320	4870	2426900	0	0	4	0	2.3	0	0	0	41.2	605000	498		3.1	-47.3		1.053
2163.71	658.59	1640000	6860000	1000000	0	6510	34200	1241600	158	0	3.9	0	2	0	0	0	59.7	7640	36					
2173.5	661.57	2250000	8300000	260000	0	10790	28600	1130	0	0	0	0	0	0	0	0	74.1							
2178.5	663.1	100000	610000	250000	0	1360	21000	3303700	0	0	0	0	0	0	0	0	30.3		157					
2189	666.3	1000000	4210000	630000	0	4420	700	150030	105	0	0	0	0	0	0	0	42.9	1430	215			-46.3		
2204.08	670.89	1070000	5180000	1360000	380	4740	2920	108700	25.4	0	3.2	0	0	0	0	0	85.2	3800	37					
2210.04	672.71	1150000	4780000	680000	180	4030	600	104900	61.5	0	1.8	0	0	0	0	0	87.4	1660	174			-47	-240	
2228.25	678.26	1450000	5730000	540000	0	5780	1020	121200	72.3	0	0	0	0	0	0	0	81.1	1680	119					
2234.25	680.09	1030000	4440000	760000	0	3470	720	99650	111	0	0	0	0	0	0	0	44.5	900	138			-46.2		
2241.42	682.27	670000	3110000	720000	120	2640	580	69990	99.2	0	1.2	0	0	0	0	0	33.5	700	121					
2256.33	686.82	430000	2330000	790000	110	2170	1020	57370	5.7	0	1.4	0	0	0	0	0	27.1	8120	56		-0.3	-46.9		1.049
2267.67	690.27	550000	2720000	770000	200	2390	500	39430	4.3	0	1.7	0	0	0	0	0	24.9	6610	79					
2278.33	693.52	250000	2490000	1600000	170	2390	510	73130	6.5	0	2.3	0	0	0	0	0	32.6	8390	144			-46.7		
2296.25	698.99	590000	3040000	940000	180	3290	2800	48960	34.2	0	1.5	0	0	0	0	0	44.2	1370	18					
2304.92	701.63	670000	3290000	910000	0	2390	450	109100	93.6	0	1.2	0	0	0	0	0	0.8	1150	244			-46.9		
2316.83	705.26	790000	3720000	890000	0	3240	640	70130	44	0	1.4	0	0	0	0	0	63.7	1550	109					
2324.38	707.56	640000	3240000	950000	0	3100	470	70400	5.9	0	1.6	0	0	0	0	0	57	9370	148			-46.8	-232	
2338.92	711.99	360000	2520000	1230000	150	1270	500	74810	8.6	0	2.7	0	0	0	0	0	27.2	6660	149					
2359.79	718.35	710000	2640000	100000	0	2290	6710	130	0	0	0	0	0	0	0	0	22.5				-11.1			
2363.25	719.41	920000	4830000	1540000	0	3980	1450	56900	8.7	0	3.5	0	0	0	0	0	44.7	4670	39					
2366.58	720.42	1020000	4780000	1150000	0	4600	7580	30300	19.2	0	4.1	1.7	0	0	0	0	54.2	1300	4			-24		
2393.08	728.5	140000	3010000	2510000	420	2770	5130	51900	28.5	1.6	4.2	1	0	0	0	0	29.5	1590	10					
2399.25	730.38	540000	3380000	1440000	240	3020	3640	26300	6.3	0	2	0	0	0	0	0	27.3	3170	7		2.2	-39	-223	1.043
2407.92	733.02	980000	6080000	2590000	1280	5280	3270	56000	14.2	0	5	0	0	0	0	0	69.8	2910	17					
2414.75	735.1	530000	2800000	920000	400	2550	700	15300	6	0	2.7	0.7	0	0	0	0	23	1760	22			-28.4		
2423.25	737.7	710000	6450000	3910000	500	5330	2520	44900	14.4	0	5.8	2.2	0	0	0	0	47.6	2230	18					
2426.75	738.76	340000	3650000	2440000	850	2790	1090	42800	15.3	0	4	1.2	0	0	0	0	78.3	2210	39			-44.2		
2446.67	744.83	440000	2200000	620000	290	2350	4240	300	1.9	1.1	1.6	0.8	0	0	0	0	36.5	90						
2454.33	747.17	110000	2140000	1760000	230	1710	710	48400	29	0	5.1	0.7	1.2	0.5	0	0	29.3	1420	68	2.5	2.6	-45	-230	1.050
2476.17	753.82	90000	2230000	1910000	0	1660	520	54700	11.8	0	2.1	0	0	0	0	0	21.8	3920	105					
2478.5	754.54	490000	2610000	850000	1030	2210	19030	350	2.5	2.2	1.2	0.9	0	0	0	0	20	90			-14.2			
2482.17	755.65	400000	1910000	480000	120	1880	330	62700	7.8	0	0.7	0	0	0	0	0	16.6	7330	189			-46.6	-235	
NA	NA	210000	790000	40000	0	590	120	40	0	0	0	0	0.2	0.4	0	0	9.8			0.5				
NA	NA	210000	790000	60000	30	760	160	250	0	0	0.3	0	0.2	0.4	0	0	10.1		2	0.5				

Table 32: Core gas compositional analyses (chemical analyses based on standards accurate to within 2%) (final 2 samples denoted as NA are drilling fluid at 1940 ft. and 2230 ft.) (Lorenson, et al, 2011)

Depth (ft)	Depth (m)	O2+Ar ppm	N2 ppm	N2 calc.	CO2 ppm	H2 ppm	CO ppm	C1 ppm	C2 ppm	C2H4 ppm	C3 ppm	C3H6 ppm	iC4 ppm	nC4 ppm	iC5 ppm	nC5 ppm	C6+ ppm	C1/C2+C3 ‰	$\delta^{13}C\ CO_2$ ‰	$\delta^{13}C1$ ‰	$\delta C1$ ‰	$\delta^{13}C2$ ppm	C1-CO2	N2 ppm	CO2 ppm	H2 ppm	C1 ppm	C2 ppm
D	**Unit**																										
2029.5	618.75	85800	302700	-3480	480	465	0	611000	0	0	0	0	0	0	0	0	15.0		-3.4	-49.5	-237		1.048	0	785	760	998400	
2033.17	619.87	52700	185100	-2960	490	413	0	761700	0	0	0	0	0	0	0	0	17.9		-3.3	-49.6	-235		1.049	0	643	542	998800	
2033.56	619.97	22800	309700	228000	4100	0	0	663400	25.5	0	0	0	0	0	0	0	0.0	26000	-15.6	-49	-243		1.035	0	*6140	0	*993800	*39.0
2053.21	625.98	66400	234900	-2050	470	469	0	698200	0	0	0	0	0	0	0	0	17.1		-5.2	-49.5	-243		1.047	0	673	671	998600	
C	**Unit**																										
2148.5	655.03	97000	345600	-550	470	435	0	556900	0	0	0	0	0	0	0	0	18.5		-9.6	-48.8	-232		1.041	0	843	780	998300	
2155.04	657.02	120000	462600	34400	370	501	0	417000	0	0	0	0	0	0	0	0	21.6		-5.4	-48.8	-249		1.046	76100	887	1108	922000	
2162.46	659.29	134400	487900	8300	1000	579	0	376700	0	0	0	0	0	0	0	0	20.5		-17.7	-48.9	-243		1.033	21500	2650	1498	974400	
2165.46	660.2	86000	312600	5700	430	431	0	601000	0	0	0	0	0	0	0	0	15.6		-10.9	-48.9	-242		1.04	9400	715	709	989200	
2168	660.98	34600	715400	592000	14600	0	0	235400	19.9	0	0.3	0	0	0	0	0	1.0	11700	-24.5	-48.8	-251		1.026	0	*58400	0	*941500	*80.0
2168.54	661.14	165200	618200	28700	860	696	0	215700	0	0	0	0	0	0	0	0	16.9		-18.4	-48.6	-260		1.032	116700	3970	2830	876900	
2177.58	663.9	166500	598700	4540	940	664	0	233800	0	0	0	0	0	0	0	0	22.3		-16.5	-48.9	-250		1.034	18900	4000	2767	974300	
2179.48	664.48	97700	352900	4250	420	385	0	549000	0	0	0	0	0	0	0	0	18.8		-14.2	-49.2	-248		1.037	7700	764	695	990800	
2179.5	664.49	82100	291500	-1480	4800	0	0	621500	61	0	0	0	0	1	0	0	1.0	10200	-8.6	-48.5	-252	-42.2	1.042	0	*7660	0	*992200	*97.4
Methane Tank and lab air blanks																											
NA	NA	36500	125800	-4450	240	342	0	837400	0	0	0	0	0	0	0	0	12.1			-41.3	-161		0	287	408	999300	
NA	NA	219100	780400	-1470	490	743	0	4	0	0	0	0	0	0	0	0	7.0										
NA	NA	219000	780300	-1210	680	638	0	7	0	0	0	0	0	0	0	0	11.9										

Table 33: Gas hydrate compositional analyses (chemical analyses based on standards accurate to within 2%) (Lorenson, et al, 2011)
* Normalized to methane

Sand Unit	Depth (ft)	Depth (m)	Chamber MPSR	He ppm	H2 ppm	Ar ppm	O2 ppm	CO2 ppm	N2 ppm	N2 calc. ppm	CO ppm	C1 ppm	C2 ppm	C3 ppm	iC4 ppm	nC4 ppm	iC5 ppm	nC5 ppm	C6+ ppm	C1/C2+C3	$\delta^{13}C1$ ‰	$\delta C1$ ‰	N2 ppm	C1 ppm	C2 ppm
D2	2025	617.2	1294	17	0	1350	20000	0	103100	26900	0	875400	46	0	0	0	0	0	95	19030	-48.02	-235.5	30700	969300	51
D1	2047	623.9	1398	0	0	393	5840	0	25400	3200	0	968000	276	0	0	0	0	0	45	3507	-48.44	-234.7	3300	994000	284
D1	2047	623.9	1295	0	0	706	9080	0	42200	7300	0	947800	166	0	0	0	0	0	47	5710	-46.61	-237.6	7700	992000	174
C2	2151	655.6	1320	14	0	174	102	0	9800	8800	0	989800	59	0	0	0	0	0	90	16776	-47.96	-229.6	8900	991000	59
C1	2161	658.7	2876	11	0	215	52	0	14100	13100	0	985200	55	0	0	0	0	0	321	17913	-48.2	-231.1	13300	986500	55

Table 34: Gas hydrate compositional analyses from MDT sampling (chemical analyses based on standards accurate to within 2%) (Lorenson, et al, 2011)

This Page Intentionally Left Blank

and to the processing and subsampling areas helps preserve remaining gas hydrate within the core (Figures 75-88). Initial core processing was accomplished onsite, primarily to ensure that time and temperature-dependent measurements and subsamples were obtained before gas hydrate completely dissociated from the core (Figures 75-78). The core was scraped to reveal sediment beneath the rind of oil-based mud (Figure 79) to allow onsite description and choosing intervals for subsampling. Various subsamples were taken (Figures 80-81) for both time/temperature-dependent onsite analyses and for later offsite analyses. During and following subsampling, an onsite description of the core was completed (Figures 79 and 80).

Depth	Gas	GC	O_2 + Ar	CO_2	N_2	CO	C_1	C_2	nC_4	iC_5	nC_5	C_6+	$\delta^{13}C_1$
Feet	Units	Date	ppm	ppm	ppm	ppm	ppm	ppm	ppm	ppm	ppm	ppm	per mil
1980	144	4/13/2007	219200	130	780400	0	241	0	1	1	1	5	
2010	0	4/13/2007	217700	420	781900	0	6	0	0	0	0	0	
2040	364	4/13/2007	207400	180	739800	0	52600	0	0	0	0	2	-49.5
2070	125	4/13/2007	210900	180	749600	0	39300	0	0	0	0	2	-48.9
2100	114	4/13/2007	215900	150	768000	0	15900	0	0	0	0	2	-47.5
2130	54	4/13/2007	218300	170	775000	0	6520	0	0	0	0	2	-47.5
2160	646	4/13/2007	200400	140	708300	0	91200	0	0	0	0	2	-49.0
2190	91	4/13/2007	218400	200	776000	0	5430	1	0	0	0	2	-49.4
2220	93	4/13/2007	217100	180	770700	0	12000	0	0	0	0	2	-49.0
2250	17	4/13/2007	219100	180	778300	0	2430	0	0	0	0	1	-48.4
2280	22	4/13/2007	218500	130	776900	0	4510	0	0	0	0	1	-48.4
2310	22	4/13/2007	219100	180	777800	0	2870	0	0	0	0	2	-48.9
2340	45	4/13/2007	218100	140	775900	0	5890	0	0	0	0	2	-50.1
2370	11	4/13/2007	219300	150	779200	0	1350	0	0	0	0	2	-49.2
2400	4	4/13/2007	219800	330	779800	0	52	0	0	0	0	2	
2430	20	4/13/2007	218100	140	779500	0	2260	0	0	0	0	2	-48.9
2460	21	4/13/2007	218700	130	778600	0	2570	0	0	0	0	2	-48.5
2490	39	4/13/2007	218400	180	777000	0	4420	0	0	0	0	2	-49.4
2520	45	4/13/2007	217300	130	774600	0	7950	0	0	0	0	2	-48.3
2550	81	4/13/2007	215600	130	772300	0	12000	0	0	0	0	2	-48.1
2580	73	4/13/2007	215600	130	773600	0	10700	0	0	0	0	2	-48.3
2610	70	4/13/2007	215900	130	774400	0	9570	0	0	0	0	2	-48.1
2640	56	4/13/2007	217200	130	774800	0	7840	0	0	0	0	2	-48.0
2670	124	4/13/2007	214000	140	770000	0	15900	0	0	0	0	2	-48.2
2700	95	4/12/2007	215600	220	771400	0	12800	0	0	0	0	2	-47.8
2730	389	4/12/2007	208000	140	743100	0	48800	0	0	0	0	2	-48.9
2760	152	4/13/2007	213400	140	766600	0	19900	0	0	0	0	2	-47.5
2790	208	4/13/2007	216700	230	772800	0	10300	0	0	0	0	2	-47.4
2820	152	4/13/2007	214200	150	765500	0	20100	0	0	0	0	2	-47.9
2850	212	4/13/2007	211100	130	761500	0	27300	0	0	0	0	2	-47.8
2880	133	4/13/2007	213300	130	768800	0	17800	0	0	0	0	2	-47.2
2910	147	4/13/2007	211900	140	768500	0	19500	0	0	0	0	1	-47.9
2940	105	4/13/2007	213800	140	772400	0	13700	0	0	0	0	2	-47.6
2970	55	4/13/2007	214300	130	773500	0	12100	0	0	0	0	2	-48.4
3000	61	4/13/2007	216500	130	775700	0	7690	0	0	0	0	2	-47.8

Table 35: 35 Mount Elbert-01 shallow formation gas data analyses, Isotech Lab (also Table 30)

Core temperature provides an indicator of gas hydrate presence (Figure 82). Over the first several minutes of onsite core processing, gas and water are actively dissociating from gas hydrate. This endothermic reaction cools the core, freezes the pore water, and helps delay gas hydrate dissociation within the innermost portion of the core. Samples of gas hydrate were placed into water (Figure 83); where gas hydrate is present, the water causes the gas to more actively dissociate from the hydrate. Headspace gas evolves and can be studied qualitatively in syringes (Figure 84) or in petri-dishes or cans (Figure 83).

Certain subsamples were acquired for further onsite processing to determine the saturation and composition of pore waters (Figures 85-88). Coring with the oil-based drilling fluid also ensured that only natural pore waters were present within the core. Samples were scraped to obtain a cleaner sediment from the innermost portion of the core and placed into a press to squeeze pure pore waters from the sample for later laboratory analyses (Figures 85-88).

A total of 261 total subsamples were processed onsite, primarily to preserve time and temperature dependent data. Eleven of these samples were preserved, four in methane-charged pressure vessels and seven in liquid nitrogen. Other samples were obtained for physical property measurements, petrophysics, water chemistry, thermal properties, and microbiological and organic geochemistry studies. Subsamples of the core were analyzed at various labs. The remaining whole core was then transported to Anchorage and stored in freezers within a refrigerated unit at the ASRC Fabrication shop.

5.3.8.8.1 Onsite Core Operations, Subsampling and Analyses

This section describes onsite core subsampling and initial analyses. Table 36 lists the core operations and subsampling field team.

Name	Function	Affiliation
Micaela Weeks	Wellsite Operations Coordinator	BPXA
Larry Vendl	Wellsite Operations Coordinator	BPXA
Bob Hunter	Shift lead, core processing	BPXA Contractor
Tim Collett	Shift lead, core processing	USGS
Bill Winters	Core processing & MDT sensor	USGS
William Waite	Core processing	USGS
Tom Lorenson	Core processing, gas sampling	USGS
Warren Agena	Drill Press, subsampling	USGS
Ray Boswell	DOE Program lead, core processing	DOE / NETL
Kelly Rose	Sedimentology, core processing	DOE / NETL
Eilis Rosenbaum	Thermal Studies, subsampling	DOE / NETL
Marta Torres	Pore Waters, subsampling	Oregon State University
Rick Colwell	Microbiology, subsampling	Oregon State University

Table 36: Core field operations team leads, functions, and affiliations (excludes OMNI, now Weatherford, staff)

Figure 75: Core barrel being lowered from rig floor to pipeshed via V-door

Figure 76: Core barrel inner liner separation in cold pipeshed processing area; rig mats placed on pipe racks provided working surface

Figure 77: Core inner barrel cutting into 3 foot segments in pipeshed with core end visible in lower left side of photo

Figure 78: Transport of 3 foot core segments in lined box via forklift from pipeshed to core processing “cold” trailer

Figure 79: Dr. Timothy Collett (USGS) scrapes and describes gas hydrate-bearing core in core processing "cold" trailer, February 2007

Figure 80: Robert Hunter (BPXA consultant) subsamples gas hydrate-bearing core in core processing "cold" trailer, February 2007

Figure 81: Foam inserts mark where core was subsampled for headspace gas, microbiology, interstitial water and physical properties (appendix A of R18 contains onsite descriptions)

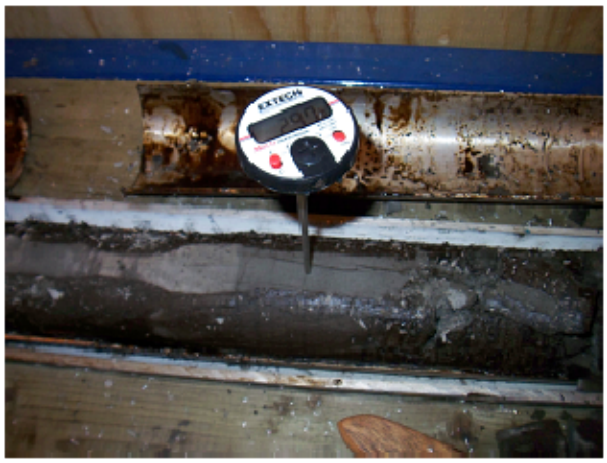

Figure 82: Temperature probe test used to show decreased temperature with time during gas hydrate dissociation in hydrate-bearing core samples during onsite subsampling

Figure 83: Gas hydrate-bearing samples in water bubble with gas escape during gas dissociation onsite testing for gas hydrate presence in core samples

Figure 84: Gas hydrate-bearing sediment placed in syringe to monitor gas escape from gas hydrate dissociation in hydrate-bearing core samples during onsite analyses

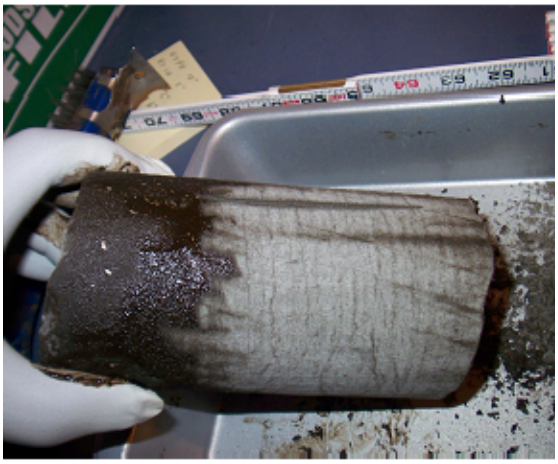

Figure 85: Whole core sample is scraped to remove oil-based drilling mud contamination

Figure 86: Cleaner innermost portion of core prior to placement into drill-press to remove formation water for later laboratory analyses

Figure 87: Marta Torres (Oregon State University) during subsampling of core for pure interstitial water samples

Figure 88: Warren Agena (USGS) and Kelly Rose (USDOE) work the drill-press to obtain interstitial water for later analyses

The shift leads arrived on the North Slope to coordinate core processing materials shipments on February 3, 2007. The drilling rig (Doyon No. 14) arrived on location February 5, 2007. The hole was drilled to the surface casing point at 1,950 feet by February 8, 2007. An 9 5/8 inch casing was emplaced to the surface casing point near the base of permafrost and successfully cemented. The water based drilling fluids were then displaced for an oil based fluid and the mud chiller was brought online. The fit-for-purpose formulated mineral oil-based drilling fluid was provided by MI-SWACO and the DrillCool engineers maintained the drilling fluids at temperatures typically below 30°F. The ReedHycalog *Corion* wireline-retrievable coring system was tripped into the hole, with the first core being recovered to the surface at 03:28 hour on February 10, 2007. The well was then continuously cored to a depth of 2,494 feet, with the last core recovered at 14:50 hour on February 12, 2007. This system delivered 85% recovery of 3-inch diameter core through 504 feet of hole. The coring team processed these cores on site, collecting and preserving 261 subsamples for analyses of pore water geochemistry, microbiology, gas chemistry, petrophysical analysis, and thermal and physical properties. In addition, 11 gas hydrate-bearing core samples were immediately transferred to either methane-charged pressure vessels or liquid nitrogen for future study of the preserved gas hydrate.

5.3.8.8.1.1 Core Receiving

Upon recovering the wireline inner core barrel at the derrick floor, the ends of the barrel were wrapped in plastic and absorbent material and lowered through the V-door to the pipeshed (Figure 75). Both the rig and the pipeshed were kept cold at near outside ambient temperatures during all core handling operations. The shoe to the inner barrel was then removed and the two 12-foot long core liners were extruded from the inner barrel (Figure 76) and cut into three foot working sections (Figure 77). The core sections were placed in a wooden box and moved to the cold core receiving lab by fork-lift (Figure 78). On average, about 20-25 minutes transpired during moving the core from the rig floor to the cold core receiving lab. Each core run was instrumented with a small pressure-temperature logger (Figure 61), from which data were downloaded at the end of core operations.

5.3.8.8.1.2 Core Processing

Upon arrival of the core in the cold core receiving lab the following procedures were conducted:

- Pick up core and move to trays
- Clip tabs on split liner (skill saw was required)
- Lay out full core length and initial inspection
- Wipe off and clean (Figure 79)
- Describe, subsample, and onsite analysis (Figures 79-88)

5.3.8.8.1.3 Core Logging

Core was processed quickly to enable subsampling prior to gas hydrate dissociation. For core measurements, it was decided to use a "core section" approach in which each "three-foot" piece of core was identified as a unique "Section" (numbered 1-8) from the "Core" run (numbered 1-23) being processed. Marker cards were placed along the side of each core section. After the field program, the individual cores and sections were assigned measured well depths from the drill pipe depths as recorded at the beginning and end of each core run. ReedHycalog *Corion* created a "Well Summary" report; a Core-Sample Depth Assignment Spreadsheet recorded the depth of each core and core subsample. The core was quickly scraped (Figure 79) to visually identify gas hydrate occurrence, physical properties, gross sedimentology and structure; this information was entered into a master core description and sample data sheet (see R18, appendix A, pp. 68-117 for scans of these field descriptions). Digital thermometers were utilized in about every other core section and the temperatures were recorded (Figure 82). Small subsamples of core were placed in water-filled dishes and cans to identify possible gas hydrate-bearing sections via observed gas bubbling (Figure 83). A gas detection monitor placed for safety within the cold core processing unit did not reveal significant measurable off-gassing during these operations.

No Thermal IR was conducted; a skate mounted system and hand held camera were available, but not employed due to processing time constraints. Similarly, all gamma ray core scanning was deferred until post field examination of the core. Plain light photo imaging (ad hoc photos) of the core were taken; these images were compiled and are part of project file records. Digital (DVD) videos were taken of the core handling and processing procedures; these videos were also complied and are part of project file records.

5.3.8.8.1.4 Gas Hydrate Core Sampling

Figure 89 depicts the core sampling plan with sample codes and sub-sample core sizes. When gas hydrate was expected, small pieces of core (typically core edge-chips) were placed in syringes to conduct a quick gas hydrate dissociation test (Figure 84). Gas hydrate samples consisting of whole round core (WRC) samples from selected gas hydrate-bearing sections were removed from the core and stored in (1) liquid nitrogen (HYLN) or (2) Parr pressure vessels (HYPV) and also frozen (see R18, appendix A, pp. 68-117 for scans of core and subsample field descriptions).

5.3.8.8.1.5 General Whole Round Core (WRC) Sampling

Head space (HS) gas samples (WRC samples) were placed in quart size cans. Microbiological (MBLN, MBRF) samples were acquired; WRC samples were removed from the core, processed, and stored in liquid nitrogen or frozen at outside ambient temperature. WRC subsamples for interstitial pore water (IW) sampling were removed from the core and transferred to the Warm Core Lab for processing (Figures 85-88). Physical property (PPMA) WRC samples (mass

properties and grain size analysis) were removed from the core and processed for storage. WRC samples were also removed for petrophysical analyses (porosity-permeability, etc.) and physical properties analyses (geotechnical, strength testing - PPOM) and frozen for shipping. WRC core samples were also collected for onsite thermal properties and conductivity (PPTHERM) analyses in the Warm Core Lab and were subsequently frozen. Core chips on one foot spacing were acquired for the State of Alaska.

5.3.8.8.1.6 Core Archiving and Storage

Gaps left by removing core subsamples were filled with styrofoam blanks labeled with sample codes described above and in Figure 89. The core was wrapped in plastic and the core liner was placed back on the core (for some of the non-gas hydrate-bearing cores below Core 10, the inner core was not wrapped in plastic). The cores were then sealed with tape, labeled, and boxed. The core was then transferred into 4x4-foot storage units and allowed to freeze at outside ambient temperature prior to transportation to the temporary core storage facility near the ASRC Fabrication shop in Anchorage.

5.3.8.8.1.7 Other Non-Core Related Samples

- Canned drilling cuttings taken by mud loggers
- Flowed gas samples, collected in ISOTUBES
- Washed drill-cuttings samples for the State of Alaska
- Mud samples for microbiological sample characterization
- Mud samples for pore water sample characterization

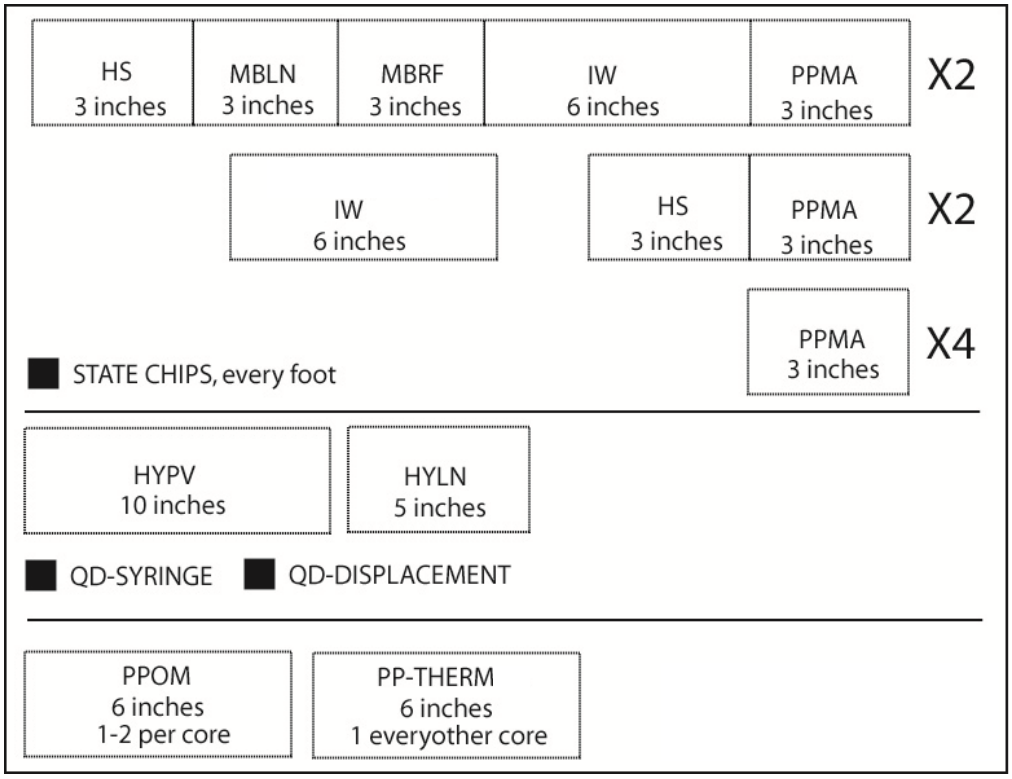

Figure 89: Core sampling plan with sample codes and sub-sample core sizes

5.3.8.8.1.8 Physical Properties Program (PPMA and PPOM)

The physical properties program in support of the Mount Elbert #1 gas hydrate stratigraphic test well was conducted to primarily study the geologic controls on the formation and presence of gas hydrate from a depth of about 2,000 feet to the bottom of coring at about 2,500 feet. More specific goals of the program include determining: (a) intrinsic formation properties (such as permeability and strength) needed by modelers for predicting behavior during gas hydrate production; (b) stress history and other properties of fine-grained "seal" materials and relating them to sedimentology; and (c) baseline index and grain size properties of host sediment and relating them to gas hydrate occurrence. Six types of samples were collected from 23 recovered cores by the physical properties team.

For index physical properties, a total of 52 2-3 inch long WRC samples (PPMA) were collected continually down hole, typically 2 to 3 samples per 24 foot-long core. When possible, excess drilling mud was removed by scraping the external surfaces of intact samples or by removing contaminated portions from unconsolidated sediment. These samples were stored in heat-sealed low-diffusion clear plastic bags and refrigerated (not frozen). Base-line physical properties, such as moisture content, grain density, porosity, bulk density, unit weight, and grain size were later determined from these samples. A challenge in this program was to mitigate the effect of drilling fluid contaminants present in some test samples.

Grain size analyses of routine samples are typically conducted by wet sieving the coarse fraction and performing a Coulter Counter analysis on the fine fraction in the USGS Sedimentology Laboratory located in Woods Hole, MA. Many of the samples recovered from the Mount Elbert #1 well are contaminated with significant to trace amounts of oil-based drilling mud and required special handling and procedures. Removing oil-based mud contaminants from samples was necessary to produce accurate results. Additional grain size analysis was conducted on trimmings from interstitial water (IW) and microbiology (MBRF) samples.

Fourteen (14) WRC samples in both coarse- and fine-grained sediment were collected for petrophysical testing by OMNI Laboratories (PPOM). These samples were 6 inches or less in length and were primarily collected as intact sediment without significant fractures or other signs of coring disturbance. Each sample was scraped to remove surficial drilling mud, wrapped in thin clear plastic and taped into a half-round aluminum liner for stability. The sample and liner were wrapped in two additional plastic bags, taped, labeled, and maintained at freezing temperatures by storing them outside the work trailers. Samples were maintained in a frozen state during shipment to OMNI Laboratories.

5.3.8.8.1.9 Gas Hydrate-Bearing Sediment Preservation (HYPV and HYLN)

Four (4) approximately 10-inch long whole-round samples of gas hydrate-bearing sandy sediment were quickly scraped to remove surficial drilling mud, wrapped in aluminum foil, placed into Parr pressure vessels (HYPV), and kept frozen. They were initially pressurized to 800 psi with 99.99% pure (Ultra High Purity) methane gas. Prior to shipping, the pressure in the vessels was increased to 900 psi after it was noticed that initial pressures had decreased to 650, 690, 700, and 750 psi, respectively. The frozen samples were shipped over land to Anchorage, with subsequent air shipment to individual researcher(s) to assess volume change behavior during dissociation and to assess behavior of the samples containing remnant gas hydrate.

Seven (7) WRC gas hydrate-bearing core samples, 5-inches in length, were wrapped in aluminum foil, placed into a labeled cloth bag, and placed into Dewar shippers filled with liquid nitrogen. The shippers were kept outside the work trailers at sub-freezing ambient temperatures. The Dewar shipper samples were later transported by air freight to designated research facilities. The JMPG volume summarizes analyses of some of these gas hydrate-bearing sediment subsamples (Kneafsey, et al, 2011and Lu, et al, 2011).

5.3.8.8.1.10 Interstitial Water (IW) Program

A total of 46 WRC samples were collected in the cold trailer and transferred to the warm lab for placement into squeezers located in the warm trailer to remove pore water for chemical analyses of interstitial water (IW). The samples, 4 to 8 inches in length, were wrapped in clear plastic film and placed into a labeled Whirl-Pak bag before being delivered to the warm trailer. The silty-clays and gas hydrate-bearing well-sorted fine-grained sands were consolidated ("cemented" by the gas hydrate) and the oil-based drilling fluid muds were easily removed from the outer sections of the sample. In poorly consolidated (typically non-gas hydrate-bearing) or fractured sands, the drilling mud penetrated the sample interior, making them difficult to fully clean. Two samples (Core 14, Section 7, 10-18 and Core 15, Section 7, 22-30) were pervasively contaminated and were deemed unsuitable for processing. Two other samples (Core 11, Section 3, 30-34 and Core 13, Section 3, 16-24) left an oily residue in the filter indicative of oil-based drilling mud contamination.

From all samples, a subsample was analyzed for grain size and the remaining cleaned sediment was loaded into stainless-steel squeezers, modified after that of Manheim and Sayles (1974). A laboratory hydraulic press was used to apply pressure to the squeezers and extract the pore water. Interstitial water was passed through a Whatman No.1 filter fitted above a Teflon frit, filtered through a 0.2µm Gelman polysulfone disposable filter, and subsequently extruded into a precleaned (10% HCl) plastic syringe attached to the bottom of the squeezer assembly. Volumes ranging from 1 to 17 cm^3 of pore water were collected.

Salinity was measured as total dissolved solids using an Index Instruments™ handheld digital refractometer. Conductivity (R_w) was measured using a Radiometer Analytical CDM 210™ conductivity meter followed by a temperature measurement. The conductivity probe was calibrated with standard KCl solutions. All Rw values were normalized to conductivity at 77^o F (25^o C).

Figure 90 illustrates initial analyses of the down-core distribution of the pore water salinity and conductivity, showing a good correlation between these parameters and documenting the presence of gas hydrate in the intervals from approximately 2,010 to 2,080 feet (Zone D) and from 2,140 to 2,220 feet (Zone C). Dissolved chloride analyses later permitted better quantification of gas hydrate occupancy in these zones; however, the presence of gas hydrate in these zones was also verified from NMR surveys and visual observation in the cores. The gas hydrate preferentially occupies these reservoir sands (zones C and D) within the formation.

Interstitial water subsamples were collected in 4 ml glass vials for subsequent analyses of dissolved Cl, and other major constituents. Depending on the volume of pore water available, additional subsamples were taken in glass vials for isotopic characterization of the pore water (oxygen and deuterium) and dissolved inorganic carbon (preserved with mercuric chloride). In

addition, subsamples were collected for analyses of dissolved volatile fatty acids (in glass vials and frozen), sulfide (in microcentrifuge tubes fixed with cadmium nitrate), ammonium (in glass vials and frozen) and minor and trace metal constituents (in acid washed nalgene bottles). The sediment sample remaining after squeezing was sealed in a plastic bag to remain available for chemical characterization of the solid phase.

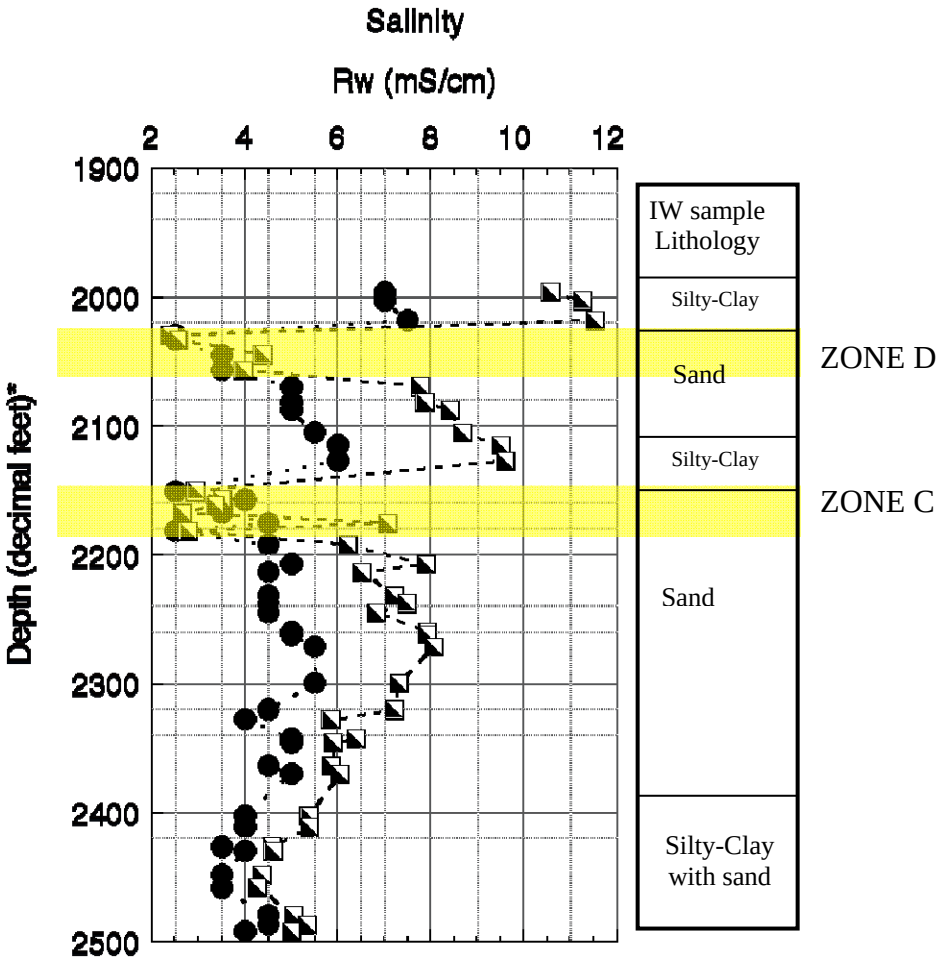

Figure 90: Distribution of salinity and conductivity in pore water samples from Mount Elbert #1

5.3.8.8.1.11Microbiological Sampling Program (MBLN and MBRF)

Collected subsamples were used to determine the influence of sediment properties such as grain size, interstitial water chemistry, or the presence of hydrates on the type and number of microbial communities in the sediments. Such data can augment computational models that describe gas hydrate-bearing sediments and were later compared to similar data collected for sediments collected from off the coast of India as a part of the NGHP coring effort. To assess sample quality, twenty four drilling mud samples as well as approximately 40 core subsamples were collected to be used to determine the degree of drilling mud invasion into the cores. Fluorescent microspheres were used to trace the presence of microbial-sized particles on the outside and inside of the cores during each core run. A preliminary assessment revealed that some of the cores are of high quality (low mud invasion) whereas some are of questionable quality due to the lack of core integrity, unconsolidated sediment (especially in the non-hydrate-bearing sands) and the associated invasion of drilling fluids. Three methods of core sampling were used for the microbiology samples: 1) preservation of intact whole round cores (this required paring of the

samples at a later date), 2) paring of the cores to remove the outside rind before storage, and 3) flaking away the outer contaminated core material and then scooping the interior of the cores from near the core centers for preservation (Figure 91). The variable consistency of the cores required these diverse approaches to help best obtain undisturbed inner core for microbiology analysis.

As a result of the Mount Elbert sampling effort, 80 samples were collected for microbiological analysis, half of them frozen in liquid nitrogen (MBLN) for molecular analyses and half of them refrigerated (MBRF) for cultivation-based experiments. The 80 samples were obtained from 45 locations within the approximately 504 feet of vertical depth cored. Based on onsite assessments, at least seven of these 45 locations contained gas hydrate, all of which occurred between 1,990 and 2,184 feet. Microbiology samples were paired with samples collected for interstitial water analysis and gas analysis.

Figure 91: Photo of core run #19, section 7, inches 1-3 after shaving the drilling fluids away from the surface and before scooping the inner portions of the core for microbiological analysis (left) and after scooping the inner portions (right).

5.3.8.8.1.12Thermal Properties and Conductivity Program (PPTHERM)

This project marked the first field deployment of NETL's thermal properties measurement device. This field program provided valuable insight into future endeavors and future directions for NETL's thermal properties measurements of gas hydrate-bearing sediments. Additional design criterions for a robust field device were developed. Thermal properties, specifically thermal conductivity and thermal diffusivity, of methane hydrate-bearing sediments, help improve gas hydrate reservoir modeling and help determine the behavior of gas hydrate in nature and during potential gas production testing. Field measurements have the potential to provide more accurate and representative data than can be acquired in the lab alone.

The mobile device performed very well in the field and thermal property measurements were successfully acquired on 5 of the 5 WRC samples collected. These samples were quickly separated from the core during initial processing in the cold trailer and brought to the warm trailer for measuring thermal conductivity. The samples were wrapped in thin plastic film, taped into aluminum half round liner for support, and labeled prior to delivery.

Modifications were made to the unit (Figure 92) that later proved successful for thermal property measurements on gas hydrate and gas hydrate-bearing sand samples formed in the laboratory. Both thermal conductivity and thermal diffusivity were obtained from one measurement.

Figure 92: Eilis Rosenbaum (left) beside the thermal properties measurement device, used to collect data. The probe's sensor (right), is placed in contact with the sample.

WRC were received intact, wrapped in thin plastic film, supported on aluminum half round liners, and labeled prior to delivery to the thermal property lab. For each sample, the oil based drilling mud (Figure 93) was scraped from a portion of the side of the WRC to expose a clean section of the sample. To ensure contact between the sample and sensor, the sample surface was smoothed by scraping. Thermal property measurements were taken by pressing the probe into the exposed side of the WRC (Figure 94). Multiple measurements were taken on five different cores, both gas hydrate-bearing and non-gas hydrate-bearing. The sediments consisted of unconsolidated silty clays, fine grained sand, and medium-grained sand; however, the gas hydrate-bearing sands were well indurated as the hydrate "cemented" the grains. Each sample was cleared of the drilling mud (Figure 94b) and frozen for shipment back to the laboratory where additional experiments took place.

Figure 93: WRC subsample covered in and invaded by drilling mud

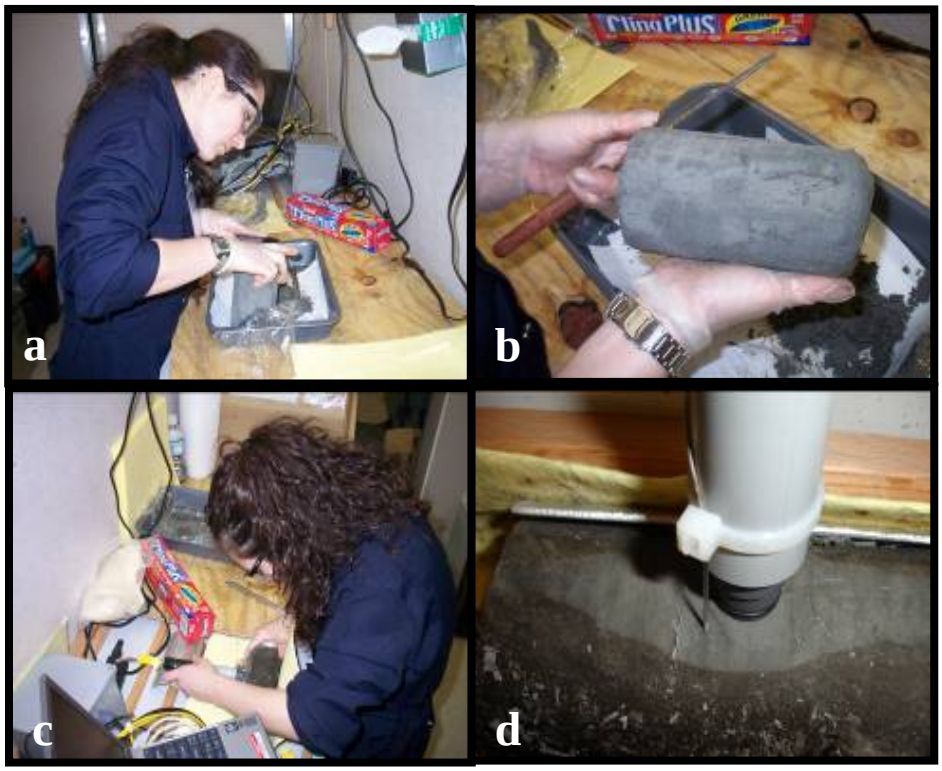

Figure 94: Sample preparation and thermal properties measurement. Drilling mud was removed prior to measurements (a and b). For time critical measurements on gas hydrate-bearing sediments, only a portion of the drilling mud was removed for measurements (c and d).

5.3.8.8.1.13List of Supplemental Information

The project files also contain additional supplementary information, including:

- ReedHycalog *Corion* "Well Summary" report
- Core-Sample Depth Assignment Spreadsheet
- Digital scans of the master core description and sample log sheets (see R18, appendix A)
- Listing of canned drill cuttings, ISOTUBES, headspace core samples, and syringe (QD) hydrate dissociation samples acquired by mud loggers or from core (Gas samples)

5.3.8.8.2 Core Transport, Storage, Imaging, and Activities

Following core acquisition, the 430 feet of recovered core was transported over land to an Anchorage, Alaska site where it was slabbed into half-sections (1 library and 1 sample set). Both sets were temporarily stored within 8 freezers within a refrigerated 220 volt connex Refer unit that was modified with a mandoor and 110 volt lighting (Figures 95-96). The dual freezer system was redundant to reduce the chance for power failure disruption. The remaining onsite subsamples were shipped to various laboratory facilities, including LBNL, NRC, PNNL, CSM, and USGS, for further analyses. Prior to slabbing, OMNI Labs ran a core gamma ray and "gapped" the core gamma to account for gaps due to both non-recovery of core and onsite core subsampling. Figure 97 illustrates the core gamma results composite for the recovered 430 feet of 503 feet cored. The core gamma was correlated to log field prints and only showed a shift of zero to three feet throughout the cored intervals. When final logs were completed by Schlumberger, the core gamma was correlated and shifted to the final log dataset. Following

modification for lighting and access, the temporary core storage facility was used extensively for additional core description, limited subsampling, core imaging, and various project activities (Figures 98-99 and 100-115).

In May, 2007, the core was sampled for Palynology studies by D. Houseknecht, USGS (Figure 98). A study of Sagavanirktok palynological biostratigraphy (Bujak, 2008) was also published in-full in the Appendix of R24, pp. 45-62.

High-resolution core scanning was performed within the Refer unit in late 2007. Geotek core scanning services were substituted for core photography due to the higher resolution images provided by Geotek versus standard core photography. The high-resolution core scans of the library set of Mount Elbert-01 core were completed in December 2007. The scans successfully recorded images better than can be observed through the naked-eye or a low-power hand-lens. Jpeg reductions of the high-resolution images and full-size images are stored within project electronic files. The Library Set of Mount Elbert-01 cores were imaged by Geotek personnel using the Geoscan IV linescan camera and automated track from Dec 5-10, 2007. All imaging was performed in the refrigerated storage unit at a temperature of 42^{o}F.

High-resolution image data were provided on a hard disk and are stored in project electronic files. The folder "mtelbert01" includes all the core images. Each folder represents a single core and folders are named ME-01-core number. Within each core folder are three sets of 16-bit TIFF core section images, two with rulers (cm and in) and one without, and a set of XML files. The XML files are used by the Geotek imaging software. The files are numbered IMsectionnumber, e.g., IM002_01.tif is an image of section number 2 in a given core. Section number "66" was used for the core catcher. TIFF files followed by an "R" have a cm ruler appended to the image left edge. Subsequent additional TIFF files were created followed by an “in” showing an inches ruler appended to the image left edge. Smaller jpeg files were created and stored in project electronic files. The folder "CoreBoxes" contains snapshots of each core box as it was opened. The folder "CoreHandling" contains pictures documenting the imaging procedure as shown in Figures 100-115. Cores invaded with oil-based drilling fluid appear very dark, but details are still visible when the brightness and contrast are adjusted.

Potential artifacts are evident on core surfaces. Cores were unlined and friable within the core storage boxes. The delicate, unlined core was very difficult to transfer to the one-third liners used to support the cores during imaging. While no core pieces were destroyed, desiccated edges tended to crumble, so cores could not be scraped. The frozen core surfaces could not be scraped to present a fresh surface for imaging. Any artifacts from cutting the core (e.g., potential smearing of clay into sands) remain in the images. Saw marks, though visible to the eye, are not visible in images due to the uniform lighting. The library set was, however, lightly sanded by OMNI prior to placement in the core boxes to remove most saw marks.

In 2011, both frozen core sections were shipped via air freight within coolers containing dry ice to DOE’s core storage freezer facility at Oregon State University in Corvallis, Oregon. The temporary core storage facility was decommissioned and later sold to ConocoPhillips.

Figure 95: 6 of 8 Freezers installed for core storage in refrigerated unit prior to temporary disconnection of unit for installation of man-door, electrical outlets. and lighting (May 16, 2007)

Figure 96: ASRC electrical and construction staff modifying core storage refrigerated unit for lighting, electrical outlet, and man-door. Extension cords visible in photo were for temporary power to freezers to keep core cold during unit modification (May 16, 2007).

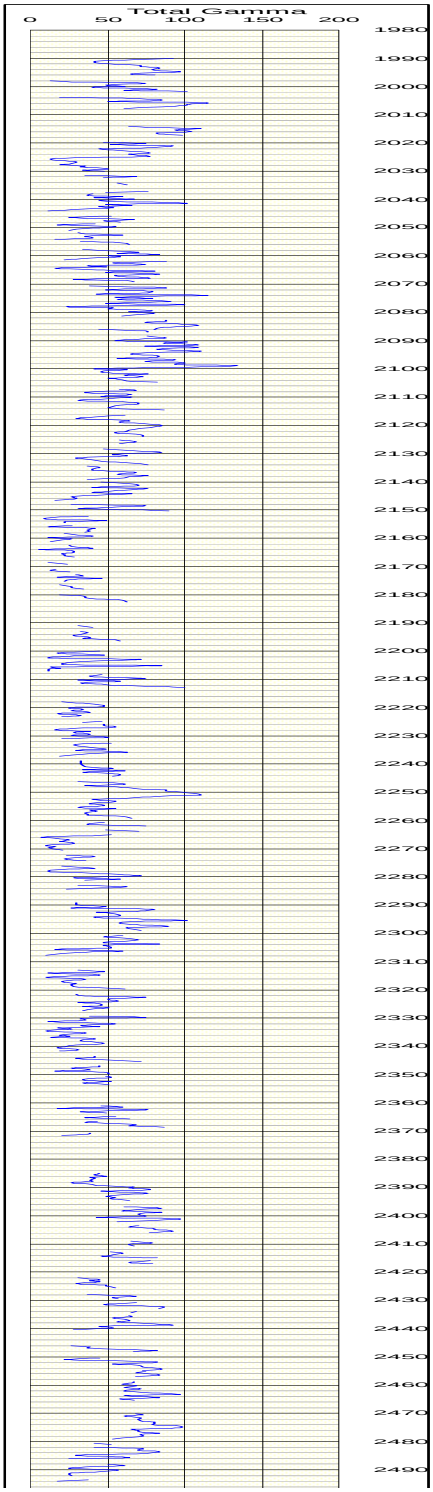

Figure 97: Core Gamma Ray results. Depth scale is 1,980 through 2,490 feet, bold lines are 10 foot intervals. Gamma scale is 0-200. Gaps in gamma correspond to core subsamples and non-recovery.

Figure 98: Dave Houseknect, USGS, views Mount Elbert-01 core, May 22, 2007

Figure 99: Core sample from Mount Elbert-01 library set ½ slab, May 22, 2007

Figure 100: Step 1: Boxes of library set core sections were removed from the freezer (temperature ~20^{o}F), one at a time

Figure 101: Step 2: The tape was slit and the boxes opened

Figure 102: Step 3: Plastic wrap, if present, was removed from the cores

Figure 103: Step 4: The core box including a hand-written label was photographed for records

Figure 104: Step 5: Core sections were carefully placed into one-third liners (see "Potential Artifacts," above)

Figure 105: Step 6: Complete placement of core sections into one-third liners

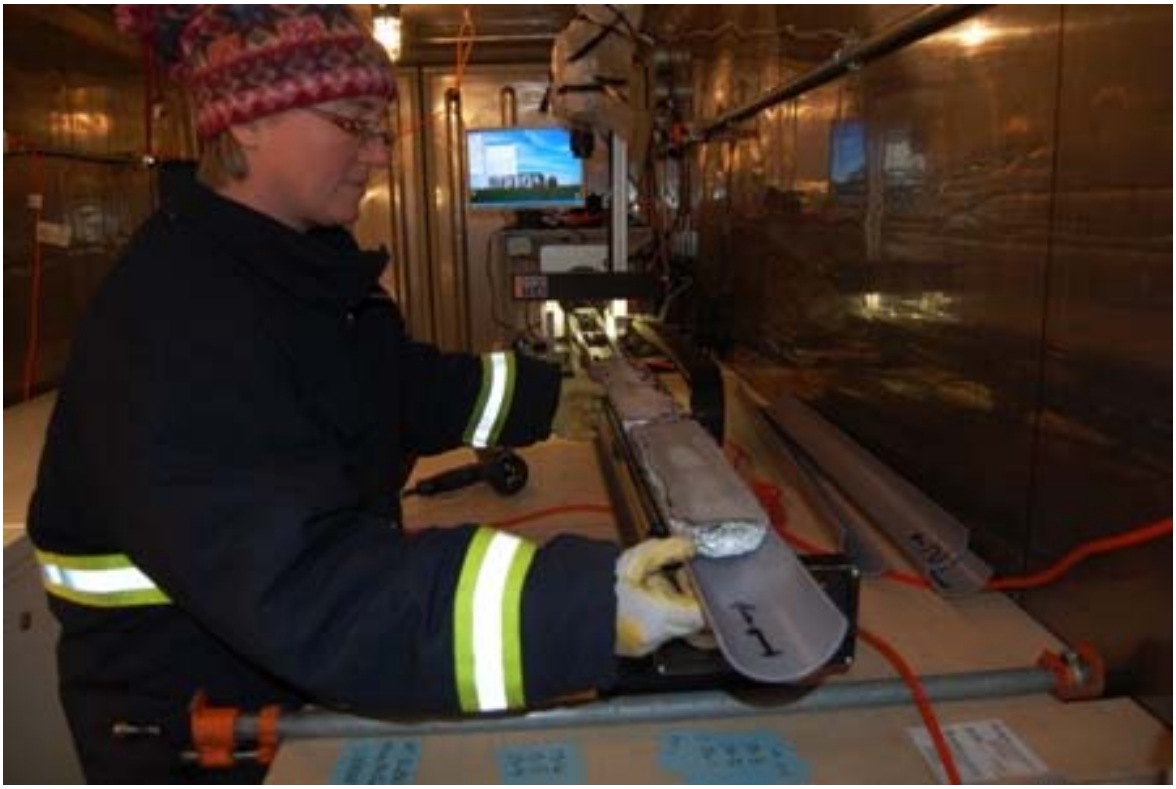

Figure 106: Step 7: Core sections in liner were placed on the Geotek imaging track

Figure 107: Step 8: Cores were scanned at a resolution of 200 pixels per centimeter at a single set of lighting and aperture conditions, and the camera was consistently calibrated with an 18% grey card so that each image is comparable with every other image

Figure 108: Step 9: Core surfaces were heated using a heat gun to melt surface frost, typically resulting in a wet surface when imaged (see "Potential Artifacts," above)

Figure 109: Step 10: Core sections within the liner were removed from the camera track

Figure 110: Step 11: The core sections in the core liner were aligned with the core box in preparation for removal

Figure 111: Step 12: The core sections were gently removed from the track in the liner and placed back into the core storage box

Figure 112: Step 13: Core sections were placed back into their storage box

Figure 113: Step 14: Plastic wrap, if present, was replaced over the core surfaces and bubble wrap (flat side to the core) was substituted if no plastic wrap was present

Figure 114: Step 15: Core storage boxes were closed with strapping tape wrapped around ends

Figure 115: Step 16: Core storage boxes were placed into a temporary storage freezer until all cores from original freezer are processed; cores were then replaced in the correct order in the original storage freezer; cores were out of the freezer for a maximum of 20 minutes at 42^{o}F

Cores were colder than the temperature at which they were imaged. The cold cores condensed moisture from the warmer air (42°F) and frosted over. The surface frost was melted using a heat gun immediately before imaging and this moisture soaked into the core, relieving the need to wet the surface of the core for imaging. However, occasional patches of ice may be present in the images. Some non-gas hydrate-bearing unconsolidated sand cores were fully invaded with oil-based drilling fluid; the melted ice could not soak into the core and formed droplets of water on the surface of the core. Large droplets were blotted with a paper towel when possible.

Cores were differentially desiccated. Cores were originally stored with plastic wrap sealing the tops of the cores, but this plastic wrap was not tightly stretched and not always present. Swirls and whorls were present in the core images, especially in clay or shale sections, due to wrinkles in the plastic wrap. Where the plastic wrap was not in contact with the cores, the cores desiccated ("freezer-burn"). Some of the desiccation was ameliorated by the melting of the condensed frost before imaging, but swirls, whorls, and drying at the edges of the core (mainly in sands) can be seen in the images.

Core thicknesses slightly differed due to erosion during acquisition. Because the cores were not always split evenly, the height of the split core also varied. Core material that departed significantly from the median core height may be slightly out of focus.

Recommendations for future core imaging work includes:
1. Cores should be imaged as soon as possible after being split
2. Cores should be scraped if possible and a wet surface imaged to bring out the fine detail in the cores
3. Consider splitting and storing cores in a liner so that they can be handled later; if cores are stored in a liner, they may not need to be frozen
4. Seal cores well against desiccation using heavy-duty plastic

5.3.8.8.3 Conventional and Special Core Analyses

Core plugs and whole core subsamples were analyzed by CTscan at OMNI laboratory and LBNL, respectively. CTscanning revealed multiple processing-associated or drilling induced fractures that complicated the mechanical rock property studies. Previous pressure-core studies by Geotek Labs (personal communication, December 2007) suggested that the “processing-associated” fractures likely propagated during dissolution of gas hydrate into free gas and water during core recovery operations at atmospheric temperatures and pressures.

OMNI Laboratory (now Weatherford Lab) studies of the Mount Elbert-01 core included conventional core analyses (porosity, permeability, etc.), special core analyses, physical property analyses, and geomechanical analyses (Tables 37-44, Figures 116-118):

1. Core Screening by CT Scanning (Appendix B): 14 Whole Core samples
2. Twin plugging of suitable whole core samples: 35 plugs acquired
3. CT Scanning of all plugs obtained from whole core plugging (Appendix B): 35 plugs plus 9 drilled at OMNI Anchorage Lab
4. Routine Properties of porosity, permeability, and grain density (Table 37, Figure 116): 16 samples
5. X-ray Diffraction (bulk & clay) – Mineral composition (Table 38): 10 samples

6. Rock Mechanics with Mohr Coulomb Failure (Tables 39-41, Figures 117-118): 2 samples, one in gas hydrate-bearing zone and one in non-gas hydrate-bearing zone
7. Laser particle size analysis (Table 42 and Appendix B): 23 samples
8. Thin Section Petrography (Tables 43-44 and Appendix B): 10 samples

Table 37 summarizes conventional core analyses. Samples were vacuum oven-dried at 140°F.

Core Number	Sample Number	Sample Depth, feet	Net Confining Stress, psi	Median Grain Size, microns	Permeability, millidarcys		Porosity, percent		Grain Density, gm/cc
					to Air	Klinkenberg	Ambient	NCS	
2	2-2-8	2017.10	572	10.27	12.2	10.1	33.2	33.1	2.70
2	2-2-21-27B	2018.35	572	6.76	4.74	3.78	32.6	32.5	2.71
2	2-5-17	2032.40	576	94.54	2100.	2020.		42.6	2.71
3	3-7-3	2045.90	580	74.55	1370.	1310.		43.0	2.71
3	3-5-28-34B	2051.45	582	88.60	1630.	1570.		42.3	2.72
5	5-8-1-6A	2106.60	597	6.94	1.46	1.15	32.0	31.9	2.72
6	6-5-30-36A	2124.75	602	25.25	145.	131.		34.2	2.72
8	8-12-12	2163.40	613	58.42	675.	636.		41.0	2.71
9	9-1-2-7A	2180.25	618	210.07	7650.	7470.		39.9	2.67
12	12-3-6-12A	2224.15	631	15.58	1.01	0.789	29.0	28.9	2.74
14	14-4-30-33A	2274.70	645	7.97	2.68	2.12	27.5	27.4	3.21
15	15-17-5	2301.10	652	62.24	815.	772.		40.1	2.71
21	21-4-30-35A	2433.35	690	12.80	1.31	1.03	29.4	29.3	2.71
22	22-4-20-23B	2454.95	696	9.99	1.34	1.06	30.4	30.3	2.70
23	23-22-7	2470.60	700	7.23	0.887	0.685	30.5	30.4	2.72
23	23-5-0-5B	2482.15	704	10.80	0.770	0.586	29.5	29.4	2.71
		Average values:		43.87	900.	871.	30.5	34.8	2.74

Table 37: Porosity, permeability, and grain density analyses (Figure 116 shows P&P cross-plot)

5.3.8.8.3.1 X-Ray Diffraction (XRD) Analyses

Table 38 summarizes X-ray diffraction (XRD) analyses results. In particular, clays may become an issue for completion and production testing design. A representative portion of each sample was dried, extracted if necessary, and then ground in a Brinkman MM-2 Retsch Mill to a fine powder. This ground sample was next loaded into an aluminum sample holder. This "bulk" sample mount was scanned with a Bruker AXS D4 Endeavor X-ray diffractometer using copper K-alpha radiation at standard scanning parameters. Computer analyses of the diffractograms provided identification of mineral phases and semiquantitative analyses of the relative abundance (in weight percent) of the various mineral phases. It should also be noted that XRD does not allow the identification of non-crystalline (amorphous) material, such as organic material and volcanic glass. An oriented clay fraction mount was also prepared for each sample from the ground powder. The samples were further size fractionated by centrifuge to separate the less than 4 micron fraction. Ultrasonic treatment was used to suspend the material and a dispersant was used to prevent flocculation when noted. The solution containing the clay fraction was then passed through a Fisher filter membrane apparatus allowing the solids to be collected on a cellulose membrane filter. These solids were then mounted on a glass slide, dried, and scanned with the Bruker AXS diffractometer. The oriented clay mount was then glycolated and another diffractogram prepared to identify the expandable, water sensitive minerals. The slide was heat-treated and scanned with the same parameters to aid in distinguishing kaolinite and chlorite.

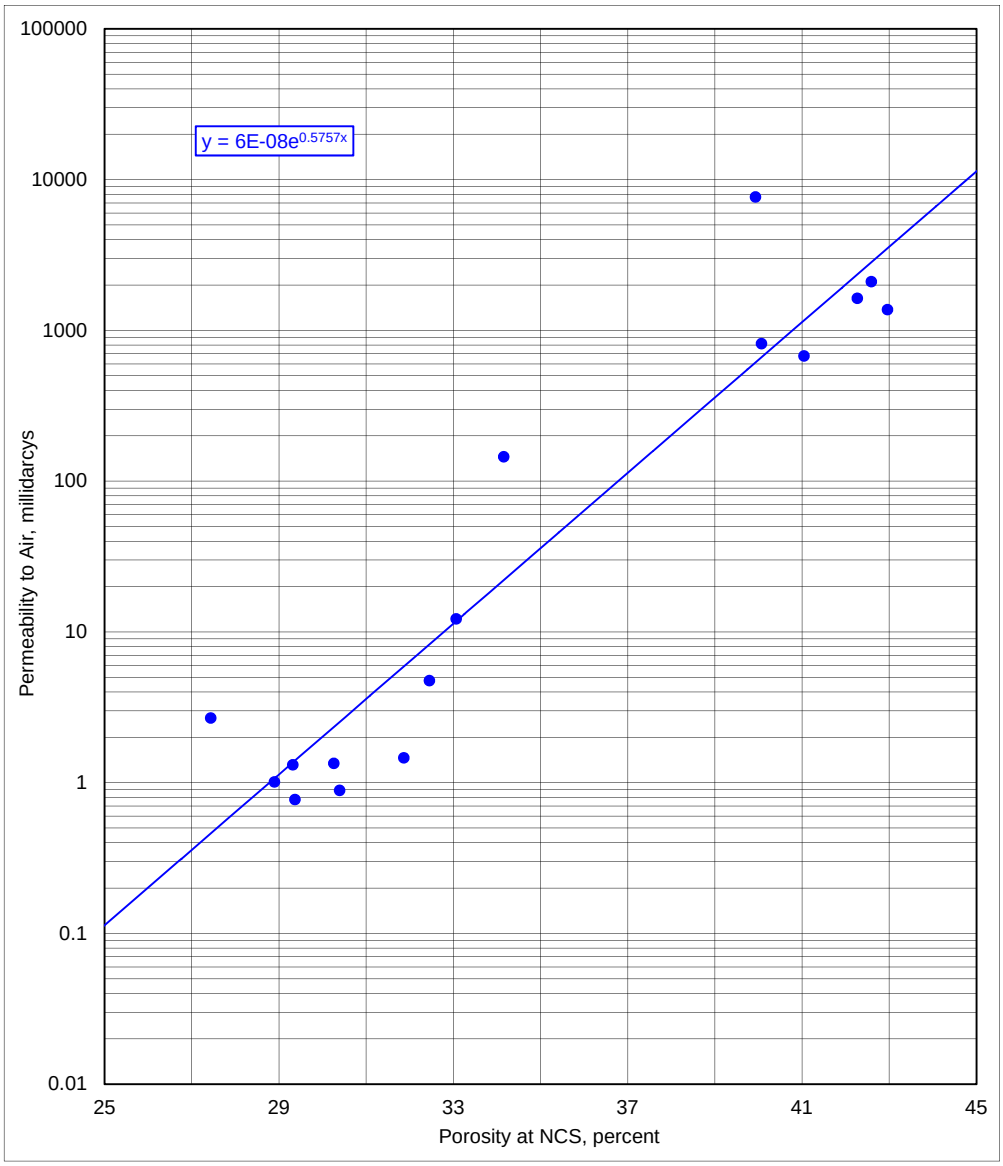

Figure 116: Porosity – Permeability cross-plot of Table 37 samples

Sample	CLAYS				CARBONATES			OTHER MINERALS						TOTALS		
	Chlorite	Kaolinite	Illite	Mx I/S*	Calcite[1]	Dol/Ank	Siderite	Quartz	K-spar	Plag.	Pyrite	Zeolite	Barite	Clays	Carb.	Other
2-2-8	12	3	13	2	0	0	Tr	54	1	6	9	0	0	30	Tr	70
2-2-21-27B	14	3	17	3	0	0	Tr	47	1	7	8	0	0	37	Tr	63
2-5-17	3	2	3	2	0	0	Tr	83	1	4	2	0	0	10	Tr	90
3-7-3	3	2	3	2	0	0	Tr	81	1	7	1	0	0	10	Tr	90
5-8-1-6A	13	4	20	4	0	0	Tr	47	1	10	1	0	0	41	Tr	59
6-5-30-36A	7	2	9	1	0	0	Tr	67	1	12	1	0	0	19	Tr	81
8-12-12	6	1	7	1	0	0	Tr	73	1	10	1	0	0	15	Tr	85
9-1-2-7A	2	1	2	Tr	0	0	Tr	90	1	3	1	0	0	5	Tr	95
12-3-6-12A	11	2	12	2	0	0	Tr	61	1	10	1	0	0	27	Tr	73
22-4-20-23B	13	3	15	3	0	0	Tr	53	1	11	1	0	0	34	Tr	66
AVERAGE	9	2	10	2	0	0	Tr	65	1	8	3	0	0	23	Tr	77

*Randomly interstratified mixed-layer illite/smectite; Approximately 90-95% expandable layers
[1]May include the Fe-rich variety

Table 38: XRD analyses results (core samples from thin sections)

5.3.8.8.3.2 Geomechanical Core Analyses

Triaxial strength measurements are shown in Table 39 and results are shown in Figure 117.

Sample No.	Depth (ft)	Confining Pressure (psi)	Compressive Strength (psi)	Static Young's Modulus ($x10^6$ psi)	Static Poisson's Ratio
2-2-21-27RMV-1	2018.30	570	not failed	0.04	0.22

Table 39: Triaxial compressive strength test (saturated with 2% KCl)

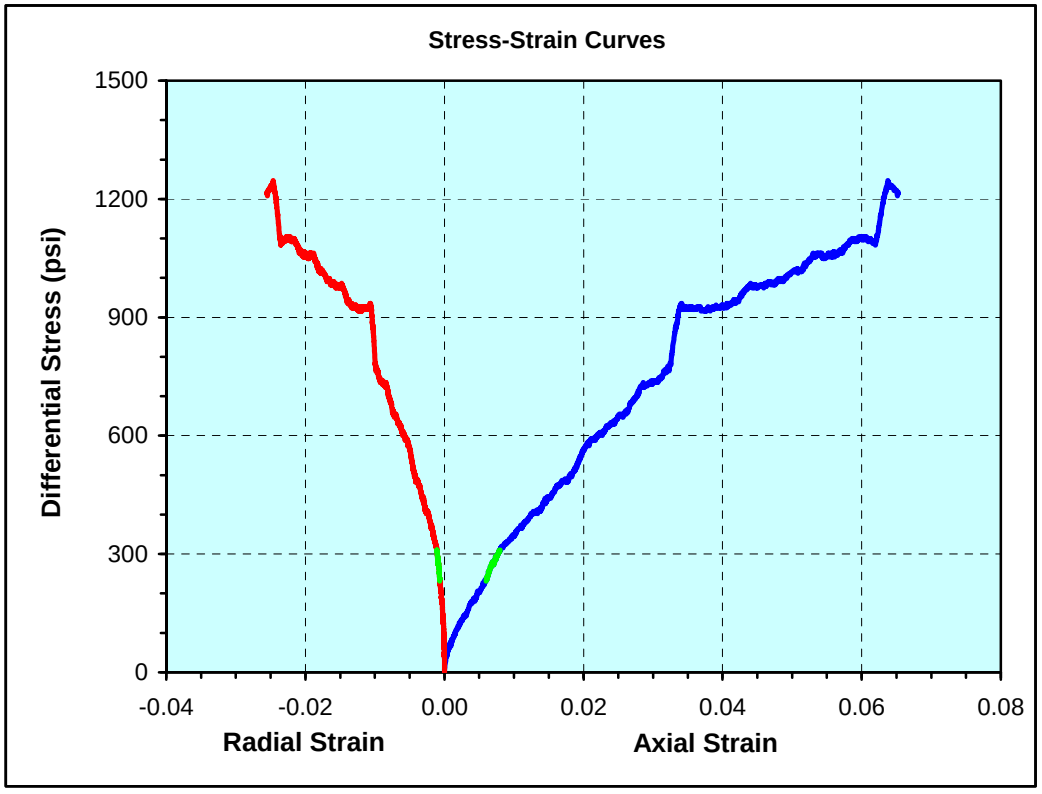

Figure 117: Triaxial Compressive Test result from Table 39 (Young's Modulus and Poisson's ratio determined at interval shown in green)

Ultrasonic velocity and elastic property measurements are shown in Table 40.

Sample No.	Depth (ft)	Confining Pressure (psi)	Bulk Density (g/cc)	Ultrasonic Wave Velocity				Dynamic Elastic Parameter			
				Compressional		Shear*		Young's Modulus ($x10^6$ psi)	Poisson's Ratio	Bulk Modulus ($x10^6$ psi)	Shear Modulus ($x10^6$ psi)
				ft/sec	µsec/ft	ft/sec	µsec/ft				
2-2-21-27RMV-1	N/A	570	2.16	6343	157.66	3858	259.17	1.05	0.21	0.59	0.43
* Best engineering judgement.											

Table 40: Ultrasonic velocities and dynamic elastic parameters measurement (2% KCl saturated)

Table 41 and Figure 118 presents rock mechanics results of Mohr-Coulomb failure analyses.

Sample No.	Depth (ft)	Confining Pressure, Pc = σ_3 (psi)	Differential Stress, $\sigma_1 - \sigma_3$ (psi)	Compressive Strength, σ_1 (psi)	Slope on σ_1 vs Pc	Unconfined Compressive Strength (psi)	Angle of Internal Friction (deg)	Coeff. of Internal Friction	Cohesion (psi)
27RMV-3	2018.30	0	74	74	1.61	114	13.5	0.24	45
27RMV-2	2018.30	285	299	584					
27RMV-1	2018.30	570	562	1132					
27RMV	2018.30	855	566	1421					

Table 41: Rock mechanics results of Mohr-Coulomb failure analyses

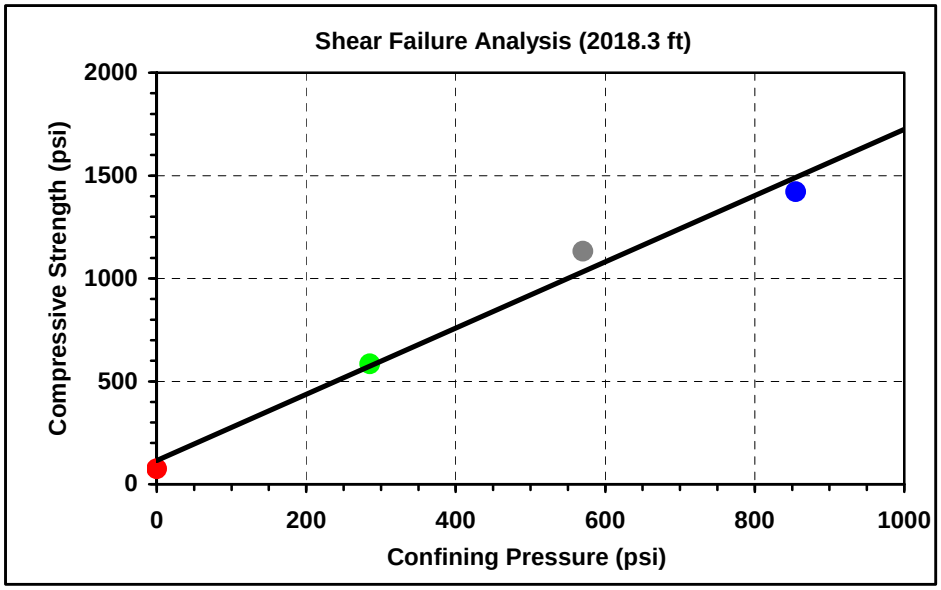

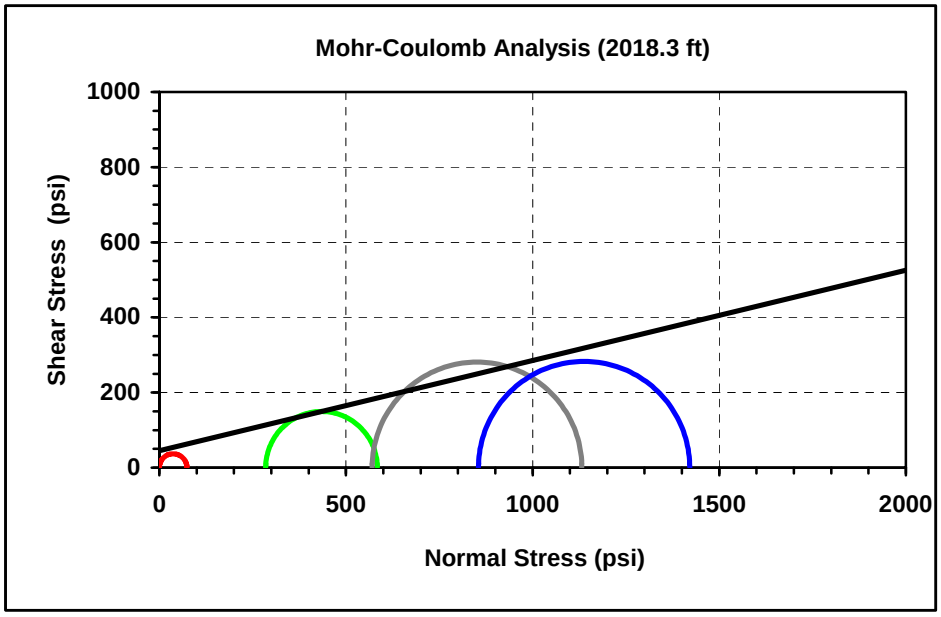

Figure 118: Mohr-Coulomb Failure analysis results (Table 41 sample)

All samples showed similar behaviors of continuous hardening and no failure. Therefore, the compressive stress of each sample taken at 2% of axial strain was used for Mohr-Coulomb analysis, even though the samples did not fail (Figure 118). The shear wave velocity was not conclusive and the reported value is the best estimate considering the sample nature.

5.3.8.8.3.3 CT Scans

OMNI Lab performed initial core plug and whole core scans as illustrated in Appendix B. LBNL performed additional scans of subsampled whole core (Appendix B) prior to core sample distribution to labs at LBNL, NRC, PNNL, CSM, and USGS. The core slices shown in these scans illustrate the ubiquitous fractures that likely propagated during core acquisition and processing procedures, probably due to dissolution of gas hydrate into free gas and water during core recovery operations at atmospheric temperatures and pressures.

5.3.8.8.3.4 Grain Size Analyses

OMNI Lab completed grain size studies on core samples as illustrated in Appendix B. Appendix B figures show both sieve and laser derived grain size charts. Most of the reservoir sands from the core are very fine- to fine-grained. Minor exceptions include coarse-grained to pebbly sands (probable transgressive lags) present in less than one-inch to ten-inch thick beds. The very fine grain size and higher clay contents would significantly affect production and completion design for sand-control during gas hydrate dissociation. Table 42 summarizes laser grain size analyses.

Core	Sample	Depth,	Sand					Silt					Clay
No.	No.	feet	Crs %	Med %	Fine %	Vf %	Total	Crs %	Med %	Fine %	Vf %	Total	Clay %
2	2-1-17	2016.00	0.0	0.0	0.5	2.7	**3.1**	7.2	13.1	20.6	24.4	65.3	31.6
2	2-2-8	2017.10	0.0	0.0	0.1	5.8	**5.9**	15.7	17.3	18.5	18.6	70.1	24.0
2	2-2-21-27B	2018.35	0.0	0.0	0.0	1.3	**1.3**	8.3	15.0	20.3	23.0	66.6	32.1
2	2-14-17	2026.70	0.0	0.3	22.9	42.6	**65.8**	14.4	5.9	5.9	3.5	29.8	4.4
2	2-5-17	2032.40	0.0	0.6	28.9	43.6	**73.1**	11.4	4.3	4.6	2.8	23.1	3.8
2	2-8-14-20A	2035.40	0.0	0.0	17.0	42.0	**58.9**	18.9	6.5	6.6	4.1	36.0	5.1
3	3-7-3	2045.90	0.0	0.0	16.2	43.6	**59.8**	16.7	5.3	6.9	4.6	33.6	6.7
3	3-5-28-34B	2051.45	0.0	0.0	16.7	60.0	**76.8**	7.5	1.9	6.0	3.3	18.7	4.5
5	5-8-1-6A	2106.60	0.0	0.0	0.0	0.5	**0.5**	4.0	15.7	25.3	22.4	67.4	32.1
6	6-5-30-36A	2124.75	0.0	0.0	0.1	12.2	**12.3**	29.6	20.8	13.0	10.6	73.9	13.8
7	Whole Core	2146.70	0.0	0.0	7.5	32.2	**39.7**	22.7	10.3	10.1	7.6	50.6	9.7
8	8-12-12	2163.40	0.0	0.0	9.6	36.7	**46.2**	24.0	7.5	7.7	6.1	45.3	8.5
8	8-5-9-13A	2169.20	0.0	0.0	13.1	44.1	**57.2**	21.9	6.0	6.2	3.8	37.9	4.9
9	9-1-2-7A	2180.25	0.5	32.4	55.7	6.9	**95.4**	0.5	1.7	0.7	0.9	3.9	0.7
12	12-3-6-12A	2224.15	0.0	0.1	1.3	5.8	**7.2**	18.6	23.9	16.4	12.1	71.0	21.8
14	14-4-30-33A	2274.70	0.0	0.0	0.0	1.2	**1.2**	8.2	18.7	22.3	21.5	70.7	28.1
15	15-17-5	2301.10	0.0	0.0	9.9	39.6	**49.5**	24.3	7.4	7.1	5.0	43.8	6.7
18	18-18-5A	2363.20	0.0	0.0	0.1	1.5	**1.6**	11.6	23.1	21.6	18.4	74.7	23.8
20	20-2-32-36A	2414.85	0.0	0.0	2.9	28.8	**31.7**	29.4	10.4	9.8	8.3	57.9	10.4
21	21-4-30-35A	2433.35	0.0	0.0	0.0	2.4	**2.4**	16.2	24.7	20.4	15.9	77.2	20.4
22	22-4-20-23B	2454.95	0.0	0.0	0.0	0.5	**0.5**	7.5	23.3	27.5	19.5	77.8	21.7
23	23-22-7	2470.60	0.0	0.0	0.0	0.3	**0.3**	3.7	14.8	27.6	26.3	72.4	27.3
23	23-5-0-5B	2482.15	0.0	0.0	0.0	1.9	**1.9**	12.2	23.0	23.0	18.3	76.5	21.6

Table 42: Laser grain size analyses summary (See Appendix B for full grain size analyses)

5.3.8.8.3.5 Core Petrography

This section documents the results of OMNI Laboratory's detailed petrographic study of conventional core plugs taken from Mount Elbert-01 core. The mineralogy, pore systems, fabric,

and texture of sediments from the sampled intervals were studied using standard thin section petrographic techniques. Included in this section are the results of ten (10) detailed thin section petrography (modal analysis) and ten (10) X-ray diffraction (XRD) analysis from the sampled interval. A summary list of the petrographic analyses by depth is provided in Table 43. The results of XRD analysis (Table 38), thin section modal analysis data (Table 44), and photographs with descriptive captions (Appendix B) are also included.

Samples selected for thin section analyses were prepared by first vacuum impregnating with blue-dyed epoxy. The samples were then mounted on an optical glass slide and cut and lapped in water to a thickness of 0.03 mm. The prepared sections were then covered with index oil and temporary cover slips, and then analyzed using standard petrographic techniques.

The samples include shales (5), a single coarse siltstone (1), and sandstones (4). The sandstones are very fine- to fine-grained. Most samples show laminations ranging from distinct shale laminations to vague zoning by grain size differential. Grain sorting ranges from very poor to well, dependent mainly on the amount of detrital clay-rich matrix present. The sandstone samples range from moderately well to well sorted, and most grains are subangular to subrounded. The fabrics observed range from massive to grain size-zoned. The coarse siltstone sample (2,124.75 feet) is vaguely-laminated and moderately sorted. The shales are typically distinctly laminated and contain abundant detrital clay-rich matrix.

Petrographic analyses of the samples indicate that they are poorly consolidated, and the sandstones show good to excellent reservoir quality. Porosity distribution is controlled primarily by sediment fabric, especially by the distribution of shale laminations. Other controlling factors include textural properties (grain size and sorting) and, to a lesser extent, distribution of various cementing agents. Primary intergranular pores and microscopic pores are the dominant pore types. A minor amount of secondary dissolution porosity also contributes to the total pore volume. This secondary porosity is created by the partial to total dissolution of chemically unstable grains such as lithic fragments and feldspars.

Sample Number	Sample Depth (feet)	Detailed Thin Section Analysis	X-Ray Diffraction Analysis	Dominant Lithology (Table 44)
2-2-8-9	2,017.10	X	X	Shale
2-2-21-27B	2,018.35	X	X	Shale
2-7-16-17	2,032.40	X	X	Litharenite ss
3-7-3	2,045.90	X	X	Litharenite ss
5-8-1-6A	2,106.60	X	X	Shale
6-5-30-36A	2,124.75	X	X	Siltstone
8-3-10-11	2,163.40	X	X	Litharenite ss
9-1-2-7A	2,180.25	X	X	Litharenite ss
12-3-6-12A	2,224.15	X	X	Sandy Shale
22-4-20-23B	2,454.95	X	X	Shale

Table 43: Thin Section Petrographic Analyses summary (sample number 2-2-8-9 corresponds to core 2, core section 2, and 8-9 inches). Note Core to Log Depth Discrepancy (depth in core-space would require shifting by up to -3 feet to approximate wireline log space).

Three (3) of the four (4) sandstones analyzed by thin section modal analysis are classified as feldspathic litharenites. One (1) sandstone (2,180.25 feet) is a fine-grained litharenite. All of these sandstones consist predominantly of quartz and lithic clasts, with minor feldspar (potassium and plagioclase varieties).

A brief description of the detrital and authigenic minerals in the four (4) sandstone samples is provided here and photos, descriptions, and tabulated data for all ten (10) samples are provided in Table 44 and Appendix B. All percentages refer to point count modal analysis data. Thin section petrography and X-ray diffraction were used for mineral identification and description. Appendix B figures provide thin section photographs representative of each thin section sample. In terms of composition, the sandstones are feldspathic litharenite to litharenite (Folk, 1980).

Quartz is the most abundant framework grain type in all of these sandstone samples. The grains are typically subangular to subrounded, with rounding increasing with greater grain size. Detrital quartz includes both monocrystalline quartz (individual crystals with non-undulose extinction; 22% to 40%, from point count modal analysis) and polycrystalline quartz (3% to 7%).

Typically, a moderate amount of feldspar grains are present in all sandstone samples, with total feldspar amount ranging from 3% to 13%. Both potassium feldspar (microcline and orthoclase; 2 to 6%) and plagioclase feldspar (1 to 8%) exist in the samples, with the plagioclase variety slightly more common. Some feldspar grains were slightly altered from dissolution, with resultant secondary intragranular porosity and microporosity.

A variety of lithic fragments (16 to 23% total) are encountered as detrital grains in the sandstone samples. The main grain types, subequal in abundance, are metamorphic, volcanic, and sedimentary chert fragments. The metamorphic fragments are typically low grade varieties such as phyllite and slate, ranging up to schist and occasional quartzite fragments. The volcanic rock fragments typically have a fine groundmass texture revealing thin feldspar laths. Sedimentary lithic fragments consist of chert, shale/mudstone, and rare siltstone/sandstone plus carbonate. Rarely, plutonic igneous grains are observed, which are represented by polycrystalline fragments consisting of both feldspar and quartz.

Other accessory detrital grains include the mica minerals muscovite (trace to 2%) and biotite (trace), carbonaceous (plant) fragments (1 to 3%; often partially altered to pyrite), and glauconite (0% to trace). Glauconite pellets are indicative of marine depositional influence. Phosphatic grains are present in trace amounts in two samples. Minor amounts (trace to 2%) of heavy minerals are present, and include clinozoisite, epidote, hornblende, opaque minerals, garnet, epidote, pyroxene, rutile, and zircon.

The amount of matrix clay is highly variable, and is directly related to rock fabric. The total range is from 0% (in several sandstone samples) to 58% in the vaguely-laminated shale from 2,106.60 feet.

Authigenic minerals in the coarse siltstone and shale samples range from 2% to 5%, and much of it is replacement pyrite, although siderite and clays are also observed. Based on point count modal analysis, the total amount of cement and authigenic replacements in these sandstones ranges from 1% to 5%.

These poorly cemented sandstones contain a wide variety of cements, albeit in very minor amounts. These include quartz overgrowths (trace), siderite (0 to 2%), pyrite (trace to 2%), Fe/Ti oxides (0 to 1%), ankerite (0% to trace), and feldspar overgrowths (0% to trace). Siderite and pyrite act as both true cements and as replacement of labile components such as mudstone fragments and biotite mica. Pyrite is also associated with the alteration of carbonaceous debris. Authigenic clays are represented by pore-lining (trace to 2%) and non-kaolin pore-filling (trace) varieties.

Thin section observations have documented that the clay mineralogy of these samples is dominantly depositional (detrital) in origin, with only very rare chloritic and/or illitic clay rims of authigenic origin. X-ray diffraction analyses reveal that the main clay mineral types in these samples are subequal illite (avg. 10%, by weight) and chlorite (avg. 9%). Kaolinite and mixed-layer illite/smectite each comprise 2% (on avg.). Overall clay mineral content ranges from 5% (2,180.25 feet) to 41% (2,106.60 feet).

5.3.8.8.3.5.1 Porosity and Reservoir Quality

The shale samples have total porosity ranging from 5% to 8%, and the coarse siltstone sample has a total porosity of 18%, reflecting its well interconnected intergranular pore system in regions free of shale laminations. The four (4) sandstones are all considered to have good to excellent reservoir quality, with porosity determined from point count modal analysis ranging from 23% (2,163.40 feet) to 31% (2,032.40 feet). Primary intergranular pores are the most abundant porosity type in the sandstones (18% to 29%). This pore type represents the original voids between detrital grains, and these have been only very slightly reduced by compaction and cementation. As a general rule, the best preservation potential for intergranular pores are in the most well sorted sediments, especially those with the lowest amount of ductile grains and matrix clay.

THIN SECTION MODAL ANALYSIS

BP Alaska
Mount Elbert-01
North Slope Borough, Alaska
Job No.: HH-36510 Sample Type: Conventional Core Plug Analyst: C. Manske

DEPTH (ft):	**2017.10**	**2018.35**	**2032.40**	**2045.90**
SAMPLE NO.:	**2-2-8-9**	**2-2-21-27B**	**2-7-16-17**	**3-7-3**
Grain Size Avg. (mm):	**0.03**	**0.02**	**0.11**	**0.09**
Grain Size Range (mm):	**<0.01-0.38**	**<0.01-0.23**	**0.03-0.38**	**0.02-0.26**
Sorting:	**Moderately Poor**	**Moderately Poor**	**Moderately Well**	**Well**
Fabric:	**Laminated**	**Laminated**	**Vaguely G.S.-zoned**	**Massive**
Rock Name (Folk, 1980):	**Shale w/ Sd./Slt. Lams.**	**Shale w/ Sd./Slt. Lams.**	**Feldspathic Litharenite**	**Feldspathic Litharenite**
FRAMEWORK GRAINS				
Quartz	**33**	**34**	**27**	**28**
Monocrystalline	31	33	22	25
Polycrystalline	2	1	5	3
Feldspar	**8**	**5**	**13**	**13**
K-Feldspar	3	2	6	5

Table 44: Continued – Thin Section Modal Analyses of core samples

Plagioclase	5	3	7	8
Lithic Fragments	**6**	**3**	**23**	**21**
Plutonic	tr	tr	1	tr
Volcanic	3	2	7	7
Metamorphic	2	1	6	8
Chert	1	tr	7	5
Mudstone	tr	tr	2	1
Carbonate	0	0	tr	0
Sandstone/Siltstone	0	0	0	0
Accessory Grains	**5**	**4**	**1**	**3**
Muscovite	5	3	1	1
Biotite	tr	1	tr	tr
Heavy Minerals*	tr	tr	tr	2
ENVIRON. INDICATORS	**7**	**9**	**1**	**2**
Carbonaceous Material	7	9	1	2
Glauconite	tr	0	0	0
Calcareous Fossils	tr	0	0	0
Phosphatic Grains	tr	tr	0	tr
DETRITAL MATRIX	**29**	**33**	**0**	**0**
CEMENT/REPLACEMENT	**4**	**4**	**4**	**3**
Pore-lining Clay	tr	1	1	1
Kaolinite	tr	tr	0	0
Other Pore-filling Clay	1	tr	tr	tr
Quartz Overgrowths	tr	tr	tr	tr
Feldspar Overgrowths	0	tr	tr	tr
Calcite	0	0	0	0
Fe-Dolomite	0	0	0	0
Ankerite	0	0	tr	0
Siderite	tr	0	2	tr
Pyrite	2	3	1	2
Fe/Ti Oxides	1	tr	0	tr
Sulfate	0	0	0	0
Bitumen	0	0	0	0
POROSITY	**8**	**8**	**31**	**30**
Primary	5	3	29	28
Secondary	tr	tr	1	tr
Microscopic	3	5	1	2
TOTALS:	**100**	**100**	**100**	**100**

*Clinozoisite, Epidote, Garnet, Hornblende, Opaques, Pyroxene, Rutile

THIN SECTION MODAL ANALYSIS

BP Alaska
Mount Elbert-01
North Slope Borough, Alaska
Job No.: HH-36510 Sample Type: Conventional Core Plug Analyst: C. Manske

DEPTH (ft):	**2106.60**	**2124.75**	**2163.40**	**2180.25**
SAMPLE NO.:	**5-8-1-6A**	**6-5-30-36A**	**8-3-10-11**	**9-1-2-7A**
Grain Size Avg. (mm):	**0.02**	**0.05**	**0.08**	**0.21**
Grain Size Range (mm):	**<0.01-0.20**	**<0.01-0.14**	**0.03-0.25**	**<0.01-0.83**
Sorting:	**Poor**	**Moderate**	**Moderately Well**	**Moderate**
Fabric:	**Vaguely-Laminated**	**Vaguely-Laminated**	**Vaguely G.S.-zoned**	**Grain Size-zoned**
Rock Name (Folk, 1980):	**Shale w/ Sd. Lenses**	**Coarse Siltstone**	**Feldspathic**	**Litharenite**

Table 44: Continued – Thin Section Modal Analyses of core samples

			Litharenite	
FRAMEWORK GRAINS				
Quartz	**18**	**38**	**45**	**46**
Monocrystalline	17	37	40	39
Polycrystalline	1	1	5	7
Feldspar	**4**	**10**	**6**	**3**
K-Feldspar	2	5	3	2
Plagioclase	2	5	3	1
Lithic Fragments	**4**	**9**	**16**	**20**
Plutonic	tr	tr	1	3
Volcanic	2	3	4	6
Metamorphic	1	2	7	3
Chert	1	1	3	7
Mudstone	tr	3	1	1
Carbonate	0	0	0	0
Sandstone/Siltstone	0	0	0	tr
Accessory Grains	**4**	**6**	**2**	**tr**
Muscovite	3	3	2	tr
Biotite	1	3	tr	tr
Heavy Minerals*	tr	0	tr	tr
ENVIRON. INDICATORS	**5**	**7**	**3**	**1**
Carbonaceous Material	5	6	3	1
Glauconite	tr	tr	0	tr
Calcareous Fossils	0	0	0	0
Phosphatic Grains	0	1	0	tr
DETRITAL MATRIX	**58**	**7**	**0**	**tr**
CEMENT/REPLACEMENT	**2**	**5**	**5**	**1**
Pore-lining Clay	tr	2	2	tr
Kaolinite	tr	0	0	0
Other Pore-filling Clay	1	1	tr	tr
Quartz Overgrowths	tr	tr	tr	tr
Feldspar Overgrowths	tr	0	tr	tr
Calcite	0	0	0	0
Fe-Dolomite	0	0	0	0
Ankerite	0	0	0	0
Siderite	tr	tr	1	0
Pyrite	1	2	2	tr
Fe/Ti Oxides	tr	tr	tr	1
Sulfate	0	0	0	0
Bitumen	0	0	0	0
POROSITY	**5**	**18**	**23**	**29**
Primary	2	12	18	27
Secondary	tr	1	3	1
Microscopic	3	5	2	1
TOTALS:	**100**	**100**	**100**	**100**

*Clinozoisite, Epidote, Hornblende, Opaques, Rutile, Zircon

THIN SECTION MODAL ANALYSIS

BP Alaska
Mount Elbert-01
North Slope Borough, Alaska
Job No.: HH-36510 Sample Type: Conventional Core Plug Analyst: C. Manske

Table 44: Continued – Thin Section Modal Analyses of core samples

DEPTH (ft):	**2224.15**	**2454.95**		
SAMPLE NO.:	**12-3-6-12A**	**22-4-20-23B**		
Grain Size Avg. (mm):	**0.05**	**0.03**		
Grain Size Range (mm):	**<0.01-0.28**	**<0.01-0.14**		
Sorting:	**Poor**	**Very Poor**		
Fabric:	**Vaguely-Laminated**	**Laminated**		
Rock Name (Folk, 1980):	**Sandy Shale**	**Shale w/ Sd. Lams.**		
FRAMEWORK GRAINS				
Quartz	**26**	**21**		
Monocrystalline	25	20		
Polycrystalline	1	1		
Feldspar	**5**	**5**		
K-Feldspar	2	2		
Plagioclase	3	3		
Lithic Fragments	**6**	**5**		
Plutonic	tr	tr		
Volcanic	3	3		
Metamorphic	1	1		
Chert	2	1		
Mudstone	tr	tr		
Carbonate	0	0		
Sandstone/Siltstone	0	0		
Accessory Grains	**6**	**5**		
Muscovite	5	3		
Biotite	1	2		
Heavy Minerals	0	0		
ENVIRON. INDICATORS	**5**	**6**		
Carbonaceous Material	5	6		
Glauconite	tr	0		
Calcareous Fossils	0	0		
Phosphatic Grains	0	0		
DETRITAL MATRIX	**41**	**45**		
CEMENT/REPLACEMENT	**3**	**5**		
Pore-lining Clay	tr	1		
Kaolinite	0	0		
Other Pore-filling Clay	tr	tr		
Quartz Overgrowths	tr	tr		
Feldspar Overgrowths	0	0		
Calcite	0	0		
Fe-Dolomite	0	0		
Ankerite	0	0		
Siderite	tr	1		
Pyrite	3	2		
Fe/Ti Oxides	0	1		
Sulfate	0	0		
Bitumen	0	0		
POROSITY	**8**	**8**		
Primary	5	3		
Secondary	tr	tr		
Microscopic	3	5		
TOTALS:	**100**	**100**		

Table 44: Thin Section Modal Analyses of core samples (OMNI Lab)

Table 44: Continued – Thin Section Modal Analyses of core samples

Secondary intragranular and grain-moldic pores result from the diagenetic alteration and partial to complete dissolution of chemically unstable detrital grains. This type of porosity ranges from trace to 3%. Most commonly, these pores are associated with partially to fully dissolved feldspars and certain lithic fragments.

Microporosity in the sandstone samples ranges from 1% to 2%, based on point count modal analysis. Micropores are associated mainly with clay minerals, such as within detrital matrix clay, mudstone fragments, altered feldspars/lithics, and pore-lining or pore-filling authigenic clay.

The good to excellent reservoir quality exemplified by the sandstones is represented by well interconnected primary intergranular pores with slight augmentation by secondary dissolution. The factors affecting reservoir character in the depth interval represented by these sandstones are: 1) rock texture and fabric, 2) the degree of cementation and 3) the degree of compaction.

5.3.8.8.3.5.2 Mineralogic Influences on Log Response

This section discusses the effects on log response of the mineralogy and associated porosity types found in these samples.

1. Resistivity Logs: The main factors that may suppress resistivity in these intervals are pore-lining and pore-filling authigenic clays and certain matrix clays. These clays have the potential to suppress resistivity by their associated bound water. This potential is considered highest in the coarse siltstone at 2,124.75 feet. Microporous (leached) grains are also found within this interval. Caution is advised in this interval when evaluating well log resistivity, especially due to various clay types and amounts.

2. Density Logs: The sandstones analyzed from this well contain a variety of high-density minerals, including the carbonates siderite and ankerite, as well as pyrite, Fe/Ti oxides, and chlorite. These constituents are found as authigenic cements and replacements, and constitute a minor portion of these sandstones. Pyrite has a very high grain density of 5.01gm/cc. It is expected that the total effect of these components will be to result in a grain density slightly above the 2.65 gm/cc sandstone (quartz) standard.

3. Gamma-Ray Log: Gamma-ray logs respond to radioactive isotopes. The clay minerals kaolinite (average 2% by weight from XRD) and chlorite (average 9% by weight from XRD) will not be detected by gamma-ray logs due to the absence of potassium in these minerals. Conversely, the mineral K-feldspar (average 1% by weight from XRD) will be detected as "clay" by gamma-ray logs due to the presence of potassium in this mineral. The total effect of these minor components is expected to result in an underestimation of rock shaliness by gamma-ray log response.

5.3.8.8.3.5.3 Formation Sensitivity Related to Fines Migration

X-ray diffraction data, supplemented by thin section results indicate that the dominant clay types are illite (average 10%) and chlorite (average 9%). Minor clay types are kaolinite (average 2%) and mixed-layer illite/smectite (average 2%). Authigenic illite is found as a fibrous or filamentous grain coating whereas chlorite typically coats grains as well. However, these clays are dominantly detrital (depositional) in origin.

Fines migration is a slight concern because of the presence of both fibrous illite and dissolution debris. Some grain-coating illite is present as fibers that protrude into pores and pore throats. Secondary dissolution debris is also observed, mainly in secondary pores. This debris is loosely attached to nearby pore walls and is rather large in size in comparison to nearby pore throats. When testing and/or producing this formation, it is recommended to avoid opening a well on too large a choke. Begin with a low flow rate and gradually increase rate as desired. Be aware that every formation and pack has a critical velocity at which fines are mobilized and production actually drops. Many wells are damaged beyond repair by ill-advised well tests run to determine the maximum rate at which a well is capable of producing.

5.3.8.8.4 Scanning Electron Microscope (SEM) Grain Scale Imaging

The JMPG Volume provides the complete documentation of these SEM studies (Stern, et al, 2011). Investigations using cryogenic SEM (CSEM), powder XRD, and gas chromatography revealed characteristics of 2 preserved gas hydrate-bearing core samples (2,033.6 feet and 2,168.5 feet, from zones D and C, respectively). Analyses revealed 99.9% methane gas forming structure I hydrate as an intergranular pore-filling material at 70-75% saturation and sporadically forming thin veins up to a diameter of tens of microns. The methane gas has carbon isotopic composition ranges consistent with onsite gas dissociated from gas hydrate samples. Pore throats within the predominantly fine grained and well sorted quartzose sands commonly range from 20-120 microns. Ice and gas bubble phases are also present within the frozen samples, perhaps due to the samples having undergone partial gas hydrate dissociation during the onsite sampling process and removal from pressure-temperature gas hydrate stability field. Artifacts from the onsite sampling procedures may have also contributed to an apparently non-equilibrium microstructure development of mesoporosity within the gas hydrate itself. However, although not the conclusion of Stern, et al (2011), they recognize the possibility that this microstructure could be typical of gas hydrate formed in sediments above the freezing point of water (below the permafrost). If this is a natural feature, then it would effectively create a tri-porosity system that would consist of this intra-hydrate mesoporosity, hydrate-filled intergranular porosity (70-75% saturation), and water-filled intergranular porosity (10-20% saturation mobile water with 5-15% immobile/irreducible water saturation).

5.3.8.8.5 Core Minipermeameter Measurements

Core analyses included minipermeameter measurements using a customized unit fabricated at UAF. Initial feasibility studies showed values and variation (Table 45) reasonably similar to conventional core analyses, and the UAF minipermeameter (Figures 119-120) was modified to enable faster measurements of the entire 430 feet of core over approximately six-inch intervals (Figures 121-123).

Over the course of this work, UAF students Aditya Deshpande and Praveen Singh applied a minipermeameter to study permeability variations on the half-slabbed Mount Elbert-01 core sample set. Figure 123 presents the minipermeameter analyses, which compare well to OMNI Laboratory's conventional poro-perm data analyses.

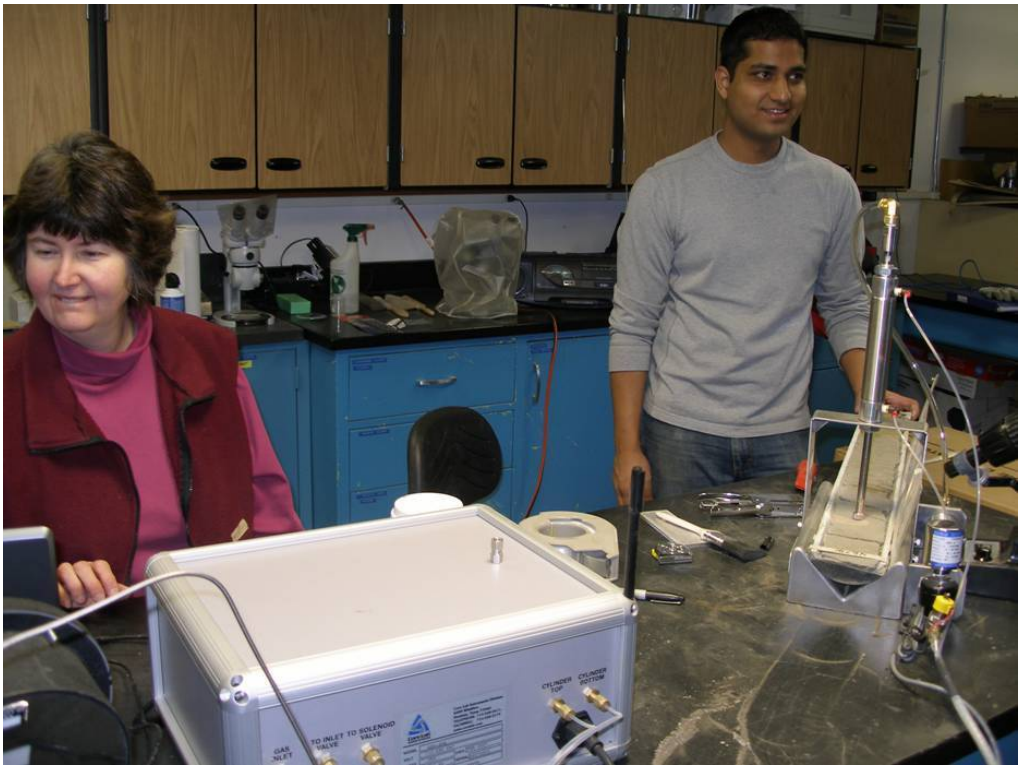

Figure 119: UAF Professor Kathy Hanks and graduate student Aditya U Deshpande at Alaska Geologic Materials Center (GMC) with minipermeameter studies of Ugnu core (March 2008)

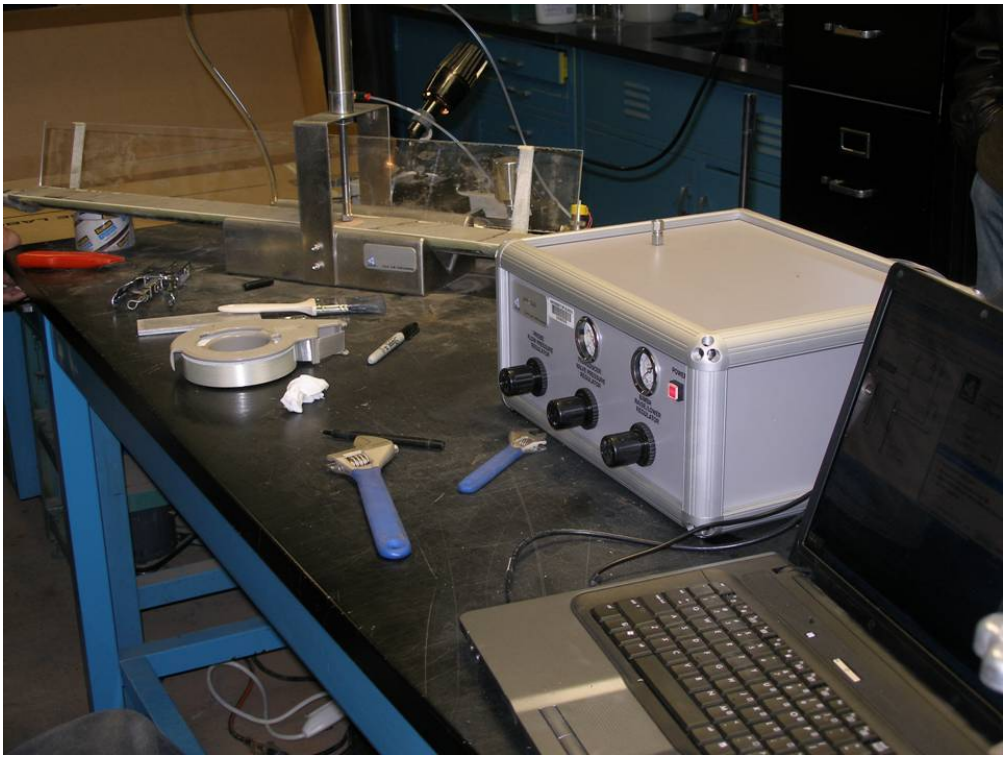

Figure 120: UAF Minipermeameter apparatus and setup, GMC (March 2008)

Figure 121: UAF Minipermeameter feasibility test setup in gas hydrate core storage unit (March 2008)

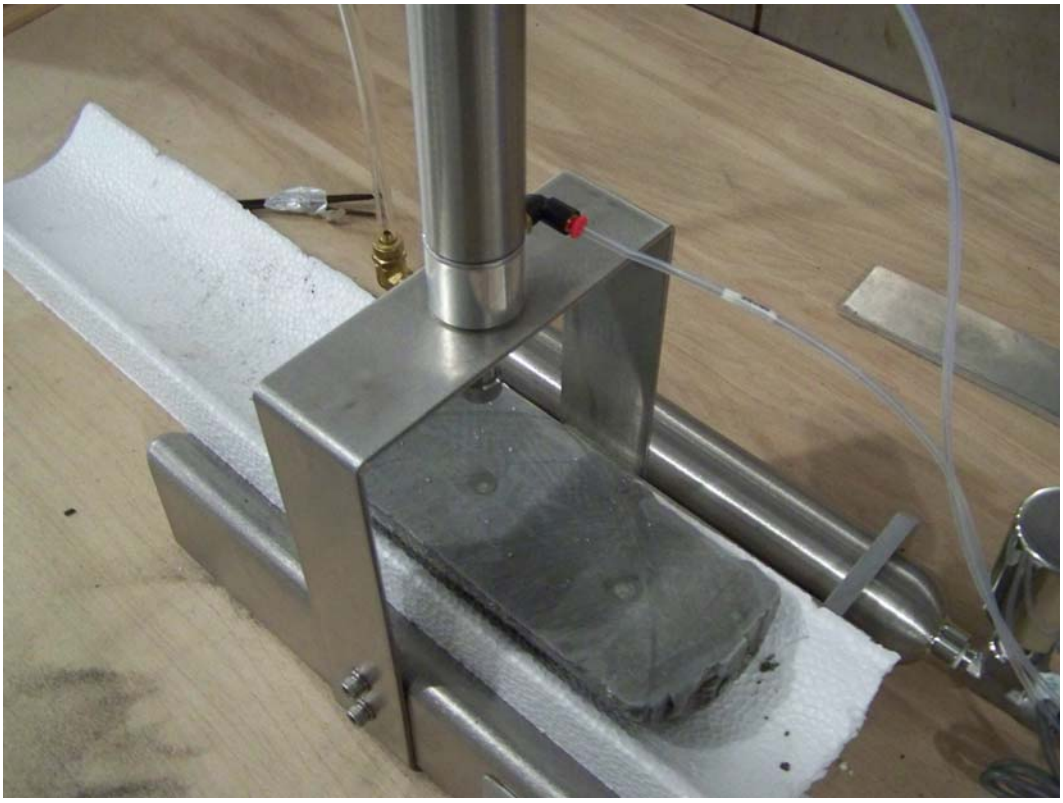

Figure 122: Mt Elbert core in minipermeameter apparatus during feasibility test (March 2008)

Core Depth	Minipermeameter Permeability (md)
2022.63	1434.0
2023.04	629.0
2023.54	738.0
2024.04	92.3
2024.75	261.0
2025.08	347.0
2026.58	2016.0
2026.63	956.0
2026.83	814.0
2027.29	-999.0
2028.25	836.0
2028.63	-999.0
2028.83	1368.0
2029.17	1635.0
2029.38	785.0
2029.63	-999.0
2143.21	526.0
2143.46	131.0
2143.50	163.0
2145.08	560.0
2149.50	2.5
2149.75	307.0
2149.92	932.0
2151.67	868.0
2151.92	1220

Table 45: UAF minipermeameter feasibility study data (-999.0 indicates inability to measure, typically due to soft sediment, fractures, and/or high reservoir quality)

5.3.8.8.6 Gas Hydrate-bearing Core Sample Relative Permeability Analyses

UAF also analyzed five (5) Mount Elbert-01 vertical plug core samples. Studies in conjunction with CoP Bartlesville Lab were accomplished from 4Q08-1Q09 in thesis work “Analysis of Permeabilities in Hydrate-Saturated Unconsolidated Core Samples” by UAF graduate student Andrew Johnson. Delicate core handling procedures were developed to help alleviate concerns that prior experiments were not performed on "native state" core samples.

Studies identified many difficulties hindering obtaining relative permeability data in gas hydrate-bearing porous media, including difficulties in handling unconsolidated cores during initial core preparation work, forming gas hydrate in the core to promote flow of both brine and methane, and obtaining simultaneous two phase flow of brine and methane necessary to quantify relative permeability using unsteady state displacement methods. Effective single phase permeabilities in unconsolidated gas hydrate samples were determined and results indicate that permeability reduction as a function of gas hydrate saturation follows a predictable trend.

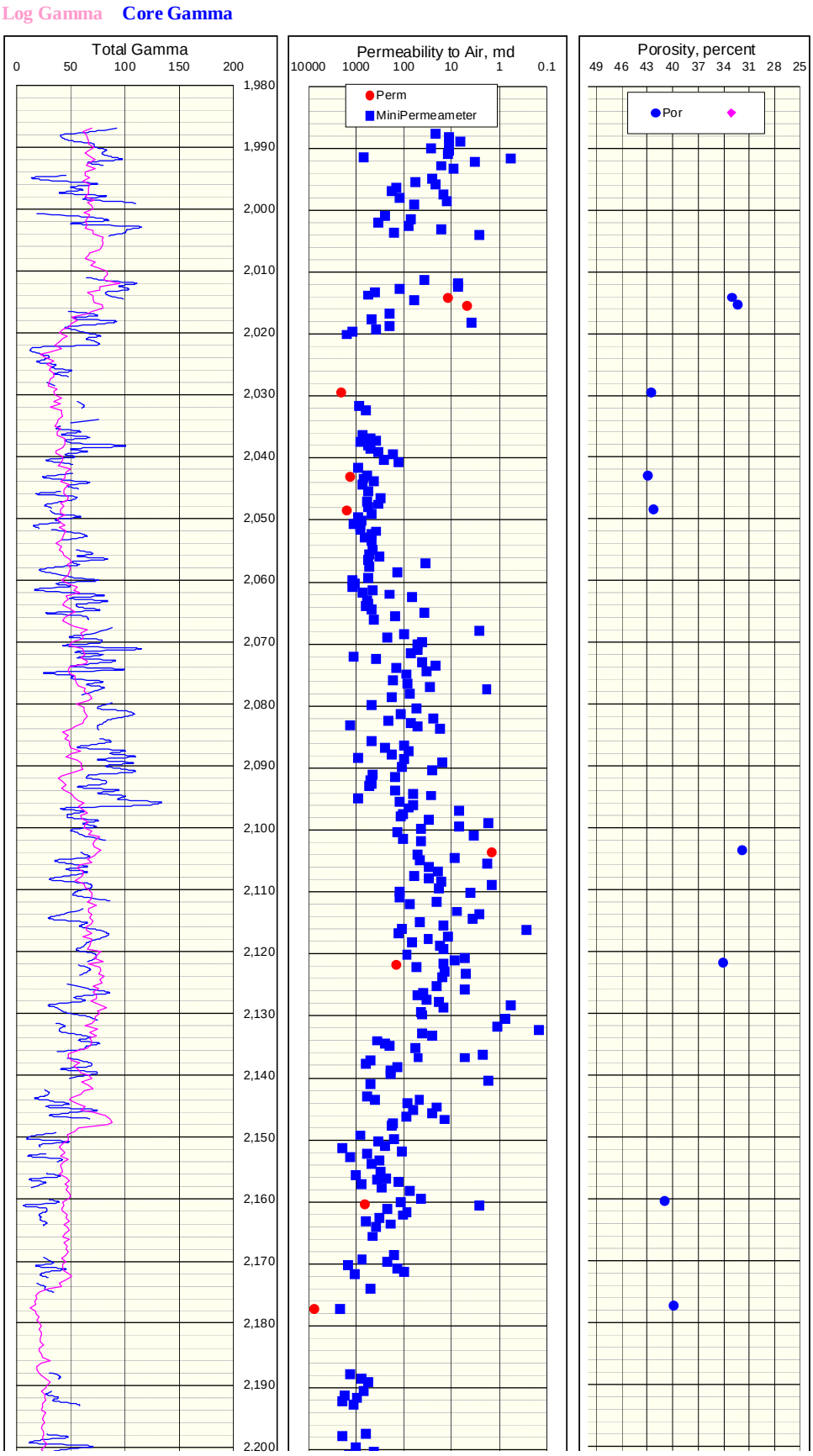

Figure 123: Continued – Minipermeameter data plotted with conventional poro-perm data

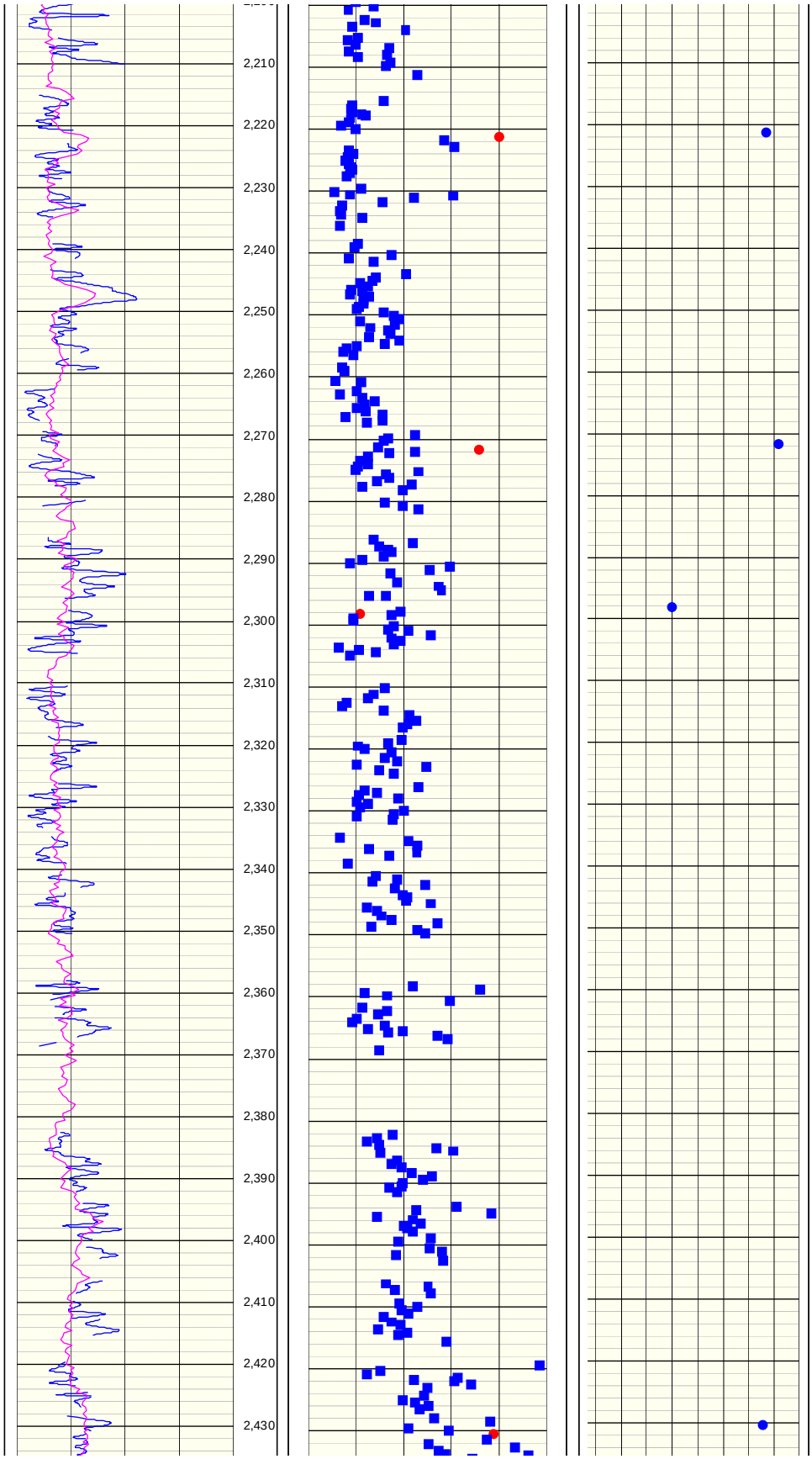

Figure 123: Continued – Minipermeameter data plotted with conventional poro-perm data

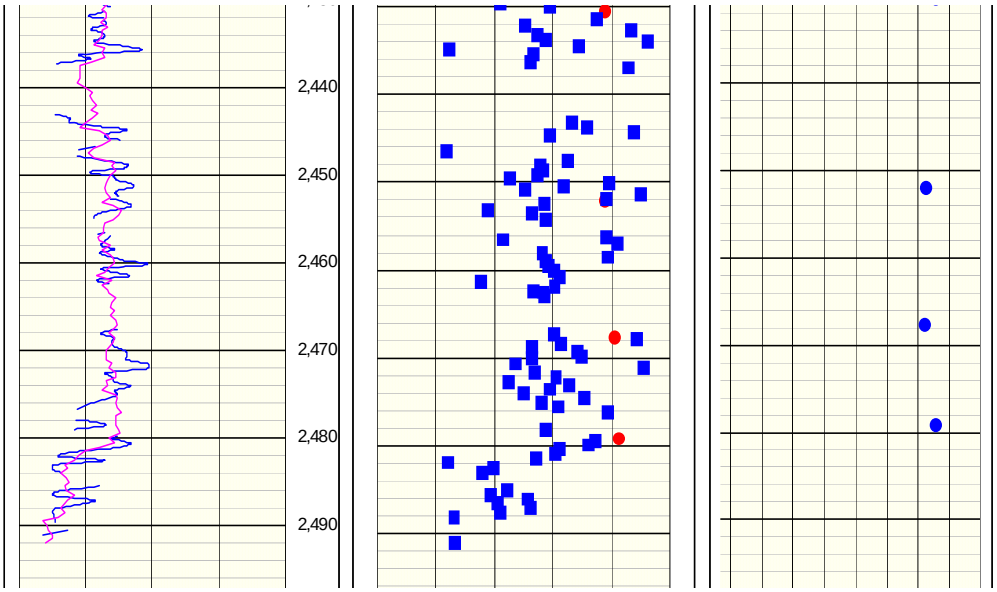

Figure 123: Minipermeameter data plotted with conventional poro-perm data in log-space (minus 3-foot shift applied to core data)

5.3.8.8.7 Core Pore Water Analyses

Dr. Marta Torres, Oregon State University, completed the pore water analyses summarized in this section. Detailed final results are published in the JMPG volume (Torres, et al, 2011). Results of pore water isotopic and compositional analyses indicate that the pore waters are very fresh (Figures 90 and 124 and Table 46), especially in the gas hydrate-bearing zones C and D.

Gas hydrate occupies up to 90% of the pore space within zones C and D. Estimates from chloride data correspond very well to gas hydrate saturation values derived from wireline log data (NMR). As shown previously in the Mallik and Cascadia margin sites, gas hydrate preferentially occupies the sand reservoir lithologies. Gas hydrate content correlates well with sand content of the sediment. The pore fluid chemistry reflects a mixture of meteoric water with formation fluids. There are no indications of a remnant seawater end-member. Pore water analyses included major and minor cations (Ba, Fe, Li, Mn, Sr, Ca, K, and Mg); anions (sulfate and chloride); water isotopes (oxygen and hydrogen) and carbon in dissolved inorganic carbon (Table 46). In addition, subsamples were provided to W. Winters (USGS) for grain size analyses and selected samples were also analyzed for carbon (inorganic and organic) and nitrogen. Only sediment samples that were deemed free of oil contamination from the drilling mud were analyzed.

The pore fluid data document the importance of acquiring a complete pore water data set in concert with log data. Both dissolved chloride and the isotopic composition of the water co-vary in gas-hydrate-bearing zones, consistent with gas hydrate dissociation during core recovery operations. Gas hydrate saturation values estimated from dissolved chloride agree with estimates based on wireline log data when gas hydrate saturation is greater than 20%; this correlation is less clear at lower saturation values. This discrepancy may reflect the effect of host sediment on parameterization of the gas saturation estimates from logs. The highest gas hydrate saturation in these permafrost regions is clearly associated with sand reservoir sequences, as also expected from theoretical and field observations in arctic and marine sediment cores. Gas hydrate, however, also occurs within finer-grained lithologies.

Core	Section	Interval (cm)	Depth top (m)	Vol. (ml)	Salinity (ppt)	Rw (mS/cm)	Cl (mM)	K (mM)	Ca (mM)	Mg (mM)	Ba (uM)	Li (uM)	Sr (uM)	$\delta^{18}O$ (‰)	δD (‰)
1	3	27-33	665.60		7.0	9.69	109.2							-20.75	-160.0
1	5	27-33	667.65	1.5	7.0	10.57								-20.23	-159.0
2	2	27-33	672.89	3.0	7.5	11.7	106.2								
2	6	24-30	676.69	11.5	2.5	2.23	22.7	0.188	0.61	0.44	13.7	7.5	11.59	-18.89	-146.0
2	7	27-33	677.75	2.5	2.5	2.39	22.1							-18.43	-147.2
3	3	28-34	681.67	12.0	3.5	4.14	40.8	0.271	1.66	1.11	38.6	11.5	20.38	-19.37	-149.6
3	7	28-34	685.76	10.0	3.5	3.54	38.1	0.299	1.42	0.90	36.4	11.3	18.33	-19.13	-147.9
4	3	25-31	689.97	18.0	5.0	6.92	78.7		4.51	2.87	107.8	21.9	44.46	-20.23	-154.5
4	7	28-34	694.03	8.5	5.0	7.06	78.3	0.713	4.34	2.68	111.9	21.2	42.41	-20.39	-154.6
5	1	21-27	695.94	11.5	5.0	8.02	81.0	0.647	4.56	2.79	125.5	21.6	44.35	-20.17	-154.6
5	7	28-34	701.86	10.0	5.5	8.02	87.6	0.819	5.20	3.10	137.5	21.1	49.6	-20.40	-155.3
6	2	28-34	705.13	8.5	6.0	9.11	91.9	0.772	5.72	3.53	146.0	22.4	53.14	-20.42	-156.0
6	6	28-34	709.14	9.5	6.0	9.05	94.7	0.831	5.90	3.52	158.4	21.4	54.5	-20.50	-156.4
7	6	20-24	716.90	6.5	2.5	2.82	24.9							-18.96	-148.8
7	8	30-34	719.19	7.0	4.0	3.46	31.4	0.382	1.09	0.60	29.9	9.9	15.13	-19.08	-149.8
8	2	31-35	720.81	9.3	3.5	3.37	29.6	0.308	0.95	0.52	26.6	8.7	13.87	-18.96	-146.9
8	4	25-29	722.67	9.0	3.5	2.5	23.2	0.197	0.68	0.38	19.8	6.8	11.59	-18.67	-146.8
8	7	14-18	725.38	18.0	4.5	6.68	68.3	0.600	3.82	2.19	52.9	19.5	39.1	-19.98	-152.8
9	1	25-29	727.54	3.5	2.5	2.74	27.3							-19.08	-149.8
10	1	30-34	731.01	12.5	4.5	5.79	67.9	0.444	3.64	2.47	122.8	16.2	41.49	-19.76	-151.4
11	5	30-34	736.04	3.5	5.0	8.33	68.4							-19.76	-151.7
11	5	28-34	738.03	6.0	4.5	5.83									
12	5	28-34	746.43	7.5	4.5	7.32	64.6	0.539	2.94	2.01	123.2	15.6	37.16		
12	7	28-34	746.10	2.5	4.5	7.38	69.4							-19.94	-155.0
13	2	26-34	748.51	4.5	4.5	6.09	70.7	0.578	3.29	2.25	126.7	16.9	40.24	-19.83	-154.7
13	7	26-34	753.49	4.1	5.0	7.86	72.7							-20.05	-153.2
13	8	18-26	754.26	3.5	5.0	7.78	73.0								
14	3	24-32	757.26	9.0	5.5	8.04	75.5		3.96	2.51	142.8	20.5	45.26		-153.5
15	4	26-34	760.82	6.0	5.5	6.92	68.8							-20.03	-154.6
16	3	26-34	766.81	4.0	4.5	7.07	65.9				132.3	14.7	37.84	-20.25	-154.0
16	6	10-12	773.65	12.5	4.0	4.69	65.6	0.525	3.05	1.93				-19.96	-154.4
17	3	16-24	776.15	10.5	5.0	5.89	65.8	0.522	3.37	1.93	142.5	14.8	39.78		
17	4	18-26	781.01	10.0	5.0	5.59	63.2	0.507	2.97	1.76	128.1	13.6	35.9	-20.34	-154.7
18	2	12-20	782.07	13.5	4.5	5.28	60.2	0.471	2.87	1.55	121.6	11.9	34.08	-20.32	-154.5
18	4	15-25	788.10	11.0	5.0	5.82	56.3	0.424	2.40	1.46	111.7	11.5	32.02	-20.34	-154.8
19	7	3-11	801.07	10.0	4.0	4.9	53.4	0.327	2.49	1.33	99.1	10.4	29.85	-20.19	-154.7
20	1	29-36	803.99	15.0	4.0	5.09	51.3	0.412	2.20	1.22	98.2	9.9	28.94		
21	2	21-28	808.99	6.0	3.5	3.63	50.1							-20.19	-155.3
21	3	26-34	810.15	11.0	4.0	3.77	49.6	0.427	2.69	1.08	92.6	8.7	27.91	-20.29	-155.4
22	2	10-19	816.32	16.0	3.5	3.51	50.5	0.431	2.68	1.45	122.9	9.7	35.33	-20.33	-154.6
22	5	21-30	819.57	6.0	3.5	3.44	46.3							-20.38	-154.9
23	4	9-17	826.74	2.0	4.5	4.37	50.2							-19.87	-154.2
23	6	26-34	829.21	6.5	4.5	4.58									
23	8	16-25	830.93	1.0	4.0	3.98	56.1							-19.76	-153.8

Table 46: Pore water chemistry results from Mt Elbert-01 core subsamples (Torres, et al, 2011)

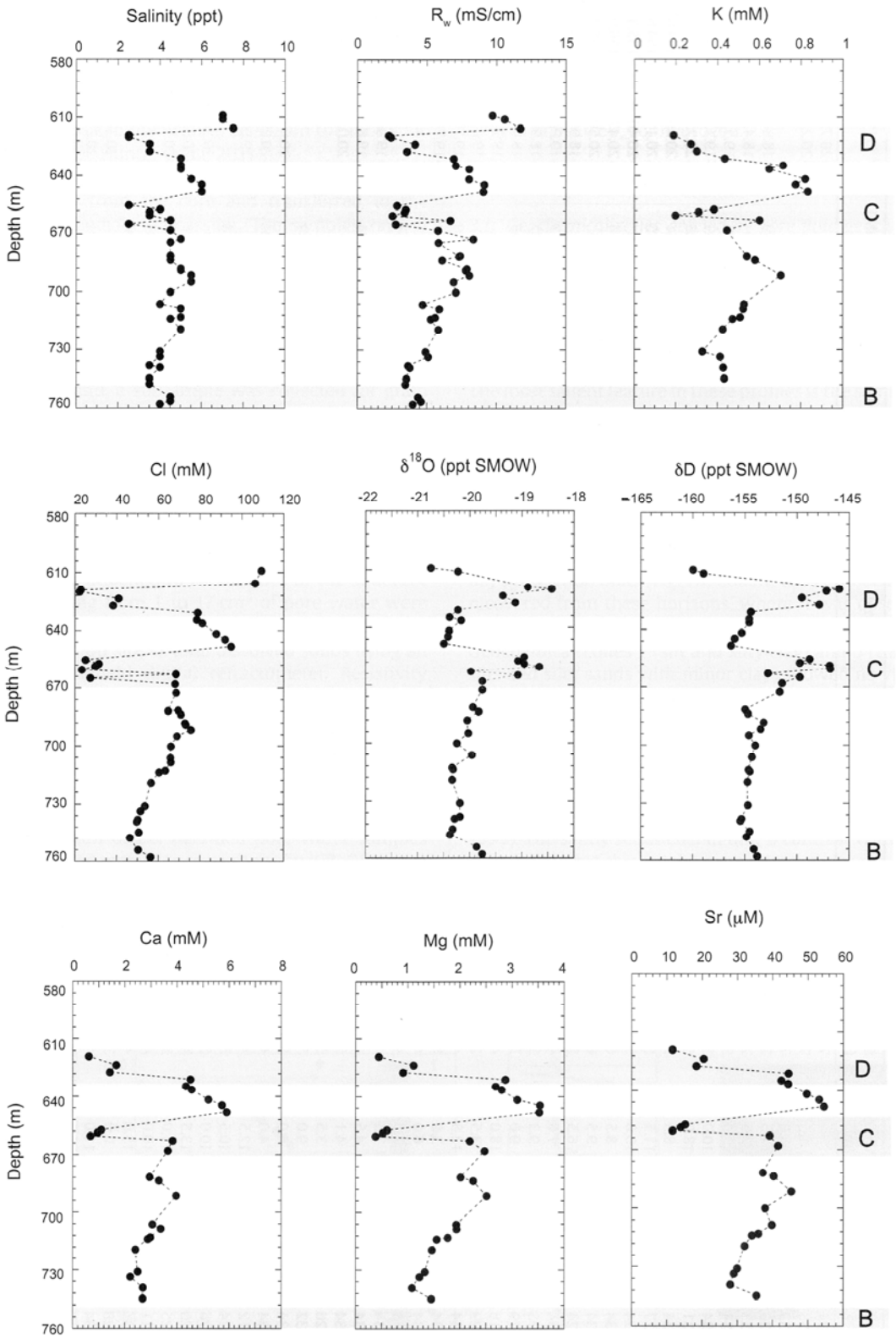

Figure 124: Pore water chemical and isotopic analyses from Mt Elbert-01 interstitial water (IW) samples (Torres, et al, 2011); zones B, C and D are shaded in gray

Interstitial water analyses conclusions include:

- Variation in BIBPF depth is a primary factor controlling the salinity profiles, as well as the distribution of dissolved ions and the isotopic composition of the formation water
- A first order approximation of a one-dimensional decay of a chloride spike generated by ion exclusion, suggest that the BIBPF deepened at the onset of the last glacial period (~100 Kyr), consistent with predictions based on thermal modeling efforts
- Dissolved chloride and isotopic data clearly demarcate the two discrete gas hydrate-bearing reservoir sands, consistent with wireline log interpretation
- Estimates based on chloride data show gas hydrate saturation in these gas hydrate-bearing zones reach values as high as 80%, consistent with log data interpretation

5.3.8.8.8 Core Microbiological Analyses

Dr. Rick Colwell, Oregon State University, completed the microbiological analyses summarized in this section. Full microbiological study results are published in the JMPG Volume in Colwell, et al. (2011). Studies detected 11 phylotypes and plans included complete DNA extractions, perform T-RFLP analysis, detect and quantify methanogen genes (mcrA), enumerate fluorescent microsphere tracers, and possibly perform whole genome amplification. Additional studies may include PhyloChip (detailed diversity information), GeoChip (detailed functional information), study link to abiotic properties in sediments, comparison to Mallik studies and other gas hydrate environments, and possibly contribution to the modeling of carbon dynamics. Microbial communities collected from gas hydrate-bearing sediments on the ANS were studied to determine how abiotic variables (e.g., grain size, gas hydrate presence, original depositional environment) may control the type and distribution of microbes in the sediments. The cores were acquired from sub-permafrost, Eocene (35-36 million years ago (MYA)) sediments laid down as a marine transgressive series within which gas hydrate is believed to have formed 1.5 MYA.

Forty samples, eight of which originally contained gas hydrate, were acquired from 606–666 meter depths. Five samples from drilling fluids acquired from the same depth range were included in the analysis as a control for contamination during the drilling and handling of cores. DNA was extracted from the samples (typically <1 ng DNA/g sediment was recovered) and then amplified using polymerase chain reaction with primers specific for bacterial and archaeal 16S rDNA. Only bacterial DNA amplicons were detected. Terminal-restriction fragment length polymorphism (t-RFLP) was used to measure bacterial diversity in the respective samples. Non-metric multidimensional scaling (NMDS) was then used to determine the abiotic variables that may have influenced bacterial diversity. NMDS analysis revealed that sediment samples were distinct from those obtained from drilling fluids suggesting that the samples were not contaminated by the drilling fluids. All samples had evidence of microbial communities and sample depth, temperature, and gas hydrate presence appeared to have some influence on community diversity. Samples sharing these environmental parameters often shared common t-RFLP profiles. Further examination of selected samples using clone libraries could help identify key taxa present in these unique sediments and could yield a better understanding of the biogeochemistry of these gas hydrate-bearing systems.

5.3.8.8.9 Core Sedimentology

DOE sedimentologist Kelly Rose initiated detailed core sedimentology studies in mid-March 2008. Results of these studies were published the JMPG volume in Rose, et al, 2011. Rose, et al (2011) contains a composite sedimentary log of the cored interval and shows sections of cored

intervals that were not recovered in black. Visual descriptions of the split core sections were completed in April 2008 within the temporary core storage unit. That study identified eight (8) lithostratigraphic subunits within the cored interval representing distinct facies relationships and packages. Subunits II and Va are predominantly very fine- to fine-grained; moderately sorted; quartz-, feldspar-, and lithic fragment-bearing sands and comprise the majority of the reservoir facies. Subunit II contains 33 feet of gas hydrate-saturated section within thinly laminated to massive and amalgamated reservoir sands. Subunits Va and upper Vb are also gas hydrate-bearing within similar lithologies that total 38 feet in thickness. However, these subunits were separated by a 6-foot thick perched water-bearing interval that appears to be composed of the same fine- to very fine-grained sand lithofacies as that of the overlying and underlying gas hydrate-bearing intervals.

The sedimentary record within the entire cored interval contains both marine and nonmarine lithofacies. The interpreted depositional environment for these reservoir facies may have been more influenced by shallower marine processes than originally interpreted based on pre-drill log and correlation interpretations of offset wells. Core lithostratigraphy and palynology confirm deposition within shallow marine and nonmarine nearshore environments during greenhouse conditions of the early to mid-Eocene and correlative with the late Paleocene to early- to mid-Eocene age Sagavanirktok formation.

5.3.9 Phase 3, Task 9 – Reservoir Modeling and Consideration of Production Test

The Phase 3a dedicated gas hydrate well stratigraphic test operations, data, and interpretations (Section 5.3.8) were used to help determine whether or not to proceed into a Phase 3b long term production test. A viable candidate site was selected in 2008 (Tables 4, 5, and 12; Figures 7 and 8), but the project was unable to proceed into Phase 3b due in part to unforeseen difficulties with funding eligibility.

5.3.9.1 Reservoir Model Code Comparison Group

Beginning in 2006, this project collaborated with an international code comparison group (CCG; Table 47). The CCG collaborated efforts to apply the leading gas hydrate numerical simulators to a series of idealized problems of increasing complexity. The CCG completed work on the initial five problems, which moved from simple 1-D heat and mass transfer problems through a complex 3-D simulation of gas hydrate dissociation in an idealized reservoir (see Fire in the Ice Newsletter, Winter, 2007). Given the lack of real-world data on gas hydrate producibility, this effort provided the best opportunity for model verification and calibration, and has resulted in meaningful improvements to the codes employed by all the members of the CCG.

Detailed results of the CCG models with application to future potential ANS long-term production testing are published in the JMPG volume (Boswell, et al, 2011, pp. 460-560). Table 48 lists average reservoir properties of gas hydrate-bearing units C and D at Mount Elbert-01 used for reservoir modeling as documented in the JMPG volume (Anderson, et al, 2011).

With the exception of RyderScott Co. and Fekete, funding for the reservoir model comparison team was separate from this project. Therefore, only general conclusions of this modeling are presented here. Study results are available in the JMPG Volume (Boswell, et al, 2011) in Anderson, et al. (2011); Kurihara, et al. (2011); Moridis, et al. (2011), Pooladi-Darvish and Hong (2011); and White, et al. (2011).

Organization	Primary Representative	Function
University of Akron	Joe Wilder	Co-coordinator
West Virginia University/NETL	Brian Anderson	Co-coordinator
Ryder Scott Co./BPXA consultant	Scott Wilson	Co-Lead STARS & Procast
LBNL	George Moridis	Lead TOUGH+Hydrate
PNNL	Mark White	Lead STOMP-HYD
Japan Oil Engineering Co.	Masanori Kurihara	Lead Japan, MH-21
Nat'l Inst. Adv. Industrial Science	Hideo Narita	Co-Lead, Japan
Fekete Associates/Univ. Calgary	Mehran Pooladi-Darvish	Co-Lead STARS
University of Tokyo	Yoshihiro Masuda	Co-Lead, Japan
DOE NETL	Kelly Rose	Support
DOE NETL	Ray Boswell	Support
USGS	Timothy Collett	Support
BPXA (contractor)	Robert Hunter	Support

Table 47: Code Comparison Group Participants and Support

As indicated in Tables 48-50, three reservoir models were constructed to compare and contrast Areas 1-3 (Figures 8 and 125). These reservoir models included:

1. Milne Point Unit - Mount Elbert-01 (Problem 7A)
2. Prudhoe Bay Unit L-106 (Problem 7B) and
3. Prudhoe Bay Unit L-106 "DOWN-DIP" (Problem 7C)

All participating reservoir simulators show remarkable agreement for gas production rates, character, and times. As expected, the warmer and deeper gas hydrate-bearing reservoirs are modeled as more productive with higher overall initial and sustained rates as well as less time required to initiate gas hydrate dissociation.

5.3.9.2 Preliminary Planning for Potential Future Production Testing

While not finalized since this project did not progress into Phase 3b, preliminary accomplishments toward planning and design of a future production test included the following:

- Incorporated relevant Mallik and other project results, documentation, and information
- Provided input to Stakeholder agreement drafts for long-term gas hydrate production test
  - Reviewed and compiled draft legal, ballot, and commercial agreement documents
- Evaluated shallow well and seismic data to select long-term production test site
  - Evaluated potential surface and subsurface locations to allow 18-24 month access
  - Evaluated trajectory plans for production test wellbore(s)
  - Initiated discussions regarding monitoring of original borehole before sidetrack
    - Determined unlikely due to regulatory and operator constraints
    - Considered tubing outside casing cemented in-place with fiber optic DTS
  - Evaluated subsurface target locations in vicinity of PBU L-106 Sagavanirktok penetration, including faulting and seismic attributes
  - Selected PBU L-pad as optimal surface and subsurface site for production testing
- Evaluated synergies with CPAI-DOE CO2 – CH4 test program (DE-NT0006553)
  - Identified, evaluated, prioritized, and considered implications of synergies
  - Received, reviewed, and approved CoP ballot for well operations and testing

  - Provided information and synergistic project information for CoP Alaska R&D
  - Evaluated, prioritized, and provided input to site selection and design criteria
  - Reviewed and provided input into site options: ice, gravel, other
  - Shared core acquisition and analyses scope and categorical breakout of costs
  - Shared core imaging and NMR measurements accomplished at LBNL
  - Shared prospect generation and other relevant documentation and techniques
- Archived 2008 project workshop and USGS Eileen accumulation documentation
- Evaluated thermal modeling and considered geomechanical aspects of testing
- Reviewed ElectroMagnetic and RadioFrequency thermal stimulation technologies
- Discussed compliance of testing with global well testing parameters
- Reviewed Mount Elbert well operations, accomplishments, and analyses for input to long-term production test drilling and data acquisition operations
- Reviewed field facility access and simultaneous operations issues

5.3.9.3 Reservoir Characterization Supporting Studies

Additional resource characterization work was completed in support of reservoir modeling studies and potential production test site evaluations within the Eileen gas hydrate accumulation. These USGS studies were presented during the March 2008 Mount Elbert data analyses and production test workshop held at the USGS Federal Center in Denver, Colorado.

Figure 125 illustrates the lateral extent of gas hydrate-bearing zones shown with Alaska North Slope field gravel roads and pads infrastructure and several key gas hydrate-bearing well penetrations. Four areas (Figure 125) were evaluated for gas hydrate-bearing reservoir properties. Areas one, two, and three were selected as input to three primary reservoir model simulations as described above in Section 5.3.9.1.

Table 48 summarizes the gas hydrate-bearing reservoir properties at the Mount Elbert-01 site. Figure 126 illustrates a schematic cross-section tie of the Mount Elbert-01 well and gas hydrate-bearing zones into the PBU L-106 Area 2.

Based on regional mapping, correlations, and log data, the PBU L-106 area contains thicker gas hydrate-bearing zones within warmer reservoirs (Figure 126, Table 49). Only Zone C reservoir properties were provided for reservoir modeling (Table 49). At L-106, Zone C contains an additional gas hydrate-bearing reservoir sand; however, this sand may be of limited lateral extent (Figure 126). If projected downdip (Figure 125) into Area 3, the reservoir temperature would increase to nearly 12^{o}C just above the gas hydrate stability field base (Table 49 and Figure 127).

It is important to note that Area 3 has no well penetrations of gas hydrate-bearing zones D or C and that this area is not accessible within the current infrastructure road and pad system.

Area four was essentially equivalent to reservoir and temperature properties in Zone D of area one, so was not independently modeled (Table 50). Table 50 compares the WSak-24 reservoir properties of Zone B to those of Mount Elbert Zone D. Note that the similar thicknesses, reservoir properties, and temperatures preclude the need to model the reservoir in Area 4. Also note that the colder temperatures are due to a deeper base-permafrost in this area (Figure 128).

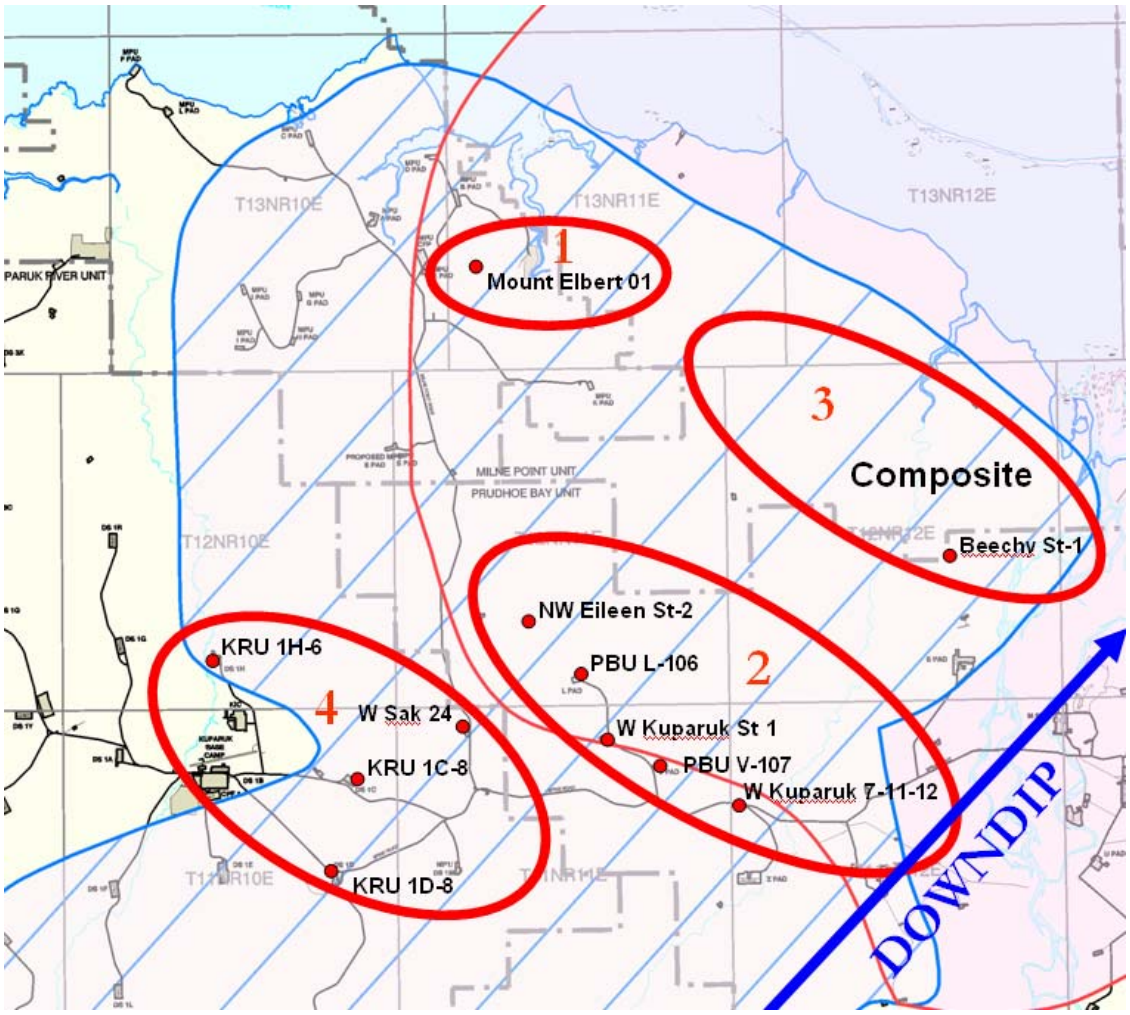

Figure 125: Map of composite lateral extent of Sagavanirktok gas hydrate-bearing zones A, B, C, D, E, and F (blue with stripes) with 4 reservoir characterization and reservoir modeling areas

Reservoir Model	Problem 7a	
Reservoir Property	**Mount Elbert Zone D**	**Mount Elbert Zone C**
Gas hydrate-bearing Reservoir (ft.)	47 (2014-2061 feet BKB)	52 (2132-2184 feet BKB)
Upper Contact	Shale contact	Shale contact
Lower Contact	Shale contact	Water Contact/perched water
Gas Hydrate Zone Saturation	65% average	65% average
Porosity	40%	35%
Intrinsic Permeability	1,000mD (NMR log)	1,000 mD (NMR log)
Gas Hydrate-bearing Permeability	0.12 mD (MDT model)	0.12 mD (MDT model)
Reservoir Temperature	2.3-2.6^{o}C (MPU D-02 basis)	3.3-3.9^{o}C (MPU D-02 basis)
Hydrostatic Pressure	6.7 MPa	7.1 MPa
Pore Water Salinity	5 ppt	5 ppt

Table 48: Reservoir properties of gas hydrate-bearing zones C and D at Mount Elbert-01

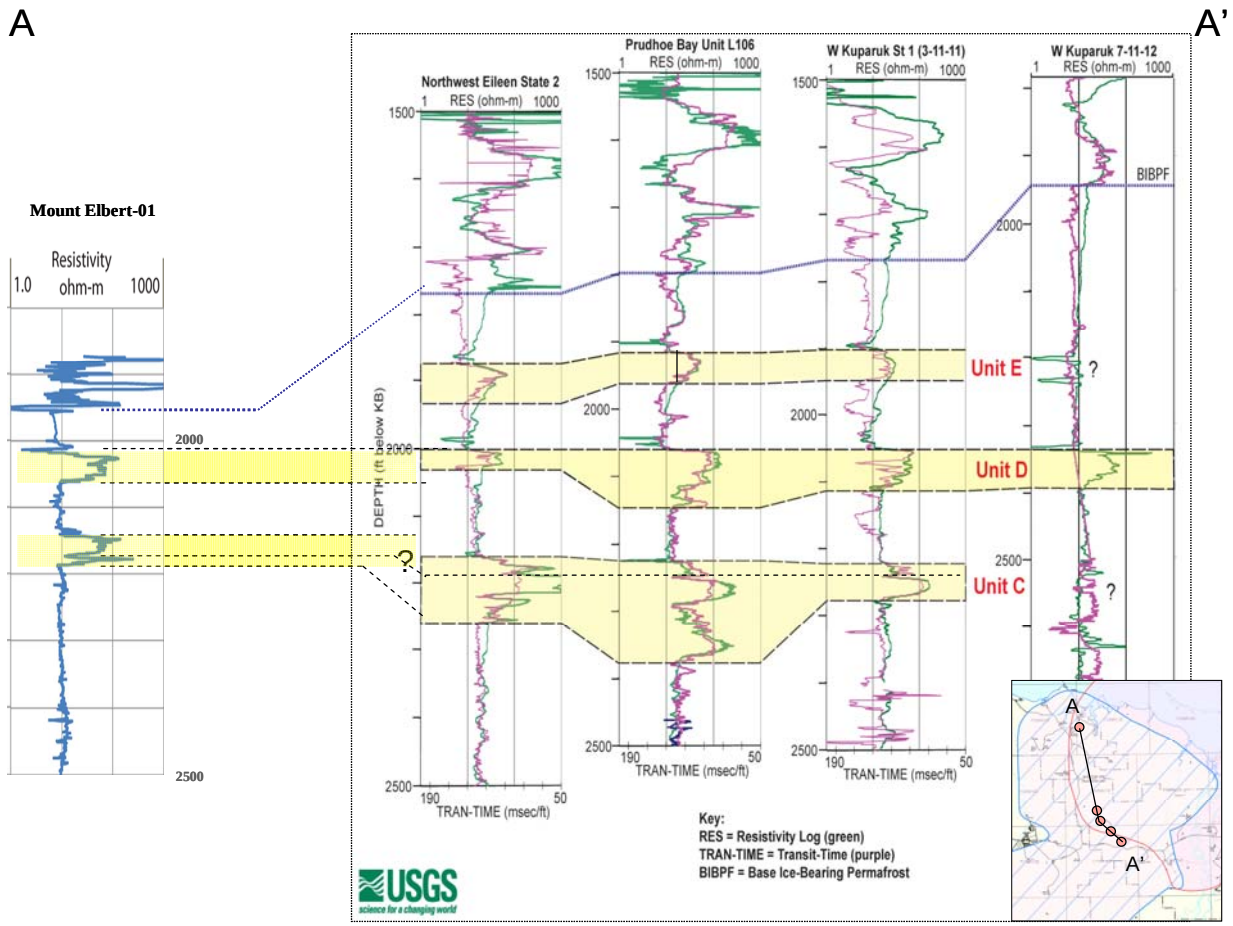

Figure 126: Schematic cross-section tie from Mount Elbert-01 Area 1 to L-106 Area 2 (R. Boswell, modified from T. Collett)

Reservoir Model	Problem 7B	Problem 7C
Reservoir Property	**L-106 Zone C1 and C2**	**"L-106 Downdip" Zone C**
Gas Hydrate-bearing Reservoir (ft)	62 (C1) & 56 (C2) = 118	120 at ~2,500 feet TVDss
Upper Contact	Shale contact	Shale contact
Lower Contact	Shale contact	Shale contact
Gas Hydrate Zone Saturation	75% average	75% average
Porosity	40%	40%
Intrinsic Permeability	1,000mD	1,000 mD
Gas Hydrate-bearing Permeability	0.12 md (MDT model)	0.12 mD (MDT model)
Reservoir Temperature	5.0-6.5^{o}C (MPU D-02 basis)	10-12^{o}C (MPU D-02 basis)
Hydrostatic Pressure	7.3-7.7 MPa	8-9 MPa
Pore Water Salinity	5 ppt	5 ppt

Table 49: L-106 Area 2 and Area 3 reservoir properties comparison

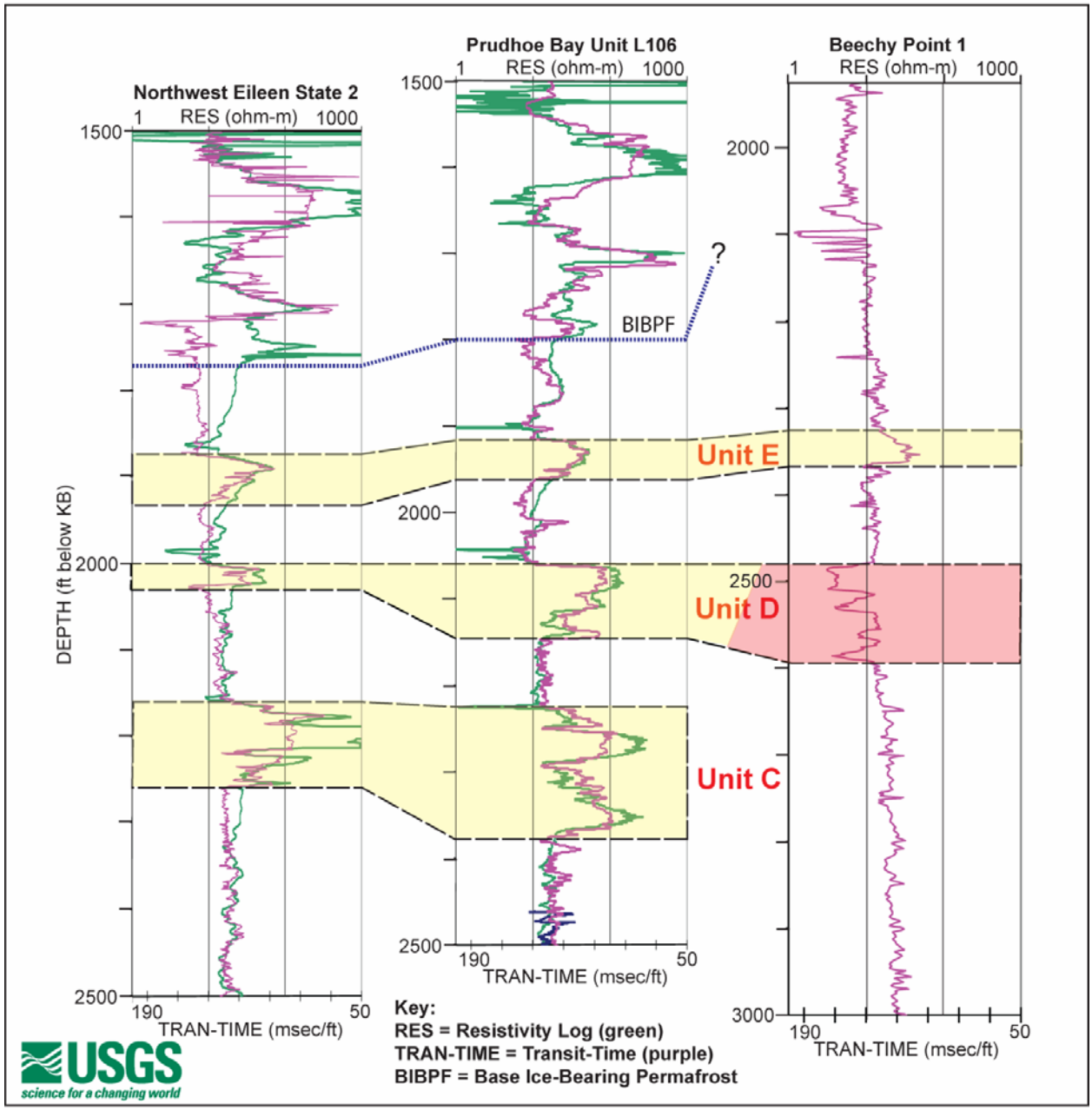

Figure 127: Cross section from PBU L-106 Area 2 to “Downdip” Area 3

Reservoir Model	Problem 7a	~ equivalent to Problem 7a
Reservoir Property	**Mount Elbert Zone D**	**KRU West Sak 24 Zone B**
Gas Hydrate-bearing Reservoir (ft)	47 (2014 – 2061 feet RKB)	40 (2260 – 2300 feet RKB)
Upper Contact	Shale contact	Shale contact
Lower Contact	Shale contact	Shale contact
Gas Hydrate Zone Saturation	65% average	65% average
Porosity	40%	40%
Intrinsic Permeability	1,000mD (NMR log)	1,000mD
Gas Hydrate-bearing Permeability	0.12 md (MDT model)	0.12 md (MDT model)
Reservoir Temperature	2.3-2.6°C (MPU D-02 basis)	2.0-3.0°C (MPU D-02 basis)
Hydrostatic Pressure	6.7 MPa	7.4-7.6 MPa
Pore Water Salinity	5 ppt	5 ppt

Table 50: Area 1 and Area 4 reservoir properties comparison

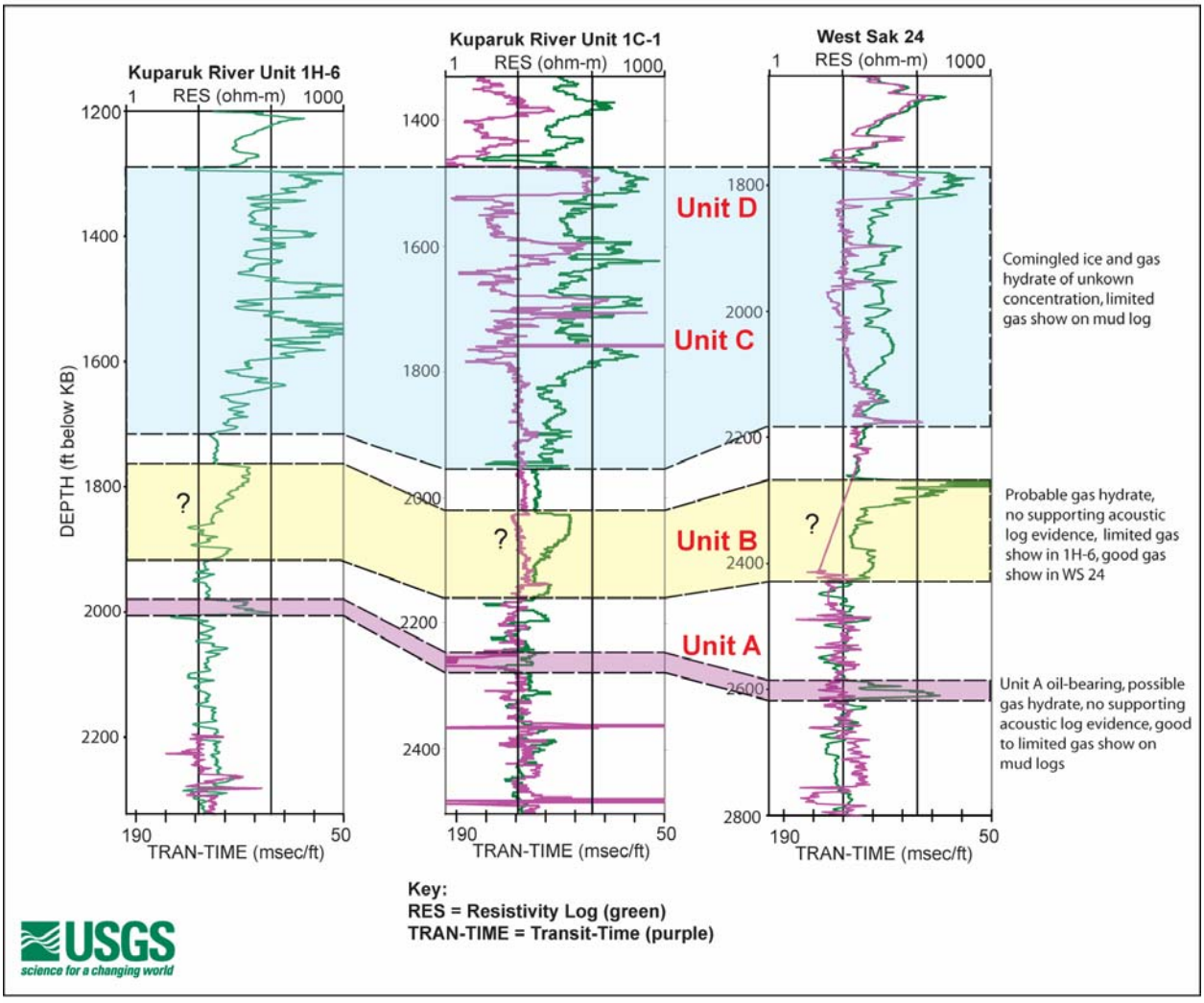

Figure 128: Cross section within KRU Area 4

6.0 CONCLUSIONS

The first ANS dedicated gas hydrate production test, NW Eileen State-02 (NWEIL-02), was drilled in 1972 within the Eileen accumulation (Figures 4, 5, 8, and 125). Since that time, ANS shallow gas hydrate-bearing reservoirs have been primarily considered a shallow drilling hazard to wells targeting deeper horizons due to a combination of factors: no ANS gas export infrastructure, assumed low-rate production potential, unknown production methods, and overall lack of production test data to validate gas hydrate resource experiments and models. Consideration of conventional ANS gas resource potential helped create industry – government alignment necessary to investigate the unconventional resource potential of the potentially large (33 to 100 TCF GIP) ANS gas hydrate accumulations beneath or near existing production infrastructure. Studies show this resource is compartmentalized both stratigraphically and structurally within the petroleum system.

The BPXA – DOE CRA enabled a better understanding of the resource potential of this ANS gas hydrate petroleum system through characterizing regional shallow reservoirs and fluids utilizing well and 3D seismic data, implementing gas hydrate experiments, and designing technology in support of gas hydrate drilling, completion, and production operations.

Following discovery of natural gas hydrate in the 1960-1970's, significant time and resources have been devoted over the past 40-50 years to study and quantify natural gas hydrate occurrence. However, only in the past decade have there been serious attempts to understand the potential production of methane from hydrate. Although significant in-place natural gas hydrate deposits have been identified and inferred, estimation of potential recoverable gas from these deposits is difficult due to the lack of empirical or even anecdotal evidence. This evidence was improved by the short-term Mallik production testing accomplished by JOGMEC in 2007-08, by the CoP Ignik-Sikumi ANS production test in 2012, and by the Nankai Trough testing by JOGMEC in 2012-13. However, long-term production testing could resolve many remaining uncertainties.

The potential to induce gas hydrate dissociation across a broad regional contact from adjacent free gas depressurization may have been observed at Messoyakha field production in Russia (Collett and Ginsberg, 1998) and possibly at East Barrow gas field in Alaska (Singh, et al., 2008). Reservoir modeling also demonstrates this potential as documented in the March 2003 CRA Quarterly report R02, in the December 2003 CRA Quarterly report R05, in the June 2006 CRA Quarterly report R15, and others.

The possibility to induce in-situ gas hydrate dissociation through producing mobile connate waters from within an under-saturated gas hydrate-bearing reservoir was postulated by Hunter in personal communication with Wilson in 2004 (documented in Howe, Wilson, and Hunter et. al., 2004). This potential to induce a depressurization drive within a gas hydrate accumulation emphasizes the importance of saturation and permeability as key variables which, when better understood, could help mitigate productivity uncertainty. A schematic regional screening study was undertaken in 2005 (Wilson et al., 2011) to evaluate ranges of potential recoverable resources given various possible production scenarios of the ANS Eileen gas hydrate accumulation, which may contain up to 33 TCF GIP. Type-well production rates modeled at

0.4-2 MMSCF/d yield potential future peak field-wide development forecast rates of up to 350-450 MMSCF/d and cumulative production up to 12 TCF gas (Wilson, et al, 2011). Individual wells could exhibit a long production character with flat declines, potentially analogous to Coalbed Methane production. Results from the various scenarios show a wide range of potential outcomes. None of these forecasts would qualify for Proved, Probable, or even Possible reserve categories using the SPE/WPC definitions, since there has yet to be a fully documented case of long-term economic production from hydrate-derived gas. Each of these categories would, by definition, require a positive economic prediction, supported by historical analogies, prudent engineering judgment, and rigorous geological characterization of the potential resource before a decision on an actual development could proceed.

BPXA conducted a comprehensive logging, coring, and well pressure testing program in collaboration with the DOE and USGS at the ANS MPU Mount Elbert location in February, 2007. Operational and data acquisition priorities for this Stratigraphic Test field program were designed to better constrain critical uncertainties of gas hydrate-bearing reservoir properties used in initial reservoir simulations (Howe et al., 2004) and regional schematic development modeling (Wilson et al., 2011) and to help assess whether or not gas produced from gas hydrate might someday become part of the broader ANS gas resource portfolio. Key data acquired included cores, logs, and wireline pressure tests (MDT) within gas hydrate-bearing reservoir sands. Analyses of the core, log, and MDT results has helped reduce the uncertainty regarding gas hydrate-bearing reservoir productivity and improved planning of Phase 3b gas hydrate production test designs, although Phase 3b operations did not proceed.

The Mount Elbert Stratigraphic Test location was selected based on detailed geologic-geophysical reservoir and fluid characterization and prospecting studies conducted primarily by the USGS (Inks et al., 2009; Lee et al., 2009; Lee et al., 2010) in collaboration with the BPXA-DOE CRA utilizing MPU 3D seismic data provided by BPXA. The 2007 field program adhered to BPXA ANS operations standards and proved the ability to safely conduct extended drilling and data acquisition operations within ANS gas hydrate-bearing reservoirs. A key element enabling drilling program success was using chilled Mineral-Oil-Based-Mud (MOBM) drilling fluid, which with proper borehole maintenance and conditioning, helped provide stable and in-gauge hole conditions for data acquisition of continuous wireline core, full wireline log suite, and extended open hole MDT within interlayered gas hydrate-bearing and water-bearing intervals beneath the permafrost. The acquired data helped calibrate reservoir models, improve recoverable resource estimates, and characterize gas hydrate-bearing porous media reservoir quality, fluid saturations, mobile versus irreducible water content, water chemistry, and microbiology. Operations proceeded safely, smoothly, on-time, and without incident.

The Mount Elbert Stratigraphic Test field operations program acquired the first significant Sagavanirktok formation core data within ANS gas hydrate-bearing reservoirs. Studies of acquired data reveal a combined 30.5 meters (100 feet) thickness of gas hydrate-bearing sediment (Lee et al., 2011a) within a complex stratigraphic-structural trap within two distinct stratigraphic units C and D (Rose et al., 2011, Boswell et al., 2011). These results conform well to the pre-drill prediction (Lee et al., 2011b). The MDT results significantly improved understanding of the in-situ petrophysics of the reservoir and provided insight into reservoir response to local depressurization through free water withdrawal and associated gas production

from gas hydrate dissociation (Anderson et al., 2011a; Pooladi-Darvish et al., 2011; Kurihara et al., 2011). Reservoir modeling indicates that the ability of the gas hydrate-bearing porous media to transmit a pressure front could be a key parameter to enable pressure-depletion drive during production testing (Wilson et al., 2011), provided temperatures do not fall below freezing, which would effectively transform the small remaining mobile water phase into an immobile ice phase. Reservoir simulations based on an idealized Mount Elbert-01 unit D geologic model have better constrained the range of possible production responses across variable gas hydrate occurrences within the Eileen accumulation and indicate these gas hydrate-bearing reservoirs may be capable of gas production through sustained dissociation by depressurization (Wilson et al., 2011; Anderson et al., 2011a, b; Moridis et al., 2011). These reservoir characterization and modeling techniques have also been applied to identify, compare, and select prospective future production test sites (Collett and Boswell, 2009; Tables 5, 49, and 50 and Figures 8 and 125).

The Mount Elbert-01 well results confirm that long-term production testing within the Eileen accumulation infrastructure area (Figures 8, 9, and 125) would better constrain what portion of a gas hydrate in-place resource might become a technically-feasible or possibly even a commercial natural gas resource. A future long-term ANS gas hydrate production test would build on the successful short-term production test conducted in March 2008 at the Mallik site in the MacKenzie Delta by the governments of Japan and Canada, which indicated the technical feasibility of gas production from gas hydrate by conventional depressurization technology (Dallimore, et al., 2008; Kurihara, et al., 2008); on the successful CO_2-injection gas hydrate production test conducted on the ANS by CoP in 2012; and on the successful 2013 depressurization test conducted by JOGMEC at the Nankai Trough (JOGMEC, 2013). Although technical production of gas from gas hydrate has been modeled and proven possible in short-term production testing at the Mallik, ANS, and Nankai Trough sites, the economic viability of gas hydrate production remains unproven. Additional data acquisition and future long-term production testing could help determine the technical feasibility of depressurization-induced or thermal-, chemical-, and/or mechanical-stimulated dissociation of gas hydrate to producible gas.

Future long-term production testing would provide a valuable dataset that cannot be obtained from existing or planned desktop research or laboratory studies. One or more of the areas shown in Figure 125 and compared in Tables 49-51 may offer the unique combination of low geologic risk, maximal operational flexibility (multiple zones), low operational risk (near-vertical wells adjacent to infrastructure) and near-term meaningful reservoir response. Test designs could initially evaluate depressurization technologies and if necessary, extend into a sequence of increasingly complex thermal, chemical, and/or mechanical stimulation procedures. Whether or not gas hydrate is capable of commercial gas production will remain a priority to help sustain future economic growth and energy security. Results from a future onshore Alaska production test might also help determine the resource potential of offshore gas hydrate accumulations in the Gulf of Mexico (GOM), Japan Nankai Trough, and other continental shelf areas.

Field Area / Parameter	MPU E-pad (area 1)	MPU B-Pad (area 1)	PBU L-pad (area 2)	PBU Kup St. 3-11-11 (area 2)	PBU Downdip L-pad (area 3)	KRU WSak-24 (area 4)	KRU 1H-Pad (area 4)
Temperature	H	H	M	M	L	H	H
Ownership	L	L	H	H	H	M-L	M-L
Gravel Access	M	M	L	L	H	L	L
Geologic	L	L	L	L	H	M	M
Data Constraints	L	L	L	M	H	M	M
Well / Drilling	L-M	L-M	M	M	H	M	M
Facilities	L	L	L	M	H	M	L
Gas Handling	H	H	H	H	H	H	H
Water Handling	L	L	L	M	H	M	L
Simultaneous Operations	L	M	H?	L	L	L	H?
Operations Linkage	L?	L?	M	M	M	L	L?
Multi-zone Options	M-H	M-H	L	L	M-H	H	H
AVERAGE	**L-M**	**L-M**	**L-M**	**M**	**M-H**	**M**	**M**

Table 51: Review of risk factors for potential long-term production test sites with area corresponding to Figures 8 and 125. H = high risk associated with this parameter (unfavorable); M = medium risk; L = low risk (after Collett and Boswell, 2009).

7.0 REFERENCES

7.1 General Project References

Anderson, B.J., Wilder, J.W., Kurihara, M., White, M.D., Moridis, G.J., Wilson, S.J., Pooladi-Darvish, M., Masuda, Y., Collett, T.S., Hunter, R.B., Narita, H., Rose, K., and Boswell, R., 2008, Analysis of modular dynamic formation test results from the Mount Elbert 01 stratigraphic test well, Milne Point Unit, North Slope, Alaska: Proceedings of the 6th International Conference on Gas Hydrates (ICGH 2008), July 6–10, 2008, Vancouver, British Columbia, Canada, 13 p. (on CD–ROM).

Boswell, R.M., Kleinberg, R., Collett, T.S., Frye, M., Exploration Priorities for Marine Gas Hydrate Resources *(gas hydrate resource pyramid)*, USDOE NETL Fire-in-the-Ice Newsletter, Summer 2007, p.11-13.

Casavant, R.R. and Gross, E., 2002, Basement Fault Blocks and Subthrust Basins? A Morphotectonic Investigation in the Central Foothills and Brooks Range, Alaska, at the SPE-AAPG: Western Region-Pacific Section Conference, Anchorage, Alaska, May 18-23, 2002.

Casavant, R.R. and Miller, S.R., 2002, Tectonic Geomorphic Characterization of a Transcurrent Fault Zone, Western Brooks Range, Alaska, at the SPE-AAPG: Western Region-Pacific Section Conference, Anchorage, Alaska, May 18-23, 2002.

Collett, T.S., 1993, Natural Gas Hydrates of the Prudhoe Bay and Kuparuk River Area, North Slope, Alaska, American Association of Petroleum Geologists Bulletin, Vol. 77, No. 5, May 1993, p. 793-812.

Collett, T.S., 1995, Gas hydrate resources of the United States, *in* Gautier, D.L., Dolton, G.L., Takahashi, K.I., and Varnes, K.L., eds., 1995 National assessment of United States oil and gas resources - results, methodology, and supporting data: U.S. Geological Survey Digital Data Series 30 (on CD–ROM).

Collett, T.S., 2001, Natural-gas hydrates: resource of the twenty-first century? In Downey, M.W., Threet, J.C. and Morgan, W.A. eds., Petroleum Provinces of the Twenty-First Century: American Association of Petroleum Geologist Memoir 74, p. 85-108.

Collett, T.S., 2001, MEMORANDUM: Preliminary analysis of the potential gas hydrate accumulations along the western margin of the Kuparuk River Unit, North Slope, Alaska (unpublished administrative report, December 6, 2001).

Collett, T.S., et al., 2001, Modified version of a multi-well correlation section between the Cirque-2 and Reindeer Island-1 wells, depicting the occurrence of the Eileen and Tarn gas hydrate and associated free-gas accumulations (unpublished administrative report).

Collett, T.S., et al., 2001, Modified version of a map that depicts the distribution of the Eileen and Tarn gas hydrate and associated free-gas accumulations (unpublished administrative report).

Collett, T.S., 2002, Methane hydrate issues – resource assessment, *In* the Proceedings of the Methane Hydrates Interagency R&D Conference, March 20-22, 2002, Washington, D.C., 30 p.

Collett, T.S., 2002, Energy resource potential of natural gas hydrates: American Association of Petroleum Geologists Bulletin, v. 86, no. 11, p. 1971-1992.

Collett, T.S., Johnson, A., Knapp, C., and Boswell, R., 2009, Natural gas hydrates – a review, *in* Collett, T., Johnson, A., Knapp, C., and Boswell, R., eds, *In* Natural Gas Hydrates - Energy Resource Potential and Associated Geologic Hazards: American Association of Petroleum Geologists Memoir 89.

Collett, T.S. and Dallimore, S.R., 2002, Detailed analysis of gas hydrate induced drilling and production hazards, *In* the Proceedings of the Fourth International Conference on Gas Hydrates, April 19-23, 2002, Yokohama, Japan, 8 p.

Collett, T.S. and Ginsberg, G.D., 1998, Gas Hydrates in the Messoyakha Gas Field of the West Siberian Basin - A Re-examination of the Geologic Evidence, International Journal of Offshore and Polar Engineering 8 (1998): pp. 22–29.

Digert, S. and Hunter, R.B., 2003, Schematic 2 by 3 mile square reservoir block model containing gas hydrate, associated free gas, and water (Figure 2 from December, 2002 Quarterly

and Year-End Technical Report, First Quarterly Report, R01: October, 2002 – December, 2002, Cooperative Agreement Award Number DE-FC26-01NT41332.

Folk, R.L., 1980, Petrology of Sedimentary Rocks, Hemphill Publishing Co., 182pp.

Geauner, S., 2009, Fault analysis, seismic facies modeling and volumetric reassessment of gas hydrates in the Milne Point Unit, North Slope, Alaska: Master of Science thesis, University of Arizona, Tucson.

Geauner, J.M., Manuel, J., and Casavant, R.R., 2003, Preliminary subsurface characterization and modeling of gas hydrate resources, North Slope, Alaska, *in*: 2003 AAPG-SEG Student Expo Student Abstract Volume, Houston, Texas.

Hagbo, C.L., 2003, Characterization of Gas hydrate Occurrences using 3D Seismic Data and Seismic Attributes, Milne Point, North Slope, Alaska, M.S. Thesis, Dept. of Geosciences, University of Arizona, Tucson, 127 pp.

Hennes, A.M., 2004, Structural Constraints on Gas Hydrate Formation and Distribution in the Milne Point, North Slope of Alaska, Prepublication Manuscript submitted in partial fulfillment for M.S. Thesis, Dept. of Geosciences, University of Arizona, Tucson, 40 pp., 19 figs., 3 tables.

Howe, S.J., 2004, Production modeling and economic evaluation of a potential gas hydrate pilot production program on the North Slope of Alaska, MS Thesis, University of Alaska Fairbanks, 141 p.

Hunter, R.B., Casavant, R. R., Johnson, R.A., Poulton, M., Moridis, G.J., Wilson, S.J., Geauner, S., Manuel, J., Hagbo, C., Glass, C.E., Mallon, K.M., Patil, S.L., Dandekar, A.Y., and Collett, T.S., 2004, Reservoir-fluid characterization and reservoir modeling of potential gas hydrate resource, Alaska North Slope, 2004 AAPG Annual Convention Abstracts with Program.

Hunter, R.B., Digert, S.A., Casavant, R.R., Johnson, R.A., Poulton, M., Glass, C., Mallon, K., Patil, S.L., Dandekar, A.Y., and Collett, T.S., 2003, Resource Characterization and Quantification of Natural Gas Hydrate and Associated Free-Gas Accumulations in the Prudhoe Bay-Kuparuk River Area, North Slope of Alaska, Poster Session at the AAPG Annual Meeting, Salt Lake City, Utah, May 11-14, 2003. Poster received EMD, President's Certificate for Excellence in Presentation.

Hunter, R.B., Pelka, G.J., Digert, S.A., Casavant, R.R., Johnson, R., Poulton, M., Glass, C., Mallon, K., Patil, S.L., Chukwu, G.A., Dandekar, A.Y., Khataniar, S., Ogbe, D.O., and Collett, T.S., 2002, Resource Characterization and Quantification of Natural Gas Hydrate and Associated Free-Gas Accumulations in the Prudhoe Bay-Kuparuk River Area on the North Slope of Alaska, presented at the Methane Hydrate Inter-Agency Conference of U.S. Department of Energy, Washington DC, March 21-23, 2002.

Hunter, R.B., Pelka, G.J., Digert, S.A., Casavant, R.R., Johnson, R.A., Poulton, M., Glass, C., Mallon, K., Patil, S.L., Chukwu, G.A., Dandekar, A.Y., Khataniar, S., Ogbe, D.O., and Collett,

T.S., 2002, Resource Characterization and Quantification of Natural Gas Hydrate and Associated Free-Gas Accumulations in the Prudhoe Bay-Kuparuk River Area on the North Slope of Alaska, at SPE-AAPG: Western Region-Pacific Section Conference, Anchorage, Alaska, May 18-23, 2002.

Hunter, R.B., 2004, Characterization of Alaska North Slope Gas Hydrate Resource Potential, Spring 2004 Fire in the Ice Newsletter, DOE National Energy Technology Laboratory.

Hunter, R.B., Digert, S.A., Wilson, S.J., Collett, T.S., and Boswell, R.M., 2007, Gas Hydrate Resource Potential, *at* AAPG Annual Meeting, Long Beach, CA, Abstracts with Programs, Received EMD Frank Kottlowski Memorial Award for best presentation.

Inks, T., Lee, M., Agena, W., Taylor, D., Collett, T., Hunter, R., and Zyrianova, M., 2009, Seismic prospecting for gas hydrate and associated free-gas prospects in the Milne Point Area of Northern Alaska; *in* Collett, T., Johnson, A., Knapp, C., and Boswell, R., eds, Natural Gas Hydrates: Energy Resource and Associated Geologic Hazards, American Association of Petroleum Geologists Memoir 89.

Jaiswal, N.J., 2004, Measurement of gas-water relative permeabilities in hydrate systems, MS Thesis, University of Alaska Fairbanks, 100 p.

JOGMEC, 2013, Japan Oil, Gas and Metals National Corporation (JOGMEC, Headquarters: Minato-ku, Tokyo, President: Hirobumi Kawano), Gas Production from Methane Hydrate Layers Confirmed in March 12, 2013 Press Release:
http://www.jogmec.go.jp/english/news/release/release0110.html

Johnson, A.C., 2009, Experimental and simulation studies in support of the Mt. Elbert gas hydrate prospect on the Alaska North Slope, M.S. Thesis, University of Alaska Fairbanks, August 2009.

Kerkar, P.B., 2005, Assessment of Formation Damage from Drilling Fluids Dynamic Filtration in Gas Hydrate Reservoirs of the North Slope of Alaska, M.S. Thesis, University of Alaska Fairbanks, August 2005.

Kvenvolden, K.A., 1988, Methane hydrate – a major reservoir of carbon in the shallow geosphere?, Chemical Geology, v. 71, p.41-51.

Lachenbruch, A.H., Galanis Jr., S.P., and Moses Jr., T.H., 1988, A Thermal Cross Section for the Permafrost and Hydrate Stability Zones in the Kuparuk and Prudhoe Bay Oil Fields, Geologic Studies in Alaska by the U.S. Geological Survey during 1987, p. 48-51.

Lee, M.W., 2002, Joint inversion of acoustic and resistivity data for the estimation of gas hydrate concentration: U.S. Geological Survey Bulletin 2190, 11 pp.

Lee, M.W., 2004, Elastic velocities of partially gas-saturated unconsolidated sediments, Marine and Petroleum Geology 21, p. 641–650.

Lee, M.W., 2005, Well-log analysis to assist the interpretation of 3-D seismic data at the Milne Point, North Slope of Alaska, U. S. Geological Survey Scientific Investigation Report SIR 2005-5048, 18 pp.

Lewis, R.E., Collett, T.S., and Lee, M.W., 2001, Integrated well log montage for the Phillips Alaska Inc., Kuparuk River Unit (Tarn Pool) 2N-349 Well (unpublished administrative report).

Khataniar, S., Kamath, V.A., Omenihu, S.D., Patil, S.L., and Dandekar, A.Y., 2002, Modeling and Economic Analysis of Gas Production from Hydrates by Depressurization Method, Canadian Journal of Chemical Engineering, Volume 80, February 2002.

Manuel, J., 2008, A chronostratigraphic framework of the Sagavanirktok Formation, North Slope Alaska: Incorporating facies characterization, reservoir continuity and dimensions in relation to gas hydrate and associated free-gas resources, M.G.Eng., M.S. Thesis, Department of Mining and Geologic Engineering, University of Arizona.

Schoderbek, D., Farrell, H., Hester, K,. Howard, J., Raterman, K., Silpngarmlert, S., Martin, K.L., Smith, B., and Klein, P., 2013, ConocoPhillips Gas Hydrate Production Test Final Technical Report, October 1, 2008–June 30, 2013, Submitted July 20, 2013, DOE Award No.: DE-NT0006553

Singh, P., Panda, M., and Stokes, P.J., 2008, Topical Report: Material Balance Study to Investigate Methane Hydrate Resource Potential in the East Pool of the Barrow Gas Field, prepared for USDOE NETL, DOE Project Number DE-FC26-06NT42962.

Sun, Y.F. and Goldberg, D., 2005, Analysis of electromagnetic propagation tool response in gas hydrate-bearing formations, *IN* Geological Survey of Canada Bulletin 585: Scientific Results from the Mallik 2002 Gas Hydrate Production Research Well Program, MacKenzie Delta, Northwest Territories, Canada, Editors S.R. Dallimore and T.S. Collett.

Walsh, T., Stokes, P., Panda, M., Morahan, T., Greet, D., Singh, P., and Patil, S., 2008, Final Report DE-FC26-06NT42962, Characterization and Quantification of the Methane Hydrate Resource Potential Associated with the Barrow Gas Fields, USDOE, NETL, 21pp.

Werner, M.R., 1987, Tertiary and Upper Cretaceous heavy-oil sands, Kuparuk River Unit area, Alaska North Slope, in Meyer, R.F., ed., Exploration for heavy crude oil and natural bitumen: American Association of Petroleum Geologists Studies in Geology 25, p. 537-547.

Westervelt, J.V., 2004, Determination of methane hydrate stability zones in the Prudhoe Bay, Kuparuk River, and Milne Point units on the North Slope of Alaska, MS Thesis, University of Alaska Fairbanks, 85 p.

Zhao, Bo, 2003, Classifying Seismic Attributes in the Milne Point Unit, North Slope of Alaska, M.S. Thesis, Dept. of Mining and Geological Engineering, University of Arizona, Tucson, 159 pp.

7.2 Selected JMPG Volume 28, Issue 2 Publication References

Anderson, B.J., Wilder, J.W., Kurihara, M., White, M.D., Moridis, G.J., Wilson, S.J., Pooladi-Darvish, M., Masuda, Y., Collett, T.S., Hunter, R.B., Narita, H., Rose, K., and Boswell, R., 2008, Analysis of modular dynamic formation test results from the Mount Elbert 01 stratigraphic test well, Milne Point Unit, North Slope, Alaska, Proceedings of the 6th International Conference on Gas Hydrates (ICGH 2008), July 6-10, 2008, Vancouver, British Columbia, Canada, 10 p.

Anderson, B.J., Hancock, S., Wilson, S.J., Collett, T.S., Boswell, R.M., Hunter, R.B., 2011 (a), Formation pressure testing at the Mount Elbert Gas Hydrate Stratigraphic Test Well, Alaska North Slope: Operational summary, history matching, and interpretations *in* Scientific results of the Mount Elbert Gas Hydrate Stratigraphic Test Well, Alaska North Slope, Ed. by Boswell, R., Collett, T., Anderson, B., and Hunter, R., Journal of Marine and Petroleum Geology, Vol. 28, Issue 2, Feb. 2011. http://www.sciencedirect.com/science/article/pii/S0264817210000462

Anderson, B.J., Kurhiara, M., Wilson, S.J., Pooladi-Darvish, M., Moridis, G., White, M., 2011 (b), Regional long-term production modeling from a single well test, Mount Elbert Gas Hydrate Stratigraphic Test Well, Alaska North Slope *in* Scientific results of the Mount Elbert Gas Hydrate Stratigraphic Test Well, Alaska North Slope, Ed. by Boswell, R., Collett, T., Anderson, B., and Hunter, R., Journal of Marine and Petroleum Geology, Vol. 28, Issue 2, Feb. 2011. http://www.sciencedirect.com/science/article/pii/S0264817210000176

Boswell, R., Collett, T.S., Hunter, R.B., and Anderson, B.J., Editors, 2011, **Thematic Set on** Scientific Results of the Mount Elbert Gas Hydrate Stratigraphic Test Well, Alaska North Slope, Journal of Marine and Petroleum Geology, Vol. 28, Issue 2, Feb. 2011. http://www.sciencedirect.com/science/journal/02648172/28/2

Boswell, R., Rose, K., Collett, T.S., Lee, M.W., Winters, W.J., Lewis, K., and Agena, W.F., 2011, Geologic controls on gas hydrate occurrence in the Mount Elbert prospect, Alaska North Slope *in* Scientific results of the Mount Elbert Gas Hydrate Stratigraphic Test Well, Alaska North Slope, Ed. by Boswell, R., Collett, T., Anderson, B., and Hunter, R., Journal of Marine and Petroleum Geology, Vol. 28, Issue 2, Feb. 2011. http://www.sciencedirect.com/science/article/pii/S0264817209002219

Bujak, J.P., 2008, Palynological Biostratigraphy of the Interval 1990-2484 feet, Mount Elbert-01 Well, Northern Alaska, July 2008 project report, 22pp, 2 plates. *Also published as Appendix to CRA DE-FC26-01NT41332 2Q2008-3Q2008 Semi-Annual Project Report R24.*

Collett, T.S., 1993, Natural gas hydrates of the Prudhoe Bay and Kuparuk River area, North Slope, Alaska, American Association of Petroleum Geologists Bulletin, v. 77, no. 5, p. 793-812.

Collett, T.S., 1995, Gas hydrate resources of the United States, *in* Gautier, D.L., Dolton, G.L., Takahashi, K.I., and Varnes, K.L., eds., 1995 National assessment of United States oil and gas resources on CD-ROM: U.S. Geological Survey Digital Data Series 30.

Collett, T., 2002, Energy resource potential of natural gas hydrates: American Association of Petroleum Geologists Bulletin, v. 86, no. 11, p. 1971-1992.

Collett T.S., Agena, W.F., Lee, M.W., Zyrianova, M.V., Bird, K.J., Charpentier, R.R., Cook, T., Houseknecht, D.W., Klett, T.R., Pollastro, R.M., and Schenk, C.J., 2008, Assessment of Gas Hydrate Resources on the North Slope, Alaska, U.S. Geological Survey, U.S. Department of the Interior, Fact Sheet 2008-3073, October 2008.

Collett, T.S. and Boswell, R.M., 2009, The Identification of Sites for Extended-term Gas Hydrate Reservoir Testing on the Alaska North Slope, USDOE NETL Fire-in-the-Ice Newsletter, Summer 2009, p.12-16.

Collett, T.S., Johnson, A., Knapp, C., Boswell, R., 2009, Natural gas hydrates – a review, *in* Collett, T., Johnson, A., Knapp, C., Boswell, R., eds, Natural Gas Hydrates - Energy Resource Potential and Associated Geologic Hazards: American Association of Petroleum Geologists Memoir 89.

Collett, T.S., Lee, M.W., Agena, W.F., Miller, J.J., Lewis, K.A., Zyrianova, M.V., Boswell, R.M., and Inks, T.L., 2011 (a), Permafrost Associated Natural Gas Hydrate Occurrences on the Alaska North Slope *in* Scientific results of the Mount Elbert Gas Hydrate Stratigraphic Test Well, Alaska North Slope, Ed. by Boswell, R., Collett, T., Anderson, B., and Hunter, R., Journal of Marine and Petroleum Geology, Vol. 28, Issue 2, Feb. 2011.
http://www.sciencedirect.com/science/article/pii/S0264817209002177

Collett, T.S., Lewis, R.E., Winters, W.J., Lee, M.W., Rose, K.K., and Boswell, R.M., 2011, Downhole well log and core montages from the Mount Elbert Gas Hydrate Stratigraphic Test Well, Alaska North Slope, *in* Scientific results of the Mount Elbert Gas Hydrate Stratigraphic Test Well, Alaska North Slope, Ed. by Boswell, R., Collett, T., Anderson, B., and Hunter, R., Journal of Marine and Petroleum Geology, Vol. 28, Issue 2, Feb. 2011.
http://www.sciencedirect.com/science/article/pii/S0264817210000759

Colwell, F., Briggs, B., and Schwartz, 2011, Microbial Community Distribution in Sediments from the Mount Elbert Gas Hydrate Stratigraphic Test Well, Alaska North Slope *in* Scientific results of the Mount Elbert Gas Hydrate Stratigraphic Test Well, Alaska North Slope, Ed. by Boswell, R., Collett, T., Anderson, B., and Hunter, R., Journal of Marine and Petroleum Geology, Vol. 28, Issue 2, Feb. 2011.
http://www.sciencedirect.com/science/article/pii/S0264817209002372

Collett, T.S. and Dallimore, S.R., 2002, Detailed analysis of gas hydrate induced drilling and production hazards, *In* the Proceedings of the Fourth International Conference on Gas Hydrates, April 19-23, 2002, Yokohama, Japan, 8 p.

Dai, S., Lee, C., and Santamarina, A., 2011, Formation history and physical properties of sediments from the Mount Elbert Gas Hydrate Stratigraphic Test Well, Alaska North Slope, *in* Scientific results of the Mount Elbert Gas Hydrate Stratigraphic Test Well, Alaska North Slope, Ed. by Boswell, R., Collett, T., Anderson, B., and Hunter, R., Journal of Marine and Petroleum Geology, Vol. 28, Issue 2, Feb. 2011.
http://www.sciencedirect.com/science/article/pii/S0264817210000644

Dallimore, S.R. and Collett, T.S., Eds., 2005. Scientific Results from the Mallik 2002 Gas Hydrate Production Research Well Program, Mackenzie Delta, Northwest Territories, Canada, *Geological Survey of Canada Bulletin* **585,** two CD-ROM set.

Dallimore, S., Wright, J.F., Nixon, F.M., Kurhiara, M., Yamamoto, K., Fugjii, T., Fujii, K., Numasawa, M., Yasuda, M., and Imasato, Y., 2008a, Geologic and Porous Media Factors Affecting the 2007 Production Response Characteristics of the JOGMEC/ NRCAN/ Aurora Mallik Gas Hydrate Production Research Well *in* Proceedings of the 6th International Conference on Gas Hydrates (ICGH 2008), July 6-10, 2008, Vancouver, British Columbia, Canada, 10 p.

Dallimore, S. R., Wright, J.F., and Yamamoto, K. 2008b, Appendix D: Update on Mallik, *in* Energy from gas hydrates: Assessing the opportunities and challenges for Canada: Ottawa, Canada, Council of Canadian Academies, p. 196-200.
http://www.scienceadvice.ca/documents/(2008-11-05)%20Report%20on%20GH.pdf

Hancock, S.H., Collett, T.S., Dallimore, S.R., Satoh, T., Inoue, T., Huenges, E., Henninges, J. and Weatherill, B., 2004, Overview of thermal-stimulation production-test results for the JAPEX/JNOC/GSC et al. Mallik 5L-38 gas hydrate production research well, *in* Scientific Results from the Mallik 2002 Gas Hydrate Production Research Well Program, Mackenzie Delta, Northwest Territories, Canada, Dallimore, S.R., and Collett, T.S., Eds., Geological Survey of Canada Bulletin 585.

Howe, S., Nanchar, N., Patil, S., Ogbe, D., Chukwu, G., Hunter, R., and Wilson, S.J., 2004, Economic Analysis and Feasibility Study of Gas Production from Alaska North Slope Gas Hydrate Resources, Presented at AAPG Hedberg Conference, Vancouver, BC.

Hunter, R.B., Collett, T.S., Boswell, R., Anderson, B.J., Digert, S.A., Pospisil, G., Baker, R., and Weeks, M., 2011, Mount Elbert Gas Hydrate Stratigraphic Test Well, Alaska North Slope: Overview of Scientific and Technical Program, *in* Scientific results of the Mount Elbert Gas Hydrate Stratigraphic Test Well, Alaska North Slope, Ed. by Boswell, R., Collett, T., Anderson, B., and Hunter, R., Journal of Marine and Petroleum Geology, Vol. 28, Issue 2, Feb. 2011.
http://www.sciencedirect.com/science/article/pii/S0264817210000619

Inks, T., Lee, M., Agena, W., Taylor, D., Collett, T., Hunter, R., and Zyrianova, M., 2009, Seismic prospecting for gas hydrate and associated free-gas prospects in the Milne Point Area of Northern Alaska; in Collett, T., Johnson, A., Knapp, C., and Boswell, R., eds, Natural Gas Hydrates: Energy Resource and Associated Geologic Hazards; American Association of Petroleum Geologists Memoir 89.

Johnson, A., Patil, S., and Dandekar, A., 2011, Experimental Investigation of Gas-Water Relative Permeability for Gas Hydrate-Bearing Sediments from the Mount Elbert Gas Hydrate Stratigraphic Test Well, Alaska North Slope, *in* Scientific results of the Mount Elbert Gas Hydrate Stratigraphic Test Well, Alaska North Slope, Ed. by Boswell, R., Collett, T., Anderson, B., and Hunter, R., Journal of Marine and Petroleum Geology, Vol. 28, Issue 2, Feb. 2011.
http://www.sciencedirect.com/science/article/pii/S0264817209002025

Kneafsey, T., Lu, H., Winters, W.J., Boswell, R., Hunter, R.B., and Collett, T.S., 2011, Examination of core samples from the Mount Elbert gas hydrate stratigraphic test well, Alaska North Slope, effects of retrieval and preservation, *in* Scientific results of the Mount Elbert Gas Hydrate Stratigraphic Test Well, Alaska North Slope, Ed. by Boswell, R., Collett, T., Anderson, B., and Hunter, R., Journal of Marine and Petroleum Geology, Vol. 28, Issue 2, Feb. 2011. http://www.sciencedirect.com/science/article/pii/S0264817209001810

Kurihara, M., Junihiro, F., Hisanao, O., Masuda, Y., Yasuda, M., Yamamoto, K., Numasawa, M., Fuji, T., Nariat, H., Dallimore, S., and Wright, F., 2008, Analyses of the JOGMEC/NRCAN/Aurora Mallik Gas Hydrate Production Test Through Numerical Simulation: Proceedings of the 6th International Conference on Gas Hydrates (ICGH 2008), July 6-10, 2008, Vancouver, British Columbia, Canada, 13 p.

Kurihara, M., Funatsu, K., Ouchi, H., Masuda, Y., Yamamoto, K., Narita, H., Dallimore, S., Collett, T., and Hancock, S., 2008, Analyses of Production Tests and MDT Tests Conducted in Mallik and Alaska Methane Hydrate Reservoirs: What can We Learn from These Well Tests?, *in* Proceedings of the 6th International Conference on Gas Hydrates (ICGH 2008), Vancouver, British Columbia, Canada, July 6-10, 2008.

Kurihara, M., Sato, A., Funatsu, K., Ouchi, H., Masuda, Y., Narita, H., and Collett, T.S., 2011, Analysis of Formation Pressure Test Results in the Mount Elbert Methane Hydrate Reservoir through Numerical Simulation *in* Scientific results of the Mount Elbert Gas Hydrate Stratigraphic Test Well, Alaska North Slope, Ed. by Boswell, R., Collett, T., Anderson, B., and Hunter, R., Journal of Marine and Petroleum Geology, Vol. 28, Issue 2, Feb. 2011. http://www.sciencedirect.com/science/article/pii/S0264817210000097

Lee, M.W., Collett, T.S., and Agena, W.F., 2008, Assessing gas-hydrate prospects on the North Slope of Alaska – Theoretical considerations: U.S. Geological Survey, Scientific Investigations Report 2008 – 5175, 28pp.

Lee, M.W., Collett, T.S., and Inks, T.L., 2009, Seismic attribute analysis for gas-hydrate and free-gas prospects on the North Slope of Alaska, *in* Collett, T., Johnson, A., Knapp, C., Boswell, R., eds, Natural Gas Hydrates - Energy Resource Potential and Associated Geologic Hazards: American Association of Petroleum Geologists Memoir 89.

Lee, M.W., Agena, W.F., Collett, T.S., and Inks, T.L., 2011 (a), Pre- and post-drill comparison of the Mount Elbert gas hydrate prospect, Alaska North Slope *in* Scientific results of the Mount Elbert Gas Hydrate Stratigraphic Test Well, Alaska North Slope, Ed. by Boswell, R., Collett, T., Anderson, B., and Hunter, R., Journal of Marine and Petroleum Geology, Vol. 28, Issue 2, Feb. 2011. http://www.sciencedirect.com/science/article/pii/S0264817209001366

Lee, M.W. and Collett, T.S., 2011 (b), In-situ gas hydrate saturation estimated from various well logs at the Mount Elbert Gas Hydrate Stratigraphic Test Well, Alaska North Slope *in* Scientific results of the Mount Elbert Gas Hydrate Stratigraphic Test Well, Alaska North Slope, Ed. by

Boswell, R., Collett, T., Anderson, B., and Hunter, R., Journal of Marine and Petroleum Geology, Vol. 28, Issue 2, Feb. 2011.
http://www.sciencedirect.com/science/article/pii/S0264817209001081

Lorenson, T.D., Collett, T.S., and Hunter, R.B., 2011, Gas geochemistry of the Mount Elbert Gas Hydrate Stratigraphic Test Well, Alaska North Slope: Implications for gas hydrate exploration in the Arctic *in* Scientific results of the Mount Elbert Gas Hydrate Stratigraphic Test Well, Alaska North Slope, Ed. by Boswell, R., Collett, T., Anderson, B., and Hunter, R., Journal of Marine and Petroleum Geology, Vol. 28, Issue 2, Feb. 2011.
http://www.sciencedirect.com/science/article/pii/S0264817210000413

Lu, H., Lorenson, T.D., Moudrakovski, I.L., Ripmeester, J.A., Collett, T.S., Hunter, R.B., and Ratcliffe, C.I., 2011, The Characteristics of Gas Hydrates Recovered from the Mount Elbert Gas Hydrate Stratigraphic Test Well, Alaska North Slope *in* Scientific results of the Mount Elbert Gas Hydrate Stratigraphic Test Well, Alaska North Slope, Ed. by Boswell, R., Collett, T., Anderson, B., and Hunter, R., Journal of Marine and Petroleum Geology, Vol. 28, Issue 2, Feb. 2011. http://www.sciencedirect.com/science/article/pii/S0264817210000048

Moridis, G.J, Silpngarmlert, S., Reagan, M.T., Collett, T.S., and Zhang, K., 2011, Gas Production from a Cold, Stratigraphically Bounded Gas Hydrate Deposit at the Mount Elbert Gas Hydrate Stratigraphic Test Well, Alaska North Slope *in* Scientific results of the Mount Elbert Gas Hydrate Stratigraphic Test Well, Alaska North Slope, Ed. by Boswell, R., Collett, T., Anderson, B., and Hunter, R., Journal of Marine and Petroleum Geology, Vol. 28, Issue 2, Feb. 2011. http://www.sciencedirect.com/science/article/pii/S0264817210000073

Moridis, G.J., Collett, T.S., Boswell, R., Kurihara, M., Reagan, M.T., Sloan, E.D., and Koh, C., 2008, Toward production from gas hydrates: assessment of resources and technology and the role of numerical simulation: Proceedings of the 2008 SPE Unconventional Reservoirs Conference, Keystone, Colorado, February, 10–12, 2008, SPE 114163, 45 p.

Pooladi-Darvish, M. and Hong, H., 2011, Use of Formation Pressure Test Results over a Hydrate Interval for Long Term Production Forecasting at the Mount Elbert Gas Hydrate Stratigraphic Test Well, Alaska North Slope: Implications of Uncertainties *in* Scientific results of the Mount Elbert Gas Hydrate Stratigraphic Test Well, Alaska North Slope, Ed. by Boswell, R., Collett, T., Anderson, B., and Hunter, R., Journal of Marine and Petroleum Geology, Vol. 28, Issue 2, Feb. 2011. http://www.sciencedirect.com/science/article/pii/S0264817210000085

Rose, K., Boswell, R., and Collett, T.S., 2011, Mount Elbert gas hydrate stratigraphic test well, Alaska North Slope: coring operations, core sedimentology, and lithostratigraphy *in* Scientific results of the Mount Elbert Gas Hydrate Stratigraphic Test Well, Alaska North Slope, Ed. by Boswell, R., Collett, T., Anderson, B., and Hunter, R., Journal of Marine and Petroleum Geology, Vol. 28, Issue 2, Feb. 2011.
http://www.sciencedirect.com/science/article/pii/S0264817210000358

Sigal, R.F., Rai, C., Sondergeld, C., Spears, B., Ebanks, W.J., Zogg, W.D., Emery, N., McCardle, G., Schweizer, R., McLeod, W., and Van Eerde, J., 2009, Characterization of a

Sediment Core from Potential Gas Hydrate Bearing Reservoirs in the Sagavanirktok, Prince Creek, and Schrader Bluff Formations of Alaska's North Slope, Part 1. Project Summary and Geological Description of Core *in* American Association of Petroleum Geologists Memoir 89, Natural Gas Hydrates - Energy Resource Potential and Associated Geologic Hazards.

Stern, L.A., Lorenson, T.D., and Pinkston, J.C., 2011, Gas hydrate characterization and grain-scale imaging of recovered cores from the Mount Elbert gas hydrate stratigraphic test well, Alaska North Slope *in* Scientific results of the Mount Elbert Gas Hydrate Stratigraphic Test Well, Alaska North Slope, Ed. by Boswell, R., Collett, T., Anderson, B., and Hunter, R., Journal of Marine and Petroleum Geology, Vol. 28, Issue 2, Feb. 2011.
http://www.sciencedirect.com/science/article/pii/S0264817209001329

Sun, Y., Goldberg, D., Collett, T.S., and Hunter, R.B., 2011, High-resolution well-log derived dielectric properties of gas-hydrate-bearing sediments, Mount Elbert Gas Hydrate Stratigraphic Test Well, Alaska North Slope *in* Scientific results of the Mount Elbert Gas Hydrate Stratigraphic Test Well, Alaska North Slope, Ed. by Boswell, R., Collett, T., Anderson, B., and Hunter, R., Journal of Marine and Petroleum Geology, Vol. 28, Issue 2, Feb. 2011.
http://www.sciencedirect.com/science/article/pii/S0264817210000590

Torres, M.E., Collett, T.S., Rose, K., Sample, J.C., Agena, W.F., and Rosenbaum, E., 2011, Pore Fluid Geochemistry from the Mount Elbert Gas Hydrate Stratigraphic Test Well, Alaska North Slope *in* Scientific results of the Mount Elbert Gas Hydrate Stratigraphic Test Well, Alaska North Slope, Ed. by Boswell, R., Collett, T., Anderson, B., and Hunter, R., Journal of Marine and Petroleum Geology, Vol. 28, Issue 2, Feb. 2011.
http://www.sciencedirect.com/science/article/pii/S0264817209001731

White, M., Wurstner, S., and McGrail, P., 2011, Numerical studies of methane production from Class 1 gas hydrate accumulations enhanced with carbon dioxide injection *in* Scientific results of the Mount Elbert Gas Hydrate Stratigraphic Test Well, Alaska North Slope, Ed. by Boswell, R., Collett, T., Anderson, B., and Hunter, R., Journal of Marine and Petroleum Geology, Vol. 28, Issue 2, Feb. 2011. http://www.sciencedirect.com/science/article/pii/S026481720900107X

Wilson, S.J., Hunter, R.B., Collett, T.S., Hancock, S., Boswell, R., Anderson, B.J., 2011, Alaska North Slope Regional Gas Hydrate Production Modeling Forecasts *in* Scientific results of the Mount Elbert Gas Hydrate Stratigraphic Test Well, Alaska North Slope, Ed. by Boswell, R., Collett, T., Anderson, B., and Hunter, R., Journal of Marine and Petroleum Geology, Vol. 28, Issue 2, Feb. 2011. http://www.sciencedirect.com/science/article/pii/S0264817210000668

Winters, W.J., Walker, M., Kwon, O., Waite, B., Torres, M., Collett, T.S., and Rose, K., 2011, Physical Properties of Sediment from the Mount Elbert Gas Hydrate Stratigraphic Test Well, Alaska North Slope *in* Scientific results of the Mount Elbert Gas Hydrate Stratigraphic Test Well, Alaska North Slope, Ed. by Boswell, R., Collett, T., Anderson, B., and Hunter, R., Journal of Marine and Petroleum Geology, Vol. 28, Issue 2, Feb. 2011.
http://www.sciencedirect.com/science/article/pii/S0264817210000103

Yamamoto, K. and Dallimore, S., 2008, Aurora-JOGMEC-NRCan Mallik 2006-2008 Gas Hydrate Research Project progress, *in* DOE-NETL Fire In the Ice Methane Hydrate Newsletter, Summer 2008, p. 1-5.
http://www.netl.doe.gov/technologies/oil-gas/publications/Hydrates/Newsletter/HMNewsSummer08.pdf#Page=1

7.3 USGS Phase 1, Task 5 MPU Prospecting Study References, 2004

Bird, K.J. and Magoon, L.B., 1987, Petroleum geology of the northern part of the Arctic National Wildlife Refuge, Northeastern Alaska: U.S. Geological Survey Bulletin 1778, 324 p.

Carman, G.J. and Hardwick, P., 1983, Geology and regional setting of the Kuparuk oil field, Alaska: American Association of Petroleum Geologists Bulletin, v. 67, no. 6, p. 1014-1031.

Collett, T.S., 1993, Natural gas hydrates of the Prudhoe Bay and Kuparuk River Area, North Slope, Alaska: American Association of Petroleum Geologists Bulletin, v. 77, no. 5, p. 793-812.

Collett, T.S., 2001, Natural-gas hydrates: Resource of the twenty-first century?, in Downey, M.W., Threet, J.C., and Morgan, W.A., eds, Petroleum provinces of the twenty-first century: American Association of Petroleum Geologists Memoir 74, p. 85-108.

Collett, T.S, Lee, M.W., Dallimore, S.R., and Agena, W.F., 1999, Seismic and well-log-inferred gas hydrate accumulations on Richards Island, *in* Dallimore, S.R., Uchida, T., and Collett, T.S., eds., Scientific results from JAPEX/JNOC/GSC Mallik 2L-38 gas hydrate research well, Mackenzie Delta, Northwest Territories, Canada: Geological Survey of Canada Bulletin 544, p. 357-376.

Collett, T.S., Subsurface temperatures and geothermal gradients on the North Slope of Alaska, *in* Cold Regions Science and Technologies, 21 (1993) Elsevier Science Publishers B.V., Amsterdam, p. 275-293.

Dillon, W.P., Lee, M.W., Fehlhaber, K., and Coleman, D.F., 1993, Gas hydrates on the Atlantic continental margin of the United States – Controls on concentration, *in* Howell, D.G., ed., The future of energy gases: U.S. Geological Survey Professional Paper 1570, p. 313-330.

Grantz, A.M., Holmes, M.L., and Kososki, B.A., 1975, Geologic framework of the Alaskan continental terrace in the Chukchi and Beaufort Seas, *in* Yorath, C.J., Parker, E.R., and Glass, D.J., eds., Canada's continental margins and offshore petroleum exploration: Canadian Society of Petroleum Geologists Memoir 4, p. 669-700.

Gray, W.C., 1979, Variable norm deconvolution: Stanford, California. Stanford University, Ph.D. thesis, 101 p.

Gryc, G., 1988, Geology and exploration of the National Petroleum Reserve in Alaska, 1974 to 1982: U.S. Geological Survey Professional Paper 1399, 940 p.

Jones, H.P. and Speers, R.G., 1976, Permo-Triassic reservoirs of Prudhoe Bay field, North Slope, Alaska, *in* J. Braunstein, ed., North American oil and gas fields: American Association of Petroleum Geologists Memoir 24, p. 23-50.

Kvenvolden, K.A., 1993, Gas hydrates as a potential energy resource – A review of their methane content, in Howell, D.G., ed., The Future of energy gases: U.S. Geological Survey Professional Paper 1570, p. 555-561.

Lee, M.W., Hutchinson, D.R., Dillon, W.P., Miller, J.J., Agena, W.F., and Swift, B.A., 1993, Method of estimating the amount of in situ gas hydrates in deep marine sediments: Marine and Petroleum Geology, v. 10, p. 493-506.

Morgridge, D.L. and Smith, W.B., 1972, Geology and discovery of Prudhoe Bay field, eastern Arctic Slope, Alaska, *in* King, R.E., ed., Stratigraphic oil and gas fields-classification, exploration methods, and case histories: American Association of Petroleum Geologists Memoir 16, p. 489-501.

Seifert, W.K., Moldowan, J.M., and Jones, J.W., 1979, Application of biological marker chemistry to petroleum exploration: Tenth World Petroleum Congress, p. 425-440.

Sloan, E.D., 1998, Clathrate hydrates of natural gases (2nd ed.): New York, Marcel Dekker Inc., 705 p.

Taylor, D.J., et al., 2003, Imaging Gas-Hydrate Bearing Zones Using 3-D Seismic Data- Milne Point, North Slope, Alaska: abstract 2003 3-D Symposium, Denver, Colorado.

Tailleur, I.L. and Weimer, P., eds., 1987, Alaskan North Slope geology: Bakersfield, California, Pacific Section, Society of Economic Paleontologists and Mineralogists and the Alaska Geological Society, Book 50, v. 1, 874 p.

7.4 University of Arizona Research Publications and Presentations

7.4.1 Project-Sponsored Thesis

Geauner, S., 2009, Fault analysis, seismic facies modeling and volumetric reassessment of gas hydrates in the Milne Point Unit, North Slope, Alaska: Master of Science thesis, University of Arizona, Tucson.

Hagbo, C.L., 2003, Characterization of Gas Hydrate Occurrences using 3D Seismic Data and Seismic Attributes, Milne Point, North Slope, Alaska, M.S. Thesis, Dept. of Geosciences, University of Arizona, Tucson, 127 pp.

Hennes, A.M., 2004, Structural Constraints on Gas Hydrate Formation and Distribution in the Milne Point, North Slope of Alaska, Prepublication Manuscript submitted in partial fulfillment for M.S. Thesis, Dept. of Geosciences, University of Arizona, Tucson, 40 pp., 19 figs., 3 tables.

Manuel, J., 2008, A chronostratigraphic framework of the Sagavanirktok Formation, North Slope Alaska: Incorporating facies characterization, reservoir continuity and dimensions in relation to

gas hydrate and associated free-gas resources, M.G.Eng., M.S. Thesis, Department of Mining and Geologic Engineering, University of Arizona.

Zhao, B., 2003, Classifying Seismic Attributes in the Milne Point Unit, North Slope of Alaska, M.S. Thesis, Department of Mining and Geological Engineering, University of Arizona, Tucson, 159 pp.

7.4.2 Professional Presentations

Casavant, R.R., Hennes, A.M., Johnson, R.A, and Collett, T.S., 2004, Structural analysis of a proposed pull-apart basin: Implications for gas hydrate and associated free-gas emplacement, Milne Point Unit, Arctic Alaska, AAPG Hedberg Conference, Gas Hydrates: Energy Resource Potential and Associated Geologic Hazards, September 12-16, 2004, Vancouver, Canada, 5 pp.

Hagbo, C. and Johnson, R.A., 2003, Delineation of gas hydrates, North Slope, Alaska, 2003 University of Arizona Dept. Geosciences Annual GeoDaze Symposium.

Hagbo, C. and Johnson, R. A., 2003, Use of seismic attributes in identifying and interpreting onshore gas hydrate occurrences, North Slope, Alaska, Eos Trans. AGU, 84, Fall Meeting.

Hennes, A. and Johnson, R.A., 2004, Structural character and constraints on a shallow, gas hydrate-bearing reservoir as determined from 3-D seismic data, North Slope, Alaska, 2004 University of Arizona Dept. Geosciences Annual GeoDaze Symposium.

7.4.3 Professional Posters

Gandler, G.L., Casavant, R.R., Johnson, R.A., Glass, C.E., and Collett, T.S., 2004, Preliminary Spatial Analysis of Faulting and Gas Hydrate-Free Gas Occurrence, Milne Point Unit, Arctic Alaska, AAPG Hedberg Conference, Gas Hydrates: Energy Resource Potential and Associated Geologic Hazards, September 12-16, 2004, Vancouver, BC, Canada, 3 pp.

Geauner, J.M., Manuel, J., and Casavant, R.R., 2003, Preliminary Subsurface Characterization and Modeling of Gas Hydrate Resources, North Slope, Alaska, *in*: Student Abstract Volume, 2003 AAPG-SEG Student Expo, Houston, Texas.

Geauner, S., Manuel, J., and Casavant, R.R., 2004, Well Log Normalization and Comparative Volumetric Analysis of Gas Hydrate and Free-Gas Resources, Central North Slope, Alaska, AAPG Hedberg Conference, Gas Hydrates: Energy Resource Potential and Associated Geologic Hazards, September 12-16, 2004, Vancouver, BC, Canada, 4 pp.

Hennes, A.M., Johnson, R.A., and Casavant, R.R., 2004, Seismic Characterization of a Shallow Gas Hydrate-Bearing Reservoir on the North Slope of Alaska, AAPG Hedberg Conference, Gas Hydrates: Energy Resource Potential and Associated Geologic Hazards, September 12-16, 2004, Vancouver, BC, Canada, 4 pp.

Hennes, A. and Johnson, R.A., 2004, Pushing the envelope of seismic data resolution: Characterizing a shallow gas hydrate reservoir on the North Slope of Alaska, 2004 University of Arizona Dept. Geosciences Annual GeoDaze Symposium.

Poulton, M.M., Casavant, R.R., Glass, C.E., and Zhao, B., 2004, Model Testing of Methane Hydrate Formation on the North Slope of Alaska with Artificial Neural Networks, AAPG Hedberg Conference, Gas Hydrates: Energy Resource Potential and Associated Geologic Hazards, September 12-16, 2004, Vancouver, BC, Canada, 2 pp.

7.4.4 Professional Publications

Casavant, R.R., 2002, Tectonic geomorphic characterization of a transcurrent fault zone, Western Brooks Range, Alaska (linkage of shallow hydrocarbons with basement deformation), SPE-AAPG: Western Region-Pacific Section Joint Technical Conference Proceedings, Anchorage, Alaska, May 18-23, 2002, p. 68.

Gandler, G.L., Casavant, R.R., Johnson, R.A., Glass, C.E., and Collett, T.S., 2004, Preliminary Spatial Analysis of Faulting and Gas Hydrate-Free Gas Occurrence, Milne Point Unit, Arctic Alaska, AAPG Hedberg Conference, Gas Hydrates: Energy Resource Potential and Associated Geologic Hazards, September 12-16, 2004, Vancouver, BC, Canada, 3 pp.

Geauner, J.M., Manuel, J., and Casavant, R.R., 2003, Preliminary Subsurface Characterization and Modeling of Gas Hydrate Resources, North Slope, Alaska; in: Student Abstract Volume, 2003 AAPG-SEG Student Expo, Houston, Texas.

Geauner, S., Manuel, J., and Casavant, R.R., 2004, Well Log Normalization and Comparative Volumetric Analysis of Gas Hydrate and Free-Gas Resources, Central North Slope, Alaska, AAPG Hedberg Conference, Gas Hydrates: Energy Resource Potential and Associated Geologic Hazards, September 12-16, 2004, Vancouver, BC, Canada, 4 pp.

Hagbo, C. and Johnson, R.A., 2003, Delineation of gas hydrates, North Slope, Alaska, 2003 University of Arizona Dept. Geosciences Annual GeoDaze Symposium.

Hagbo, C. and Johnson, R.A., 2003, Use Of Seismic Attributes In Identifying And Interpreting Onshore Gas Hydrate Occurrences, North Slope, Alaska, EOS Trans. AGU, 84, Fall Meeting, Suppl., Abstract OS42B-06.

Hennes, A.M. and Johnson, R.A., 2004, Structural character and constraints on a shallow, gas hydrate-bearing reservoir as determined from 3-D seismic data, North Slope, Alaska, 2004 University of Arizona Dept. Geosciences Annual GeoDaze Symposium.

Hennes, A.M. and Johnson, R.A., 2004, Pushing the envelope of seismic data resolution: Characterizing a shallow gas hydrate reservoir on the North Slope of Alaska, 2004 University of Arizona Dept. Geosciences Annual GeoDaze Symposium.

Hennes, A.M., Johnson, R.A., and Casavant, R.R., 2004, Seismic Characterization of a Shallow Gas Hydrate-Bearing Reservoir on the North Slope of Alaska, AAPG Hedberg Conference, Gas Hydrates: Energy Resource Potential and Associated Geologic Hazards, September 12-16, 2004, Vancouver, BC, Canada, 4 pp.

Johnson, R.A., 2003, Shallow Natural-Gas Hydrates Beneath Permafrost: A Geophysical Challenge To Understand An Unconventional Energy Resource, News From Geosciences, University of Arizona, Department Of Geosciences Newsletter, V. 8, No. 2, p. 4-6.

Poulton, M.M., Casavant, R.R., Glass, C.E., and Zhao, B., 2004, Model Testing of Methane Hydrate Formation on the North Slope of Alaska with Artificial Neural Networks, AAPG Hedberg Conference, Gas Hydrates: Energy Resource Potential and Associated Geologic Hazards, September 12-16, 2004, Vancouver, BC, Canada, 2 pp.

7.4.5 Artificial Neural Network References

Bishop, C., 1995, Neural Networks for Pattern Recognition: Oxford Press.

Broomhead, D. and Lowe, D., 1988, Multivariable functional interpolation and adaptive networks: Complex Systems, 2, 321-355.

Casavant, R.R., 2001, Morphotectonic Investigation of the Arctic Alaska Terrane: Implications to Basement Architecture, Basin Evolution, Neotectonics and Natural Resource Management: Ph.D thesis, University of Arizona, 457 p.

Casavant, R.R., Hennes, A., Johnson, R.A., and Collett, T.S., 2004, Structural analysis of a proposed pull-apart basin: Implications for gas hydrate and associated free-gas emplacement, Milne Point Unit, Arctic Alaska: AAPG Hedberg Conference, Gas Hydrates: Energy Resource Potential and Associated Geologic Hazards, September 12-16, 2004, Vancouver, BC, Canada.

Collett, T., Bird, K., Kvenvolden, K., and Magoon, L., 1988, Geologic interrelations relative to gas hydrates within the North Slope of Alaska: USGS Open File Report, 88-389.

Darken, C. and Moody, J., 1990, Fast adaptive K-means clustering: Some empirical results: IEEE INNS International Joint Conference on Neural Networks, 233-238.

Gandler, G., Casavant, R., Glass, C., Hennes, A., Hagbo, C., and Johnson, R., 2004, Preliminary Spatial Analysis of Faulting and Gas Hydrate Occurrence Milne Point Unit, Arctic Alaska: AAPG Hedberg Conference, Gas Hydrates: Energy Resource Potential and Associated Geologic Hazards, September 12-16, 2004, Vancouver, BC, Canada.

Geauner, S., Manuel, J., Casavant, R., Glass, C., and Mallon, K., 2004,Well Log Normalization and Comparative Volumetric Analyses of Gas Hydrate and Free-gas Resources, Central North Slope, Alaska: AAPG Hedberg Conference, Gas Hydrates: Energy Resource Potential and Associated Geologic Hazards, September 12-16, 2004, Vancouver, BC, Canada.

Girosi, F. and Poggio, T., 1990, Networks and the best approximation property: Biological Cybernetics, 63, 169-176.

Glass, C.E., 2003, Estimating pore fluid concentrations using acoustic and electrical log attributes, Interim Report, UA Gas Hydrate Project.

Hashin, Z. and Shtrikman, S., 1963, A variational approach to the theory of the elastic behavior of multiphase materials, Journal of the Mechanics and Physics of Solids, Vol. 11, p. 127-140.

Haykin, S., 1994, Neural Networks, A Comprehensive Foundation: Macmillan.

Light, W., 1992, Some aspects of radial basis function approximation, in Singh, S., Ed., Approximation Theory, Spline Functions and Applications: NATO ASI series, 256, Kluwer Academic Publishers, 163-190.

Mavco, G., Mukerji, T., and Dvorkin, J., 1988, The rock physics handbook, Cambridge University Press.

Moody, J. and Darken, C., 1989, Fast learning in networks of locally-tuned processing units: Neural Computation, 1, 281-294.

Musavi, M., Ahmed, W., Chan, K., Faris, K., and Hummels, D., 1992, On the training of radial basis function classifiers: Neural Networks, 5, 595-603.

Poggio, T. and Girosi, F., 1989, A theory of networks for approximation and learning: A.I. Memo No. 1140 (C.B.I.P . Paper No. 31), Massachusetts Institute of Technology, Artificial Intelligence Laboratory.

Poulton, M., 2002, Neural networks as an intelligence amplification tool: A review of applications: Geophysics, vol. 67, no. 3, pp. 979-993.

Poulton, M., (Ed.), 2001, Computational Neural Networks for Geophysical Data Processing: Pergamon, Amsterdam, 335p.

Powell, M., 1987, Radial basis functions for multivariable interpolation: A review, in Mason, J. and Cox, M., Eds., Algorithms for Approximation: Clarendon Press.

Zell, A., 1994, Simulation Neuronaler Netze: AddisonWesley.

7.4.6 University of Arizona Final Report References

Abu-Hamdeh, N.H. and Reeder, R.C., 2000, Soil thermal conductivity - effects of density, moisture, salt concentration, and organic matter: Soil Science Society of America Journal, v. 64, p. 1285-1290.

Alaska Oil and Gas Conservation Commission, 1981, Mud Log Baroid Logging Systems, Sohio Alaska West Sak No. 16 and West Sak No. 17, Anchorage, AK.

Archie, G.E., 1942, The electrical resistivity log as an aid in determining some reservoir characteristics: Journal of Petroleum Technology, v. 5, p. 1-8.

Bishop, C., 1995, Neural Networks for Pattern Recognition: Oxford Press.

Bird, K.J., 1985, The framework geology of the North Slope of Alaska as related to oil-source rock correlations, in Magoon, L.B. and Claypool, G.E., eds., Alaska North Slope oil-rock correlation study; analysis of North Slope Crude: AAPG Studies in Geology, v. 20, p. 3-29.

Bird, K.J. and Magoon, L.B., 1987, Petroleum geology of the northern part of the Arctic National Wildlife Refuge, northeastern Alaska Bulletin, Washington, D.C., U.S. Geological Survey.

Bond, L.O., Alger, R.P., and Schmidt, A.W., 1972, Well log applications in coal mining and rock mechanics: Transactions of the American Institute of Mining, Metallurgical and Petroleum Engineers, v. 250, p. 355-362.

Bouvier, J.D., Kaars-Sijpesteijn, C.H., Kluesner, D.F., Onyejekwe, C.C., and Van Der Pal, R.C., 1989, Three-Dimensional Seismic Interpretation and Fault Sealing Investigations, Nun River Field, Nigeria: AAPG Bulletin, v. 73, n. 11, p. 1397-1414.

Broomhead, D. and Lowe, D., 1988, Multivariable functional interpolation and adaptive networks: Complex Systems, 2, 321-355.

Carman, G.J. and Hardwick, P., 1983, Geology and Regional Setting of Kuparuk Oil Field, Alaska, AAPG Bulletin, v. 67, n. 6, p. 1014-1031.

Casavant, R.R., 2001, Morphotectonic Investigation of the Arctic Alaska Terrane: Implications to Basement Architecture, Basin Evolution, Neotectonics and Natural Resource Management: Ph.D. thesis, University of Arizona, 457 p.

Casavant, R.R., 2004, Reservoir-Fluid Characterization and Reservoir Modeling of Potential Gas Hydrate Resources, Alaska North Slope, Calgary, AB, Canada, Canadian Society of Petroleum Geologists Technical Conference, June 1, 2004.

Casavant, R.R. and Gross, E., 2002, Basement Fault Blocks and Subthrust Basins? A Morphotectonic Investigation in the Central Foothills and Brooks Range, Alaska: Western Region-Pacific Section Conference, Anchorage, Alaska, May 18-23, 2002.

Casavant, R.R., Hennes, A.M., Johnson, R.A., and Collett, T.S., 2004, Structural analysis of a proposed pull-apart basin: Implications for gas hydrate and associated free-gas emplacement, Milne Point Unit, Arctic Alaska, AAPG Hedberg Conference, Gas Hydrates: Energy Resource Potential and Associated Geologic Hazards, September 12-16, 2004, Vancouver, BC, Canada, 5 pp.

Casavant, R.R. and Miller, S.R., 2002, Tectonic geomorphic characterization of a transcurrent fault zone, Western Brooks Range, Alaska (linkage of shallow hydrocarbons with basement deformation), SPE-AAPG: Western Region-Pacific Section Joint Technical Conference Proceedings, Anchorage, Alaska, May 18-23, 2002, p. 68.

Casavant, R.R. and Mallon, K.M., 1999, Facies and reservoir characterization of the Morrow Sandstones (Lower Pennsylvanian), White City Penn Gas Pool, Eddy County, southeastern New Mexico. Symposium of the Oil and Gas fields of southeastern New Mexico, 1999 Supplement "Pennsylvanian Gas Field", Roswell, NM, Roswell Geological Society.

Casavant, R.R. and Miller, S.R., 1999, Is the Western Brooks Range on the move?, Abstracts with Program, Geological Society of America, 1999 Annual meeting, Denver, CO, v. 31, n. 7, p. 474.

Collett, T.S., 1983, Detection and evaluation of natural gas hydrates from well logs, Prudhoe Bay, Alaska, Masters thesis, University of Alaska, Fairbanks, 77 p.

Collett, T.S., 1993, Natural Gas Hydrates of the Prudhoe Bay and Kuparuk River Area, North Slope, Alaska, AAPG Bulletin, v. 77, n. 5, p. 793-812.

Collett, T.S., 1997, Gas hydrate resources of northern Alaska, Bulletin of Canadian Petroleum Geology, v. 45, p. 317-338.

Collett, T.S., 1998, Gas hydrates of northern Alaska – a potential energy resource or just a nuisance?, Alaska Geology, v. 28, p. 1-5.

Collett, T.S. and Kvenvolden, K.A., 1987, Evidence of naturally occurring gas hydrates on the North Slope of Alaska, U.S. Geological Survey Open-File Report, v. 87-255, p. 8 pp.

Collett, T.S., Bird, K.J., Kvenvolden, K.A., and Magoon, L.B., 1988, Geologic interrelations relative to gas hydrates within the North Slope of Alaska, U.S. Geological Survey Open-File Report, v. 88-389, p. 150 p.

Collett, T.S., Bird, K.J., and Magoon, L.B., 1993, Subsurface temperatures and geothermal gradients on the North Slope of Alaska: Cold Regions Science and Technology, v. 21, p. 275-293.

Collett, T.S., Lewis, R.E., Dallimore, S.R., Lee, M.W., Mroz, T.H., and Uchida, T., 1999, Detailed evaluation of gas hydrate reservoir properties using JAPEX/JNOC/GSC Mallik 2L-38 gas hydrate research well downhole well-log displays: Scientific Results from JAPEX/JNOC/GSC Mallik 2L-38 Gas Hydrate Research Well, Mackenzie Delta, Northwest Territories, Canada, p. 295-311.

Dallimore, S.R., 1992, Borehole logs from joint GSC-industry Mackenzie Delta geology-permafrost transect, Geological Survey of Canada Open File Report, p. 3 Sheets.

Dallimore, S.R. and Collett, T.S., 1995, Intrapermafrost gas hydrates from a deep core hole in the Mackenzie Delta, Northwest Territories, Canada: Geology, v. 23, n. 6, p. 527-530.

Dallimore, S.R., Uchida, T., and Collett, T.S., 1999, Scientific results from JAPEX/JNOC/GSC Mallik 2L-38 Gas Hydrate Research Well, Mackenzie Delta, Northwest Territories, Canada, v. 544, Geological Survey of Canada Bulletin, 403 pp.

Darken, C. and Moody, J., 1990, Fast adaptive K-means clustering: Some empirical results: IEEE INNS International Joint Conference on Neural Networks, p. 233-238.

Davidson, D.W., El-Defrawy, M.K., Fuglem, M., and Judge, A., 1978, Natural gas hydrates in northern Canada, Proceedings of the 3rd International Conference on Permafrost, National Research Council of Canada.

Deming, D., Sass, J.H., Lachenbruch, A.H., and De Rito, R.F., 1992, Heat flow and subsurface temperature as evidence for basin-scale ground-water flow, North Slope of Alaska, Geological Society of America Bulletin, v. 104, p. 528-542.

Dennis, J., Gay, D., and Welsch, R., 1981, An adaptive nonlinear least-squares algorithm: ACM Transactions on Mathematical Software, 7, 3, 348-368.

Doughty, P., 2003, Clay smear seals and fault sealing potential of an exhumed growth fault, Rio Grande Rift, New Mexico: AAPG Bulletin, 87(3), p. 427-444.

Dooley, T. and McClay, K., 1997, Analog modeling of pull-apart basins: American Association of Petroleum Geologists, v. 81, n. 11, p. 1804-1826.

Galate, J.W. and Goodman, M.A., 1982, Review and evaluation of evidence of in-situ gas hydrates in the National Petroleum Reserve in Alaska, U.S. Geological Survey unpublished report, Contract No. 14-08-000119148, p. 102.

Gandler, G.L., Casavant, R.R., Johnson, R.A., Glass, C.E., and Collett, T.S., 2004, Preliminary Spatial Analysis of Faulting and Gas Hydrates-Free Gas Occurrence, Milne Point Unit, Arctic Alaska, AAPG Hedberg Conference, Gas Hydrates: Energy Resource Potential and Associated Geologic Hazards, September 12-16, 2004, Vancouver, BC, Canada, 3 pp.

Geauner, S., Manuel, J., and Casavant, R.R., 2003, Preliminary subsurface characterization and modeling of gas hydrate resources, North Slope, Alaska, , in: 2003 AAPG-SEG Student Expo Student Abstract Volume, Houston, Texas.

Geauner, S., Manuel, J., Casavant, R.R., Glass, C.E., and Mallon, K., 2004, Well Log Normalization and Comparative Volumetric Analyses of Gas Hydrate and Free-gas Resources, Central North Slope, Alaska: AAPG Hedberg Conference, Gas Hydrates: Energy Resource Potential and Associated Geologic Hazards, September 12-16, 2004, Vancouver, Canada, 4 pp.

Geauner, S., 2009, Fault analysis, seismic facies modeling and volumetric reassessment of gas hydrates in the Milne Point Unit, North Slope, Alaska, Master of Science thesis, University of Arizona, Tucson.

Geman, S., Bienenstock, E., and Doursat, R., 1992, Neural networks and the bias/variance dilemma: Neural Computation, 4, 1-58.

Girosi, F. and Poggio, T., 1990, Networks and the best approximation property: Biological Cybernetics, 63, 169-176.

Glass, C.E., 2003, Estimating pore fluid concentrations using acoustic and electrical log attributes, Interim Report, University of Arizona, Gas Hydrate Project.

Glass, C.E. and Casavant, R.R., *(2007)*, Using thermal conductivity modeling and wireline petrophysical logs to identify intrapermafrost gas hydrate: *draft manuscript* submitted to Journal of Geophysical Research.

Glass, C.E. and Casavant, R.R., *(2009)*, Estimating permafrost thinning on the central North Slope of Alaska using well bore temperature and petrophysical wireline logs: *draft manuscript.*

Glass, C.E. and Casavant, R.R., *(2009)*, Expert system for estimating gas hydrate concentrations using petrophysical wireline logs on the central Alaskan North Slope: *draft manuscript.*

Glass, C.E. and Casavant, R.R., *(2009)*, Estimating the base of the permafrost and base of the hydrate stability field using simulated well bore temperature logs: *draft manuscript.*

Grantz, A., Eittreim, S., and Dinter, D.A., 1979, Geology and Tectonic Development of the Continental Margin of North Alaska, Tectonophysics, v.59, p. 263-291.

Grantz, A., May, S.D., and Dinter, D.A., 1988, Geologic framework, petroleum potential, and environmental geology of the United States Beaufort and northeasternmost Chukchi Seas, in Gyrc, G., ed., Geology and Exploration of the National Petroleum Reserve in Alaska, 1974 to 1982, Washington, D.C., U.S. Geological Survey Professional Paper, p. 231-256.

Grantz, A., May, S., and Hart, P., 1994, Geology of the Arctic continental margin of Alaska, in Plafker, G. and Berg, H.C. eds., The Geology of Alaska, Boulder, Colorado, Geological Society of America, The Geology of North America, v. G-1, p. 17-48.

Grollimund, B. and Zoback, M.D., 2003, Impact of glacially induced stress changes on fault-seal integrity offshore Norway, AAPG Bulletin, v. 87, n. 3, p. 493-506.

Gryc, G., Ed., 1988, Geology and Exploration of the National Petroleum Reserve in Alaska, 1974 to 1982, Washington D.C., U.S. Geological Survey Professional Paper.

Hagbo, C.L., 2003, Characterization of Gas Hydrate Occurrences using 3D Seismic Data and Seismic Attributes, Milne Point, North Slope, Alaska, M.S. Thesis, Department of Geosciences, University of Arizona, Tucson, 127 pp.

Hagbo, C. and Johnson, R.A., 2003, Use of Seismic Attributes in Identifying and Interpreting Onshore Gas Hydrate Occurrences, North Slope, Alaska (abs.), Eos Transaction American Geophysical Union 84 (46), Fall Meeting Suppl., Abstract OS42B-06, 2003.

Hagbo, C. and Johnson, R.A., 2003, Delineation of gas hydrates, North Slope, Alaska, 2003 University of Arizona Department of Geosciences Annual GeoDaze Symposium presentation.

Hashin, Z. and Shtrikman, S., 1963, A variational approach to the theory of the elastic behavior of multiphase materials, Journal of the Mechanics and Physics of Solids, v. 11, p. 127-140.

Haykin, S., 1994, Neural Networks, A Comprehensive Foundation: Macmillan.

Hennes, A.M., 2004, Structural Constraints on Gas Hydrate Formation and Distribution in the Milne Point, North Slope of Alaska, Prepublication Manuscript submitted in partial fulfillment for M.S. Thesis, Dept. of Geosciences, University of Arizona, Tucson, 40 pp., 19 figs., 3 tables.

Hennes, A.M. and Johnson, R.A., 2004, Pushing the envelope of seismic data resolution: Characterizing a shallow gas hydrate reservoir on the North Slope of Alaska, 2004 University of Arizona Department of Geosciences Annual GeoDaze Symposium.

Hennes, A.M. and Johnson, R.A., 2004, Structural character and constraints on a shallow, gas hydrate-bearing reservoir as determined from 3-D seismic data, North Slope, Alaska, University of Arizona Department of Geosciences Annual GeoDaze Symposium presentation.

Hennes, A.M., Johnson, R.A., and Casavant, R.R., 2004, Seismic Characterization of a Shallow Gas Hydrate-Bearing Reservoir on the North Slope of Alaska, AAPG Hedberg Conference, Gas Hydrates: Energy Resource Potential and Associated Geologic Hazards, September 12-16, 2004, Vancouver, BC, Canada, 4 pp.

Hertz, J., Krogh, A., and Palmer, R.G., 1991, Introduction to the Theory of Neural Computation: Addison Wesley.

Holder, G.D., Malone, R.D., and Lawson, W.F., 1987, Effects of gas composition and geothermal properties on the thickness and depth of natural gas hydrate zone, Journal of Petroleum Technology 39(9), p.1147-1152.

Hubbard, R.J., Edrich, S.P., and Rattey, R.P., 1987, Geologic evolution and hydrocarbon habitat of the Arctic Alaska microplate, *in* Tailleur, I. and Weimer, P. eds., Alaskan North Slope Geology, Bakersfield, CA, Society of Economic Paleontologists and Mineralogists, Pacific Section, and Alaska Geological Society, p.797-830.

Hunter, R.B., Pelka, G.J., Digert, S.A., Casavant, R.R., Johnson, R.A., Poulton, M.M, Glass, C.E., Mallon, K., Patil, S.L., Chukwu, G.A., Dandekar, A.Y., Khataniar, S., Ogbe, D.O., and Collett, T.S., 2002, Resource Characterization and Quantification of Natural Gas Hydrate and Associated Free-Gas Accumulations in the Prudhoe Bay-Kuparuk River Area on the North Slope

of Alaska, presented at the Methane Hydrate Inter-Agency Conference of US Department of Energy, Washington DC, March 21-23, 2002.

Hunter, R.B., Pelka, G.J., Digert, S.A., Casavant, R.R., Johnson, R.A., Poulton, M.M., Glass, C.E., Mallon, K., Patil, S.L., Chukwu, G.A., Dandekar, A.Y., Khataniar, S., Ogbe, D.O., and Collett, T.S., 2002, Resource Characterization and Quantification of Natural Gas Hydrate and Associated Free-Gas Accumulations in the Prudhoe Bay-Kuparuk River Area on the North Slope of Alaska, at the SPE-AAPG: Western Region-Pacific Section Conference, Anchorage, Alaska, May 18-23, 2002, p. 81-82.

Hunter, R.B., Digert, S.A., Casavant, R.R., Johnson, R.A., Poulton, M.M., Glass, C.E., Mallon, K., Patil, S.L., Dandekar, A.Y., and Collett, T.S., 2003, Resource Characterization and Quantification of Natural Gas Hydrate and Associated Free-Gas Accumulations in the Prudhoe Bay-Kuparuk River Area, North Slope of Alaska, Poster Session at the AAPG Annual Meeting, Salt Lake City, Utah, May 11-14, 2003. Poster received EMD President's Certificate for Excellence in Presentation.

Hunter, R.B., Casavant, R.R., Johnson, R.A., Poulton, M.M., Moridis, G.J., Wilson, S.J., Geauner, S., Manuel, J., Hagbo, C., Glass, C.E., Mallon, K.M., Patil, S.L., Dandekar, A., and Collett, T.S., 2004, Reservoir-fluid characterization and reservoir modeling of potential gas hydrate resource, Alaska North Slope, 2004 AAPG Annual Convention Abstracts with Program.

Hunter, R.B., Collett, T.S., Patil, S.L., Casavant, R.R., and Mroz, T.H., 2004, Characterization, Appraisal and Economic Viability of Alaska North Slope Gas Hydrate Accumulations, Vancouver, BC, Canada, American Association of Petroleum Geologists Hedberg Research Conference, September 12-16.

Hunter, R.B., Collett, T.S., Wilson, S.J., Inks, T., Casavant, R.R., Johnson, R.A., Poulton, M.M., Mallon, K., Patil, S.L., and Dandekar, A., 2005, Gas Hydrate Prospect Development and Production Modeling, Alaska North Slope, Calgary, AB, Canada, American Association of Petroleum Geologists Annual Meeting, June 19-22.

Hyndman, R.D. and Spence, G.D., 1992, A Seismic Study of Methane Hydrate Marine Bottom Simulating Reflectors: Journal of Geophysical Research, v. 97, n. B5, p. 6683-6698.

Johnson, R.A., 2003, Shallow Natural-Gas Hydrates Beneath Permafrost: A Geophysical Challenge To Understand An Unconventional Energy Resource, News From Geosciences, Department Of Geosciences Newsletter, V. 8, No. 2, p. 4-6.

Jones, H. P. and Speers, R.G., 1976, Permo-Triassic reservoirs of Prudhoe Bay Field, North Slope, Alaska, Memoir - AAPG(24): 23-50.

Khairkhah, D., Pooladi-Darvish, M., Bishnoi, P.R., Collett, T.S., and Dallimore, S.R., 1999, Production potential of the Mallik field reservoir in Dallimore, S.R., Uchida, T. and Collett, T.S. eds., Scientific Results from JAPEX/JNOC/GSC Mallik 2L-38 Gas Hydrate Research Well,

Mackenzie River Delta, Northwest Territories, Canada, Geological Survey of Canada Bulletin 544, p. 377-390.

Knipe, R.J., 1997, Juxtaposition and Seal Diagrams to Help Analyze Fault Seals in Hydrocarbon Reservoirs: American Association of Petroleum Geologists Bulletin, v. 81, n. 2, p. 187-195.

Koleodye, B.A., Aydin, A., and May, E., 2003, A new process-based methodology for analysis of shale smear along normal faults in the Niger Delta, AAPG Bulletin, v. 87, n. 3, p. 445-463.

Krantz, R.W., 1995, The transpressional strain model applied to strike-slip, oblique-convergent and oblique-divergent deformation, Journal of Structural Geology, v. 17, n. 8, p. 1125-1137.

Kvenvolden, K.A., 1993, A Primer on Gas Hydrates in Howell, D.G. ed., The Future of Energy Gases, U.S. Geological Survey Professional Paper 1570, p. 279-291.

Kvenvolden, K.A. and McMenamin, M.A., 1980, Hydrates of natural gas - a review of their geologic occurrence, U.S. Geological Survey Circular, v. 825, p. 11p.

Lachenbruch, A.H., Galanis, P.S., and Moses, T.H., 1987, A Thermal Cross Section for the Permafrost and Hydrate Stability Zones in the Kuparuk and Prudhoe Bay Oil Fields, in Galloway, J.P. and Hamilton, T.D., eds., Geologic Studies in Alaska by the U.S. Geological Survey during 1987, USGS Geological Survey Circular 1016, p. 48-51.

Lachenbruch, A.H., Sass, J.H., Marshall, B.V., and Moses, T.H., 1982, Permafrost heat flow, and the geothermal regime at Prudhoe Bay, Alaska, Journal of Geophysical Research, v. 87, p. 9310-9316.

Lachenbruch, A.H., Sass, J.H., Lawver, L.A., Brewer, M.C., Marshall, B.V., Munroe, R.J., Kennelly, J.P., Galanis, S.P., and Moses, T.H., 1987, Temperature and depth of permafrost on the Alaskan Arctic Slope, *in* Tailleur, I. and Weimer, P., eds., Alaska North Slope Geology, v.2, Pacific Section Society of Economic Paleontologists and Mineralogists, p. 545-558.

Lamorey, G., 2003, West Arctic Ice Sheet Antarctic Glaciological Data Center Catalog.

Lee, M.W., 1999, Methods of generating synthetic acoustic logs from resistivity logs for gas hydrate-bearing sediments, *in* U.S. Geological Survey Bulletin, (Issues 1074-1097).

Lee, M.W., Hutchinson, D.R., Collett, T.S., and Dillon, W.P., 1996, Seismic velocities for hydrate-bearing sediments using weighted equation, Journal of Geophysical Research, v. 101, n. B9, p. 20,347-20,358.

Lee, M.W. and Collett, T.S., 1999, Amount of gas hydrate estimated from compressional and shear-wave velocities at the JAPEX/JNOC/GSC Mallik 2L-38 gas hydrate research well, *in* Dallimore, S.R., Uchida, T., and Collett, T.S. eds., Scientific results from JAPEX/JNOC/GSC Mallik 2L-38 gas hydrate research well, Mackenzie Delta, Northwest Territories, v. 544, Canada Geological Survey of Canada Bulletin p. 313-322.

Light, W., 1992, Some aspects of radial basis function approximation, *in* Singh, S., Ed., Approximation Theory, Spline Functions and Applications: NATO ASI series, 256, Kluwer Academic Publishers, 163-190.

Makogon, Y.F., 1981, Hydrates of natural gas: Tulsa, OK, Penn Well Publishing Company, 237p.

Manuel, J., 2008, A chronostratigraphic framework of the Sagavanirktok Formation, North Slope Alaska: Incorporating facies characterization, reservoir continuity and dimensions in relation to gas hydrate and associated free-gas resources, M.G.Eng., M.S. Thesis, Department of Mining and Geologic Engineering, University of Arizona.

Mavco, G., Mukerji, T., and Dvorkin, J., 1988, The rock physics handbook, Cambridge University Press.

Mendes, N., Fernandes, C.P., Philippi, P.C., and Lamberts, R., 2001, Moisture content influence on thermal conductivities of porous building materials: Seventh International IBPSA Conference, p. 957-963.

Meyer, V., Nicol, A., Childs, C., Walsh, J.J., and Watterson, J., 2002, Progressive localization of strain during the evolution of a normal fault population, Journal of Structural Geology, v. 24, p. 1215-1231.

Mitchell, K., Casavant, R., and Manuel, J., 2003, Regional characterization of the Cretaceous Nanushuk Group: Preliminary assessment for coal-bed methane potential in arctic Alaska, American Association of Petroleum Geologists-SEG Student Expo, Houston, TX, October 5-6, 2003.

Michelli, C., 1986, Interpolation of scattered data: distance matrices and conditionally positive definite functions, Constructive Approximations, 2, 11-22.

Moody, J. and Darken, C., 1989, Fast learning in networks of locally-tuned processing units, Neural Computation, 1, 281-294.

Moore, T., Wallace, W., Bird, K., Karl, S., Mull, C., and Dillon, J., 1994, Geology of Northern Alaska, *in* Plafker, G. and Berg, H.C., eds., The Geology of Alaska, Boulder, Colorado, Geological Society of America, The Geology of North America, v. G-1, p. 49-140.

Morgridge, D.L. and Smith, W.B., 1972, Geology and discovery of Prudhoe Bay field, eastern Arctic Slope, Alaska, American Association of Petroleum Geologists Memoir 16: 489-501.

Musavi, M., Ahmed, W., Chan, K., Faris, K., and Hummels, D., 1992, On the training of radial basis function classifiers, Neural Networks, 5, 595-603.

Ohara, T., Dallimore, S.R., and Fercho, E., 1999, Drilling operations, JAPEX/JNOC/GSC Mallik 2L-38 gas hydrate research well, *in* Dallimore, S.R., Uchida, T., and Collett, T.S., eds., Scientific results from JAPEX/JNOC/GSC Mallik 2L-38 Gas Hydrate Research Well, Mackenzie Delta, Northwest Territories, Canada, , v. 544, Geological Survey of Canada Bulletin, p. 19-30.

Osterkamp, T.E. and Payne, M.W., 1981, Estimates of permafrost thickness from well logs in northern Alaska: Cold Regions Science and Technology, v.5, p.13-17.

Poggio, T. and Girosi, F., 1989, A theory of networks for approximation and learning, A.I. Memo No. 1140 (C.B.I.P . Paper No. 31), Massachusetts Institute of Technology, Artificial Intelligence Laboratory.

Poggio, T. and Girosi, F., 1990a, Regularization algorithms for learning that are equivalent to multilayer networks, Science, 247, pp.978-982.

Poggio, T. and Girosi, F., 1990b, Networks for approximation and learning, Proceedings of the IEEE, 78, pp.1481-1497.

Poulton, M., (Ed.), 2001, Computational Neural Networks for Geophysical Data Processing, Pergamon, Amsterdam, 335 pp.

Poulton, M., 2002, Neural networks as an intelligence amplification tool: A review of applications, Geophysics, vol. 67, no. 3, pp. 979-993.

Poulton, M.M., Casavant, R.R., Glass, C.E., and Zhao, B., 2004, Model Testing of Methane Hydrate Formation on the North Slope of Alaska With Artificial Neural Networks, AAPG Hedberg Conference, Gas Hydrates: Energy Resource Potential and Associated Geologic Hazards, September 12-16, 2004, Vancouver, BC, Canada, 2 pp.

Poulton, M.M. and Meisberger, D., *draft manuscript (2009),* Artificial neural network analysis and gas hydrate characterization, Milne Point Unit, Alaskan North Slope.

Powell, M., 1987, Radial basis functions for multivariable interpolation: A review, *in* Mason, J. and Cox, M., Eds., Algorithms for Approximation, Clarendon Press.

Rawlinson, S.E., 1993, Surficial geology and morphology of the Alaskan central Arctic Coastal Plain, Alaska Division of Geological and Geophysical Surveys Report of Investigations, v. 93-1, n.172.

Reister, D.B., 2003, Using measured velocity to estimate gas hydrates concentration, Geophysics, v. 68, p. 884-891.

Roberts, S.B., 1991, Subsurface cross section showing coal beds in the Sagavanirktok Formation, vicinity of Prudhoe Bay, East-Central North Slope, Alaska, U.S. Geological Survey.

Saxena, R.S., 1979, Facies Models and Subsurface Exploration Methods for the Analysis of Deltaic and other Associated Sandstone Reservoirs, 233 pp.

Slack, G.A., 1980, Thermal conductivity, Physics Review, v.B, p.3065.

Sloan, E.D., 1990, Clathrate hydrates of natural gases, New York, Marcel Dekker, 641 pp.

Spath, H., 1980, Cluster Analysis Algorithms for Data Reduction and Classification of Objects, Elis Horwood Publishers.

Stein, J.A., Johnson, R.A., Casavant, R.R., and Warren, M.B., *2007*, Calibration and analysis of methane hydrate beneath Alaska's North Slope using spectral decomposition of 3-D seismic reflection data, *manuscript submitted to* American Geophysical Union.

Tikhonov, A. and Arsenin, V., 1977, Solutions of Ill-Posed Problems, W.H.Winston.

Tye, R.S., 2004, Geomorphology: An approach to determining subsurface reservoir dimensions, American Association of Petroleum Geologists, Bulletin 88(8), p.1123-1147.

U.S. Geological Survey, 1989, U.S. Geological Survey's Borehole Temperature Logs from Arctic Alaska, pre-1989, U.S. Geological Survey.

Van Wagoner, J.C., Mitchum, R.M., Campion, K.M., and Rahmanian, V.D., 1990, Siliciclastic Sequence Stratigraphy in Well Logs, Cores, and Outcrops: Concepts for High-Resolution Correlation of Time and Facies, Tulsa, OK, American Association of Petroleum Geologists Methods in Exploration Series, No. 7, 55pp.

Waite, W.F., Gilbert, L.Y., Winters, W.J., and Mason, D.H., 2004, Thermal property measurements in tetrahydrofuran (THF) hydrate between -25 and +4°C and their application to methane, EOS Transactions, American Geophysical Union, abstract # OS41C-0489.

Weimer, P., 1987, Northern Alaska Exploration - the past dozen years, *in* Tailleur, I. and Weimer, P., eds., Alaskan North Slope Geology, Bakersfield, CA, Pacific Section, Society of Economic Paleontologists and Mineralogists, 1: 31-39.

Werner, M.R., 1987, Tertiary and Upper Cretaceous heavy-oil sands, Kuparuk River Unit area, Alaska North Slope, in Meyer, R.F., ed., Exploration for heavy crude oil and natural bitumen: American Association of Petroleum Geologists Studies in Geology 25, p. 537-547.

Wright, J.F., Dallimore, S.R., and Nixon, M.F., 1999, Influences of grain size and salinity on pressure-temperature thresholds for methane hydrate stability *in* JAPEX/JNOC/GSC Mallik 2L-38 gas hydrate research-well sediments: Scientific Results from JAPEX/JNOC/GSC Mallik 2L-38 Gas Hydrate Research Well, Mackenzie Delta, Northwest Territories, Canada, p. 229-240.

Wyllie, M.R., Gregory, A.R., and Gardner, G.H.F., 1958, An experimental investigation of factors affecting elastic wave velocities in porous media, Geophysics, v.23, p.459-493.

Yakushev, V.S. and Collett, T.S., 1992, Gas hydrates in arctic regions: Risk to drilling and production, 2nd International Offshore and Polar Engineering Conference, p.669-673.

Yielding, G., Freeman, B., and Heedham, D.T., 1997, Quantitative Fault Seal Prediction, AAPG Bulletin, v. 81, n. 6, p. 897-917.

Yielding, G., Overland, J.A., and Byberg, G., 1999, Characterization of Fault Zones for Reservoir Modeling: An Example from the Gullfaks Field, Northern North Sea, American Association of Petroleum Geologists, Bulletin, v. 83, n.6, p. 925-951.

Zell, A., 1994, Simulation Neuronaler Netze, Addison Wesley.

Zhao, B., 2003, Classifying Seismic Attributes in the Milne Point Unit, North Slope of Alaska, MS Thesis, University of Arizona, 159 p.

7.5 University of Alaska Fairbanks Research References

7.5.1 Project-Sponsored Thesis

Howe, S.J., 2004, Production modeling and economic evaluation of a potential gas hydrate pilot production program on the North Slope of Alaska, MS Thesis, University of Alaska Fairbanks, 141 p.

Jaiswal, N.J., 2004, Measurement of gas-water relative permeabilities in hydrate systems, MS Thesis, University of Alaska Fairbanks, 100 p.

Johnson, A.C., 2009, Experimental and simulation studies in support of the Mt. Elbert gas hydrate prospect on the Alaska North Slope, MS Thesis, University of Alaska Fairbanks.

Kerkar, P.B., 2005, Assessment of Formation Damage from Drilling Fluids Dynamic Filtration in Gas Hydrate Reservoirs of the North Slope of Alaska, MS Thesis, University of Alaska Fairbanks, August 2005.

Westervelt, J.V., 2004, Determination of methane hydrate stability zones in the Prudhoe Bay, Kuparuk River, and Milne Point units on the North Slope of Alaska, MS Thesis, University of Alaska Fairbanks, 85 p.

7.5.2 Gas Hydrate Phase Behavior and Relative Permeability References

ASTM, 2000, Standard Test Method for Permeability of Granular Soils (constant head) D 2434-68, American Society for Testing and Materials, Annual Book of ASTM Standards, West Conshohocken, PA, 202-206.

Dvorkin, J., Helgerud, M.B., Waite, W.F., Kirby, S.H., and Nur, A., 2000, Introduction to Physical Properties and Elasticity Models, *in* Natural Gas Hydrate in Oceanic and Permafrost Environments, edited by Max, M.D., pp. 245-260, Kluwer, Dordrecht.

Gash, B.W., 1991, Measurement of Rock Properties in Coal for Coalbed Methane Production, Paper 22909 presented at the 1991 SPE Annual Technical conference and Exhibition, Dallas, October 6-9, 1991.

Johnson, E.F., Bossler, D.P., and Neumann, V.O., 1959, Calculation of Relative Permeability from Displacement Experiments, Trans. AIME, 216, 370- 372.

Jones, S.C. and Roszelle, W.O., 1978, Graphical Techniques for Determining Relative Permeability from Displacement Experiments, JPT, May 1978, p. 807-817.

Joseph, W.W. and Duane, H.S., 2002, Upper Limits on the Rates of Dissociation of Clathrate Hydrates to Ice and Free Gas, J. Phys. Chem. B., May 2002, 106, p. 6298-6302.

Makogon, Y.F., Makogon, T.Y., and Holditch, S.A., 1998, Several Aspects of the Kinetics and Morphology of Gas Hydrates, Proceedings of the International Symposium on Methane Hydrates: Resources in the Near Future?, Chiba City, Japan, October 20-22, 1998.

Masuda, Y., Ando, S., Ysukui, H., and Sato, K., 1997, Effect of Permeability on Hydrate Decomposition in Porous Media, International Workshop on Gas Hydrate Studies, Tsukuba, Japan, March 4-6, 1997.

Mehrad, N., 1989, Measurement of gas permeability in hydrate saturated unconsolidated cores, MS Thesis, University of Alaska, Fairbanks.

Owens, W.W., Parrish, D.R., and Lamoreausx, W.E., 1956, An Evaluation of Gas Drive Method for Determining Relative Permeability Relationships, Trans., AIME 207, p. 275-280.

Scheidegger, A.E., 1998, The Physics of Flow Through Porous Media, Macmillan, New York.

Sloan, E.D., 1998, Clathrate Hydrates of Natural Gases, Marcel Dekker, New York.

Spangenberg, W., 2001, Modeling of the influence of gas hydrate content on the electrical properties of porous sediments, J of Geophys. Res B., 106, p. 6535-6549.

Stern, L.A., Kirby, S.H., Durham, W.B., Circone, S., and Waite, W.F., 2000, Laboratory synthesis of pure methane hydrate suitable for measurement of physical properties and decomposition behavior *in* Natural Gas Hydrate in Oceanic and Permafrost Environments, ed. by Max, M.D., pp. 323-348, Kluwer, Dordrecht.

Toth, J., Bodi, T., Szucs, P., and Civan, F., 2000, Analytical Techniques for Determination of Relative Permeability from Displacement Experiments, Progress in Mining and Oilfield Chemistry, Vol-2, 91-100.

Westervelt, J.V., 2004, Determination of methane hydrate stability zones in the Prudhoe Bay, Kuparuk River, and Milne Point units on the North Slope of Alaska, MS Thesis, University of Alaska Fairbanks.

Wilder, J.W., Seshadri, K., and Smith, D.H., 2001, Modeling Hydrate Formation in Media with Broad Pore Size Distributions, Langmuir 17, p. 6729-6735.

Winters, W.J., Dillon, W.P., Pecher, I.A., and Mason, D.H., 2000, GHASTLI-Determining physical properties of sediment containing natural and laboratory formed gas hydrate *in* Natural Gas Hydrate in Oceanic and Permafrost Environments, edited by Max, M.D., pp. 311-322, Kluwer, Dordrecht.

7.5.3 Drilling Fluid Evaluation and Formation Damage References

Collett, T.S., 1998, Well Log Characterization of Sediments in Gas Hydrate-Bearing Reservoirs, SPE 49298, presented at SPE Annual Technical Conference and Exhibition, New Orleans, Louisiana, September 27-30, 1998.

Collett, T.S., Bird, K.J., and Magoon, L.B., 1988, Subsurface Temperatures and Geothermal Gradients on the North Slope of Alaska, SPE 19024, Society of Petroleum Engineers.

Collett, T.S., 1993, Natural Gas Hydrates of the Prudhoe Bay and Kuparuk River Area North Slope, Alaska, American Association of Petroleum Geologists, Bull., V. 77, No. 5, pp. 793-812.

Dallimore, S.R., Uchida, T., and Collett, T.S., 1999, Scientific Results from JAPEX/JNOC/GSC Mallik 2L-38 Gas Hydrate Research Well, Mackenzie Delta, Northwest Territories, Canada, Geological Survey of Canada Bulletin 544.

Dvorkin, J., Helgerud, M.B., Waite, W.F., Kirby, S.H., and Nur, A., 2000, Introduction to Physical Properties and Elasticity Models, in Natural Gas Hydrate in Oceanic and Permafrost Environments, edited by Max, M.D., pp. 245-260, Kluwer, Dordrecht.

Ginsburg, G., Soloviev, V., Matveeva, T., and Andreeva, I., 2000, Sediment Grain Size Control on Gas Hydrate Presence, Sites 994, 995, and 997, *in* Proceedings of the Ocean Drilling Program, Scientific Results, Leg 164, edited by Paull, C.K., Matsumoto, R., Wallace, P.J., and Dillon, W.P., Chapter 24, Ocean Drilling Program, College Station, Texas, 2000.

Kamath, V.A. and Patil, S.L., 1994, Description of Alaskan Gas Hydrate Resources and Current Technology, studies by University of Alaska Fairbanks.

Kerkar, P.B., 2005, Assessment of Formation Damage from Drilling Fluids Dynamic Filtration in Gas Hydrate Reservoirs of the North Slope of Alaska, MS Thesis, University of Alaska Fairbanks, August 2005.

Marshall, D.S., Gray, R., and Byrne, M., 1997, Development of a Recommended Practice for Formation Damage Testing, SPE 38154, presented at the SPE European Formation Damage Conference, Hague, Netherlands, June 2-3, 1997.

Matsumoto, R., 2002, Comparison of Marine and Permafrost Gas Hydrates: Examples from Nankai Trough and Mackenzie Delta, *in* Proceedings of the Fourth International Conference on Gas Hydrates, Yokohama, May 19-23, 2002.

Murlidharan, V., Putra, E., and Schechter, D.S., 2002, Investigating the Changes in Matrix and Fracture Properties and Fluid Flow under Different Stress-state Conditions, MS Thesis, Texas A&M University.

Shipboard Scientific Party, 2002, Leg 204 Preliminary Report, Drilling Gas Hydrates on Hydrate Ridge, Cascadia Continental Margin, ODP Texas A&M University, December 2002, Available at: http://www-odp.tamu.edu/publications/prelim/204_prel/204PREL.PDF

Winters, W.J., Dallimore, S.R., Collett, T.S., Katsube, T.J., Jenner, K.A., Cranston, R.E., Wright, J.F., Nixon, F.M., and Uchida, T., 1999, Physical properties of sediments from the JAPEX/JNOC/GSC Mallik 2L-38 Gas Hydrate Research Well", *in* Geological Survey of Canada Bulletin 544, Scientific Results from JAPEX/JNOC/GSC Mallik 2L-38 Gas Hydrate Research Well, Mackenzie Delta, Northwest Territories, Canada, edited by Dallimore, S.R. , Uchida, T., and Collett, T.S., Geological Survey of Canada, Ottawa, 1999.

Yousif, M.H., Abass, H.H., Selim, M.S., and Sloan, E.D., 1991, Experimental and Theoretical Investigation of Methane-Gas hydrate Dissociation in Porous Media; SPE 18320, SPE Reservoir Engineering, February 1991, p. 69-76.

7.5.4 Supplemental Formation Damage Prevention References

Anselme, M.J., Reijnhout, M.J., Muijs, H.M., and Klomp, U.C., 1993, World Pat. WO 93/25798.

Belavadi, M.N., 1994, Experimental Study of the Parameters Affecting Cutting Transportation in a Vertical Wellbore Annulus, MS Thesis, University of Alaska, Fairbanks, September, 1994.

Bennion, D.B., Thomas, F.B., and Bietz, R.F., 1996, Low permeability Gas Reservoirs: Problems, Opportunities and Solution for Drilling, Completion, Simulation and Production, SPE 35577, May 1996.

Bennion, D.B., Thomas, F.B., and Bietz, R.F., 1996, Formation Damage and Horizontal Wells-A Productivity Killer?, SPE 37138; International Conference on Horizontal Well Technology, Calgary; Nov. 1996.

Bennion, D.B., Thomas, F.B., and Bietz, R.F., 1995, Underbalanced Drilling and Formation Damage- Is it a Total Solution?, The Journal of Canadian Petroleum Tech., Vol. 34 (9) November 1995.

Bennion, D.B., Thomas F.B., Bietz, R.F., and Bennion, D.W., 1995, Advances in Laboratory Core Flow Evaluation to minimize Formation Damage Concerns with Vertical/Horizontal Drilling Application; CAODC; Vol. 95 (105).

Bennion, D.B., Thomas, F.B, Jamaluddin, K.M., and Ma, T.Y., 1998, Using Underbalanced Drilling to Reduce Invasive Formation Damage and Improve Well Productivity- An Update, Petroleum Society of CIM, PTS 98-58.

Chadwick J., 1995, Exploration in permafrost, Mining Magazine, February, 1995.

Chen, W., Patil S.L., Kamath, V.A., and Chukwu, G.A., 1998, Role of Lecithin in Hydrate Formation/Stabilization in Drilling Fluids, JNOC, October 20, 1998.

Chilingarian, G.V. and Vorabutr, P., 1983, Drilling and drilling fluids, Elsevier, NY.

Cohen, J.H. and Williams, T.E., 2002, Hydrate Core Drilling Tests: Topical Report, Maurer Technology Inc., Houston, Texas, November 2002.

Crowell, E.C., Bennion, D.B., Thomas, F.B., and Bennion, D.W., 1992, The Design and Use of Laboratory Tests to Reduce Formation Damage in Oil and Gas Reservoirs, 13th Annual Conference of the Ontario Petroleum Institute.

Dallimore, S.R., Uchida, T., and Collett, T.S., 1999, Scientific Results from JAPEX/JNOC/GSC Mallik 2L-38 Gas Hydrate Research Well, Mackenzie Delta, Northwest Territories, Canada, Geological Survey of Canada Bulletin 544, February, 1999.

Drill Cool Systems Canada Inc., www.drillcool.com.

Duncum, S.N., Edwards, A.R., and Osborne, C.G., 1993, Eur. Pat. 536,950.

Francis, P.A., Eigner, M.R.P., Patey, I.T.M., and Spark, I.S.C., 1995, Visualization of Drilling-Induced Formation Damage Mechanisms using Reservoir Conditions Core Flood Testing, paper SPE 30088 presented at the European Formation Damage Conference, The Hague, May 15-16, 1995.

Fu, S.B., Cenegy, L.M., and Neff, C.S., 2001, A Summary of Successful Field Application of a Kinetic Hydrate Inhibitor, SPE 65022.

Hammerschmidt, E.G., 1934, Ind.Eng.Chem., 26, 851.

Howard, S.K., 1995, Formate Brines for Drilling and Completion: State of the Art, SPE 30498.

I.F.P. patents: Fr.Pats. 2,625,527; 2,625,547; 2,625,548; 2,694,213; 2,697,264. Eur. Pats. 594,579; 582,507323,775; 323307. US Pat. 5,244,878. Can.Pat. 2,036,084.

Jamaluddin, A.K.M., Bennion D.B., Thomas, F.B., and Ma, T.Y., 1998, Application of Heat Treatment to Enhance Permeability in Tight Gas Reservoirs, Petroleum Society of CIM, Paper No. 98-01.

Kalogerakis, N., Jamaluddin, A.K.M., Dholabhai, P.D., and Bishnoi, P.R., 1993, Effect of Surfactants on Hydrate Formation Kinetics, SPE 25188.

Kamath V.A., Mutalik P.N., Sira, J.H., and Patil, S.L., 1991, Experimental Study of Brine Injection and Depressurization Methods for Dissociation of Gas Hydrate, SPE Formation Evaluation, December 1991.

Kastube, T.J., Dallimore, S.R., et. al., 1999, Gas Hydrate Investigation in Northern Canada, JAPEX, Vol. 8; No. 5.

Kelland, M.A., Svartaas, T.M., and Dybvik, L.A., 1994, Control of Hydrate Formation by Surfactants and Polymers, SPE 28506, p. 431-438.

Kotkoskie, T.S., Al-Ubaidi, B., Wildeman, T.R., and Sloan, E.D., 1990, Inhibition of Gas Hydrates in Water-Based Drilling Mud, SPE 20437.

Kutasov, I.M., 1995, Salted drilling mud helps prevent casing collapse in permafrost, Oil and Gas Journal, July 31, 1995.

Marshall, D.S., Gray, R., and Byrne, M., 1997, Development of a Recommended Practice for Formation Damage Testing, SPE 38154, Presented at the SPE European Formation Damage Conference, Netherlands, June 2-3, 1997.

Maury, V. and Guenot, A., 1995, Practical Advantages of Mud Cooling Systems for Drilling, SPE Drilling and Completion, March 1995.

Max, M.D., 2000, Natural Gas Hydrate in Oceanic and Permafrost Environments, Kluwer Academic Publishers, Boston.

Muijs, H.M., Beers, N.C., Van Om, N.M., Kind, C.E., and Anselme, M.J., 1992, Can. Pat. 2,036,084.

Oort, E.V., Friedheim, J.M., and Toups, B., 1999, Drilling faster with Water-Base Mud, American Association of Drilling Engineers – Annual Technical Forum, March 30-31, 1999.

Paez, J.E., Blok, R., Vaziri, H., and Islam, M.R., 2001, Problems in Hydrates: Mechanisms and Elimination Methods, SPE 67322.

Pooladi-Darvish, M. and Hong, H., 2003, A Numerical Study on Gas Production from Formations Containing Gas Hydrates, Canadian International Petroleum Conference, Calgary, June 10-12, 2003.

Reijnhout, M.J., Kind, C.E., and Klomp, U.C., 1993, Eur. Pat. 526,929.

Robinson, L., 1977, Mud equipment manual, Handbook 1: Introduction to drilling mud system, Gulf Publishing Company, Houston.

Sasaki, K., Akibayashi, S., and Konno, S., 1998, Thermal and Rheological properties of Drilling Fluids and an Estimation of Heat Transfer Rate at Casing pipe, JNOC-TRC, Japan; October 20-22, 1998.

Schofield, T.R., Judis, A., and Yousif, M., 1997, Stabilization of In-Situ Hydrates Enhances Drilling Performance and Rig Safety, SPE 32568, Drilling and Completion.

Sira, J.H., Patil, S.L., and Kamath, V.A., 1990, Study of Hydrate Dissociation by Methanol and Glycol Injection; SPE 20770.

Sloan, E.D., 1994, World Pat. WO 94/12761.

Spence, G.D. and Hyndman, R.D., 2001, The challenge of Deep ocean Drilling for Natural Gas Hydrate, Geoscience Canada, Vol.28 (4), December, 2001.

Sumrow, M., 2002, Synthetic-based muds reduce pollution discharge, improve drilling, Oil and Gas Journal, December 23, 2002.

Szczepanski, R., Edmonds, B., et. al., 1998, Research provides clues to hydrate formation and drilling-hazard solutions, Oil and Gas Journal, Vol. 96(10), Mar 9, 1998.

Toshiharu, O., Yuriko M., et. al., 1998, Kinetic Control of Methane Hydrates in Drilling Fluids, JNOC-TRC, October 20-22, 1998.

Urdahl, O., Lund, A., Moerk, P., and Nilsen, T.N, 1995, Inhibition of Gas Hydrate Formation by means of Chemical Additives: Development of an Experimental Set-up for Characterization of Gas Hydrate Inhibitor Efficiency with respect to Flow Properties and Deposition, Chem. Eng. Sci., 50(5), 863.

Maury, V. and Guenot, A., 1993, Practical Advantages of Mud Cooling Systems for Drilling, SPE 25732.

Vincent, M. and Guenot, A., 1995, Practical Advantages of Mud Cooling System for Drilling, SPE Drilling and Completion, March 1995.

Weidong, C., Patil, S.L., Kamath, V.A., and Chukwu, G.A., 1998, Role of Lecithin in Hydrate Formation/Stabilization in Drilling Fluids, JNOC-TRC, October 20-22, 1998.

Yuliev, A.M. and Gazov, D., 1972, 10, 17-19, Russia.

Zakharov, A.P., 1992, Silicon-based additives improve mud Rheology, Oil and Gas Journal, August 10, 1992.

7.5.5 Coring Technology References

Amann, H., et al., 2002, First Successful Deep-Sea Operations of OMEGA-MAC, the Multiple Auto Corer, during the OTEGA-I campaign on Hydrate Ridge, Fachgebiet Maritime Technik, August 2002.

Carroll, J., 2002, Natural Gas Hydrates: A Guide for Engineers, Gulf Professional Publishing, October 30, 2002.

Dickens, G.R., Wallace, P.J., Paull, C.K., and Borowski, W.S., 2000, Detection of Methane Gas Hydrate in the Pressure Core Sampler (PCS): Volume-Pressure-Time Relations During Controlled Degassing Experiments, *in* Proc. of the Ocean Drilling Program, Vol. 164.

Francis, T.J.G., 2001, The HYACINTH project and pressure coring in the Ocean Drilling Program, Internal Document: Geotek, Ltd. July 2001.

Hohnberg, H.J., et al., 2003, Pressurized Coring of Near-Surface Gas Hydrate Sediment on Hydrate Ridge: The Multiple Autoclave Corer, and First Results from Pressure Core X-Ray CT Scans, Geophysical Research Abstracts, Vol. 5, European Geophysical Society.

"HYACE", 2003, [www] http://www.tu-berlin.de/fb10/MAT/hyace/description/describe.htm.

Manheim, F.T. and Sayles, F.L., 1974, Composition and origin of interstitial waters of marine sediments based on deep sea drill cores, *In* Goldberg, E.D., (Ed.), The Sea, (Vol. 5): New York (Wiley), pp. 527-568.

"Methane Hydrate Recovery", [www]http://www.mh21japan.gr.jp/english/mh/05kussaku.html#e

"Methane Hydrates: A US Department of Energy Website". www.fossil.energy.gov.

"Natural Gas Demand": [www] www.naturalgas.org/business/demand.asp.

"Patent No. 6,214,804: The Pressure-Temperature Coring System". U.S. Patent Office. [www]http://patft.uspto.gov/netacgi/nph-Parser?Sect1=PTO1&Sect2=HITOFF&d=PALL&p=1&u=/netahtml/srchnum.htm&r=1&f=G&l=50&s1=6,216,804.WKU.&OS=PN/6,216,804&RS=PN/6,216,804. Viewed July 14, 2003.

Rack, F.R, In-Situ Sampling and Characterization of Naturally Occurring Marine Hydrate Using the D/V JOIDES Resolution, Joint Oceanographic Institute, Cooperative Agreement DE-FC-26-01NT41329.

Shukla, K., et al., 2002, Overview on Hydrate Coring/Handling/Analysis, Westport Technology Center International, Prepared for DOE on December 12, 2002 under award No. DE-PS26-NT40869-1.

7.6 Reservoir and Economic Modeling References

Brown, G., Storer, D., and McAllister, K., 2003, Monitoring Horizontal Producers and Injectors during Cleanup and Production Using Fiber-Optic-Distributed Temperature Measurements, SPE 84379.

Ji, C., Ahmadi, G., and Smith, D.H., 2003; Constant rate natural gas production from a well in a hydrate reservoir, Energy Conversion and Management 44, p. 2403-2423.

Ji, C, Ahmadi, G., and Smith, D.H., 2001, Natural gas production from hydrate decomposition by depressurization, Chemical Eng. science 56, p. 5801-5814.

Howe, S.J., 2004, Production modeling and economic evaluation of a potential gas hydrate pilot production program on the North Slope of Alaska, MS Thesis, University of Alaska Fairbanks, 141 p.

Howe, S.J., Nanchary, N.R., Patil S.L., Ogbe D.O., Chukwu G.A., Hunter R.B and Wilson S.J., 2004, Production Modeling and Economic Evaluation of a Potential Gas Hydrate Pilot Production Program on the North Slope of Alaska.

Howe, S.J., Nanchary, N.R., Patil, S.L., Ogbe D.O., Chukwu, G.A., Hunter, R.B., and Wilson, S.J., 2004, Economic Analysis and Feasibility study of Gas Production from Alaska North Slope Gas Hydrate Resources, Presentation at the AAPG Hedberg Conference in Vancouver, September 2004.

Jaiswal, N.J., 2003, Measurement of Relative Permeabilities for Gas Hydrate Systems, Received third prize in International Thermal Operations and Heavy-Oil Symposium and SPE Regional Meeting Bakersfield, California, USA.

Jaiswal, N.J., Dandekar, A.Y., Patil, S.L., and Chukwu, G.C., 2003, Measurement of Relative Permeability for Gas hydrate System, *at* 54th Arctic Science Conference, September 23, 2003.

Jaiswal, N.J., Westervelt, J.V., Patil, S.L., Dandekar, A.Y., Nanchary, N.R., Tsunemori, P., and Hunter, R.B., 2004, Phase Behavior and Relative Permeability of Gas-Water-Hydrate System, AAPG Hedberg Conference, Vancouver, September 2004.

Johnson, A.C., 2009, Experimental and simulation studies in support of the Mt. Elbert gas hydrate prospect on the Alaska North Slope, MS Thesis, University of Alaska Fairbanks.

McGuire, P.L., 1982, Recovery of gas from hydrate deposits using conventional technology, SPE/DOE 10832, *in* Proc. Unconventional Natural Gas Recovery Symposium Pittsburgh, PA, pp. 373-387, Society of Petroleum Engineers, Richardson Texas.

McGuire, P.L., 1982, Methane hydrate gas production by thermal stimulation, *in* Proceedings of the 4th Canadian Permafrost Conference, pp.356-362.

Moridis, G.J., 2002, Numerical Studies of Gas Production from Methane Hydrates, SPE 75691, presented at the SPE Gas Technology Symposium, Calgary, Alberta, Canada, 30 April – 2 May.

Moridis, G.J. and Collett, T.S., 2004, Gas Production from Class 1 Hydrate Accumulations, *in* Taylor, C. and Qwan, J., eds., Recent Advances in the Study of Gas Hydrates, Sec.I, V.6, Springer, USA, pp. 75-88.

Moridis, G.J., Collett, T.S., Dallimore, S.R., Satoh, T., Hancock, S., and Weatherill, B., 2003, Numerical simulation studies of gas production scenarios from hydrate accumulations at the Mallik site, Mackenzie Delta, Canada, *In* Mori, Y.S., Ed., Proceedings of the Fourth International Conference on Gas Hydrates, May 19-23, 2003, Yokohama, Japan, pp. 239-244.

Nanchary, N.R., Patil S.L., and Dandekar A.Y., Numerical Simulation of Gas Production from Hydrate Reservoirs by Depressurization, Journal of Petroleum Science and Engineering (Elsevier publication), *Draft Manuscript.*

Nanchary, N.R., Patil, S.L., Dandekar, A.Y., and Hunter, R.B., Numerical Modeling of Gas Hydrate Dissociation in Porous Media, AAPG Hedberg Conference in Vancouver, September 2004.

Swinkles, W.J.A.M. and Drenth, R.J.J., 1999, Thermal Reservoir Stimulation Model of Prediction from Naturally Occurring Gas Hydrate Accumulations, Society of Petroleum Engineers, SPE 56550, 13 p.

Tsunemori, P., 2003, Phase Behavior of Natural Gas from Gas Hydrates, Received first in International Thermal Operations and Heavy-Oil Symposium and SPE Regional Meeting Bakersfield, California, USA.

Tsypkin, G.G., 1992, Appearance of two moving phase transition boundaries in the dissociation of gas hydrates in strata, Dokl. Ross. Akad. Nauk. 323. 52-57 (in Russian).

Tsypkin, G.G., 1991, Effect of liquid phase mobility on gas hydrate dissociation in reservoirs. Izvestiya Akad. Nauk SSSR. Mekh. Zhidkosti i Gaza. 4: 105-114 (in Russian).

Westervelt, J.V., 2004, Determination of methane hydrate stability zones in the Prudhoe Bay, Kuparuk River, and Milne Point units on the North Slope of Alaska, MS Thesis, University of Alaska Fairbanks, 85 p.

Yousif, M.H., Abass, H.H., Selim, M.S., and Sloan, E.D., 1991, Experimental and Theoretical Investigation of Methane-Gas hydrate Dissociation in Porous Media; SPE 18320, SPE Reservoir Engineering, February 1991, p. 69-76.

7.7 Regional Schematic Modeling Scenario Study References

Collett, T.S., 1993, Natural Gas Hydrates of the Prudhoe Bay and Kuparuk River Area, North Slope, Alaska, AAPG Bulletin, Vol. 77, No. 5, May, 1993, p 793-812.

Howe, S.J., Nanchary, N.R., Patil, S.L., Ogbe, D.O., Chukwu, G.A., Hunter, R.B., and Wilson, S.J., 2004, Economic Analysis and Feasibility study of Gas Production from Alaska North Slope Gas Hydrate Resources, Presentation at the AAPG Hedberg Conference in Vancouver, September 2004.

Hancock, S.H., Collett, T.S., Dallimore, S.R., Satoh, T., Inoue, T., Huenges, E., Henninges, J., and Weatherill, B., 2004, Overview of thermal-stimulation production-test results for the JAPEX/JNOC/GSC et al. Mallik 5L-38 gas hydrate production research well, *in* Scientific Results from the Mallik 2002 Gas Hydrate Production Research Well Program, Mackenzie Delta, Northwest Territories, Canada, Dallimore, S.R. and Collett, T.S., Eds., Geological Survey of Canada Bulletin 585.

Sturgeon-Berg, R., 1996, Permeability Reduction Effects Due to Methane and Natural Gas Flow through Wet Porous Media, Colorado School of Mines, MS Thesis, T- 4920, September 1996.

Howe, S.J., 2004, Production modeling and economic evaluation of a potential gas hydrate pilot production program on the North Slope of Alaska, MS Thesis, University of Alaska Fairbanks, 141 p.

Hong, H., Pooladi-Darvish, M., and Bishnoi, P.R., 2003, Analytical Modeling of Gas Production from Hydrates in Porous Media, Journal of Canadian Petroleum Technology (JCPT), November 2003, Vol. 42 (11) p. 45-56.

7.8 Short Courses

Natural Gas Hydrates, by Collett, T.S. (USGS) and Patil, S.L. (UAF), 2002, A Short Course at the SPE-AAPG: Western Region-Pacific Section Conference, Anchorage, Alaska, May 18-23, 2002, Sponsored by Alaska Division of Geological and Geophysical Surveys and West Coast Petroleum Technology Transfer Council, Anchorage, Alaska.

7.9 Websites

There are no external project-sponsored websites. Project information is available on the DOE website: http://www.netl.doe.gov/research/oil-and-gas/methane-hydrates
A project internal website was developed for storage, transfer, and organization of project-related files, results, and studies. Project electronic and hardcopy files will be maintained.

8.0 LIST OF ACRONYMS AND ABBREVIATIONS

Acronym	Denotation
2D	Two Dimensional (seismic or reservoir data)
3D	Three Dimensional (seismic or reservoir data)
AAPG	American Association of Petroleum Geologists
AAT	Alaska Arctic Terrane (plate tectonics)
AGS	Alaska Geological Society
AEO	Arctic Energy Office (DOE AETDL)
AETDL	Alaska Energy Technology Development Laboratory (DOE AEO)
ADEC	Alaska Department of Environmental Conservation
AES	ASRC Energy Services, E&P Technology
ANL	Argonne National Laboratory
ANN	Artificial Neural Network
ANS	Alaska North Slope
AOGCC	Alaska Oil and Gas Conservation Commission
AOI	Area of Interest
ASRC	Arctic Slope Regional Corporation
ATP	Authority to Proceed (BP-internal)
AVO	Amplitude versus Offset (seismic data analysis technique)
ASTM	American Society for Testing and Materials
BGHSZ	Base of Gas Hydrate Stability Zone
BHA	Bottom Hole Assembly; equipment at bottom hole during drilling operations
BIBPF	Base of Ice-Bearing Permafrost

BLM	U.S. Bureau of Land Management
BMSL	Base Mean Sea Level
BOP	Blow Out Preventer, well control equipment
BP	BP or BPXA
BPTA	BP Transportation (Alaska), Inc.
BPXA	BP Exploration (Alaska), Inc.
CCG	Code Comparison Group, International reservoir modeling team
CMR	Combinable Magnetic Resonance log (wireline logging tool – see also NMR)
CNOOC	China National Offshore Oil Corporation
CoP	ConocoPhillips, Inc.
COR	Contracting Officer's Representative (DOE NETL)
CPAI	ConocoPhillips Alaska, Inc. (or CoP)
CRA	Cooperative Research Agreement (commonly in reference to BP/DOE project)
CSM	Colorado School of Mines
DOE	U.S. Department of Energy
DOI	U.S. Department of Interior
DGGS	Alaska Division of Geological and Geophysical Surveys
DNR	Alaska Department of Natural Resources
DST	Drill Stem Test, a measure of potential well productivity
DTS	Distributed Temperature Survey (used to monitor hydrate dissociation)
EM	Electromagnetic (referencing potential in-situ thermal stimulation technology)
EPT	Electromagnetic Propagation Tool for geophysical wireline logging
ERD	Extended Reach Drilling (commonly horizontal and/or multilateral drilling)
ESP	Electrical Submersible Pump
EUR	Expected Ultimate Recovery
FBHP	Flowing Bottom-Hole Pressure (during MDT wireline production testing)
FBHT	Flowing Bottom-Hole Temperature
FEL	Front-End Loading, reference to effective pre-project operations planning
FG	Free Gas (commonly referenced in association with and below gas hydrate)
GEOS	UA Department of Geology and Geophysics
GH	Gas Hydrate
GIP	Gas-in-Place
GMC	Geological Materials Center, State of Alaska in Eagle River, Alaska
GOM	Gulf of Mexico (typically referring to Chevron Gas Hydrate project JIP)
GR	Gamma Ray (well log)
GSC	Geological Survey of Canada
GTL	Gas to Liquid
GSA	Geophysical Society of Alaska
HP	Hewlett Packard
HSE	Health, Safety, and Environment (typically pertaining to field operations)
JBN	Johnson-Bossler-Naumann method (of gas-water relative permeabilities)
JIP	Joint Industry Participating (group/agreement), ex. Chevron GOM project
JNOC	Japan National Oil Corporation
JOGMEC	Japan Oil, Gas, and Metals National Corporation (reorganized from JNOC 1/04)
JSA/JRA	Job Safety Assessment/Job Risk Assessment; part of BP HSE operations protocol
KRU	Kuparuk River Unit

LBNL	Lawrence Berkeley National Laboratory
LDD	Generic term referencing Logging During Drilling (also LWD and MWD)
LDEO	Lamont-Dougherty Earth Observatory
LN	Liquid Nitrogen
LNG	Liquefied Natural Gas
LSND	Low Solids Non Dispersed (KCl drilling mud system)
MD	Measured Depth (in well)
MDT	Modular Dynamics Testing wireline tool for downhole production testing data
MGE	UA Department of Mining and Geological Engineering
MOBM	Mineral Oil-Based Mud drilling fluid used to improve safety and data acquisition
MPU	Milne Point Unit
MSFL	Micro-spherically focused log (wireline log indication of formation permeability)
MYA	Million Years Ago (also MYBP, Million Years Before Present)
NAS	National Academy of Sciences (National Research Council of the National Academies)
NETL	National Energy Technology Laboratory
NGHP	India National Gas Hydrate Program
NMDS	Non-metric Multidimensional Scaling (microbiology)
NMR	Natural Magnetic Resonance (wireline or LDD tool – see also CMR)
NRC	National Research Council of Canada
OBM	Oil Based Mud, drilling fluid
ONGC	Oil and Natural Gas Corporation Limited (India)
PBU	Prudhoe Bay Unit
PNNL	Pacific Northwest National Laboratory
POOH	Pull out of Hole; pulling drillpipe or wireline from borehole during operations
POS	Pump-out Sub (pertaining to MDT tool)
PPE	Personal Protective Equipment
SCAL	Special Core Analyses, references analyses beyond basic porosity/permeability
SEM	Scanning Electron Microscope (also CSEM, Cryogenic SEM)
SPE	Society of Petroleum Engineers
TCF	Trillion Cubic Feet of Gas at Standard Conditions
TCM	Trillion Cubic Meters of Gas at Standard Conditions
TD	Total Depth (of well), typically in MD
T-D	Time-Depth (referencing time to depth conversion of seismic data)
TVDss	Total Vertical Depth, measured below subsea datum
t-RFLP	Terminal-Restriction Fragment Length Polymorphism (microbiology)
UA	University of Arizona (or Arizona Board of Regents)
UAF	University of Alaska, Fairbanks
USGS	United States Geological Survey
USDOE	United States Department of Energy
Vp	Velocity of primary seismic wave component
Vs	Velocity of shear seismic wave component (commonly useful to identify GH)
VSP	Vertical Seismic Profile
WOO	Well-of-Opportunity

9.0 APPENDIX A: UNIVERSITY OF ARIZONA FINAL REPORT EXCERPTS

Under the leadership of Principle Investigators Dr. Robert Casavant, Dr. Roy Johnson, and Dr. Mary Poulton, the University of Arizona (UA) completed significant reservoir and fluid characterization studies from 2002 through 2008. This Appendix summarizes an edited version of significant accomplishments achieved by these UA studies. An Interval-of-interest (IOI) was initially established between lithostratigraphic markers PS-36 and L-31A (Figure A1). However, due to time constraints and resource limitations, the IOI was later shortened to encompass primarily the USGS Zone C unit (Figure A1). Therefore, analyses and interpretation of USGS Zone D and Zone B horizons were limited. In addition, log pattern analyses and paleo-depositional environment interpretations within Zone C sand packages suggest more fluvial and less marine-influence than prior studies. Mount Elbert-01 core sedimentology and palynology descriptions were not available to UA at the time of this work; lithostratigraphic interpretation of the Mount Elbert core indicates the B, C, and D unit sands are shallow marine to shoreface sands interbedded with marine and nonmarine lithofacies. Importantly, however, the well log-based cross-sections, isopach maps, and net sand maps within the Eileen accumulation Zone C chronostratigraphic correlation intervals were used to interpret distribution, geometry, and volumetrics of these gas hydrate-, associated free gas-, and water-bearing reservoir sands.

9.1 Regional Geologic Framework

A robust petroleum system is in place for the generation and emplacement of shallow gas hydrate and associated free-gas resources (Collett et al., 1988) on the central North Slope of Alaska. Current interpretations place these resources within the eastern portions of the Kuparuk River and the Milne Point units (KRU, MPU), and along the western edge the Prudhoe Bay Unit (PBU) (Collett et al., 1988). The majority of reservoirs are contained within a thick interval of Late Cretaceous to Late Tertiary stacked sequences of fluvio-deltaic and nearshore marine gravels, sands, and shales.

Regional structural mapping within the MPU and KRU indicates that gas hydrate and free-gas occur along the highly faulted, northeast-dipping flank of a large anticlinal structure (Casavant, 2001; Hennes, Johnson, and Casavant, 2004) This southeast-plunging antiform lies along a regional east-west trending basement antiform, known as the Barrow Arch, which coincides with the northern rifted margin of the Arctic Alaska terrane (AAT) that rifted and docked into its present position during the mid-late Mesozoic. Fault reactivation and structural inversion along weakened and long-lived basement fault blocks beneath the MPU and KRU areas have been linked to basinal fluid migration and variations in permafrost thickness. Periodic crustal shortening along the southern margin of the terrane continues to reactivate basement deformation across the major structural provinces (Casavant, 2001), which included continued segmentation and rotation of the Barrow Arch. Figure A2 illustrates the geologic setting of the study area.

Interpretations of 3-D seismic data within the MPU (Hennes, Johnson, and Casavant, 2004) and KRU (Casavant, 2001) reveal that the shallow package of gas hydrate-bearing sediments are extensively deformed by north- and north-northeast trending syn- and post-depositional faults. The presence of a diffuse and segmented northwest-trending structural hingeline can also be identified on seismic maps by (1) the alignment of termini of north- and north-northeast-trending faults, (2) alignment of inflections, jogs or offset of fault sets, (3) the offset/termination of some

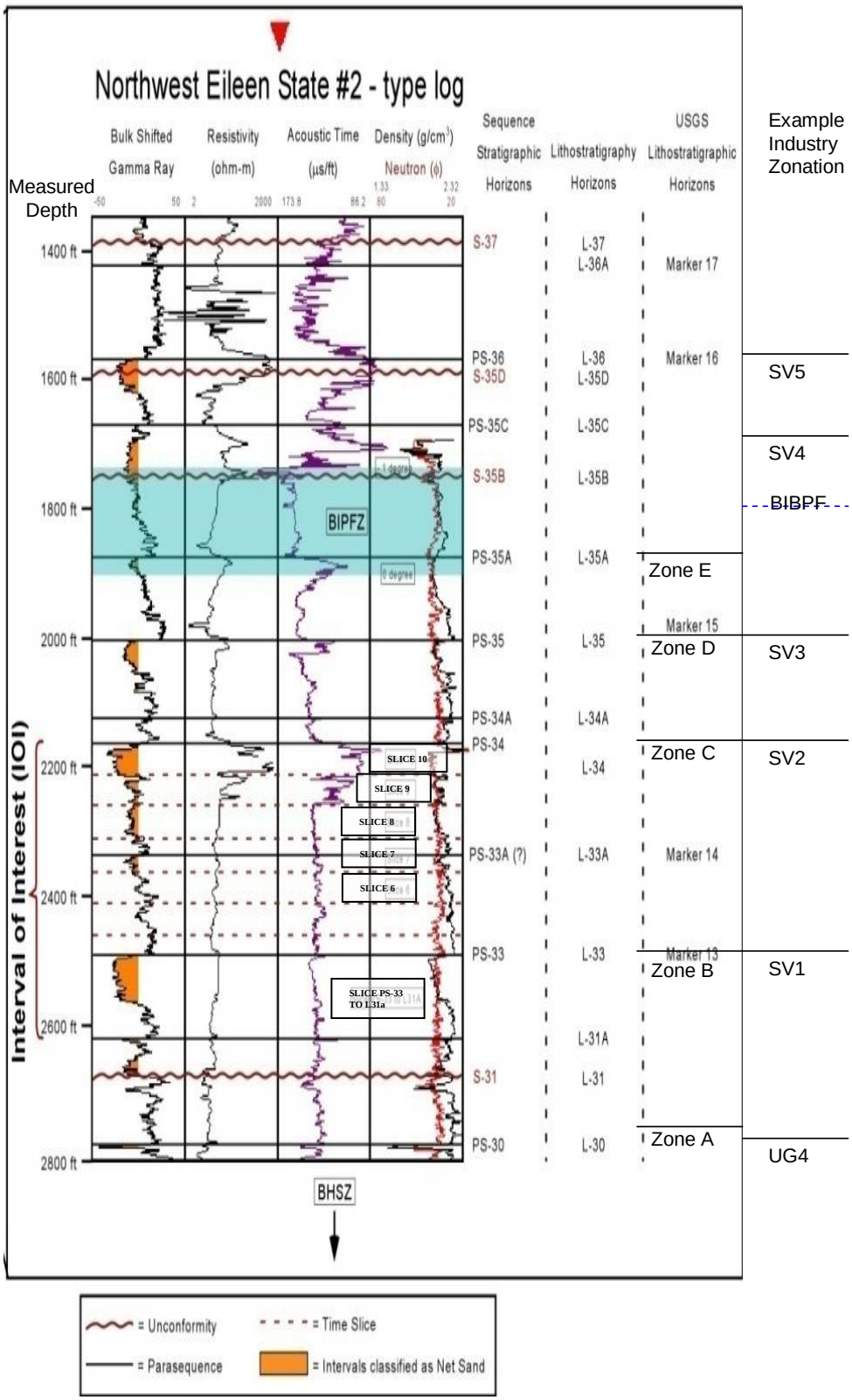

Figure A1: Type Log Northwest Eileen State #2, Eileen Accumulation showing UA, USGS, and industry zonation for the Sagavanirktok formation. UA chronostratigraphic slices 6-10 occur within Zone C as shown in the small boxes between the PS-33 and PS-34 horizons.

graben structures, and (4) first-order changes in the structural attitude of stratigraphic units downflank, although no Northwest-trending offset is resolvable in the vertical seismic sections. These hingelines have been linked to deeper fault zones that segment oil reservoirs and define important oil-water contacts within deeper Cretaceous-age reservoirs (Werner, 1987).

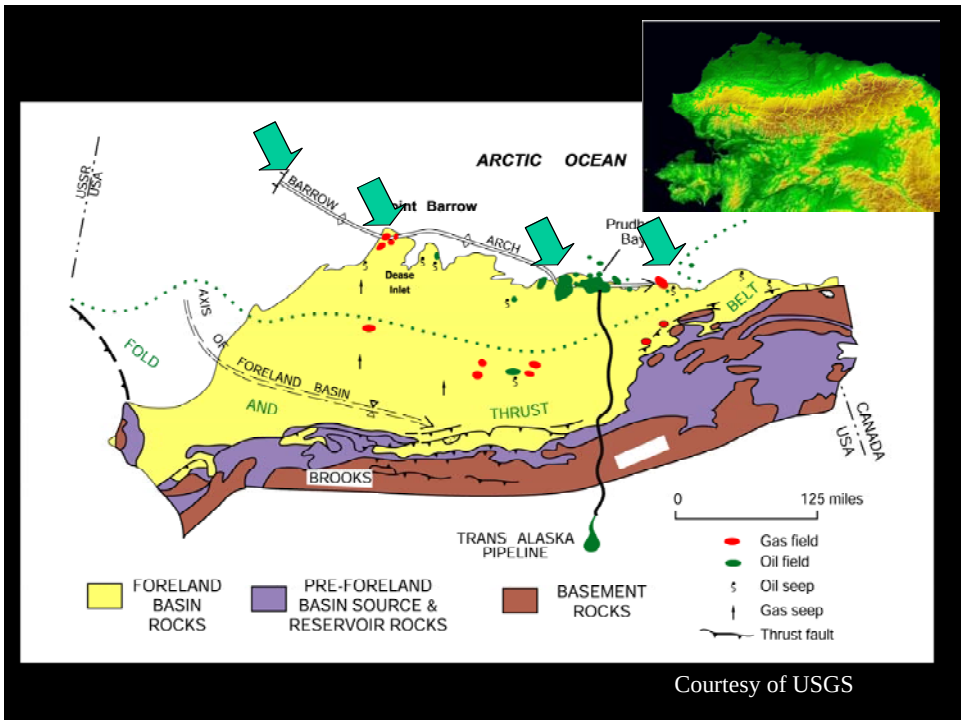

Figure A2: Generalized geologic setting of Arctic Alaska. The Barrow Arch approximates the northern margin of the rifted Arctic Alaska Terrane. Note that the majority of major gas and oil fields occur along the flank of the arch and/or in locations where major bends or offset occur along its axial trend.

Shallow fault displacements, vertical morphologies, and plan-view distribution suggest that the MPU area is dominated by down-to-the-east northeast-trending and down-to-the-north northwest-trending systems of normal faulting. A similar conjugate set has been illustrated in numerous studies.

Regional stratigraphic and geophysical studies show that periodic reactivation along basement block boundaries resulted in localized sagging and structural inversion along zones of weakened crust that were constrained to the margins of basement blocks. In numerous locales across the AAT, a morphotectonic analysis suggests that basement faulting has long influenced the morphology and location of both modern and ancient fluvio-deltaic, nearshore marine systems, and upward migration of fluids and heat-flow (Casavant, 2001; Rawlinson, 1993; Casavant and Miller, 1999a). Structural mapping of shallow seismic sequences within the MPU area revealed a certain degree of spatial correlation between subsurface structure and geomorphic features at the surface as was proposed in earlier studies (Casavant, 2001; Rawlinson, 1993). Such spatial associations suggest the influence of shallow basement control on the morphology of coastal and fluvial elements across the Arctic coastal plains.

Seismic attribute analysis and geologic mapping confirm that reservoir continuity is controlled both by fault compartmentalization and by changes in facies type and geometry. Regional lithostratigraphic and chronostratigraphic correlations show these impacts of depositional facies on reservoir continuity. Lithostratigraphic correlation across the study area confirmed the presence of at least six distinct correlative gas hydrate-bearing units defined in earlier studies (Collett et al., 1988). The sequence stratigraphic framework in this study implies a higher degree of reservoir heterogeneity than those in previous studies. The distribution and quality of reservoir sands relates not only to rapid changes in depositional environments and facies, but also to the preservation and erosion of units that can be linked to numerous intraformational unconformities and other structural features (Casavant et al, 2004; Manuel, 2008). This study of facies, sand body dimensions, and related seismic facies mapping helped develop a more accurate reservoir description model needed for estimating volumetric and recovery factors (Manuel, 2008).

Generally, Eileen accumulation gas hydrate-bearing reservoirs appear to be influenced by a combination of structural-stratigraphic trapping on the upper flanks and axes of structural highs, where the presence and thickness of porous and permeable reservoir facies is adequate. This is not unlike constraints required to develop the petroleum system for deeper, oil-prone marine and fluvial sandstone and conglomerate deposits encountered in the area. Gas hydrate forms within the hydrate stability pressure-temperature window defined by modeling. This study shows that the base of the ice-bearing permafrost undulates as a function of lithology and thermal gradients. The expert system and neural network used for well log analyses did not find evidence of gas hydrate in wells outside the favorable geologic areas identified in this report.

9.2 Lithostratigraphic Correlations

A lithostratigraphic framework was developed during initial studies which identified several regionally distinguishable geologic horizons based principally on correlating similar petrophysical well log patterns. Most of these lithostratigraphic horizons compared well with previous lithostratigraphic work (Collett et al., 1988; Figure A1).

This study interpreted changes in well log character across the AOI below and above major horizons. These changes were later interpreted in facies characterization studies as different depositional environments ranging from onshore fluvial point bars to offshore marine mouthbars and prodelta shales (Figure A3 and Table 18). Variations in depositional settings were not obvious in the early stages, but as work progressed into mapping lateral changes in sand quality, quantity, and connecting potential reservoir bodies, these discrepancies warranted reconstruction of the stratigraphic framework. Initial net sand and facies characterization maps connected thin interbedded and abundantly rich sand bodies together over large areas. Both fluvial and marine sand bodies displayed an unrealistic amount of connectivity in a fashion that is not demonstrated in modern depositional environments (Casavant et al., 2004). Realizing the shortcomings of this early lithostratigraphic framework, a chronostratigraphic (sequence stratigraphic) framework (Van Wagoner et al., 1990) was constructed as discussed below.

9.3 Chronostratigraphic (Sequence Stratigraphic) Correlation

In a chronostratigraphic framework, correlating time equivalent units is accomplished by identifying major sequence and parasequence units. A diagram emphasizing this process is provided in Figure A4. Several sequence and parasequence units were identified within the Interval of Interest (IOI – Figure A1), which are displayed in cross-section in Figures A3, A5, and A6.

9.3.1 Interval of Interest (IOI) and Correlation Summary

The regional IOI was defined in this study to extend from parasequence marker 34 (PS-34) down to lithostratigraphic marker 31A (L-31A). This interval contained the most prominent and thickest gas hydrate-bearing sand unit (USGS Zone C) that was cored in the Northwest Eileen State #2 well (Figure A1). Although some minor sand-rich intervals above and below the IOI also contain gas hydrate, these were not evaluated in this study due to time and program resource limitations.

Correlation studies revealed that most defined lithostratigraphic boundaries coincided with chronostratigraphic boundaries. All seventeen regional cross-sections (Figure A7) used the PS-36 marker as their stratigraphic datum (e.g. Figure A6). Examination of various cross-sections throughout the AOI revealed some general trends. An increase in interval thickness is shown to progress from southwest to northeast over the AOI. Spatial relationships, such as the termination of parasequence units by unconformities and changes in log character, are interpreted to relate to structurally-controlled depositional changes that are predominately oriented in the same direction. This spatial relationship suggests that there is a significant connection between the timing of structural and stratigraphic events.

9.3.2 Sequences

Identifying major sequence units was one key element used to create this chronostratigraphic framework. A sequence by definition is a relatively conformable succession of genetically related strata bounded at its top and base by unconformities and/or their correlative conformities (Van Wagoner et al., 1990). An unconformity is a surface separating younger from older strata, along which there is evidence of subaerial erosional truncation or non-deposition and, in some areas, correlative submarine erosion or subaerial exposure, with a significant hiatus indicated (Van Wagoner et al., 1990).

During initial efforts to identify regional sequence units, unconformable surfaces were identified by conducting a pattern analysis of the natural gamma ray log. For this analysis, seventeen cross-sections were generated over the AOI (Figure A7). These cross-sections were oriented parallel and perpendicular to the regional strike and dip (Figures A7 and A8). For each cross-section generated, a large transparency was overlain to help group the natural gamma ray log response. Four separate groups of patterns were decided upon to classify the gamma ray log response: coarsening up, fining up, sandy, and shale-rich intervals. This gross classification approach was initially performed to help reveal any major patterns. An example of this procedure is given in Figure A9 with corresponding colors to emphasize classified intervals.

Initial interval grouping was conducted on similar gamma ray log responses greater than 60 feet. This data corresponds to the black arrows in Figure A9. After reviewing these initial results, many intervals were generally interpreted as under-classified. Acknowledging this interpretation,

a second and more refined pattern analysis was conducted as shown by the red arrows in Figure A9. This analysis appeared to reveal more of the rapidly changing nature displayed in the gamma ray log. Blocky shades of color were added to this pattern analysis to enhance changing behaviors.

From this initial work, interpretation of intraformational unconformities commenced. The criteria for classifying an unconformity was to identify an interval that displayed interpreted pattern characteristics of a fluvial unit, usually classified as a fining-up or sand-rich interval, lying directly above and truncating a marine unit, usually classified as a coarsening-up, sandy, or shale-rich interval. This approach was adopted in this work because of the abrupt behavior observed as sea level rapidly drops during the transition period from a high to low stand system tract, as described by Van Wagoner, et al (1990).

A number of intraformational unconformities were interpreted and correlated across the AOI. Some of the interpreted unconformities could only be locally correlated. Other unconformity horizons were difficult and sometimes impossible to correlate, particularly in fluvially-dominated regions. These studies were iterative and all unconformity horizons underwent a number of circular well log "ties" throughout the AOI. From this research, three well-defined regional intraformational unconformities were identified and labeled as S-31, S-35B and S-35D (Figures A3, A5, and A6). Besides juxtaposing fluvial units deposited over marine deposits, some of these unconformity horizons truncate underlying lower parasequence units. This is especially evident in the stratigraphic cross-sections provided in Figures A3, A5, and A6. More localized unconformable surfaces maybe present within the AOI, but evidence for their regional extent was not noted from the well log patterns. It is recommended that future confirmation of these well log-based sequence boundaries be obtained through high-resolution seismic interpretation and core descriptions wherever possible.

9.3.3 Parasequences

Identifying parasequence boundaries began after identifying major sequence boundaries. By definition, a parasequence is a relatively conformable succession of genetically related beds or bedsets bounded by marine-flooding surfaces or their correlative surfaces (Van Wagoner et al., 1990).

Within the IOI, several marine-flooding surfaces were observed (Figure A6). A marine-flooding surface on the natural gamma ray well logs typically exhibits a more radioactive (higher gamma ray) reading relative to the shale unit within which it usually resided. Difficulties emerged in correlating maximum flooding surfaces throughout the AOI, mostly due to the rapidly changing gamma ray log character from well to well. Some of this behavior could be attributed to inconsistencies from using different well log tools to acquire the data and others may be due to well logs being run after metal casing was installed, which "muted" the log response. Moreover, a larger part was dependent on the lateral position in which the well resided relative to the paleodepositional environment in which the unit was deposited, which became more evident during the facies characterization mapping.

Instead of correlating the maximum marine-flooding surface, correlation of the base of the marine shale that contained the maximum marine-flooding surface was completed. This action was warranted because many maximum flooding surfaces were complicated to identify, due to

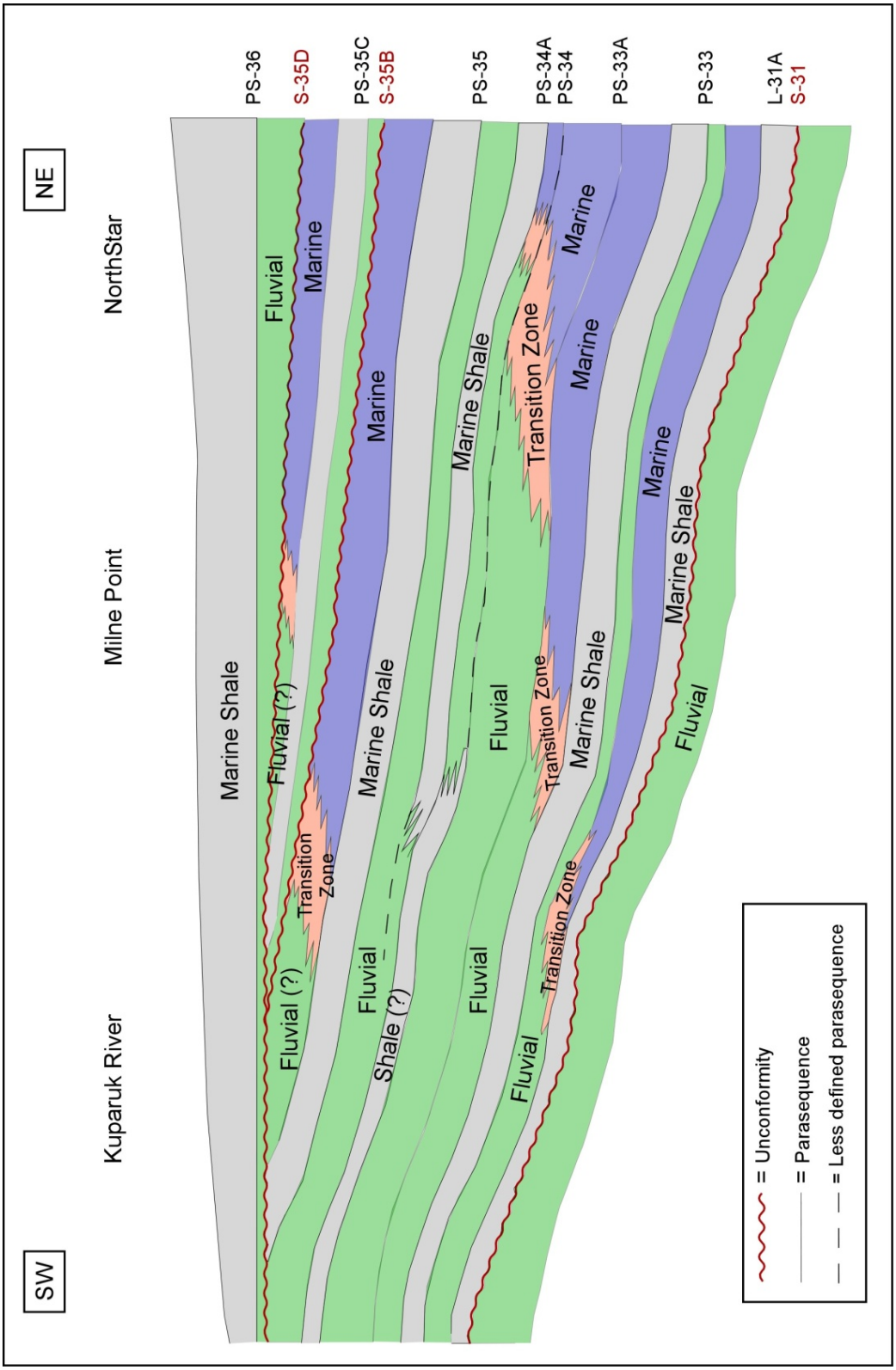

Figure A3: A diagrammatic stratigraphic cross-section representing the interpreted depositional environments that exist throughout the AOI. This cross-section was interpreted from the stratigraphic cross-section in Figure A6.

the reasons previously given, and some did not appear to extend into up-dip fluvial-dominated regions. In many instances the maximum marine-flooding surfaces were in approximately the same position as the base of the marine shale unit that encased them. A detailed figure using the parasequence 36 marker as a stratigraphic datum shows multiple parasequence units extending across the AOI (Figure A6).

Several major parasequence boundaries are identified in the AOI. Within these, one boundary contained an anomalous shale-like surface, labeled PS-34, which correlated well throughout most of the AOI. This surface is interpreted as a coastal plain mudstone or tidal flat mud based on its lateral occurrence, abrupt truncation, and pinch out behavior. Correlating this horizon in the northwest portion of the AOI was difficult because the sandy nature of this horizon rapidly changes to the northwest. This horizon is the only parasequence marker that displays this behavior. In finalizing the boundaries of each parasequence unit, numerous circular well "ties" were completed to verify the accuracy of the lateral correlations for each boundary.

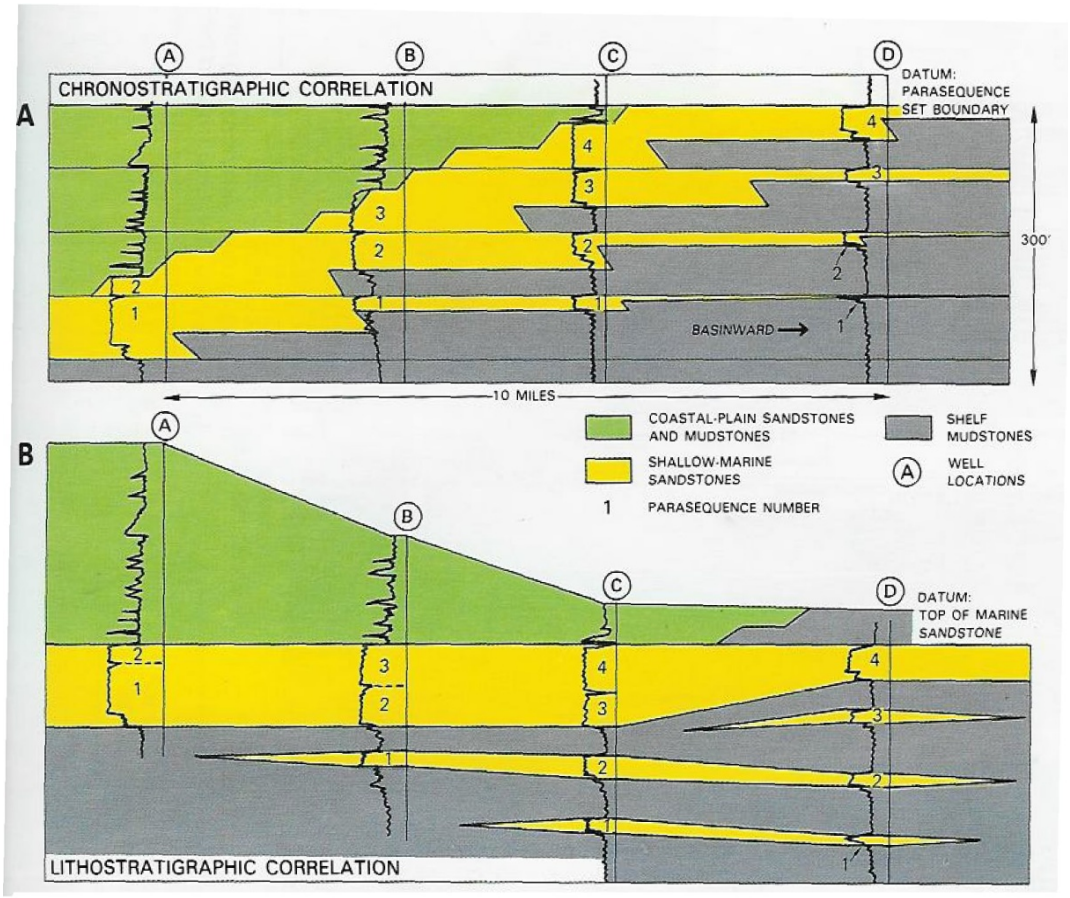

Figure A4: A diagrammatic sketch cross-section representing the drastic differences between a lithostratigraphic and chronostratigraphic framework system (Van Wagoner 1990).

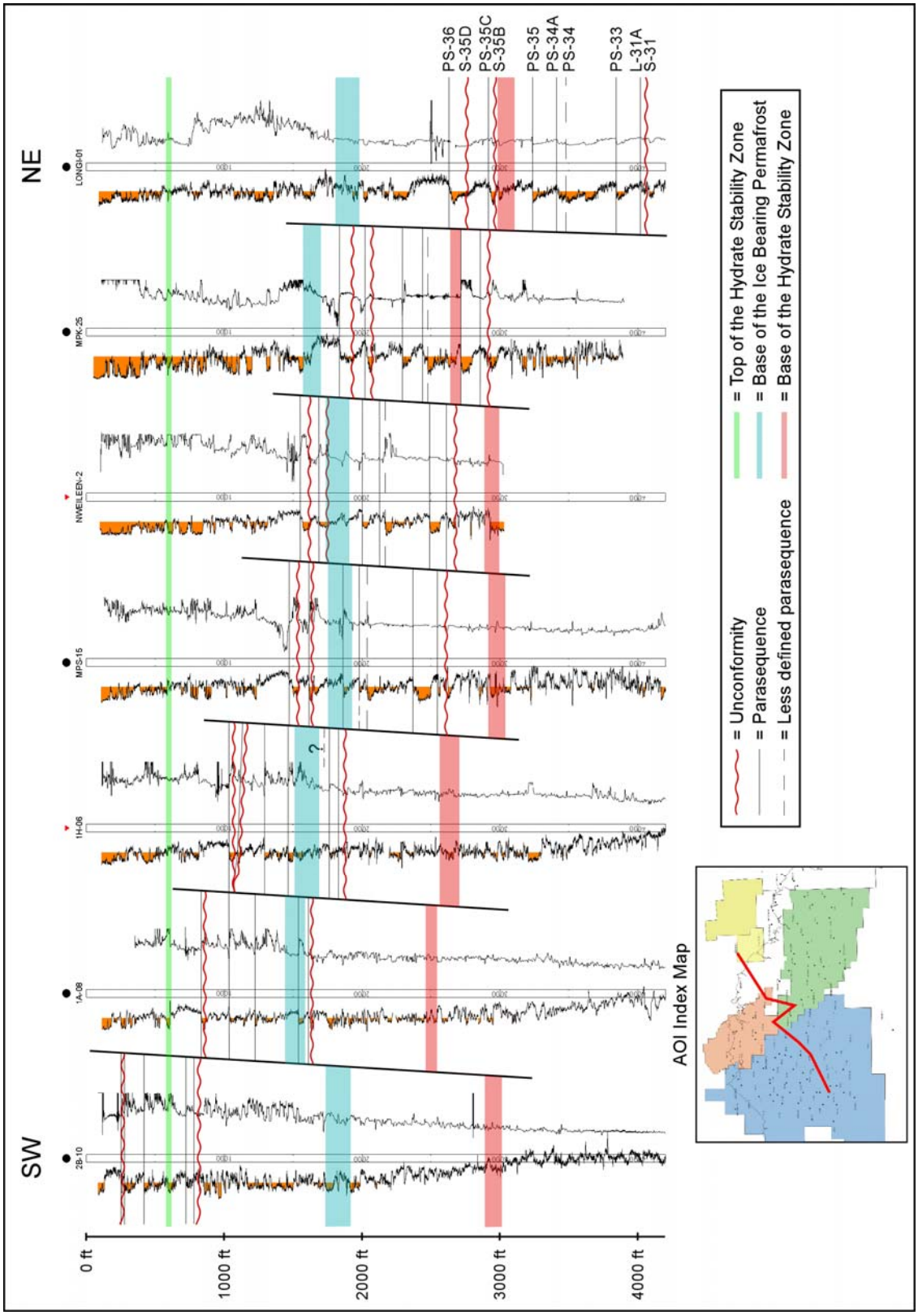

Figure A5: A northeast oriented structural cross-section, showing the PS-36 datum and other horizons, illustrates identified sequence and parasequence horizons in their present day position

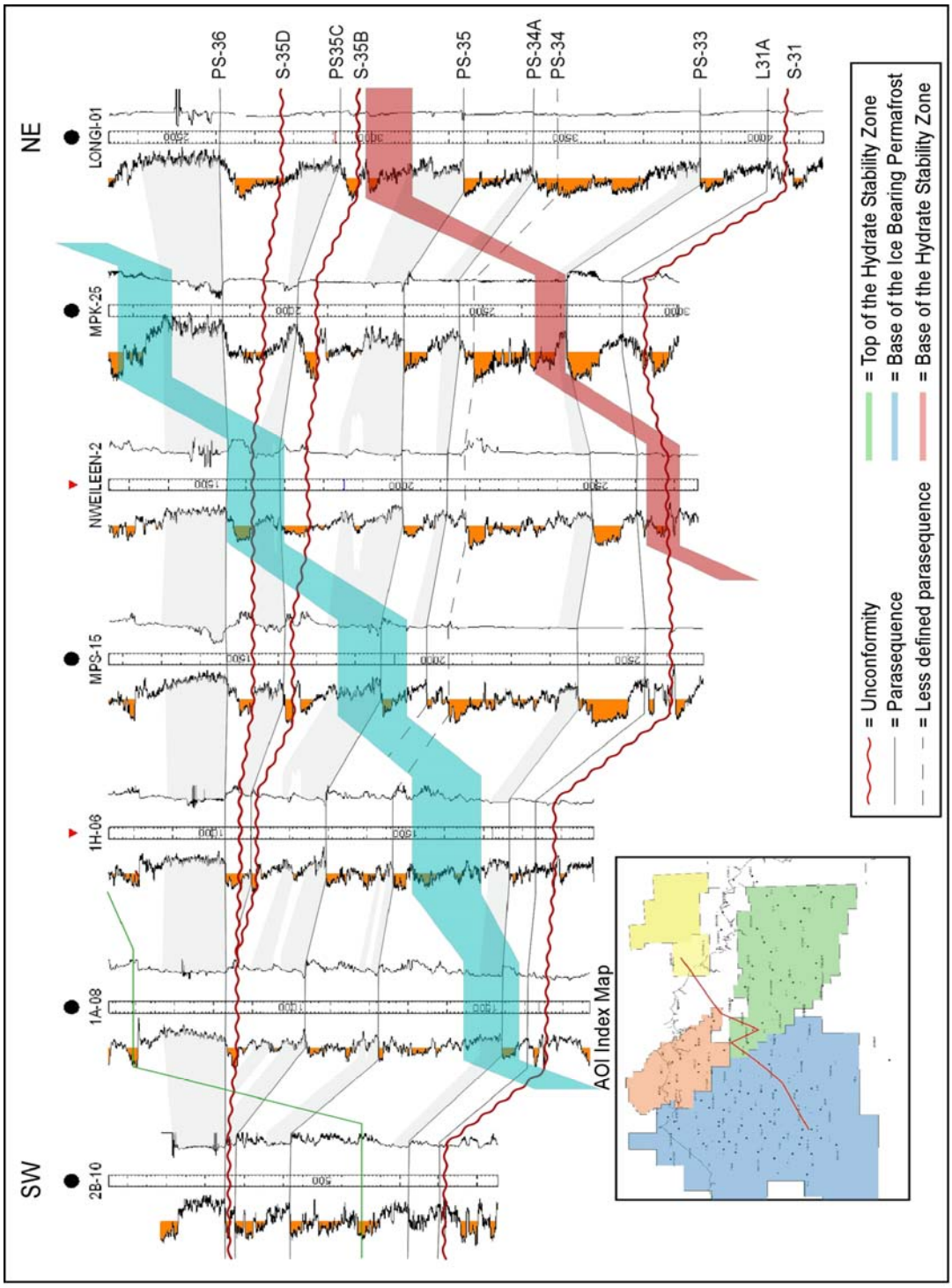

Figure A6: A northeast oriented stratigraphic cross-section, using PS-36 marker as the stratigraphic datum, illustrates sequence and parasequence horizons in the AOI. This cross-section provides a good example of the complexity encountered during the correlation studies. Note the number of lower parasequence units terminated by the upper unconformities. The green, blue and red areas respectively represent the intersection of the Top Hydrate Stability Zone (THSZ), Base Ice-bearing Permafrost Zone (BIPFZ) and Base Hydrate Stability Zone (BHSZ) in this cross-section.

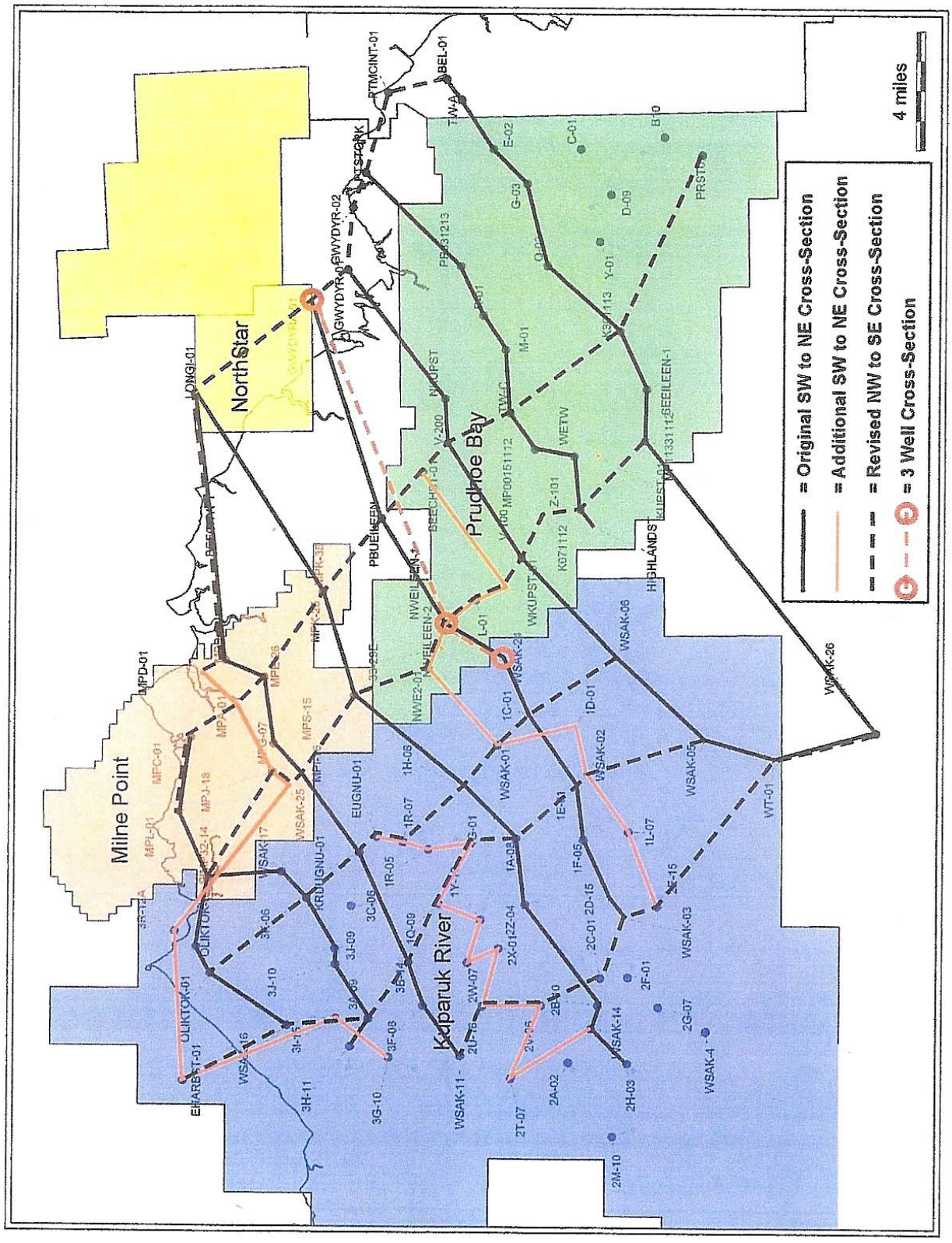

Figure A7: A cross-section base map displaying the location of all cross-sections generated in this study. The three well cross-section displays the location of the wells used in Figure A9.

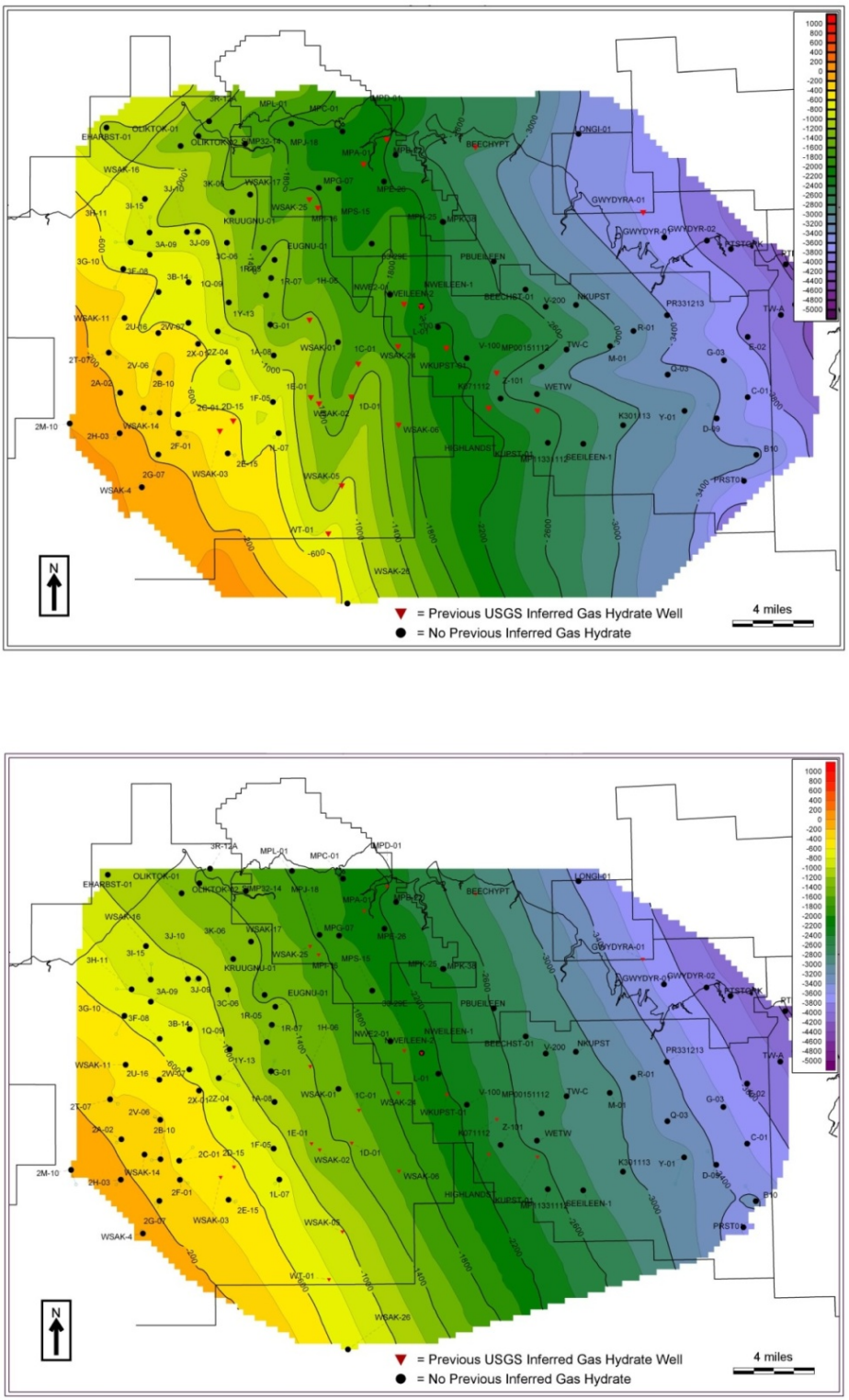

Figure A8: Two structural contour maps on parasequence 34 horizon are displayed. The upper map represents a hand-contoured map of this horizon by R. Casavant. The lower map was generated using GeoPlus Corporation – PETRA computer program. Notice the difference in contour interval location between both maps.

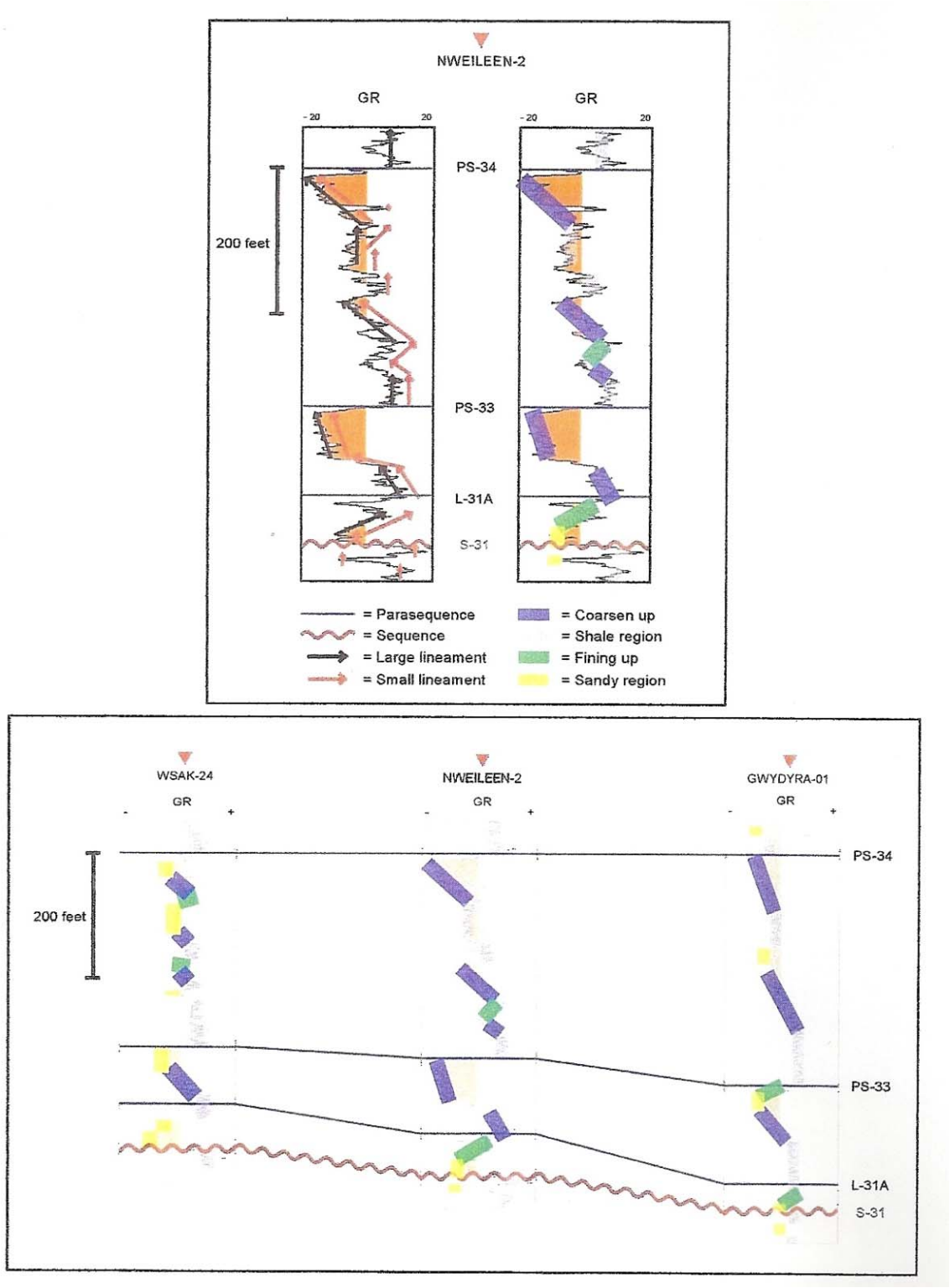

Figure A9: An illustration presenting the log pattern analysis conducted in this study. The Northwest Eileen State #2 type log was used to provide a detailed example of the pattern analysis and a three well cross-section (Figure A7) with corresponding colors to provide a visual example of this research method.

More parasequence boundaries were identified in the AOI than discussed above. Many were locally present and not regional in extent. One notable parasequence boundary, labeled PS-33A, presented difficulties in the correlation phase, especially within the KRU, due to the dominant surrounding fluvial deposits. The importance of this boundary did not manifest itself at this point in the study, but during the net sand mapping phase the importance of this boundary became more apparent (Net Sand – Time Slice 8, Section 9.5.5.4).

9.4 Structural Characterization

Three separate fault maps across the AIO were compiled and sutured together to create one regional composite fault map for these studies (Figure A10). The first fault map was obtained using thesis work by Hagbo (2003). This map covers the MPU area (orange in Figure A10). The location of the faults mapped in this unit was completed by using fault trace maps created on lithostratigraphic 34 and 33 horizons (Hagbo, 2003). These fault trace maps were chosen because this interval is equivalent to the IOI. The average distance between each fault location on both horizon maps was used in the final placement for all faults displayed within the MPU area. Throughout the MPU area, the majority of faults appear nearly vertical in all seismic sections (Geauner, personal communication) and many of the fault traces for both horizons reside on top of one another.

The second fault map covers the majority of the KRU (blue in Figure A10) and was compiled from previous research (Casavant, 2001). These faults were interpreted from a black and white artificially-illuminated IHS (intensity, hue, saturation) image of the fault structure at the top of the Kuparuk River Formation at depths ranging from 5,800-6,200 feet below mean sea level.

The third fault map was a compilation of faults from Carman and Hardwick (1983). These faults were imaged at depths ranging from 8,500-9,200 feet below mean sea level in the PBU (green in Figure A10). Selected fault traces were digitized for this study.

During the compilation phase, the KRU and PBU fault maps were geographically registered with one another. This manual manipulation of the data can inherently introduce some errors into the map. In addition, although shallow seismic data shows that most faults are near vertical, no adjustment of each data set to a common datum was made. In evaluating the quality of this regional composite fault map, some observations were noted. The north-south fault trends that exist in the MPU area, when extended south, align well with deeper faults present within the KRU area. The northwest-trending zone (labeled in many figures as NW2) within the MPU area is also a dominant trend within the PBU area. Hennes' (2004) thesis observed that fault throw decreases and fault terminations are noted in this region. Projecting the PBU area faults into the MPU area, the location of major faults are approximately the same as those within the northwest trending zone. This spatial relationship suggests that deep seated faults extend from both the KRU and PBU areas into the MPU area and that issues such as fault frequency and termination are connected with deeper structure (Casavant, 2001; Casavant et al., 2004).

One regional structural map was created for the IOI at the top of the parasequence 34 marker. This map was produced using GeoPlus Corporation - PETRA mapping software modular. A highly connected least squares algorithm was employed to create this contour map. Analyzing the map reveals a structural northwest-trending strike with a regional dip down-to-the-northeast

(Figure A8 – lower figure). Besides the pronounced first-order northwest-striking fabric expressed in the map, no other obvious trends were noted.

This computer-generated map contrasts with a variety of second-order features that are interpreted to exist when a detailed hand-contoured map was generated using the same data (Figure A8 – upper figure). A structural hand-contoured map, provided by R. Casavant, was digitally recreated in PETRA using guided contour lines and control points (Figure A8). Visual examination of this map revealed an oval shaped north-oriented basin interpreted to exist in the south-central part of the MPU. This area is proposed to contain a pull-apart basin (Figure A11) that may be under-represented by the computer generated structural map (Casavant et al., 2004). Mapping also inferred the continuation of the MPU basin complex southward into the KRU area, which may contain additional gas hydrate-bearing sands. This area in which Casavant and others (2004) proposed potential gas hydrate-bearing-sands to be related to another pull-apart basin, is further investigated in the net sand and net pay sections of this report.

9.5 Chronostratigraphic Slice, Net Sand, and Facies Mapping

9.5.1 Net Sand

All wells within the AOI were analyzed to determine a net sand cutoff value on an individual well basis. For each well, all gamma ray (GR) logs were printed between the PS-36 and L-31A markers. Data between these horizons was chosen to determine a net sand cutoff since the original IOI extended up to the parasequence 36 horizon boundary. Due to time and resource constraints, the thickness of the IOI was later shortened.

9.5.2 Facies Characterization

Facies characterization is a method of identifying specific log response patterns from downhole geophysical tools that correspond to specific depositional environments that are relevant to the geologic setting being investigated (Figures A12 and A13). In this study, the geologic setting in the AOI was in many ways similar to other fluvio-deltaic, nearshore marine siliciclastic systems described by other researchers (Saxena, 1979; Van Wagoner et al., 1990). Using all the available log data for each well, eight general classification categories were generated and listed as follows: coastal plain mud/siltstone, point bar, fluvial channel, interbedded fringe, distributary mouth bar channel, distributary mouth bar, prodelta shale, and marine shale (also see Figure A3 and Table 18). Along with these classification categories, many intervals also expressed an additional fringy character on the logs. This fringy expression correlated with wells located near or within a transition zone between fluvial to marine environments (Figure A13). When this behavior was identified, an additional fringy description was added to the end of an initial characterization category (e.g. “distributary mouth bar fringe”). Examples of the facies characterization procedure are shown in Figures A12 and A13 with a corresponding net sand and paleodepositional map in Figure A13. This classification method is later combined and interpreted with all the net sand and paleodepositional maps to help determine the lateral continuity of potential reservoirs.

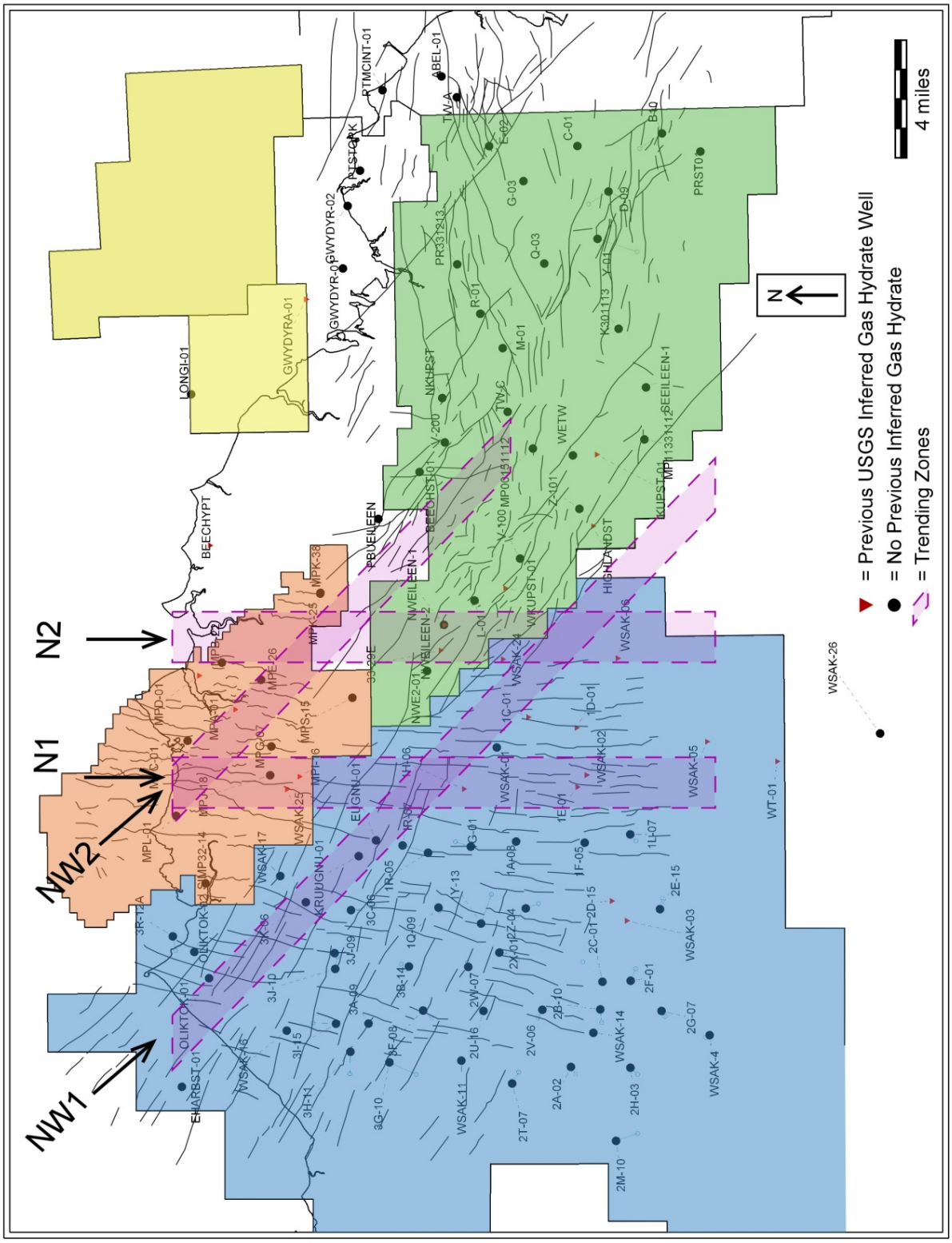

Figure A10: A composite fault map across the AOI. This fault map was created by combining three separate data sets together. The faults in the MPU (orange) were taken from Hagbo (2003). Faults for the KRU (blue) are taken from Casavant (2001). Faults from the PBU (green) were compiled from previous work (Carman and Hardwick, 1983).

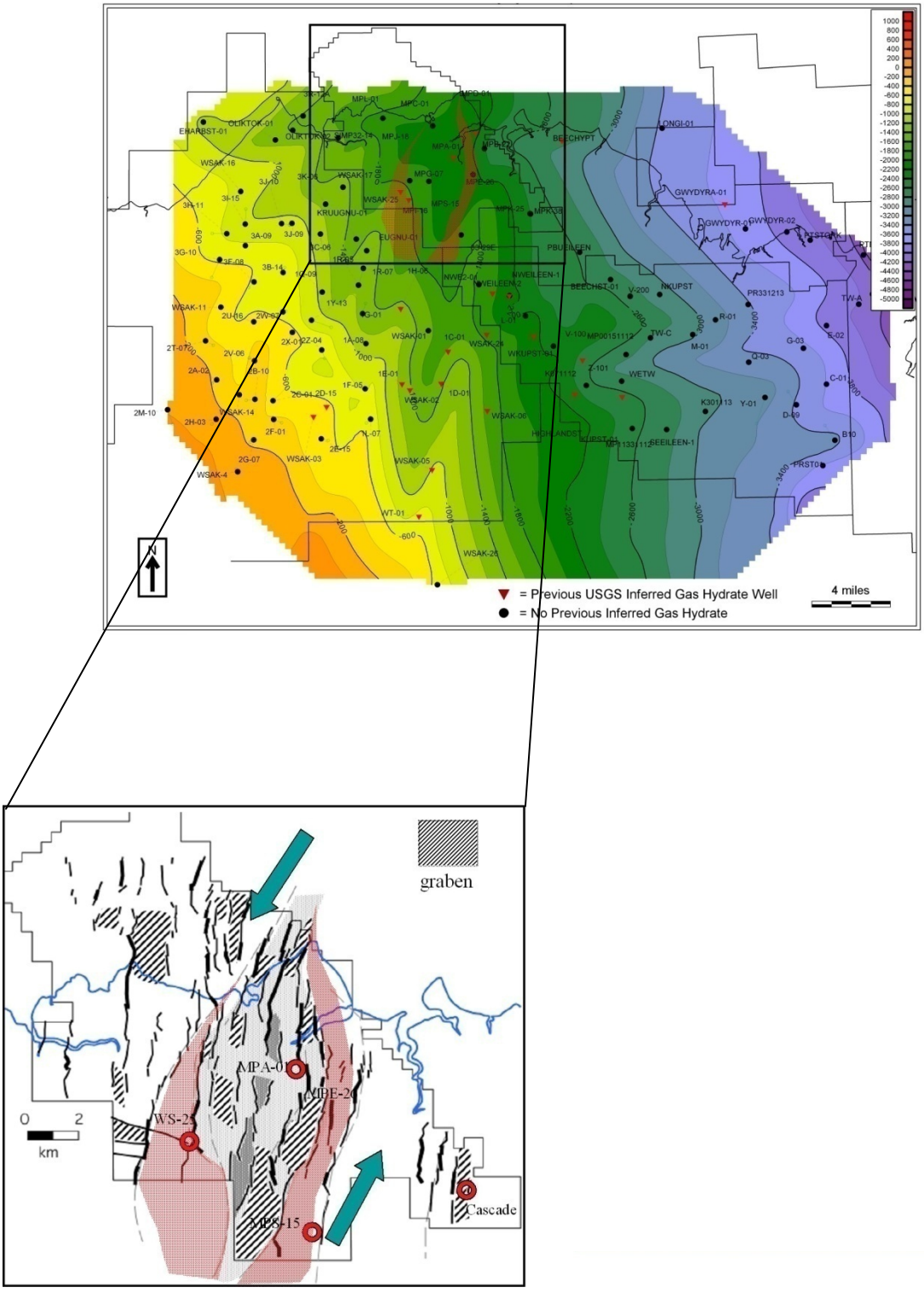

Figure A11: A diagram relating hand-contoured structure map to the proposed pull-apart basin that is inferred to exist in the MPU (Casavant, 2004)

9.5.3 Time Slice Horizons

Time slice mapping is a simplified method of breaking down a complex three-dimensional data set into interpretable two-dimensional map products (Casavant et al., 1999). In creating a time slice map, time slice horizons must be defined. Once all sequence and parasequence boundaries were identified, all boundary markers were imported into PETRA from working cross-sections. Once imported, 50-foot true vertical depth time slice horizons were computed between each parasequence set in the IOI. A time slice horizon is a marker that is calculated below a parasequence boundary within the chronostratigraphic framework. This horizon is intended to "slice" the interval incrementally into smaller genetically related sections to help reveal lateral and vertical variations within the reservoir (Figure A4). Figure A1 shows these time slice horizons within the IOI in relation to industry and USGS horizon nomenclature.

Grouping of parasequence and time slice horizons defined the time slice intervals for mapping purposes. These intervals are labeled as follows from deep to shallow: Slice L-31A to PS-33; Slices 6, 7, 8, 9, 10; and PS-34. Slices 6 through PS-34 incrementally divide the top 250 feet below the PS-34 horizon. The lower time slice horizons (Slices 5, 4, 3, 2, and 1) in the parasequence bounded by the PS-34 to PS-33 markers are not displayed in this study since the majority of the maps generated show large areas rich in shale content. The stratigraphic position of the time slices are shown as small boxes on the type log within the IOI in Figure A1. These slices correspond to reservoir sand intervals B and C of the USGS zonation (Collett et al., 1988).

9.5.4 Net Sand and Facies Characterization Mapping

Evaluation of the lateral and vertical distributions of potential reservoir sands within the AOI resulted in generation of net sand and facies characterization maps. Using the time slice horizons described above along with the GR_SAND_SHALE curve and PETRA's computing capabilities, net sand totals for each time slice interval were calculated. For all depths that registered GR readings beneath the 0 API GR cutoff value, these interval lengths were classified as net sand regions and consequently their thicknesses were summed to provide the total net sand footage for that interval. After all the net sand footages were calculated for every interval, initial net sand contour maps were generated using PETRA. In these initial maps, a highly connected – least squares algorithm was employed. The intention of creating these maps was to gain a sense of the sand distribution, but these maps were not used as final net sand maps since their appearance was a direct function of a mathematical algorithm and since they did not incorporate geologic information that influence sand distribution (e.g. faulting, facies type, Figures A10 and A12-14).

Quality control standards were addressed next based on the appearance of the initial contour maps. Areas with closely spaced wells that displayed drastic differences in net sand totals were first re-evaluated to verify the accuracy of the totals. In most cases, abrupt changes in sand thickness also reflected changes in structure and stratigraphy, so totals were left unchanged. In only a few wells, net sand cutoff values were either over- or under-estimated. In these situations, adjustment of the net sand cutoff value was necessary and sand totals for all intervals were recalculated. In other circumstances, such as two or more wells originating from the same well pad (e.g. MPU K-25 and MPU K-38), the average net sand totals between these wells was used to represent the net sand content for the area. Since producing a regional analysis of sand distribution was a key objective, using the average values in closely-spaced wells was deemed acceptable. If more localized mapping of net sand distribution is ever required, contouring both

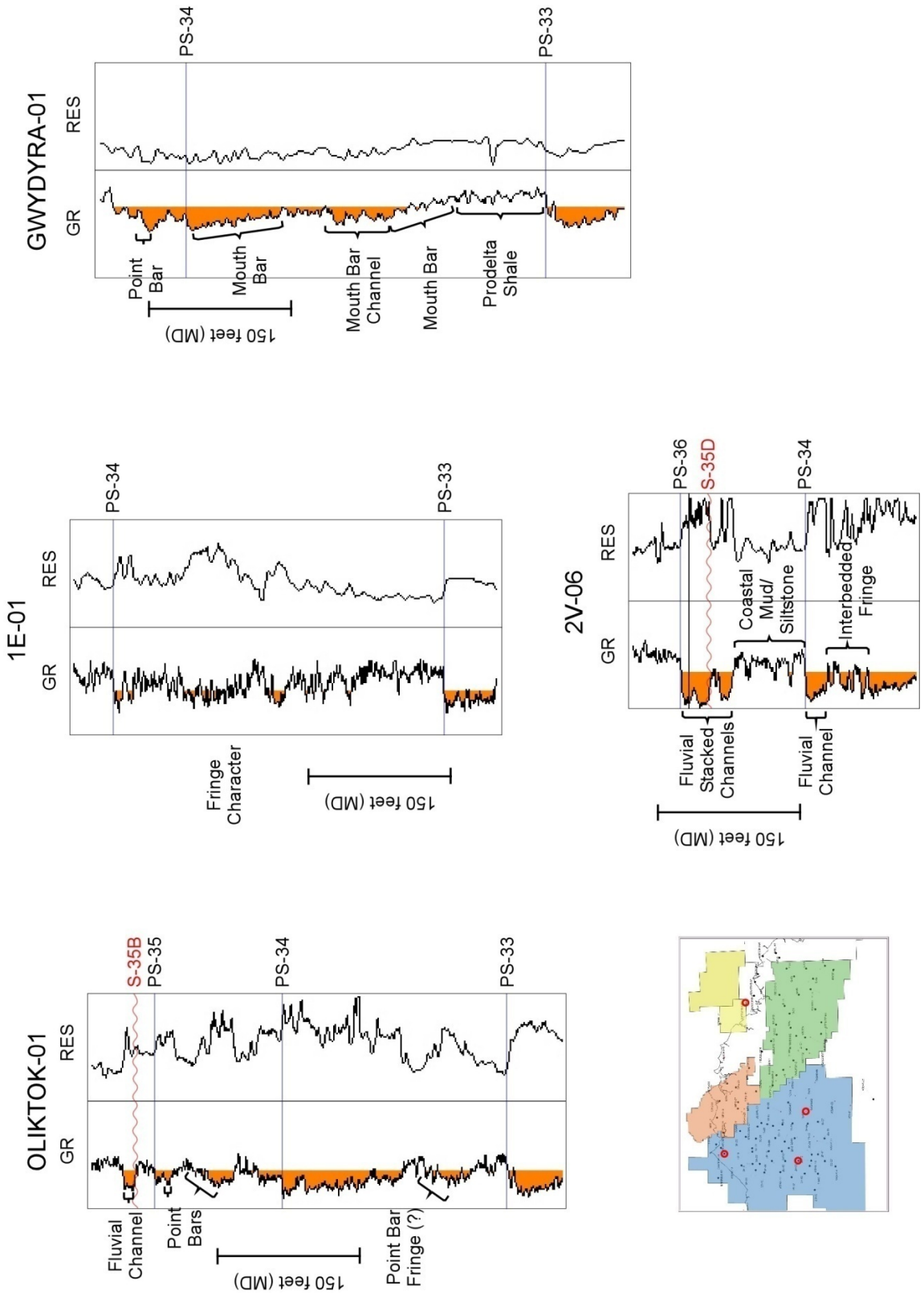

Figure A12: A facies characterization map providing well log based examples of the classification categories used during the facies characterization phase of this study

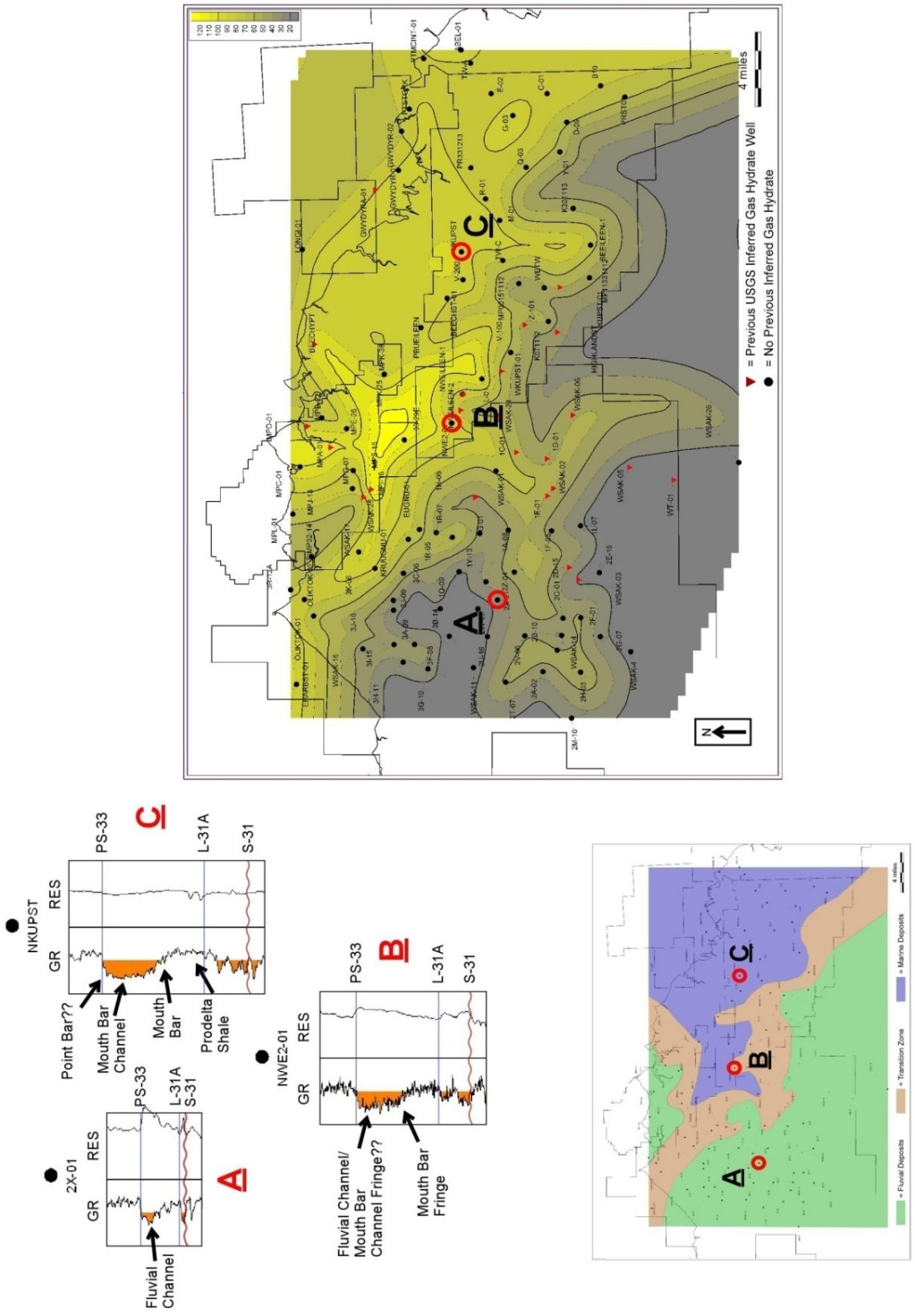

Figure A13: Diagram relating facies characterization to sand content and paleo-deposition

values independent of each other is recommended to reflect local structure and stratigraphic changes. Other cases that warranted quality control measures occurred when two GR logging runs had been merged together within one of the time slice intervals. The interval totals above and below the GR log merge used different cutoff values and were evaluated separately. In these cases, net sand totals for that interval were not used.

Once all quality control checks were complete, interpretation of facies types was performed for each interval. For many time slice map intervals, more than one facies type was present, which suggested that two or more depositional episodes occurred within the map intervals. An attempt to slice the intervals into smaller units (less than 50 feet) to have only one depositional episode represented proved to be impractical since variations at this scale could not be tracked over large distances. In many cases, more than one facies type was interpreted. To simplify this situation, the dominant facies type was labeled on all maps. A strong correlation between facies type and net sand was discovered and hand-contouring of net sand totals followed (Figure A14).

Several versions of hand-contoured net sand maps were created. Each map reflected different sand thickness trends and displayed various ways of contouring the same data. Certain trends imposed such as favoring regions where either sand or shale was interpreted, based on structural-stratigraphic research (Collett et al., 1988; Hagbo, 2003; Hennes, 2004; Casavant et al., 2004). Other factors taken into account in net sand mapping included adjustments based on structural and stratigraphic changes that occurred consistently over multiple time slice maps. These areas are referred to as “trending zone” in this report and in map figures. Contouring in areas with little well control was influenced by all factors mentioned above along with the facies characterization displayed in certain regions. An example of using the facies characterization to help contour net sand maps was especially relevant in more fluvially-influenced areas where sand-rich intervals were interpreted to not connect over large distances as commonly shown in models of modern depositional environments. Evenly spaced contour lines were drawn to display gradational changes. This was done to help compensate for areas in which the low well density and regional-scale facies characterization analysis precluded more precise definition. Thus, the tightening or spreading apart of contour lines was not warranted in those areas. Final maps were created to incorporate geologic interpretations and major trends that existed in multiple map versions. When digitizing the final net sand maps, control lines and points were used to help constrain the map grids and to best replicate the final hand-contoured maps. Although a highly connected – least square algorithm was used for gridding, its influence on the final outcome was minimal.

9.5.5 Time Slice Mapping

This section describes each series of time slice maps for all horizons within the IOI. Starting from the lowest section and moving upward, this discussion reveals study results in chronological order.

9.5.5.1 Time Slice between PS-33 to S-31A

The PS-33 to S-31A maps are located in Figures A15 and A16. Figure A1 shows the stratigraphic position of this interval. The color scales for these maps differ from the rest of the time slice horizon maps because this is the only series of maps generated that includes multiple parasequence horizons. All the other map slices were at higher resolution and subject to the 50-

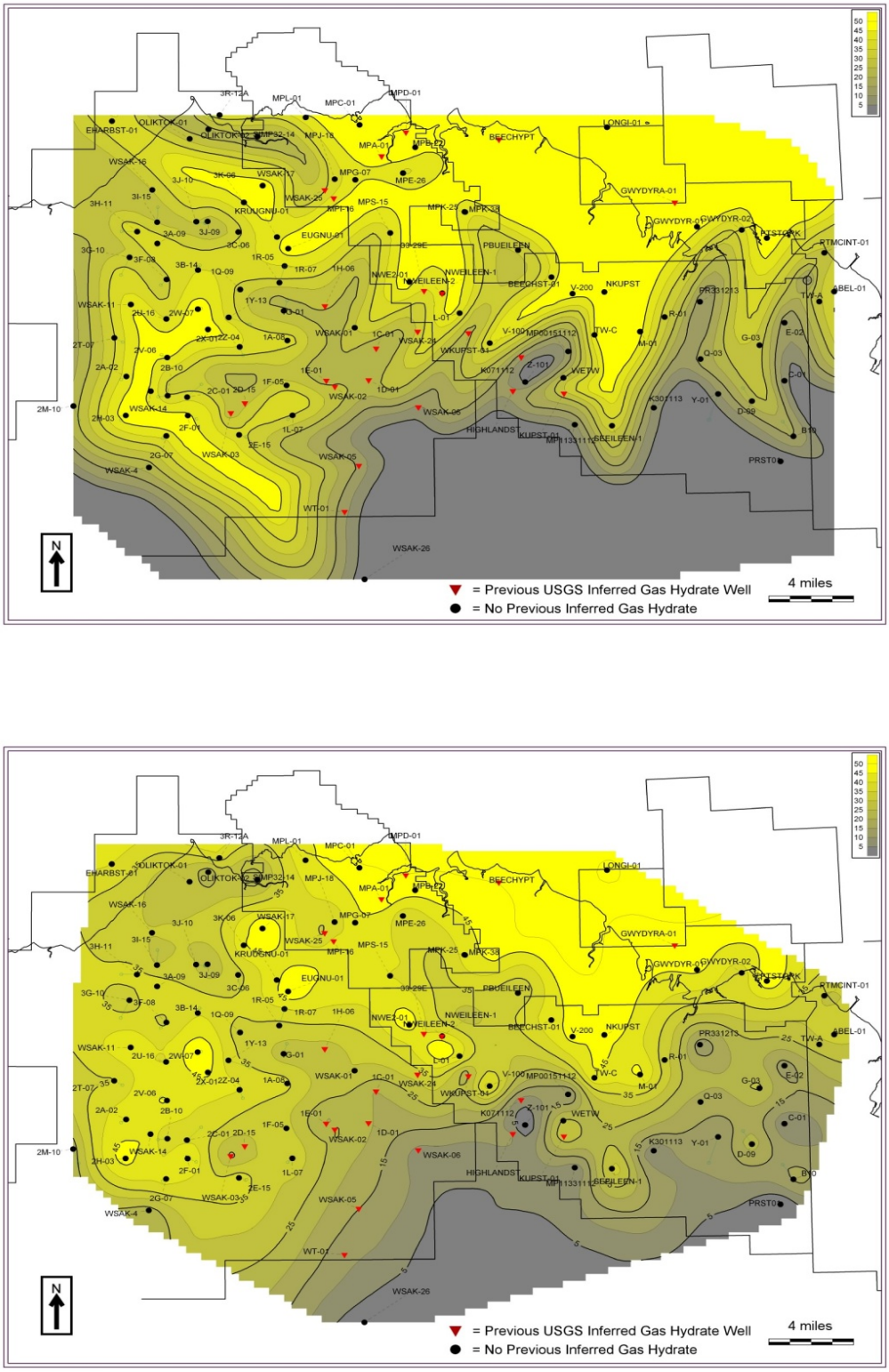

Figure A14: Two Slice 8 contour maps displaying major differences in net sand. Both maps use the same data but the hand contoured map contains numerous control lines and points to display character that reveals major geologic interpretations.

foot interval condition imposed on them. Caution must be used if this slice map is compared to the other thinner time slice maps above it (Slices 6-10, Figure A1).

A general trend noted in slice PS-33 to L-31A revealed a regional increase in net sand from southwest to northeast over the AOI (Figure A16). This increase correlates well with an increase of thickness in the gross isopach map and with the regional strike and dip displayed in the structure map (Figure A15). Within the KRU area, the east-west higher sand content trend (marked as C – Figure A16) is also present as a thicker region in the gross isopach map (Figure A15, lower). Facies characterization for this sand body classified this area as containing fluvial channel deposits (marked as A - Figure A13 and marked as C - Figure A16). The areas north and south of this sandy region within the KRU area are higher in shale content; facies characterization analysis classified these regions as shales and interbedded sands that were different in character from thicker marine units to the northeast and east. Multiple stacked channels are interpreted to exist in this area. The connectivity of units within the sand-rich area is most likely not as broad as the net sand map displays due to the nature of fluvial channel migration, incising channels, meandering orientations and lateral width displayed in modern fluvial environments. Also present in these maps are a northwest-oriented sand body connecting with the previously described east-west trending body within the KRU area. This area displays the same fluvial characteristics and is interpreted to be physically connected with the east-west trending sand-rich body. Moving to the boundary between KRU and MPU, a large regional change occurs in the northwest-trending zone 1, labeled as NW1. An increase in sand content (Figure A16) and isopach thickness (Figure A15, lower) characterizes this zone.

Coupling this behavior with the orientation of major deep seated faults within the PBU area (Figure A10) and extending their orientation northwestward supports the notion that structural faulting influenced deposition. Within the NW1 area, both fluvial and marine facies deposits are interpreted from this facies characterization study, which suggests that this was a transitional zone between both depositional environments (Figure A16). The NW1 zone exhibits much stratigraphic changes in many of the maps created for this interval. Another northwest-trending zone, labeled as NW2 in Figure A16, also influences the distribution of facies on many maps. Contours lines reflect increases in isopach thickness and sand content within this zone. The trend and stratigraphic character of NW2 also implies that structural faulting influenced deposition in this area. Comparing the magnitude of changes displayed between NW1 and NW2 reveals that NW1 was more influenced by structural control than NW2.

For the north-south trending zone, labeled N1, structural and stratigraphic changes and contour deflections occur within this region, but are less pronounced than those within the northwest-trending zones. In the marine section of the facies map, sand bodies were more correlative and connected, and their facies patterns (Figure A13) reflected that of modern distributary mouth bar deposits (Saxena, 1979; Tye, 2004). The south boundary for all net sand maps shows a laterally extensive shale region. This interpretation also reflects a decrease of the data that was available to the study. The limited available data suggest that one or two north-trending sand-rich corridors may also be present in this area.

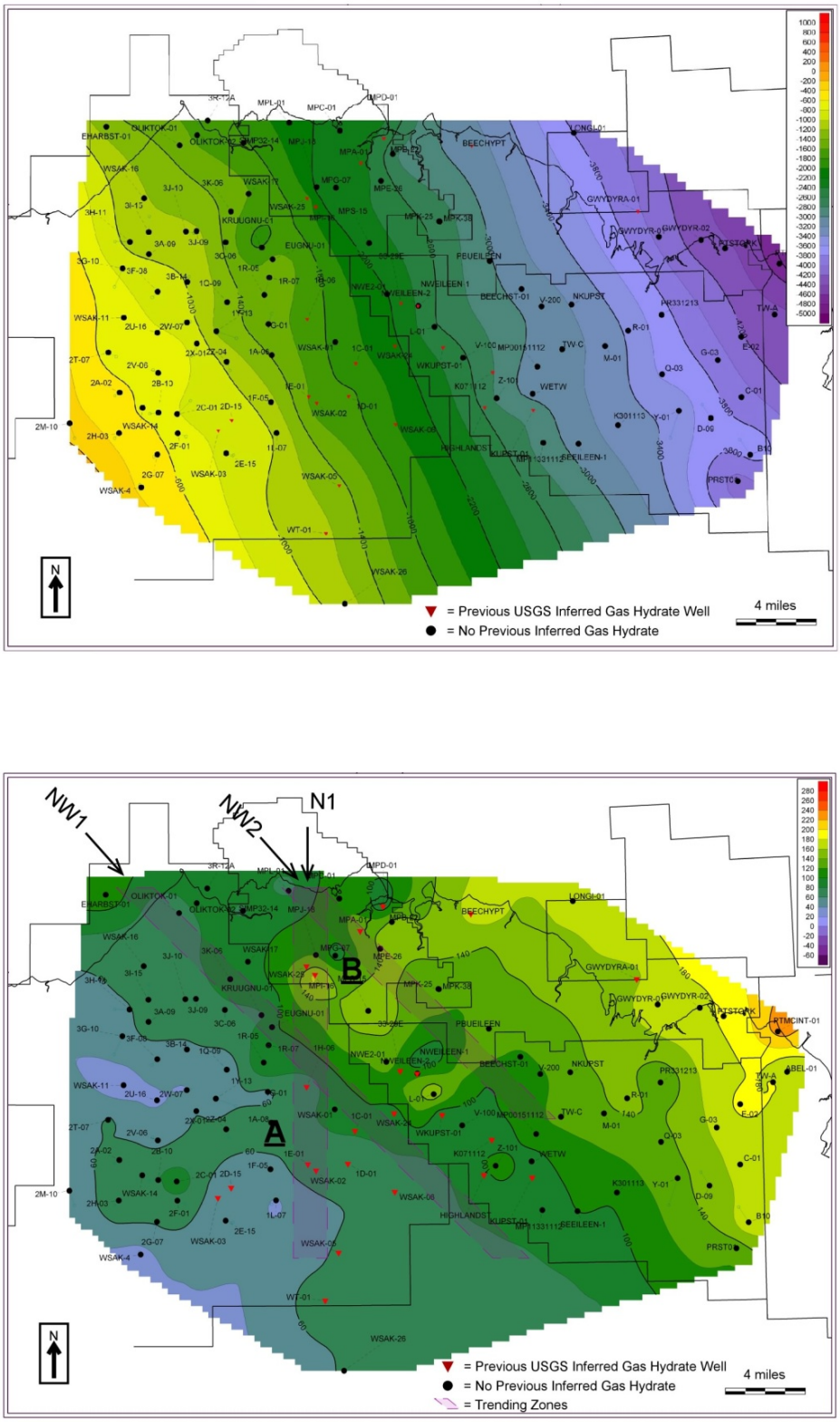

Figure A15: The upper map is a structure map on the parasequence 33 marker. The lower map is a computer generated gross isopach map between parasequence 33 and lithostratigraphic 31A (S-31) markers.

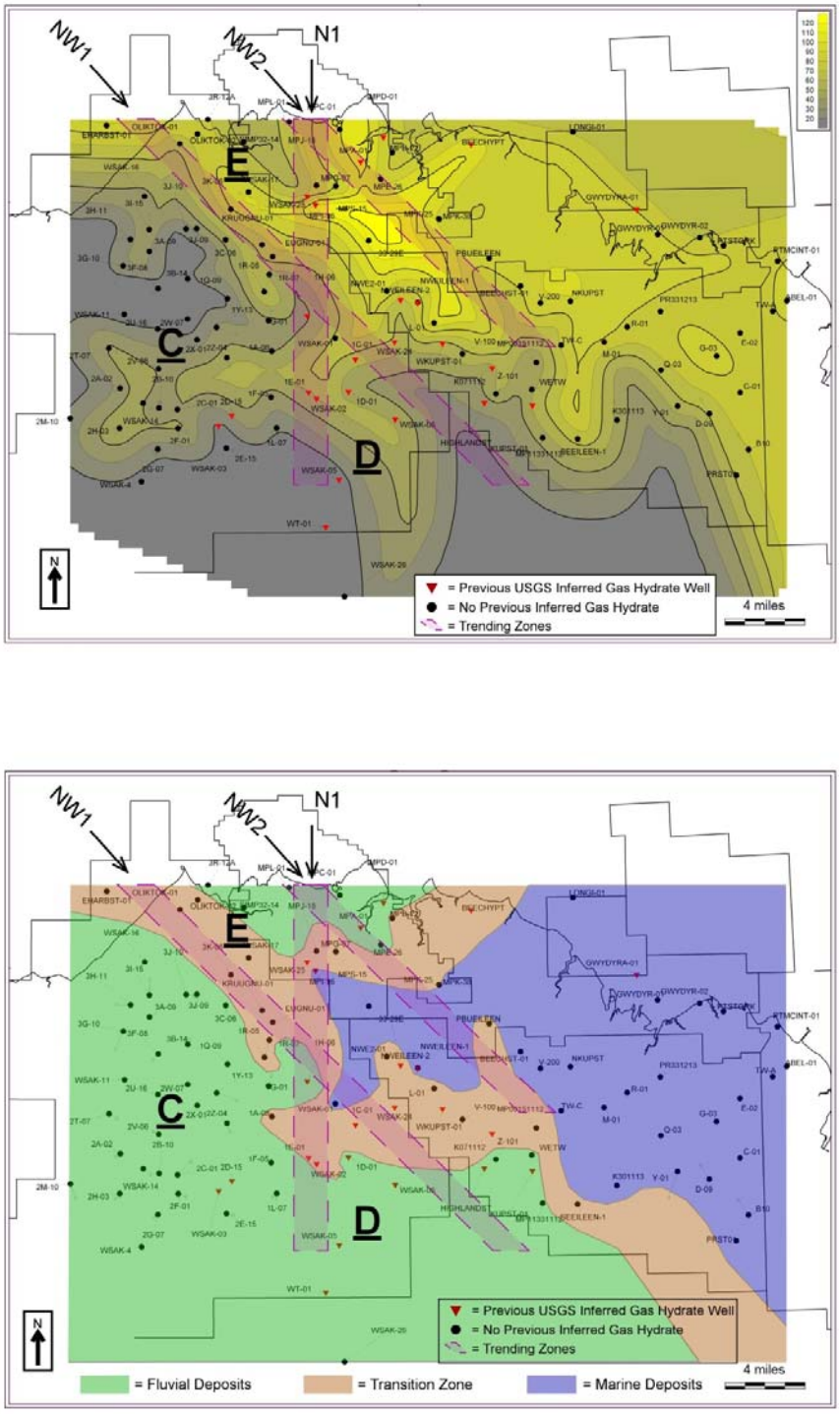

Figure A16: The upper map is a hand contoured net sand map between parasequence 33 and lithostratigraphic 31A marker generated during the net sand phase of this study. The lower map is an interpreted paleo-reconstruction map for this same interval. The interpretations displayed in this map are from the facies characterization study.

9.5.5.2 Time Slice 6

Time slice 6 is the lowest of the time slice intervals between the PS-33 to PS-34 markers (Figure A1). This slice shown in Figure A17 represents the lower 250 to 200 foot interval beneath the PS-34 marker. This interval is interpreted to reside completely below PS-33A marker, which displayed variations in the regional correlation across the AOI. In the northwest and southeast portions of the area, shale-rich regions exist and cover large areas of the KRU and PBU, respectively (Figure A17). This marine shale contains the maximum flooding surface that lies on top of the PS-33 marker. Many sand-rich areas within the KRU have wells in which previous USGS studies inferred gas hydrate-bearing sands at lower intervals below PS-33 and Slice 6 (Collett, 1993). These wells are represented by a red triangle on all time slice maps. Note how all of these wells reside in the sand-rich regions within the KRU area that were mapped in time slice 6 (Figure A17). NW1 and NW2 zones are also strongly expressed in the map and bound the largest sand-rich region within the KRU and MPU areas. A large part of this sand-rich region coincides with the location of an interpreted pull apart basin (Figure A11; Casavant et al., 2004). For NW1, an increase in net sand content appears to trend from the southwest to northeast along the zone. Recall that this same behavior was displayed in the lower PS-33 to L-31A time slice maps. In time slice 6, facies characterization places the transitional zone between marine and fluvial deposits further northeastward compared to the stratigraphically lower map (compare Figures A16 and A17). The migration of the transition zone to the east, suggests that the river systems and the paleo-shoreline are prograding oceanward during the deposition of time slice 6. Within the KRU area, fluvial channel facies characterization still correlated well with an increase in sand content and dominates the southwest portion of the AOI. The meandering-like nature of this sand body is interpreted to be strongly controlled by a northwest-trending fault fabric, which corresponds to deeper basement structure as previously mentioned. The higher east-west sand content trend displayed within the KRU area from the prior maps (Figure A16) is still present, but has less of an influence in this slice (Figure A17). The more dominant trend within the KRU area is the northwest-trending sand-rich zones comprised of fluvial channels.

In the southern part of the KRU, WSAK-26 displayed a large pronounced sand interval for this time slice. During the cross-section phase of this study, this sand body in WSAK-26 was originally placed below the PS-33 horizon marker, but a more detailed investigation disagreed with that interpretation. This sand body seemed to be anomalous to the AOI, and occurred only within a few southern wells. Development of this sand southward is possible, but connectivity within the AOI is questionable and the southern part of the net sand map should be viewed with caution.

In the northern part of the AOI, east of the MPU, another interpreted fluvial channel is shown on the net sand map (Figure A17 – BEECHYPT area). This sand body is anomalous because this is the only well that contained interpreted fluvial deposits, unlike the marine facies that dominate this region. The sand in the PBU area (labeled G in Figure A17), classified as marine deposits, is interpreted to be sourced from a fluvial channel to the west or northwest in this area. Deposit G resembles a modern distributary mouth bar.

In the southwestern part of the PBU, an interpreted fluvial sand deposit is present in PRST01 (labeled H in Figure A17). Wells close to this area are shale-rich and do not exhibit any sand

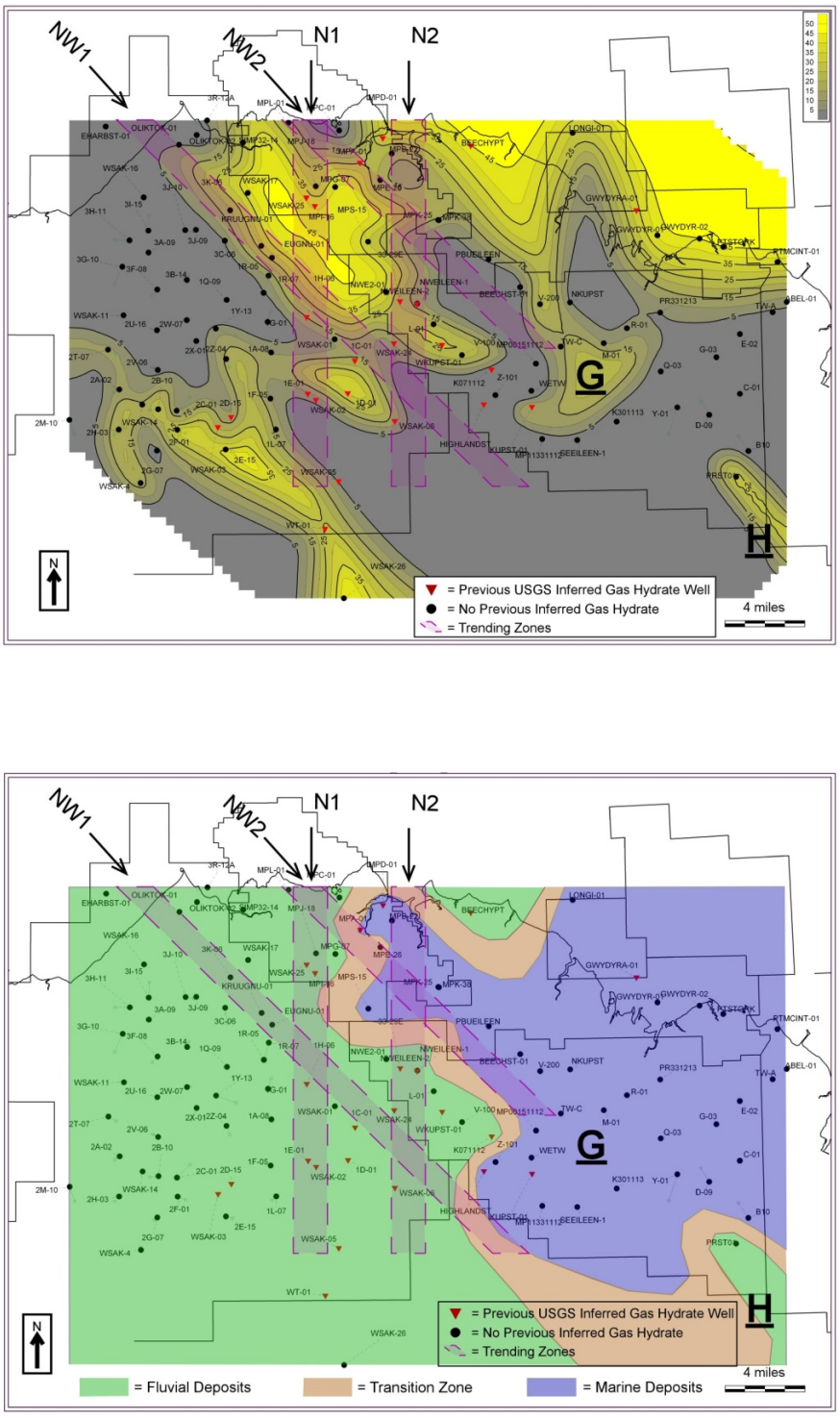

Figure A17: The upper map is a hand-contoured net sand map of time slice 6 generated during the net sand phase of this study. The lower map is an interpreted paleo-reconstruction map for this same interval. The interpretation displayed in this map is from the facies characterization study.

development. This isolated fluvial sand was hypothesized to exist near the paleo-coastline with a channel entering the ocean in another area, which may explain why no distributary mouth bar sands are interpreted in nearby wells. The north-south-trending zones N1 and N2 are substantially less pronounced compared to the northwest-trending zones NW1 and NW2. NW2 slightly expresses itself in a linear fashion in the northwestern PBU, where the boundary between sand- and shale-rich sands is located. In the MPU, net sand total for the WSAK-25 well was omitted due to difficulties in contouring a very small shale-prone region inside a predominantly sandy area. This area should be viewed with caution since WSAK-25 is still a valid data point.

9.5.5.3 Time Slice 7

Time slice 7 resides 200 to 150 feet below the PS-34 marker. This interval is interpreted to reside completely below the PS-33A marker, which as mentioned earlier, was difficult to correlate regionally. Sand development improved in the time slice interval 7 in comparison to time slice 6 (compare Figure A17 and A18). The predominant sand/shale relationship in the NW1 zone is still evident, with multiple wells displaying lower sand content to the southwest of this zone. No obvious sand channel development is noted between the large sand body (up to 40 feet thick) in the middle of the KRU (labeled I) and the other northwest-trending sand body northeast of NW1. In the reservoir characterization analysis, fluvial channel deposits are present on both sides of this minor northwest-trending shale zone, but no obvious connection was determined to exist with the data available. The link between both sand bodies is uncertain, but contours do encroach into the thinner shale region across which potential channel connections could exist. The NW2 zone has less of a signature compared to the NW1 zone, but deflections in contour lines do occur in the net sand map in the southeast part of the AOI. The facies characterization analysis for time slice 7 shows that the transition zone has again moved eastward compared to intervals below. This suggests that the river systems and paleo-shoreline prograde oceanward during deposition of time slice 7. The KRU east-west-trending thicker sand feature (area I) is again evident with good channel development present in the logs as was also seen in PS-33 to L-31A time slice maps (compare Figure A16 area C and Figure A18 area I).

9.5.5.4 Time Slice 8

Time slice 8 resides 150 to 100 feet below the PS-34 marker (Figure A1). This interval is interpreted to reside within both an upper and lower parasequence set that is not easily correlated across the area. The PS-33A to PS-34 interval likely contains this upper parasequence set, based on the vertical location of this interval for the majority of wells that were evaluated. An important point to remember is that interpretations generated from this time slice are a combination of two parasequence sets and results may be misleading. Overall, sand development and distribution increases again relative to lower intervals (Figure A19). The predominant shale region south of NW1 is only slightly apparent in the net sand map. Multiple fluvial channels are interpreted throughout the AOI in this time slice. Their frequency is probably related to the combination effect displayed by joining two parasequence data sets together. From the abundance of channels that are noted, the net sand map displays a jagged contour nature. The N1 zone appears to mildly influence net sand contour lines in both the KRU and MPU areas. Within the PBU, multiple fluvial channels are generally oriented north-south. A small area within the northeastern-most part of the AOI still contains marine distributary mouth bar facies (Figure A19). From the facies characterization across most of the AOI, it is still apparent that the river systems are prograding northeastward as the transition zone and paleo-shoreline move further to the northeast, compared to stratigraphically lower intervals (Figure A19).

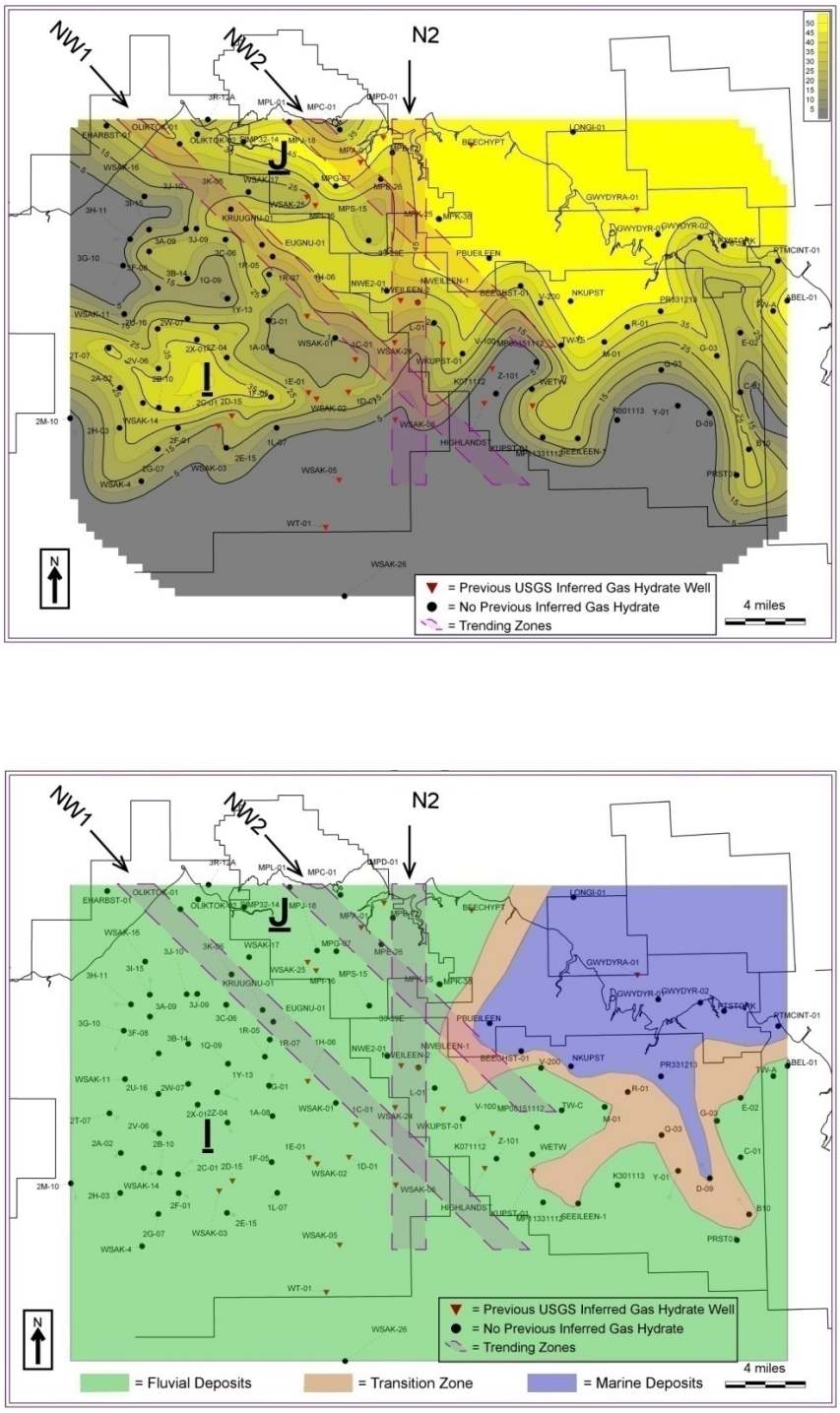

Figure A18: The upper map is a hand contoured net sand map of time slice 7 generated during the net sand phase of this study. The lower map is an interpreted paleo-reconstruction map for this same interval. The interpretation displayed in this map is from the facies characterization study.

9.5.5.5 Time Slice 9

Time slice 9 resides 100 to 50 feet below the PS-34 marker (Figure A1). This interval is hosted entirely between the PS-33A to PS-34 correlation markers, which is in the upper parasequence set that is not easily correlated across the area. An overall increase in sand content is noted (Figure A20). The shale-prone region southwest of the NW1 zone is no longer a major feature. Significant sand-prone regions are now located throughout the northern KRU area where once a strong northwest-trending shale region existed within stratigraphically lower sections. The NW2 zone exhibits a minor influence on the net sand contour map within the PBU area (Figure A20). The interpreted jagged multiple channel contour behavior displayed in time slice 8 is still present, but is not as pronounced in this net sand map. Within the PBU area, multiple potential channel areas are interpreted and are oriented northeastward, pointing towards the marine sand facies region. Log-based facies analysis reveals no significant change from the stratigraphically lower paleodepositional map in terms of the fluvial, transition, and marine deposit distributions (compare Figures A19 and A20). Fluvial deposits still dominate much of the AOI except for a small marine area identified in the northeastern part of the AOI. Since the transition zone did not move laterally, progradation either slowed or stopped completely. More adequate well density in the northeastern portion of the AOI would help better resolve this issue.

9.5.5.6 Time Slice 10

Time slice 10 represents the interval from 50 feet below the PS-34 correlation marker up to the marker (Figure A1). The most pronounced sand content for the IOI is displayed in this time slice (Figure A21). The shale-prone region southwest of the NW1 zone is represented as a minor shale region appearing within the KRU area. Good sand development is displayed in many northern areas throughout the AOI. The north-south-trending N1 and N2 structural zones slightly manifest themselves within the KRU and PBU areas by deflecting net sand map contours (Figure A21). Facies characterization analysis reveals no vital location changes from the stratigraphically lower paleodepositional map (Figure A20). The large sand-rich areas on time slice 10 are interpreted as fluvial deposits (Figure A21). Spatial connectivity between individual sand bodies associated with this fluvially-dominated time slice is likely considerably less than what is illustrated.

9.5.5.7 Interval above Time Slice 10

Between the PS-34 to PS-34A correlation markers, a retrogradational sequence is interpreted to exist in the northeast part of the AOI. Evidence of this transition is displayed in the cross-section shown in Figure A6. Examining the increasing gamma ray readings and the step back nature of the smaller distributary mouth bars interpreted in the LONGI-01 well above the PS-34 correlation marker indicates a likely association with a retrograde or transgressive phase of deposition. However, strong evidence of this sequence is not always expressed in other wells throughout the AOI. Furthermore, facies characterization analysis of this unit does not support this hypothesis because no major paleodepositional movements occur within this interval. In the next higher parasequence set between PS-34A to PS-35, all sand-rich areas were interpreted as fluvial deposits (Figures A6 and A3), which contradicts this retrogradational interpretation. Therefore, this parasequence behavior is debatable.

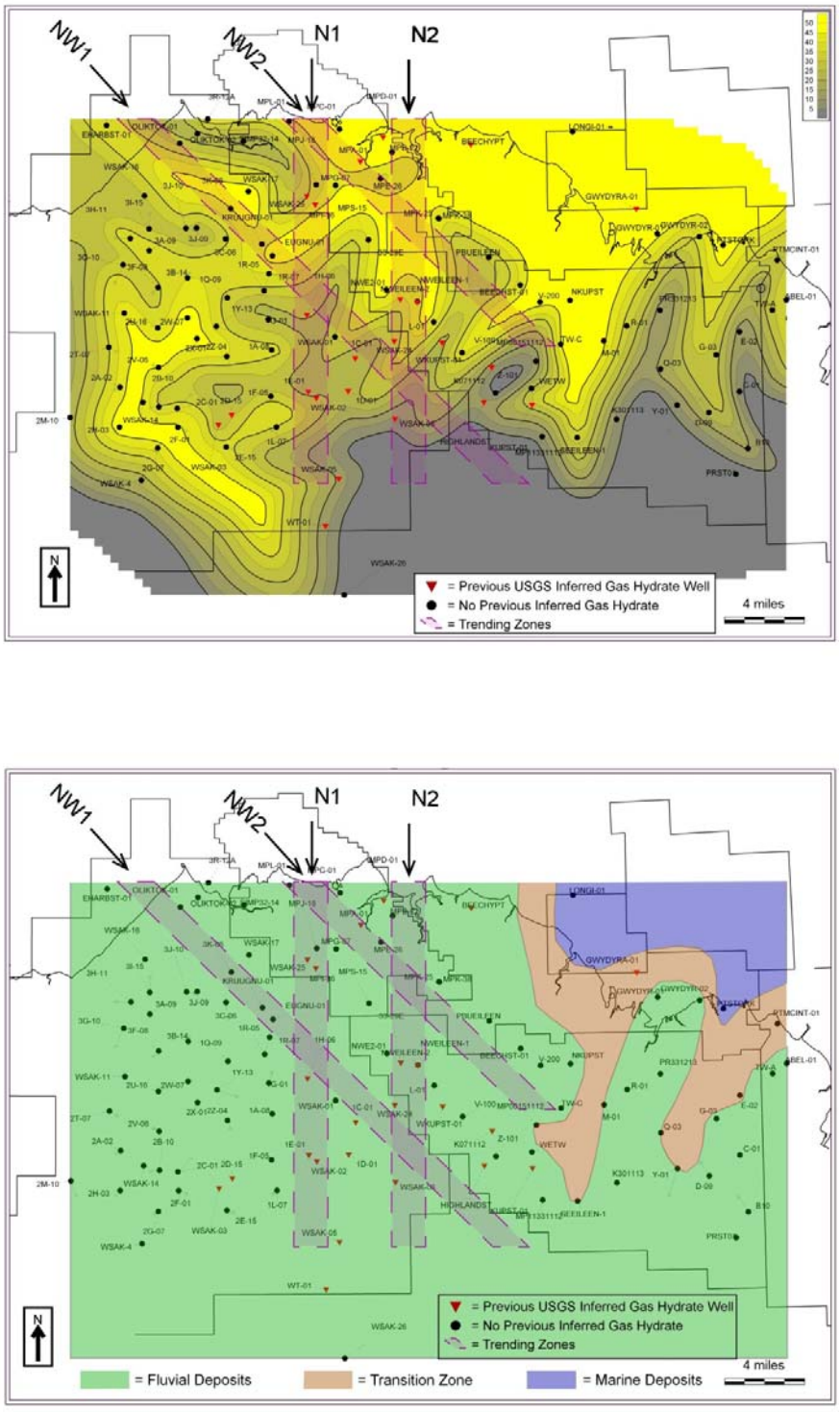

Figure A19: The upper map is a hand contoured net sand map of time slice 8 generated during the net sand phase of this study. The lower map is an interpreted paleo-reconstruction map for this same interval. The interpretation displayed in this map is from the facies characterization study.

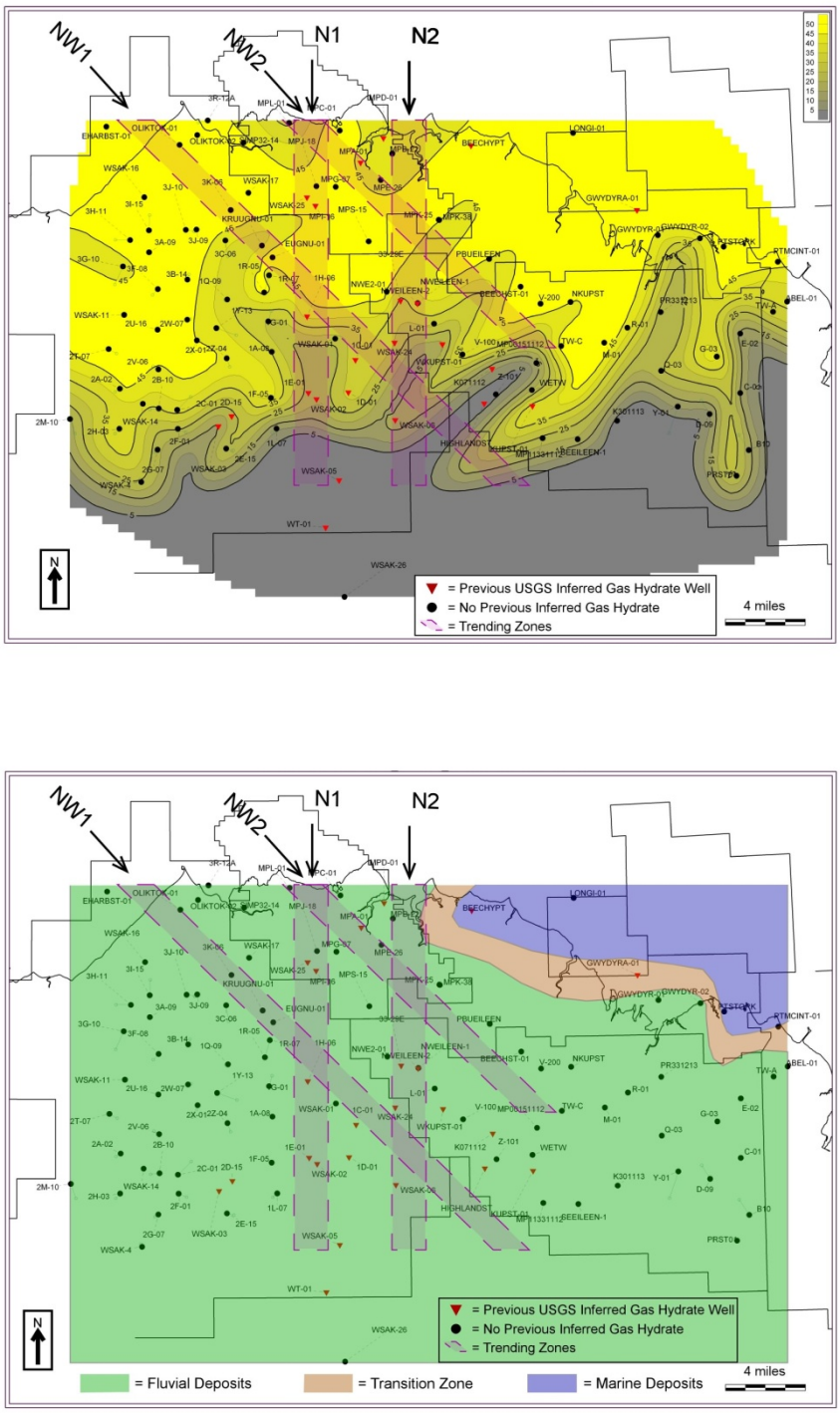

Figure A20: The upper map is a hand contoured net sand map of time slice 9 generated during the net sand phase of this study. The lower map is an interpreted paleo-reconstruction map for this same interval. The interpretation displayed in this map is from the facies characterization study.

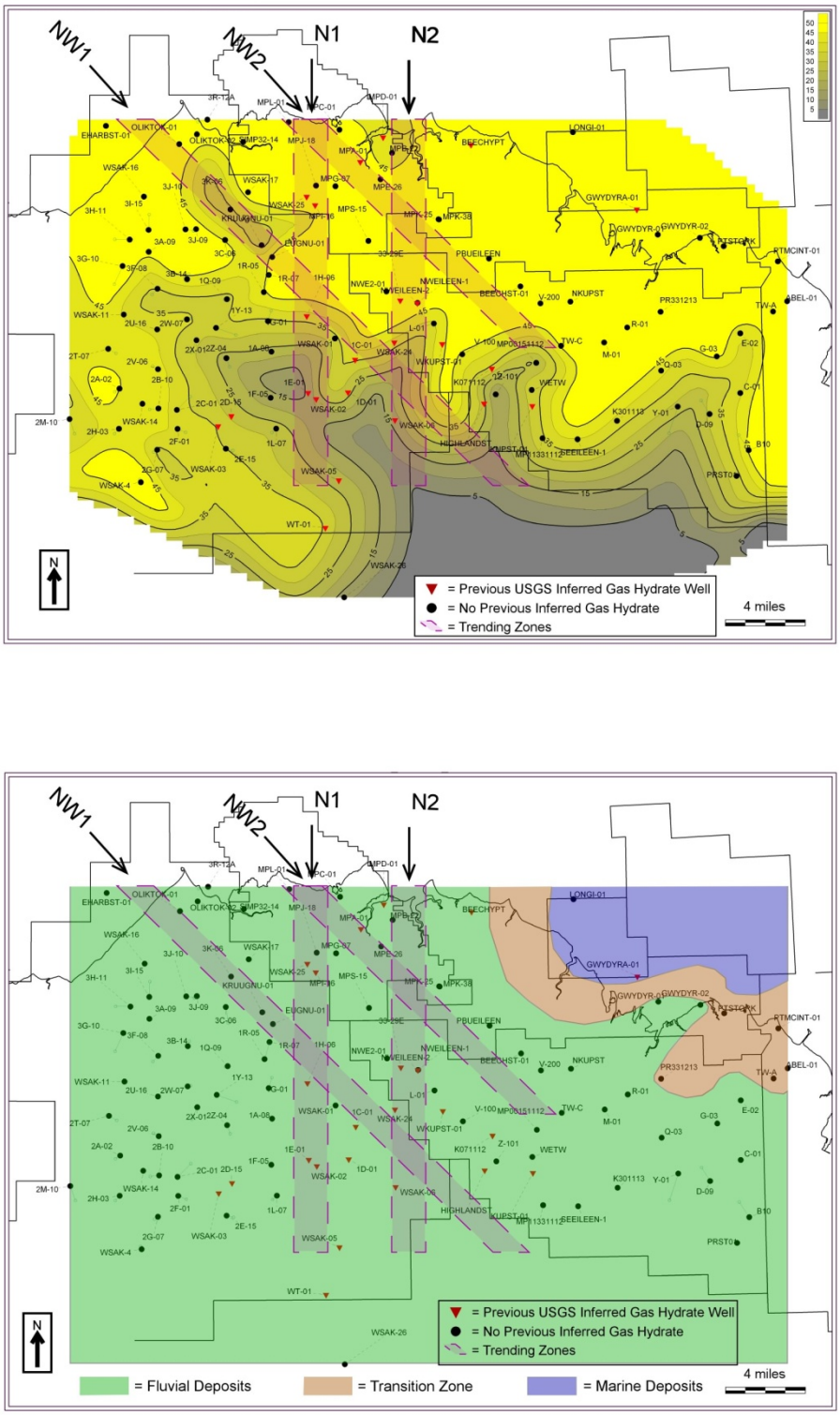

Figure A21: The upper map is a hand contoured net sand map of time slice 10 generated during the net sand phase of this study. The lower map is an interpreted paleo-reconstruction map for this same interval. The interpretation displayed in this map is from the facies characterization study.

Also present above the PS-34 marker is an anomalous shale-rich area located in the southwest part of the AOI, mainly within the KRU (Figure A3). Based on the opposite lateral location and the pinching out behavior displayed towards the northeast (Figures A6 and A3), this shale unit was hypothesized to be a coastal plain mud or siltstone. No well-developed sand intervals are displayed throughout this shale unit within the KRU region. This may suggest that a major change in the river system locations occurred during this time. This is one proposed explanation of why no sand-rich fluvial deposits are associated with this interval within the KRU area. Combining this observation with the retrogradational hypothesis observed in LONGI-01, dramatic changes in sediment deposition orientation may have been present during this time. No consensus was agreed upon to describe the data results observed in this parasequence set.

An additional important point to mention is that for a few mostly MPU-area wells, gas hydrate-bearing reservoirs are interpreted to exist between the PS-34 to PS-34A correlation markers. Since gas hydrate-bearing sands in slice 10 and above the parasequence set are laterally connected for intervals that were identified to contain gas hydrate between the PS-34 and PS-34A markers, these net pay values were added to slice 10.

9.5.6 Paleosol Horizon Alternative Interpretation

Well log-based stratigraphic interpretation within the MPU reveals the presence of potential single and stacked paleosol units that may be alternatively interpreted as potential gas hydrate-bearing reservoir zones in previous studies. A lack of available core data and cuttings for analysis keeps this alternate paleosol interpretation speculative. The interpreted paleosols appear as one and/or several relatively thin resistive zones that are characterized by low GR readings and are immediately overlain by above-normal velocity and bulk density responses. Thicknesses of individual resistive units (possibly ankerite or calcite cemented beds) range from 1-4 meters. These units can be interleaved with shale zones comprising what is commonly referred to as a paleosol stack, which commonly produce intermittent, but relatively strong impedance contrasts along sequence boundaries in seismic data. These vary in thickness within the MPU area and appear to reach thicknesses of 5 meters or more (e.g. ~ 1,930 feet MD in MPB-02). The paleosol interpretation might explain the notable lack of increase in background or “total” gas seen on mud logs across these previously interpreted “gas hydrate-bearing” zones within the MPU. Similar intervals have been correlated and noted in many other wells within the KRU and PBU areas. Reviews of any available core and/or sample descriptions, drilling exponents, and porosity log litho-identification and MSFL analysis would prove most useful in validating this preliminary interpretation. Although this data had been requested early in the project, little was available for study.

Table A1 lists the MPU wells that were interpreted to contain potential paleosol intervals based on well log interpretations. Paleosol horizon interpretations were based on petrophysical calculations where relevant logs were available and were based on correlative horizons where logs for complete petrophysical analysis were not available.

Well	USGS-zone	UA-zone	Comment
MPU B-02	E	L_35a - 35	
MPU E-26	E	L_35a – 35	
MPU A-01	E	L_35a – 35	Possible thicker paleosol stack interbeds
MPU K-38	E	L_35a - 35	Possible thicker paleosol stack interbeds
MPU B-02	C	L_34 – 33	2 meter interval may correlate to 3-4 meter interval interpreted above gas hydrate in NWEileen-02
MPU B-01	E	L_35a - 35	Logs for complete petrophysical analysis not available
Kavea32-25	E	L_35a - 35	Logs for complete petrophysical analysis not available
MPU D-01	E	L_35a - 35	Logs for complete petrophysical analysis not available
MPU A-01	E	L_35a - 35	Logs for complete petrophysical analysis not available
MPU K-25	E	L_35a - 35	Logs for complete petrophysical analysis not available
Cascade-01	E	L_35a - 35	Logs for complete petrophysical analysis not available
WSak-25	E	L_35a - 35	Logs for complete petrophysical analysis not available
MPU B-01	D	L_35 – 34	Logs for complete petrophysical analysis not available
MPU B-01	C	L_34 – 33	Logs for complete petrophysical analysis not available

Table A1: Interpreted Possible Paleosol Intervals within MPU Area Wells

The chronostratigraphic or sequence stratigraphic analysis shows that these interpreted paleosol units are commonly linked to the upper beds of incised channel deposits or upper units of point bar parasequences that overlie intraformational unconformities. This spatial relationship and their regional correlativity also makes these units ideal indicators for detailed sequence boundary interpretation. The latter are critical to accurate chronostratigraphic correlations that ultimately lead to more accurate characterization of reservoir connectivity, production modeling, refinement of volumetric assessments, and paleodepositional reconstructions. Studies were planned (but not conducted) to assess the relations between potential paleosol horizons within the MPU area and the adjacent Eileen accumulation area (within KRU and PBU) and their potential linkage to underlying northwest-trending fault zones and, in some locations, to syndepositional north-northeast-trending faulting. Both are expressed as reactivated structural areas that could have been associated with subaerial exposure, erosion and subsequent formation of paleosol units that were interpreted to occur within the gas hydrate stability zone within the MPU area. Their role in possibly constraining or indicating gas hydrate and free gas occurrences is not fully understood.

9.5.7 Net Pay Estimations

Due to the common overestimation of net pay totals observed using the expert system, manual interpretation of net pay commenced. In determining final net pay totals for each well, all net pay intervals were defined to meet the following standard log conditions:

Gamma Ray: Net pay must reside within an interval that is classified as net sand according to the net sand study.

Caliper: Net pay that resides within intervals that contain sudden caliper increases (washouts) will be evaluated on an individual well basis. All other intervals are considered valid data points.

Resistivity: An increase in resistivity not related to changes in lithology, but related to pore fluid changes, is required for net pay to exist.

Acoustic time: For gas hydrate-bearing reservoirs, an increase in acoustic time from background responses must be present for net pay to exist. For associated free gas, a decrease in acoustic time from background responses must be present for net pay to exist.

Density: For gas hydrate-bearing reservoirs, a density response is not one of the primary logs used in determining net pay, but any response with the combination of the previous log responses may be classified as net pay depending on the circumstances. For associated free gas, a decrease in the density log creating a cross-over effect with the neutron log will be classified as net pay.

Neutron: For gas hydrate-bearing reservoirs, a neutron response is not one of the primary logs used in determining net pay, but any response with the combination of the previous log responses maybe classified as net pay depending on the circumstances. For associated free gas, an increase in the neutron log creating a cross-over effect with the density log will be classified as net pay.

Using the above outlined primary log responses, the Expert System (ES) and the location of the wells relative to the Top Hydrate Stability Zone (THSZ), Base Ice-bearing Permafrost Zone (BIPFZ), and Base Hydrate Stability Zone (BHSZ), manual interpretations of net pay for each time slice were visually determined. During the manual interpretation phase, a transitional trend of net pay was discovered to exist. This trend evolved in lateral space from areas with well-developed net pay “shows” to moderate net pay “shows” then onto slight “shows” and finally to no “shows” intervals. These trends later became classification categories for all net pay intervals. Every identified net pay interval that contained gas hydrate or associated free gas on a slice map demonstrated this lateral trend. This lateral observation was mapped for all interval slices and net pay strength categories were assigned to each location in an attempt to emphasize the strength of the net pay show indicators. Along with the classification of net pay based on the strength of the shows, when a well contained an incomplete set of petrophysical logs, an additional asterisk was placed on the map disclosing this condition. For areas that contained well-developed to moderate shows, net pay interval footages were determined and were recorded on the slice maps. Defining net pay for an interval classified as slight shows were difficult since no sharp petrophysical log responses were present. Only gradational and subtle changes were noticed in the data. Due to this effect, no net pay values were calculated for these intervals.

Once all net pay totals were recorded, correcting the measured depth to a true vertical depth for all net pay intervals was initiated using the directional survey data. Since all petrophysical log data is displayed in measured depth, the true vertical and measured depth values for each time slice horizon were exported from PETRA into a Microsoft Excel spreadsheet. In Excel, a ratio between measured depth and true vertical depth was calculated for each interval containing net pay. Using these ratios calculated as a multiplier, net pay footages were converted from measured depth to true vertical depth by multiplying these numbers together. For the vast majority of cases, no change occurred between measured and true vertical depth for net pay values. Only in a few intervals were minor changes required.

9.5.8 Net Pay Mapping

After determining final net pay footages for all slice map intervals, contouring of net pay maps began. Incorporating all geologic trends discussed earlier, net pay maps for each interval were highly constrained. During the creation of all net pay maps, the corresponding net sand map was used, as a transparent background, to help define the shape and lateral limits of these maps. During the contouring process, no net pay contour was allowed to be greater than the corresponding net sand contour for each interval evaluated. This condition eliminated the possibility of having areas display larger net pay values than their corresponding net sand values. The below discussion reviews all net pay maps created and also explains why certain contour shapes, orientations, and lateral extent of contour lines were chosen.

9.5.8.1 Net Pay Map between PS-33 to L31A

Two separate potential associated free gas- and gas hydrate-bearing reservoirs exist in this deepest studied interval. The first resides within the eastern MPU area and the second within the south-central part of the PBU (Figure A22). For the MPU, well-developed gas shows are identified in the MPU K-25 and MPU K-38 wells. In the MPU K-38 well, a near complete set of petrophysical logs were available. In this well, the gas crossover effect is present and covers almost the entire sand interval. In the MPU K-25 well, an incomplete set of petrophysical logs were available. A strong resistivity response was displayed and is similar in nature to the response seen in the MPU K-38 well, which contained an obvious gas crossover effect on the neutron-density porosity log. Leaning towards a conservative estimate of net pay totals, the net pay for this area was determined to be 60 feet. This number was estimated by examining net pay totals from both wells and using the more conservative number. Other nearby wells did not demonstrate any well-developed to moderate associated free gas or gas hydrate shows for this region. Since these wells are the only conclusive evidence of net pay for this extensively sand-rich area, the shape of this reservoir was guided by the net sand maps and by the BHSZ. The Mount Elbert prospect lies in a structurally higher area than the MPU K-pad and is fault bounded. The gas show displayed in the MPU K-pad could be the down-dip associated free gas source providing methane to the structurally higher gas hydrate reservoir within the Mt Elbert prospect. This occurrence is supported by early gas hydrate and associated free gas models (Collett, 1988). With the BHSZ between this prospect and the MPU K-pad, a decrease in the amount of free gas is interpreted as one moves up-dip above the BHSZ. Within and on the opposite sides of this zone, the amount of gas hydrate increases in the same fashion as the associated free gas decreases (Figure A22). This contour effect illustrates that gas is continuously present throughout this area, but just changes its physical state from associated free gas to gas hydrate. Sand-rich areas east of the MPU K-pad could potentially contain associated free gas, but net pay contours do not extend far into this region as no well data is available. The south end of this prospect does not extend much further past the MPU boundaries due to the lack of available well log data. Associated free gas- and gas hydrate-bearing reservoirs could exist in these areas based on the net sand map and facies characterization results, but these regions are not interpreted to connect to the MPU K-pad gas shows, using a more conservative approach. For the PBU area, three wells contained well-developed to moderate gas and/or gas hydrate shows. In WETW and KUPST-01, well-developed gas shows were illustrated with density and neutron logs displaying the gas crossover effect. In K071112, a moderate increase in resistivity is present. The acoustic log for this interval is invalid due to the straight line nature that was displayed, so the interpretation of gas hydrate-bearing reservoirs was made based on its location relative to the BHSZ. Other wells in the area had either slight to no gas shows.

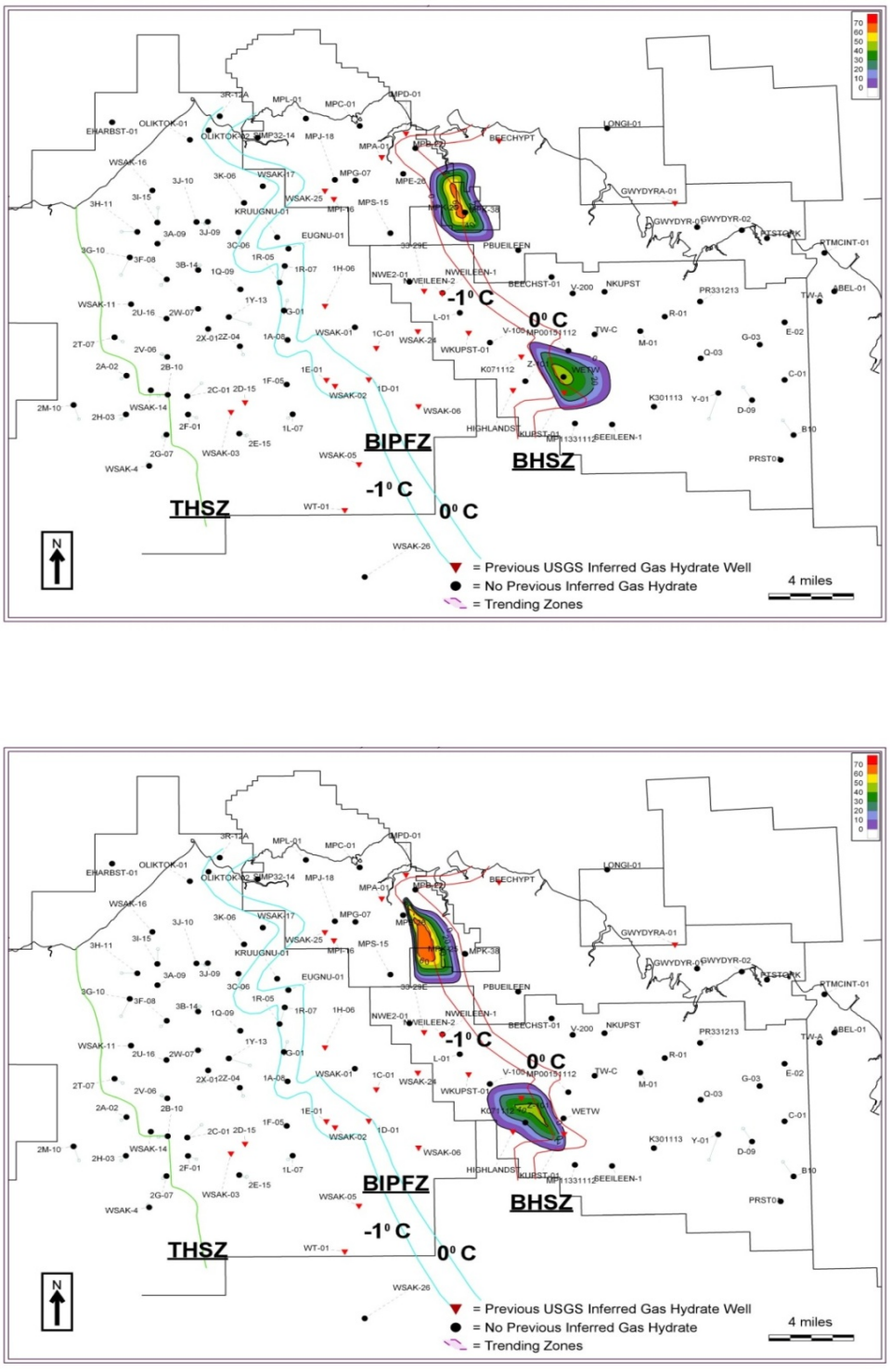

Figure A22: The upper map is a hand contoured net pay map of the PS-33 to L-31A interval and represents associated free gas that is inferred to exist in this interval. The lower map is a hand-contoured net pay map of gas hydrate-bearing reservoirs inferred to exist within the interval.

The lateral extent of this reservoir is controlled by nearby wells that contained no gas shows. Net sand contours between the associated free gas- and gas hydrate-bearing areas are divided by a shale-prone region (Figure A16). Examining a three well cross-section revealed this shale appears to be a function of less sand development and does not imply there is a physical boundary between these wells. Connectivity between the three wells is probable and gas hydrate located structurally above a down dip associated gas-bearing reservoir is inferred. Due to the lack of seismic data, net pay contours were constrained by well density and net sand map trends.

9.5.8.2 Net Pay Map Within Time Slice 6

One potential gas hydrate-bearing reservoir exists near the intersection of the MPU, KRU and PBU. Three wells define the amount of net pay for this reservoir with strengths ranging from moderately to slightly developed (Figure A23). In WSAK-24, a minor resistivity response coupled with a sudden drop in acoustic time and defined by a moderate gas show is interpreted as gas hydrate within this interval. Slight shows from 1C-01 and NWE2-01 were also documented. Analyzing the well locations against the net sand map shows primarily under-developed sand areas (Figure A17). Facies analysis displays fluvial channels with interbedded shales as the predominant sediment type within the net pay intervals. Sand development improves to the Northwest and structurally up-dip from all well penetrations. A relationship relating increases in sand quality to increases in net pay was assumed. Using this interpreted relationship, areas structurally up-dip within better developed sand-prone regions had contours representing more net pay without well data support. This more aggressive approach was taken since all wells in this interval with net pay shows were in structurally down-dip locations in less sand-rich areas. Using the surrounding well data, net sand contour patterns, BIPFZ and all trending zone boundaries, the reservoir lateral extent was defined and a final net pay contour map was generated (Figure A23). No associated free gas was identified within this interval.

9.5.8.3 Net Pay Map Within Time Slice 7

One potential gas hydrate-bearing reservoir is interpreted to reside within the time slice 7 map (Figure A24) in approximately the same location as the gas hydrate-bearing reservoir displayed in the time slice 6 map (Figure A23). The four wells used in determining net pay values for this interval display a moderate to slight strength response. Time slice 7 in 1H-06 resides above the BIPFZ, which could be related to the formation of ice, but this interval was interpreted to contain gas hydrate due to the similar log responses compared to the other wells. WSAK-24 is the only well that possessed an acoustic log, which shows a slight decrease coupled with an increase in resistivity in the potential reservoir interval. This behavior suggests the presence of gas hydrate. For the NWE2-01 and 33-29E wells, only gamma ray and resistivity logs were available. Comparing the resistivity character of both wells to the WSAK-24 response, similar resistivity patterns emerged. In the facies characterization analysis, fluvial channels and point bars were identified throughout the net pay interval. According to the trends displayed in the net sand map, these intervals are most likely connected based on their lateral extent and similar facies patterns. The NW1 zone bounded net pay contours on the south portion of this reservoir (Figure A24). On the west and east boundaries lie the N1 and N2 zones, respectively. For the north boundary, a more shale-rich region is present with no gas hydrate indications in those wells. On the southwest portion of the net pay area, migration of contours southward is drawn to integrate the potential higher sand-rich areas interpreted from the net sand study (Figure A18). Reservoir volumes from this map are considered to be upper limit estimates since no pronounced gas hydrate indications were present. No associated free gas shows were seen in time slice 7.

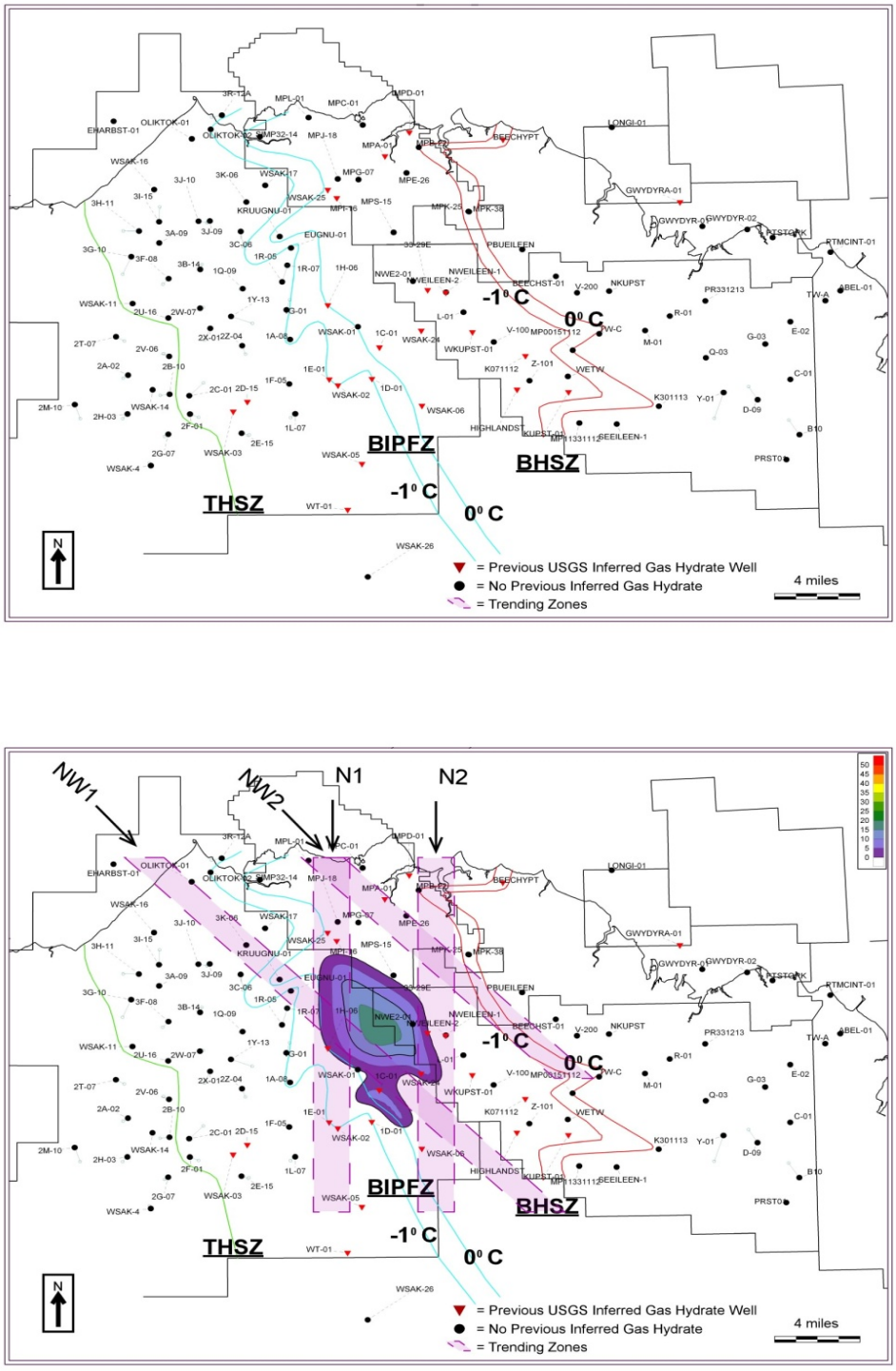

Figure A23: The upper map represents the associated free gas that is inferred to exist in this Time-slice 6 interval. The lower map is a hand contoured net pay map for gas hydrate-bearing reservoirs that are inferred to exist within this interval. On both maps, the three major transition zones are present.

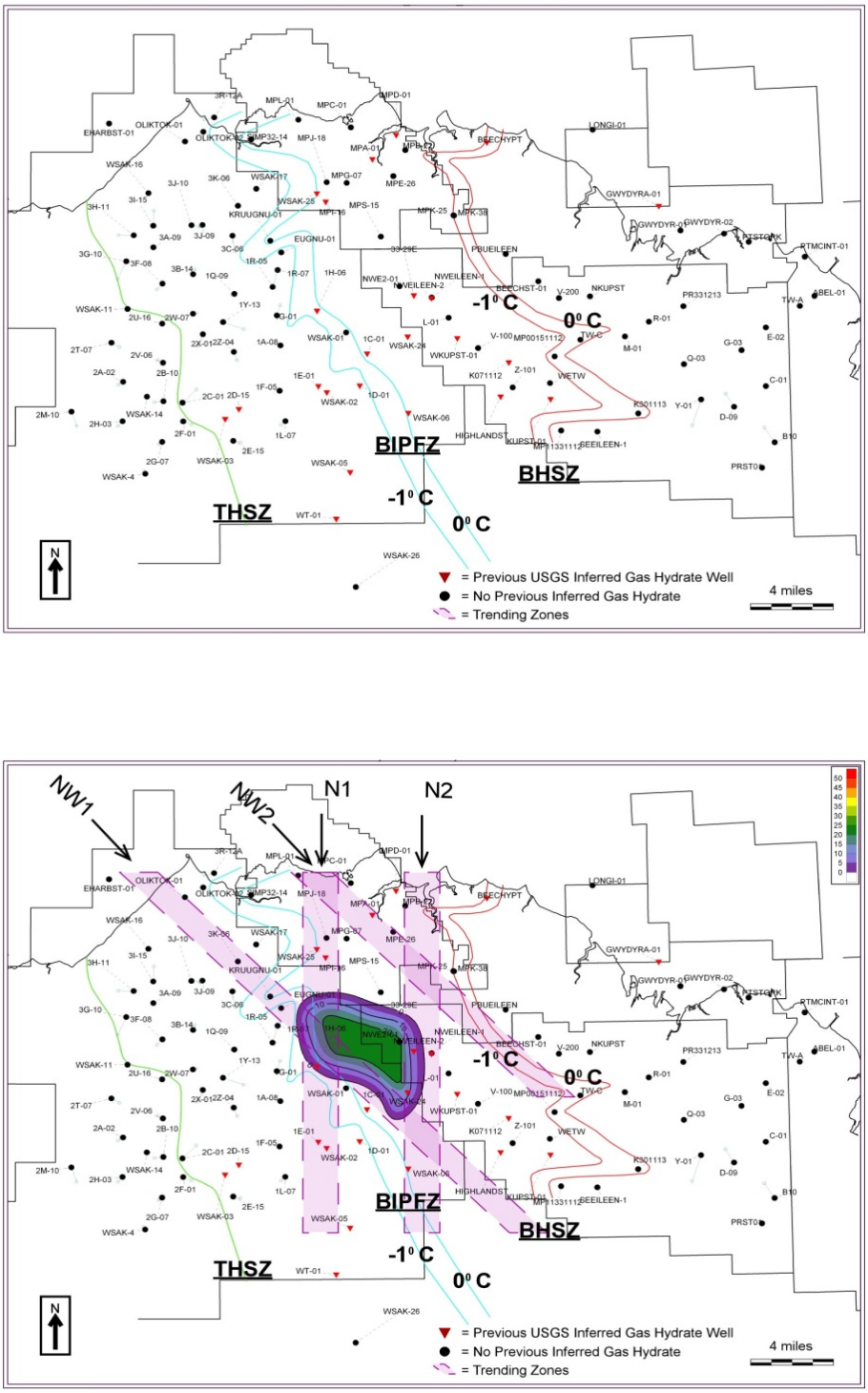

Figure A24: The upper map is a hand contoured net pay map of time slice 7. This map shows no associated free gas is inferred to exist in this interval. The lower map is a hand contoured net pay map for gas hydrate-bearing reservoirs that are inferred to exist within this interval. On both maps, the three major transition zones are present.

9.5.8.4 Net Pay Map Within Time Slice 8

One potential gas hydrate-bearing and one associated free gas-bearing reservoir are present in the time slice 8 map (Figure A25). The gas hydrate reservoir located in the northwest part of the PBU is defined by two wells. The L-01 well was not evaluated for net pay in this study because the gamma ray log was the only petrophysical log available in this well. Instead, logs for an additional well (L-106) were obtained near the end of this study and were used to determine net pay for this interval. Visual comparison of the gamma ray character for both wells display an almost identical pattern and correlation horizons between the two wells was straightforward. The distance between the two wells is relatively close and acknowledging the fact that the gamma ray responses are similar, net pay identified in L-106 was assumed to be present in L-01. L-106 contained a full suite of petrophysical logs. A moderate resistivity response displayed in this interval suggested the presence of gas hydrate. In NWE2-01, an incomplete set of petrophysical logs was available. Only the gamma ray and resistivity surveys were present. Similar resistivity log behavior was illustrated and compared well with responses observed in the L-106 well. Although this response was not as strong, compared to the L-106 data, defining net pay for the NWE2-01 was feasible. The horseshoe-shaped reservoir geometry is strongly influenced by the net sand contour map and by no gas indications present in either the 33-29E or Northwest Eileen State #2 wells. This volume should be considered the upper limit of gas hydrate for this interval. No associated free gas-bearing reservoir co-existed with this gas hydrate-bearing reservoir.

In the central part of the PBU, the MP00151112 and the K091112 wells were used to identify a small gas show. On the net pay map, only the MP00151112 well is displayed. The K091112 well is located in relatively the same location as the MP00151112, but was not chosen to be displayed because of complications that arose from wells being spaced too closely together. Using incomplete petrophysical log sets from both wells that included the gamma ray, resistivity, acoustic and density curves, this interval was evaluated. A slight to moderate resistivity response is illustrated with an increase in acoustic time and decrease in the density log for the K091112 well. Since the MP00151112 well was chosen to represent the area, projecting the net pay identified from the K091112 well visually verified that both the gamma ray and resistivity responses over this interval were similar. No other nearby well contained any net pay indications, so the lateral extent of this reservoir is assumed to be limited as shown in the map (Figure A25).

9.5.8.5 Net Pay Map Within Time Slice 9

Two small associated free gas- and one fairly large gas hydrate-bearing reservoirs are interpreted to be present within the time slice 9 map (Figure A26). The large associated free gas- and gas hydrate-bearing reservoir, located within the northwest portion of the PBU, is defined by four wells. Two well-developed gas hydrate shows occur within the Northwest Eileen State #1 and #2 wells. In the 1972 Northwest Eileen State #2 well, gas hydrate was cored and tested (DST) within this interval. This interval (Figure A1) is within the USGS C Unit (Collett et al., 1988). While resistivity increases, acoustic time decreases in this interval. This behavior represents a classic example of gas hydrate petrophysical log response. Density and neutron logs do not display dramatic changes within this interval. In the Northwest Eileen State #1, similar resistivity increases are observed, but the acoustic, density and neutron logs are of poor quality. Considering the relative short distance between these wells and similar gamma ray and resistivity

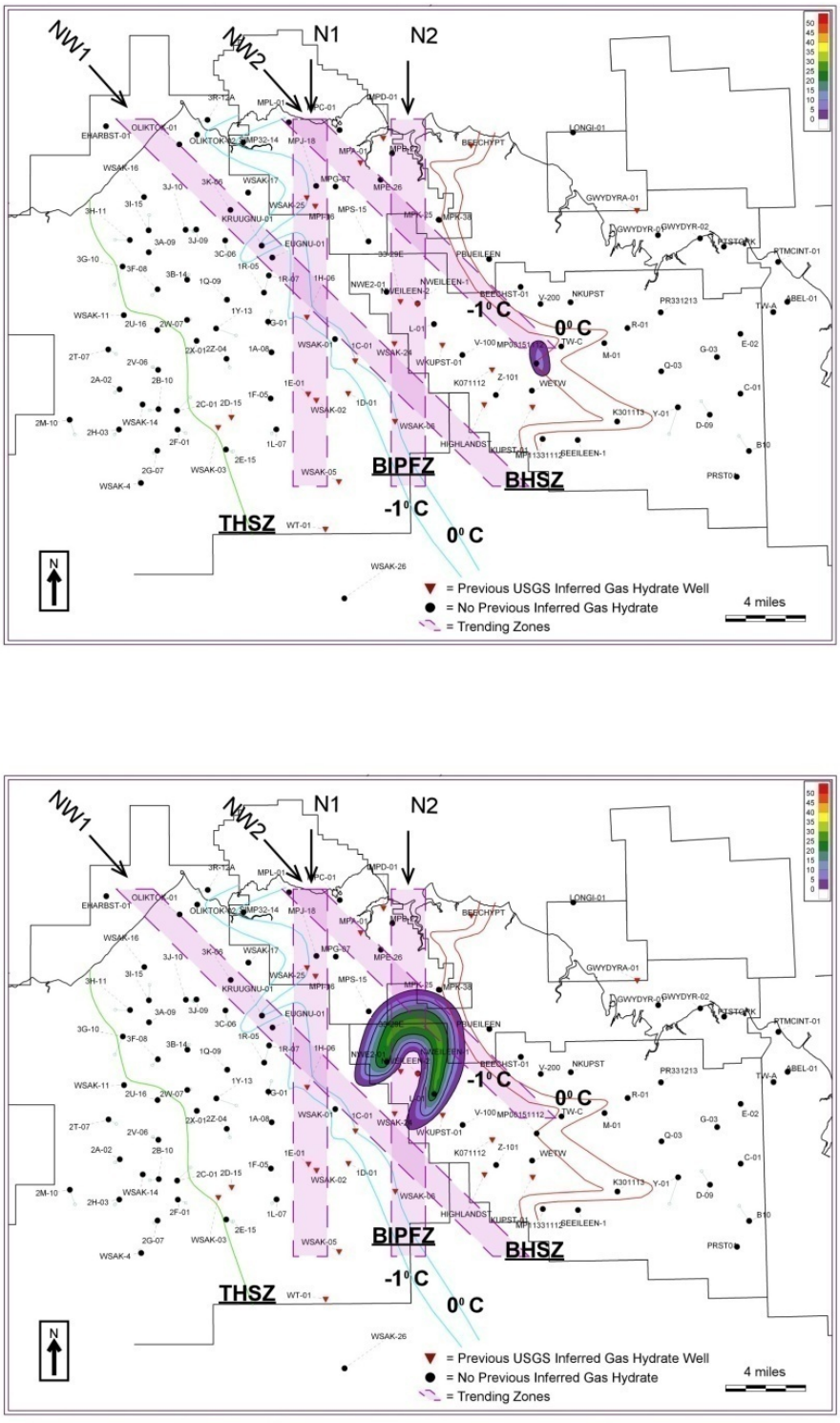

Figure A25: The upper map is a hand contoured net pay map of time slice 8. This map represents the associated free gas that is inferred to exist in this interval. The lower map is a hand contoured net pay map for gas hydrate-bearing reservoirs that are inferred to exist within this interval. On both maps, the three major transition zones are present.

log behavior, assuming gas hydrate is also present in the Northwest Eileen State #1 was deemed acceptable. In the NWE2-01 and 33-29E wells, only gamma ray and resistivity logs were available. A moderate resistivity increase was displayed in both wells. These intervals were classified to have moderate gas hydrate indications and net pay footages were recorded. The structural up-dip location relative to the Northwest Eileen State wells provides a plausible pathway for migration of gas to have occurred into the NWE2-01 and 33-29E well region prior to the later conversion of gas into gas hydrate. All four wells in this region were inferred to contain gas hydrate. Facies characterization analysis reveals this region to be sand-rich with fringe channel and point bar deposits. Connectivity between these areas is likely due to the sand-rich nature of this interval, but the lateral extent may not be as expansive as drawn considering the limited dimensions of sands bodies typically associated with fluvial deposits. No dense well control is available in this area. Based on the strong log responses indicated, the net pay area interpretation was extended beyond well control. The north and south boundaries of the net pay region were constrained by wells with no gas hydrate indications. The west and east boundaries were controlled by the BIPFZ and BHSZ, respectively. In the southern part of the net pay map, a contour inflection is displayed to show the influence of the net sand map on this interval. Towards the east, the associated free gas corresponding with the gas hydrate-bearing reservoir is displayed. This associated free gas interpretation is not constrained by well control. Assuming that the lateral extent of this reservoir may potentially cross the BHSZ boundary, this smaller area would be the down dip gas associated with this gas hydrate-bearing reservoir as predicted in early gas hydrate models (Collett, 1988) and similar to the inferred reservoir behavior between the PS-33 to L-31A markers. The location of the BHSZ below the MPU K-pad is estimated and does not contain good well control for constraining purposes. This zone may lie further westward than drawn, but its exact location is uncertain. Depending on the true location of this zone, the amount of associated free gas inferred in this region can significantly change.

In the central part of the PBU area, a small gas show is again present in the MP00151112 and K091112 wells. Associated free gas was first determined in K091112 and then projected into the MP00151112 with similar log behavior as seen in time slice 8 (Figure A25). The lateral extent of this reservoir is limited since no surrounding wells demonstrate any net pay indications. The limited and small gas show is expressed as a small oval-shaped area on the map.

9.5.8.6 Net Pay Map Within Time Slice 10

One each intra-permafrost-, gas hydrate- and associated free gas-bearing reservoirs exist on the time slice 10 map (Figures A27 and A28). This slice contains the best defined net pay shows and laterally covers the largest area of potential reservoir within the AOI.

Beginning with the associated free gas reservoir, two wells contain gas indications. Evaluating the well-developed to moderate gas indications in PBUEILEEN and BEECHST-01, resistivity and acoustic time log measurements increase along with density logs decreasing throughout this interval. PBUEILEEN was the only well with a neutron log. The typical density and neutron crossover gas effect was present in this well. Well density in this area is minimal. Using the limited well control available, the BHSZ and the up-dip structural trend toward the southwest, a radial decreasing contour map was drawn that corresponds to the gas hydrate contour map (Figure A27).

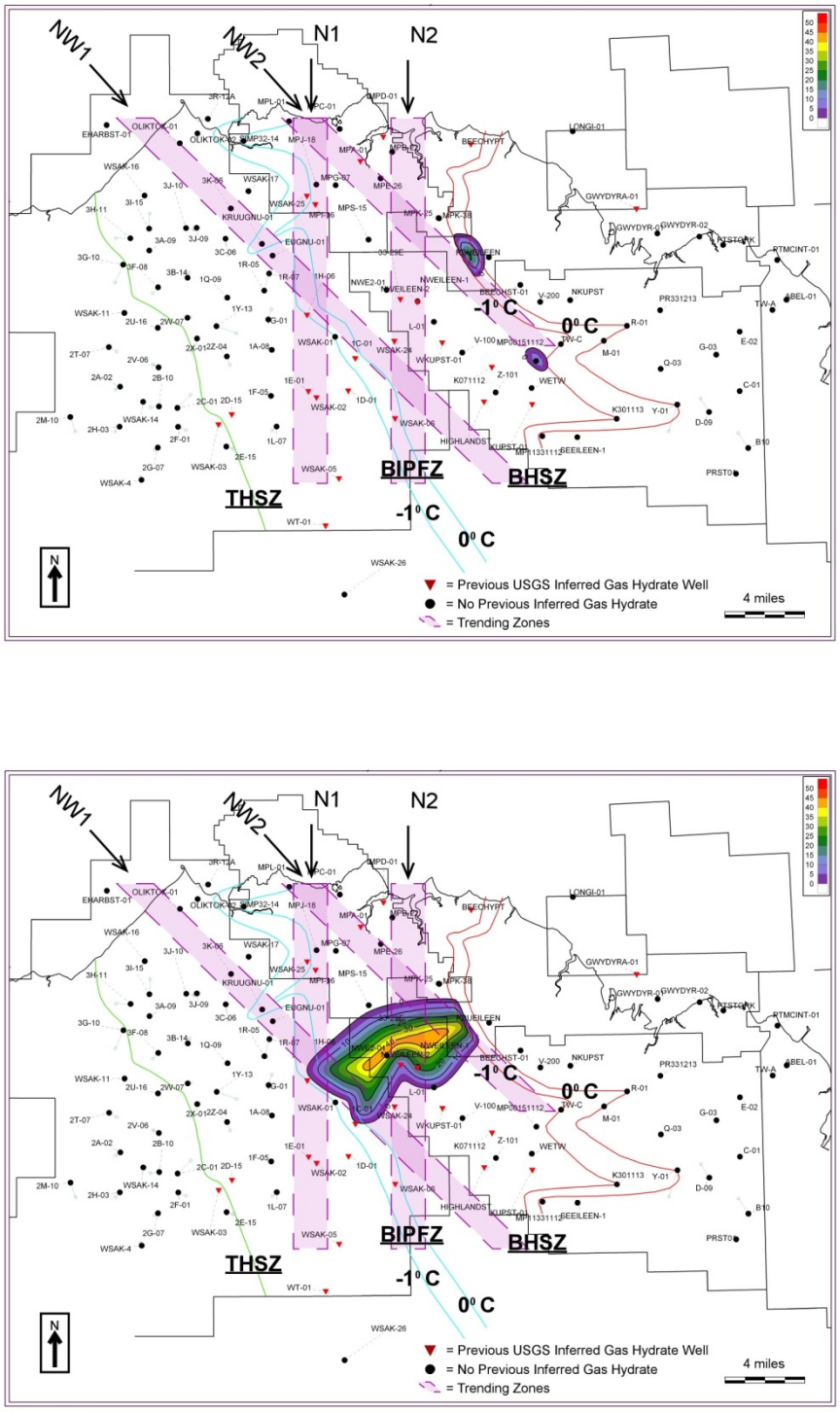

Figure A26: The upper map is a hand contoured net pay map of time slice 9. This map represents the associated free gas that is inferred to exist in this interval. The lower map is a hand contoured net pay map for gas hydrate-bearing reservoirs that are inferred to exist within this interval. On both maps, the three major transition zones are present.

In the gas hydrate-bearing reservoir, fifteen wells were identified with shows ranging in strength from well-developed to slight. The well-developed shows reside in the northwest portion of the PBU and are derived from the Northwest Eileen State #1, Northwest Eileen State #2, 33-29E, L-106 and WKUPST-01 wells. In this slice, gas hydrate cores were recovered from Northwest Eileen State #2. Another well-developed to moderate show is interpreted to exist in the MPA-01 well. This well has the only strong show within the MPU. Net pay contours were controlled by well density in many areas. In the southern part of the map, an abrupt termination of contours exist which was highly influenced by the V-107 well. The nearby WKUPST-01 and HIGHLANDST wells did contain sufficient amounts of net pay. Based on their location and the magnitude of net pay, a fault interpretation between these wells is presumed. The inferred fault at this location is oriented northwest, based on the net pay contour map and fault trends displayed. This direction appeared to align semi-parallel with the trending zones present in this study. A consistent contour thickness was still maintained for the area despite this condition. The lower extension of net pay beyond the HIGHLANDST well was projected from net sand trends in this area.

Along the east part of the net pay map, no well control was present and contour thickness limited the lateral extent of the pay for this region. Since no data is present between the BIPFZ and net pay contour map, this area could contain additional gas hydrate resources. Recognizing that this area is structurally up-dip to proven gas hydrate-bearing zones that are stratigraphically connected, migration of gas up-dip into these locations is conceivable. Along the west part of the map, the BHSZ controls contour behavior for this region. The phase transition occurring within the BHSZ correlates with the associated free gas contour map to illustrate the presence of gas throughout this zone. Physical connection of both reservoirs is assumed for this area. On the north end in the MPU, well control and contour thickness dictate net pay contour behavior. A thicker net pay region is extended southward with no supporting well data. Contours were drawn in this manner to reflect the pull-apart basin (Figure A11) inferred by Casavant (2004). For the entire reservoir within the MPU, five wells contain net pay values above the PS-34 horizon. These wells include MPB-01, MPA-01, MPJ-18, NWE2-01 and WSAK-24.

The intra-permafrost net pay map is a direct function of the net sand map for this interval. Identical resistivity well log responses from all wells are observed between the THSZ and BIPFZ. Attempting to identify net pay in this area using only a well log based analysis is infeasible since ice and gas hydrate cannot be distinguished from each other. Recognizing from Lachenbruch (1988) that intra-permafrost gas hydrate does exist, assuming gas hydrate-bearing prospects in this region is probable. Making a second assumption that net pay is a function of sand quality, net pay contours for this area were generated. Acknowledging that this area is located structurally up-dip and is stratigraphically connected to the largest and best developed reservoir in the IOI and that inferred gas hydrate-bearing reservoirs exist at greater depths according to the previous USGS studies (Collett et al., 1988 - red triangles on map figures), the source providing methane to this region is plausible. The parameters constraining the limits of this reservoir are the THSZ, BIPFZ, trends in the net sand map, and the location of USGS-inferred lower gas hydrate-bearing reservoirs. No net pay contour extended past these boundaries. Gas volumes from this area are to be viewed with extreme caution since these assumptions only imply its existence.

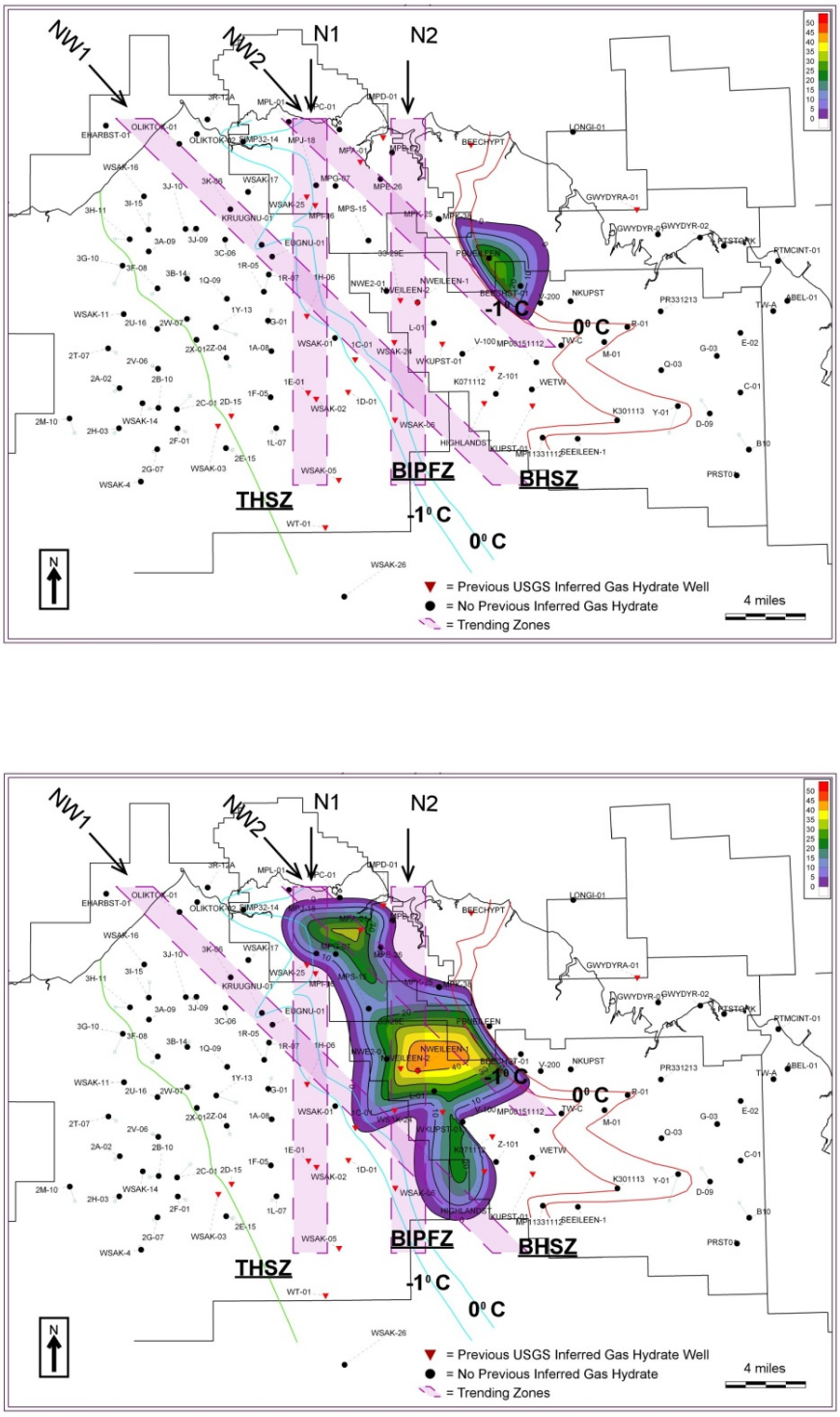

Figure A27: The upper map is a hand contoured net pay map of time slice 10. This map represents the associated free gas that is inferred to exist in this interval. The lower map is a hand contoured net pay map for gas hydrate-bearing reservoirs that are inferred to exist within this interval. On both maps, the three major transition zones are present.

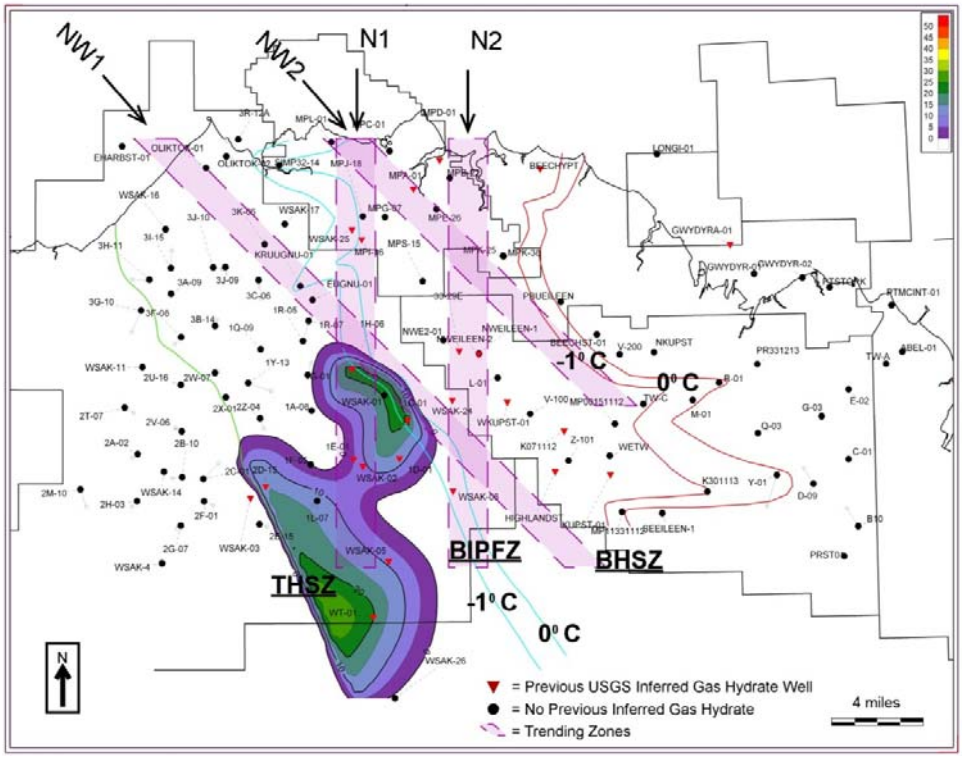

Figure A28: This map displays the hand contoured regions that are inferred to contain intra-permafrost gas hydrate-bearing reservoirs within time slice 10. Since identification of gas hydrate solely using petrophysical well logs is impractical in this area, the results displayed in this map should be viewed with extreme caution.

9.6 Volumetric Assessment for the Area and Intervals of Interest

The following volumetric analysis is from the work of Manuel (2008) from well log and other geologic data. After all net pay maps were created, total rock volumes from all maps were calculated. Using the net pay contour maps and PETRA's volumetric calculation capabilities, volume totals for areas that contained positive contour values were computed. Each volume total was generated using a grid refinement of three and average porosity, gas saturation, gas expansion factors and other volumetric parameters as provided below. Raw volumes in cubic square feet were generated from PETRA and were exported into a Microsoft Excel spreadsheet. These volumes are recorded in Tables A2 and A3, documented by interval. Both associated free gas (Table A2) and gas hydrate (Table A3) volumetrics were generated. The equations used to quantify the amount of original-gas-in-place (OGIP) for gas hydrate- and associated free gas-bearing reservoirs are listed below.

9.6.1 Associated Free Gas Volumetrics

$OGIP_G$ = Volume total * ϕ * B_g * S_g

Volume total = Computed utilizing net pay contour maps and PETRA computing capabilities

ϕ = Average porosity, taken from USGS MPU seismic and volumetric study (36%)

B_g = Free gas expansion factor, taken from USGS MPU seismic and volumetric study (108)

S_g = Gas saturation, taken from USGS MPU seismic and volumetric study (70%)

Volumetrics for Chronostratigraphy Framework in AOI area
Associated Free Gas Volumetrics

1	2	3	4	5
Interval Unit	Data Area (ft^2)	Volume (ft^3)	Reservoir Volume (ft^3)	Original Gas-In-Place (tcf)
Slice 10	418,989,139.49	4,455,513,544.17	1,603,984,875.90	0.121
Slice 9	83,812,607.24	546,777,721.94	196,839,979.90	0.015
Slice 8	39,775,400.79	122,256,197.84	44,012,231.22	0.003
Slice 7	0.00	0.00	0.00	0.000
Slice 6	0.00	0.00	0.00	0.000
Slice M4 to L31A	476,313,708.72	11,109,044,594.64	3,999,256,054.07	0.302

Total Reservoir Volume (bcf) = 5.84

Total Gas Volume (tcf) = 0.44

Total Gas Volume (x 10^{12} m^3) = 0.01252

Static Variables	
Porosity =	36%
B_G =	108
Gas Saturation =	70%

(1) Interval unit defined by gas hydrate team
(2) Data area of net pay for each unit calculated in GeoPlus - PETRA volumetric program
(3) Volume of reservoir rock computed in GeoPlus-PETRA volumetric program
(4) Reservoir Rock Volume = Volume * Porosity
(5) OGIP volume calculated assuming a gas saturation of 70 % and a B_G expansion factor of 108.

Note: Porosity, B_G and Gas Saturation values were taken from USGS Milne Point seismic volumetric study to produce comparable volumetric numbers

Assumed 35.3 ft^3 = 1 m^3

Table A2: Free Gas-in-place Volumetrics calculations total 0.44 TCF for chronostratigraphic framework in IOI within AOI (Figure A1) from Manuel (2008)

Volumetrics for Chronostratigraphy Framework in AOI
Gas Hydrate Volumetrics

1	2	3	4	5	Static Variables	
Interval Unit	Data Area (ft^2)	Volume (ft^3)	Reservoir Volume (ft^3)	Original Gas-In-Place (tcf):		
Slice 10	2,488,199,686.68	40,724,439,557.19	15,475,287,031.73	2.157	Porosity =	38%
Slice 9	899,687,933.01	16,646,464,963.44	6,325,656,686.11	0.882	B_{GH} =	164
Slice 8	648,523,815.31	8,391,902,527.30	3,188,922,960.37	0.445	Gas Saturation =	85%
Slice 7	743,768,460.56	9,289,901,619.59	3,530,162,615.44	0.492		
Slice 6	857,382,533.33	6,049,729,635.31	2,298,897,261.42	0.320		
Slice M4 to L31A	441,641,750.83	11,399,232,628.77	4,331,708,398.93	0.604		
Permafrost Slice 10	2,092,833,531.56	23,243,667,664.36	8,832,593,712.46	1.231		

Total Reservoir Volume (bcf) = 43.98

Total Gas Volume (tcf) = 6.131 4.900

Total Gas Volume (x 10^{12} m^3) = 0.174

(1) Interval unit defined by gas hydrate team
(2) Data area of net pay for each unit calculated in GeoPlus - PETRA volumetric program
(3) Volume of reservoir rock computed in GeoPlus-PETRA volumetric program
(4) Reservoir Rock Volume = Volume * Porosity
(5) OGIP volume calculated assuming a gas saturation of 85% and a B_{GH} expansion factor of 164 as suggested by Collett (1993) and Sloan (1990)

Note: Porosity and B_{GH} values were taken from USGS Milne Point seismic volumetric study to produce comparable volumetric numbers

Assumed 35.3 ft^3 = 1 m^3

Table A3: Gas Hydrate Gas-in-place Volumetrics calculations total 6.1 TCF for chronostratigraphic framework in IOI within AOI (Figure A1) from Manuel (2008). This compares to 8.9 TCF risked gas-in-place from the Eileen accumulation regional schematic modeling documented in Quarterly Report 15 (R15). The 4.9 TCF is gas hydrate volume gas-in-place below ice-bearing permafrost (IBPF).

9.6.2 Gas Hydrate Volumetrics

$OGIP_{GH}$ = Volume total * ϕ * B_{gh} * S_{gh}

Volume total = Computed utilizing net pay contour maps and PETRA computing capabilities

ϕ = Average porosity, from USGS MPU seismic and volumetric study (38%)

B_{gh} = Gas hydrate expansion factor, from USGS study and Sloan (1990) (164)

S_{gh} = Gas saturation, assumed to be 85% from Collett (1988 and 1993) studies

9.6.3 Volumetrics Discussion

In an attempt to compare volumetric results to the USGS MPU study (Task 5), porosity, expansion and saturation values for both gas hydrate and associated free gas were used from Collett (1988 and 1993). The only parameter not directly used from the USGS volumetric study was the gas expansion factor for gas hydrate. This parameter was from Sloan (1990).

The original gas-in-place (OGIP) for all gas hydrate-bearing reservoirs studied within the IOI is 6.131 trillion cubic feet (TCF). Subtracting the intra-permafrost interval due to the ambiguity between ice and gas hydrate identification, the modified OGIP is 4.900 TCF. The greatest volumes of gas reside in slice 10 (uppermost Zone C). This interval overall contains the best development of net pay and covers a large area. The second largest gas volumes calculated are within the inferred intra-permafrost reservoir. This reservoir is based on assumptions of gas migration pathways and the presence of intra-permafrost gas hydrate-bearing reservoirs. No unambiguous gas indications can be proven with the data provided, but if this phenomenon does exist, then gas volumes in this area could be immense. Slice 9 contains the third largest calculated gas volumes. This reservoir is physically connected with Slice 10 and provides a favorable area for potential future gas hydrate production. In slices 8, 7 and 6, less pronounced reservoirs exist and are located beneath the reservoirs identified in Slices 10 and 9. Between the PS-33 to L-31A markers, an inferred reservoir exists in the southeast section of the MPU from USGS seismic analysis. This strong response is a combination of seismic interpreted gas hydrate-bearing reservoirs and a large associated free gas interval identified in the MPU K-pad area. Also, at the western boundary of the PBU, another reservoir resides within this interval.

The OGIP for all associated free gas reservoirs studied within the IOI is 0.44 trillion cubic feet (TCF). The largest volumes of free gas reside between the PS-33 to L-31A markers. The MPU reservoir is defined by two closely spaced wells in the MPU K-pad area and by the Mount Elbert prospect near its northwest boundary. Another less pronounced reservoir in the PBU exists within this interval. Combining both reservoirs, approximately 68% of the free gas volume is contained in this slice. Since three wells, two from the same well pad, define majority of the net pay for the IOI, assuming the largest gas volumes reside in this interval should be done with caution due to the lack of data available. The second largest free gas reservoir is present within slice 10. This associated free gas is inferred to be the down-dip gas source related to the pronounced gas hydrate-bearing reservoir within this interval. The other two free gas-bearing reservoirs in Slice 9 and 8 contribute only minor volumes and should not be viewed as primary targets. Combining all gas hydrate and associated free gas OGIP totals, the GIP within the IOI is 6.571 TCF. Acknowledging that only well-defined and moderate gas indications contributed to the final total, then the shale prone, interbedded sand, and marginal reservoirs could add significant amounts to the final gas totals, but these were not quantified in this study.

10.0 APPENDIX B: MT ELBERT-01 CORE PROPERTIES

10.1 Grain Size Data

Figures B1-B20 illustrate grain size data from sieve and laser analyses for Mt Elbert-01 cores.

SIEVE ANALYSIS

Conventional Core

U.S. Geological Survey - MA
Mt. Elbert 01 PPMA Samples

Core Run: 1
Core Section: 3
Sample Top-Bottom, In.: 33-36
File: HH-36917

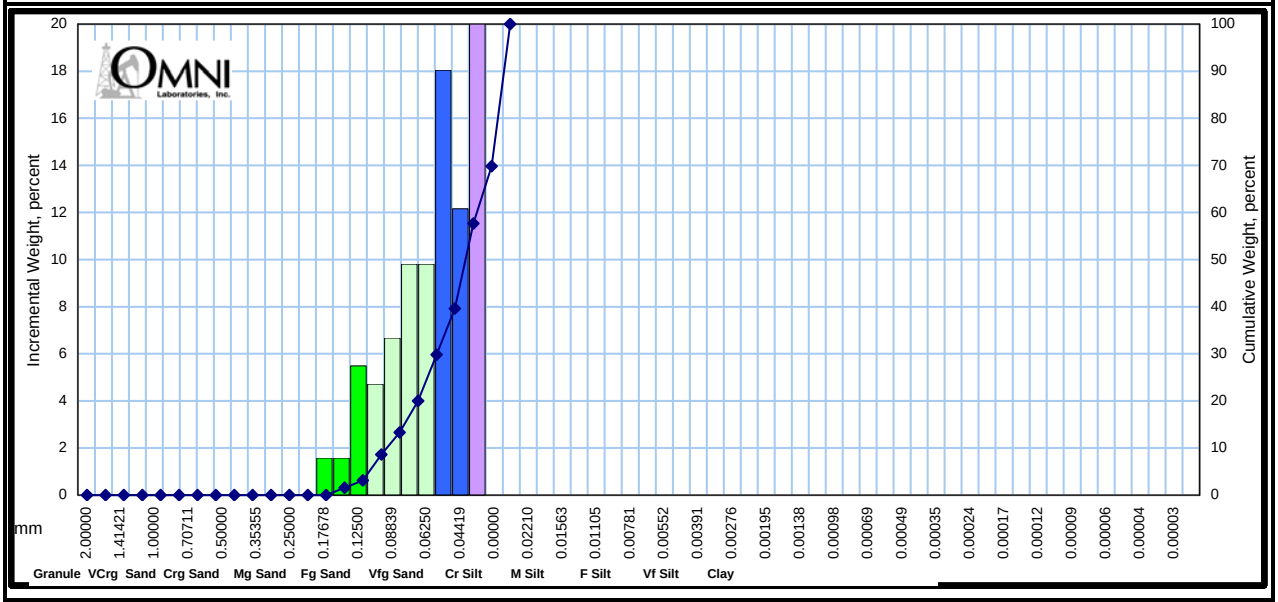

Wentworth Size Class	Mesh Size Inches	Mesh Size Millimeters	Phi of Screen	U.S. Sieve No.	Incremental Weight, percent	Cumulative Weight, percent
Granule	0.078740	2.00000	- 1.00	10	0.0	0.0
VCg Sand	0.066212	1.68179	- 0.75	12	0.0	0.0
	0.055678	1.41421	- 0.50	14	0.0	0.0
	0.046819	1.18921	- 0.25	16	0.0	0.0
	0.039370	1.00000	0.00	18	0.0	0.0
Cg Sand	0.033106	0.84090	0.25	20	0.0	0.0
	0.027839	0.70711	0.50	25	0.0	0.0
	0.023410	0.59460	0.75	30	0.0	0.0
	0.019685	0.50000	1.00	35	0.0	0.0
Mg Sand	0.016553	0.42045	1.25	40	0.0	0.0
	0.013919	0.35355	1.50	45	0.0	0.0
	0.011705	0.29730	1.75	50	0.0	0.0
	0.009843	0.25000	2.00	60	0.0	0.0
Fg Sand	0.008277	0.21022	2.25	70	0.0	0.0
	0.006960	0.17678	2.50	80	1.6	1.6
	0.005852	0.14865	2.75	100	1.6	3.1
	0.004921	0.12500	3.00	120	5.5	8.6
Vfg Sand	0.004138	0.10511	3.25	140	4.7	13.3
	0.003480	0.08839	3.50	170	6.7	20.0
	0.002926	0.07433	3.75	200	9.8	29.8
	0.002461	0.06250	4.00	230	9.8	39.6
C Silt	0.002069	0.05256	4.25	270	18.0	57.6
	0.001740	0.04419	4.50	325	12.2	69.8
Pan				<325	30.2	100.0

Description	Sieve Size	Weight Percent
Granule	10	0.0
Very Coarse Sand	18	0.0
Coarse Sand	35	0.0
Medium Sand	60	0.0
Fine Sand	120	8.6
Very Fine Sand	230	31.0
Coarse Silt	0	30.2
Pan	<325	30.2

Cumulative Volume Percent greater than			
	Phi	Particle Size	
Percentile	Value	Inches	Millimeters
5	2.8301	0.0055	0.1406
10	3.0686	0.0047	0.1192
16	3.3449	0.0039	0.0984
25	3.6221	0.0032	0.0812
50	4.1387	0.0022	0.0568
75	4.6043	0.0016	0.0411
84	4.8051	0.0014	0.0358
90	4.5422	0.0017	0.0429
95	4.6374	0.0016	0.0402

Measure	Trask, mm	Folk, phi	Inches
Median	0.0568	4.1387	0.0022
Mean	0.0612	4.0962	0.0024
Sorting	1.4055	0.6389	
Skewness	1.0360	-0.2677	
Kurtosis	0.2629	0.7541	

Figure B1: Grain Size Sieve Analysis, Core 1, Section 3, 33 to 36 inches

LASER GRAIN SIZE ANALYSIS

Conventional Core

U.S. Geological Survey - MA
Mt. Elbert 01 PPMA Samples

Core Run: 1
Core Section: 3
Sample Top-Bottom, In.: 33-36
File: HH-36917

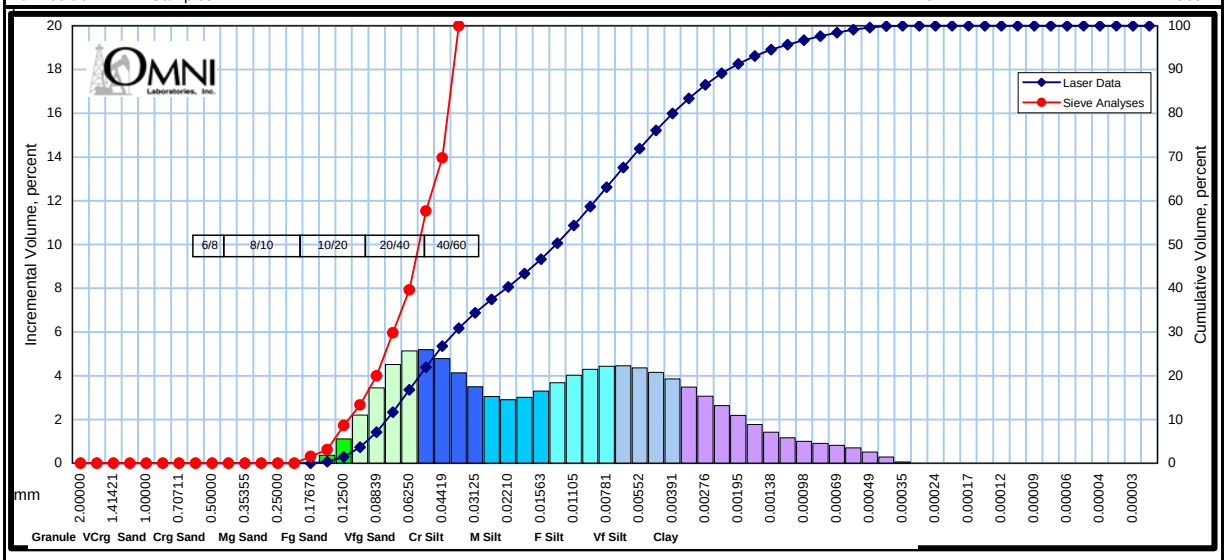

Wentworth Size Class	Mesh Size Inches	Mesh Size Millimeters	Phi of Screen	U.S. Sieve No.	Incremental Volume, percent	Cumulative Volume, percent
Granule	0.078740	2.00000	- 1.00	10	0.0	0.0
VCg Sand	0.066212	1.68179	- 0.75	12	0.0	0.0
	0.055678	1.41421	- 0.50	14	0.0	0.0
	0.046819	1.18921	- 0.25	16	0.0	0.0
	0.039370	1.00000	0.00	18	0.0	0.0
Cg Sand	0.033106	0.84090	0.25	20	0.0	0.0
	0.027839	0.70711	0.50	25	0.0	0.0
	0.023410	0.59460	0.75	30	0.0	0.0
	0.019685	0.50000	1.00	35	0.0	0.0
Mg Sand	0.016553	0.42045	1.25	40	0.0	0.0
	0.013919	0.35355	1.50	45	0.0	0.0
	0.011705	0.29730	1.75	50	0.0	0.0
	0.009843	0.25000	2.00	60	0.0	0.0
Fg Sand	0.008277	0.21022	2.25	70	0.0	0.0
	0.006960	0.17678	2.50	80	0.0	0.0
	0.005852	0.14865	2.75	100	0.4	0.4
	0.004921	0.12500	3.00	120	1.1	1.5
Vfg Sand	0.004138	0.10511	3.25	140	2.2	3.7
	0.003480	0.08839	3.50	170	3.4	7.1
	0.002926	0.07433	3.75	200	4.5	11.6
	0.002461	0.06250	4.00	230	5.1	16.8
C Silt	0.002069	0.05256	4.25	270	5.2	22.0
	0.001740	0.04419	4.50	325	4.8	26.8
	0.001463	0.03716	4.75	400	4.1	30.9
	0.001230	0.03125	5.00	450	3.5	34.4
M Silt	0.001035	0.02628	5.25	500	3.1	37.5
	0.000870	0.02210	5.50	635	2.9	40.4
	0.000732	0.01858	5.75		3.0	43.4
	0.000615	0.01563	6.00		3.3	46.7
F Silt	0.000517	0.01314	6.25		3.7	50.3
	0.000435	0.01105	6.50		4.0	54.4
	0.000366	0.00929	6.75		4.3	58.7
	0.000308	0.00781	7.00		4.4	63.1
Vf Silt	0.000259	0.00657	7.25		4.5	67.6
	0.000217	0.00552	7.50		4.4	71.9
	0.000183	0.00465	7.75		4.2	76.1
	0.000154	0.00391	8.00		3.9	80.0
Clay	0.000129	0.00329	8.25		3.5	83.4
	0.000109	0.00276	8.50		3.1	86.5
	0.000091	0.00232	8.75		2.6	89.1
	0.000077	0.00195	9.00		2.2	91.3
	0.000065	0.00164	9.25		1.8	93.1
	0.000054	0.00138	9.50		1.4	94.5
	0.000046	0.00116	9.75		1.2	95.7
	0.000038	0.00098	10.00		1.0	96.7
	0.000032	0.00082	10.25		0.9	97.6
	0.000027	0.00069	10.50		0.8	98.4
	0.000023	0.00058	10.75		0.7	99.1
	0.000019	0.00049	11.00		0.5	99.6
	0.000016	0.00041	11.25		0.3	99.9
	0.000014	0.00035	11.50		0.1	100.0
	0.000011	0.00029	11.75		0.0	100.0
	0.000010	0.00024	12.00		0.0	100.0
	0.000008	0.00021	12.25		0.0	100.0
	0.000007	0.00017	12.50		0.0	100.0
	0.000006	0.00015	12.75		0.0	100.0
	0.000005	0.00012	13.00		0.0	100.0
	0.000004	0.00010	13.25		0.0	100.0
	0.000003	0.00009	13.51		0.0	100.0
	0.000003	0.00007	13.74		0.0	100.0
	0.000002	0.00006	14.00		0.0	100.0
	0.000002	0.000051	14.26		0.0	100.0
	0.000002	0.000043	14.51		0.0	100.0
	0.000001	0.000036	14.76		0.0	100.0
	0.000001	0.000031	14.98		0.0	100.0
	0.000001	0.000026	15.23		0.0	100.0
	TOTALS				100.0	100.0

Description	Sieve Size	Volume Percent
Granule	10	0.0
Very Coarse Sand	18	0.0
Coarse Sand	35	0.0
Medium Sand	60	0.0
Fine Sand	120	1.5
Very Fine Sand	230	15.3
Coarse Silt	450	17.6
Medium Silt		12.3
Fine Silt		16.4
Very Fine Silt		16.8
Clay		20.0
	Total	100.0

Cumulative Volume Percent greater than			
	Phi	Particle Size	
Percentile	Value	Inches	Millimeters
5	3.3509	0.0039	0.0980
10	3.6590	0.0031	0.0792
16	3.9570	0.0025	0.0644
25	4.3977	0.0019	0.0474
50	6.2188	0.0005	0.0134
75	7.6721	0.0002	0.0049
84	8.2823	0.0001	0.0032
90	8.8316	0.0001	0.0022
95	9.5851	0.0001	0.0013

Measure	Trask, mm	Folk, phi	Inches
Median	0.0134	6.2188	0.0005
Mean	0.0262	6.1527	0.0010
Sorting	3.1106	2.0259	
Skewness	1.2904	0.0170	
Kurtosis	0.2763	0.7803	

Figure B2: Grain Size Laser Analysis, Core 1, Section 3, 33 to 36 inches

SIEVE ANALYSIS

Conventional Core

U.S. Geological Survey - MA
Mt. Elbert 01 PPMA Samples

Core Run: 2
Core Section: 7
Sample Top-Bottom, In.: 33-36
File: HH-36917

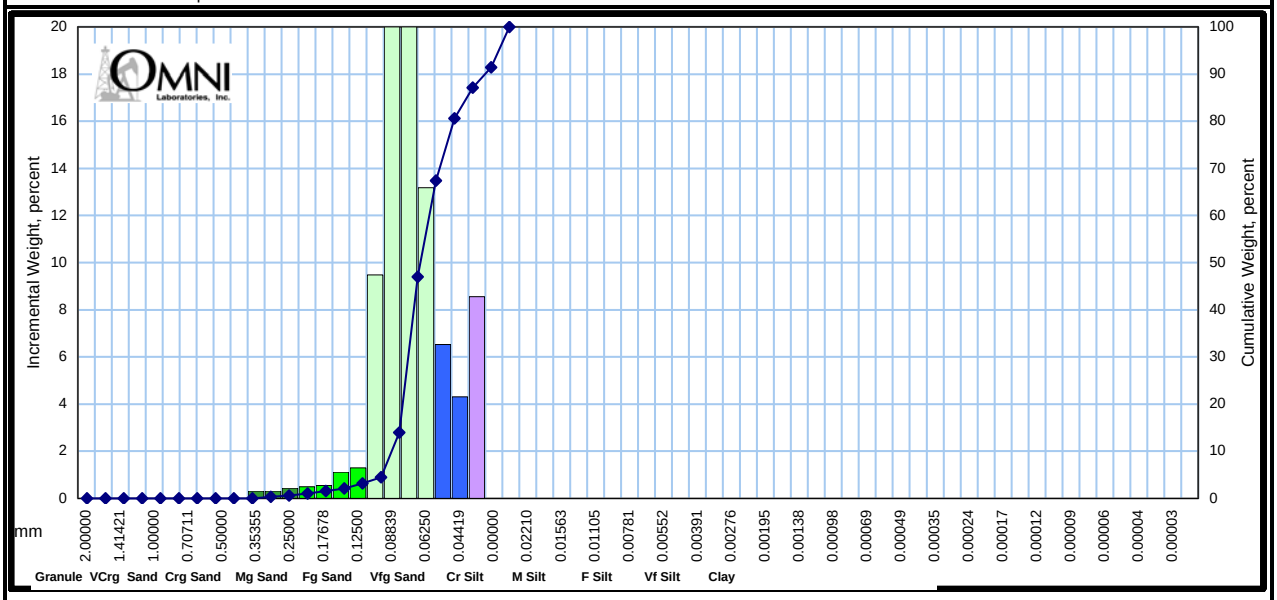

Wentworth Size Class	Mesh Size Inches	Mesh Size Millimeters	Phi of Screen	U.S. Sieve No.	Incremental Weight, percent	Cumulative Weight, percent
Granule	0.078740	2.00000	- 1.00	10	0.0	0.0
VCg Sand	0.066212	1.68179	- 0.75	12	0.0	0.0
	0.055678	1.41421	- 0.50	14	0.0	0.0
	0.046819	1.18921	- 0.25	16	0.0	0.0
	0.039370	1.00000	0.00	18	0.0	0.0
Cg Sand	0.033106	0.84090	0.25	20	0.0	0.0
	0.027839	0.70711	0.50	25	0.0	0.0
	0.023410	0.59460	0.75	30	0.0	0.0
	0.019685	0.50000	1.00	35	0.0	0.0
Mg Sand	0.016553	0.42045	1.25	40	0.0	0.0
	0.013919	0.35355	1.50	45	0.3	0.3
	0.011705	0.29730	1.75	50	0.3	0.6
	0.009843	0.25000	2.00	60	0.4	1.0
Fg Sand	0.008277	0.21022	2.25	70	0.5	1.5
	0.006960	0.17678	2.50	80	0.6	2.1
	0.005852	0.14865	2.75	100	1.1	3.2
	0.004921	0.12500	3.00	120	1.3	4.5
Vfg Sand	0.004138	0.10511	3.25	140	9.5	14.0
	0.003480	0.08839	3.50	170	33.0	47.0
	0.002926	0.07433	3.75	200	20.4	67.4
	0.002461	0.06250	4.00	230	13.2	80.6
C Silt	0.002069	0.05256	4.25	270	6.5	87.1
	0.001740	0.04419	4.50	325	4.3	91.4
Pan				<325	8.6	100.0

Description	Sieve Size	Weight Percent
Granule	10	0.0
Very Coarse Sand	18	0.0
Coarse Sand	35	0.0
Medium Sand	60	1.0
Fine Sand	120	3.4
Very Fine Sand	230	76.1
Coarse Silt	0	10.8
Pan	<325	8.6

Cumulative Volume Percent greater than			
	Phi	Particle Size	
Percentile	Value	Inches	Millimeters
5	3.0123	0.0049	0.1239
10	3.1398	0.0045	0.1135
16	3.2641	0.0041	0.1041
25	3.3288	0.0039	0.0995
50	3.5343	0.0034	0.0863
75	3.8884	0.0027	0.0675
84	4.1247	0.0023	0.0573
90	4.5422	0.0017	0.0429
95	4.6374	0.0016	0.0402

Measure	Trask, mm	Folk, phi	Inches
Median	0.0863	3.5343	0.0034
Mean	0.0835	3.6410	0.0033
Sorting	1.2140	0.4614	
Skewness	0.9022	0.3649	
Kurtosis	0.2268	1.1902	

Figure B3: Grain Size Sieve Analysis, Core 2, Section 7, 33 to 36 inches

LASER GRAIN SIZE ANALYSIS

Conventional Core

U.S. Geological Survey - MA
Mt. Elbert 01 PPMA Samples

Core Run: 2
Core Section: 7
Sample Top-Bottom, In.: 33-36
File: HH-36917

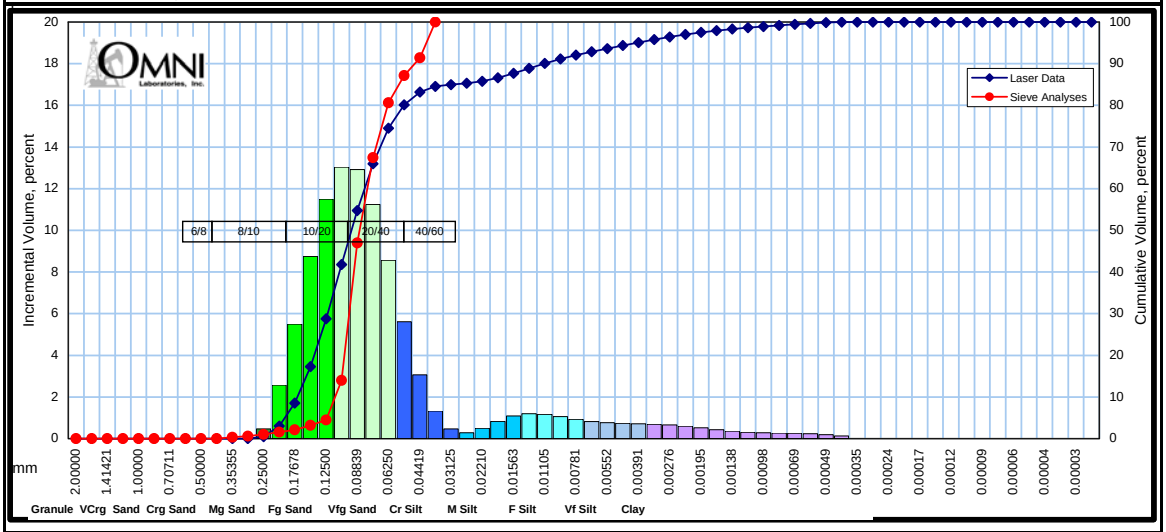

Wentworth Size Class	Mesh Size Inches	Mesh Size Millimeters	Phi of Screen	U.S. Sieve No.	Incremental Volume, percent	Cumulative Volume, percent
Granule	0.078740	2.00000	- 1.00	10	0.0	0.0
VCg Sand	0.066212	1.68179	- 0.75	12	0.0	0.0
	0.055678	1.41421	- 0.50	14	0.0	0.0
	0.046819	1.18921	- 0.25	16	0.0	0.0
	0.039370	1.00000	0.00	18	0.0	0.0
Cg Sand	0.033106	0.84090	0.25	20	0.0	0.0
	0.027839	0.70711	0.50	25	0.0	0.0
	0.023410	0.59460	0.75	30	0.0	0.0
	0.019685	0.50000	1.00	35	0.0	0.0
Mg Sand	0.016553	0.42045	1.25	40	0.0	0.0
	0.013919	0.35355	1.50	45	0.0	0.0
	0.011705	0.29730	1.75	50	0.0	0.0
	0.009843	0.25000	2.00	60	0.5	0.5
Fg Sand	0.008277	0.21022	2.25	70	2.6	3.0
	0.006960	0.17678	2.50	80	5.5	8.5
	0.005852	0.14865	2.75	100	8.7	17.3
	0.004921	0.12500	3.00	120	11.5	28.8
Vfg Sand	0.004138	0.10511	3.25	140	13.0	41.8
	0.003480	0.08839	3.50	170	12.9	54.7
	0.002926	0.07433	3.75	200	11.2	66.0
	0.002461	0.06250	4.00	230	8.6	74.5
C Silt	0.002069	0.05256	4.25	270	5.6	80.1
	0.001740	0.04419	4.50	325	3.1	83.2
	0.001463	0.03716	4.75	400	1.3	84.5
	0.001230	0.03125	5.00	450	0.5	85.0
M Silt	0.001035	0.02628	5.25	500	0.3	85.3
	0.000870	0.02210	5.50	635	0.5	85.8
	0.000732	0.01858	5.75		0.8	86.6
	0.000615	0.01563	6.00		1.1	87.7
F Silt	0.000517	0.01314	6.25		1.2	88.9
	0.000435	0.01105	6.50		1.2	90.1
	0.000366	0.00929	6.75		1.1	91.1
	0.000308	0.00781	7.00		0.9	92.0
Vf Silt	0.000259	0.00657	7.25		0.8	92.9
	0.000217	0.00552	7.50		0.8	93.6
	0.000183	0.00465	7.75		0.7	94.4
	0.000154	0.00391	8.00		0.7	95.1
Clay	0.000129	0.00329	8.25		0.7	95.8
	0.000109	0.00276	8.50		0.7	96.4
	0.000091	0.00232	8.75		0.6	97.0
	0.000077	0.00195	9.00		0.5	97.5
	0.000065	0.00164	9.25		0.4	98.0
	0.000054	0.00138	9.50		0.4	98.3
	0.000046	0.00116	9.75		0.3	98.6
	0.000038	0.00098	10.00		0.3	98.9
	0.000032	0.00082	10.25		0.3	99.2
	0.000027	0.00069	10.50		0.3	99.4
	0.000023	0.00058	10.75		0.2	99.7
	0.000019	0.00049	11.00		0.2	99.9
	0.000016	0.00041	11.25		0.1	100.0
	0.000014	0.00035	11.50		0.0	100.0
	0.000011	0.00029	11.75		0.0	100.0
	0.000010	0.00024	12.00		0.0	100.0
	0.000008	0.00021	12.25		0.0	100.0
	0.000007	0.00017	12.50		0.0	100.0
	0.000006	0.00015	12.75		0.0	100.0
	0.000005	0.00012	13.00		0.0	100.0
	0.000004	0.00010	13.25		0.0	100.0
	0.000003	0.00009	13.51		0.0	100.0
	0.000003	0.00007	13.74		0.0	100.0
	0.000002	0.00006	14.00		0.0	100.0
	0.000002	0.000051	14.26		0.0	100.0
	0.000002	0.000043	14.51		0.0	100.0
	0.000001	0.000036	14.76		0.0	100.0
	0.000001	0.000031	14.98		0.0	100.0
	0.000001	0.000026	15.23		0.0	100.0
	TOTALS				100.0	100.0

Description	Sieve Size	Volume Percent
Granule	10	0.0
Very Coarse Sand	18	0.0
Coarse Sand	35	0.0
Medium Sand	60	0.5
Fine Sand	120	28.3
Very Fine Sand	230	45.7
Coarse Silt	450	10.5
Medium Silt		2.7
Fine Silt		4.3
Very Fine Silt		3.0
Clay		4.9
	Total	100.0

Cumulative Volume Percent greater than			
	Phi	Particle Size	
Percentile	Value	Inches	Millimeters
5	2.3534	0.0077	0.1957
10	2.5448	0.0067	0.1714
16	2.7141	0.0060	0.1524
25	2.9183	0.0052	0.1323
50	3.4010	0.0037	0.0947
75	4.0110	0.0024	0.0620
84	4.6099	0.0016	0.0410
90	6.4769	0.0004	0.0112
95	7.9593	0.0002	0.0040

Measure	Trask, mm	Folk, phi	Inches
Median	0.0947	3.4010	0.0037
Mean	0.0972	3.5750	0.0038
Sorting	1.4604	1.3233	
Skewness	0.9156	0.4508	
Kurtosis	0.2194	2.1025	

Figure B4: Grain Size Laser Analysis, Core 2, Section 7, 33 to 36 inches

SIEVE ANALYSIS

Conventional Core

U.S. Geological Survey - MA
Mt. Elbert 01 PPMA Samples

Core Run: 3
Core Section: 3
Sample Top-Bottom, In.: 34-36
File: HH-36917

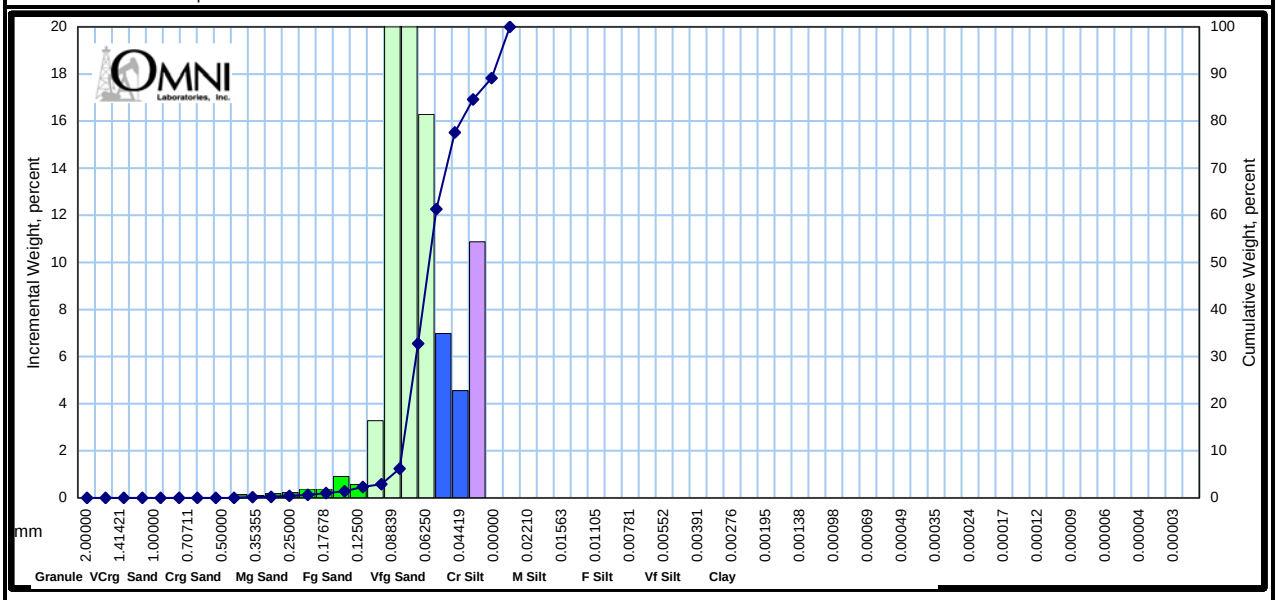

Wentworth Size Class	Mesh Size Inches	Mesh Size Millimeters	Phi of Screen	U.S. Sieve No.	Incremental Weight, percent	Cumulative Weight, percent
Granule	0.078740	2.00000	- 1.00	10	0.0	0.0
VCg Sand	0.066212	1.68179	- 0.75	12	0.0	0.0
	0.055678	1.41421	- 0.50	14	0.0	0.0
	0.046819	1.18921	- 0.25	16	0.0	0.0
	0.039370	1.00000	0.00	18	0.0	0.0
Cg Sand	0.033106	0.84090	0.25	20	0.0	0.0
	0.027839	0.70711	0.50	25	0.0	0.0
	0.023410	0.59460	0.75	30	0.0	0.0
	0.019685	0.50000	1.00	35	0.0	0.0
Mg Sand	0.016553	0.42045	1.25	40	0.1	0.1
	0.013919	0.35355	1.50	45	0.1	0.2
	0.011705	0.29730	1.75	50	0.2	0.4
	0.009843	0.25000	2.00	60	0.2	0.7
Fg Sand	0.008277	0.21022	2.25	70	0.4	1.0
	0.006960	0.17678	2.50	80	0.4	1.4
	0.005852	0.14865	2.75	100	0.9	2.3
	0.004921	0.12500	3.00	120	0.6	2.9
Vfg Sand	0.004138	0.10511	3.25	140	3.3	6.2
	0.003480	0.08839	3.50	170	26.6	32.8
	0.002926	0.07433	3.75	200	28.5	61.3
	0.002461	0.06250	4.00	230	16.3	77.6
C Silt	0.002069	0.05256	4.25	270	7.0	84.6
	0.001740	0.04419	4.50	325	4.6	89.1
Pan				<325	10.9	100.0

Description	Sieve Size	Weight Percent
Granule	10	0.0
Very Coarse Sand	18	0.0
Coarse Sand	35	0.0
Medium Sand	60	0.7
Fine Sand	120	2.2
Very Fine Sand	230	74.7
Coarse Silt	0	11.5
Pan	<325	10.9

Cumulative Volume Percent greater than			
	Phi	Particle Size	
Percentile	Value	Inches	Millimeters
5	3.1555	0.0044	0.1122
10	3.2834	0.0040	0.1027
16	3.3374	0.0039	0.0989
25	3.4224	0.0037	0.0933
50	3.6458	0.0031	0.0799
75	3.9573	0.0025	0.0644
84	4.2280	0.0021	0.0534
90	4.5422	0.0017	0.0429
95	4.6374	0.0016	0.0402

Measure	Trask, mm	Folk, phi	Inches
Median	0.0799	3.6458	0.0031
Mean	0.0788	3.7371	0.0031
Sorting	1.2037	0.4472	
Skewness	0.9407	0.3229	
Kurtosis	0.2416	1.1356	

Figure B5: Grain Size Sieve Analysis, Core 3, Section 3, 34 to 36 inches

LASER GRAIN SIZE ANALYSIS

Conventional Core

U.S. Geological Survey - MA
Mt. Elbert 01 PPMA Samples

Core Run: 3
Core Section: 3
Sample Top-Bottom, In.: 34-36
File: HH-36917

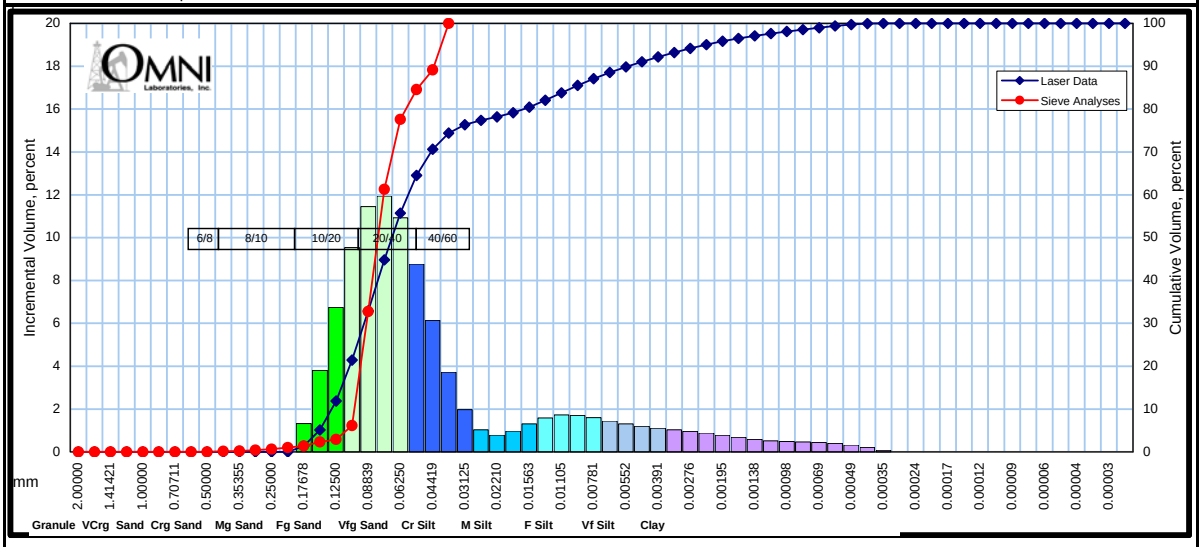

Wentworth Size Class	Mesh Size Inches	Mesh Size Millimeters	Phi of Screen	U.S. Sieve No.	Incremental Volume, percent	Cumulative Volume, percent
Granule	0.078740	2.00000	- 1.00	10	0.0	0.0
VCg Sand	0.066212	1.68179	- 0.75	12	0.0	0.0
	0.055678	1.41421	- 0.50	14	0.0	0.0
	0.046819	1.18921	- 0.25	16	0.0	0.0
	0.039370	1.00000	0.00	18	0.0	0.0
Cg Sand	0.033106	0.84090	0.25	20	0.0	0.0
	0.027839	0.70711	0.50	25	0.0	0.0
	0.023410	0.59460	0.75	30	0.0	0.0
	0.019685	0.50000	1.00	35	0.0	0.0
Mg Sand	0.016553	0.42045	1.25	40	0.0	0.0
	0.013919	0.35355	1.50	45	0.0	0.0
	0.011705	0.29730	1.75	50	0.0	0.0
	0.009843	0.25000	2.00	60	0.0	0.0
Fg Sand	0.008277	0.21022	2.25	70	0.0	0.0
	0.006960	0.17678	2.50	80	1.3	1.3
	0.005852	0.14865	2.75	100	3.8	5.1
	0.004921	0.12500	3.00	120	6.7	11.9
Vfg Sand	0.004138	0.10511	3.25	140	9.5	21.4
	0.003480	0.08839	3.50	170	11.5	32.9
	0.002926	0.07433	3.75	200	11.9	44.8
	0.002461	0.06250	4.00	230	10.9	55.7
C Silt	0.002069	0.05256	4.25	270	8.8	64.5
	0.001740	0.04419	4.50	325	6.1	70.6
	0.001463	0.03716	4.75	400	3.7	74.4
	0.001230	0.03125	5.00	450	2.0	76.4
M Silt	0.001035	0.02628	5.25	500	1.0	77.4
	0.000870	0.02210	5.50	635	0.8	78.2
	0.000732	0.01858	5.75		1.0	79.2
	0.000615	0.01563	6.00		1.3	80.5
F Silt	0.000517	0.01314	6.25		1.6	82.1
	0.000435	0.01105	6.50		1.7	83.8
	0.000366	0.00929	6.75		1.7	85.5
	0.000308	0.00781	7.00		1.6	87.1
Vf Silt	0.000259	0.00657	7.25		1.5	88.6
	0.000217	0.00552	7.50		1.3	89.9
	0.000183	0.00465	7.75		1.2	91.1
	0.000154	0.00391	8.00		1.1	92.2
Clay	0.000129	0.00329	8.25		1.0	93.2
	0.000109	0.00276	8.50		1.0	94.2
	0.000091	0.00232	8.75		0.9	95.1
	0.000077	0.00195	9.00		0.8	95.8
	0.000065	0.00164	9.25		0.7	96.5
	0.000054	0.00138	9.50		0.6	97.1
	0.000046	0.00116	9.75		0.5	97.6
	0.000038	0.00098	10.00		0.5	98.1
	0.000032	0.00082	10.25		0.5	98.6
	0.000027	0.00069	10.50		0.4	99.0
	0.000023	0.00058	10.75		0.4	99.4
	0.000019	0.00049	11.00		0.3	99.7
	0.000016	0.00041	11.25		0.2	99.9
	0.000014	0.00035	11.50		0.1	100.0
	0.000011	0.00029	11.75		0.0	100.0
	0.000010	0.00024	12.00		0.0	100.0
	0.000008	0.00021	12.25		0.0	100.0
	0.000007	0.00017	12.50		0.0	100.0
	0.000006	0.00015	12.75		0.0	100.0
	0.000005	0.00012	13.00		0.0	100.0
	0.000004	0.00010	13.25		0.0	100.0
	0.000003	0.00009	13.51		0.0	100.0
	0.000003	0.00007	13.74		0.0	100.0
	0.000002	0.00006	14.00		0.0	100.0
	0.000002	0.000051	14.26		0.0	100.0
	0.000002	0.000043	14.51		0.0	100.0
	0.000001	0.000036	14.76		0.0	100.0
	0.000001	0.000031	14.98		0.0	100.0
	0.000001	0.000026	15.23		0.0	100.0
	TOTALS				100.0	100.0

Description	Sieve Size	Volume Percent
Granule	10	0.0
Very Coarse Sand	18	0.0
Coarse Sand	35	0.0
Medium Sand	60	0.0
Fine Sand	120	11.9
Very Fine Sand	230	43.9
Coarse Silt	450	20.6
Medium Silt		4.1
Fine Silt		6.6
Very Fine Silt		5.1
Clay		7.8
	Total	100.0

Cumulative Volume Percent greater than			
	Phi	Particle Size	
Percentile	Value	Inches	Millimeters
5	2.7395	0.0059	0.1497
10	2.9362	0.0051	0.1307
16	3.1117	0.0046	0.1157
25	3.3266	0.0039	0.0997
50	3.8586	0.0027	0.0689
75	4.8051	0.0014	0.0358
84	6.5211	0.0004	0.0109
90	7.5182	0.0002	0.0055
95	8.7239	0.0001	0.0024

Measure	Trask, mm	Folk, phi	Inches
Median	0.0689	3.8586	0.0027
Mean	0.0677	4.4971	0.0027
Sorting	1.6693	1.7591	
Skewness	0.7502	0.5940	
Kurtosis	0.2552	1.6589	

Figure B6: Grain Size Laser Analysis, Core 3, Section 3, 34 to 36 inches

SIEVE ANALYSIS

Conventional Core

U.S. Geological Survey - MA
Mt. Elbert 01 PPMA Samples

Core Run: 4
Core Section: 7
Sample Top-Bottom, In.: 34-36
File: HH-36917

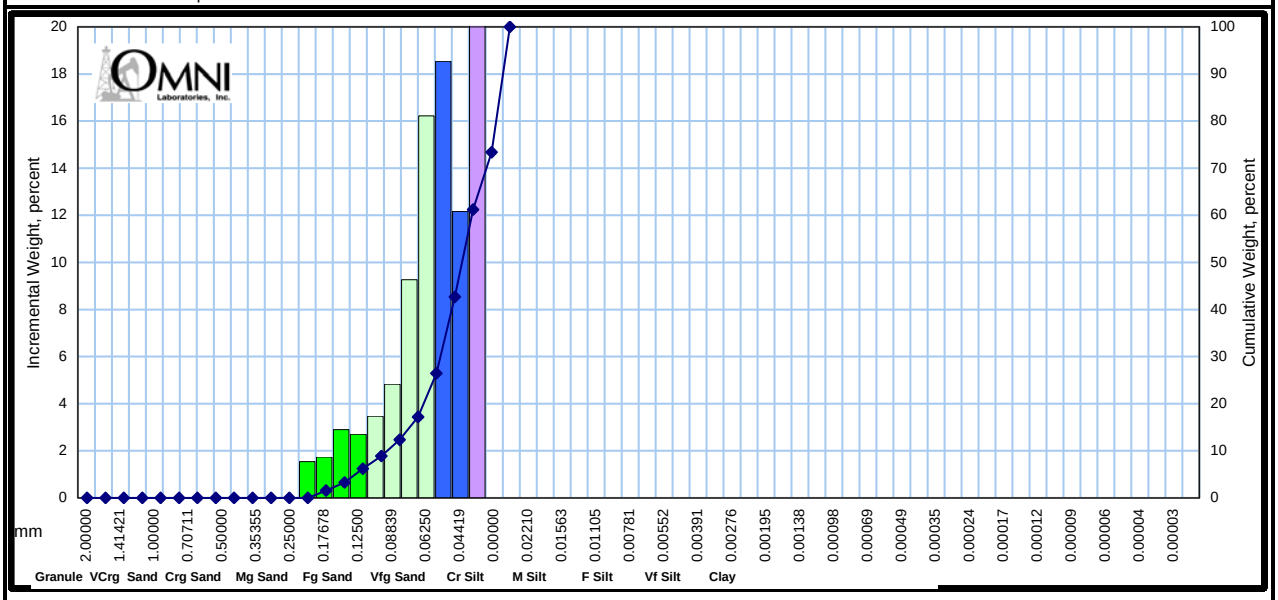

Wentworth Size Class	Mesh Size Inches	Mesh Size Millimeters	Phi of Screen	U.S. Sieve No.	Incremental Weight, percent	Cumulative Weight, percent
Granule	0.078740	2.00000	- 1.00	10	0.0	0.0
VCg Sand	0.066212	1.68179	- 0.75	12	0.0	0.0
	0.055678	1.41421	- 0.50	14	0.0	0.0
	0.046819	1.18921	- 0.25	16	0.0	0.0
	0.039370	1.00000	0.00	18	0.0	0.0
Cg Sand	0.033106	0.84090	0.25	20	0.0	0.0
	0.027839	0.70711	0.50	25	0.0	0.0
	0.023410	0.59460	0.75	30	0.0	0.0
	0.019685	0.50000	1.00	35	0.0	0.0
Mg Sand	0.016553	0.42045	1.25	40	0.0	0.0
	0.013919	0.35355	1.50	45	0.0	0.0
	0.011705	0.29730	1.75	50	0.0	0.0
	0.009843	0.25000	2.00	60	0.0	0.0
Fg Sand	0.008277	0.21022	2.25	70	1.5	1.5
	0.006960	0.17678	2.50	80	1.7	3.3
	0.005852	0.14865	2.75	100	2.9	6.2
	0.004921	0.12500	3.00	120	2.7	8.9
Vfg Sand	0.004138	0.10511	3.25	140	3.5	12.4
	0.003480	0.08839	3.50	170	4.8	17.2
	0.002926	0.07433	3.75	200	9.3	26.4
	0.002461	0.06250	4.00	230	16.2	42.7
C Silt	0.002069	0.05256	4.25	270	18.5	61.2
	0.001740	0.04419	4.50	325	12.2	73.4
Pan				<325	26.6	100.0

Description	Sieve Size	Weight Percent
Granule	10	0.0
Very Coarse Sand	18	0.0
Coarse Sand	35	0.0
Medium Sand	60	0.0
Fine Sand	120	8.9
Very Fine Sand	230	33.8
Coarse Silt	0	30.7
Pan	<325	26.6

Cumulative Volume Percent greater than			
	Phi	Particle Size	
Percentile	Value	Inches	Millimeters
5	2.6431	0.0063	0.1601
10	3.0759	0.0047	0.1186
16	3.4347	0.0036	0.0925
25	3.7080	0.0030	0.0765
50	4.0938	0.0023	0.0586
75	4.5365	0.0017	0.0431
84	4.7549	0.0015	0.0370
90	4.5422	0.0017	0.0429
95	4.6374	0.0016	0.0402

Measure	Trask, mm	Folk, phi	Inches
Median	0.0586	4.0938	0.0023
Mean	0.0598	4.0945	0.0024
Sorting	1.3326	0.6322	
Skewness	0.9614	-0.2267	
Kurtosis	0.2209	0.9865	

Figure B7: Grain Size Sieve Analysis, Core 4, Section 7, 34 to 36 inches

LASER GRAIN SIZE ANALYSIS

Conventional Core

U.S. Geological Survey - MA
Mt. Elbert 01 PPMA Samples

Core Run: 4
Core Section: 7
Sample Top-Bottom, In.: 34-36
File: HH-36917

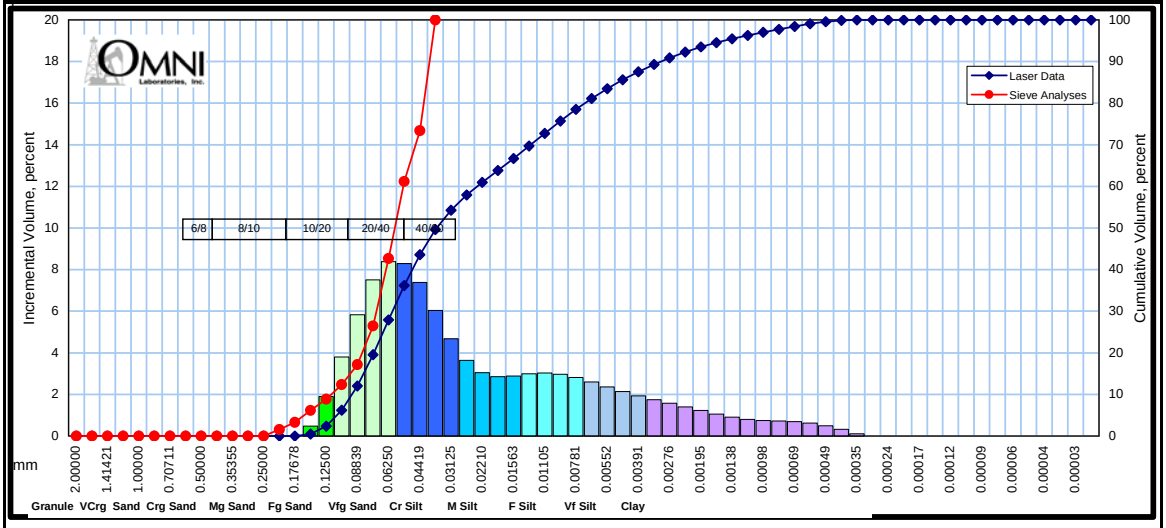

Wentworth Size Class	Mesh Size Inches	Mesh Size Millimeters	Phi of Screen	U.S. Sieve No.	Incremental Volume, percent	Cumulative Volume, percent
Granule	0.078740	2.00000	- 1.00	10	0.0	0.0
VCg Sand	0.066212	1.68179	- 0.75	12	0.0	0.0
	0.055678	1.41421	- 0.50	14	0.0	0.0
	0.046819	1.18921	- 0.25	16	0.0	0.0
	0.039370	1.00000	0.00	18	0.0	0.0
Cg Sand	0.033106	0.84090	0.25	20	0.0	0.0
	0.027839	0.70711	0.50	25	0.0	0.0
	0.023410	0.59460	0.75	30	0.0	0.0
	0.019685	0.50000	1.00	35	0.0	0.0
Mg Sand	0.016553	0.42045	1.25	40	0.0	0.0
	0.013919	0.35355	1.50	45	0.0	0.0
	0.011705	0.29730	1.75	50	0.0	0.0
	0.009843	0.25000	2.00	60	0.0	0.0
Fg Sand	0.008277	0.21022	2.25	70	0.0	0.0
	0.006960	0.17678	2.50	80	0.0	0.0
	0.005852	0.14865	2.75	100	0.5	0.5
	0.004921	0.12500	3.00	120	1.9	2.4
Vfg Sand	0.004138	0.10511	3.25	140	3.8	6.2
	0.003480	0.08839	3.50	170	5.8	12.0
	0.002926	0.07433	3.75	200	7.5	19.5
	0.002461	0.06250	4.00	230	8.4	27.9
C Silt	0.002069	0.05256	4.25	270	8.3	36.2
	0.001740	0.04419	4.50	325	7.4	43.6
	0.001463	0.03716	4.75	400	6.0	49.6
	0.001230	0.03125	5.00	450	4.7	54.3
M Silt	0.001035	0.02628	5.25	500	3.6	57.9
	0.000870	0.02210	5.50	635	3.0	61.0
	0.000732	0.01858	5.75		2.8	63.8
	0.000615	0.01563	6.00		2.9	66.7
F Silt	0.000517	0.01314	6.25		3.0	69.7
	0.000435	0.01105	6.50		3.0	72.7
	0.000366	0.00929	6.75		3.0	75.7
	0.000308	0.00781	7.00		2.8	78.5
Vf Silt	0.000259	0.00657	7.25		2.6	81.1
	0.000217	0.00552	7.50		2.4	83.5
	0.000183	0.00465	7.75		2.1	85.6
	0.000154	0.00391	8.00		1.9	87.5
Clay	0.000129	0.00329	8.25		1.7	89.3
	0.000109	0.00276	8.50		1.6	90.9
	0.000091	0.00232	8.75		1.4	92.3
	0.000077	0.00195	9.00		1.2	93.5
	0.000065	0.00164	9.25		1.1	94.6
	0.000054	0.00138	9.50		0.9	95.5
	0.000046	0.00116	9.75		0.8	96.3
	0.000038	0.00098	10.00		0.7	97.0
	0.000032	0.00082	10.25		0.7	97.8
	0.000027	0.00069	10.50		0.7	98.4
	0.000023	0.00058	10.75		0.6	99.1
	0.000019	0.00049	11.00		0.5	99.6
	0.000016	0.00041	11.25		0.3	99.9
	0.000014	0.00035	11.50		0.1	100.0
	0.000011	0.00029	11.75		0.0	100.0
	0.000010	0.00024	12.00		0.0	100.0
	0.000008	0.00021	12.25		0.0	100.0
	0.000007	0.00017	12.50		0.0	100.0
	0.000006	0.00015	12.75		0.0	100.0
	0.000005	0.00012	13.00		0.0	100.0
	0.000004	0.00010	13.25		0.0	100.0
	0.000003	0.00009	13.51		0.0	100.0
	0.000003	0.00007	13.74		0.0	100.0
	0.000002	0.00006	14.00		0.0	100.0
	0.000002	0.000051	14.26		0.0	100.0
	0.000002	0.000043	14.51		0.0	100.0
	0.000001	0.000036	14.76		0.0	100.0
	0.000001	0.000031	14.98		0.0	100.0
	0.000001	0.000026	15.23		0.0	100.0
	TOTALS				100.0	100.0

Description	Sieve Size	Volume Percent
Granule	10	0.0
Very Coarse Sand	18	0.0
Coarse Sand	35	0.0
Medium Sand	60	0.0
Fine Sand	120	2.4
Very Fine Sand	230	25.5
Coarse Silt	450	26.4
Medium Silt		12.4
Fine Silt		11.8
Very Fine Silt		9.0
Clay		12.5
	Total	100.0

Cumulative Volume Percent greater than			
	Phi	Particle Size	
Percentile	Value	Inches	Millimeters
5	3.1806	0.0043	0.1103
10	3.4172	0.0037	0.0936
16	3.6327	0.0032	0.0806
25	3.9089	0.0026	0.0666
50	4.7616	0.0015	0.0369
75	6.6813	0.0004	0.0097
84	7.5492	0.0002	0.0053
90	8.3480	0.0001	0.0031
95	9.3523	0.0001	0.0015

Measure	Trask, mm	Folk, phi	Inches
Median	0.0369	4.7616	0.0015
Mean	0.0382	5.3145	0.0015
Sorting	2.6139	1.9142	
Skewness	0.4773	0.4556	
Kurtosis	0.3138	0.9123	

Figure B8: Grain Size Laser Analysis, Core 4, Section 7, 34 to 36 inches

SIEVE ANALYSIS

Conventional Core

U.S. Geological Survey - MA
Mt. Elbert 01 PPMA Samples

Core Run: 7
Core Section: 2
Sample Top-Bottom, In.: 33-35
File: HH-36917

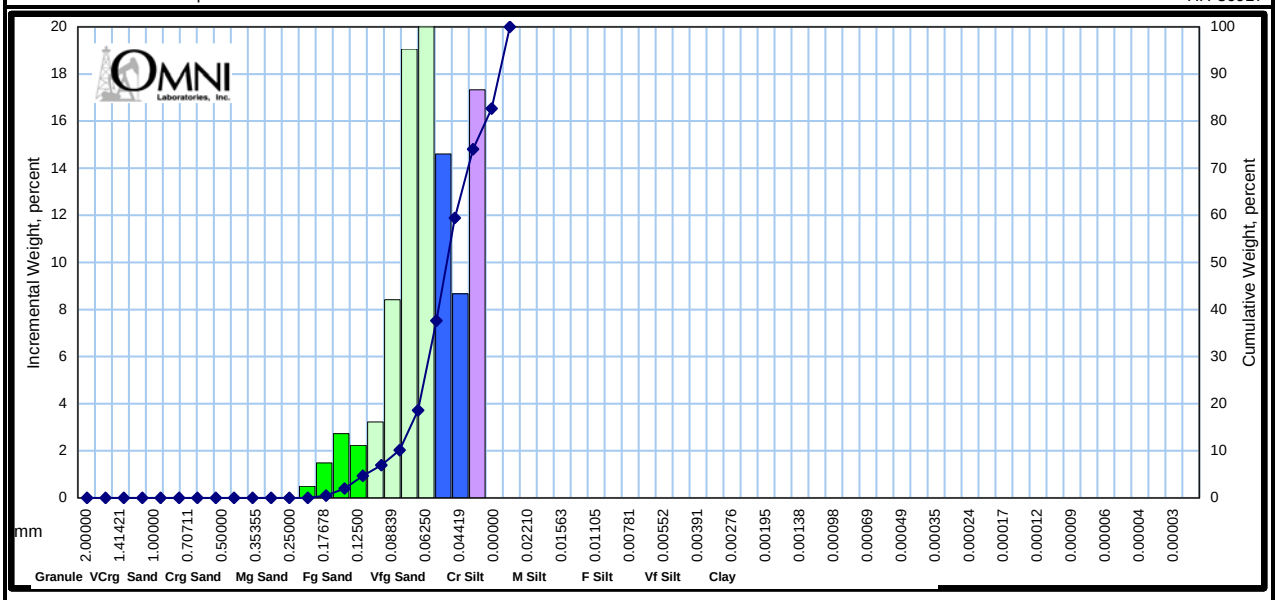

Wentworth Size Class	Mesh Size Inches	Mesh Size Millimeters	Phi of Screen	U.S. Sieve No.	Incremental Weight, percent	Cumulative Weight, percent
Granule	0.078740	2.00000	- 1.00	10	0.0	0.0
VCg Sand	0.066212	1.68179	- 0.75	12	0.0	0.0
	0.055678	1.41421	- 0.50	14	0.0	0.0
	0.046819	1.18921	- 0.25	16	0.0	0.0
	0.039370	1.00000	0.00	18	0.0	0.0
Cg Sand	0.033106	0.84090	0.25	20	0.0	0.0
	0.027839	0.70711	0.50	25	0.0	0.0
	0.023410	0.59460	0.75	30	0.0	0.0
	0.019685	0.50000	1.00	35	0.0	0.0
Mg Sand	0.016553	0.42045	1.25	40	0.0	0.0
	0.013919	0.35355	1.50	45	0.0	0.0
	0.011705	0.29730	1.75	50	0.0	0.0
	0.009843	0.25000	2.00	60	0.0	0.0
Fg Sand	0.008277	0.21022	2.25	70	0.5	0.5
	0.006960	0.17678	2.50	80	1.5	2.0
	0.005852	0.14865	2.75	100	2.7	4.7
	0.004921	0.12500	3.00	120	2.2	6.9
Vfg Sand	0.004138	0.10511	3.25	140	3.2	10.1
	0.003480	0.08839	3.50	170	8.4	18.6
	0.002926	0.07433	3.75	200	19.1	37.6
	0.002461	0.06250	4.00	230	21.8	59.4
C Silt	0.002069	0.05256	4.25	270	14.6	74.0
	0.001740	0.04419	4.50	325	8.7	82.7
Pan				<325	17.3	100.0

Description	Sieve Size	Weight Percent
Granule	10	0.0
Very Coarse Sand	18	0.0
Coarse Sand	35	0.0
Medium Sand	60	0.0
Fine Sand	120	6.9
Very Fine Sand	230	52.5
Coarse Silt	0	23.3
Pan	<325	17.3

Cumulative Volume Percent greater than			
	Phi	Particle Size	
Percentile	Value	Inches	Millimeters
5	2.7809	0.0057	0.1455
10	3.2375	0.0042	0.1060
16	3.4191	0.0037	0.0935
25	3.5797	0.0033	0.0836
50	3.8867	0.0027	0.0676
75	4.2765	0.0020	0.0516
84	4.5455	0.0017	0.0428
90	4.5422	0.0017	0.0429
95	4.6374	0.0016	0.0402

Measure	Trask, mm	Folk, phi	Inches
Median	0.0676	3.8867	0.0027
Mean	0.0676	3.9504	0.0027
Sorting	1.2731	0.5629	
Skewness	0.9443	-0.0107	
Kurtosis	0.2538	1.0919	

Figure B9: Grain Size Sieve Analysis, Core 7, Section 2, 33 to 35 inches

LASER GRAIN SIZE ANALYSIS

Conventional Core

U.S. Geological Survey - MA
Mt. Elbert 01 PPMA Samples

Core Run: 7
Core Section: 2
Sample Top-Bottom, In.: 33-35
File: HH-36917

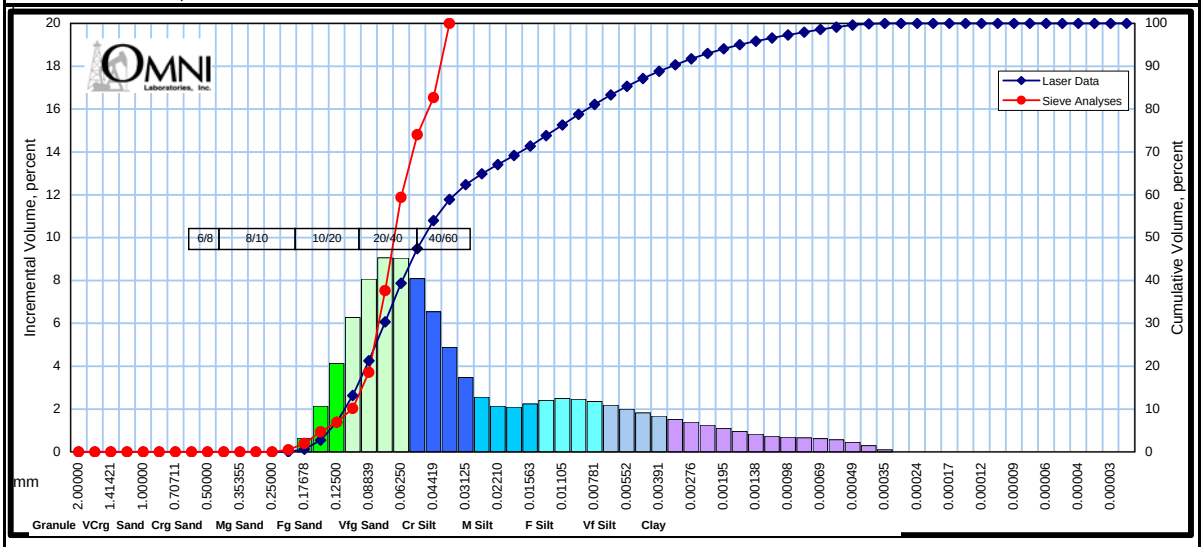

Wentworth Size Class	Mesh Size Inches	Mesh Size Millimeters	Phi of Screen	U.S. Sieve No.	Incremental Volume, percent	Cumulative Volume, percent
Granule	0.078740	2.00000	- 1.00	10	0.0	0.0
VCg Sand	0.066212	1.68179	- 0.75	12	0.0	0.0
	0.055678	1.41421	- 0.50	14	0.0	0.0
	0.046819	1.18921	- 0.25	16	0.0	0.0
	0.039370	1.00000	0.00	18	0.0	0.0
Cg Sand	0.033106	0.84090	0.25	20	0.0	0.0
	0.027839	0.70711	0.50	25	0.0	0.0
	0.023410	0.59460	0.75	30	0.0	0.0
	0.019685	0.50000	1.00	35	0.0	0.0
Mg Sand	0.016553	0.42045	1.25	40	0.0	0.0
	0.013919	0.35355	1.50	45	0.0	0.0
	0.011705	0.29730	1.75	50	0.0	0.0
	0.009843	0.25000	2.00	60	0.0	0.0
Fg Sand	0.008277	0.21022	2.25	70	0.0	0.0
	0.006960	0.17678	2.50	80	0.6	0.6
	0.005852	0.14865	2.75	100	2.1	2.8
	0.004921	0.12500	3.00	120	4.1	6.9
Vfg Sand	0.004138	0.10511	3.25	140	6.3	13.2
	0.003480	0.08839	3.50	170	8.1	21.3
	0.002926	0.07433	3.75	200	9.1	30.3
	0.002461	0.06250	4.00	230	9.0	39.4
C Silt	0.002069	0.05256	4.25	270	8.1	47.5
	0.001740	0.04419	4.50	325	6.5	54.0
	0.001463	0.03716	4.75	400	4.9	58.9
	0.001230	0.03125	5.00	450	3.5	62.4
M Silt	0.001035	0.02628	5.25	500	2.6	64.9
	0.000870	0.02210	5.50	635	2.1	67.1
	0.000732	0.01858	5.75		2.1	69.2
	0.000615	0.01563	6.00		2.2	71.4
F Silt	0.000517	0.01314	6.25		2.4	73.8
	0.000435	0.01105	6.50		2.5	76.3
	0.000366	0.00929	6.75		2.5	78.8
	0.000308	0.00781	7.00		2.4	81.1
Vf Silt	0.000259	0.00657	7.25		2.2	83.3
	0.000217	0.00552	7.50		2.0	85.3
	0.000183	0.00465	7.75		1.8	87.1
	0.000154	0.00391	8.00		1.7	88.8
Clay	0.000129	0.00329	8.25		1.5	90.3
	0.000109	0.00276	8.50		1.4	91.7
	0.000091	0.00232	8.75		1.3	93.0
	0.000077	0.00195	9.00		1.1	94.1
	0.000065	0.00164	9.25		1.0	95.0
	0.000054	0.00138	9.50		0.8	95.9
	0.000046	0.00116	9.75		0.7	96.6
	0.000038	0.00098	10.00		0.7	97.3
	0.000032	0.00082	10.25		0.7	98.0
	0.000027	0.00069	10.50		0.6	98.6
	0.000023	0.00058	10.75		0.6	99.2
	0.000019	0.00049	11.00		0.5	99.6
	0.000016	0.00041	11.25		0.3	99.9
	0.000014	0.00035	11.50		0.1	100.0
	0.000011	0.00029	11.75		0.0	100.0
	0.000010	0.00024	12.00		0.0	100.0
	0.000008	0.00021	12.25		0.0	100.0
	0.000007	0.00017	12.50		0.0	100.0
	0.000006	0.00015	12.75		0.0	100.0
	0.000005	0.00012	13.00		0.0	100.0
	0.000004	0.00010	13.25		0.0	100.0
	0.000003	0.00009	13.51		0.0	100.0
	0.000003	0.00007	13.74		0.0	100.0
	0.000002	0.00006	14.00		0.0	100.0
	0.000002	0.000051	14.26		0.0	100.0
	0.000002	0.000043	14.51		0.0	100.0
	0.000001	0.000036	14.76		0.0	100.0
	0.000001	0.000031	14.98		0.0	100.0
	0.000001	0.000026	15.23		0.0	100.0
	TOTALS				100.0	100.0

Description	Sieve Size	Volume Percent
Granule	10	0.0
Very Coarse Sand	18	0.0
Coarse Sand	35	0.0
Medium Sand	60	0.0
Fine Sand	120	6.9
Very Fine Sand	230	32.5
Coarse Silt	450	23.0
Medium Silt		9.0
Fine Silt		9.7
Very Fine Silt		7.7
Clay		11.2
	Total	100.0

Cumulative Volume Percent greater than			
	Phi	Particle Size	
Percentile	Value	Inches	Millimeters
5	2.8955	0.0053	0.1344
10	3.1282	0.0045	0.1144
16	3.3375	0.0039	0.0989
25	3.5996	0.0032	0.0825
50	4.3336	0.0020	0.0496
75	6.3610	0.0005	0.0122
84	7.3245	0.0002	0.0062
90	8.1838	0.0001	0.0034
95	9.2285	0.0001	0.0017

Measure	Trask, mm	Folk, phi	Inches
Median	0.0496	4.3336	0.0020
Mean	0.0473	4.9985	0.0019
Sorting	2.6039	1.9563	
Skewness	0.4080	0.5231	
Kurtosis	0.3170	0.9399	

Figure B10: Grain Size Laser Analysis, Core 7, Section 2, 33 to 35 inches

SIEVE ANALYSIS

Conventional Core

U.S. Geological Survey - MA
Mt. Elbert 01 PPMA Samples

Core Run: 7
Core Section: 6
Sample Top-Bottom, In.: 24-26
File: HH-36917

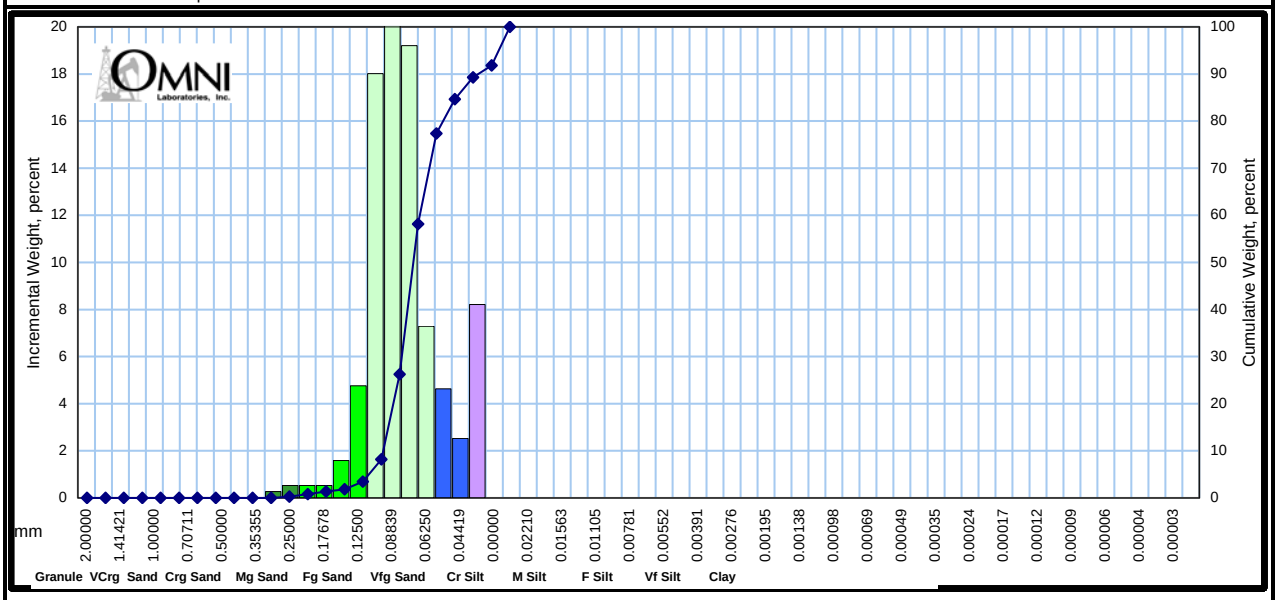

Wentworth Size Class	Mesh Size Inches	Mesh Size Millimeters	Phi of Screen	U.S. Sieve No.	Incremental Weight, percent	Cumulative Weight, percent
Granule	0.078740	2.00000	- 1.00	10	0.0	0.0
VCg Sand	0.066212	1.68179	- 0.75	12	0.0	0.0
	0.055678	1.41421	- 0.50	14	0.0	0.0
	0.046819	1.18921	- 0.25	16	0.0	0.0
	0.039370	1.00000	0.00	18	0.0	0.0
Cg Sand	0.033106	0.84090	0.25	20	0.0	0.0
	0.027839	0.70711	0.50	25	0.0	0.0
	0.023410	0.59460	0.75	30	0.0	0.0
	0.019685	0.50000	1.00	35	0.0	0.0
Mg Sand	0.016553	0.42045	1.25	40	0.0	0.0
	0.013919	0.35355	1.50	45	0.0	0.0
	0.011705	0.29730	1.75	50	0.3	0.3
	0.009843	0.25000	2.00	60	0.5	0.8
Fg Sand	0.008277	0.21022	2.25	70	0.5	1.3
	0.006960	0.17678	2.50	80	0.5	1.9
	0.005852	0.14865	2.75	100	1.6	3.4
	0.004921	0.12500	3.00	120	4.8	8.2
Vfg Sand	0.004138	0.10511	3.25	140	18.0	26.2
	0.003480	0.08839	3.50	170	31.9	58.1
	0.002926	0.07433	3.75	200	19.2	77.4
	0.002461	0.06250	4.00	230	7.3	84.6
C Silt	0.002069	0.05256	4.25	270	4.6	89.3
	0.001740	0.04419	4.50	325	2.5	91.8
Pan				<325	8.2	100.0

Description	Sieve Size	Weight Percent
Granule	10	0.0
Very Coarse Sand	18	0.0
Coarse Sand	35	0.0
Medium Sand	60	0.8
Fine Sand	120	7.4
Very Fine Sand	230	76.4
Coarse Silt	0	7.2
Pan	<325	8.2

Cumulative Volume Percent greater than			
	Phi	Particle Size	
Percentile	Value	Inches	Millimeters
5	2.8269	0.0055	0.1409
10	3.0230	0.0048	0.1230
16	3.1028	0.0046	0.1164
25	3.2316	0.0042	0.1065
50	3.4320	0.0036	0.0927
75	3.7170	0.0030	0.0760
84	3.9764	0.0025	0.0635
90	4.5422	0.0017	0.0429
95	4.6374	0.0016	0.0402

Measure	Trask, mm	Folk, phi	Inches
Median	0.0927	3.4320	0.0036
Mean	0.0913	3.5037	0.0036
Sorting	1.1832	0.4927	
Skewness	0.9431	0.2890	
Kurtosis	0.1899	1.5286	

Figure B11: Grain Size Sieve Analysis, Core 7, Section 6, 24 to 26 inches

LASER GRAIN SIZE ANALYSIS

Conventional Core

U.S. Geological Survey - MA
Mt. Elbert 01 PPMA Samples

Core Run: 7
Core Section: 6
Sample Top-Bottom, In.: 24-26
File: HH-36917

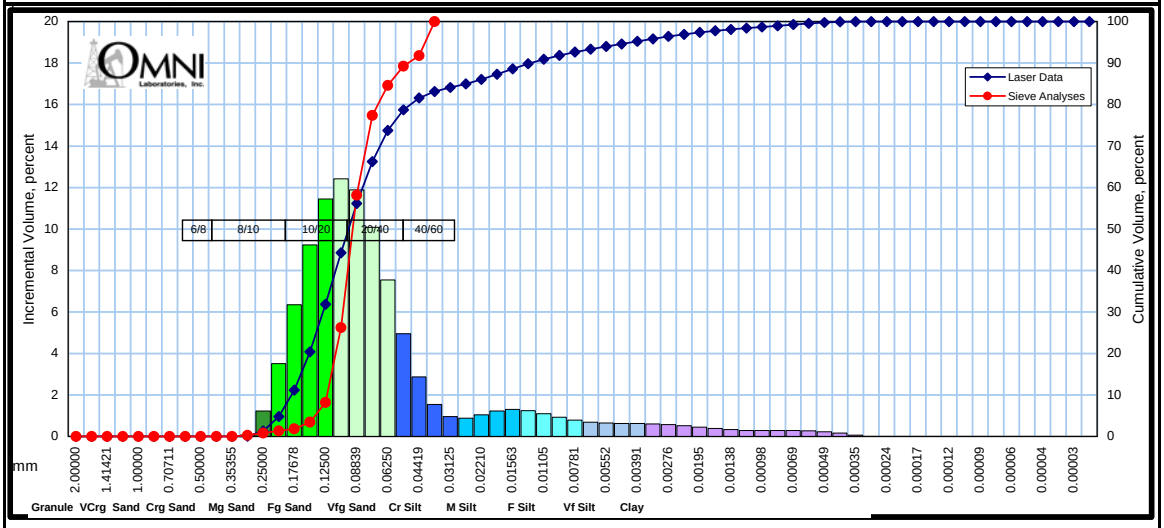

Wentworth Size Class	Mesh Size Inches	Mesh Size Millimeters	Phi of Screen	U.S. Sieve No.	Incremental Volume, percent	Cumulative Volume, percent
Granule	0.078740	2.00000	- 1.00	10	0.0	0.0
VCg Sand	0.066212	1.68179	- 0.75	12	0.0	0.0
	0.055678	1.41421	- 0.50	14	0.0	0.0
	0.046819	1.18921	- 0.25	16	0.0	0.0
	0.039370	1.00000	0.00	18	0.0	0.0
Cg Sand	0.033106	0.84090	0.25	20	0.0	0.0
	0.027839	0.70711	0.50	25	0.0	0.0
	0.023410	0.59460	0.75	30	0.0	0.0
	0.019685	0.50000	1.00	35	0.0	0.0
Mg Sand	0.016553	0.42045	1.25	40	0.0	0.0
	0.013919	0.35355	1.50	45	0.0	0.0
	0.011705	0.29730	1.75	50	0.1	0.1
	0.009843	0.25000	2.00	60	1.2	1.3
Fg Sand	0.008277	0.21022	2.25	70	3.5	4.8
	0.006960	0.17678	2.50	80	6.3	11.2
	0.005852	0.14865	2.75	100	9.2	20.4
	0.004921	0.12500	3.00	120	11.4	31.8
Vfg Sand	0.004138	0.10511	3.25	140	12.4	44.3
	0.003480	0.08839	3.50	170	11.9	56.2
	0.002926	0.07433	3.75	200	10.1	66.2
	0.002461	0.06250	4.00	230	7.5	73.8
C Silt	0.002069	0.05256	4.25	270	5.0	78.7
	0.001740	0.04419	4.50	325	2.9	81.6
	0.001463	0.03716	4.75	400	1.5	83.2
	0.001230	0.03125	5.00	450	1.0	84.1
M Silt	0.001035	0.02628	5.25	500	0.9	85.0
	0.000870	0.02210	5.50	635	1.1	86.1
	0.000732	0.01858	5.75		1.2	87.3
	0.000615	0.01563	6.00		1.3	88.6
F Silt	0.000517	0.01314	6.25		1.2	89.8
	0.000435	0.01105	6.50		1.1	90.9
	0.000366	0.00929	6.75		0.9	91.9
	0.000308	0.00781	7.00		0.8	92.6
Vf Silt	0.000259	0.00657	7.25		0.7	93.3
	0.000217	0.00552	7.50		0.6	94.0
	0.000183	0.00465	7.75		0.6	94.6
	0.000154	0.00391	8.00		0.6	95.2
Clay	0.000129	0.00329	8.25		0.6	95.9
	0.000109	0.00276	8.50		0.6	96.4
	0.000091	0.00232	8.75		0.5	96.9
	0.000077	0.00195	9.00		0.5	97.4
	0.000065	0.00164	9.25		0.4	97.8
	0.000054	0.00138	9.50		0.3	98.1
	0.000046	0.00116	9.75		0.3	98.4
	0.000038	0.00098	10.00		0.3	98.7
	0.000032	0.00082	10.25		0.3	99.0
	0.000027	0.00069	10.50		0.3	99.3
	0.000023	0.00058	10.75		0.3	99.5
	0.000019	0.00049	11.00		0.2	99.8
	0.000016	0.00041	11.25		0.2	99.9
	0.000014	0.00035	11.50		0.1	100.0
	0.000011	0.00029	11.75		0.0	100.0
	0.000010	0.00024	12.00		0.0	100.0
	0.000008	0.00021	12.25		0.0	100.0
	0.000007	0.00017	12.50		0.0	100.0
	0.000006	0.00015	12.75		0.0	100.0
	0.000005	0.00012	13.00		0.0	100.0
	0.000004	0.00010	13.25		0.0	100.0
	0.000003	0.00009	13.51		0.0	100.0
	0.000003	0.00007	13.74		0.0	100.0
	0.000002	0.00006	14.00		0.0	100.0
	0.000002	0.000051	14.26		0.0	100.0
	0.000002	0.000043	14.51		0.0	100.0
	0.000001	0.000036	14.76		0.0	100.0
	0.000001	0.000031	14.98		0.0	100.0
	0.000001	0.000026	15.23		0.0	100.0
	TOTALS				100.0	100.0

Description	Sieve Size	Volume Percent
Granule	10	0.0
Very Coarse Sand	18	0.0
Coarse Sand	35	0.0
Medium Sand	60	1.3
Fine Sand	120	30.5
Very Fine Sand	230	41.9
Coarse Silt	450	10.3
Medium Silt		4.5
Fine Silt		4.1
Very Fine Silt		2.6
Clay		4.8

Cumulative Volume Percent greater than			
	Phi	Particle Size	
Percentile	Value	Inches	Millimeters
5	2.2552	0.0082	0.2095
10	2.4577	0.0072	0.1820
16	2.6355	0.0063	0.1609
25	2.8505	0.0055	0.1386
50	3.3623	0.0038	0.0972
75	4.0454	0.0024	0.0606
84	4.9594	0.0013	0.0321
90	6.2774	0.0005	0.0129
95	7.8920	0.0002	0.0042

Measure	Trask, mm	Folk, phi	Inches
Median	0.0972	3.3623	0.0038
Mean	0.0996	3.6524	0.0039
Sorting	1.5130	1.4350	
Skewness	0.8880	0.4909	

Figure B12: Grain Size Laser Analysis, Core 7, Section 6, 24 to 26 inches

SIEVE ANALYSIS

Conventional Core

U.S. Geological Survey - MA
Mt. Elbert 01 PPMA Samples

Core Run: 8
Core Section: 2
Sample Top-Bottom, In.: 35-37
File: HH-36917

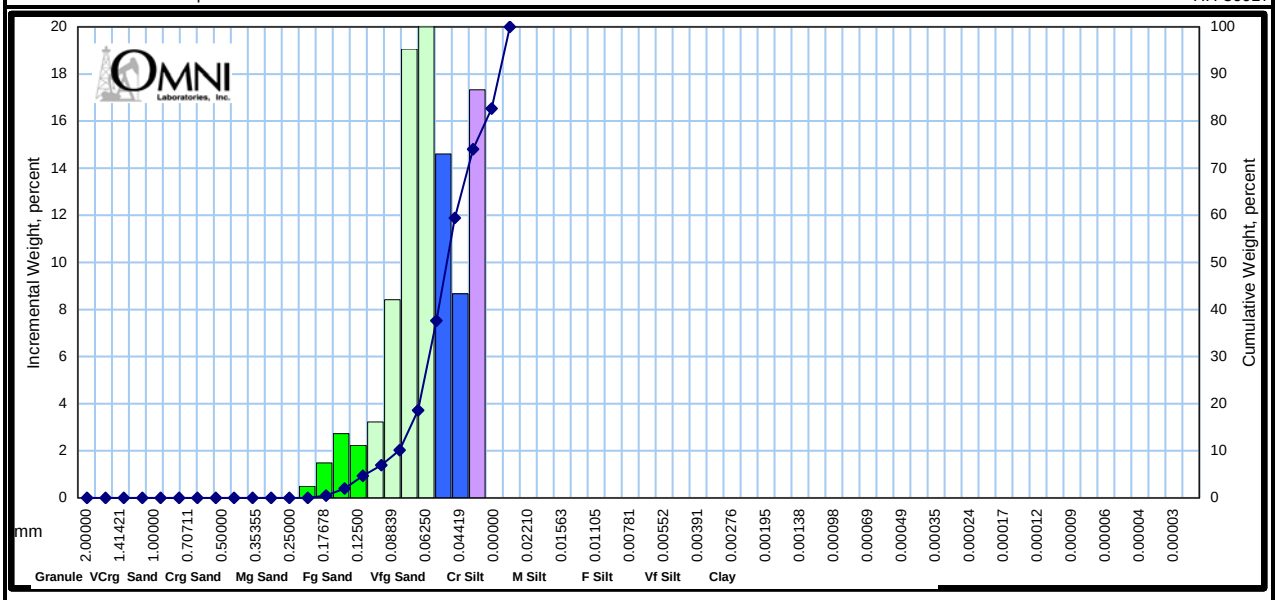

Wentworth Size Class	Mesh Size Inches	Mesh Size Millimeters	Phi of Screen	U.S. Sieve No.	Incremental Weight, percent	Cumulative Weight, percent
Granule	0.078740	2.00000	- 1.00	10	0.0	0.0
VCg Sand	0.066212	1.68179	- 0.75	12	0.0	0.0
	0.055678	1.41421	- 0.50	14	0.0	0.0
	0.046819	1.18921	- 0.25	16	0.0	0.0
	0.039370	1.00000	0.00	18	0.0	0.0
Cg Sand	0.033106	0.84090	0.25	20	0.0	0.0
	0.027839	0.70711	0.50	25	0.0	0.0
	0.023410	0.59460	0.75	30	0.0	0.0
	0.019685	0.50000	1.00	35	0.0	0.0
Mg Sand	0.016553	0.42045	1.25	40	0.0	0.0
	0.013919	0.35355	1.50	45	0.0	0.0
	0.011705	0.29730	1.75	50	0.0	0.0
	0.009843	0.25000	2.00	60	0.0	0.0
Fg Sand	0.008277	0.21022	2.25	70	0.0	0.0
	0.006960	0.17678	2.50	80	0.4	0.4
	0.005852	0.14865	2.75	100	1.8	2.2
	0.004921	0.12500	3.00	120	1.6	3.8
Vfg Sand	0.004138	0.10511	3.25	140	2.8	6.5
	0.003480	0.08839	3.50	170	8.3	14.9
	0.002926	0.07433	3.75	200	14.5	29.3
	0.002461	0.06250	4.00	230	17.8	47.1
C Silt	0.002069	0.05256	4.25	270	18.0	65.1
	0.001740	0.04419	4.50	325	14.1	79.2
Pan				<325	20.8	100.0

Description	Sieve Size	Weight Percent
Granule	10	0.0
Very Coarse Sand	18	0.0
Coarse Sand	35	0.0
Medium Sand	60	0.0
Fine Sand	120	3.8
Very Fine Sand	230	43.4
Coarse Silt	0	32.1
Pan	<325	20.8

Cumulative Volume Percent greater than			
	Phi	Particle Size	
Percentile	Value	Inches	Millimeters
5	3.1063	0.0046	0.1161
10	3.3490	0.0039	0.0981
16	3.5184	0.0034	0.0873
25	3.6709	0.0031	0.0785
50	4.0370	0.0024	0.0609
75	4.4205	0.0018	0.0467
84	4.6415	0.0016	0.0401
90	4.5422	0.0017	0.0429
95	4.6374	0.0016	0.0402

Measure	Trask, mm	Folk, phi	Inches
Median	0.0609	4.0370	0.0024
Mean	0.0626	4.0656	0.0025
Sorting	1.2967	0.5128	
Skewness	0.9881	-0.0697	
Kurtosis	0.2881	0.8371	

Figure B13: Grain Size Sieve Analysis, Core 8, Section 2, 35 to 37 inches

LASER GRAIN SIZE ANALYSIS

Conventional Core

U.S. Geological Survey - MA
Mt. Elbert 01 PPMA Samples

Core Run: 8
Core Section: 2
Sample Top-Bottom, In.: 35-37
File: HH-36917

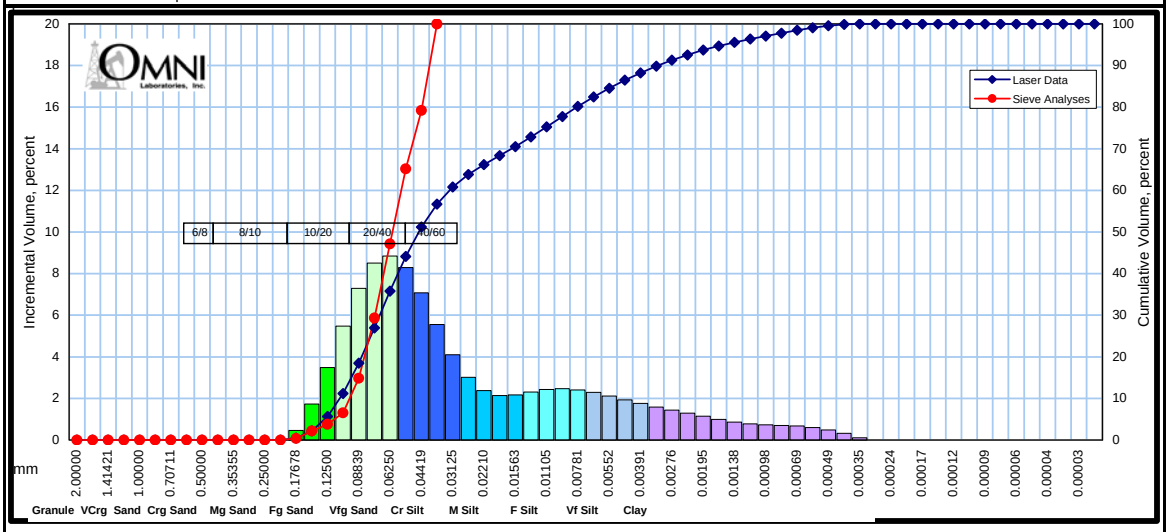

Wentworth Size Class	Mesh Size Inches	Mesh Size Millimeters	Phi of Screen	U.S. Sieve No.	Incremental Volume, percent	Cumulative Volume, percent
Granule	0.078740	2.00000	- 1.00	10	0.0	0.0
VCg Sand	0.066212	1.68179	- 0.75	12	0.0	0.0
	0.055678	1.41421	- 0.50	14	0.0	0.0
	0.046819	1.18921	- 0.25	16	0.0	0.0
	0.039370	1.00000	0.00	18	0.0	0.0
Cg Sand	0.033106	0.84090	0.25	20	0.0	0.0
	0.027839	0.70711	0.50	25	0.0	0.0
	0.023410	0.59460	0.75	30	0.0	0.0
	0.019685	0.50000	1.00	35	0.0	0.0
Mg Sand	0.016553	0.42045	1.25	40	0.0	0.0
	0.013919	0.35355	1.50	45	0.0	0.0
	0.011705	0.29730	1.75	50	0.0	0.0
	0.009843	0.25000	2.00	60	0.0	0.0
Fg Sand	0.008277	0.21022	2.25	70	0.0	0.0
	0.006960	0.17678	2.50	80	0.5	0.5
	0.005852	0.14865	2.75	100	1.7	2.2
	0.004921	0.12500	3.00	120	3.5	5.7
Vfg Sand	0.004138	0.10511	3.25	140	5.5	11.2
	0.003480	0.08839	3.50	170	7.3	18.4
	0.002926	0.07433	3.75	200	8.5	26.9
	0.002461	0.06250	4.00	230	8.8	35.8
C Silt	0.002069	0.05256	4.25	270	8.3	44.1
	0.001740	0.04419	4.50	325	7.1	51.2
	0.001463	0.03716	4.75	400	5.5	56.7
	0.001230	0.03125	5.00	450	4.1	60.8
M Silt	0.001035	0.02628	5.25	500	3.0	63.8
	0.000870	0.02210	5.50	635	2.4	66.2
	0.000732	0.01858	5.75		2.1	68.4
	0.000615	0.01563	6.00		2.2	70.5
F Silt	0.000517	0.01314	6.25		2.3	72.8
	0.000435	0.01105	6.50		2.4	75.3
	0.000366	0.00929	6.75		2.5	77.7
	0.000308	0.00781	7.00		2.4	80.2
Vf Silt	0.000259	0.00657	7.25		2.3	82.4
	0.000217	0.00552	7.50		2.1	84.6
	0.000183	0.00465	7.75		1.9	86.5
	0.000154	0.00391	8.00		1.8	88.2

Wentworth Size Class	Mesh Size Inches	Mesh Size Millimeters	Phi of Screen	U.S. Sieve No.	Incremental Volume, percent	Cumulative Volume, percent
Clay	0.000129	0.00329	8.25		1.6	89.8
	0.000109	0.00276	8.50		1.4	91.3
	0.000091	0.00232	8.75		1.3	92.6
	0.000077	0.00195	9.00		1.1	93.7
	0.000065	0.00164	9.25		1.0	94.7
	0.000054	0.00138	9.50		0.9	95.6
	0.000046	0.00116	9.75		0.8	96.4
	0.000038	0.00098	10.00		0.7	97.1
	0.000032	0.00082	10.25		0.7	97.8
	0.000027	0.00069	10.50		0.7	98.5
	0.000023	0.00058	10.75		0.6	99.1
	0.000019	0.00049	11.00		0.5	99.6
	0.000016	0.00041	11.25		0.3	99.9
	0.000014	0.00035	11.50		0.1	100.0
	0.000011	0.00029	11.75		0.0	100.0
	0.000010	0.00024	12.00		0.0	100.0
	0.000008	0.00021	12.25		0.0	100.0
	0.000007	0.00017	12.50		0.0	100.0
	0.000006	0.00015	12.75		0.0	100.0
	0.000005	0.00012	13.00		0.0	100.0
	0.000004	0.00010	13.25		0.0	100.0
	0.000003	0.00009	13.51		0.0	100.0
	0.000003	0.00007	13.74		0.0	100.0
	0.000002	0.00006	14.00		0.0	100.0
	0.000002	0.000051	14.26		0.0	100.0
	0.000002	0.000043	14.51		0.0	100.0
	0.000001	0.000036	14.76		0.0	100.0
	0.000001	0.000031	14.98		0.0	100.0
	0.000001	0.000026	15.23		0.0	100.0
	TOTALS				100.0	100.0

Description	Sieve Size	Volume Percent
Granule	10	0.0
Very Coarse Sand	18	0.0
Coarse Sand	35	0.0
Medium Sand	60	0.0
Fine Sand	120	5.7
Very Fine Sand	230	30.1
Coarse Silt	450	25.0
Medium Silt		9.7
Fine Silt		9.6
Very Fine Silt		8.1
Clay		11.8
	Total	100.0

Cumulative Volume Percent greater than			
	Phi	Particle Size	
Percentile	Value	Inches	Millimeters
5	2.9562	0.0051	0.1289
10	3.1992	0.0043	0.1089
16	3.4167	0.0037	0.0936
25	3.6891	0.0031	0.0775
50	4.4488	0.0018	0.0458
75	6.4635	0.0004	0.0113
84	7.4220	0.0002	0.0058
90	8.2653	0.0001	0.0033
95	9.3178	0.0001	0.0016

Measure	Trask, mm	Folk, phi	Inches
Median	0.0458	4.4488	0.0018
Mean	0.0444	5.0958	0.0017
Sorting	2.6157	1.9652	
Skewness	0.4190	0.5077	
Kurtosis	0.3133	0.9398	

Figure B14: Grain Size Laser Analysis, Core 8, Section 2, 35 to 37 inches

SIEVE ANALYSIS

Conventional Core

U.S. Geological Survey - MA
Mt. Elbert 01 PPMA Samples

Core Run: 8
Core Section: 4
Sample Top-Bottom, In.: 29-31
File: HH-36917

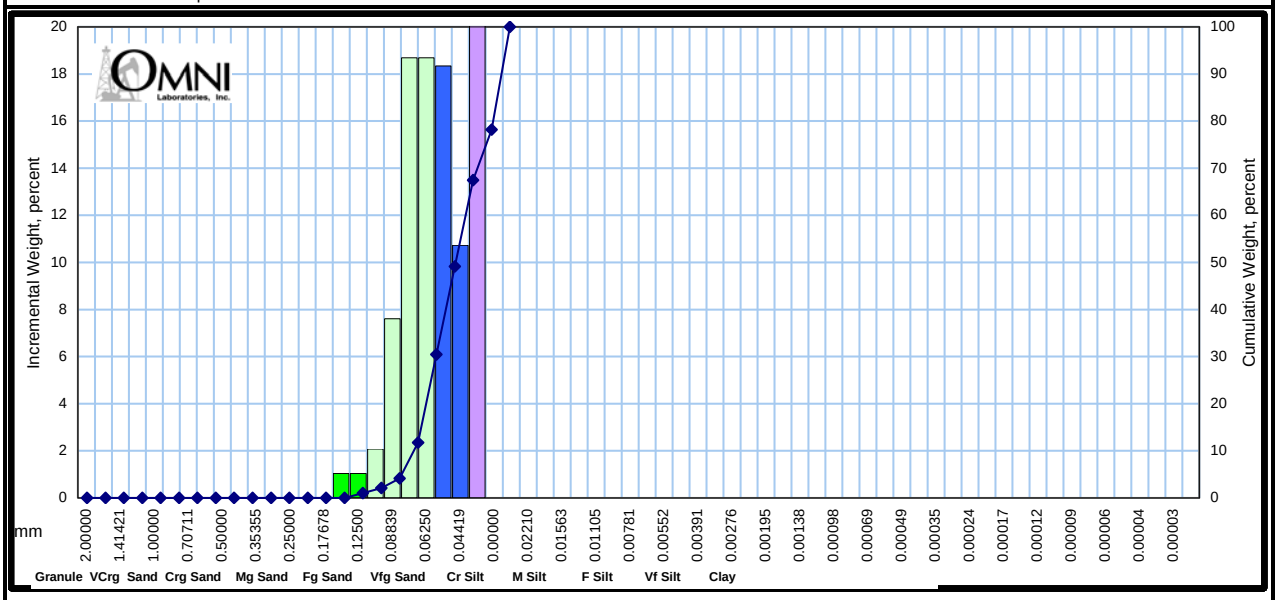

Wentworth Size Class	Mesh Size Inches	Mesh Size Millimeters	Phi of Screen	U.S. Sieve No.	Incremental Weight, percent	Cumulative Weight, percent
Granule	0.078740	2.00000	- 1.00	10	0.0	0.0
VCg Sand	0.066212	1.68179	- 0.75	12	0.0	0.0
	0.055678	1.41421	- 0.50	14	0.0	0.0
	0.046819	1.18921	- 0.25	16	0.0	0.0
	0.039370	1.00000	0.00	18	0.0	0.0
Cg Sand	0.033106	0.84090	0.25	20	0.0	0.0
	0.027839	0.70711	0.50	25	0.0	0.0
	0.023410	0.59460	0.75	30	0.0	0.0
	0.019685	0.50000	1.00	35	0.0	0.0
Mg Sand	0.016553	0.42045	1.25	40	0.0	0.0
	0.013919	0.35355	1.50	45	0.0	0.0
	0.011705	0.29730	1.75	50	0.0	0.0
	0.009843	0.25000	2.00	60	0.0	0.0
Fg Sand	0.008277	0.21022	2.25	70	0.0	0.0
	0.006960	0.17678	2.50	80	0.0	0.0
	0.005852	0.14865	2.75	100	1.0	1.0
	0.004921	0.12500	3.00	120	1.0	2.1
Vfg Sand	0.004138	0.10511	3.25	140	2.1	4.2
	0.003480	0.08839	3.50	170	7.6	11.8
	0.002926	0.07433	3.75	200	18.7	30.4
	0.002461	0.06250	4.00	230	18.7	49.1
C Silt	0.002069	0.05256	4.25	270	18.3	67.5
	0.001740	0.04419	4.50	325	10.7	78.2
Pan				<325	21.8	100.0

Description	Sieve Size	Weight Percent
Granule	10	0.0
Very Coarse Sand	18	0.0
Coarse Sand	35	0.0
Medium Sand	60	0.0
Fine Sand	120	2.1
Very Fine Sand	230	47.1
Coarse Silt	0	29.1
Pan	<325	21.8

Cumulative Volume Percent greater than			
	Phi	Particle Size	
Percentile	Value	Inches	Millimeters
5	3.2758	0.0041	0.1032
10	3.4381	0.0036	0.0923
16	3.5530	0.0034	0.0852
25	3.6725	0.0031	0.0784
50	4.0109	0.0024	0.0620
75	4.4208	0.0018	0.0467
84	4.6646	0.0016	0.0394
90	4.5422	0.0017	0.0429
95	4.6374	0.0016	0.0402

Measure	Trask, mm	Folk, phi	Inches
Median	0.0620	4.0109	0.0024
Mean	0.0626	4.0762	0.0025
Sorting	1.2961	0.4842	
Skewness	0.9516	0.0483	
Kurtosis	0.3216	0.7458	

Figure B15: Grain Size Sieve Analysis, Core 8, Section 4, 29 to 31 inches

LASER GRAIN SIZE ANALYSIS

Conventional Core

U.S. Geological Survey - MA
Mt. Elbert 01 PPMA Samples

Core Run: 8
Core Section: 4
Sample Top-Bottom, In.: 29-31
File: HH-36917

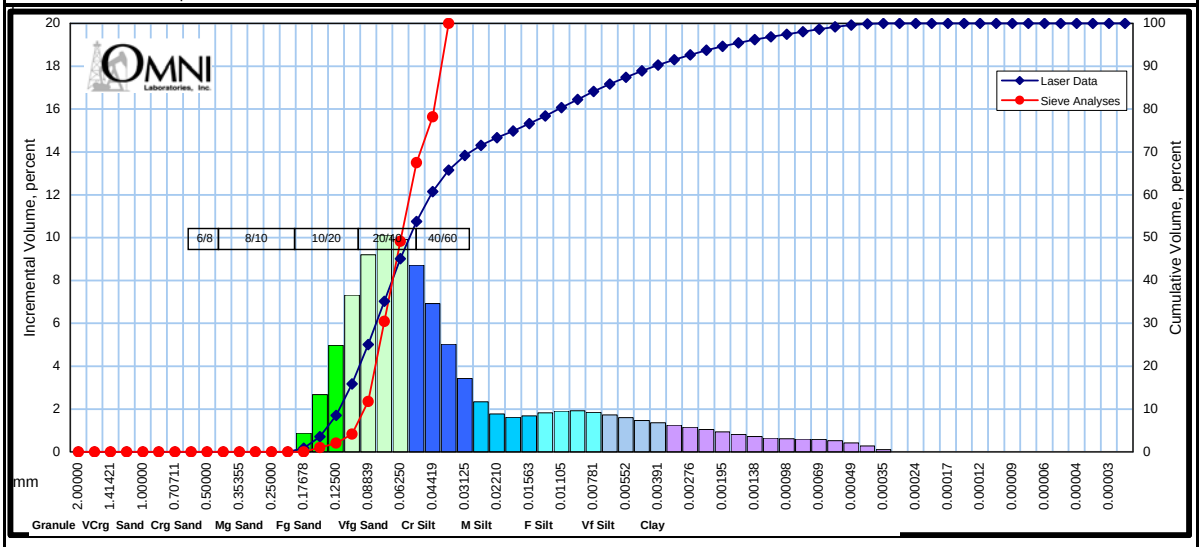

Wentworth Size Class	Mesh Size Inches	Mesh Size Millimeters	Phi of Screen	U.S. Sieve No.	Incremental Volume, percent	Cumulative Volume, percent
Granule	0.078740	2.00000	- 1.00	10	0.0	0.0
VCg Sand	0.066212	1.68179	- 0.75	12	0.0	0.0
	0.055678	1.41421	- 0.50	14	0.0	0.0
	0.046819	1.18921	- 0.25	16	0.0	0.0
	0.039370	1.00000	0.00	18	0.0	0.0
Cg Sand	0.033106	0.84090	0.25	20	0.0	0.0
	0.027839	0.70711	0.50	25	0.0	0.0
	0.023410	0.59460	0.75	30	0.0	0.0
	0.019685	0.50000	1.00	35	0.0	0.0
Mg Sand	0.016553	0.42045	1.25	40	0.0	0.0
	0.013919	0.35355	1.50	45	0.0	0.0
	0.011705	0.29730	1.75	50	0.0	0.0
	0.009843	0.25000	2.00	60	0.0	0.0
Fg Sand	0.008277	0.21022	2.25	70	0.0	0.0
	0.006960	0.17678	2.50	80	0.9	0.9
	0.005852	0.14865	2.75	100	2.7	3.6
	0.004921	0.12500	3.00	120	5.0	8.5
Vfg Sand	0.004138	0.10511	3.25	140	7.3	15.9
	0.003480	0.08839	3.50	170	9.2	25.1
	0.002926	0.07433	3.75	200	10.1	35.2
	0.002461	0.06250	4.00	230	9.9	45.1
C Silt	0.002069	0.05256	4.25	270	8.7	53.8
	0.001740	0.04419	4.50	325	6.9	60.7
	0.001463	0.03716	4.75	400	5.0	65.8
	0.001230	0.03125	5.00	450	3.4	69.2
M Silt	0.001035	0.02628	5.25	500	2.3	71.5
	0.000870	0.02210	5.50	635	1.8	73.3
	0.000732	0.01858	5.75		1.6	74.9
	0.000615	0.01563	6.00		1.7	76.6
F Silt	0.000517	0.01314	6.25		1.8	78.4
	0.000435	0.01105	6.50		1.9	80.3
	0.000366	0.00929	6.75		1.9	82.3
	0.000308	0.00781	7.00		1.8	84.1
Vf Silt	0.000259	0.00657	7.25		1.7	85.8
	0.000217	0.00552	7.50		1.6	87.4
	0.000183	0.00465	7.75		1.5	88.9
	0.000154	0.00391	8.00		1.4	90.3
Clay	0.000129	0.00329	8.25		1.3	91.5
	0.000109	0.00276	8.50		1.2	92.7
	0.000091	0.00232	8.75		1.0	93.7
	0.000077	0.00195	9.00		0.9	94.7
	0.000065	0.00164	9.25		0.8	95.5
	0.000054	0.00138	9.50		0.7	96.2
	0.000046	0.00116	9.75		0.7	96.9
	0.000038	0.00098	10.00		0.6	97.5
	0.000032	0.00082	10.25		0.6	98.1
	0.000027	0.00069	10.50		0.6	98.7
	0.000023	0.00058	10.75		0.5	99.2
	0.000019	0.00049	11.00		0.4	99.6
	0.000016	0.00041	11.25		0.3	99.9
	0.000014	0.00035	11.50		0.1	100.0
	0.000011	0.00029	11.75		0.0	100.0
	0.000010	0.00024	12.00		0.0	100.0
	0.000008	0.00021	12.25		0.0	100.0
	0.000007	0.00017	12.50		0.0	100.0
	0.000006	0.00015	12.75		0.0	100.0
	0.000005	0.00012	13.00		0.0	100.0
	0.000004	0.00010	13.25		0.0	100.0
	0.000003	0.00009	13.51		0.0	100.0
	0.000003	0.00007	13.74		0.0	100.0
	0.000002	0.00006	14.00		0.0	100.0
	0.000002	0.000051	14.26		0.0	100.0
	0.000002	0.000043	14.51		0.0	100.0
	0.000001	0.000036	14.76		0.0	100.0
	0.000001	0.000031	14.98		0.0	100.0
	0.000001	0.000026	15.23		0.0	100.0
	TOTALS				100.0	100.0

Description	Sieve Size	Volume Percent
Granule	10	0.0
Very Coarse Sand	18	0.0
Coarse Sand	35	0.0
Medium Sand	60	0.0
Fine Sand	120	8.5
Very Fine Sand	230	36.6
Coarse Silt	450	24.1
Medium Silt		7.4
Fine Silt		7.5
Very Fine Silt		6.2
Clay		9.7
	Total	100.0

Cumulative Volume Percent greater than			
	Phi	Particle Size	
Percentile	Value	Inches	Millimeters
5	2.8320	0.0055	0.1404
10	3.0523	0.0047	0.1205
16	3.2495	0.0041	0.1052
25	3.4935	0.0035	0.0888
50	4.1294	0.0022	0.0571
75	5.7548	0.0007	0.0185
84	6.9759	0.0003	0.0079
90	7.9386	0.0002	0.0041
95	9.0869	0.0001	0.0018

Measure	Trask, mm	Folk, phi	Inches
Median	0.0571	4.1294	0.0022
Mean	0.0537	4.7849	0.0021
Sorting	2.1896	1.8793	
Skewness	0.5037	0.5564	
Kurtosis	0.3016	1.1336	

Figure B16: Grain Size Laser Analysis, Core 8, Section 4, 29 to 31 inches

SIEVE ANALYSIS

Conventional Core

U.S. Geological Survey - MA
Mt. Elbert 01 PPMA Samples

Core Run: 12
Core Section: 3
Sample Top-Bottom, In.: 21-23
File: HH-36917

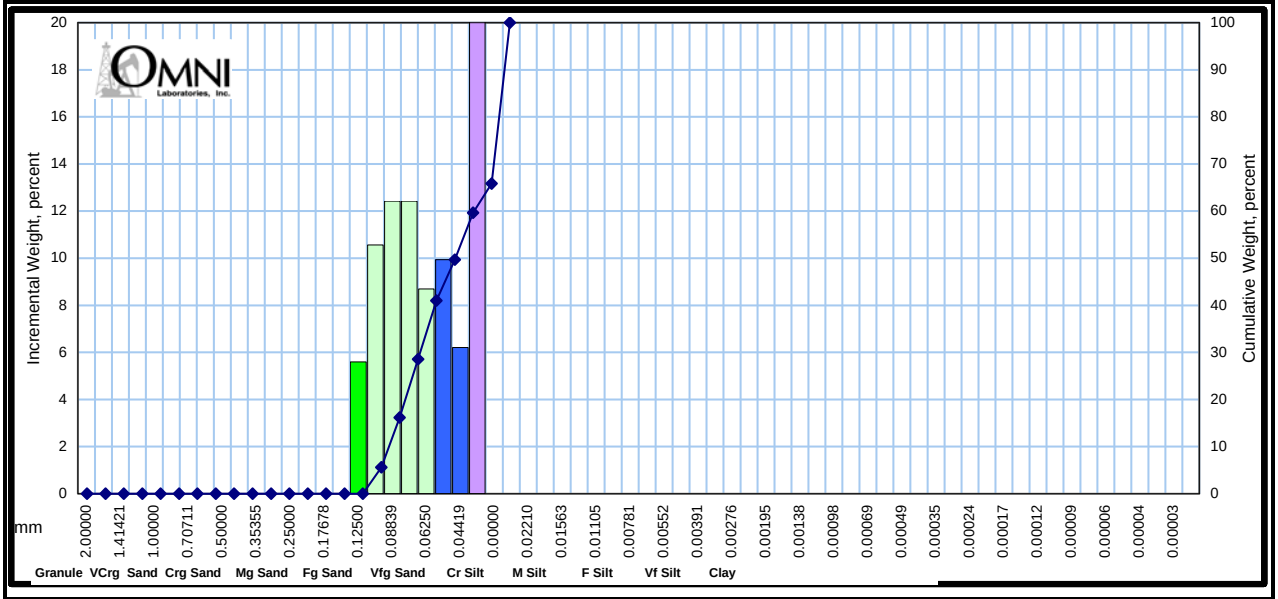

Wentworth Size Class	Mesh Size Inches	Mesh Size Millimeters	Phi of Screen	U.S. Sieve No.	Incremental Weight, percent	Cumulative Weight, percent
Granule	0.078740	2.00000	- 1.00	10	0.0	0.0
VCg Sand	0.066212	1.68179	- 0.75	12	0.0	0.0
	0.055678	1.41421	- 0.50	14	0.0	0.0
	0.046819	1.18921	- 0.25	16	0.0	0.0
	0.039370	1.00000	0.00	18	0.0	0.0
Cg Sand	0.033106	0.84090	0.25	20	0.0	0.0
	0.027839	0.70711	0.50	25	0.0	0.0
	0.023410	0.59460	0.75	30	0.0	0.0
	0.019685	0.50000	1.00	35	0.0	0.0
Mg Sand	0.016553	0.42045	1.25	40	0.0	0.0
	0.013919	0.35355	1.50	45	0.0	0.0
	0.011705	0.29730	1.75	50	0.0	0.0
	0.009843	0.25000	2.00	60	0.0	0.0
Fg Sand	0.008277	0.21022	2.25	70	0.0	0.0
	0.006960	0.17678	2.50	80	0.0	0.0
	0.005852	0.14865	2.75	100	0.0	0.0
	0.004921	0.12500	3.00	120	5.6	5.6
Vfg Sand	0.004138	0.10511	3.25	140	10.6	16.1
	0.003480	0.08839	3.50	170	12.4	28.6
	0.002926	0.07433	3.75	200	12.4	41.0
	0.002461	0.06250	4.00	230	8.7	49.7
C Silt	0.002069	0.05256	4.25	270	9.9	59.6
	0.001740	0.04419	4.50	325	6.2	65.8
Pan				<325	34.2	100.0

Description	Sieve Size	Weight Percent
Granule	10	0.0
Very Coarse Sand	18	0.0
Coarse Sand	35	0.0
Medium Sand	60	0.0
Fine Sand	120	5.6
Very Fine Sand	230	44.1
Coarse Silt	0	16.1
Pan	<325	34.2

Cumulative Volume Percent greater than			
	Phi	Particle Size	
Percentile	Value	Inches	Millimeters
5	2.9715	0.0050	0.1275
10	3.0992	0.0046	0.1167
16	3.2462	0.0041	0.1054
25	3.4236	0.0037	0.0932
50	4.0072	0.0024	0.0622
75	4.6661	0.0016	0.0394
84	4.8502	0.0014	0.0347
90	4.5422	0.0017	0.0429
95	4.6374	0.0016	0.0402

Measure	Trask, mm	Folk, phi	Inches
Median	0.0622	4.0072	0.0024
Mean	0.0663	4.0345	0.0026
Sorting	1.5382	0.6534	
Skewness	0.9492	-0.0961	
Kurtosis	0.3647	0.5495	

Figure B17: Grain Size Sieve Analysis, Core 12, Section 3, 21 to 23 inches

LASER GRAIN SIZE ANALYSIS

Conventional Core

U.S. Geological Survey - MA
Mt. Elbert 01 PPMA Samples

Core Run: 12
Core Section: 3
Sample Top-Bottom, In.: 21-23
File: HH-36917

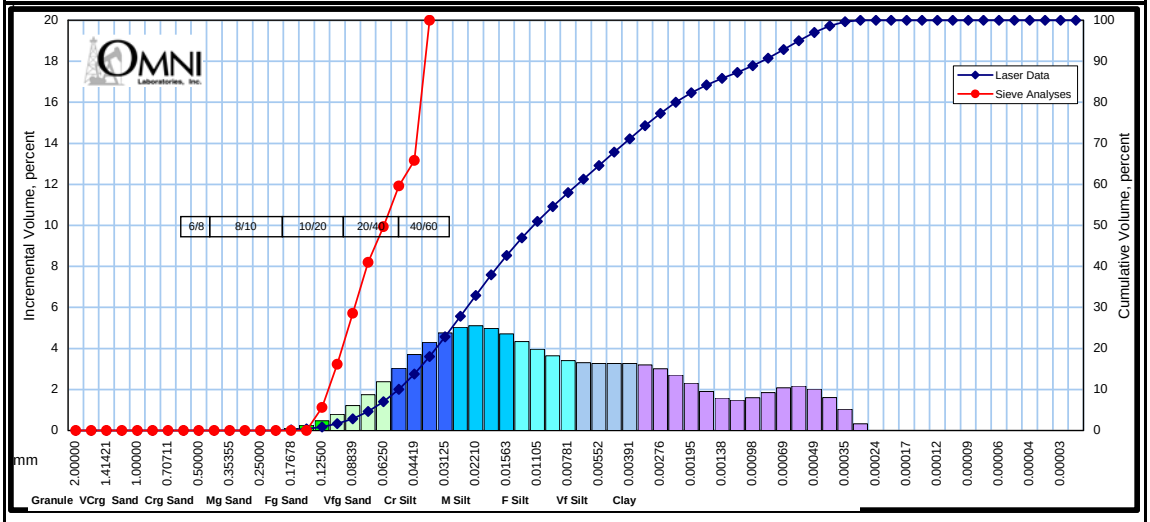

Wentworth Size Class	Mesh Size Inches	Mesh Size Millimeters	Phi of Screen	U.S. Sieve No.	Incremental Volume, percent	Cumulative Volume, percent
Granule	0.078740	2.00000	- 1.00	10	0.0	0.0
VCg Sand	0.066212	1.68179	- 0.75	12	0.0	0.0
	0.055678	1.41421	- 0.50	14	0.0	0.0
	0.046819	1.18921	- 0.25	16	0.0	0.0
	0.039370	1.00000	0.00	18	0.0	0.0
Cg Sand	0.033106	0.84090	0.25	20	0.0	0.0
	0.027839	0.70711	0.50	25	0.0	0.0
	0.023410	0.59460	0.75	30	0.0	0.0
	0.019685	0.50000	1.00	35	0.0	0.0
Mg Sand	0.016553	0.42045	1.25	40	0.0	0.0
	0.013919	0.35355	1.50	45	0.0	0.0
	0.011705	0.29730	1.75	50	0.0	0.0
	0.009843	0.25000	2.00	60	0.0	0.0
Fg Sand	0.008277	0.21022	2.25	70	0.0	0.0
	0.006960	0.17678	2.50	80	0.1	0.1
	0.005852	0.14865	2.75	100	0.3	0.4
	0.004921	0.12500	3.00	120	0.5	0.9
Vfg Sand	0.004138	0.10511	3.25	140	0.8	1.7
	0.003480	0.08839	3.50	170	1.2	2.9
	0.002926	0.07433	3.75	200	1.8	4.6
	0.002461	0.06250	4.00	230	2.4	7.0
C Silt	0.002069	0.05256	4.25	270	3.0	10.0
	0.001740	0.04419	4.50	325	3.7	13.8
	0.001463	0.03716	4.75	400	4.3	18.1
	0.001230	0.03125	5.00	450	4.8	22.8
M Silt	0.001035	0.02628	5.25	500	5.0	27.9
	0.000870	0.02210	5.50	635	5.1	33.0
	0.000732	0.01858	5.75		5.0	37.9
	0.000615	0.01563	6.00		4.7	42.7
F Silt	0.000517	0.01314	6.25		4.3	47.0
	0.000435	0.01105	6.50		4.0	51.0
	0.000366	0.00929	6.75		3.6	54.6
	0.000308	0.00781	7.00		3.4	58.0
Vf Silt	0.000259	0.00657	7.25		3.3	61.3
	0.000217	0.00552	7.50		3.3	64.6
	0.000183	0.00465	7.75		3.3	67.9
	0.000154	0.00391	8.00		3.3	71.1

Wentworth Size Class	Mesh Size Inches	Mesh Size Millimeters	Phi of Screen	U.S. Sieve No.	Incremental Volume, percent	Cumulative Volume, percent
Clay	0.000129	0.00329	8.25		3.2	74.3
	0.000109	0.00276	8.50		3.0	77.3
	0.000091	0.00232	8.75		2.7	80.0
	0.000077	0.00195	9.00		2.3	82.4
	0.000065	0.00164	9.25		1.9	84.3
	0.000054	0.00138	9.50		1.6	85.8
	0.000046	0.00116	9.75		1.5	87.3
	0.000038	0.00098	10.00		1.6	88.9
	0.000032	0.00082	10.25		1.8	90.8
	0.000027	0.00069	10.50		2.1	92.9
	0.000023	0.00058	10.75		2.2	95.0
	0.000019	0.00049	11.00		2.0	97.0
	0.000016	0.00041	11.25		1.6	98.6
	0.000014	0.00035	11.50		1.0	99.7
	0.000011	0.00029	11.75		0.3	100.0
	0.000010	0.00024	12.00		0.0	100.0
	0.000008	0.00021	12.25		0.0	100.0
	0.000007	0.00017	12.50		0.0	100.0
	0.000006	0.00015	12.75		0.0	100.0
	0.000005	0.00012	13.00		0.0	100.0
	0.000004	0.00010	13.25		0.0	100.0
	0.000003	0.00009	13.51		0.0	100.0
	0.000003	0.00007	13.74		0.0	100.0
	0.000002	0.00006	14.00		0.0	100.0
	0.000002	0.000051	14.26		0.0	100.0
	0.000002	0.000043	14.51		0.0	100.0
	0.000001	0.000036	14.76		0.0	100.0
	0.000001	0.000031	14.98		0.0	100.0
	0.000001	0.000026	15.23		0.0	100.0
	TOTALS				100.0	100.0

Description	Sieve Size	Volume Percent
Granule	10	0.0
Very Coarse Sand	18	0.0
Coarse Sand	35	0.0
Medium Sand	60	0.0
Fine Sand	120	0.9
Very Fine Sand	230	6.1
Coarse Silt	450	15.8
Medium Silt		19.8
Fine Silt		15.4
Very Fine Silt		13.1
Clay		28.9
	Total	100.0

Cumulative Volume Percent greater than			
	Phi	Particle Size	
Percentile	Value	Inches	Millimeters
5	3.7870	0.0029	0.0724
10	4.2402	0.0021	0.0529
16	4.6279	0.0016	0.0404
25	5.1023	0.0011	0.0291
50	6.4290	0.0005	0.0116
75	8.2940	0.0001	0.0032
84	9.2011	0.0001	0.0017
90	10.1372	0.0000	0.0009
95	10.7344	0.0000	0.0006

Measure	Trask, mm	Folk, phi	Inches
Median	0.0116	6.4290	0.0005
Mean	0.0161	6.7527	0.0006
Sorting	3.0228	2.1959	
Skewness	0.6886	0.2259	
Kurtosis	0.2492	0.8921	

Figure B18: Grain Size Laser Analysis, Core 12, Section 3, 21 to 23 inches

SIEVE ANALYSIS

Conventional Core

U.S. Geological Survey - MA
Mt. Elbert 01 PPMA Samples

Core Run: 19
Core Section: 4
Sample Top-Bottom, In.: 32-34
File: HH-36917

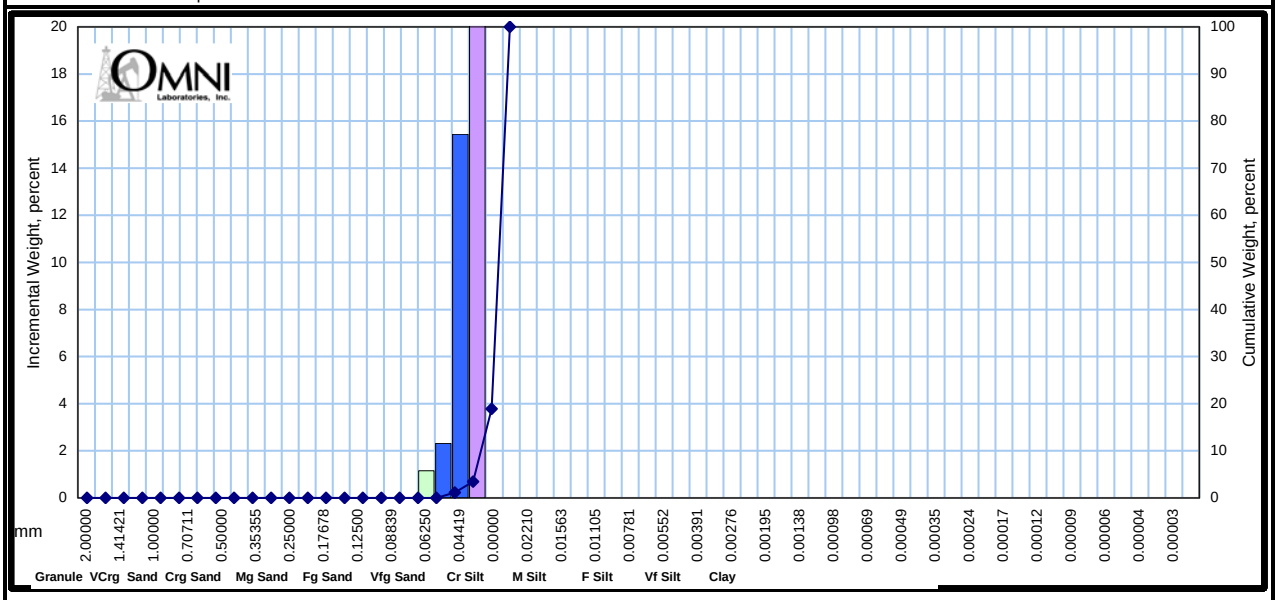

Wentworth Size Class	Mesh Size Inches	Mesh Size Millimeters	Phi of Screen	U.S. Sieve No.	Incremental Weight, percent	Cumulative Weight, percent
Granule	0.078740	2.00000	- 1.00	10	0.0	0.0
VCg Sand	0.066212	1.68179	- 0.75	12	0.0	0.0
	0.055678	1.41421	- 0.50	14	0.0	0.0
	0.046819	1.18921	- 0.25	16	0.0	0.0
	0.039370	1.00000	0.00	18	0.0	0.0
Cg Sand	0.033106	0.84090	0.25	20	0.0	0.0
	0.027839	0.70711	0.50	25	0.0	0.0
	0.023410	0.59460	0.75	30	0.0	0.0
	0.019685	0.50000	1.00	35	0.0	0.0
Mg Sand	0.016553	0.42045	1.25	40	0.0	0.0
	0.013919	0.35355	1.50	45	0.0	0.0
	0.011705	0.29730	1.75	50	0.0	0.0
	0.009843	0.25000	2.00	60	0.0	0.0
Fg Sand	0.008277	0.21022	2.25	70	0.0	0.0
	0.006960	0.17678	2.50	80	0.0	0.0
	0.005852	0.14865	2.75	100	0.0	0.0
	0.004921	0.12500	3.00	120	0.0	0.0
Vfg Sand	0.004138	0.10511	3.25	140	0.0	0.0
	0.003480	0.08839	3.50	170	0.0	0.0
	0.002926	0.07433	3.75	200	0.0	0.0
	0.002461	0.06250	4.00	230	1.2	1.2
C Silt	0.002069	0.05256	4.25	270	2.3	3.5
	0.001740	0.04419	4.50	325	15.4	18.9
Pan				<325	81.1	100.0

Description	Sieve Size	Weight Percent
Granule	10	0.0
Very Coarse Sand	18	0.0
Coarse Sand	35	0.0
Medium Sand	60	0.0
Fine Sand	120	0.0
Very Fine Sand	230	1.2
Coarse Silt	0	17.8
Pan	<325	81.1

Cumulative Volume Percent greater than			
	Phi	Particle Size	
Percentile	Value	Inches	Millimeters
5	4.2728	0.0020	0.0517
10	4.3504	0.0019	0.0490
16	4.4493	0.0018	0.0458
25	4.5446	0.0017	0.0429
50	4.7437	0.0015	0.0373
75	4.9747	0.0013	0.0318
84	5.0679	0.0012	0.0298
90	4.5422	0.0017	0.0429
95	4.6374	0.0016	0.0402

Measure	Trask, mm	Folk, phi	Inches
Median	0.0373	4.7437	0.0015
Mean	0.0373	4.7536	0.0015
Sorting	1.1608	0.2099	
Skewness	0.9781	-0.7673	
Kurtosis	0.9052	0.3473	

Figure B19: Grain Size Sieve Analysis, Core 19, Section 4, 32 to 34 inches

LASER GRAIN SIZE ANALYSIS

Conventional Core

U.S. Geological Survey - MA
Mt. Elbert 01 PPMA Samples

Core Run: 19
Core Section: 4
Sample Top-Bottom, In.: 32-34
File: HH-36917

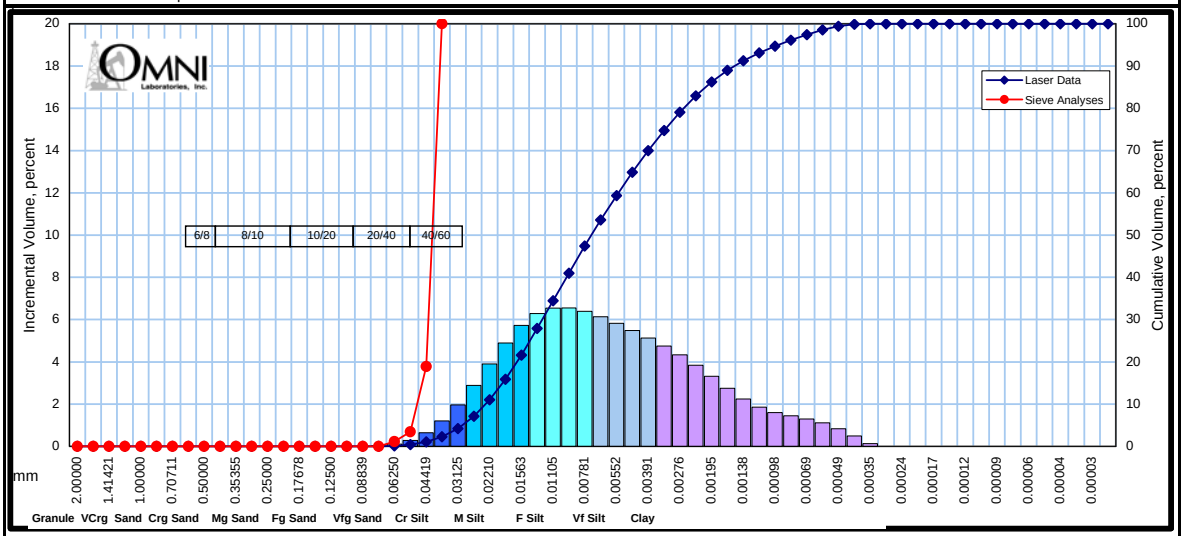

Wentworth Size Class	Mesh Size Inches	Mesh Size Millimeters	Phi of Screen	U.S. Sieve No.	Incremental Volume, percent	Cumulative Volume, percent
Granule	0.078740	2.00000	- 1.00	10	0.0	0.0
VCg Sand	0.066212	1.68179	- 0.75	12	0.0	0.0
	0.055678	1.41421	- 0.50	14	0.0	0.0
	0.046819	1.18921	- 0.25	16	0.0	0.0
	0.039370	1.00000	0.00	18	0.0	0.0
Cg Sand	0.033106	0.84090	0.25	20	0.0	0.0
	0.027839	0.70711	0.50	25	0.0	0.0
	0.023410	0.59460	0.75	30	0.0	0.0
	0.019685	0.50000	1.00	35	0.0	0.0
Mg Sand	0.016553	0.42045	1.25	40	0.0	0.0
	0.013919	0.35355	1.50	45	0.0	0.0
	0.011705	0.29730	1.75	50	0.0	0.0
	0.009843	0.25000	2.00	60	0.0	0.0
Fg Sand	0.008277	0.21022	2.25	70	0.0	0.0
	0.006960	0.17678	2.50	80	0.0	0.0
	0.005852	0.14865	2.75	100	0.0	0.0
	0.004921	0.12500	3.00	120	0.0	0.0
Vfg Sand	0.004138	0.10511	3.25	140	0.0	0.0
	0.003480	0.08839	3.50	170	0.0	0.0
	0.002926	0.07433	3.75	200	0.0	0.0
	0.002461	0.06250	4.00	230	0.1	0.1
C Silt	0.002069	0.05256	4.25	270	0.3	0.4
	0.001740	0.04419	4.50	325	0.6	1.1
	0.001463	0.03716	4.75	400	1.2	2.3
	0.001230	0.03125	5.00	450	2.0	4.2
M Silt	0.001035	0.02628	5.25	500	2.9	7.1
	0.000870	0.02210	5.50	635	3.9	11.0
	0.000732	0.01858	5.75		4.9	15.9
	0.000615	0.01563	6.00		5.7	21.6
F Silt	0.000517	0.01314	6.25		6.3	27.9
	0.000435	0.01105	6.50		6.5	34.4
	0.000366	0.00929	6.75		6.6	41.0
	0.000308	0.00781	7.00		6.4	47.4
Vf Silt	0.000259	0.00657	7.25		6.1	53.5
	0.000217	0.00552	7.50		5.8	59.4
	0.000183	0.00465	7.75		5.5	64.9
	0.000154	0.00391	8.00		5.1	70.0
Clay	0.000129	0.00329	8.25		4.8	74.7
	0.000109	0.00276	8.50		4.3	79.1
	0.000091	0.00232	8.75		3.8	82.9
	0.000077	0.00195	9.00		3.3	86.2
	0.000065	0.00164	9.25		2.8	89.0
	0.000054	0.00138	9.50		2.2	91.2
	0.000046	0.00116	9.75		1.9	93.1
	0.000038	0.00098	10.00		1.6	94.7
	0.000032	0.00082	10.25		1.4	96.1
	0.000027	0.00069	10.50		1.3	97.4
	0.000023	0.00058	10.75		1.1	98.5
	0.000019	0.00049	11.00		0.8	99.4
	0.000016	0.00041	11.25		0.5	99.9
	0.000014	0.00035	11.50		0.1	100.0
	0.000011	0.00029	11.75		0.0	100.0
	0.000010	0.00024	12.00		0.0	100.0
	0.000008	0.00021	12.25		0.0	100.0
	0.000007	0.00017	12.50		0.0	100.0
	0.000006	0.00015	12.75		0.0	100.0
	0.000005	0.00012	13.00		0.0	100.0
	0.000004	0.00010	13.25		0.0	100.0
	0.000003	0.00009	13.51		0.0	100.0
	0.000003	0.00007	13.74		0.0	100.0
	0.000002	0.00006	14.00		0.0	100.0
	0.000002	0.000051	14.26		0.0	100.0
	0.000002	0.000043	14.51		0.0	100.0
	0.000001	0.000036	14.76		0.0	100.0
	0.000001	0.000031	14.98		0.0	100.0
	0.000001	0.000026	15.23		0.0	100.0
	TOTALS				100.0	100.0

Description	Sieve Size	Volume Percent
Granule	10	0.0
Very Coarse Sand	18	0.0
Coarse Sand	35	0.0
Medium Sand	60	0.0
Fine Sand	120	0.0
Very Fine Sand	230	0.1
Coarse Silt	450	4.1
Medium Silt		17.4
Fine Silt		25.8
Very Fine Silt		22.6
Clay		30.0
	Total	100.0

Cumulative Volume Percent greater than			
	Phi	Particle Size	
Percentile	Value	Inches	Millimeters
5	5.0695	0.0012	0.0298
10	5.4338	0.0009	0.0231
16	5.7467	0.0007	0.0186
25	6.1282	0.0006	0.0143
50	7.0949	0.0003	0.0073
75	8.2534	0.0001	0.0033
84	8.8159	0.0001	0.0022
90	9.3438	0.0001	0.0015
95	10.0383	0.0000	0.0010

Measure	Trask, mm	Folk, phi	Inches
Median	0.0073	7.0949	0.0003
Mean	0.0088	7.2192	0.0003
Sorting	2.0887	1.5201	
Skewness	0.8755	0.1531	
Kurtosis	0.2551	0.9582	

Figure B20: Grain Size Laser Analysis, Core 19, Section 4, 32 to 34 inches

10.2 Petrography Data and Photomicrographs

Figures B21-B40 illustrate Mt Elbert-01 core sample photomicrographs. Sample descriptions and interpretations are also included.

Sample Depth: 2017.10 Feet, Sample Number: 2-2-8-9
Lithology: Shale
Fabric and Texture: Sand-/Silt-Laminated
Framework Grains: Mainly quartz (Plate 1B; C-D5); moderate potassium (Plate 1B; A-B7) and plagioclase (Plate 1B; K5.5) feldspar; minor lithics (Plate 1B; D-E15); elongate plant fragments (Plate 1B; B10)
Matrix: Clay-rich; organic-bearing; laminated (across Plate 1A from F-G)
Cements and Replacement Minerals: Pyrite (Plate 1B; A-B3.5); recrystallized clay matrix (Plate 1B)
Pore System and Reservoir Quality: Minor intergranular (Plate 1B; E-F12) and micropores (Plate 1B; area of H-J9)

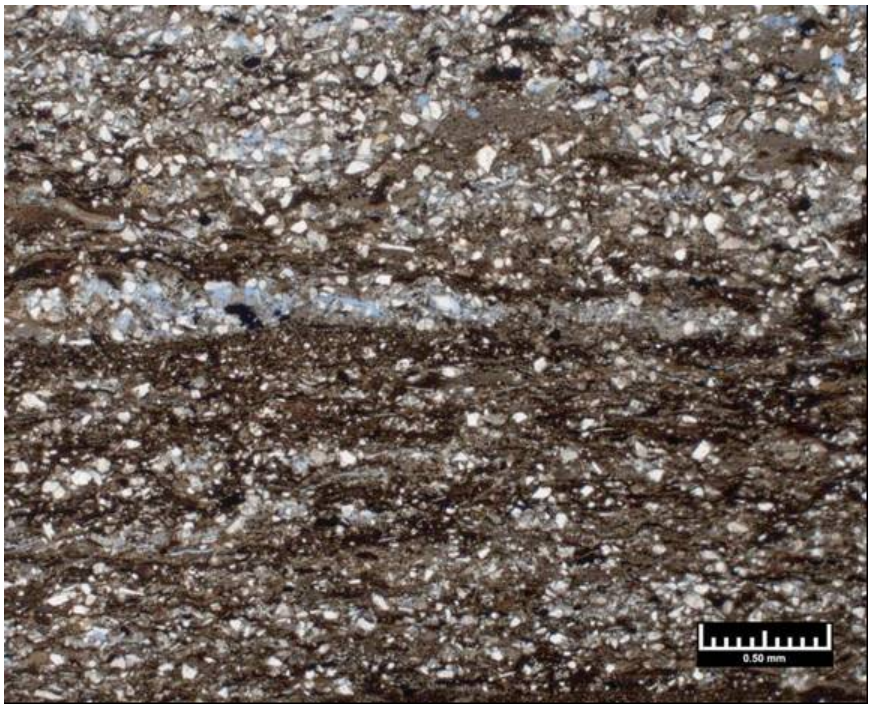

Figure B21: Photomicrograph of Sample Depth: 2017.10 Feet Sample Number: 2-2-8-9 Magnification: A: 40X

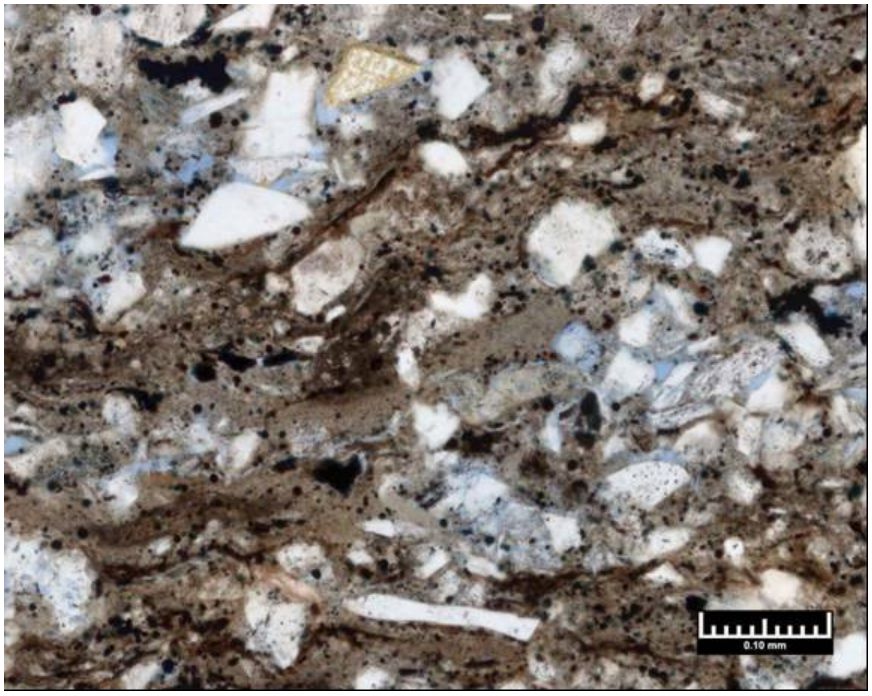

Figure B22: Photomicrograph of Sample Depth: 2017.10 Feet Sample Number: 2-2-8-9 Magnification: B: 200X

Sample Depth: 2018.35 Feet, Sample Number: 2-2-21-27B
Lithology: Shale
Fabric and Texture: Sand-/Silt-Laminated
Framework Grains: Mainly quartz (Plate 2A; G9); moderately potassium (Plate 2B; G11); minor lithics
Matrix: Clay rich; organic-bearing; laminated (across Plate 2A from G-H)
Cements and Replacement Minerals: Pyrite (Plate 2B; E-F4.5; recrystallized clay matrix (Plate 2B; G5)
Pore System and Reservoir Quality: Dominant micropores, minor intergranular porosity (Plate 2B; G-H5)

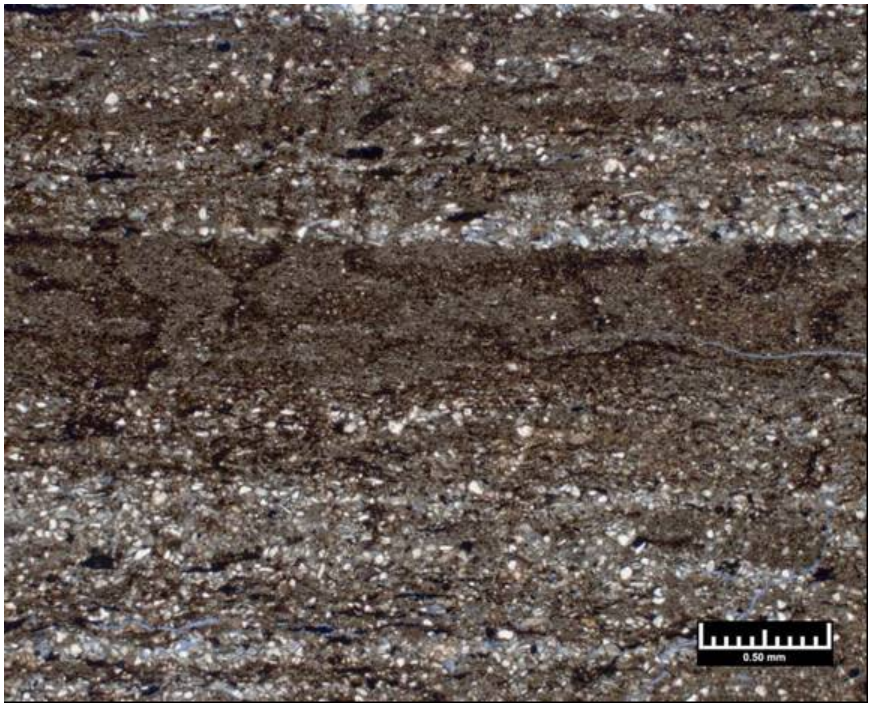

Figure B23: Photomicrograph of Sample Depth: 2018.35 Feet Sample Number: 2-2-21-27B Magnification: A: 40X

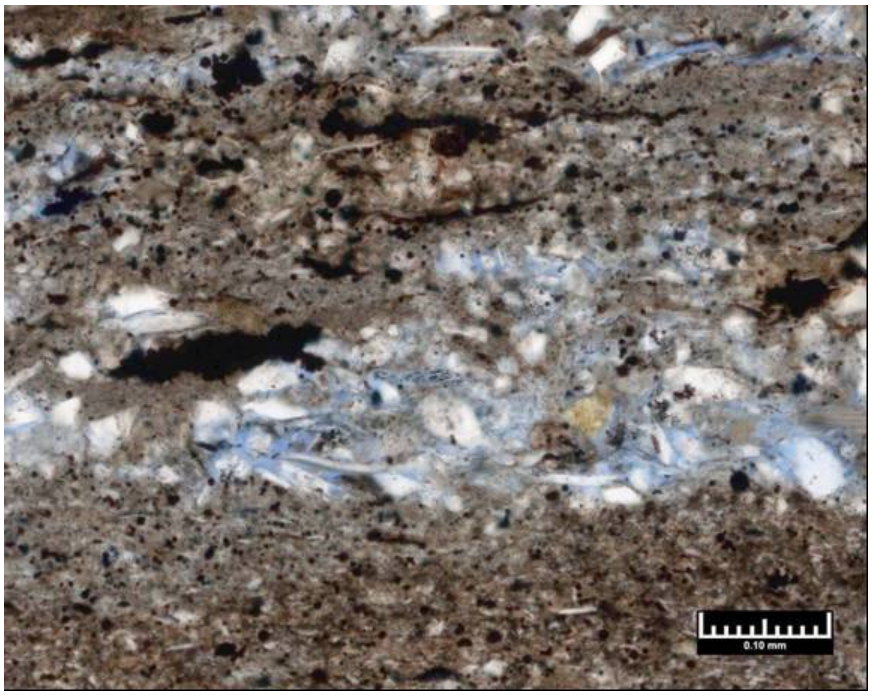

Figure B24: Photomicrograph of Sample Depth: 2018.35 Feet Sample Number: 2-2-21-27B Magnification: B: 200 X

Sample Depth: 2032.40 Feet, Sample Number: 2-7-16-17
Lithology: Sandstone
Fabric and Texture: Vaguely Grain size-zoned
Framework Grains: Mainly quartz (Plate 3A; B 5.5); sub-dominant lithics (Plate 3B; B-C11.5); moderate potassium (Plate 3B; H5)
Matrix: None
Cements and Replacement Minerals: Pyrite (Plate 3B; H7); pore-lining clay (Plate 3B; C1)
Pore System and Reservoir Quality: Dominant intergranular porosity (Plate 3B; E9.5)

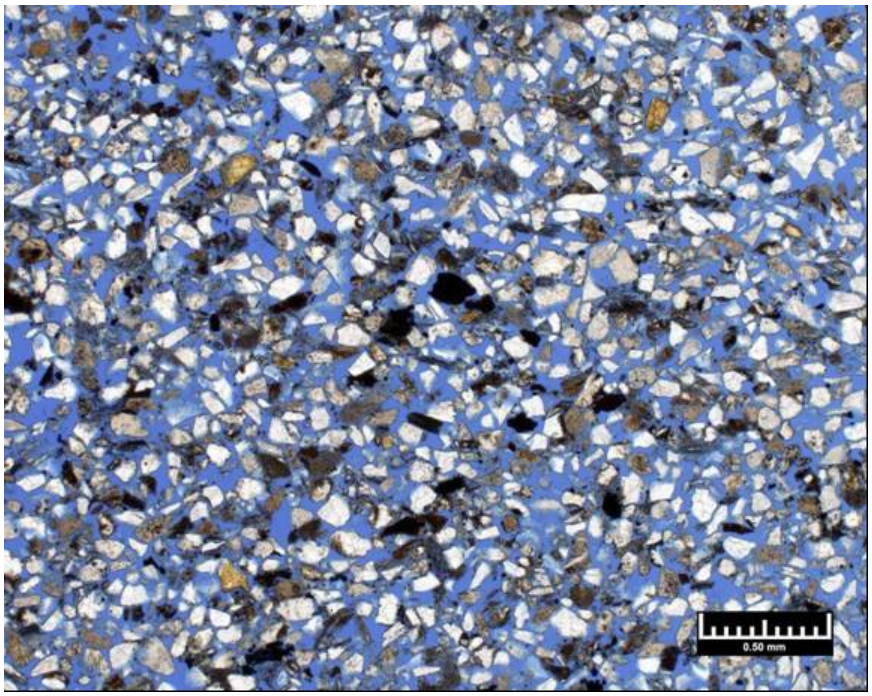

Figure B25: Photomicrograph of Sample Depth: 2032.40 Feet Sample Number: 2-7-16-17 Magnification: A: 40X

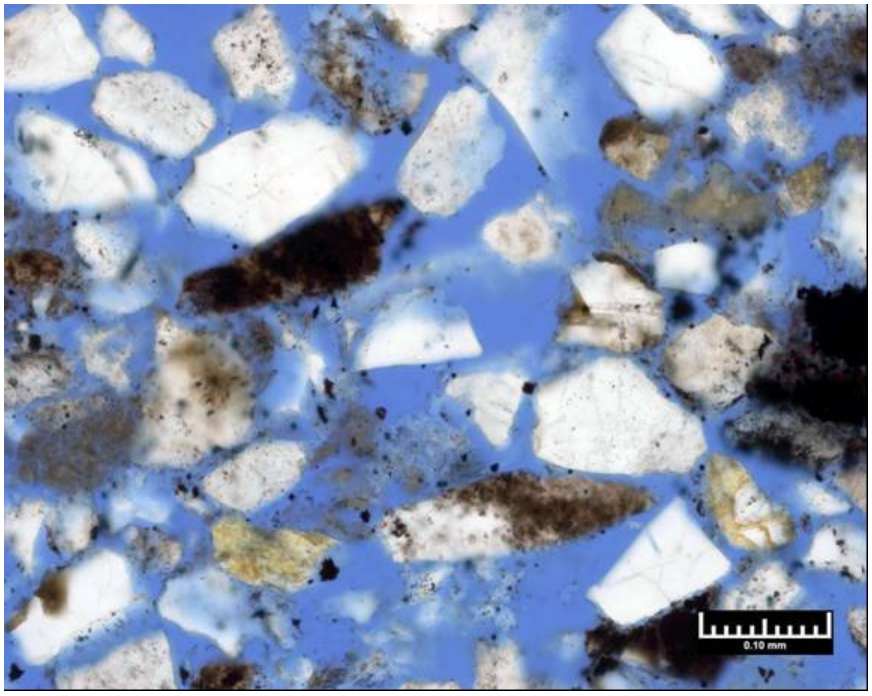

Figure B26: Photomicrograph of Sample Depth: 2032.40 Feet Sample Number: 2-7-16-17 Magnification: B: 200X

Sample Depth: 2045.90 Feet, Sample Number: 3-7-3
Lithology: Sandstone
Fabric and Texture: Massive, very fine-grained, well sorted
Framework Grains: Mainly quartz (Plate 4A; E11); moderate lithics (Plate 4B; E4.5); minor plagioclase (Plate 4A;G9) and potassium feldspars
Matrix: None
Cements and Replacement Minerals: Pyrite (Plate 4B; F12) ; pore-lining clay (Plate 4B; H5.5)
Pore System and Reservoir Quality: Dominant intergranular (Plate 4B; G9); minor microporosity (Plate 4B; within grain at D11)

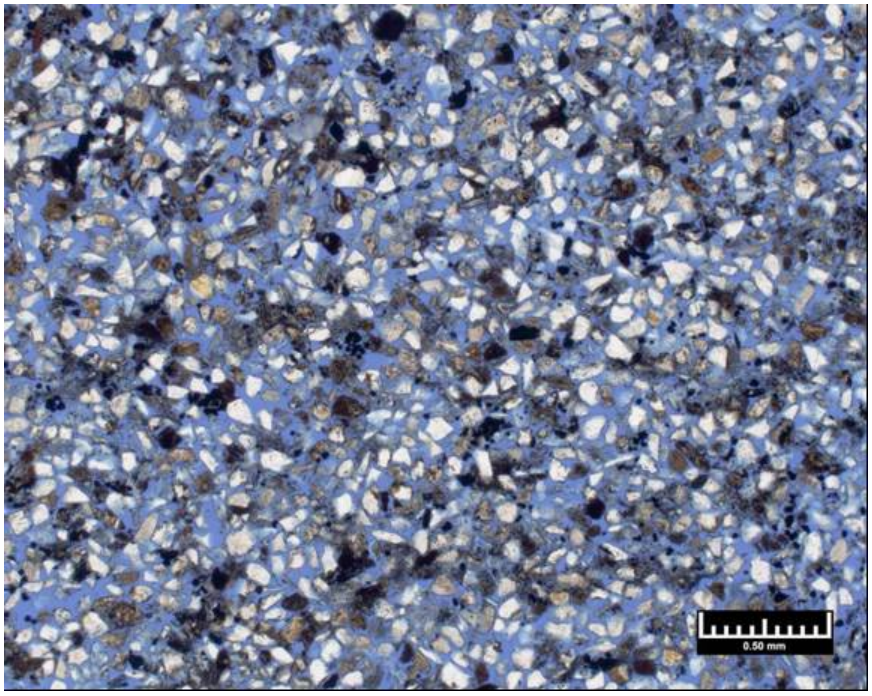

Figure B27: Photomicrograph of Sample Depth: 2045.90 Feet Sample Number: 3-7-3 Magnification: A: 40X

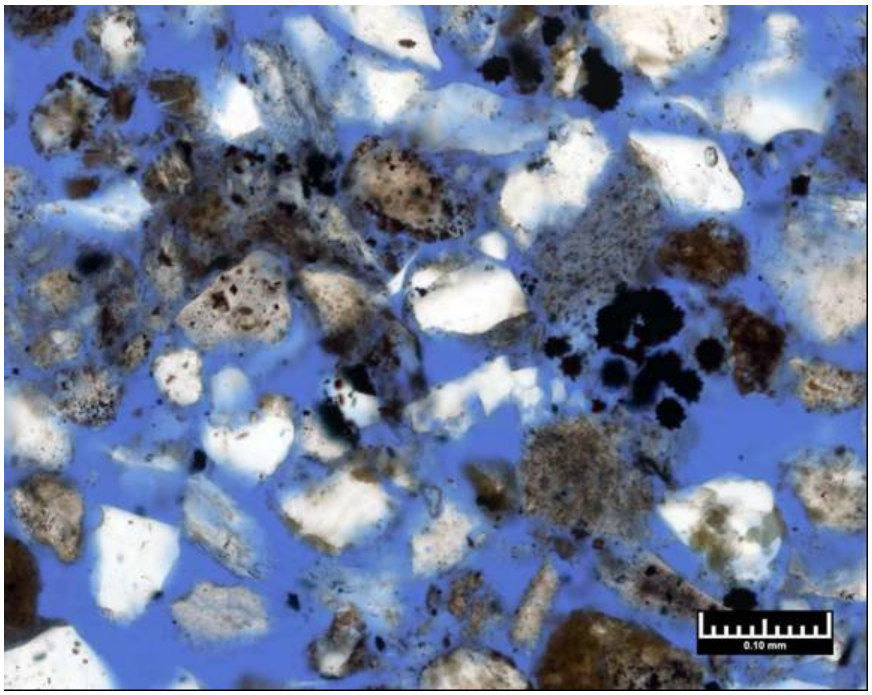

Figure B28: Photomicrograph of Sample Depth: 2045.90 Feet Sample Number: 3-7-3 Magnification: B: 200 X

Sample Depth: 2106.60 Feet, Sample Number: 5-8-1-6A
Lithology: Shale
Fabric and Texture: Vaguely-Laminated; Burrowed
Framework Grains: Dominant quartz (Plate 5A; C6); moderate lithics (Plate 5B; H7), minor potassium feldspar (Plate 5B; B3)
Matrix: Detrital (Plate 5A; brownish fine material)
Cements and Replacement Minerals: Pyrite (Plate 5B; J10)
Pore System and Reservoir Quality: Subequal microporosity (within matrix); and intergranular porosity (Plate 5B; E6)

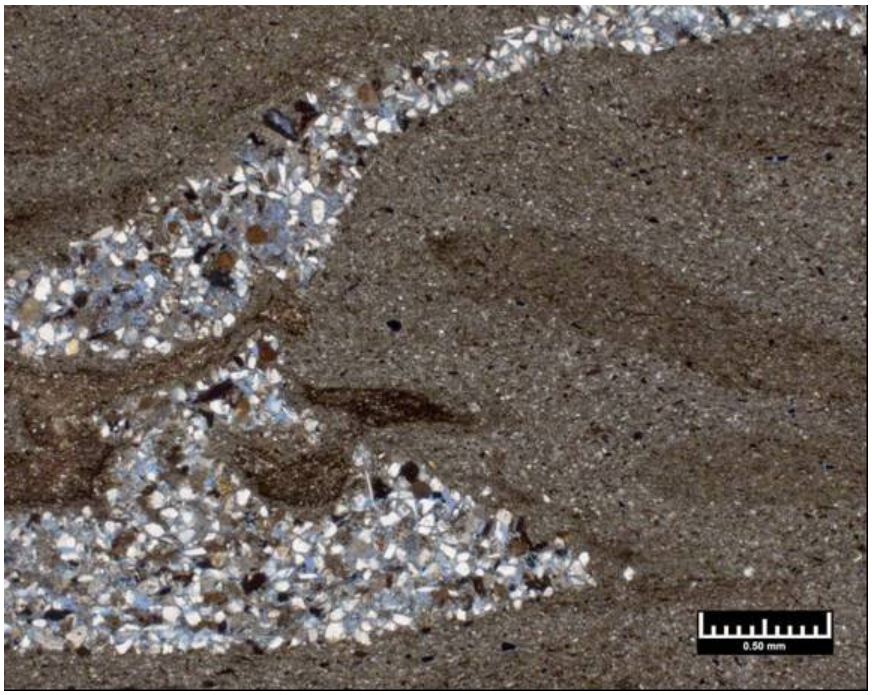

Figure B29: Photomicrograph of Sample Depth: 2106.60 Feet Sample Number: 5-8-1-6A Magnification: A: 40X

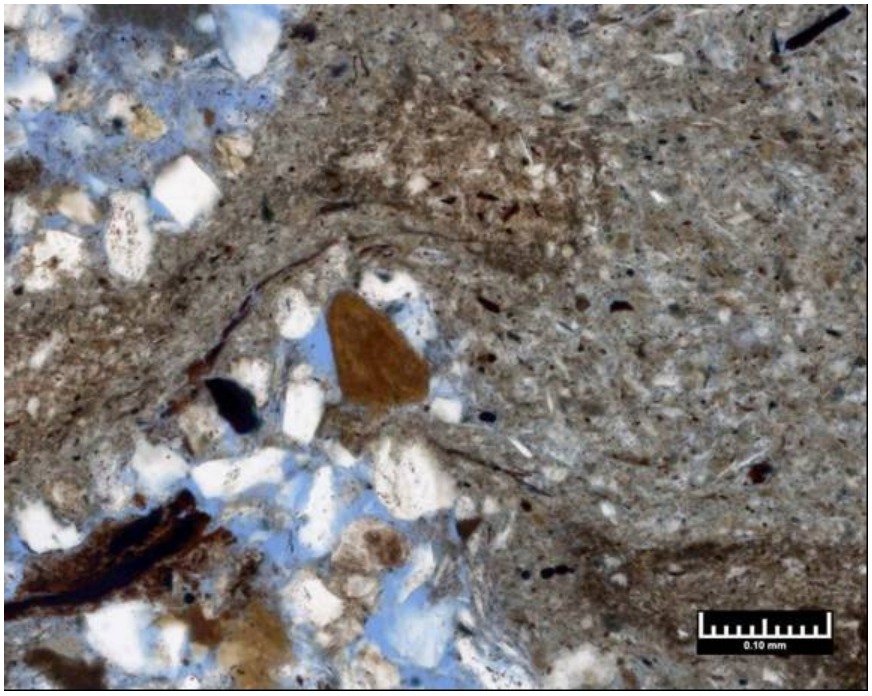

Figure B30: Photomicrograph of Sample Depth: 2106.60 Feet Sample Number: 5-8-1-6A Magnification: B: 200X

Sample Depth: 2124.75 Feet, Sample Number: 6-5-30-36A
Lithology: Siltstone
Fabric and Texture: Vaguely-Laminated
Framework Grains: Mainly quartz (Plate 6A;F8); moderate plagioclase (Plate 6B;F5) and lesser potassium feldspar; minor lithics (Plate 6A; B-C12.5)
Matrix: Depositional; clay-rich; minor very fine sand grains
Cements and Replacement Minerals: Pore-lining clay (Plate 6B; D8.5); pyrite (Plate 6B; K11.5)
Pore System and Reservoir Quality: Dominant intergranular (Plate 6B;B7.5); moderate microporous (Plate 6B; G6)

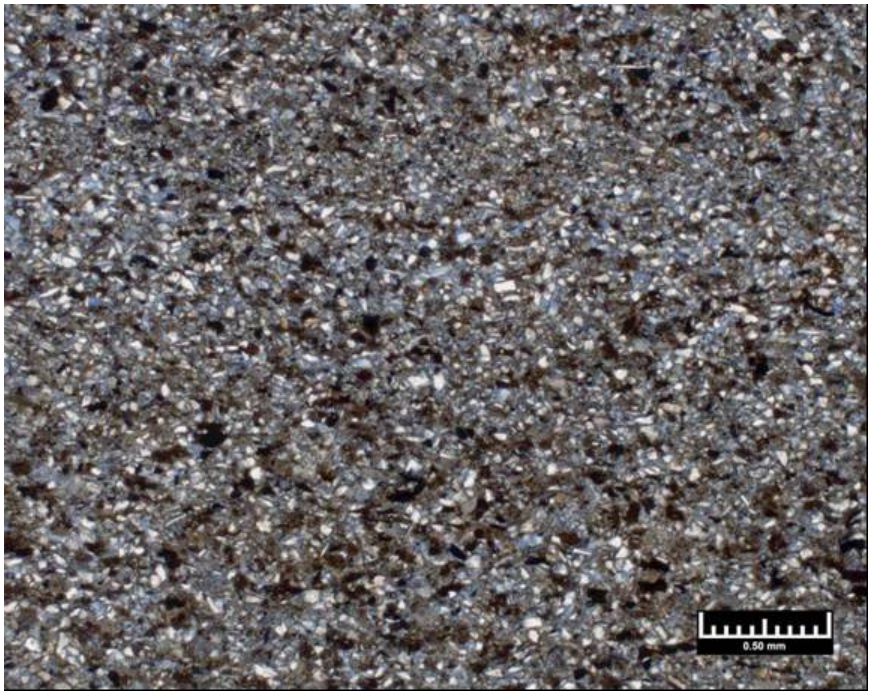

Figure B31: Photomicrograph of Sample Depth: 2124.75 Feet Sample Number: 6-5-30-36A Magnification: A: 40X

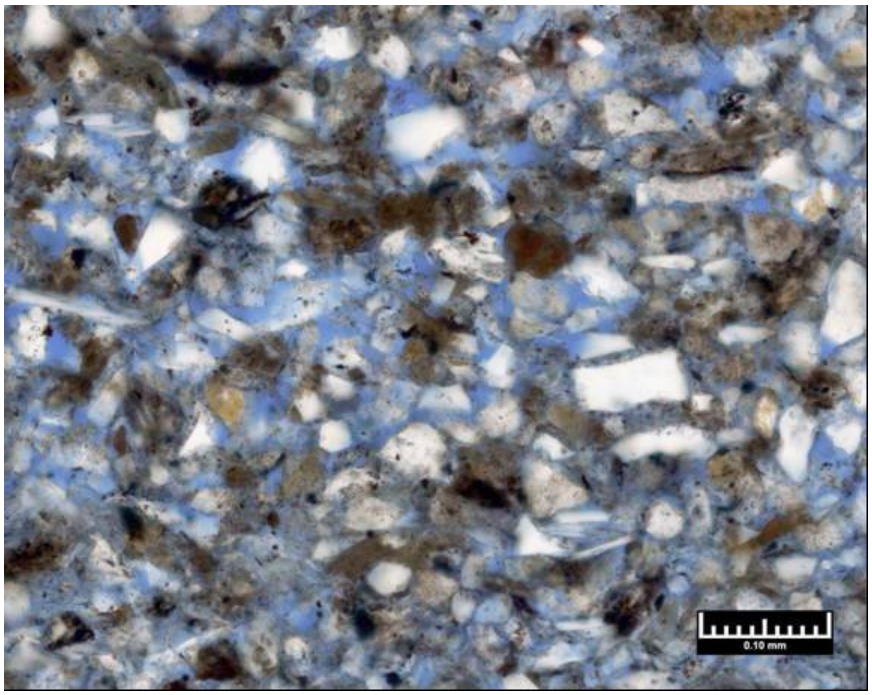

Figure B32: Photomicrograph of Sample Depth: 2124.75 Feet Sample Number: 6-5-30-36A Magnification: B: 200X

Sample Depth: 2163.40 Feet, Sample Number: 8-3-10-11
Lithology: Sandstone
Fabric and Texture: Vaguely Grain Size-zoned
Framework Grains: Mainly quartz (Plate 7A; C10); moderate lithics (Plate 7B; E5); minor potassium and plagioclase (Plate 7B; B6) feldspars
Matrix: None
Cements and Replacement Minerals: Pyrite (Plate 7B; E9); pore-lining clay (Plate 7B; B10.5)
Pore System and Reservoir Quality: Dominant intergranular (Plate 7B; D5); minor microporous (within pore-lining clays)

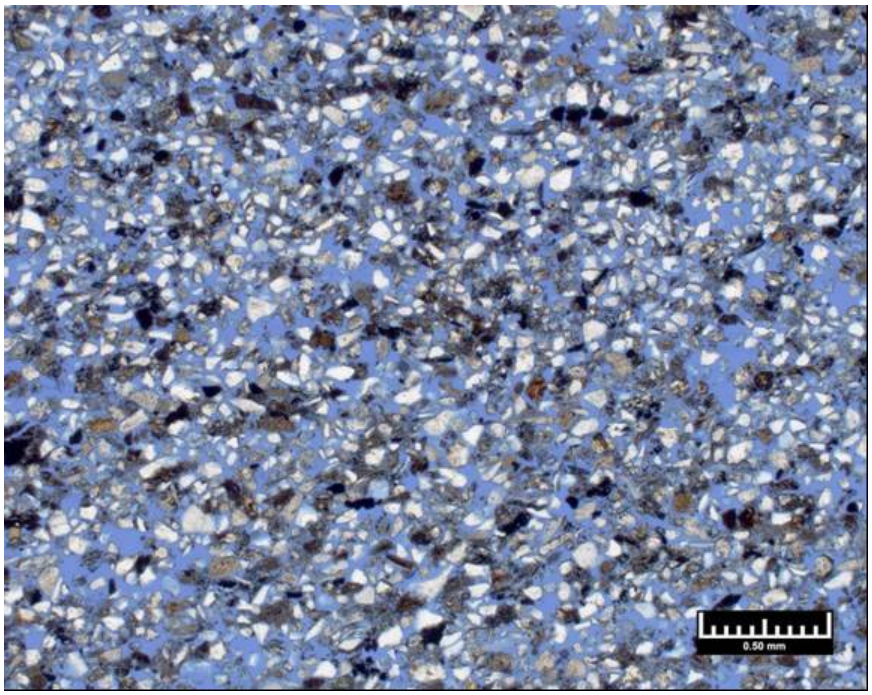

Figure B33: Photomicrograph of Sample Depth: 2163.40 Feet Sample Number: 8-3-10-11 Magnification: A: 40X

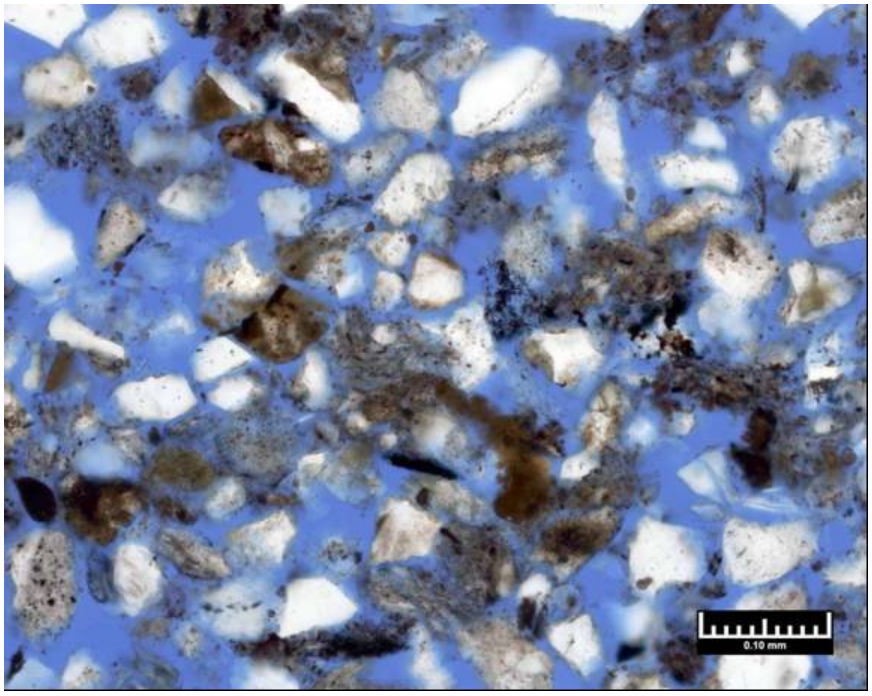

Figure B34: Photomicrograph of Sample Depth: 2163.40 Feet Sample Number: 8-3-10-11 Magnification: B: 200X

Sample Depth: 2180.25 Feet, Sample Number: 9-1-2-7A
Lithology: Sandstone
Fabric and Texture: Grain Size-zoned
Framework Grains: Mostly quartz (Plate 8A; H11); common lithics (Plate 8B; C11); minor plagioclase (Plate 8A; H-J3) feldspar
Matrix: None
Cements and Replacement Minerals: Minor pyrite (Plate 8B; F10)
Pore System and Reservoir Quality: Dominant primary intergranular (Plate 8B; E12); minor secondary intragranular porosity (Plate 8B; G-H6.5) and microporous (associated with clays)

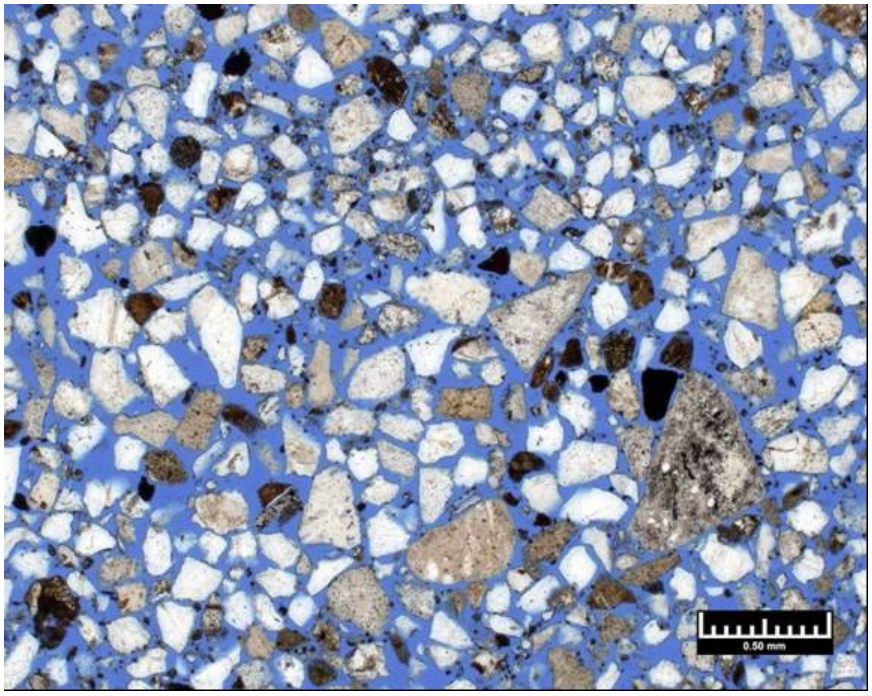

Figure B35: Photomicrograph of Sample Depth: 2180.25 Feet Sample Number: 9-1-2-7A Magnification: A: 40X

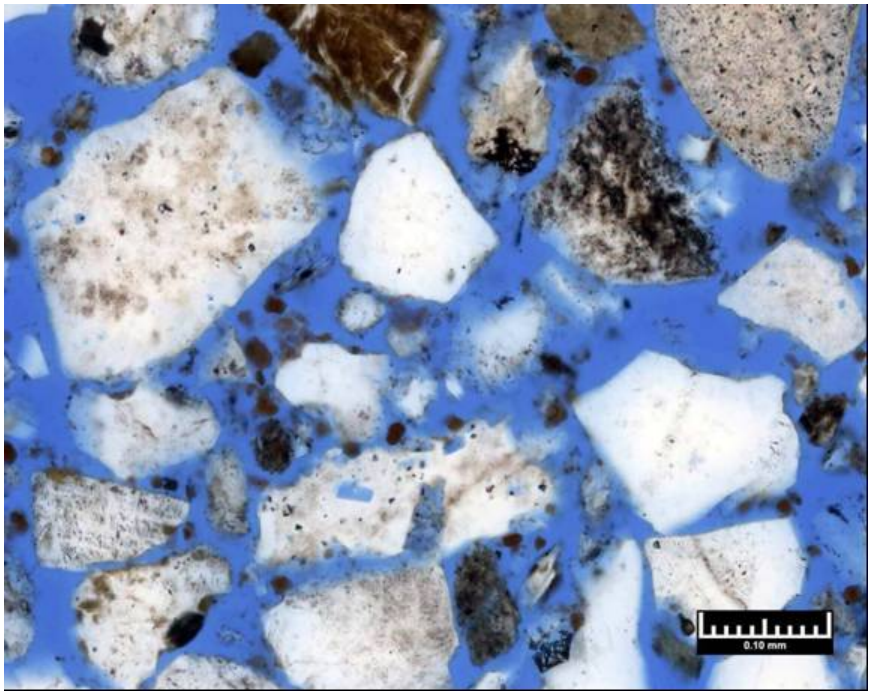

Figure B36: Photomicrograph of Sample Depth: 2180.25 Feet Sample Number: 9-1-2-7A Magnification: B: 200X

Sample Depth: 2224.15 Feet, Sample Number: 12-3-6-12A
Lithology: Shale
Fabric and Texture: Sandy; Vaguely-Laminated
Framework Grains: Mostly quartz (Plate 9A; E-F7); moderate lithics (Plate 9B: D9); minor plagioclase (D-E13) and potassium feldspars
Matrix: Detrital; brownish; clay-rich
Cements and Replacement Minerals: Pyrite (Plate 9B; E10)
Pore System and Reservoir Quality: Minor intergranular (elsewhere in thin section); moderate microporous (Plate 9B: C-D8.5); rare secondary intragranular (Plate 9B; G10)

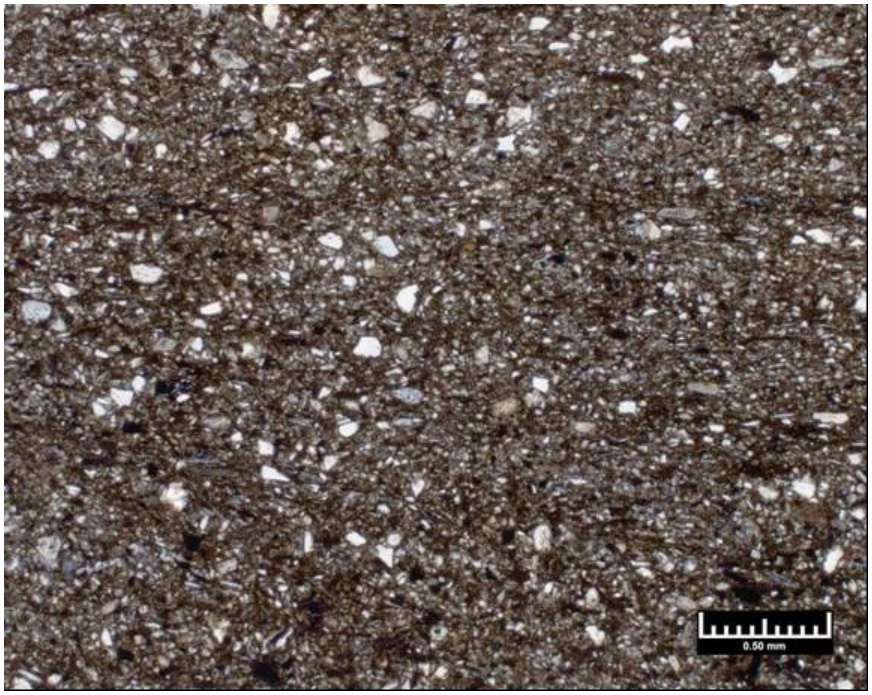

Figure B37: Photomicrograph of Sample Depth: 2224.15 Feet Sample Number: 12-3-6-12A Magnification: A: 40X

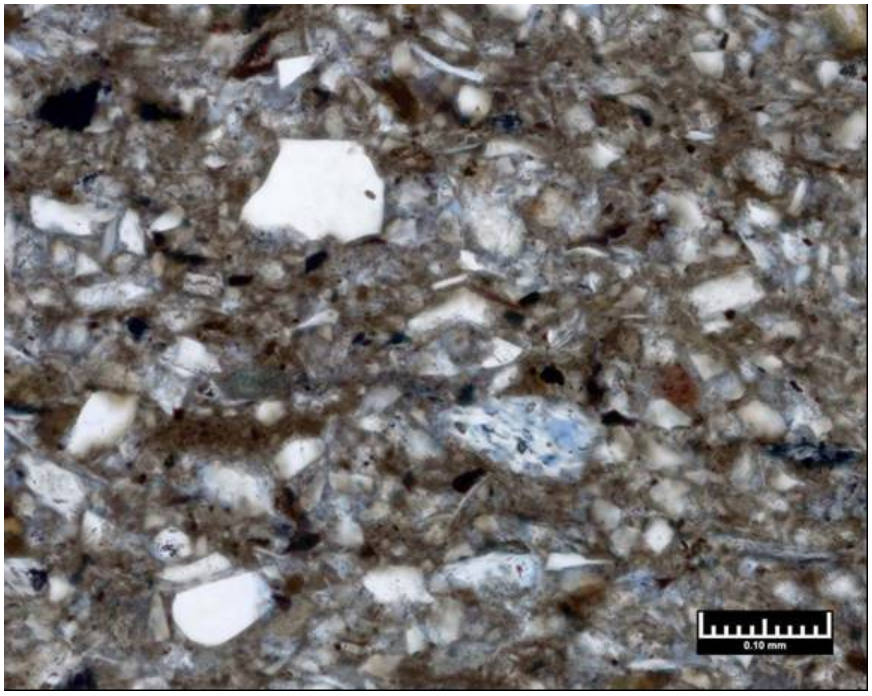

Figure B38: Photomicrograph of Sample Depth: 2224.15 Feet Sample Number: 12-3-6-12A Magnification: B: 200X

Sample Depth: 2454.95 Feet, Sample Number: 22-4-20-23B
Lithology: Shale
Fabric and Texture: Sand-Laminated
Framework Grains: Mostly quartz (Plate 10A; C13); moderate lithic fragments (Plate 10B; F4); minor muscovite mica (Plate 10B; F6); rare zircon (Plate 10B; E-F8)
Matrix: Detrital; clay-rich; organic-bearing
Cements and Replacement Minerals: Pyrite (Plate 10B; B14); minor siderite and Fe/Ti oxides
Pore System and Reservoir Quality: Dominate microporosity (Plate 10B; E9); moderate intergranular porosity (Plate 10B; F10)

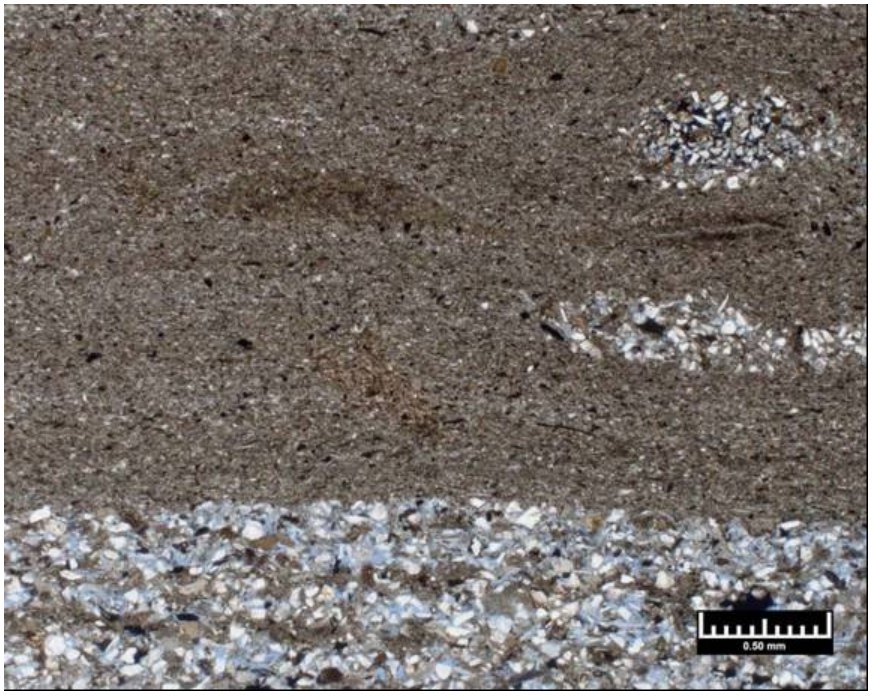

Figure B39: Photomicrograph of Sample Depth: 2454.95 Feet Sample Number: 22-4-20-23B Magnification: A: 40X

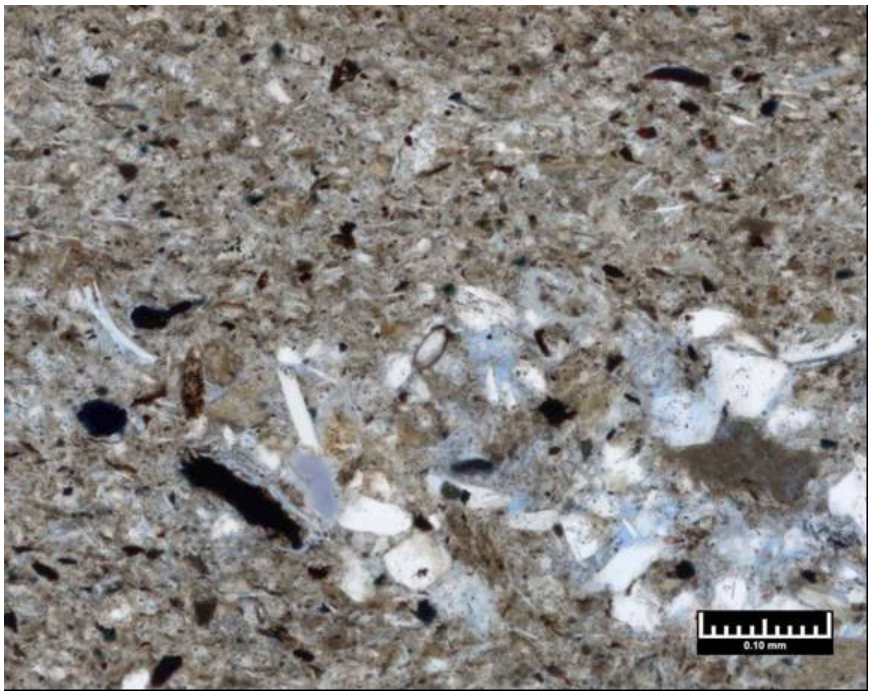

Figure B40: Photomicrograph of Sample Depth: 2454.95 Feet Sample Number: 22-4-20-23B Magnification: A: 200X

10.3 CT Scans

Figures B41-B63 illustrate CT scans performed at OMNI Labs (now Weatherford). Figures B64-B73 illustrate whole core scans performed by LBNL prior to core sample analyses.

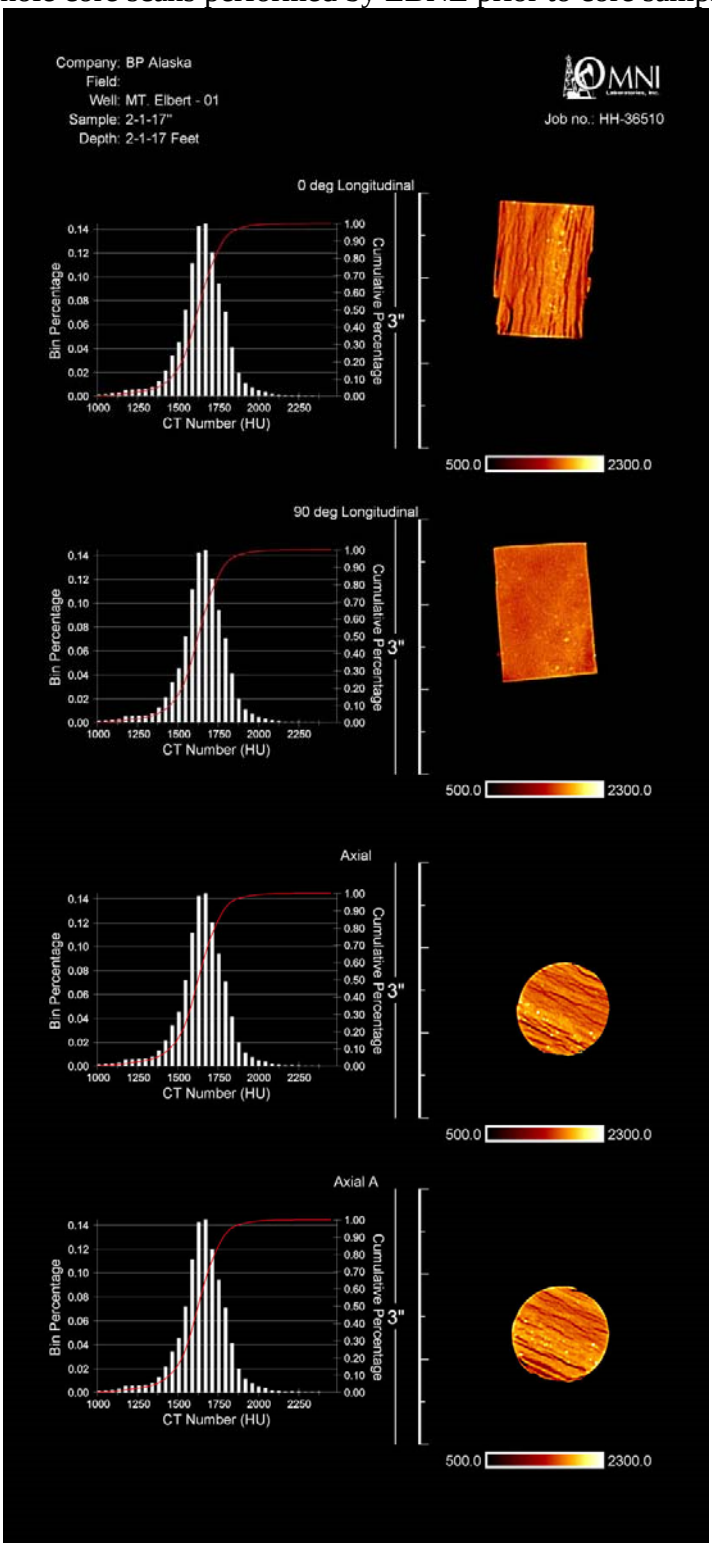

Figure B41: CTscan of core sample, Core 2, Section 1, 17 inches

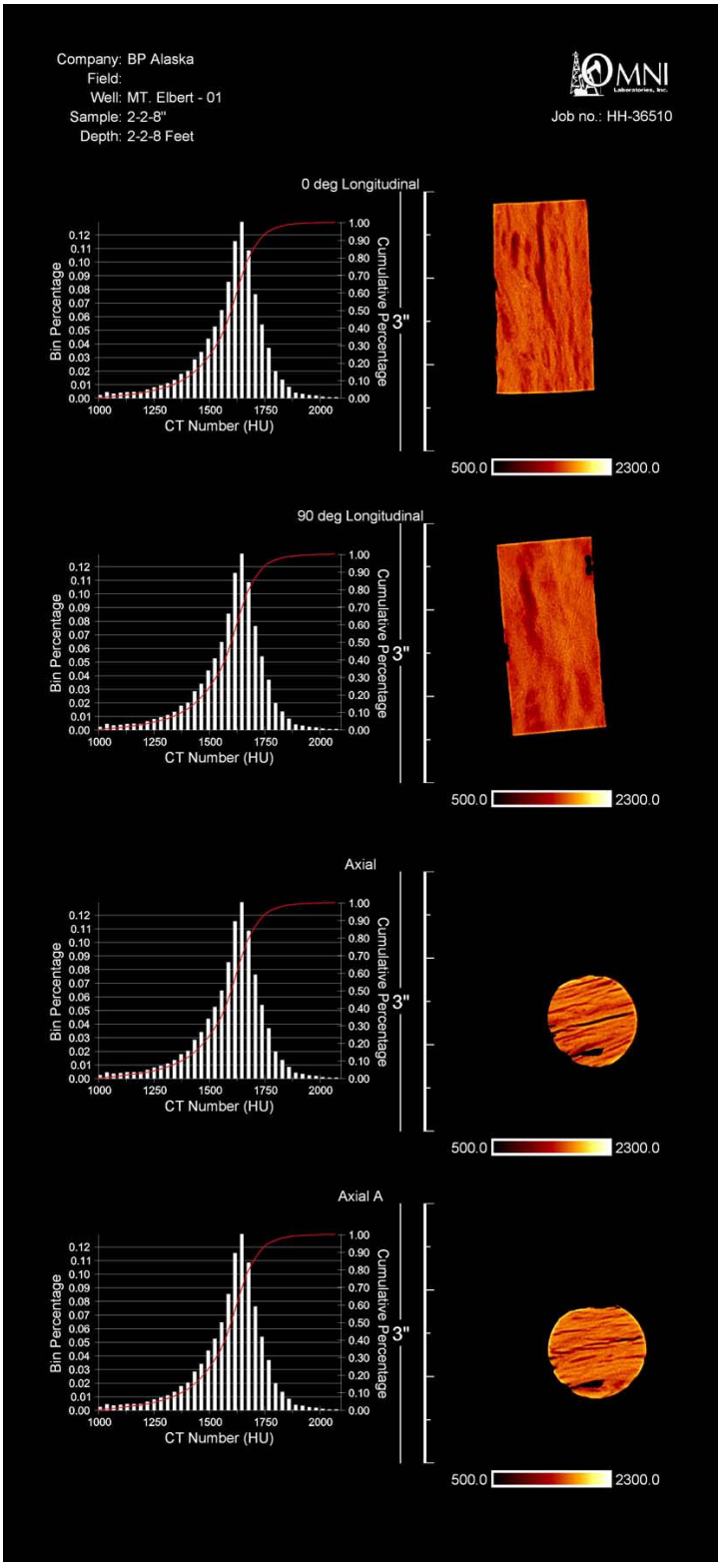

Figure B42: CTscan of core sample, Core 2, Section 2, 8 inches

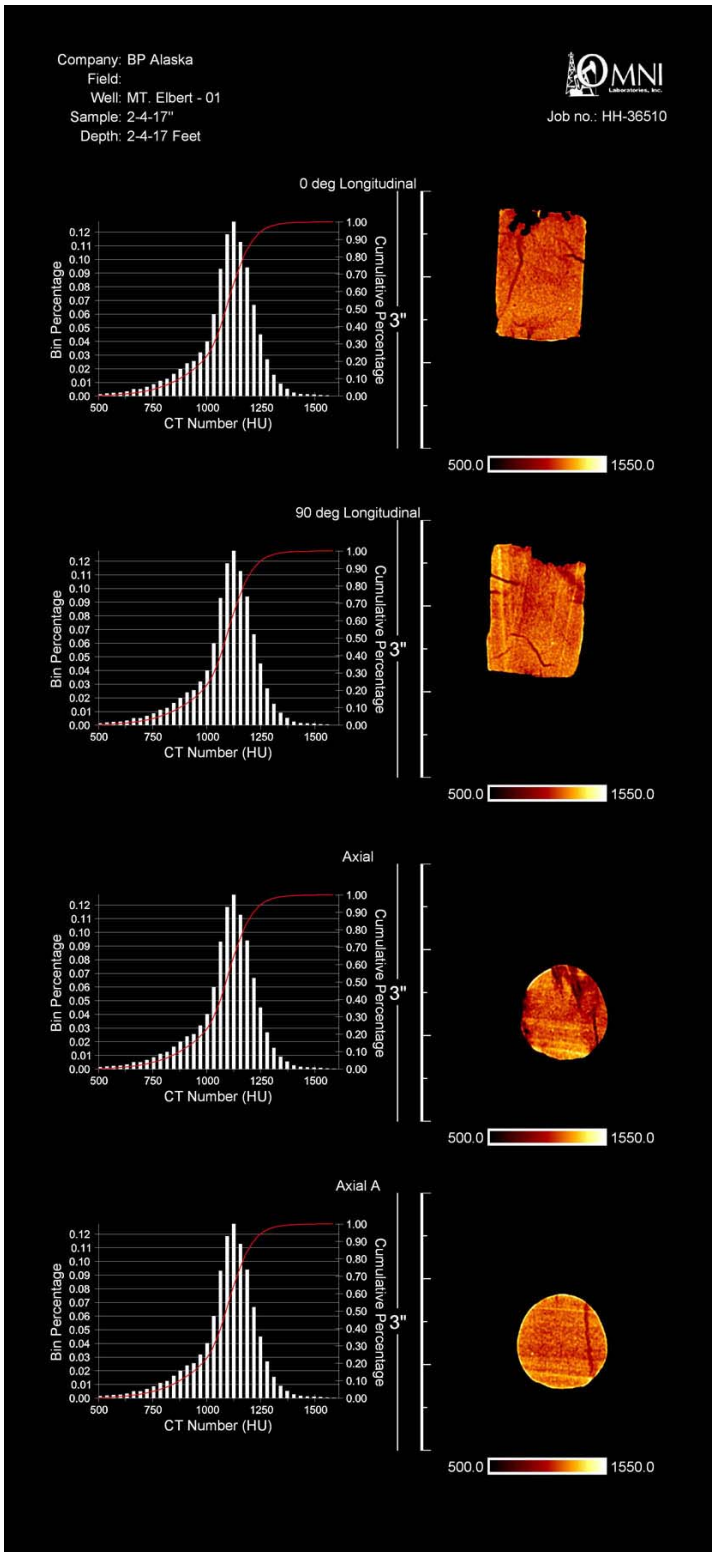

Figure B43: CTscan of core sample, Core 2, Section 4, 17 inches

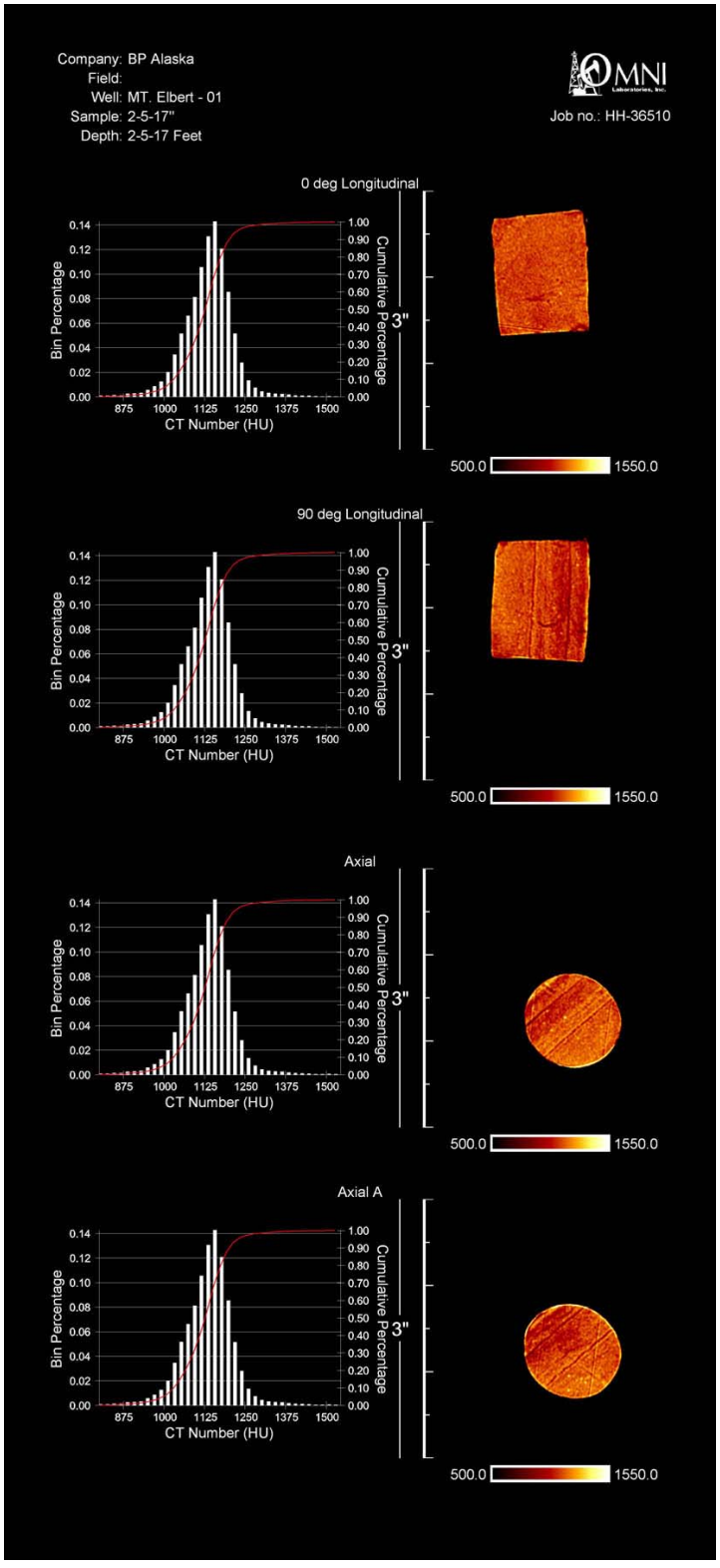

Figure B44: CTscan of core sample, Core 2, Section 5, 17 inches

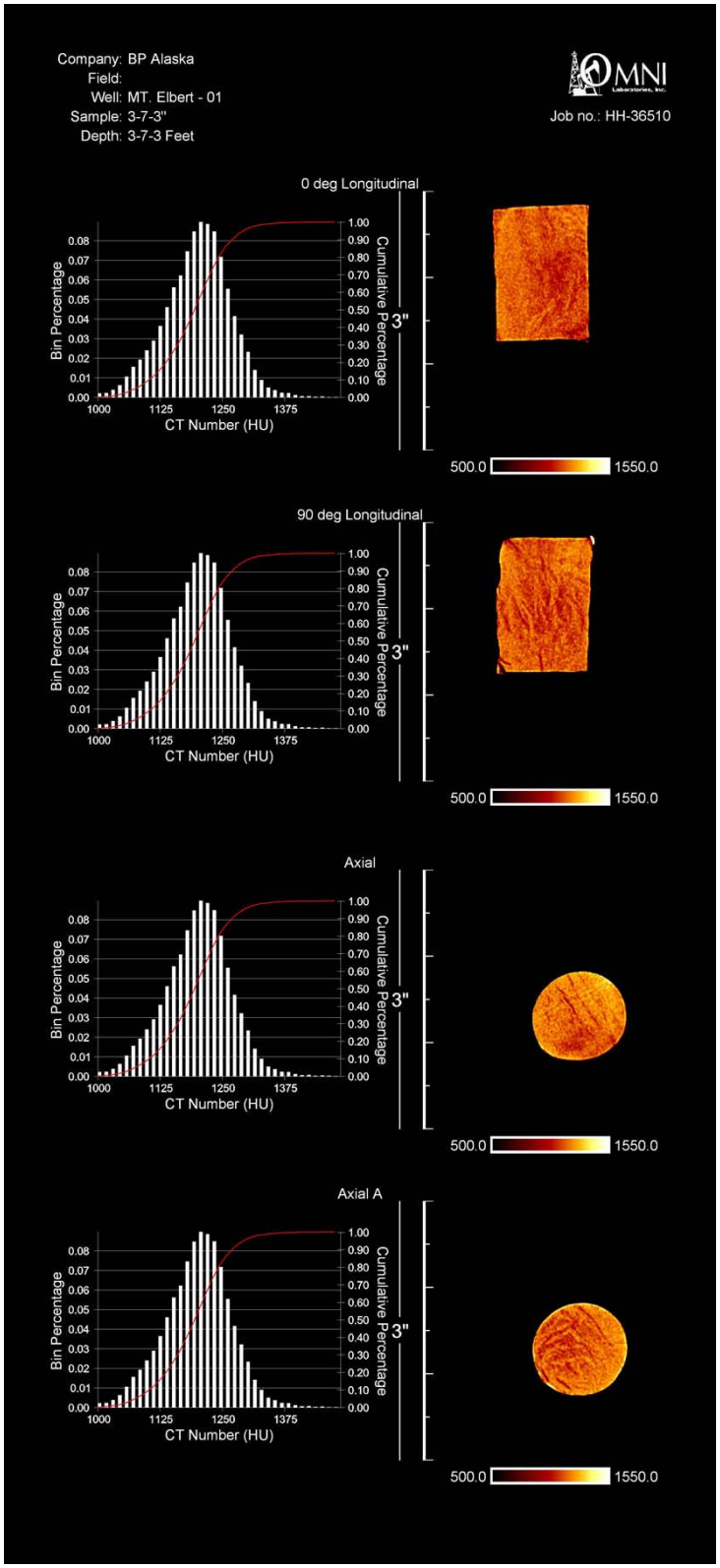

Figure B45: CTscan of core sample, Core 3, Section 7, 3 inches

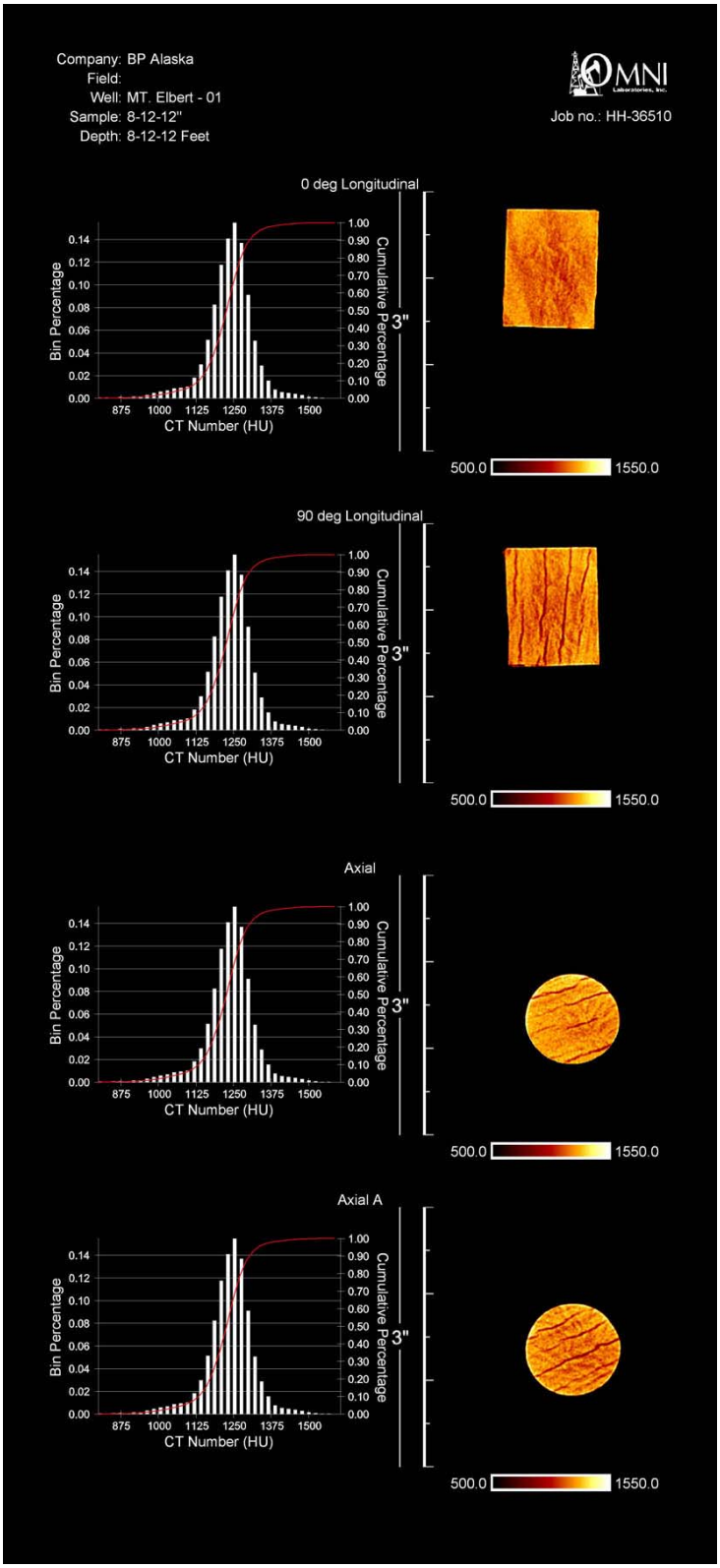

Figure B46: CTscan of core sample, Core 8, Section 12, 12 inches

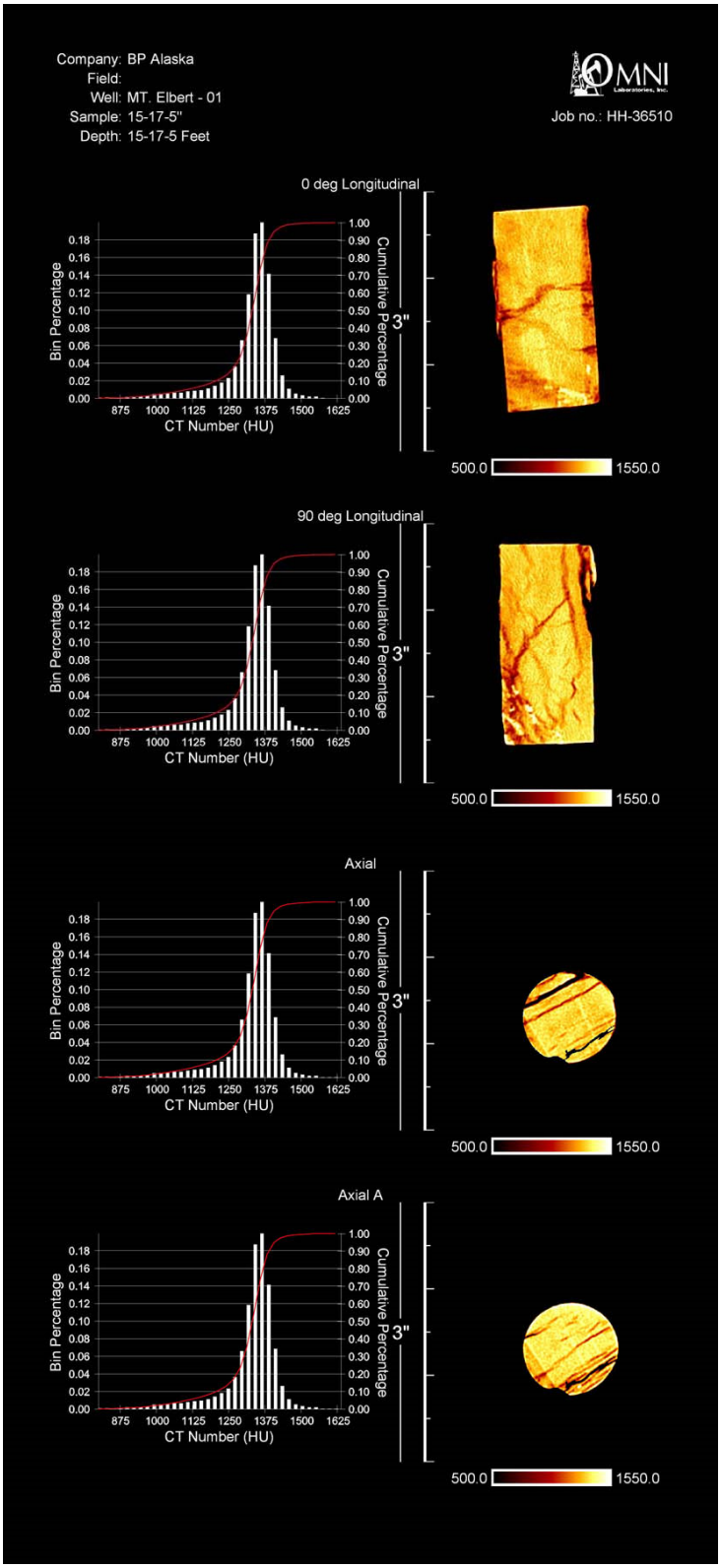

Figure B47: CTscan of core sample, Core 15, Section 17, 5 inches

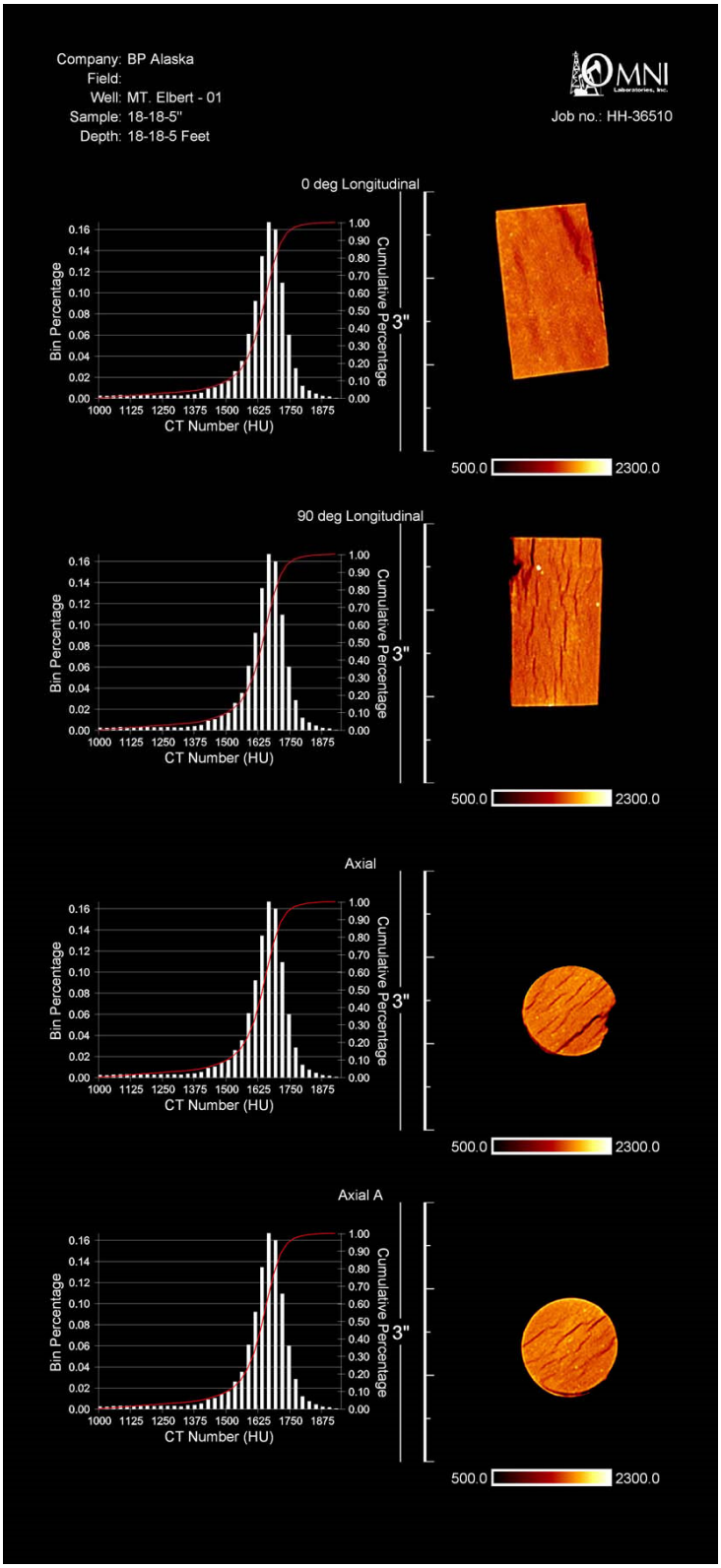

Figure B48: CTscan of core sample, Core 18, Section 18, 5 inches

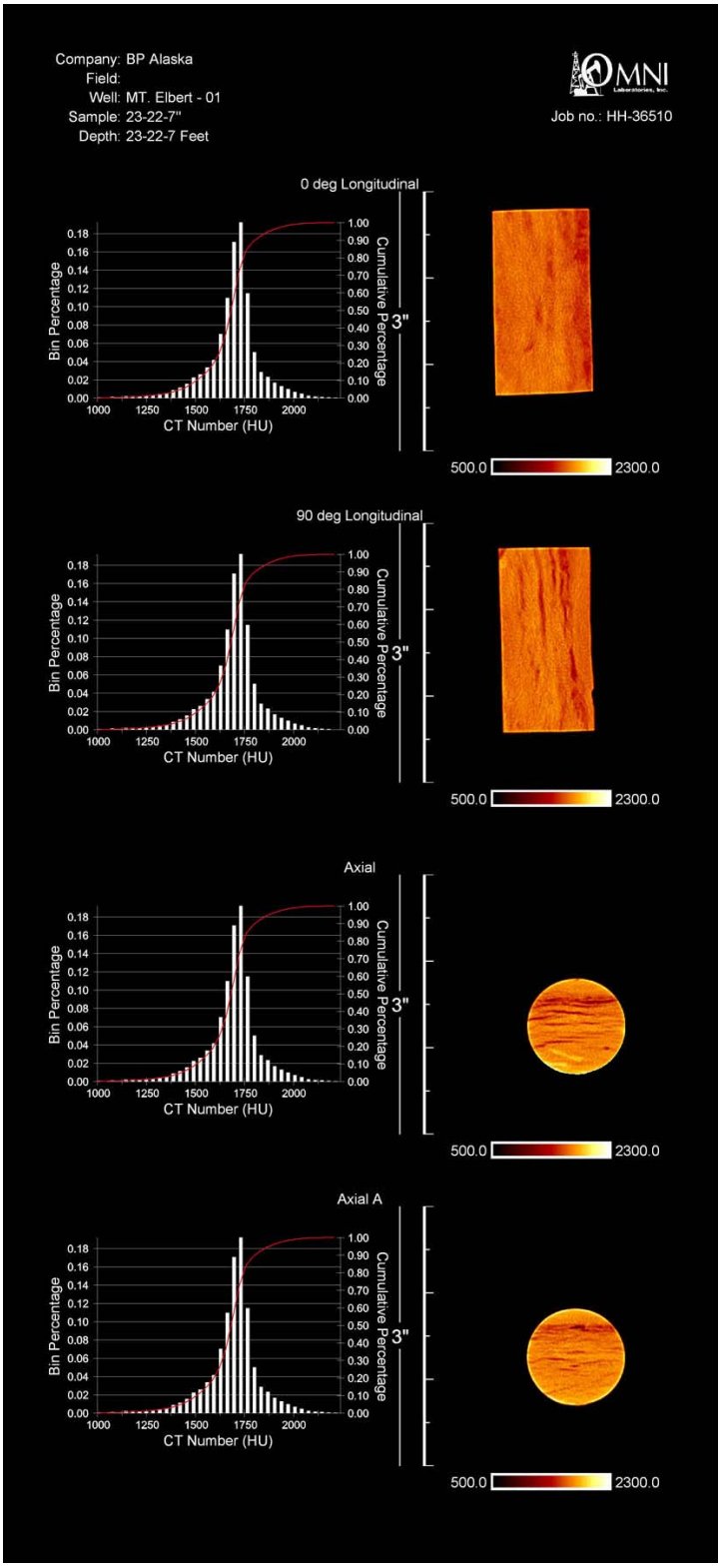

Figure B49: CTscan of core sample, Core 23, Section 22, 7 inches

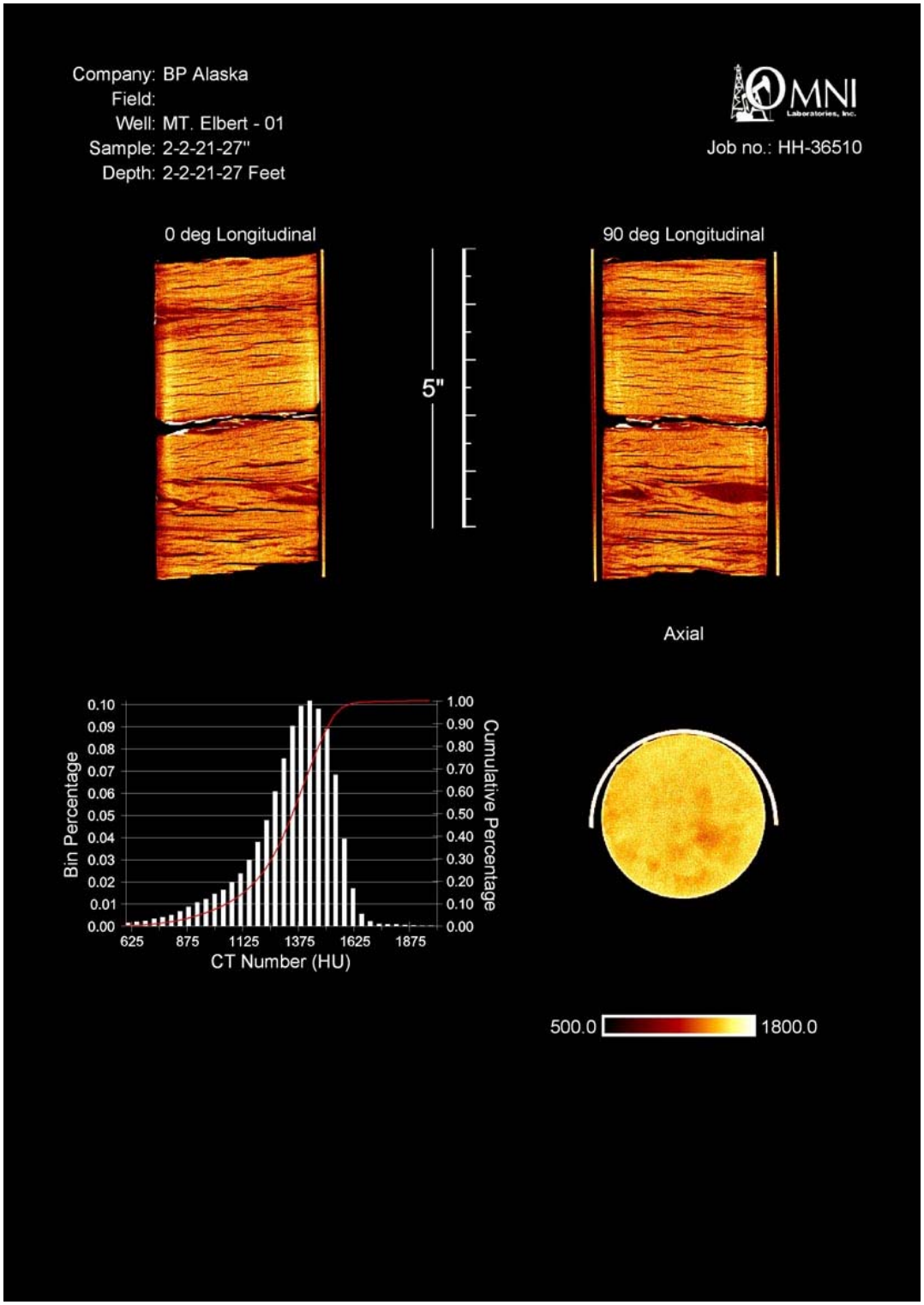

Figure B50: CTscan of core sample, Core 2, Section 2, 21 to 27 inches

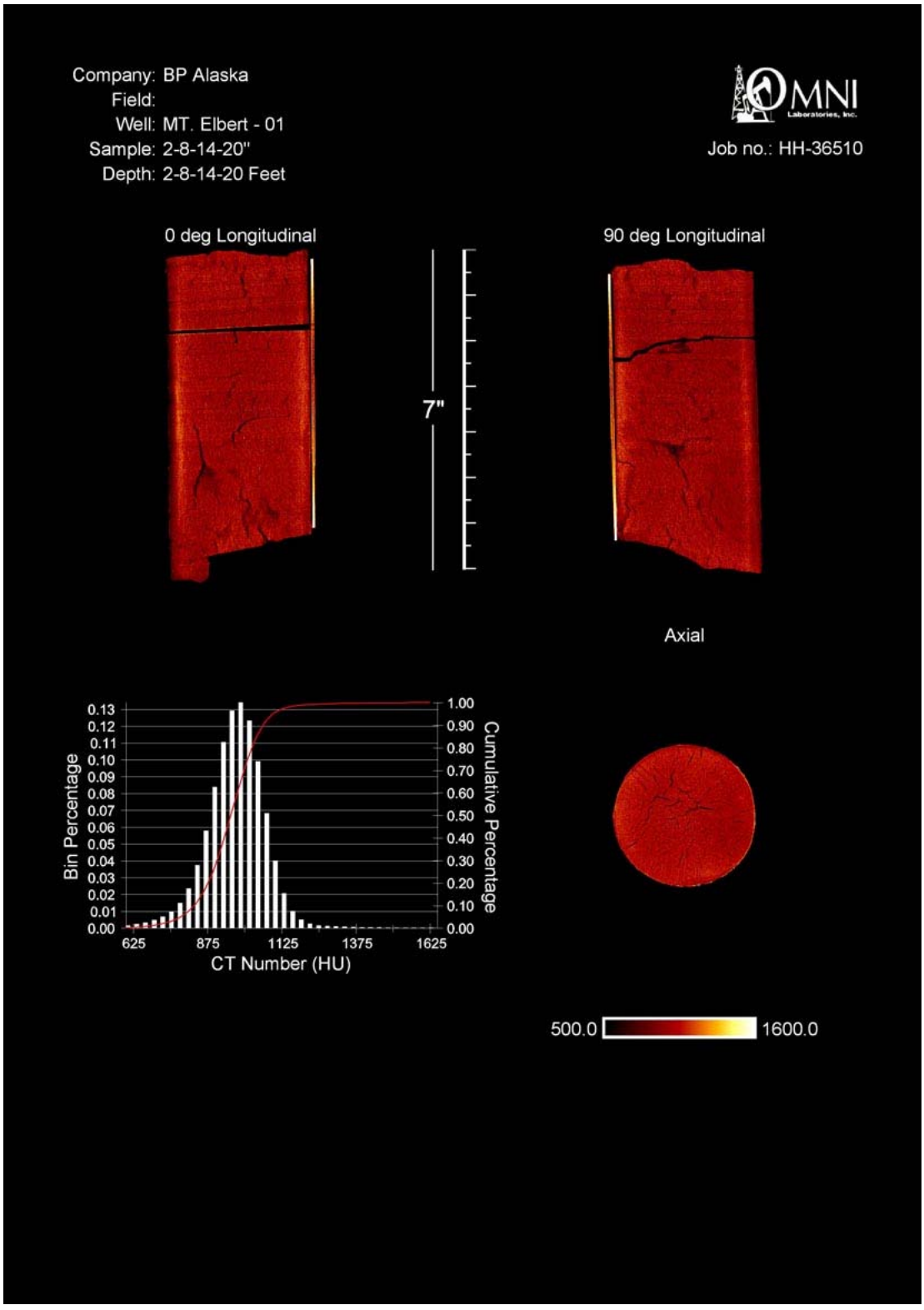

Figure B51: CTscan of core sample, Core 2, Section 8, 14 to 20 inches

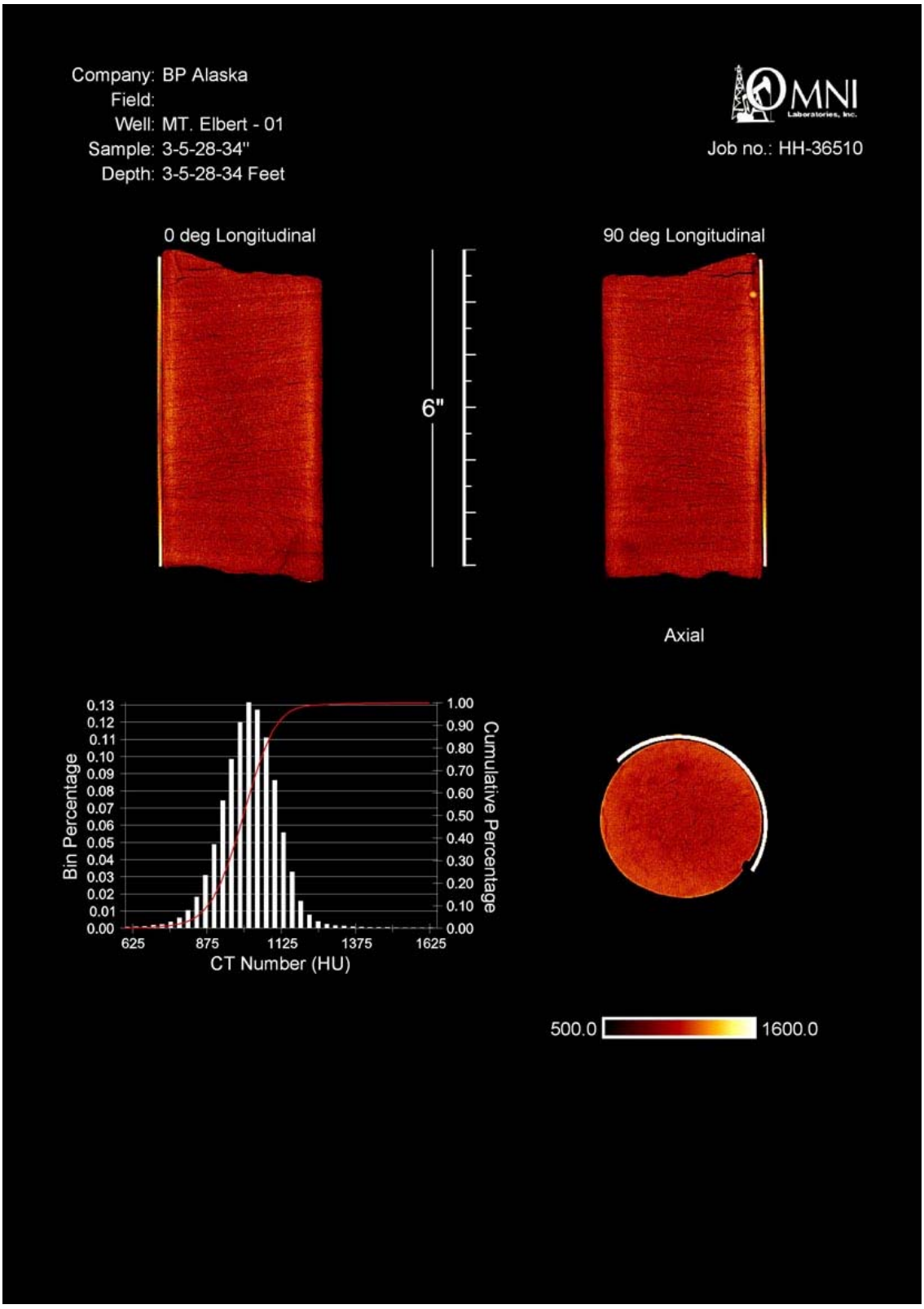

Figure B52: CTscan of core sample, Core 3, Section 5, 28 to 34 inches

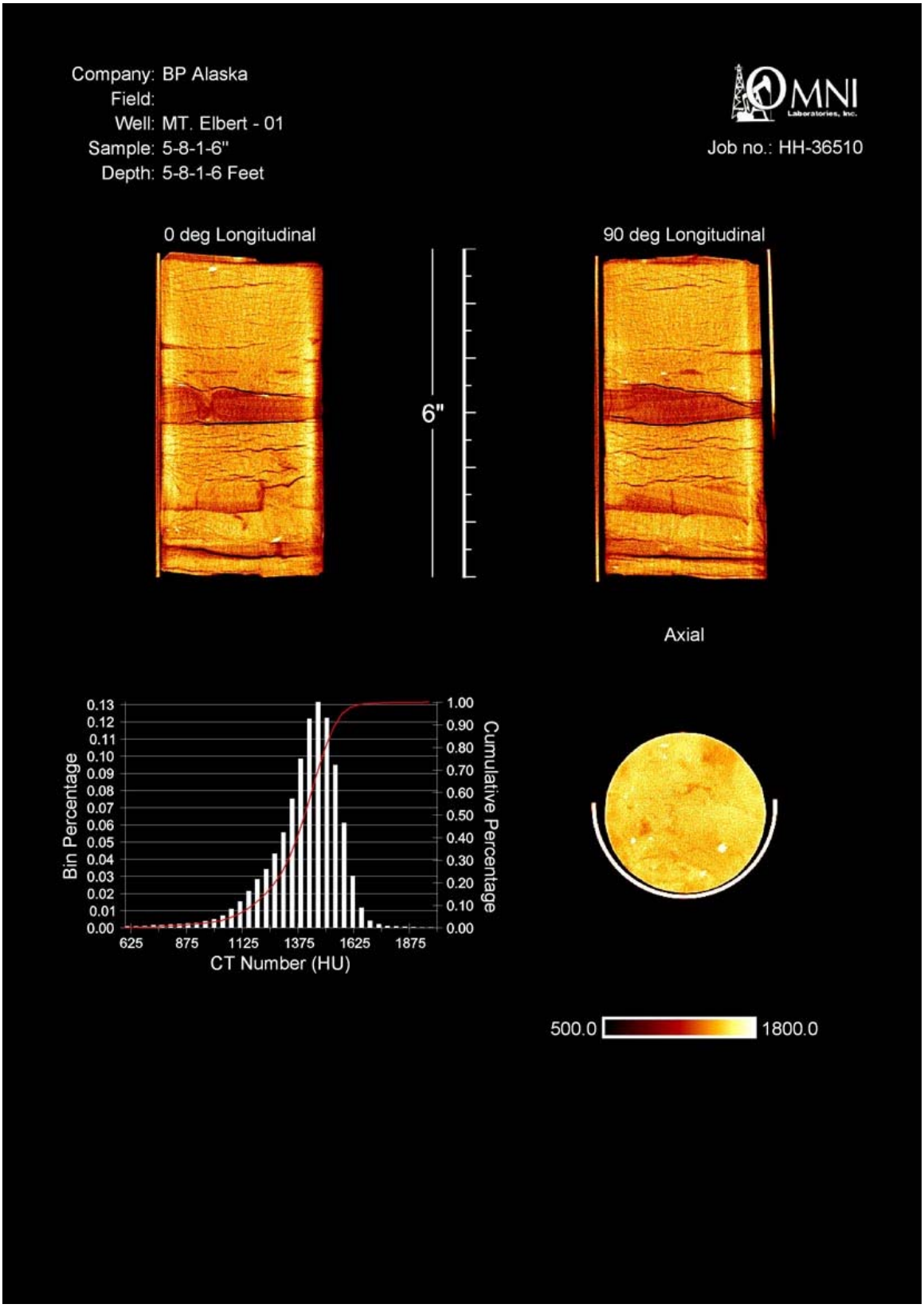

Figure B53: CTscan of core sample, Core 5, Section 8, 1 to 6 inches

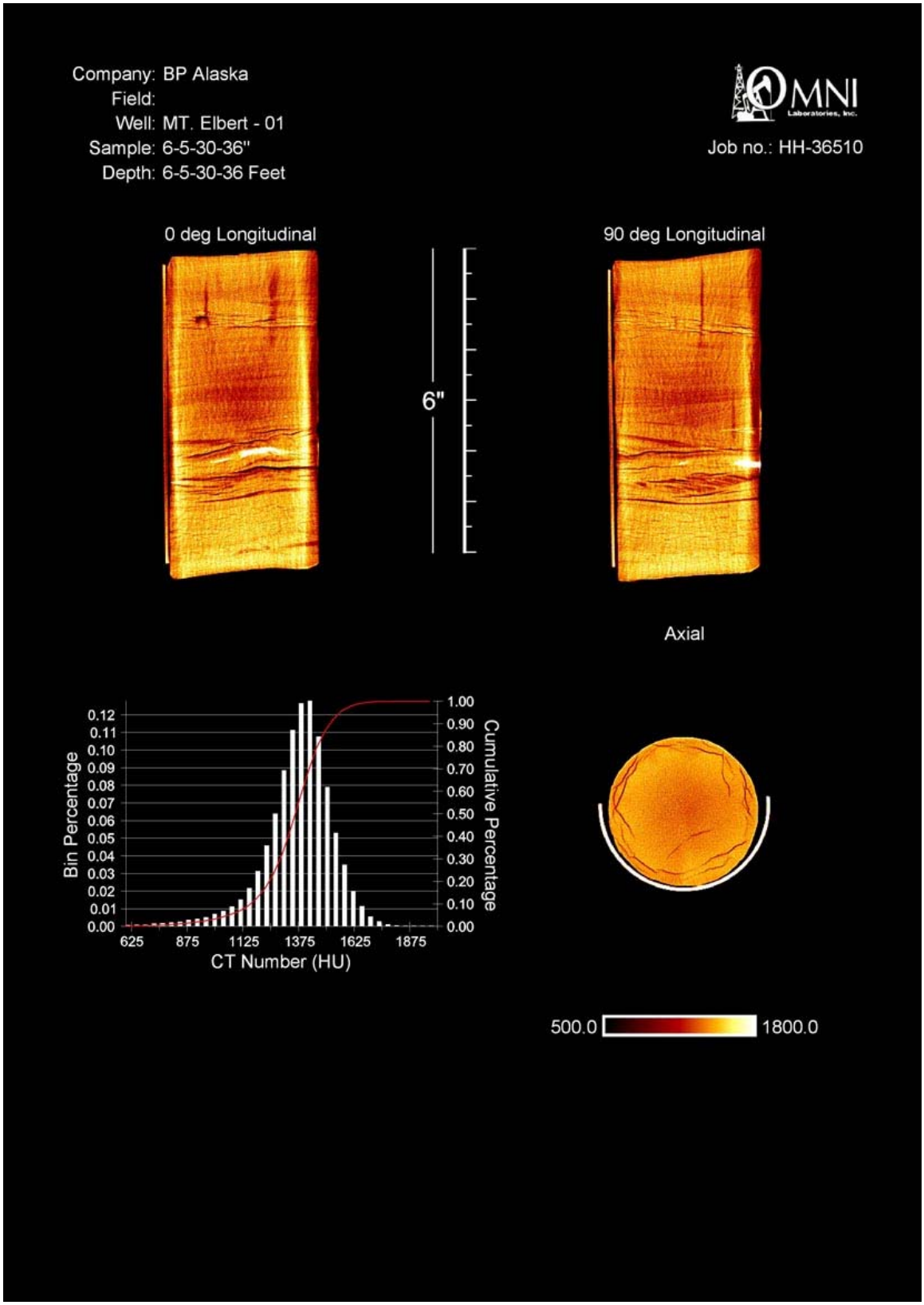

Figure B54: CTscan of core sample, Core 6, Section 5, 30 to 36 inches

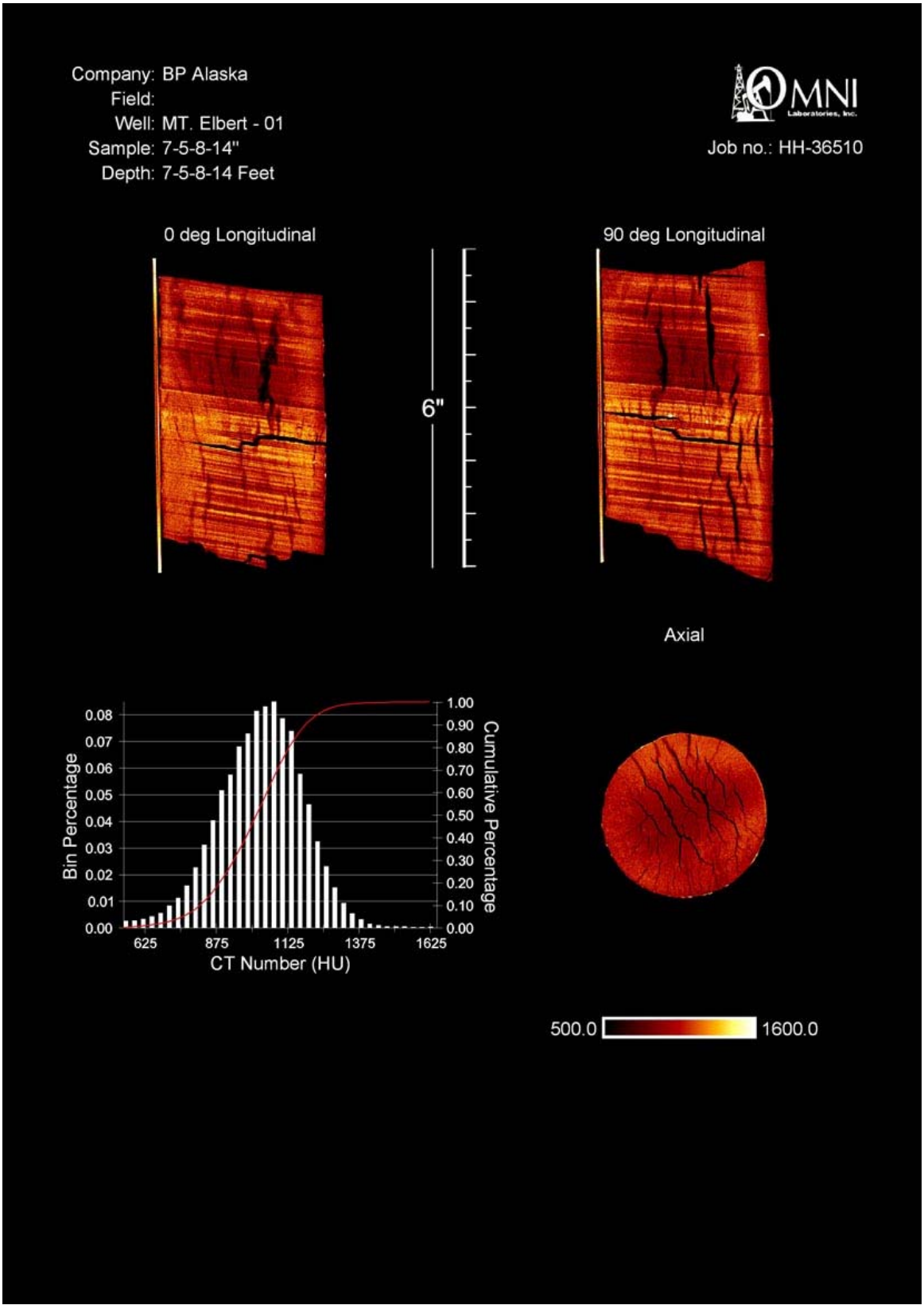

Figure B55: CTscan of core sample, Core 7, Section 5, 8 to 14 inches

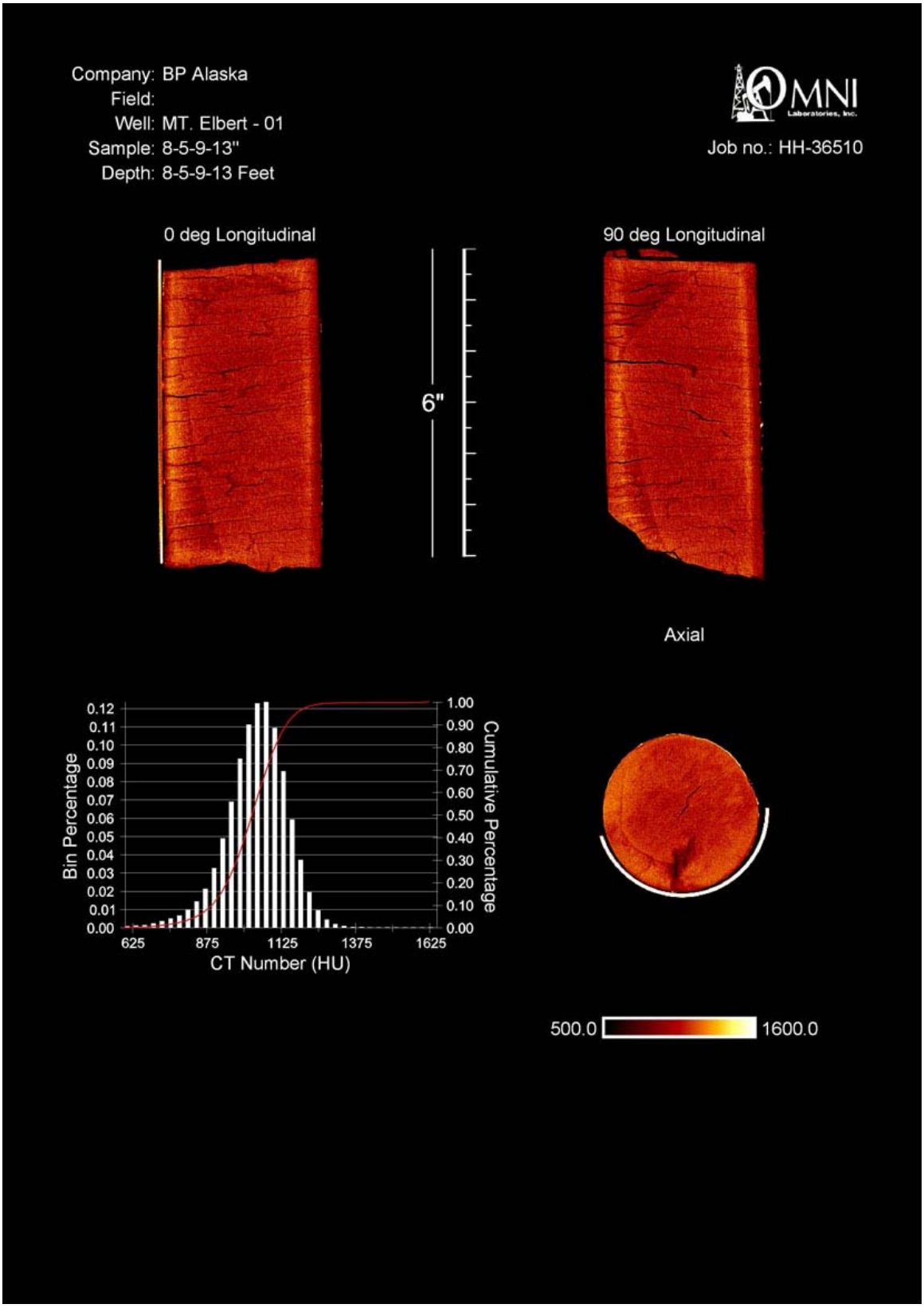

Figure B56: CTscan of core sample, Core 8, Section 5, 9 to 13 inches

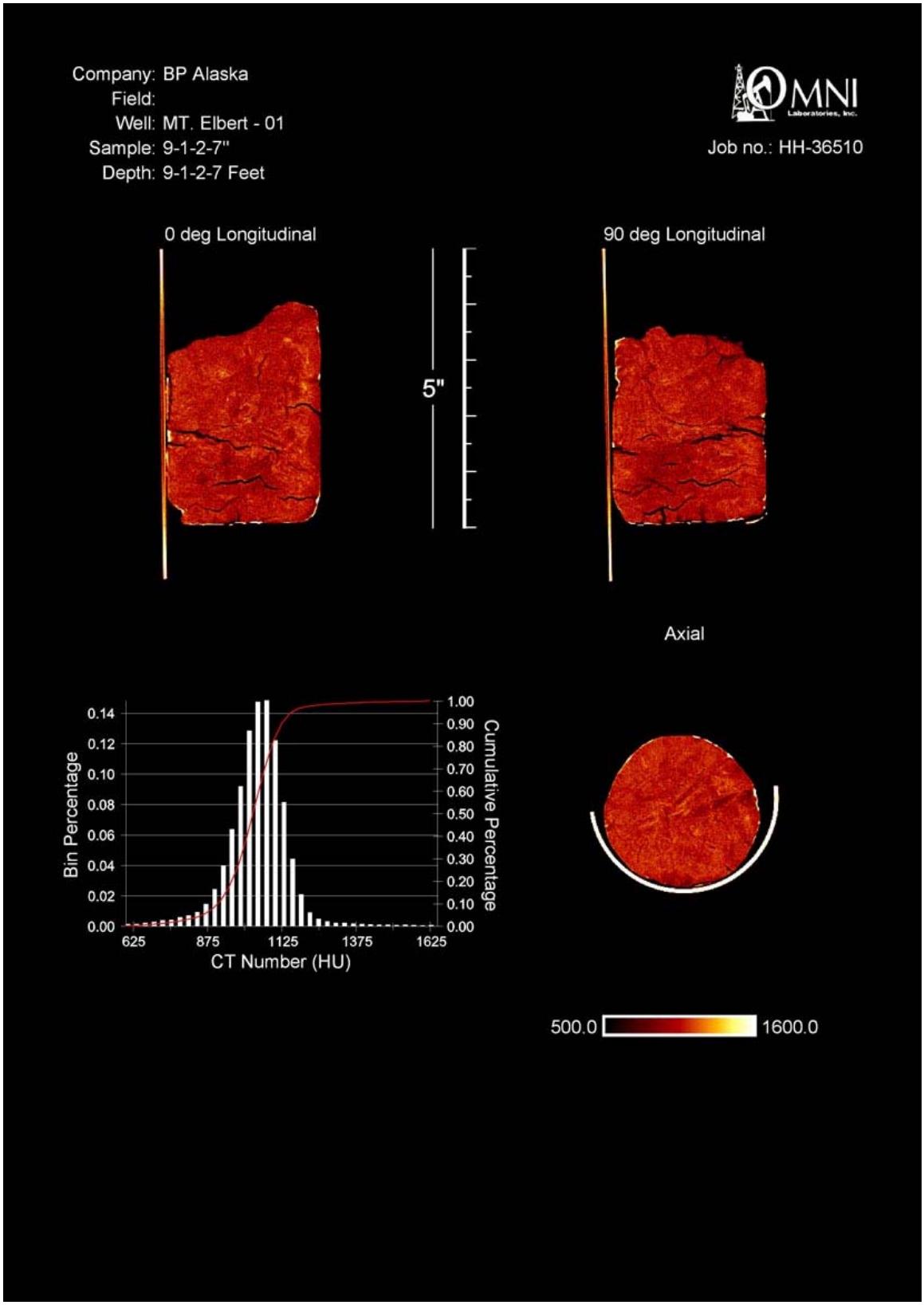

Figure B57: CTscan of core sample, Core 9, Section 1, 2 to 7 inches

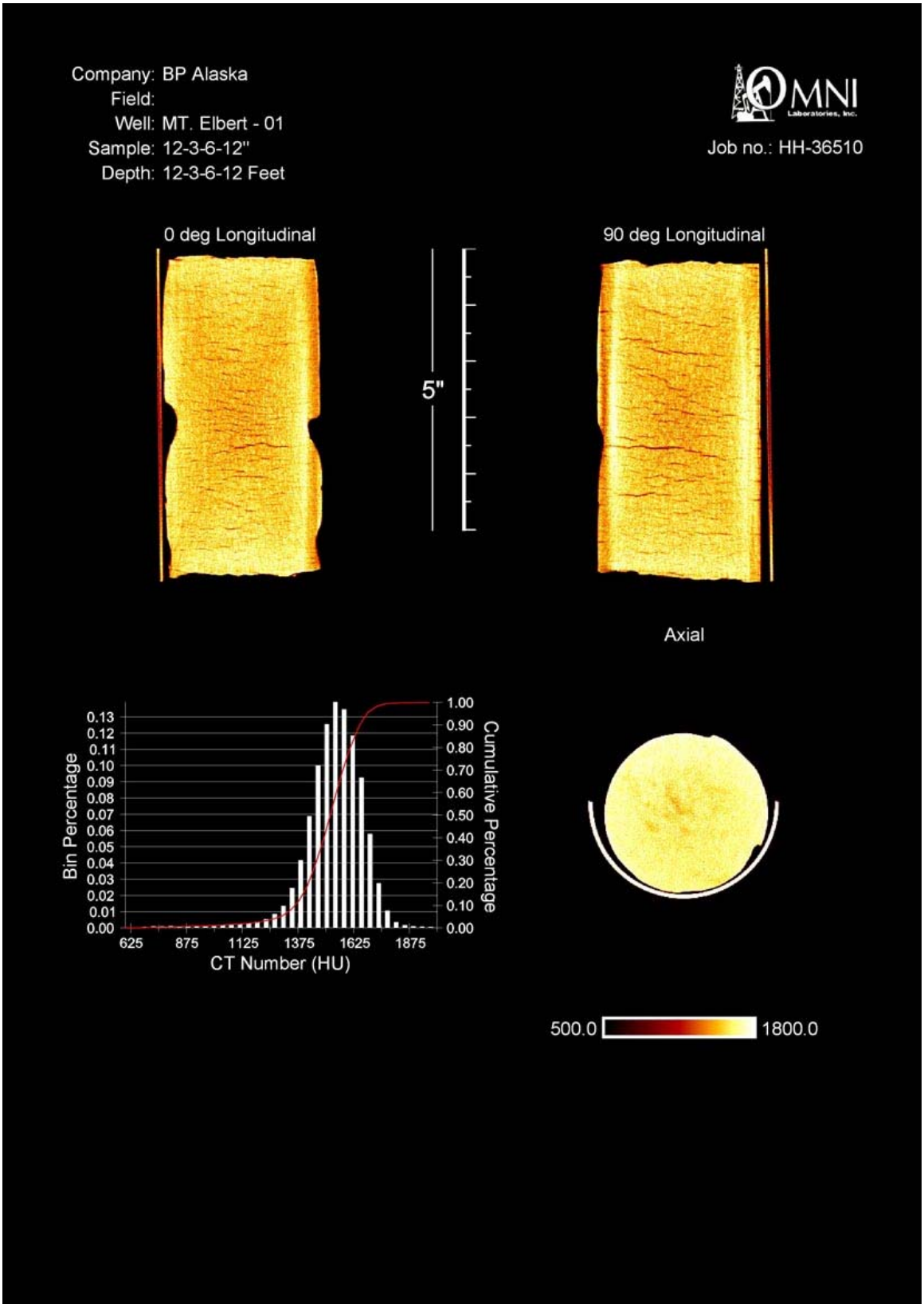

Figure B58: CTscan of core sample, Core 12, Section 3, 6 to 12 inches

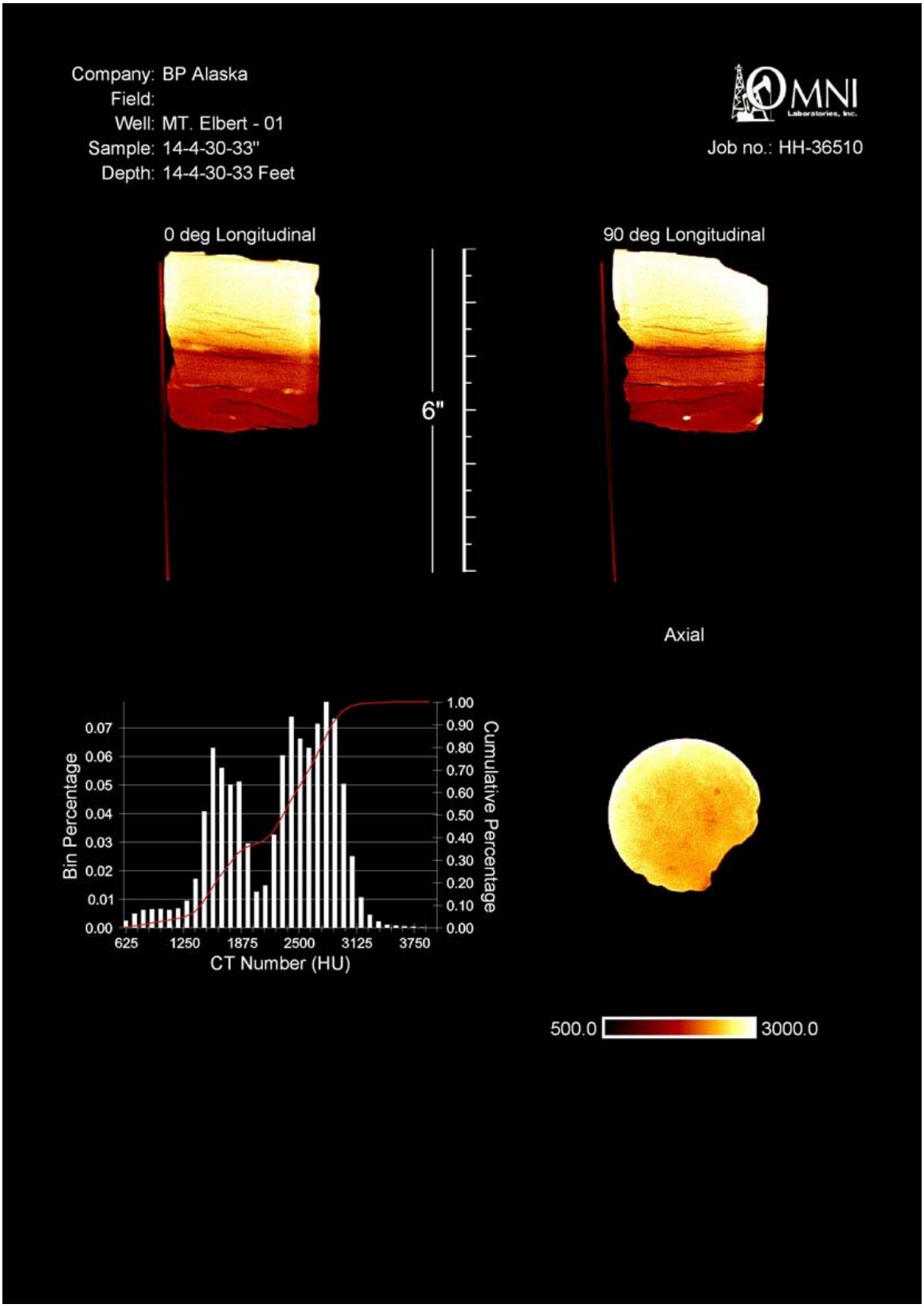

Figure B59: CTscan of core sample, Core 14, Section 4, 30 to 33 inches

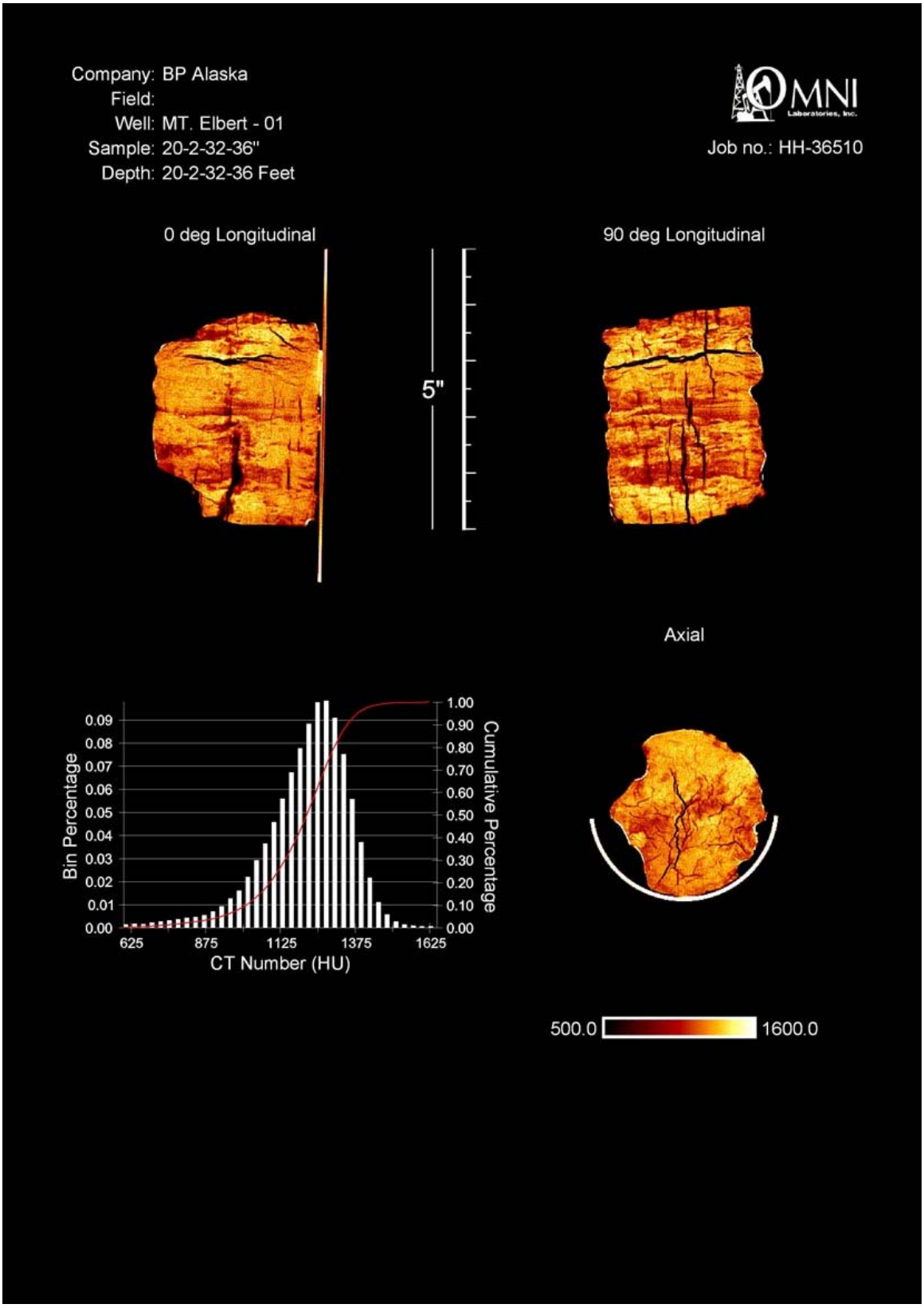

Figure B60: CTscan of sample, Core 20, Section 2, 32 to 36 inches

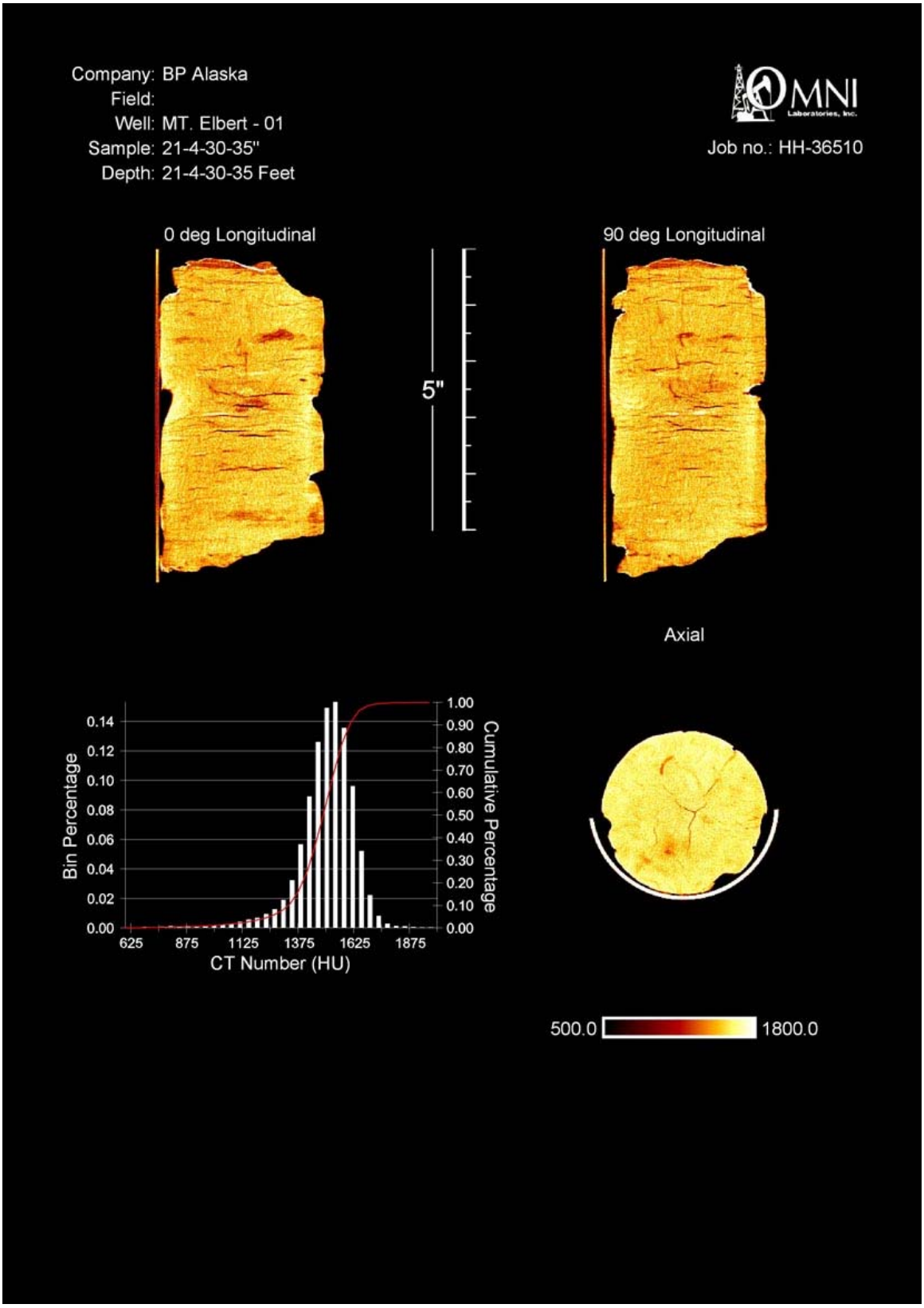

Figure B61: CTscan of core sample, Core 21, Section 4, 30 to 35 inches

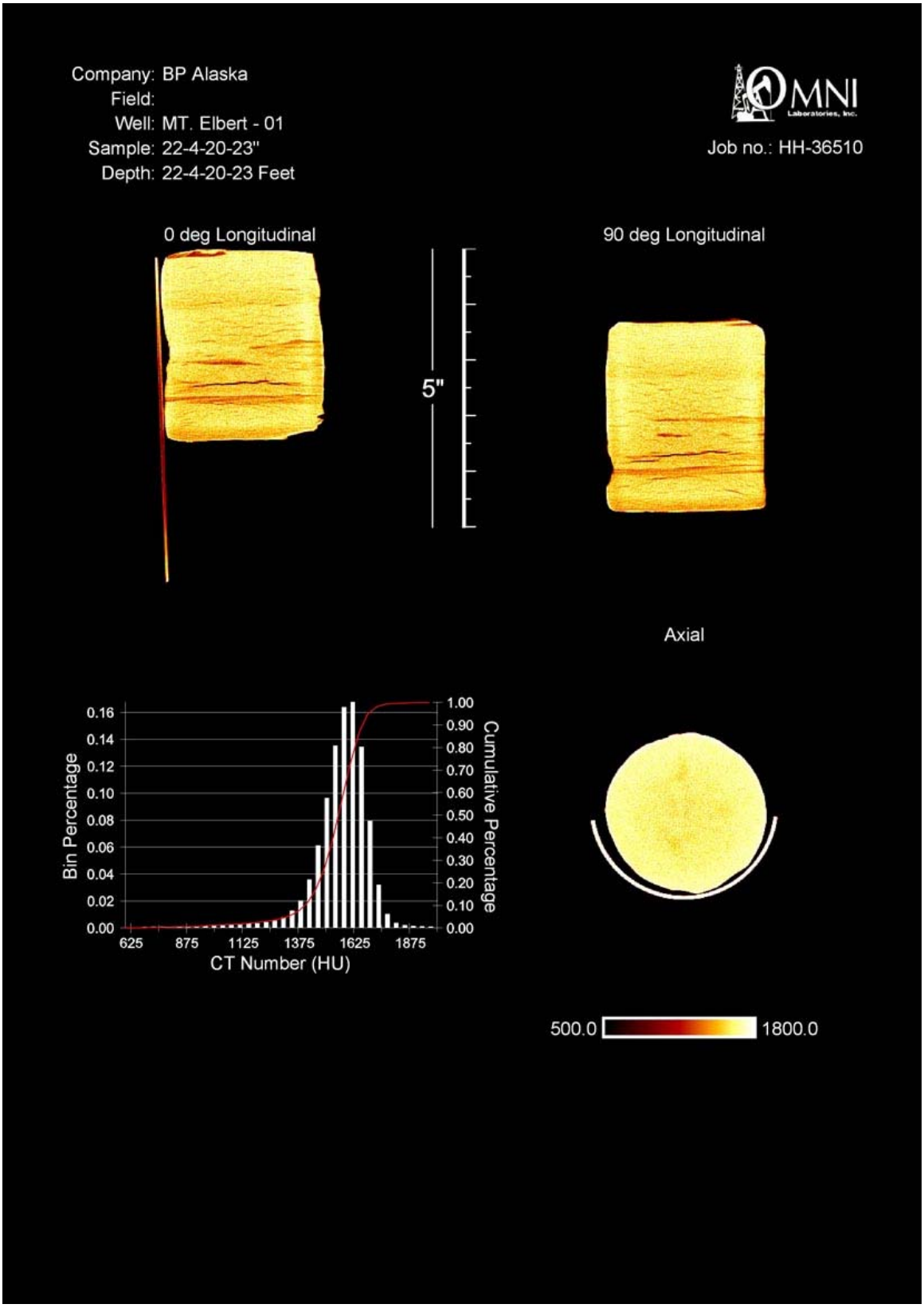

Figure B62: CTscan of core sample, Core 22, Section 4, 20 to 23 inches

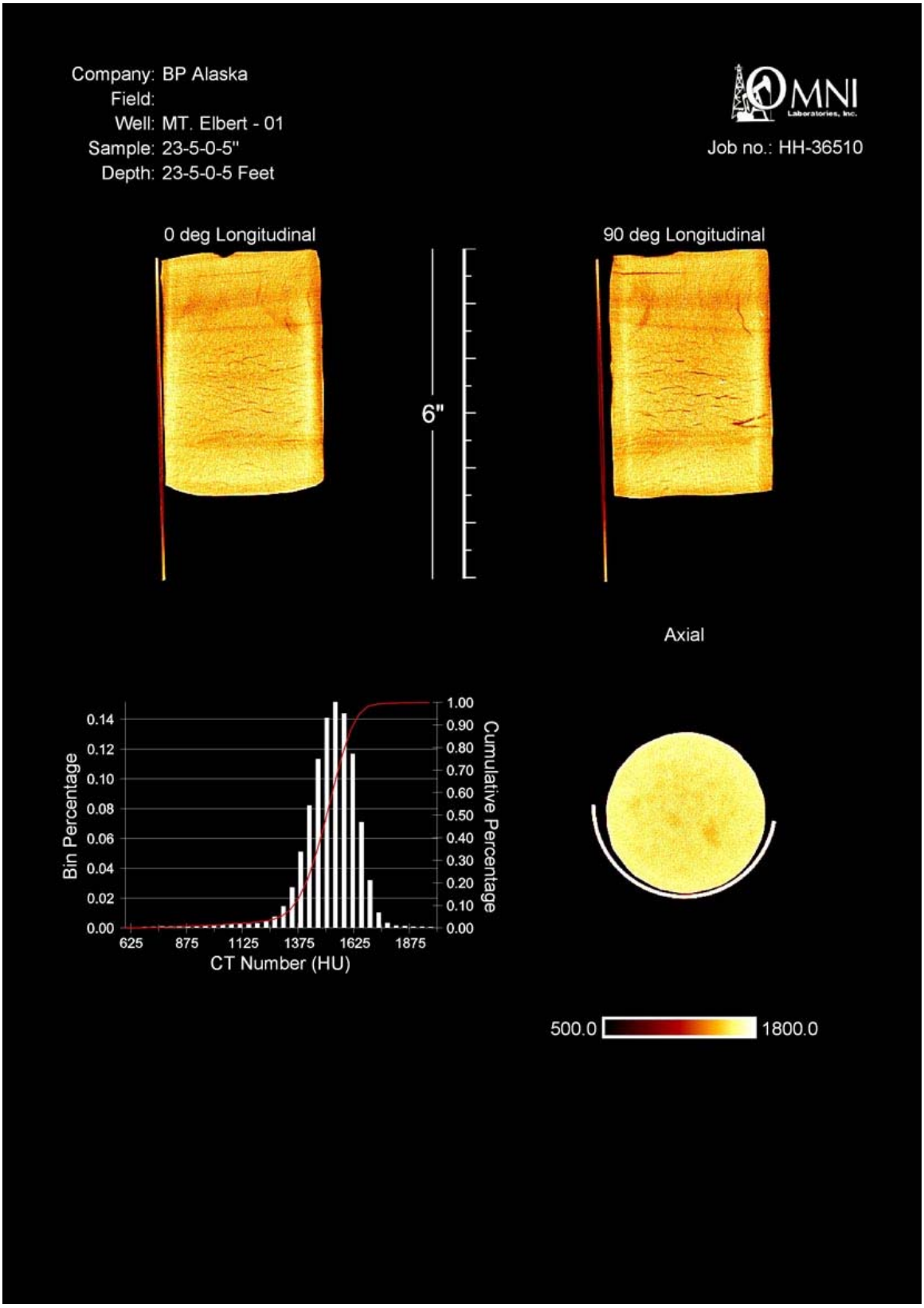

Figure B63: CTscan of core sample, Core 23, Section 5, 0 to 5 inches

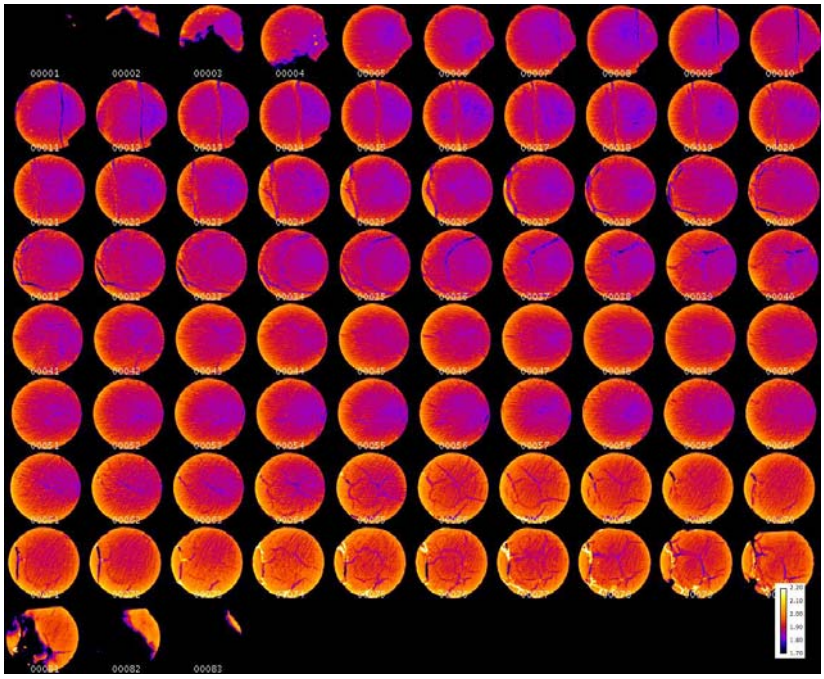

Figure B64: LBNL CTscan slices of Core 2, Section 7, 20 to 30 inches

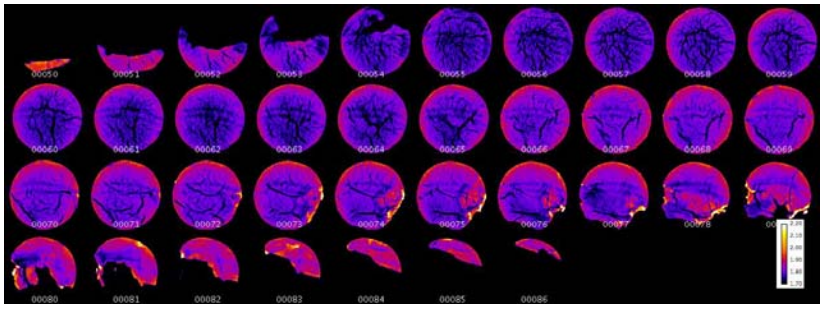

Figure B65: LBNL CTscan slices of Core 2, Section 8, 26 to 31 inches

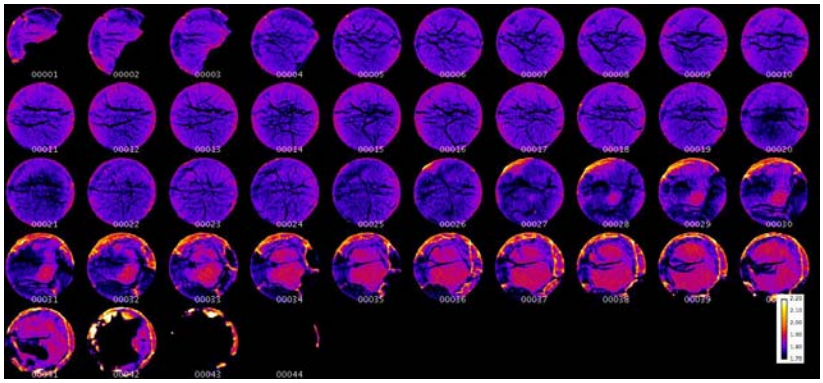

Figure B66: LBNL CTscan slices of Core 2, Section 8, 31 to 36 inches

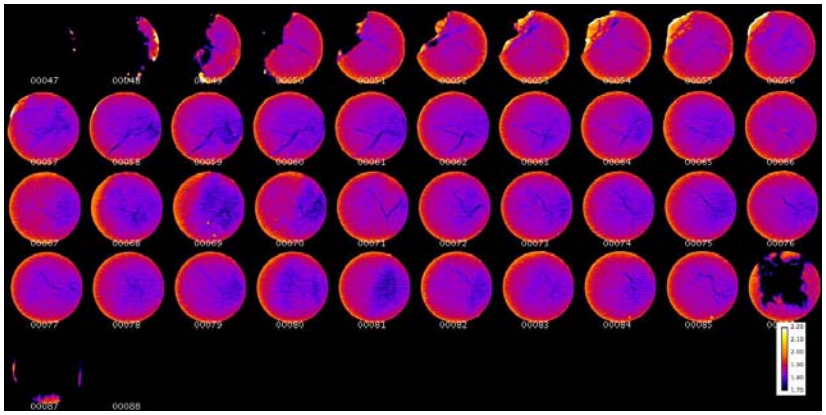

Figure B67: LBNL CTscan slices of Core 3, Section 4, 31 to 36 inches

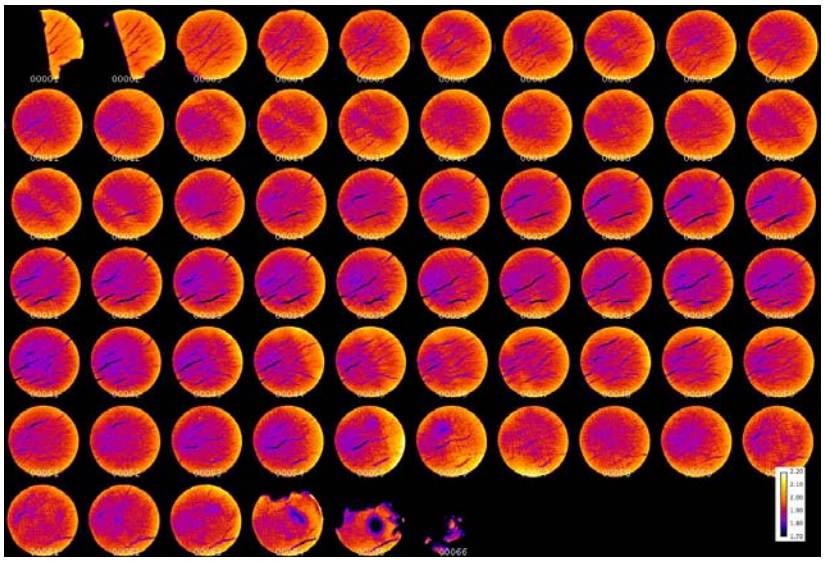

Figure B68: LBNL CTscan slices of Core 7, Section 5, 14 to 22 inches

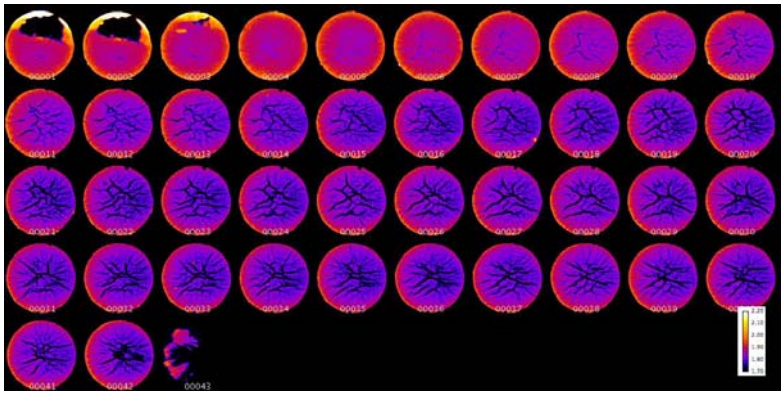

Figure B69: LBNL CTscan slices of Core 7, Section 6, 31 to 36 inches

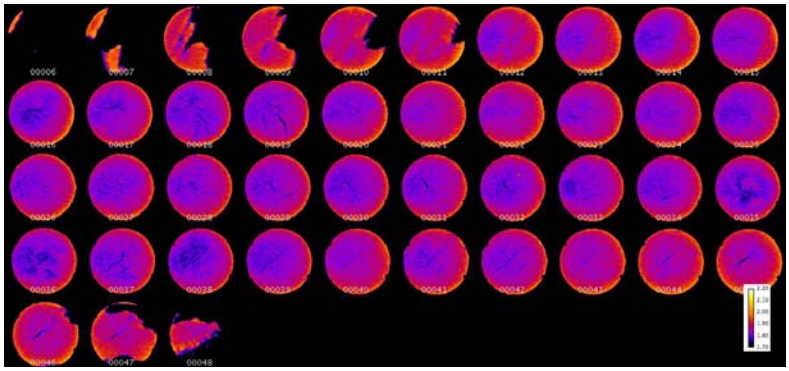

Figure B70: LBNL CTscan slices of Core 8, Section 4, 31 to 36 inches

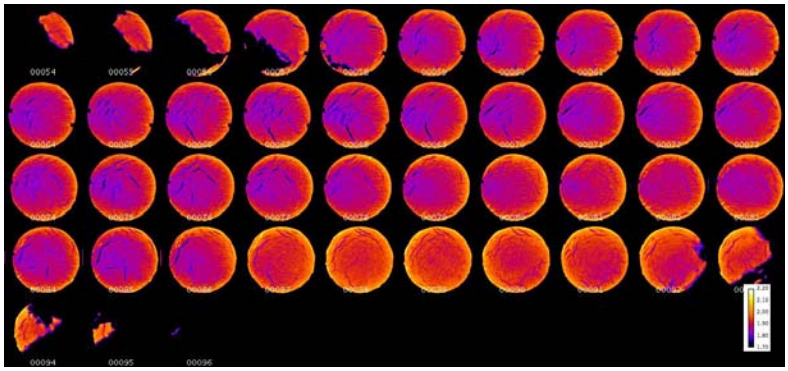

Figure B71: LBNL CTscan slices of Core 8, Section 5, 31 to 36 inches

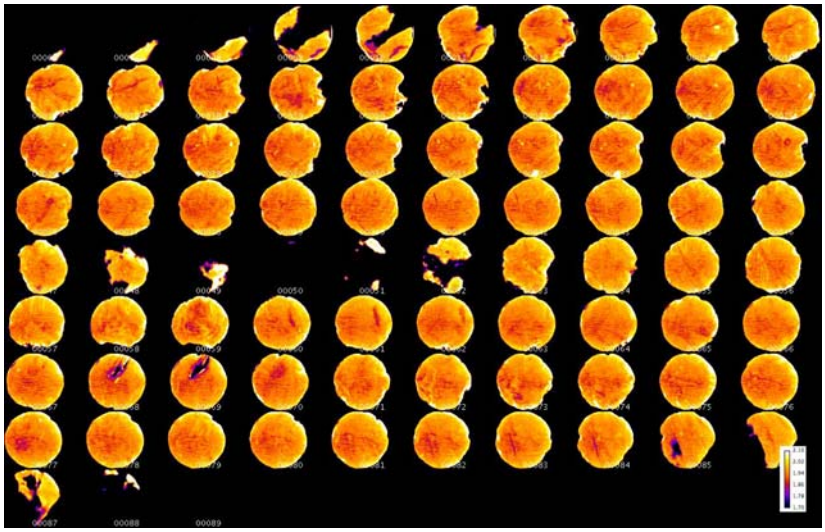

Figure B72: LBNL CTscan slices of Core 9, Section 1, 7 to 17 inches

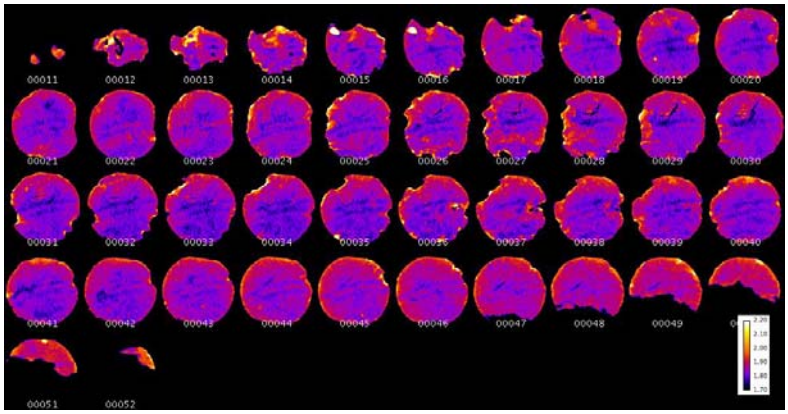

Figure B73: LBNL CTscan slices of Core 9, Section 1, 31 to 36 inches

National Energy Technology Laboratory

626 Cochrans Mill Road
P.O. Box 10940
Pittsburgh, PA 15236-0940

3610 Collins Ferry Road
P.O. Box 880
Morgantown, WV 26507-0880

One West Third Street, Suite 1400
Tulsa, OK 74103-3519

1450 Queen Avenue SW
Albany, OR 97321-2198

Visit the NETL website at:
www.netl.doe.gov

Customer Service:
1-800-553-7681